SECTION 5.9: OCEANOGRAPHY AND COASTAL ENGINEERING	
File name: SAR230013-RP-CE-002-R1 TSSR Section 5.9 Update	
Author declaration:	I declare that appropriate diligence and quality assurance was applied in the compilation of this report. As such I am confident in the results here described and the conclusions drawn.  ..... Name: Stephen Luger Date: 2025/01/27
Peer Reviewer:	I declare that this report has undergone independent peer review by myself, that comments were addressed to my satisfaction, and that as such, it is considered fit for publication.  ..... Name: Chris Fleming Date: 2025/01/27
Project Manager Authorisation:	 ..... Name: Andy McClarty Date: 2025/01/28
Eskom Acceptance:	 ..... Name: Date: 2025-01-30

CONTROLLED DISCLOSURE

When downloaded from the EDS database, this document is uncontrolled and the responsibility rests with the user to ensure it is in line with the authorised version on the database.

AMENDMENT RECORD			
Rev	**Draft**	**Date**	**Description**
0	11	April 2015	Section 5.9 (Oceanography and Coastal Engineering) of the Site Safety Report authorised by Eskom Senior Management.
0a		27 January 2025	Section 5.9 updated to reflect the latest regulations, requirements and guidelines. Includes additional oceanographic data, updated climate change and improved methodologies.

CONTROLLED DISCLOSURE

When downloaded from the EDS database, this document is uncontrolled and the responsibility rests with the user to ensure it is in line with the authorised version on the database.

EXECUTIVE SUMMARY

Purpose and Scope

Oceanography and coastal engineering studies have been undertaken for the planned development of new nuclear installation(s) (NIs) at the Thyspunt site. The purpose of this section of this SSR is to identify the requirements and to demonstrate the technical acceptability of the site with regard to coastline stability, flooding from the sea, integrity of cooling water supply and thermal plume dispersion. Design considerations for seawater cooling water intake and outfall layouts are provided.

Climate Change

The effect of climate change on all relevant oceanographic and coastal engineering parameters has been included. For sea level rise (SLR) values of 0.14 m, 1.38 m and 1.76 m have been applied for the key dates of 2034, 2114, and 2134, respectively. An additional high-end SLR scenario, which incorporates processes which are deeply uncertain but cannot be ruled out, was considered as a high-end sea level rise scenario of 3.28 m for only the 2134 date, and is referred to as the '2134 High SLR' scenario throughout Section 5.9. The applied changes for the other parameters besides SLR are provided in the main report.

Nearshore Waves

The results indicate a rough wave climate with significant wave heights (the mean of the highest one-third of waves) up to 14.7 m in a depth of 55 m directly offshore of the site. These waves will need to be accounted for in the design of all coastal structures at the site during the SAR and engineering design phases, e.g., intake structures, outfall structures and revetments.

Coastline Stability

Coastline stability at the site has been assessed including sea level rise, wave climate change and cross-shore storm erosion. The maximum horizontal erosion line in front of the new NIs is provided in the main report.

- The coastline erosion increases over time due to climate change which causes sea level rise and associated coastline recession, a rotated wave climate, and increases in storm wave height and storm surge.
- The erosion is more severe in Thysbaai than on the rocky coastline in the west, driven by recession due to sea level rise and coastline changes due to wave climate change which affect sandy coastlines.
- In 2034 only the 1E-8 y^{-1} storm erosion line extends onto a small section of the Nuclear Installation Corridor near the centre of the rocky coastline west of Thyspunt.

CONTROLLED DISCLOSURE

When downloaded from the EDS database, this document is uncontrolled and the responsibility rests with the user to ensure it is in line with the authorised version on the database.

- By 2134 the Nuclear Installation Corridor is exceeded by the erosion lines for all storms with exceedance frequencies of 1E-2 y^{-1} and lower, at a limited number of locations along the rocky coastline west of Thyspunt and within Thysbaai.
- The 2134 High SLR scenario increases the erosion along the entire site, most substantially within Thysbaai. The erosion lines for all storms with exceedance frequencies of 1E-2 y^{-1} and lower extend onto the Nuclear Installation Corridor along the majority of Thysbaai and along the westernmost half of the rocky coastline west of Thyspunt.
- It will thus be necessary to move the position of the new NIs landward, or to design appropriate coastal protection such as revetments.
- Note that these erosion lines show the extent of erosion of the topography which will threaten safety related structures, systems and components (SSCs) at the site. Wave run-up and flooding due to storm waves or tsunamis may extend further inland than these erosion lines. Flooding is discussed below.
- Further engineering studies should be undertaken to ensure that the outfall structures can withstand the predicted coastline erosion over the operating life of the plant.

Flooding from the Sea

Flooding from the sea can occur due to:

- Storm wave run-up combined with sea level rise, high tides, positive storm surge and wave set-up; and
- Tsunami run-up combined with sea level rise, high tides and positive storm surge.

No tsunami results are presented in this SSR and it is recommended that an updated Tsunami Hazard Analysis (THA) be undertaken for Thyspunt and that this SSR should then be updated once these results are available. In the interim the flooding from the sea is based on the storm wave run-up only, as described below.

The results show the following:

- The flooding hazard increases over time due to climate change which causes sea level rise and associated coastline recession, a rotated wave climate, and increases in storm wave height and storm surge.
- The best estimate maximum vertical run-up level in 2034 due to the 1E-8 y^{-1} storm is 13.3 m msl, increasing to 17.6 m msl in 2134, and 21.0 m msl for the 2134 High SLR scenario.
- The maximum wave run-up for all modelled frequencies in 2034 and both 2134 scenarios occurred along the exposed rocky coastline to the west of Thyspunt, while Thysbaai to the east of Thyspunt experienced significant landward flooding due to coastline recession.

CONTROLLED DISCLOSURE

When downloaded from the EDS database, this document is uncontrolled and the responsibility rests with the user to ensure it is in line with the authorised version on the database.

- The flood lines extend into the estimated position of the Nuclear Installation Corridor for all three climate change scenarios. In 2034 the flood lines reach Nuclear Installation Corridor for exceedance frequencies of 1E-4 y^{-1} and lower, increasing to exceedance frequencies of 1E-2 y^{-1} and lower in 2134.
- The SSCs will need to be placed landward of the maximum flood lines, or alternatively protective structures such as revetments and wave walls will need to be placed in front of the SSCs. The SSCs will also need to be placed landward of the maximum erosion lines described above.

Extreme Low Water Levels

Extreme low water levels at the cooling water intakes can occur due to:

- Storm wave drawdown combined with low tides and negative storm surge; and
- Tsunami drawdown combined with low tides and negative storm surge.

No tsunami results are presented in this SSR and it is recommended that an updated THA be undertaken for Thyspunt and that this SSR should then be updated once these results are available. In the interim the extreme low water levels are based on the storm wave drawdown only.

If a tunnel intake in a depth of -30 m msl is selected for the new NIs, then the results show that the intake should be designed to accommodate a best estimate minimum water level of -7.6 m msl, which is driven by the 1E-8 y^{-1} storm event in 2134.

Thermal Plume Dispersion and Recirculation

It is proposed that the new NIs will be cooled using a once-through seawater cooling system. A conceptual layout for the seawater cooling intake and outfall system has been developed and thermal plume dispersion modelling has been performed to demonstrate the technical feasibility of the site. The concept considers offshore tunnel intakes at a depth of −30 m msl and an outfall channel discharging at −5 m msl.

The PPE specifies that the maximum ΔT of the re-circulated cooling water between the discharge and the intake should be less than 1.5°C.

The results show the worst case 99th percentile ΔT at the intakes is 0.51°C, which is below the specified 1.5°C maximum allowable ΔT at the intakes.

Extreme Seawater Temperatures

The PPE also specifies a maximum cooling water intake temperature for the new NIs of 30°C. The results show that the exceedance frequency of the maximum specified PPE intake temperature of 30°C is 7.8E-51 y^{-1} (in 2034) and 7.9E-11 y^{-1} (in 2134), thus the intake temperature at the site will be less than the maximum specified in the PPE.

CONTROLLED DISCLOSURE

When downloaded from the EDS database, this document is uncontrolled and the responsibility rests with the user to ensure it is in line with the authorised version on the database.

Sedimentation at Intakes

The results show the following for the proposed tunnel intakes:

- For operational conditions the volume of sand drawn into the tunnel intakes which will have to be removed from the proposed landside intake basins is less than 2 900 m^3/y.
- A maintenance dredging programme will be required to prevent excessive sedimentation in the basin and to keep a sufficient buffer for storm events.
- For extreme storm events the sand volume increases significantly and the 1E-2 y^{-1} storm event results in similar sand volumes over the 5.4-day event as the annual maintenance dredging requirements. The intake basin will need to be designed to accommodate these sediment volumes without blocking the pumps.

Blockage of Intakes and Biofouling

Based on the KNPS and worldwide experience it can be concluded that the new NIs intakes could be designed to cope with the marine species found at the site and to minimise the risk of complete blockage of the intake.

Future Work

The estimation of the influence of climate change has been based on the most reliable scientific information available at the time that this study was undertaken, but must be continually reassessed as new data and research results become available (at least every five years). The SSR would only need to be updated should one of the relevant climate change parameters change significantly.

Marine geotechnical surveys and additional numerical modelling will be required as part of future engineering design studies of the intake and outfall structures.

The scope of work for this update of the SSR excluded an updated Tsunami Hazard Analysis. Since tsunamis will pose a significant hazard to the site, it is recommended that an updated THA be undertaken for Thyspunt and that this SSR should then be updated once these results are available.

CONTROLLED DISCLOSURE

When downloaded from the EDS database, this document is uncontrolled and the responsibility rests with the user to ensure it is in line with the authorised version on the database.

CONTENTS

EXECUTIVE SUMMARY 5.9-3
5.9 OCEANOGRAPHY AND COASTAL ENGINEERING 5.9-19
5.9.1 Introduction 5.9-19
5.9.2 Definitions and Abbreviations 5.9-19
5.9.3 Purpose and Scope 5.9-25
5.9.4 Regulatory Framework 5.9-27
5.9.5 Requirements Documents and Guides 5.9-28
5.9.6 Approach to Evaluation 5.9-29
5.9.6.1 Oceanographic Monitoring 5.9-29
5.9.6.2 Extreme Value Analysis 5.9-35
5.9.6.3 Numerical Modelling 5.9-36
5.9.6.4 Conceptual Design for New NIs 5.9-38
5.9.7 Climate Change 5.9-38
5.9.7.1 Introduction 5.9-38
5.9.7.2 Sea Level Rise 5.9-39
5.9.7.3 Seawater Temperature 5.9-40
5.9.7.4 Storm Surge and Long Waves 5.9-41
5.9.7.5 Waves 5.9-41
5.9.7.6 Currents 5.9-42
5.9.7.7 Summary 5.9-43
5.9.8 Physical Description of the Site 5.9-43
5.9.9 Hydrographic Conditions 5.9-52
5.9.9.1 Tidal Levels 5.9-52
5.9.9.2 Storm Surge 5.9-55
5.9.9.3 Long Waves 5.9-63
5.9.9.4 Currents 5.9-70
5.9.9.5 Seawater Temperature 5.9-77
5.9.9.6 Salinity 5.9-87
5.9.9.7 Suspended Sediment 5.9-87
5.9.9.8 Waves 5.9-89
5.9.9.9 Waterspouts 5.9-104
5.9.10 Joint Probability 5.9-105

CONTROLLED DISCLOSURE

When downloaded from the EDS database, this document is uncontrolled and the responsibility rests with the user to ensure it is in line with the authorised version on the database.

5.9.10.1 Introduction 5.9-105
5.9.10.2 Methodology 5.9-106
5.9.10.3 Waves and Positive Storm Surge 5.9-107
5.9.10.4 Waves and Negative Storm Surge 5.9-109
5.9.10.5 Waves and currents 5.9-110
5.9.11 Sediment Transport 5.9-113
5.9.11.1 Long-Term Coastline Trends 5.9-113
5.9.11.2 Present-Day Sediment Budget 5.9-126
5.9.11.3 Recession due to Sea Level Rise 5.9-131
5.9.11.4 Coastline Changes due to Wave Climate Change 5.9-139
5.9.11.5 Erosion and Sedimentation due to Storms 5.9-144
5.9.11.6 Erosion and Sedimentation due to Outfall Structure 5.9-151
5.9.11.7 Resultant Coastline Stability 5.9-152
5.9.11.8 Suspended Sand at Intakes 5.9-163
5.9.12 Storm Wave Run-Up and Drawdown 5.9-165
5.9.12.1 Introduction 5.9-165
5.9.12.2 Example Outputs 5.9-165
5.9.12.3 Maximum Flood Lines 5.9-168
5.9.12.4 Maximum Vertical Run-Up 5.9-173
5.9.12.5 Minimum Vertical Drawdown 5.9-175
5.9.13 Tsunamis 5.9-177
5.9.13.1 Introduction 5.9-177
5.9.13.2 Initial Tsunami Hazard Analysis Undertaken for the Previous Thyspunt SSR in 2012 ..... 5.9-178
5.9.13.3 Deterministic Tsunami Hazard Analysis Undertaken for the Duynefontyn SSR in 2022 ..... 5.9-179
5.9.13.4 Probabilistic Tsunami Hazard Analysis Undertaken for the Duynefontyn SSR in 2024 ..... 5.9-180
5.9.13.5 Conclusions and Recommendations for Tsunamis 5.9-183
5.9.14 Flooding from the Sea 5.9-183
5.9.15 Extreme Low Water Levels 5.9-184
5.9.16 Thermal Plume Dispersion 5.9-184
5.9.16.1 Introduction 5.9-184
5.9.16.2 Discharge Characteristics 5.9-184

CONTROLLED DISCLOSURE

When downloaded from the EDS database, this document is uncontrolled and the responsibility rests with the user to ensure it is in line with the authorised version on the database.

5.9.16.3 Engineering Concept for Intake and Outfall Structures 5.9-185
5.9.16.4 Damage to Cooling Water Intake and Outfall Structures 5.9-187
5.9.16.5 Dispersion Modelling 5.9-188
5.9.16.6 Thermal Recirculation 5.9-197
5.9.16.7 Extreme Seawater Temperatures at Intakes 5.9-198
5.9.17 Blockage of Intakes and Biofouling 5.9-199
5.9.18 Uncertainties and Future Work 5.9-204
5.9.19 Monitoring Programme 5.9-205
5.9.20 Management System 5.9-205
5.9.21 Conclusions 5.9-212
5.9.21.1 Climate Change 5.9-212
5.9.21.2 Nearshore Waves 5.9-213
5.9.21.3 Coastline Stability 5.9-214
5.9.21.4 Flooding from the Sea 5.9-215
5.9.21.5 Extreme Low Water Levels 5.9-217
5.9.21.6 Thermal Plume Dispersion and Recirculation 5.9-219
5.9.21.7 Extreme Seawater Temperatures 5.9-219
5.9.21.8 Sedimentation at Intakes 5.9-220
5.9.21.9 Blockage of Intakes and Biofouling 5.9-221
5.9.22 References 5.9-222
APPENDIX 5.9.A: NUMERICAL MODEL DETAILS 5.9-231

CONTROLLED DISCLOSURE

When downloaded from the EDS database, this document is uncontrolled and the responsibility rests with the user to ensure it is in line with the authorised version on the database.

TABLES

Table 5.9-1: Definitions 5.9-19

Table 5.9-2: Abbreviations.....5.9-23

Table 5.9-3: PPE Parameters for new NIs Relevant to Oceanography and Coastal Engineering 5.9-27

Table 5.9-4: Coordinates of Oceanographic Instruments. 5.9-30

Table 5.9-5: Coordinates of Beach Profile Measurements. 5.9-32

Table 5.9-6: Summary of Oceanographic Monitoring Programme 5.9-34

Table 5.9-7: Overview of Numerical Models Used. 5.9-37

Table 5.9-8: Climate Change Applied for Each Oceanographic Parameter and Date. 5.9-43

Table 5.9-9: Tidal Constituents at Thyspunt (Baseline Date is 2013.5). 5.9-54

Table 5.9-10: Predicted Tidal Levels at Thyspunt (Baseline Date is 2013.5). 5.9-55

Table 5.9-11: Extreme Positive Storm Surge and Maximum Still Water Levels. .5.9-61

Table 5.9-12: Extreme Negative Storm Surge and Minimum Still Water Levels. .5.9-62

Table 5.9-13: Extreme Long Wave Amplitudes. 5.9-69

Table 5.9-14: Summary of Measured Current Speeds. 5.9-73

Table 5.9-15: Extreme Depth-Averaged Current Speed at Site B Including Climate Change (Water Depth -30.8 m msl).....5.9-76

Table 5.9-16: Statistics of Measured Hourly Seawater Temperature. 5.9-79

Table 5.9-17: Seasonal Percentiles of Measured Seawater Temperature Stratification. 5.9-79

Table 5.9-18: Location and Depth of Thermistor String at Middelbank. 5.9-80

Table 5.9-19: Extreme Maximum Seawater Temperatures. 5.9-86

Table 5.9-20: Summary of Measured Total Suspended Solids. 5.9-88

Table 5.9-21: Summary of Measured Waves. 5.9-93

Table 5.9-22: Extreme Wave Parameters at Point 1 in a Depth of -55 m msl. ..5.9-103

Table 5.9-23: Categories of Dependence (Petroliagkis, et al., 2016). 5.9-107

Table 5.9-24: Joint Exceedance Frequency of Wave Height and Positive Storm Surge for χ = 0.344. .....5.9-109

Table 5.9-25: Joint Exceedance Frequency of Wave Height and Negative Storm Surge for χ = 0.042. .....5.9-110

Table 5.9-26: Joint Exceedance Frequency of Wave Height and Current Speed for χ = 0.167. .....5.9-112

CONTROLLED DISCLOSURE

When downloaded from the EDS database, this document is uncontrolled and the responsibility rests with the user to ensure it is in line with the authorised version on the database.

Table 5.9-27: Present-Day Sediment Budget. 5.9-130

Table 5.9-28: Sand Volume Drawn into Cooling Water Intake Tunnels for 10 000 MWe Power Station. 5.9-165

Table 5.9-29: Extreme Flooding Due to Storm Waves. 5.9-173

Table 5.9-30: Extreme Low Water Levels Due to Storm Waves.....5.9-176

Table 5.9-31: Results of the Deterministic THA at the New NIs at the Duynefontyn Site. 5.9-180

Table 5.9-32: Frequency of Occurrence and Volume of Landslide Events for Each Volcanic Flank Collapse Source. 5.9-182

Table 5.9-33: Results of the Probabilistic THA at the New NIs at the Duynefontyn Site. 5.9-182

Table 5.9-34: Discharge Characteristics. 5.9-185

Table 5.9-35: Intake and Outfall Configuration. 5.9-187

Table 5.9-36: Recirculation at the Intakes. 5.9-198

Table 5.9-37: Extreme Maximum Seawater Temperatures at the Intakes (Including Recirculation). 5.9-199

Table 5.9-38: Marine Species Found at the Site. 5.9-200

Table 5.9-39: Summary of Major Debris Events at KNPS Since 1997 (EPRI, 2021). 5.9-200

Table 5.9-40: Summary of Measured Biofouling Thickness. 5.9-203

Table 5.9-41: Summary of Activities, Links and Quality Requirements. 5.9-207

Table 5.9-42: Regulatory Compliance Matrix. 5.9-209

Table 5.9-43: Climate Change Applied for Each Oceanographic Parameter and Date. 5.9-213

Table 5.9-44: Extreme Wave Parameters at a Depth of -55 m msl in Front of the Site. 5.9-214

Table 5.9-45: Extreme Flooding Due to Storm Waves. 5.9-216

Table 5.9-46: Extreme Low Water Levels Due to Storm Waves.....5.9-218

Table 5.9-47: Recirculation at the Intakes. 5.9-219

Table 5.9-48: Extreme Maximum Seawater Temperatures at the Intakes (Including Recirculation). 5.9-220

Table 5.9-49: Sand Volume Drawn into Cooling Water Intake Tunnels.....5.9-220

CONTROLLED DISCLOSURE

When downloaded from the EDS database, this document is uncontrolled and the responsibility rests with the user to ensure it is in line with the authorised version on the database.

FIGURES

Figure 5.9-1: Location of Oceanographic Instruments.....5.9-30

Figure 5.9-2: Location of Beach Profile Measurements.....5.9-31

Figure 5.9-3: SLR Projections at Thyspunt for the Upper End of the Likely Range of the SSP5-8.5 and SSP5-8.5 High SLR Scenarios.....5.9-40

Figure 5.9-4: Site Location Including Multi-Beam Bathymetry Offshore of the Site. 5.9-46

Figure 5.9-5: Bathymetry and Topography at the Site Showing the Location of the Nuclear Installation Corridor. 5.9-47

Figure 5.9-6: Seabed Features Offshore of the Site (Adapted from Fugro, (2006)). 5.9-48

Figure 5.9-7: Sediment Thickness at the Site. Also Shown are the Measured Borehole Locations. 5.9-49

Figure 5.9-8: Measured Sediment Grain Size Offshore and Along the Beach. ...5.9-51

Figure 5.9-9: Measured Hourly Water Levels at Thyspunt. 5.9-53

Figure 5.9-10: Measured Water Level, Predicted Tide and Storm Surge at Thyspunt for the Entire Dataset (Top) and Detail for a Storm Event in 2009 (Bottom).....5.9-56

Figure 5.9-11: Measured Water Level, Predicted Tide and Storm Surge at Gqeberha (Port Elizabeth) for the Entire Dataset (Top), Detail for 2020 (Top Middle), the May 1984 Storm (Bottom Middle) and the June 2017 Storm (Bottom).....5.9-57

Figure 5.9-12: Scatter Comparison of Measured Storm Surge at Thyspunt and Gqeberha for the Overlapping Period.....5.9-58

Figure 5.9-13: Extreme Value Analysis of Scaled Positive Storm Surge Residuals at Gqeberha (Baseline Date is 2001). 5.9-59

Figure 5.9-14: Extreme Value Analysis of Scaled Negative Storm Surge Residuals at Gqeberha (Baseline Date is 2001). 5.9-60

Figure 5.9-15: Locations of Tide Gauges 5.9-64

Figure 5.9-16: Propagation of a Meteo-Tsunami Event Measured Along the South African Coast.....5.9-65

Figure 5.9-17: Extreme Value Analysis of Positive Long Wave Amplitude (Baseline Date is 2014.5). 5.9-67

Figure 5.9-18: Extreme Value Analysis of Negative Long Wave Amplitude (Baseline Date is 2014.5). 5.9-68

Figure 5.9-19: Time-Series of Measured Currents at Site A (Water Depth -13.2 m msl). 5.9-71

Figure 5.9-20: Time-Series of Measured Currents at Site B (Water Depth -30.8 m msl). 5.9-72

CONTROLLED DISCLOSURE

When downloaded from the EDS database, this document is uncontrolled and the responsibility rests with the user to ensure it is in line with the authorised version on the database.

Figure 5.9-21: Measured Current Roses at Sites A and B. 5.9-73

Figure 5.9-22: Extreme Value Analysis of Depth-Averaged Current Speed at Site B (Depth -30.8 m msl) (Baseline Date is 2013).....5.9-75

Figure 5.9-23: Time-Series of Measured Seawater Temperatures and Stratification at All Sites. Bottom Plots Show the Results for 2018 in More Detail. 5.9-78

Figure 5.9-24: Location of Thermistor String at Middelbank. 5.9-80

Figure 5.9-25: Time-Series of Seawater Temperatures Measured at Site B and Middelbank. 5.9-81

Figure 5.9-26: Percentile Comparison of the Seawater Temperatures Measured at Site B and Middelbank for the Overlapping Period Between 2008 and 2011. .....5.9-82

Figure 5.9-27: Scatterplot and Q-Q Comparison of the Seawater Temperature Measured at Site B and Middelbank.....5.9-83

Figure 5.9-28: Time-Series of the Combined Seawater Temperatures at Site B (Water Depth -30.8 m msl) and Middelbank (Water Depth -27 m msl) Used for the EVA. The Blue Dots Show the Events Selected for the EVA, i.e., the Extreme Value Series..5.9-84

Figure 5.9-29: Extreme Value Analysis of Seawater Temperatures at Site B (Water Depth -30.8 m msl) and Middelbank (Water Depth -27 m msl) (Baseline Date is 2008). 5.9-85

Figure 5.9-30: Total Suspended Solids Sampling Locations. 5.9-87

Figure 5.9-31: Total Suspended Solids Distribution in Water Column. 5.9-88

Figure 5.9-32: Time-Series of Measured Wave Parameters at Site A (Water Depth -13.2 m msl).....5.9-90

Figure 5.9-33: Time-Series of Measured Wave Parameters at Site B (Water Depth -30.8 m msl).....5.9-91

Figure 5.9-34: Wave Roses at Site A and Site B.....5.9-92

Figure 5.9-35: Example Instantaneous Wave Refraction. 5.9-95

Figure 5.9-36: Time-Series of 10 Years (2000-2009) of Modelled Operational Wave Parameters at Point 1 (-55 m msl).....5.9-96

Figure 5.9-37: Time-Series of 1 Year (2009) of Modelled Operational Wave Parameters at Point 1 (-55 m msl).....5.9-97

Figure 5.9-38: 3D Scatterplot of 10 Years (2000-2009) of Modelled Operational Wave Parameters at Point 1 (-55 m msl).....5.9-98

Figure 5.9-39: Scatterplot Showing Relationship between Wave Height and Period at Point 1 from Modelled Storms between 1979 and 2024.....5.9-100

Figure 5.9-40: Scatterplot Showing Relationship between Wave Height and Direction at Point 1 from Modelled Storms between 1979 and 2024. The 5th, 50th, and 95th

CONTROLLED DISCLOSURE

When downloaded from the EDS database, this document is uncontrolled and the responsibility rests with the user to ensure it is in line with the authorised version on the database.

Percentiles of MWD_p were Determined from the H_{m0}-MWD_p Distribution for Waves Exceeding the 1 y^{-1} Exceedance Frequency H_{m0}. 5.9-100

Figure 5.9-41: Scatterplot Showing Relationship between Wave Height and Directional Spreading at Point 1 from Modelled Storms between 1979 and 2024. The 50th Percentile of DSD_p was Determined from the H_{m0}-DSD_p Distribution for Waves Exceeding the 1 y^{-1} Exceedance Frequency H_{m0}. 5.9-101

Figure 5.9-42: Extreme Value Analysis of Wave Height at Point 1 in a Depth of -55 m msl (Baseline Date is 2001.5). 5.9-102

Figure 5.9-43: Scatterplot of Wave Height and Storm Surge at Thyspunt. 5.9-108

Figure 5.9-44: Dependence Parameter χ of Wave Height and Positive Storm Surge at Thyspunt.....5.9-108

Figure 5.9-45: Dependence Parameter χ of Wave Height and Negative Storm Surge. 5.9-110

Figure 5.9-46: Scatterplot of Measured Wave Height and Depth-Averaged Current Speed at Thyspunt. 5.9-111

Figure 5.9-47: Dependence Parameter χ of Wave Height and Current Speed at Thyspunt.....5.9-112

Figure 5.9-48: Historical Images of the Cape St. Francis Headland in 1961 (Top) and 2023 (Bottom).....5.9-114

Figure 5.9-49: Historical Aerial and Satellite Images of Oyster Bay. 5.9-116

Figure 5.9-50: Historical Aerial and Satellite Images of Thysbaai. 5.9-116

Figure 5.9-51: Measured Beach Profiles at Profile 03: Western End of Oyster Bay. 5.9-117

Figure 5.9-52: Measured Beach Profiles at Profile 10: Eastern End of Oyster Bay.5.9-118

Figure 5.9-53: Measured Beach Profiles at Profile 27: Western End of Thysbaai...5.9-118

Figure 5.9-54: Measured Beach Profiles at Profile 38: Eastern End of Thysbaai....5.9-119

Figure 5.9-55: Horizontal Movement of the +2 m msl Level Over Time on Oyster Bay. 5.9-120

Figure 5.9-56: Horizontal Movement of the +2 m msl Level Over Time on Thysbaai. 5.9-120

Figure 5.9-57: Historical Wetted Line Along Oyster Bay (Top) and Thysbaai (Bottom) from 1961 to 2023. .....5.9-121

Figure 5.9-58: Horizontal Movement of the Wetted Line from Historical Images Over Time on Oyster Bay.....5.9-122

CONTROLLED DISCLOSURE

When downloaded from the EDS database, this document is uncontrolled and the responsibility rests with the user to ensure it is in line with the authorised version on the database.

Figure 5.9-59: Horizontal Movement of the Wetted Line from Historical Images Over Time on Thysbaai. 5.9-122

Figure 5.9-60: Horizontal Movement of the Coastline from Satellite Imagery Over Time on Oyster Bay. 5.9-123

Figure 5.9-61: Horizontal Movement of the Coastline from Satellite Imagery Over Time on Thysbaai. 5.9-124

Figure 5.9-62: Long-Term Coastline Trends from Measured Beach Profile Surveys, Historical Wetted Lines from Aerial Imagery and Digital Earth Africa Coastlines (2024). 5.9-125

Figure 5.9-63: Example Results of Operational Conditions During a Large Wave Event Showing Instantaneous Waves, Currents, Sediment Transport, and Surface Elevation. The Sediment Transport Vectors are Plotted on a Log Scale. 5.9-127

Figure 5.9-64: Annual Net Transport Including Vectors (Plotted on a Log Scale) for the Present-Day Case. 5.9-128

Figure 5.9-65: Annual Bed Level Change Including Annual Net Transport Vectors (Plotted on a Log Scale) for the Present-Day Case 5.9-128

Figure 5.9-66: Location of Profiles 1 to 33 Used to Calculate the Sediment Budget at the Site. 5.9-129

Figure 5.9-67: Cumulative Transport for Profiles 6 and 30 for the Present-Day Case. Positive Transport is Eastward. 5.9-129

Figure 5.9-68: Net Transport per Profile for the Present-Day Case. Positive Transport is Eastward. 5.9-130

Figure 5.9-69: Schematic representation of the Bruun Rule, modified after Hands (1983). 5.9-133

Figure 5.9-70: Plan View of Cross-Shore Profiles Used in the Coastline Stability Analysis. 5.9-135

Figure 5.9-71: Comparison of Cross-Shore Profiles Along Thysbaai. 5.9-136

Figure 5.9-72: Example of Profile Recession due to Sea Level Rise for Profile 107 for the 2134 High SLR Scenario. Also Shown are the Cumulative Coastline Changes due to Wave Climate Change 5.9-137

Figure 5.9-73: Example of Profile Recession due to Sea Level Rise for Profile 347 for the 2134 High SLR Scenario. Also Shown are the Cumulative Coastline Changes due to Wave Climate Change 5.9-138

Figure 5.9-74: Cumulative Bed Level Change After 10 Years for the 2134 Scenario. 5.9-140

Figure 5.9-75: Cumulative Bed Level Change After 10 Years for the 2134 High SLR Scenario. 5.9-141

CONTROLLED DISCLOSURE

When downloaded from the EDS database, this document is uncontrolled and the responsibility rests with the user to ensure it is in line with the authorised version on the database.

Figure 5.9-76: Coastline Changes due to Wave Climate Change: 2134. Positive Values Indicate Accretion and Negative Values Indicate Erosion. 5.9-142

Figure 5.9-77: Coastline Changes due to Wave Climate Change: 2134 High SLR. Positive Values Indicate Accretion and Negative Values Indicate Erosion. 5.9-143

Figure 5.9-78: Bed Level Change Including Net Transport Vectors (Plotted on a Log Scale) for the 1E-8 y^{-1} 2034 Scenario. 5.9-144

Figure 5.9-79: Bed Level Change Including Net Transport Vectors (Plotted on a Log Scale) for the 1E-8 y^{-1} 2134 Scenario. 5.9-145

Figure 5.9-80: Bed Level Change Including Net Transport Vectors (Plotted on a Log Scale) for the 1E-8 y^{-1} 2134 High SLR Scenario. 5.9-145

Figure 5.9-81: Profile 108 Cross-Shore Erosion Results for Storm Surge Dominant Cases. 5.9-147

Figure 5.9-82: Profile R18 Cross-Shore Erosion Results for Storm Surge Dominant Cases. 5.9-148

Figure 5.9-83: Interpolated Storm Erosion for the 2134 High SLR scenario and 1E-8 y^{-1} Storm. 5.9-150

Figure 5.9-84: Annual Bed Level Change Including Annual Net Transport Vectors (Plotted on a Log Scale) for the Present-Day Operational Case Including the Outfall Structure. 5.9-151

Figure 5.9-85: Bed Level Change Including Net Transport Vectors (Plotted on a Log Scale) for the 1E-8 y^{-1} 2034 Storm Case Including the Outfall Structure. 5.9-152

Figure 5.9-86: Pre-Storm Bathymetry Adjusted for Sea Level Rise: 2034. .....5.9-154

Figure 5.9-87: Pre-Storm Bathymetry Adjusted for Sea Level Rise: 2134. .....5.9-155

Figure 5.9-88: Pre-Storm Bathymetry Adjusted for Sea Level Rise: 2134 High SLR. 5.9-156

Figure 5.9-89: Pre-Storm Bathymetry Adjusted for Sea Level Rise and Wave Climate Change: 2134 High SLR. 5.9-157

Figure 5.9-90: Post-Storm Bathymetry Adjusted for Sea Level Rise, Wave Climate Change and 1E-8 y^{-1} Storm: 2134 High SLR. 5.9-158

Figure 5.9-91: Erosion Lines for the Labelled Storm Frequencies: 2034. The Contours Indicate the Pre-Storm Bathymetry. 5.9-160

Figure 5.9-92: Erosion Lines for the Labelled Storm Frequencies: 2134. The Contours Indicate the Pre-Storm Bathymetry. 5.9-161

Figure 5.9-93: Erosion Lines for the Labelled Storm Frequencies: 2134 High SLR. The Contours Indicate the Pre-Storm Bathymetry. 5.9-162

Figure 5.9-94: Example of Modelled Vertical Profile of Suspended Sand in -30 m msl at the Peak of the 1E-8 y^{-1} Storm. 5.9-164

CONTROLLED DISCLOSURE

When downloaded from the EDS database, this document is uncontrolled and the responsibility rests with the user to ensure it is in line with the authorised version on the database.

Figure 5.9-95: Instantaneous Water Surface Elevation (Top) and Profiles of Water Surface Elevation with Orbital Velocities for the 1E-8 y^{-1} Wave-Dominated Storm Case in 2034. .....5.9-167

Figure 5.9-96: Instantaneous Water Surface Elevation (Contours) and Depth-Averaged Currents (Vectors) at the Bay to the West of the Site for the 1E-8 y^{1} Wave-Dominated Storm Case in 2034. .....5.9-168

Figure 5.9-97: Definition Sketch for Vertical Run-Up Level and the Horizontal Flood Line. 5.9-169

Figure 5.9-98: Maximum Flood Lines Due to Storm Wave Run-Up for the Labelled Storm Frequencies in 2034. .....5.9-170

Figure 5.9-99: Maximum Flood Lines Due to Storm Wave Run-Up for the Labelled Storm Frequencies in 2134. .....5.9-171

Figure 5.9-100: Maximum Flood Lines Due to Storm Wave Run-Up for the Labelled Storm Frequencies in 2134, High SLR. 5.9-172

Figure 5.9-101: Vertical Run-Up Levels Due to Storm Waves.....5.9-174

Figure 5.9-102: Extreme Low Water Levels at the Intakes Due to Storm Waves. ...5.9-177

Figure 5.9-103: Location of Each Volcanic Flank Collapse Tsunami Source. ...5.9-181

Figure 5.9-104: Tunnel Intakes and Channel Outfall. 5.9-185

Figure 5.9-105: Schematic Diagram Showing the Main Components for an Offshore Tunnel Intake Configuration. 5.9-186

Figure 5.9-106: Example of Instantaneous ΔT and Currents Near Surface with the Plume Moving East. 5.9-189

Figure 5.9-107: Example of Instantaneous ΔT and Currents Near Seabed with the Plume Moving East. 5.9-190

Figure 5.9-108: Example of Instantaneous ΔT and Currents Near Surface with the Plume Moving South. 5.9-191

Figure 5.9-109: Example of Instantaneous ΔT and Currents Near Seabed with the Plume Moving South. 5.9-192

Figure 5.9-110: Example of Instantaneous ΔT and Currents Near Surface with the Plume Moving West. 5.9-193

Figure 5.9-111: Example of Instantaneous ΔT and Currents Near Seabed with the Plume Moving West. 5.9-194

Figure 5.9-112: 99th Percentile ΔT Near Surface.....5.9-195

Figure 5.9-113: 99th Percentile ΔT Near Seabed.....5.9-196

Figure 5.9-114: Recirculation at Intakes. 5.9-197

CONTROLLED DISCLOSURE

When downloaded from the EDS database, this document is uncontrolled and the responsibility rests with the user to ensure it is in line with the authorised version on the database.

Figure 5.9-115: Thyspunt Biofouling After 3.7 Months at 3 m Depth (Left) and After 5.6 Months in 10 m Depth (Right).....5.9-203

Figure 5.9-116: Duynefontyn Biofouling After 6 Months at 8 m Depth (Left) and After 14 Months in 10 m Depth (Right).....5.9-204

CONTROLLED DISCLOSURE

When downloaded from the EDS database, this document is uncontrolled and the responsibility rests with the user to ensure it is in line with the authorised version on the database.

5.9 OCEANOGRAPHY AND COASTAL ENGINEERING

5.9.1 Introduction

This section of this Site Safety Report (SSR) presents the results from the oceanography and coastal engineering studies undertaken for the planned development of new nuclear installation(s) (NIs) at the Thyspunt site, based on the Technical Requirements Specification (Eskom, 2023) and the Technical Specification for this section (Eskom, In Progress).

This section complements the remaining sections of ***Chapter 5*** (Site Characteristics) related to the site characteristics and provides input for the identification of external hazards associated with coastline stability, flooding from the sea and integrity of cooling water supplies in ***Chapter 6*** (Evaluation of External Events). Hazards associated with flooding from the land are addressed in ***Section 5.10*** (Hydrology and Hydraulics).

5.9.2 Definitions and Abbreviations

The definitions and abbreviations used in this section are provided in ***Table 5.9-1*** and ***Table 5.9-2***, respectively.

Table 5.9-1: Definitions

Definition	Explanation
Aeolian transport	The process by which sediment is transported by wind.
Alluvial transport	The process by which sediment is transported by river or stream flow.
Antecedent still water level	The still water level that existed before the arrival of the tsunami.
Astronomical Tide	The periodic rising and falling of the water level that results from gravitational attraction of the moon, sun and other astronomical bodies acting upon the rotating earth.
Atmospheric pressure	The force per unit area exerted by an atmospheric column (the entire body of air above the specified area).
Barometer	A device used to measure atmospheric pressure.
Bathymetry	Level of the seabed relative to a defined datum.
Beach profile	Intersection of the beach level with a vertical plane perpendicular to the coastline.
Benthic	Organisms living on the bed of the water body.
Best estimate	In the context of Extreme Value Analysis, the best estimate refers to the estimate from the original data, i.e., the most probable estimate.
Biofouling	The undesirable accumulation of micro-organisms, plants, algae, and animals on submerged structures.

CONTROLLED DISCLOSURE

When downloaded from the EDS database, this document is uncontrolled and the responsibility rests with the user to ensure it is in line with the authorised version on the database.

Bottom friction	The effect of the roughness of the seabed on currents or wave orbital velocities.
Coastline	The line that forms the boundary between the land and the sea.
Coriolis force	A force that as a result of the earth's rotation deflects moving objects.
Cross-shore	Perpendicular to the shoreline or coastline.
Current	Flow of water in a specific direction.
Current direction	The direction towards which the current is flowing, measured clockwise from true north.
Deep water wave	A deep water wave has a wavelength to water depth ratio less than 2. A shallow water has this ratio exceeding 25. A transitional water wave lies in between shallow and deep water waves.
Directional Standard Deviation (DSD)	A measure of the directional spreading of the waves, calculated from the two-dimensional wave spectrum.
Directional Standard Deviation at T_p (DSD_p)	A measure of the directional spreading of the waves at the peak wave frequency, calculated from the two-dimensional wave spectrum.
Drawdown	The minimum water level resulting from a storm wave or a tsunami wave.
Eddy viscosity	A model viscosity used to account for unresolved turbulent processes.
Erosion line	The most landward extent where any erosion of the topography occurs.
Exceedance frequency	The frequency that an event with a certain value will be exceeded in a given time period.
Flather boundary	A Flather boundary is when both the water surface elevation and the current are specified on the boundary of a hydrodynamic model.
Flood depth	The depth of water above the ground level due to flooding. Flood depth = flood level – ground level.
Flood level	The water surface elevation relative to a fixed datum due to flooding. Flood level = ground level + flood depth.
Flood line	The most landward point flooded by wave run-up.
Grain size	D_N is the diameter for which N% of the sediment, by mass, has a smaller diameter, e.g., D_{50} is the median grain diameter.
Gaussian	Relating to the Gauss distribution (also called the normal distribution).
Hindcast	Historical modelled data that provides information for the analysis of atmospheric and marine environments at specific sites.
Hydrodynamics	The movement of fluid.
Hydrostatic and non-hydrostatic models	Hydrostatic models assume a static vertical pressure distribution equal to that of water at rest. Non-hydrostatic models consider the effect of dynamic pressure and are thus appropriate for situations with significant vertical acceleration.
Intertidal zone	The area of the shore that lies between the highest normal high tide and the lowest normal low tide.

CONTROLLED DISCLOSURE

When downloaded from the EDS database, this document is uncontrolled and the responsibility rests with the user to ensure it is in line with the authorised version on the database.

Joint probability	The statistical measure that calculates the likelihood of two parameters (e.g., waves and storm surge) occurring together at the same time. The joint probability depends on the site-specific level of dependence between parameters.
Littoral drift	The term used for the longshore transport of sediments, along the upper shoreface due to the action of breaking waves and longshore currents.
Long waves	Fluctuations in still water level with periods between 8 and 60 min. Long waves typically include: edge waves, bound waves, tsunamis (generated by geophysical phenomena such as earthquakes) and meteo-tsunamis (generated by atmospheric pressure fluctuations).
Longshore	Moving parallel to the shoreline or coastline.
Mean Sea Level (MSL)	Throughout Section 5.9 the vertical datum used is mean sea level (msl), also known as Land Levelling Datum (LLD).
Mean wave direction (MWD)	The mean direction calculated from the full two-dimensional wave spectrum by weighting the energy at each direction and frequency. Wave direction is defined as the direction from which the wave is coming, measured clockwise from true north.
Mean wave direction at T_p (MWD_p)	The mean direction calculated from the two-dimensional wave spectrum at the peak wave frequency. Wave direction is defined as the direction from which the wave is coming, measured clockwise from true north.
Mean wave period (T_m)	The spectral estimate of the mean wave period, calculated from the ratio between the zeroth and first spectral moments.
Meteo-tsunami	A long-period wave generated by atmospheric pressure fluctuations.
Nearshore	Close to the shore, e.g., water depths up to approximately 30 m.
Nikuradse roughness	A method for specifying bottom friction in spectral wave models, where the dissipation coefficient depends on the wave hydrodynamic conditions.
Nowcast	Refers to modelled weather data for the present time, rather than in the past or future.
Nuclear terrace	Elevated platform on which the containment buildings and other key installations are located.
Operational	Operational conditions are those occurring normally, e.g., up to once per year, as opposed to extreme conditions which occur less than once per year.
Peak wave period (T_p)	The wave period with the maximum wave energy density in the wave energy spectrum.
Probable Maximum Tsunami (PMT)	The PMT is that tsunami for which the impact at the site is derived from the use of best available scientific information to arrive at a set of scenarios reasonably expected to affect the nuclear power plant site, taking into account (1) appropriate consideration of the most severe of the natural phenomena that have been historically reported for the site and surrounding area, with sufficient margin for the limited accuracy, quantity, and period of time in which the historical data have been accumulated; (2) appropriate combinations of the effects of normal and accident conditions with the effects of the natural phenomena; and (3) the importance of the safety functions to be performed.
Reanalysis	A process of historical observational meteorological data assimilation and assessment to generate long term global climate models.
RCP	Representative Concentration Pathway used for climate change scenarios.

CONTROLLED DISCLOSURE

When downloaded from the EDS database, this document is uncontrolled and the responsibility rests with the user to ensure it is in line with the authorised version on the database.

Run-up	The maximum vertical run-up level, defined as the highest ground or building level flooded by the storm or tsunami wave. Depending on the topography this point may or may not coincide with the maximum flood line.
Salinity	The measure of all the salts dissolved in water.
Sand budget	The analysis of the erosion or accretion rate of sediment at a specific location by considering the factors that affect the transport of sediment along a coast, e.g., longshore and cross-shore transport, dredging, aeolian and alluvial transport.
Sedimentation	The process of transportation and deposition of sediment particles onto the bottom of a body of water.
Seiche	An oscillation of an enclosed or semi-enclosed body of water in response to an atmospheric, oceanographic or seismic disturbing force.
Semi-diurnal	Having a tidal cycle that experiences two high tides and two low tides during a one-day period.
Scour	The removal of sediment around coastal structures during extreme storm events due to fast flowing water and waves.
Shallow water wave	A shallow water has a wavelength to water depth ratio exceeding 25. A deep water wave has this ratio less than 2. A transitional water wave lies in between shallow and deep water waves.
Sigma coordinates	In 3D numerical grids, sigma coordinates represent vertical coordinates as a function of total water depth, i.e., layer thickness varying from horizontal grid point to grid point.
Significant wave height (H_{m0})	The energy-based significant wave height, defined by $H_{m0} = 4\sqrt{m_0}$, where m_0 is the zeroth moment of the wave energy spectrum. H_{m0} is approximately equal to the mean of the highest one-third of waves in a sea state having a typical duration of 20 minutes.
Still Water Level (SWL)	The water level in the absence of waves.
Storm surge	The influence of meteorological effects such as winds and barometric pressure that result in the actual sea level being above or below the predicted astronomical tide level.
Stratification	The water column contains water layers with different densities due to the different salinities, temperatures and suspended sediment concentrations. The less dense water layers lay on top of the higher density layers.
Surf-beat	The long period (typically more than 60 s) oscillation of the water line on the beach, related to the infragravity waves in the surf zone.
Swell (waves)	Waves that are generated far offshore in the deep sea that propagate onshore and make up the low frequency part of the wave spectrum, defined in this study as wave periods in the range 30 s > T > 6 s.
Synthetic tide	In this context a water surface elevation time-series generated using one tidal constituent.
Time domain significant wave height (H_s)	The mean of the highest one-third of waves in a sea state having a typical duration of 20 minutes.
Topography	Level of the land relative to a defined datum.

CONTROLLED DISCLOSURE

When downloaded from the EDS database, this document is uncontrolled and the responsibility rests with the user to ensure it is in line with the authorised version on the database.

Tsunami	A long-period wave caused by an underwater disturbance such as a volcano, submarine landslide or earthquake.
Upwelling	Upwelling is when the surface water is displaced offshore by wind blowing alongshore over the ocean and is then replaced by cold water from below.
Water surface elevation	Level of the water surface relative to a defined datum.
Wave direction	The direction from which the wave is coming, measured clockwise from true north.
Wave refraction	The process by which the height and direction of a wave moving in shallow water at an angle to the bed contours is changed.
Wave set-up	An increase in water level due to breaking waves.
Wave shoaling	The increase in wave height as waves propagate into shallower depth.
Wind direction	The direction from which the wind is coming, measured clockwise from true north.
Wind set-up	An increase in water level due to onshore winds.

Table 5.9-2: Abbreviations

Abbreviation	Explanation
2D	Two-dimensional
3D	Three-dimensional
ADCP	Acoustic Doppler Current Profiler
AR6	6th Assessment Report from the IPCC
CD: NGI	Chief Directorate: National Geo-Spatial Information
CGS	Council for Geoscience
COTS	Commercial-Off-The-Shelf software
CRF	Circulating Water System
DGPS	Differential Global Positioning System
DHI	Danish Hydraulics Institute
DSD	Directional Standard Deviation
DTHA	Duynefontyn Tsunami Hazard Analysis
EMCWF	European Center for Medium-Range Weather Forecasts
EPRI	Electric Power Research Institute
EVA	Extreme Value Analysis
FM	Flexible Mesh
HAT	Highest Astronomical Tide
HBD	Headland Bypass Dunefield
HYCOM	HYbrid Coordinate Ocean Model

CONTROLLED DISCLOSURE

When downloaded from the EDS database, this document is uncontrolled and the responsibility rests with the user to ensure it is in line with the authorised version on the database.

IAEA	International Atomic Energy Agency
IMOS	Australia's Integrated Marine Observing System
IPCC	Intergovernmental Panel for Climate Change
KNPS	Koeberg Nuclear Power Station
LAT	Lowest Astronomical Tide
LiDAR	Light Detection and Ranging
LLD	Land Levelling Datum
MHWN	Mean High Water Neaps
MHWS	Mean High Water Springs
ML	Mean (Tidal) Level
MLWN	Mean Low Water Neap
MLWS	Mean Low Water Spring
MSL	Mean Sea Level
MWD	Mean Wave Direction
NCEP	National Centers for Environmental Prediction
NIs	Nuclear Installation(s)
NNR	National Nuclear Regulator
NOAA	(United States) National Oceanic and Atmospheric Administration
NRC	(United States) Nuclear Regulatory Commission
NS	Navier-Stokes
PMT	Probable Maximum Tsunami
PPE	Plant Parameter Envelope
PTHA	Probabilistic Tsunami Hazard Analysis
RCPs	Representative Concentration Pathways
RMS	Root-Mean-Square
SAR	Safety Analysis Report
SBEACH	Storm-induced BEAch Change model
SLR	Sea Level Rise
SOPs	Standard Operating Procedures
SSCs	Structures, Systems and Components
SSR	Site Safety Report
STPQ3D	Quasi Three-Dimensional Sediment Transport Model
SWL	Still Water Level
TSS	Total Suspended Solids
V&V	Verification and Validation

CONTROLLED DISCLOSURE

When downloaded from the EDS database, this document is uncontrolled and the responsibility rests with the user to ensure it is in line with the authorised version on the database.

WANO	World Association of Nuclear Operators

5.9.3 Purpose and Scope

The purpose of this section of this SSR is to identify the requirements and to demonstrate the technical acceptability of the site with regard to coastline stability, flooding from the sea, integrity of cooling water supply and thermal plume dispersion. Design considerations for seawater cooling water intake and outfall layouts for the new NIs are also provided. The scope of work for this update of the SSR excluded an updated Tsunami Hazard Analysis (THA). This SSR will thus need to be updated once an updated THA has been undertaken.

The layout and structure of this section is provided below, including a brief description of the contents of the main subsections and the linkages between them:

- 5.9.1 Introduction
- 5.9.2 Definitions and Abbreviations
- 5.9.4 Regulatory Framework
- 5.9.5 Requirements Documents and Guides
- 5.9.6 Approach to Evaluation: The approach combined oceanographic measurements, extreme value analysis, detailed numerical modelling studies and conceptual engineering design.
- 5.9.7 Climate Change: The effect of climate change on all relevant oceanographic and coastal engineering parameters has been estimated and the changes are described in this subsection. These changes have then been applied as described in the subsection relevant to each parameter.
- 5.9.8 Physical Description of the Site: The topography at the site, the bathymetry offshore, the seabed features, and sediment characteristics are described.
- 5.9.9 Hydrographic Conditions: This section characterises the hydrographic conditions at the site based on measurements and numerical modelling. These conditions comprise tides, storm surge, long waves, currents, seawater temperature, salinity, suspended sediment, waves, and waterspouts. These hydrographic conditions are used as inputs to the sediment transport modelling, storm wave run-up and drawdown, and thermal plume dispersion, as described in the subsections that follow.

CONTROLLED DISCLOSURE

When downloaded from the EDS database, this document is uncontrolled and the responsibility rests with the user to ensure it is in line with the authorised version on the database.

- 5.9.10 Joint Probability: This section describes the joint probabilities between the hydrographic conditions, where relevant.
- 5.9.11 Sediment Transport: In order to assess the potential instability of the coastline near the site, the following physical processes and timescales have been evaluated by analysing measured data and modelling: long-term coastline trends, the present-day sediment budget, recession due to sea level rise, coastline changes due to wave climate change, erosion and sedimentation due to storms, and erosion and sedimentation due to the outfall structure. and cross-shore erosion. Modelling was also performed to estimate the volume of sand drawn into the tunnel intakes, should these be selected for the new NIs.
- 5.9.12: Storm Wave Run-Up and Drawdown: This section describes the wave modelling undertaken to estimate the maximum flood lines, maximum vertical run-up, and minimum vertical drawdown due to storms.
- 5.9.13 Tsunamis: Since the scope of work for this update of the SSR excluded an updated Tsunami Hazard Analysis (THA), tsunami hazard information from previous analyses is summarised. This SSR will thus need to be updated once an updated THA has been undertaken.
- 5.9.14 Flooding from the Sea: No tsunami results are presented in this SSR. In the interim the flooding from the sea is based on the storm wave run-up only, as described in Subsection 5.9.12.
- 5.9.15 Extreme Low Water Levels: No tsunami results are presented in this SSR. In the interim the extreme low water levels are based on the storm wave drawdown only, as described in Subsection 5.9.12.
- 5.9.16 Thermal Plume Dispersion: This section describes an engineering concept for intake and outfall structures for the new NIs, dispersion modelling of the thermal plumes, thermal recirculation and extreme seawater temperatures at the intakes.
- 5.9.17 Blockage of Intakes and Biofouling: This section describes potential mechanisms for blockage of the intakes including biofouling.
- 5.9.18: Uncertainties and Future Work
- 5.9.19: Monitoring Programme
- 5.9.20: Management System
- 5.9.21 Conclusions.

The details of the numerical modelling are provided in Appendix 5.9.A, with only the model results included in the body of the report.

The evaluation of the site took into account the relevant Plant Parameter Envelope (PPE) values for the new NIs (Eskom, 2024a), as given below.

CONTROLLED DISCLOSURE

When downloaded from the EDS database, this document is uncontrolled and the responsibility rests with the user to ensure it is in line with the authorised version on the database.

Table 5.9-3: PPE Parameters for new NIs Relevant to Oceanography and Coastal Engineering

PPE Parameter	Definition	Enveloping Limits(s)
Plant design life	The designed lifetime of the plant, including planned midlife refurbishments	60 y + 20 y life extension
Maximum flood or tsunami (terrace height)	Design assumption regarding the difference in elevation between finished plant grade and the water level due to the probable maximum flood (or tsunami).	The terrace height must be such that the new NIs terrace is elevated above design basis flooding hazards.
Cooling Water Flow Rate	Total cooling water flow rate through the condenser (also the rate of withdrawal from and return to the water source)	76 m^3/s per 1708 MWe unit
Cooling Water Temperature Rise	Temperature rise across the condenser (temperature of water out minus temperature of water in)	12°C
Cooling Water Temperature Range	The range of water temperatures at the intake	-0.5°C to 30°C
Maximum increase in the cooling water source	Design value for the maximum temperature increase in the cooling water source.	The intake and the outfall configuration should not result in a net rise in CW. The maximum increase in the temperature of the recirculated water should be less than 1.5°C. Increases in the water temperature will most likely be limited by environmental issues for each specific site.

It is assumed that the new NIs will become operational from 2034, will operate for 60 y, which will be extended to 80 y (i.e., up to 2114), after which a decommissioning period of 20 y will follow (i.e., up to 2134). Therefore, this section assesses the following dates with respect to climate change:

- 2034: start of operations;
- 2114: end of operations;
- 2134: end of decommissioning period.

5.9.4 Regulatory Framework

The legal and regulatory basis for the overall SSR process is outlined in ***Chapter 2*** of this SSR. The current national regulations specifically relevant to an oceanography and coastal engineering investigation to be taken into account for site selection are Regulation R.927: Regulations on Licensing of Sites for New Nuclear Installations (Department of Energy, 2011) which requires that the SSR provides the following:

CONTROLLED DISCLOSURE

When downloaded from the EDS database, this document is uncontrolled and the responsibility rests with the user to ensure it is in line with the authorised version on the database.

"4(5) Natural phenomena and potential man-made hazards must be appropriately accounted for in the design of the new nuclear installation(s) …";

"5(3) The characteristics of the site relevant to the design assessment, risk and dose calculations, including inter alia:

(a) external events;

(b) meteorological data;

(f) projections of the above data commensurate with the design life of the nuclear installation(s)".

5.9.5 Requirements Documents and Guides

The following National Nuclear Regulator (NNR) Requirements Documents were taken into account where applicable:

- RD-0034, Quality and Safety Management Requirements for Nuclear Installations (NNR, 2008);
- RG-0011, Interim Guidance on the Siting of Nuclear Facilities (NNR, 2016a);
- RG-0016, Guidance on the Verification and Validation of Evaluation and Calculation Models used in Safety and Design Analyses (NNR, 2016b);
- PP-0014, Consideration of External Events for Nuclear Installations (NNR, 2014).

The following international guides were consulted to ensure that the work follows international best practice:

- IAEA Safety Guide No. SSG-18, Meteorological and Hydrological Hazards in Site Evaluation for Nuclear Installations (IAEA, 2011);
- IAEA Safety Guide No. NS G 1.9, Design of the Reactor Coolant System and Associated Systems in Nuclear Power Plants (IAEA, 2004);
- US Nuclear Regulatory Commission (US NRC), Regulation 1.27, Ultimate Heat Sink for Nuclear Power Plants (NRC, 2015);
- US NRC, Regulatory Guide 1.59, Design Basis Floods for Nuclear Power Plants (NRC, 1977);
- US NRC, Regulatory Guide 1.70, Standard Format and Content of Safety Analysis Reports for Nuclear Power Plants (NRC, 1978);
- US NRC, Regulatory Guide 1.206, Combined License Applications for Nuclear Power Plants (NRC, 2007a);

CONTROLLED DISCLOSURE

When downloaded from the EDS database, this document is uncontrolled and the responsibility rests with the user to ensure it is in line with the authorised version on the database.

- US NRC, Regulatory Guide 1.102, Flood Protection for Nuclear Power Plants (NRC, 1976);
- US NRC, NUREG-0800, Part 2.4.5, Probable Maximum Surge and Seiche Flooding (NRC, 2007b);
- US NRC, NUREG-0800, Part 2.4.6, Probable Maximum Tsunami Hazards (NRC, 2007c);
- US NRC, NUREG-0800, Part 2.4.11, Low Water Considerations (NRC, 2007d);
- US NRC, NUREG/CR-7046 (PNNL-20091), Design-Basis Flood Estimation for Site Characterization at Nuclear Power Plants in the United States of America (NRC, 2011);
- US NRC, NUREG/CR-7223, Tsunami Hazard Assessment: Best Modeling Practices and State-of-the-Art Technology (NRC, 2016).

5.9.6 Approach to Evaluation

The approach to the site evaluation combined oceanographic measurements, extreme value analysis, detailed numerical modelling studies and conceptual engineering design, as detailed below.

5.9.6.1 Oceanographic Monitoring

A comprehensive oceanographic data collection programme has been implemented at the site. The objective of this programme is to provide baseline data for:

- evaluation of the site and NIs safety;
- design of coastal structures at the site, e.g., intakes and outfalls;
- calibration and validation of the numerical models to confirm that models are accurate and can thus be used for estimation of both frequent and rare events.

The programme was initiated during the original SSR from 2008 to 2013 and then extended from 2017 until 2019. Details are provided in Thyspunt SSR Ch 5.9: 2 Yrs Oceanographic Monitoring Data (PRDW, 2019).

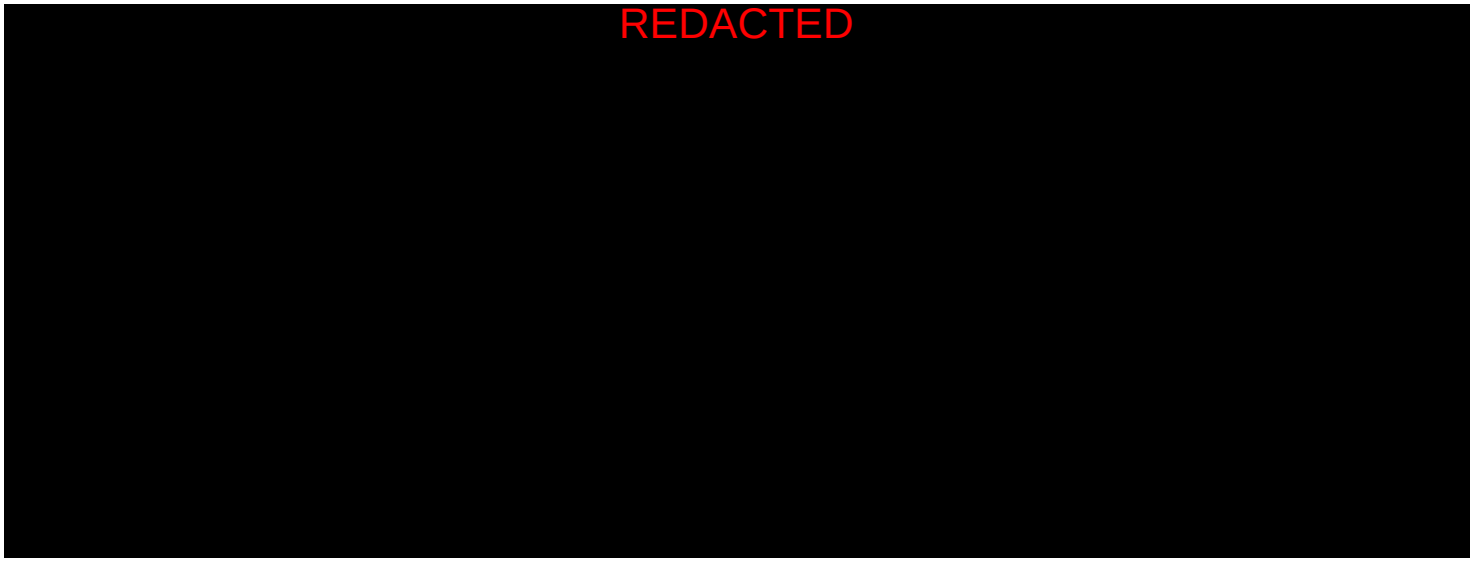
A further extension commenced in 2024 which is scheduled to end in November 2028. Data measured up to March 2019 is included in this report, with the exception of the beach profile surveys and associated measurement of the wave run-up debris line on Thysbaai from March 2024. The locations of the instruments deployed at the Thyspunt site are provided in ***Figure 5.9-1*** and ***Table 5.9-4.*** The locations of beach profile measurements are provided in ***Figure 5.9-2*** and ***Table 5.9-5.***

CONTROLLED DISCLOSURE

When downloaded from the EDS database, this document is uncontrolled and the responsibility rests with the user to ensure it is in line with the authorised version on the database.



Figure 5.9-1: Location of Oceanographic Instruments.



(1) Position from February 2008 to March 2009
(2) Position from April 2009 onwards
(3) Position from February 2008 to July 2008
(4) Position from July 2008 onwards

CONTROLLED DISCLOSURE

When downloaded from the EDS database, this document is uncontrolled and the responsibility rests with the user to ensure it is in line with the authorised version on the database.

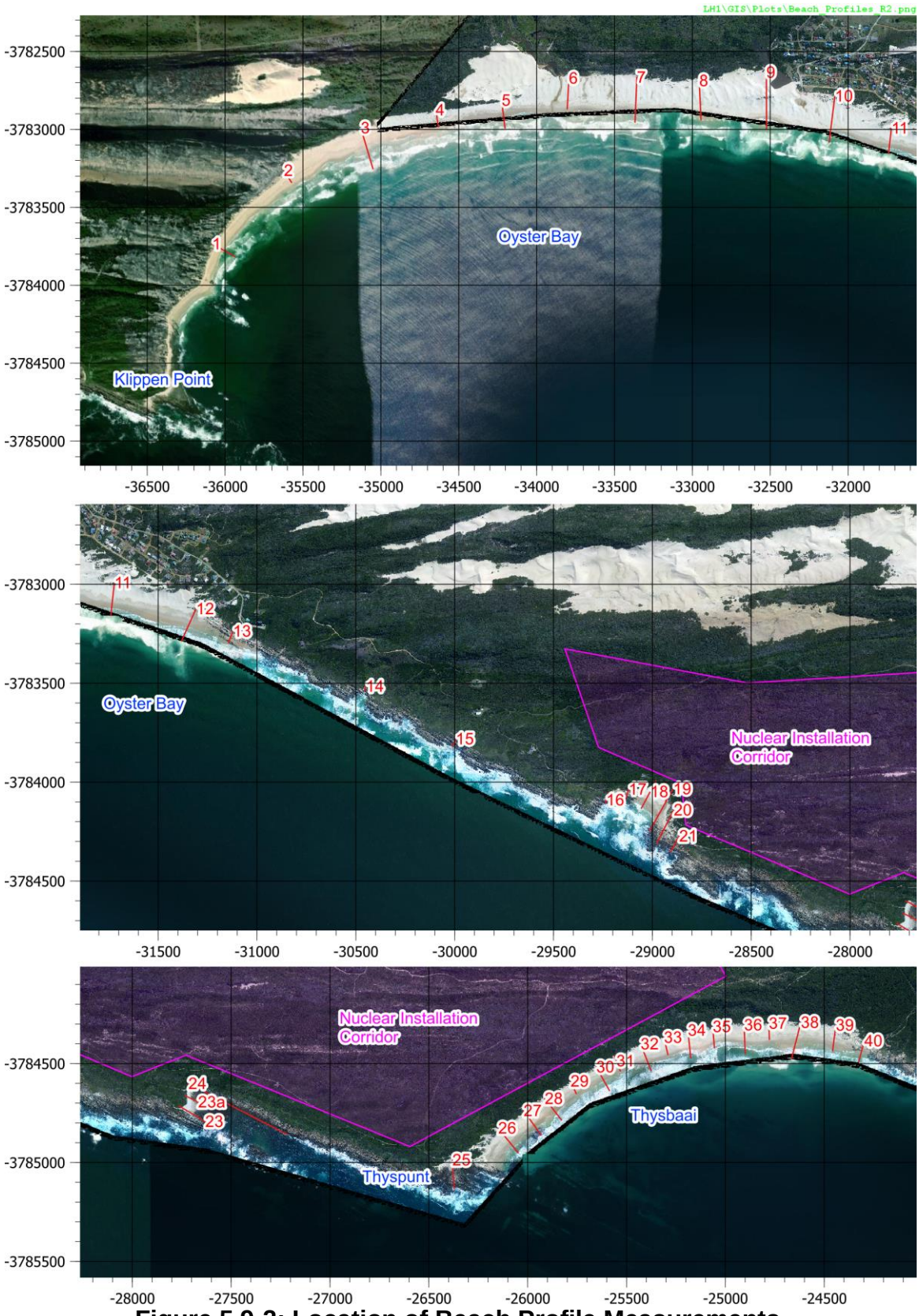


Figure 5.9-2: Location of Beach Profile Measurements.

CONTROLLED DISCLOSURE

When downloaded from the EDS database, this document is uncontrolled and the responsibility rests with the user to ensure it is in line with the authorised version on the database.

Table 5.9-5: Coordinates of Beach Profile Measurements.

Profile	Position	Profile	Position
1	24.6086°E, -34.1804°S	21 (1)	24.6868°E, -34.1855°S
2 (1)	24.6136°E, -34.1761°S	23 (1)	24.6990°E, -34.1894°S
3	24.6190°E, -34.1737°S	23a	24.6992°E, -34.1890°S
4 (1)	24.6242°E, -34.1727°S	24 (1)	24.6994°E, -34.1885°S
5	24.6288°E, -34.1721°S	25 (1)	24.7136°E, -34.1919°S
6 (1)	24.6335°E, -34.1709°S	26	24.7164°E, -34.1906°S
7	24.6382°E, -34.1708°S	27	24.7178°E, -34.1898°S
8 (1)	24.6426°E, -34.1710°S	28	24.7189°E, -34.1892°S
9	24.6472°E, -34.1706°S	29 (1)	24.7203°E, -34.1884°S
10	24.6520°E, -34.1720°S	30	24.7217°E, -34.1877°S
11	24.6559°E, -34.1738°S	31 (1)	24.7227°E, -34.1872°S
12	24.6604°E, -34.1751°S	32	24.7242°E, -34.1867°S
13 (1)	24.6624°E, -34.1761°S	33 (1)	24.7254°E, -34.1864°S
14 (1)	24.6697°E, -34.1786°S	34	24.7267°E, -34.1861°S
15 (1)	24.6746°E, -34.1810°S	35 (1)	24.7281°E, -34.1859°S
16 (1)	24.6830°E, -34.1835°S	36	24.7298°E, -34.1858°S
17 (1)	24.6841°E, -34.1833°S	37 (1)	24.7312°E, -34.1858°S
18	24.6854°E, -34.1832°S	38	24.7329°E, -34.1857°S
19	24.6863°E, -34.1836°S	39 (1)	24.7349°E, -34.1859°S
20 (1)	24.6862°E, -34.1846°S	40	24.7364°E, -34.1866°S

Notes:

(1) Profiles only surveyed once during the first set of surveys in 2008

Since sites A1 and A2 have similar depths and are only 170 m apart, the data measured at these two sites are combined into one data set (called Site A, with a mean deployment depth of -13.2 m msl) for the statistical analyses described in this report. Although Sites B1 and B2 are 956 m apart in the alongshore direction, they are located a similar distance offshore of the reef in the cross-shore direction (see ***Figure 5.9-1***) and the water depths at the two sites differ by only 10 per cent. For these reasons, the data measured at these two sites are combined into one data set (called Site B with a mean depth of -30.8 m msl) for the statistical analyses described in this report.

The oceanographic monitoring programme is summarised in ***Table 5.9-6***. The programme has been reviewed and updated over time, e.g., the

CONTROLLED DISCLOSURE

When downloaded from the EDS database, this document is uncontrolled and the responsibility rests with the user to ensure it is in line with the authorised version on the database.

Acoustic Doppler Current Profiler (ADCP) at Site A was replaced with a temperature sensor after August 2010.

CONTROLLED DISCLOSURE

When downloaded from the EDS database, this document is uncontrolled and the responsibility rests with the user to ensure it is in line with the authorised version on the database.

Table 5.9-6: Summary of Oceanographic Monitoring Programme

Location	Instrument	Parameters	Sampling Interval	Start Date	End Date	Valid Data
Site A	Acoustic Doppler Current Profiler (ADCP)	Current speed and direction at 0.3 m and 0.4 m depth intervals	10 min	Feb 2008	Aug 2010	1.41 y
		Waves: 2D spectrum, significant wave height (H_{m0}), peak wave period (T_p), mean wave direction (MWD)	1 h	Feb 2008	Aug 2010	1.75 y
	Temperature sensor	Water temperature	10 min	Feb 2008	Mar 2019	5.94 y
	Conductivity sensor	Salinity	10 min	Mar 2011	Feb 2012	0.33 y
	Asbestos plate	Biofouling thickness	3.7 months	Jul 2008	Oct 2008	2 plates
			5.6 months	Jun 2009	Dec 2009	2 plates
Site B	Acoustic Doppler Current Profiler (ADCP)	Current speed and direction at 0.5 m depth intervals	10 min	Apr 2008	Mar 2019	5.41 y
		Waves: 2D spectrum, H_{m0}, T_p, MWD	1 h	Apr 2008	Mar 2019	5.47 y
	Temperature sensor	Water temperature	10 min	Apr 2008	Mar 2019	6.79 y
	Conductivity sensor	Salinity	10 min	Apr 2008	Dec 2011	2.16 y
	Asbestos plate	Biofouling thickness	5.6 months	Jun 2009	Dec 2009	2 plates
Site C	Temperature and pressure sensor	Water temperature	10 min	Jul 2008	Mar 2019	5.96 y
		Water level	1 s	Jul 2017	Mar 2019	1.43 y
			1 h	Feb 2008	Mar 2019	6.02 y
Airshed Weather Station	Anemometer	Wind speed, wind gusts and direction on a 10 m high mast	1 h averaged	Jan 2008	Mar 2019	5.36 y
	Barometer	Atmospheric pressure (for water level correction)	1 h	Jan 2008	Mar 2019	5.36 y
Beach Profiles 1 to 40	Survey using Differential Global Positioning System (DGPS)	Beach level	Quarterly until Jul 2009, annually in 2010, 2018, 2019 and 2024, twice in 2012	Jan 2008	Mar 2024	13 surveys
Depths between -10 and -30 m and beach	Grab samples and sieve analysis	Sediment grain size distribution	Once off	Apr 2008	Apr 2008	51 samples
Depths between -4 and -28 m	Niskin bottle and laboratory analysis	Total suspended solids (TSS)	Variable	Jul 2008	Feb 2010	66 samples

CONTROLLED DISCLOSURE

When downloaded from the EDS database, this document is uncontrolled and the responsibility rests with the user to ensure it is in line with the authorised version on the database.

The results of these measurements are described in ***Subsections 5.9.9*** and ***5.9.11.1*** below. Further details of the monitoring programme are provided in the Oceanographic Monitoring Report (PRDW, 2019).

5.9.6.2 Extreme Value Analysis

In line with Eskom's external hazards requirements (Eskom, 2011) and the NNR defined risk categories (NNR, 2014), the external hazards have been quantified for the following frequencies of exceedance: 1E-2, 1E-4, 1E-5, 1E-6, 1E-7 and 1E-8 y^{-1}.

The frequency of exceedance is related to return period as follows:

$$\text{Frequency of exceedance} = \frac{1}{return\ period} \qquad \text{Equation 5.9.1}$$

An event with a frequency of exceedance of 1E-2 y^{-1} means that, on average, the frequency of this event being exceeded in one year is 1E-2. Equivalently, the event will have a return period of 100 y and will, on average, be exceeded once every 100 y.

Extreme value analyses (EVAs) were undertaken using the MIKE Extreme Value Analysis software (DHI, 2024a) and (DHI, 2024b). The theorical basis and the V&V of the EVA software is described in the supporting V&V Report (PRDW, 2022a).

The analysis was performed by fitting a 3-parameter Weibull distribution using the method of moments to an extreme value series extracted from the input time-series. The extreme value series was selected using the 'peaks over threshold' method (also called the 'partial duration series'), with the threshold defined as the value that is exceeded 4 times per year on average, except for currents and temperature where a more accurate fit was achieved using 3 times per year. To ensure independence, two successive events were extracted only if the time between the events exceeded 48 hours.

The uncertainty was calculated using the Jackknife method (DHI, 2024b), in which the analysis is repeated n times, where n is the number of data points in the extreme values series, with one data point excluded at a time. The output of the uncertainty analysis is the mean and standard deviation of the estimate for each frequency of exceedance. The estimate is assumed to be normally distributed which allows the 5th and 95th percentile estimates to be calculated. Note that it is only the estimate for each frequency of exceedance that is assumed to be normally distributed, whilst the data is assumed to follow the Weibull distribution.

For each frequency of exceedance the following four estimates are provided:

CONTROLLED DISCLOSURE

When downloaded from the EDS database, this document is uncontrolled and the responsibility rests with the user to ensure it is in line with the authorised version on the database.

- Best estimate = the estimate from the original data set, i.e., the most probable estimate;
- Mean estimate = the mean estimate from the Jackknife resampling;
- 5th percentile = mean - 1.645 × standard deviation;
- 95th percentile = mean + 1.645 × standard deviation.

The frequencies of exceedance were estimated by performing EVAs on long-term time-series of the following datasets as described in the indicated subsections:

- Storm surge (***Subsection 5.9.9.2***);
- Long waves (***Subsection 5.9.9.3***);
- Currents (***Subsection 5.9.9.4***);
- Seawater temperature (***Subsection 5.9.9.5***);
- Waves (***Subsection 5.9.9.8***).

Recent IAEA guidance is that hazards cannot be estimated with sufficient accuracy for return periods more than three to four times the length of the sample period (IAEA, 2011). The datasets used for the EVAs have a maximum duration of 45.5 y, implying that frequencies less than approximately 6E−3 y^{-1} need to be interpreted with caution. In the case of datasets with shorter durations the accuracy will reduce proportionally. The uncertainty for each dataset is indicated by the 5th and 95th percentiles from the EVA analysis, which shows how the uncertainty increases for lower exceedance frequencies, see for example ***Figure 5.9-42***.

5.9.6.3 Numerical Modelling

Numerical modelling has been undertaken to extend the duration of the measured oceanographic parameters and to simulate the coastal processes required to quantify the hazards at the site.

The modelling was undertaken using the MIKE suite of software developed by DHI A/S in Denmark. This is Commercial-Off-The-Shelf (COTS) software and was selected for its large international user base, large number of integrated models suitable for analysis of the required physical processes, high quality of available Verification and Validation (V&V) documentation, dedicated user support, and the experience of the PRDW staff in the use of the software. The MIKE software was first released commercially in 1985 and has been under constant development since then.

The models have undergone V&V as per the requirements contained in NSIP02761 (Eskom, 2020) and RG-0016 (NNR, 2016b). The V&V of models is described in a supporting report (PRDW, 2022a). As part of the

When downloaded from the EDS database, this document is uncontrolled and the responsibility rests with the user to ensure it is in line with the authorised version on the database.

V&V the models have been calibrated against site-specific data measured as part of the Thyspunt monitoring programme, as described in ***Appendix 5.9.A***.

Table 5.9-7 provides an overview of the numerical models used. The applications of the models are described in the User Guides, whilst detailed descriptions of the application areas, governing mathematical equations, numerical space and time discretisation, solution methods, and references are provided in the Scientific Documentation. Hyperlinks to these documents are included in the references. The model results are provided in the subsections indicated, whilst the details of the numerical modelling are provided in the indicated appendices.

Table 5.9-7: Overview of Numerical Models Used.

Model Name	User Guide	Scientific Documentation	Physical Processes Simulated	Subsection	Appendix
MIKE 21 Flow	(DHI, 2024c)	(DHI, 2024d)	Wave setup at Site C	***5.9.9.1***	***5.9.A.1***
MIKE Spectral Waves	(DHI, 2024e)	(DHI, 2024f)	Wave refraction, shoaling and breaking	***5.9.9.8***	***5.9.A.2***
MIKE 21 Sand Transport	(DHI, 2024g)	(DHI, 2024h)	Present-day sediment budget Coastline changes due to wave climate change Erosion and sedimentation due to storms Erosion and sedimentation due to outfall structure	***5.9.11.2*** ***5.9.11.4*** ***5.9.11.5*** ***5.9.11.6***	***5.9.A.3***
SBEACH	(USACE, 1996a)	(USACE, 1989) (USACE, 1990)	Cross-shore beach erosion	***5.9.11.5***	***5.9.A.4***
MIKE Littoral Processes	(DHI, 2024i)	(DHI, 2024j)	Suspended sand concentration	***5.9.11.8***	***5.9.A.5***
MIKE 3 Wave	(DHI, 2024k)	(DHI, 2024l)	Storm wave run-up and drawdown	***5.9.12.2***	***5.9.A.6***
MIKE 3 Flow	(DHI, 2024m)	(DHI, 2024n)	Three-dimensional hydrodynamics and thermal plume dispersion	***5.9.16.5***	***5.9.A.7***

To rationalise the number of cases whilst still resolving the impact of climate change, the models were run for the two key dates shown in bold below (the 2114 date was assessed for climate change but was not simulated in the models):

- **2034: start of operations;**
- 2114: end of operations;
- **2134: end of decommissioning period.**

CONTROLLED DISCLOSURE

When downloaded from the EDS database, this document is uncontrolled and the responsibility rests with the user to ensure it is in line with the authorised version on the database.

The 2134 date was assessed for two sea level rise (SLR) scenarios as described in ***Subsection 5.9.7***.

Siting requires consideration of site suitability to the end of decommissioning, not just the end of operations. Since climate change results in all key parameters becoming progressively worse over time (refer to ***Subsection 5.9.7***), the model results for 2134 will conservatively envelope those for 2114.

The models were run for the following four exceedance frequencies: 1E-2, 1E-4, 1E-6 and 1E-8 y^{-1}. These exceedance frequencies accounted for the joint probability of the relevant input parameters applied in the model, as described in ***Subsection 5.9.9.9***. The best estimate values were used as the model inputs.

The results for all modelled cases are available as spatial plots. The results for the intermediate exceedance frequencies of 1E-5 and 1E-7 y^{-1} were obtained by interpolation of the model results and these results are included in the figures and tables of key output parameters, e.g., maximum wave run-up.

5.9.6.4 Conceptual Design for New NIs

The conceptual engineering design was limited to developing a conceptual layout for the seawater cooling intake and outfall system. No engineering feasibility studies were performed for the SSR and this conceptual layout thus serves only to demonstrate the technical feasibility of the layout in terms of:

- thermal plume dispersion;
- recirculation;
- sediment transport around the structures;
- suspended sediments drawn into the intake.

5.9.7 Climate Change

5.9.7.1 Introduction

The effect of climate change on all relevant oceanographic and coastal engineering parameters has been estimated. The effect of climate change was evaluated over both the operating life and the decommissioning period of the proposed new NIs at the site. The primary guidance is taken from the latest publications from the Intergovernmental Panel for Climate Change (IPCC), along with peer-reviewed journal articles where IPCC projections are outdated or unavailable. IPCC publications up to the Sixth Assessment Report (AR6) (IPCC, 2021) were considered.

CONTROLLED DISCLOSURE

When downloaded from the EDS database, this document is uncontrolled and the responsibility rests with the user to ensure it is in line with the authorised version on the database.

The AR6 presents climate change projections for a range of scenarios called Shared Socioeconomic Pathways (SSPs), which span a wide range of plausible societal and climatic futures and are an update to the Representative Concentration Pathways (RCPs) used in previous reports of the IPCC. The SSPs are based on different greenhouse gas and air pollutant concentration trajectories over the 21st century and are all plausible and illustrative with no probabilities attached. The most conservative pathway (SSP5-8.5), representing very high warming and high carbon dioxide emissions driven by fossil-fuelled development, was adopted for climate change projections. Where projections for SSP5-8.5 were not available, the projections for the nominally corresponding RCP8.5 used in earlier IPCC assessments was used.

For conservatism the upper end of the confidence intervals was applied where these are available in the projections. Projections from the AR6 are typically provided as a mean and a likely range, where the likely range is defined as the region between the 17th to 83rd percentile.

Projections are given relative to a baseline period, which for AR6 is typically 1995-2014. The oceanographic and coastal engineering parameters used in ***Section 5.9*** are based on different datasets available over different periods. For each parameter the baseline date was taken as the middle of the period of available data at the site. Projections derived from literature were converted relative to the baseline date for each parameter.

5.9.7.2 Sea Level Rise

Projections for sea level rise (SLR) were obtained from the AR6, which provides the regional relative sea level rise up to 2150 relative to the baseline period of 1995-2014 (mid-point 2004.5). The projections at Thyspunt were extracted at the nearest node to the site (24°E, 35°S) and were converted from the 2004.5 baseline date to the baseline date for mean tidal level at Thyspunt of 2013.5 (see ***Subsection 5.9.9.1***).

SLR projections were extracted for the upper end of the likely range (83rd percentile) for SSP5-8.5. This projection incorporates only those processes in which the AR6 has at least medium confidence (a qualitative measure of the validity of a finding based on the type, amount, quality, and consistency of evidence and the degree of agreement), consistent with earlier IPCC publications. There is therefore a 17% likelihood that the processes in which there is at least medium confidence will generate outcomes above the upper end of the likely range. To inform decision making for stakeholders with a low risk tolerance, the AR6 also presents high-end sea level projections, which incorporate processes which are deeply uncertain but cannot be ruled out. These include ice-sheet projections based on Structured Expert Judgement and projections from an Antarctic Ice Sheet model that includes

CONTROLLED DISCLOSURE

When downloaded from the EDS database, this document is uncontrolled and the responsibility rests with the user to ensure it is in line with the authorised version on the database.

the marine ice cliff instability (a specific uncertain process not generally included in ice-sheet models). This projection for the SSP5-8.5 scenario was considered as a high-end sea level rise scenario for only the 2134 date, and is referred to as the '2134 High SLR' scenario throughout this ***Section 5.9***. Only the SLR projection differs between the 2134 and 2134 High SLR scenarios.

The SLR projections for Thyspunt relative to the 2013.5 mean level is presented in ***Figure 5.9-3*** and ***Table 5.9-8***.

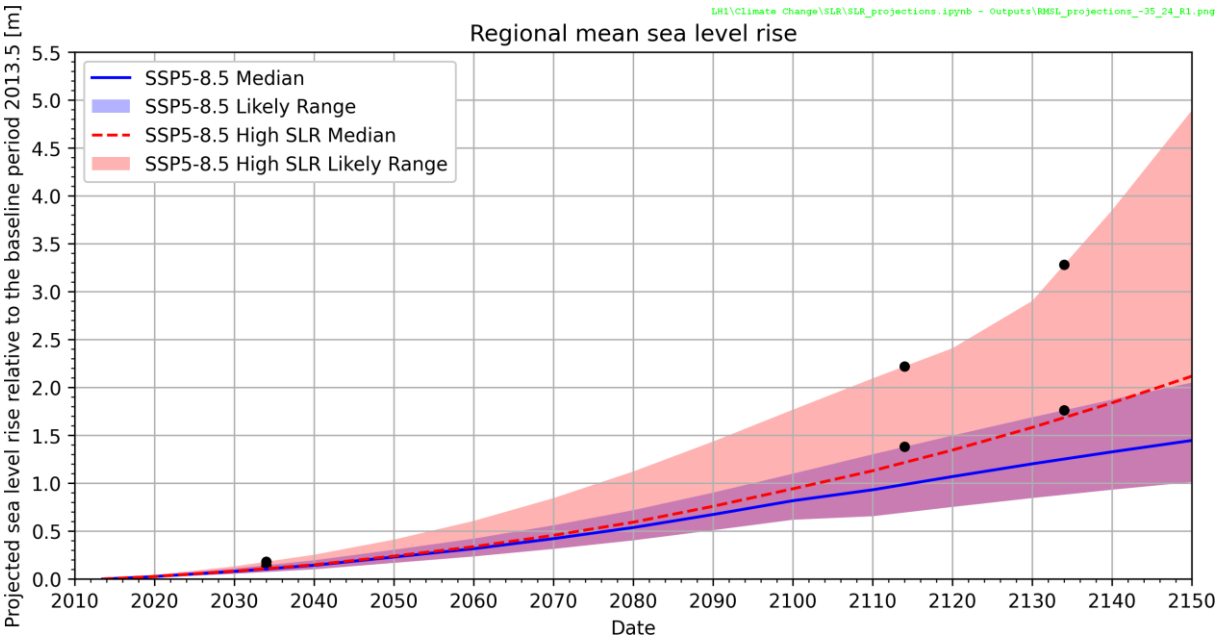


Figure 5.9-3: SLR Projections at Thyspunt for the Upper End of the Likely Range of the SSP5-8.5 and SSP5-8.5 High SLR Scenarios.

5.9.7.3 Seawater Temperature

Projections for sea surface temperature were obtained from the Interactive Atlas of the AR6. Projected changes were extracted at the nearest node to Thyspunt for the near term (2021-2040), medium term (2041-2060) and long term (2081-2100) time slices under SSP5-8.5 using the multi-model mean from 27 models in the Coupled Model Intercomparison Project 6 (CMIP6). The projections were converted from the AR6 baseline date of 2004.5 to the baseline date for seawater temperature at the site (2008, see ***Subsection 5.9.9.5***), and were then interpolated and extrapolated to the required dates using a second order polynomial fit. The results are presented in ***Table 5.9-8***.

CONTROLLED DISCLOSURE

When downloaded from the EDS database, this document is uncontrolled and the responsibility rests with the user to ensure it is in line with the authorised version on the database.

5.9.7.4 Storm Surge and Long Waves

The AR6 concludes that SLR is the main driver for changes in extreme sea water levels, while contributions from storm surge and waves are non-negligible. Projections for storm surge were assessed using the results of a study by Vousdoukas et al. (2018) (also referenced in AR6) who used global hydrodynamic and wave models forced by an ensemble of six global climate models in a probabilistic assessment of the impacts of climate change on extreme sea water levels. The outputs of this study include projected changes in the contribution of combined storm surge and wave set-up for events with a 1E-2 y^{-1} exceedance frequency along the global coastline relative to a baseline period of 1980-2014. The results for RCP8.5 indicate small changes at Thyspunt for the median projection (-0.6% by 2050 and +0.6% by 2100) with positive changes at the 95th percentile (+1.7% by 2050 and +3.5% by 2100). The 95th percentile projections were converted to the baseline date for storm surge at the site (2001; see ***Subsection 5.9.9.2***) and interpolated and extrapolated to the required dates using a linear fit. The results are included in ***Table 5.9-8***. It is noted that these projections include a component of wave set-up which cannot be separated from the storm surge component. However, since the projected changes in extreme wave height exceed those derived here, the projections that include a component of wave set-up envelope the increases for storm surge alone.

Considering that long waves such as meteo-tsunamis are generated by the same physical processes as storm surge, i.e., wind and atmospheric pressure, the same projections were used for these events. The projections are given in ***Table 5.9-8*** relative to a baseline date of 2014.5, appropriate for long wave events at the site (see ***Subsection 5.9.9.3***).

5.9.7.5 Waves

A global ensemble of wave climate projections has been published (Morim, et al., 2020) under the Coordinated Wave Climate Experiment Phase 2 (COWCLIP 2.0). The ensemble archive comprises 148 global wave climate simulations from 10 state-of-the-art studies from different international climate research groups, including both dynamical and statistical wind-wave modelling methods. The ensemble includes mean and exceedance statistics of significant wave height (H_{m0}), mean wave period (T_m) and mean wave direction (MWD) for present (1979-2004) and future (2081-2100) time slices. An analysis of this ensemble by Morim et al. (2019) informed projected changes in mean wave conditions.

Ensemble-mean projections for RCP8.5 at the future time slice were extracted offshore of Thyspunt for the annual mean H_{m0}, annual mean T_m, and annual mean MWD. Projections at the required dates were linearly interpolated or extrapolated from the available data and converted to the

CONTROLLED DISCLOSURE

When downloaded from the EDS database, this document is uncontrolled and the responsibility rests with the user to ensure it is in line with the authorised version on the database.

baseline date of 2004.5, appropriate for the operational wave climate (see ***Subsection 5.9.9.8***). The projections for H_{m0} indicated a small negative trend and was conservatively set to zero. Projections for T_m were negligible (<0.1%) and were also taken as zero. Projections for MWD indicate an anti-clockwise rotation in operational wave direction.

Projections for global changes in extreme wave heights have been determined from a seven-member subset of the wave model ensemble described above (Meucci, et al., 2020). For each of a present-day (1979-2005) and future time slice (2081-2100), extreme wave heights were determined by fitting an exponential distribution to the 1 000 highest wave heights pooled from the seven models (after bias-correction). The projected changes for the 1E-2 y^{-1} exceedance frequency significant wave height (H_{m0}) were linearly interpolated or extrapolated to the required dates, and converted to a baseline date of 2001.5, as appropriate for the extreme wave climate at the site (see ***Subsection 5.9.9.8***). The associated increase in wave period was determined based on wave period being proportional to the square root of the wave height based theoretically on limiting the wave steepness and confirmed by measurements at the site (see ***Figure 5.9-39***).

5.9.7.6 Currents

Coastal hydrodynamics are highly variable and site-specific and are challenging to model at sufficient resolution over long timescales. The currents measured at Thyspunt were found to include forcings from wind stress, waves, and the Agulhas Current (see ***Subsection 5.9.9.4***). In lieu of available projections for currents, the change in current speed was derived from projections for the underlying forcings. Although the AR6 reports an intensification of the Agulhas Current Extension west of Southern Africa under SSP5-8.5, it indicates a reduction in the surface speeds of the Agulhas Current along the east coast of South Africa (noting that projections in this area are presented as having low model agreement). Projected changes in the Agulhas Current offshore of Thyspunt are therefore not conclusive. Projected changes in wind speed used in ***Section 5.8*** indicate a reduction in mean wind speeds in the near-future (2021-2040) and zero change in the far future (2071-2099) under RCP8.5, and conservatively no changes in wind speeds are applied. The change in current speeds due to climate change was therefore based on the increase in extreme wave heights (discussed above). The change was calculated to be proportional to the square root of the increase in wave height, based on the relationship between longshore wave-driven currents and the breaking wave height (USACE, 2002a). The resulting projections are given in ***Table 5.9-8*** relative to the baseline date of 2013, appropriate for the current measurements at Thyspunt (see ***Subsection 5.9.9.4***).

CONTROLLED DISCLOSURE

When downloaded from the EDS database, this document is uncontrolled and the responsibility rests with the user to ensure it is in line with the authorised version on the database.

5.9.7.7 Summary

Based on the discussion above, ***Table 5.9-8*** shows the climate change applied in ***Section 5.9***.

Table 5.9-8: Climate Change Applied for Each Oceanographic Parameter and Date.

Parameter	Description	Scenario	Units	Baseline date	2034	2114	2134
Sea level rise	Regional relative sea level rise	SSP5-8.5 83rd percentile	m	2013.5	0.14	1.38	1.76
		SSP5-8.5 High SLR 83rd percentile	m	2013.5	0.18	2.22	3.28
Seawater temperature	Sea surface temperature	RCP8.5 mean, (No uncertainty ranges available)	°C	2008.0	0.50	3.34	4.35
Storm surge	Extreme positive	RCP8.5, 95th percentile	%	2001.0	1.07	3.85	4.56
	Extreme negative		%	2001.0	1.07	3.85	4.56
Long waves	Extreme positive	RCP8.5, 95th percentile	%	2014.5	0.63	3.40	4.10
	Extreme negative		%	2014.5	0.63	3.40	4.10
Wave height	Extreme in deep water offshore	RCP8.5 mean, (No uncertainty ranges available)	%	2001.5	1.91	6.62	7.80
	Mean in deep water offshore		%	2004.5	0.0	0.0	0.0
Wave period	Extreme in deep water offshore	RCP8.5 mean, (No uncertainty ranges available)	%	2001.5	Base on H_{m0}-T_P relationship		
	Mean in deep water offshore		%	2004.5	0.0	0.0	0.0
Wave direction	Extreme in deep water offshore	RCP8.5 mean, (No uncertainty ranges available)	deg, pos clockwise	2001.5	Not available		
	Mean in deep water offshore			2004.5	-1.1	-4.0	-4.8
Current speed	Extreme depth-averaged wave-driven longshore current	RCP8.5 mean, (No uncertainty ranges available)	%	2013.0	0.61	2.91	3.48

In general, climate change projections must be continually reassessed as new data and research results become available (at least every five years). The SSR would only need to be updated should one of the relevant climate change parameters change significantly.

5.9.8 Physical Description of the Site

The topography at the site and the bathymetry offshore of the site were obtained from the following sources:

CONTROLLED DISCLOSURE

When downloaded from the EDS database, this document is uncontrolled and the responsibility rests with the user to ensure it is in line with the authorised version on the database.

- C-MAP Electronic Charts and available local surveys in areas surrounding Thyspunt (DHI, 2024o);
- Multi-beam bathymetric surveys offshore (Fugro, 2006) and inshore (Fugro, 2007) of Thyspunt by Fugro Survey Africa;
- Multi-beam bathymetric survey inshore of Thyspunt by Tritan Survey (2008);
- Beach profiles by Tritan Survey (2024); and
- Light Detection and Ranging (LiDAR) survey of the Thyspunt site and upper beach by Southern Mapping Geospatial (SRK, 2011).

The bedrock elevations at the site were inferred from the following sources:

- The side-scan sonar surveys by Fugro Survey Africa (2006) & (2007);
- The multi-beam bathymetric survey by Tritan Survey (2008);
- The LiDAR survey by Southern Mapping Geospatial (SRK, 2011);
- Borehole measurements (***Section 5.15***);
- Geoscientific characterization of data at Thyspunt produced by Claassen and De Wit (2017); and
- Satellite images.

The borehole measurements and geoscientific characterization data provided the bedrock elevations on land which were supplemented with the LiDAR survey where exposed bedrock was visible on satellite images. Offshore, the bedrock elevations were inferred from the side-scan sonar surveys and multi-beam bathymetric survey. Where no bedrock could be identified, the sediment thickness was assumed to not be limited. The combined set of data was thus interpolated and extrapolated to create an estimate of the sediment thickness for use in the coastline stability analysis only.

Throughout ***Section 5.9*** the vertical datum used is mean sea level (msl) also known as Land Levelling Datum (LLD).

The horizontal coordinate system is WG25 defined as follows:

- Map projection: Gauss Conformal
- Datum: Hartebeesthoek 94
- Spheroid: WGS84
- Scale factor: 1
- Central meridian: 25°E

CONTROLLED DISCLOSURE

When downloaded from the EDS database, this document is uncontrolled and the responsibility rests with the user to ensure it is in line with the authorised version on the database.

- Reference system: WG25
- Co-ordinates: Eastings (X, increasing eastwards)
- Northings (Y, increasing northwards)
- Distance units: metres.

Figure 5.9-4 shows the site location including the multi-beam bathymetry offshore of the site while ***Figure 5.9-5*** shows the bathymetry offshore and the topography at the site. ***Figure 5.9-6***, and ***Figure 5.9-7*** present the seabed features, bedrock elevations and sediment thickness at the site.

CONTROLLED DISCLOSURE

When downloaded from the EDS database, this document is uncontrolled and the responsibility rests with the user to ensure it is in line with the authorised version on the database.

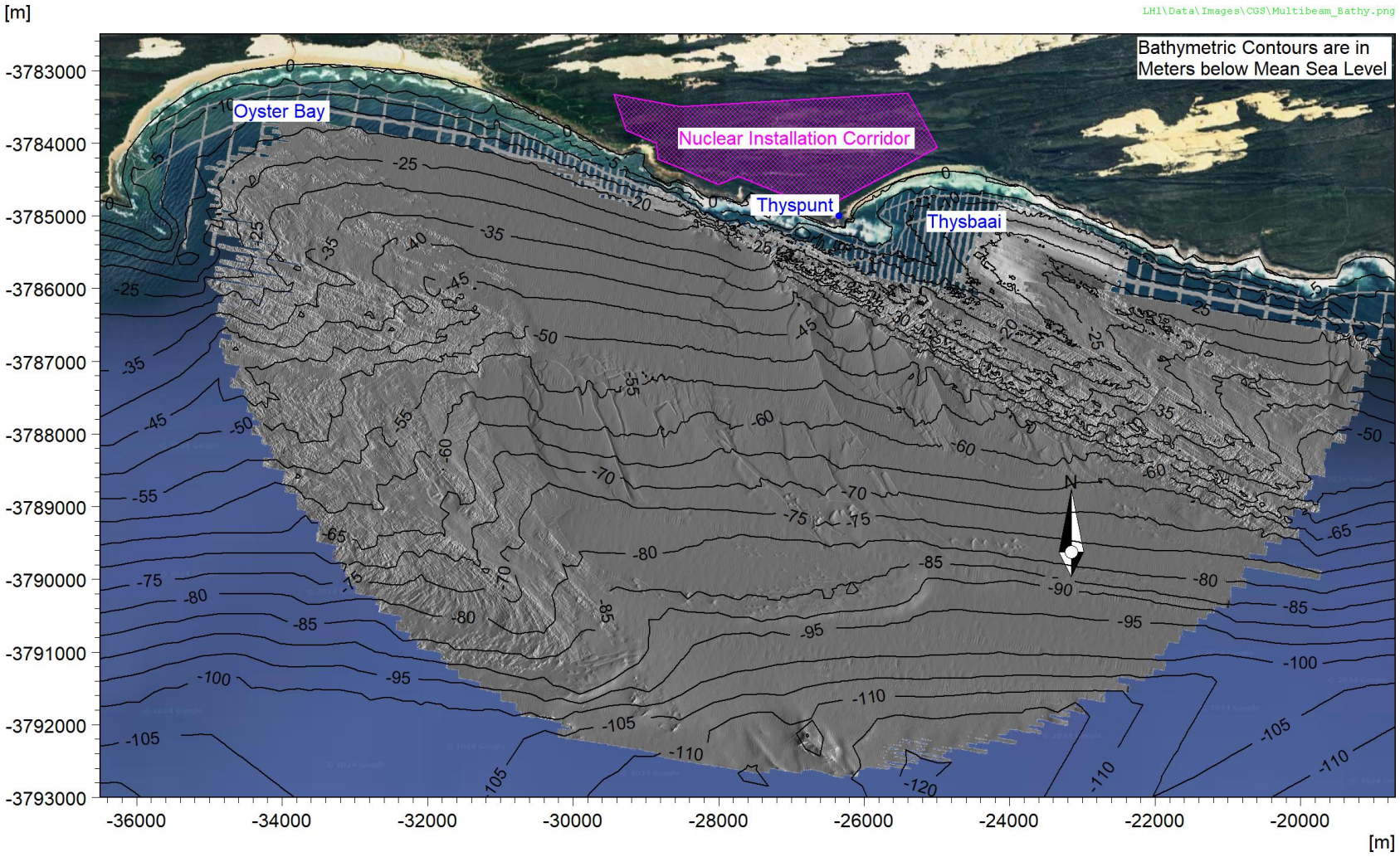


Figure 5.9-4: Site Location Including Multi-Beam Bathymetry Offshore of the Site.

CONTROLLED DISCLOSURE

When downloaded from the EDS database, this document is uncontrolled and the responsibility rests with the user to ensure it is in line with the authorised version on the database.

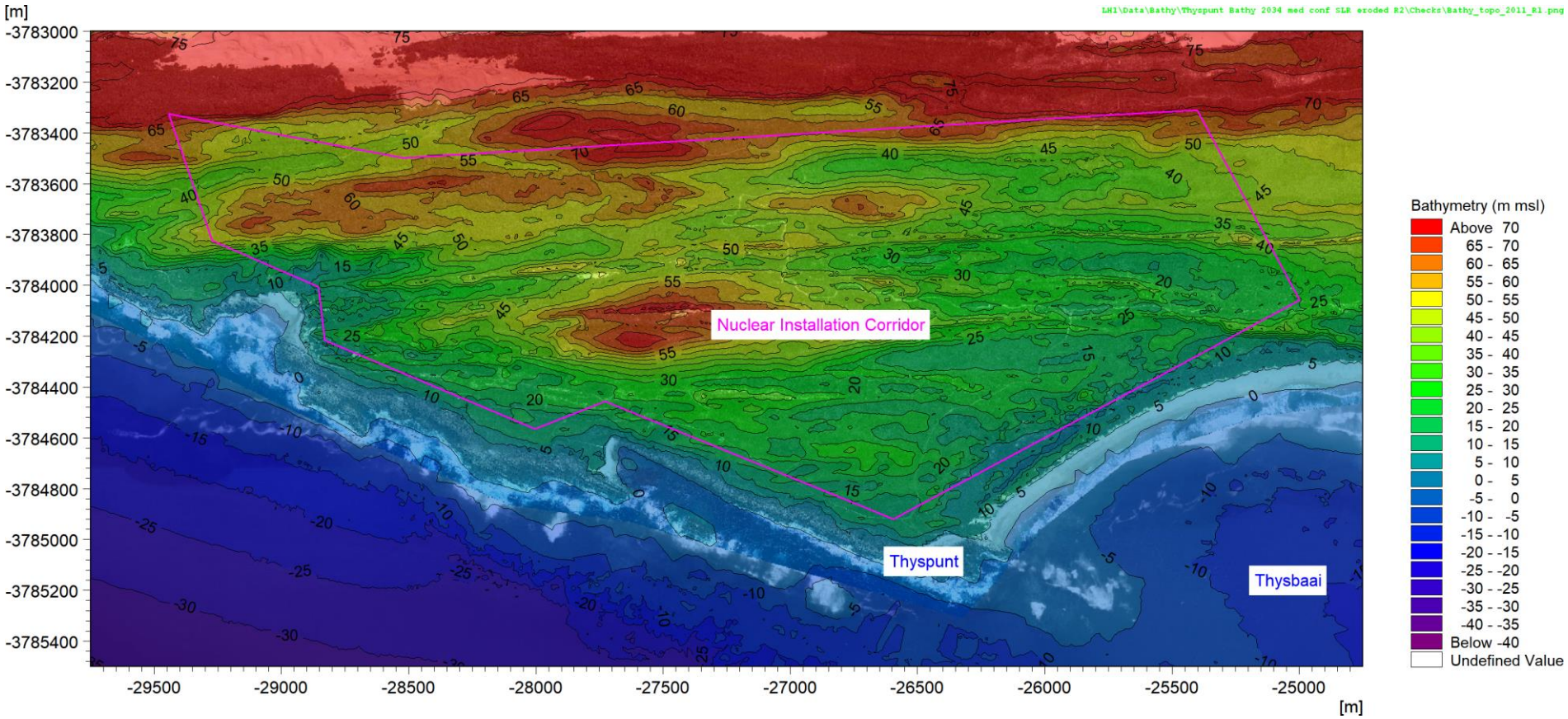


Figure 5.9-5: Bathymetry and Topography at the Site Showing the Location of the Nuclear Installation Corridor.

CONTROLLED DISCLOSURE

When downloaded from the EDS database, this document is uncontrolled and the responsibility rests with the user to ensure it is in line with the authorised version on the database.

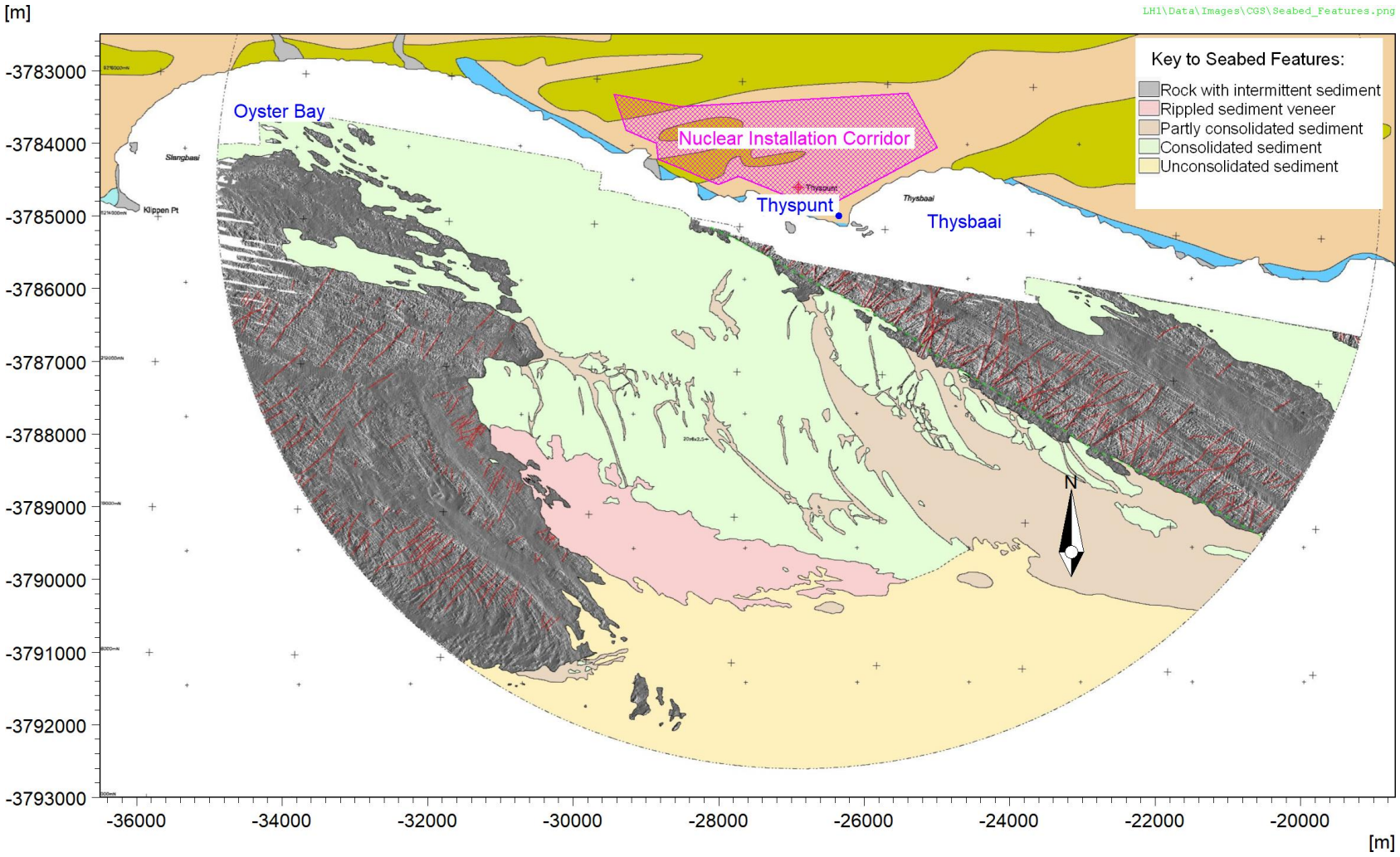


Figure 5.9-6: Seabed Features Offshore of the Site (Adapted from Fugro, (2006)).

CONTROLLED DISCLOSURE

When downloaded from the EDS database, this document is uncontrolled and the responsibility rests with the user to ensure it is in line with the authorised version on the database.

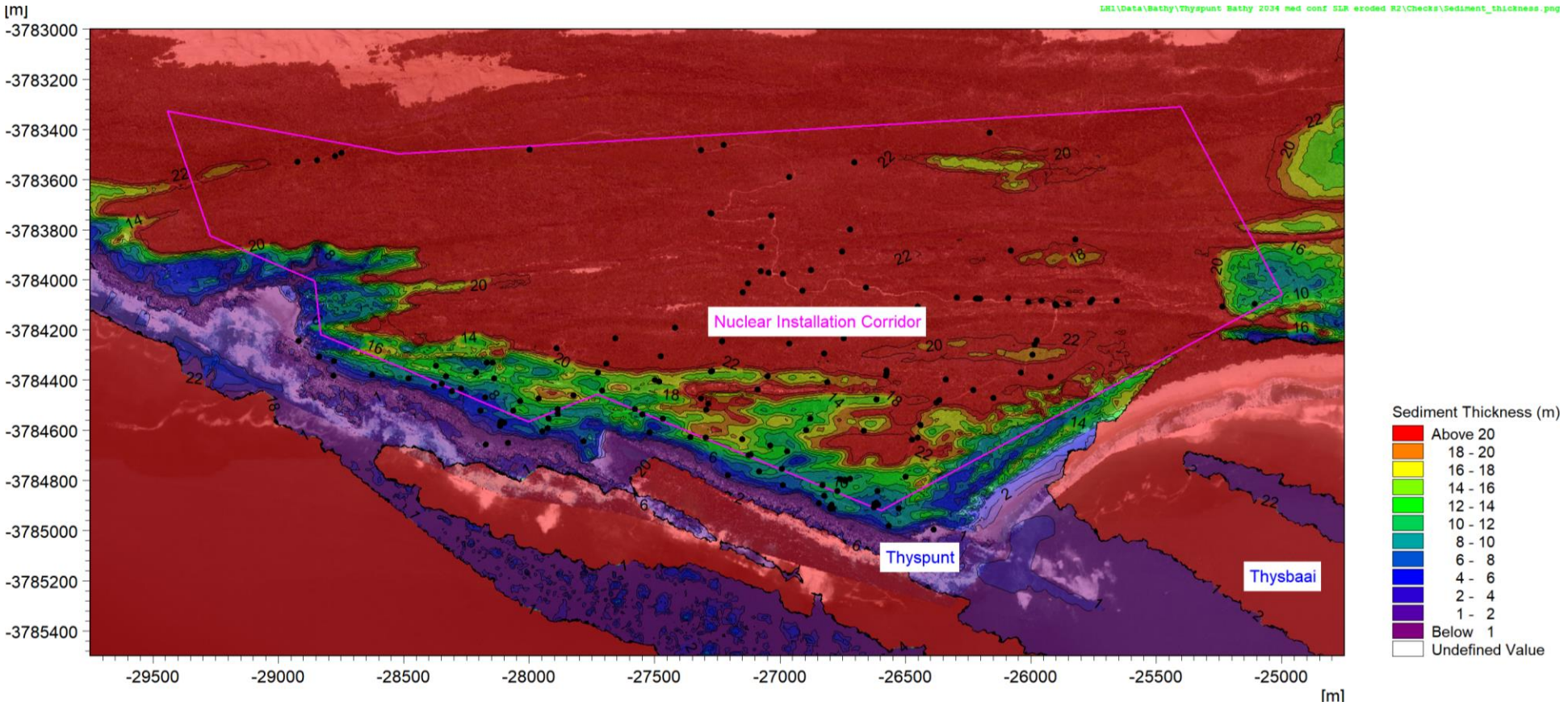


Figure 5.9-7: Sediment Thickness at the Site. Also Shown are the Measured Borehole Locations.

CONTROLLED DISCLOSURE

When downloaded from the EDS database, this document is uncontrolled and the responsibility rests with the user to ensure it is in line with the authorised version on the database.

Notable physical features of the site shown in the figures above include:

- The site is located on an exposed section of coastline that faces towards the prevailing south-south-westerly deep sea swell waves.
- The site is adjacent to a predominantly rocky coastline on the west and the sandy Thysbaai beach on the east separated by the rocky Thyspunt headland.
- Vegetated dunes exist landward of the exposed rocks along the coastline west of Thyspunt, typically above 4 m msl.
- A vegetated shore-parallel dune exists along Thysbaai beach. At its eastern end the beach meets an east-west dune ridge, with a crest level exceeding 25 m msl.
- On the west of the site to the Thyspunt headland, the inshore seabed is predominantly rocky with intermittent sediment. Within Thysbaai the seabed is mostly sandy with intermittent rock which becomes more prominent further offshore.
- A wide band of rock with intermittent sediment is the main seabed feature south of the site, extending from the point at Thyspunt and progressing in a south-easterly direction offshore of Thysbaai beach as a submerged rocky point. Additional geological information is presented in ***Section 5.13*** (Geology).
- Seabed slopes vary along the site with steeper slopes evident on the exposed rocky outcrops and gentler slopes on Thysbaai beach. The average seabed slope in Thysbaai is 1:30 (refer to ***Subsection 5.9.11.2***).

Sediment samples have been collected from the nearshore (depths between -10 and -30 m msl) and from the beach at the high and low water marks (see ***Figure 5.9-8***). The sand on the beaches has a D_{50} of between 0.2 mm and 0.4 mm and a grading of approximately 1.3, defined as $(D_{84}/D_{16})^{0.5}$. Further offshore the D_{50} is generally 0.1 to 0.2 mm, except on the reef where larger sized gravel and shell fragments have been found.

CONTROLLED DISCLOSURE

When downloaded from the EDS database, this document is uncontrolled and the responsibility rests with the user to ensure it is in line with the authorised version on the database.

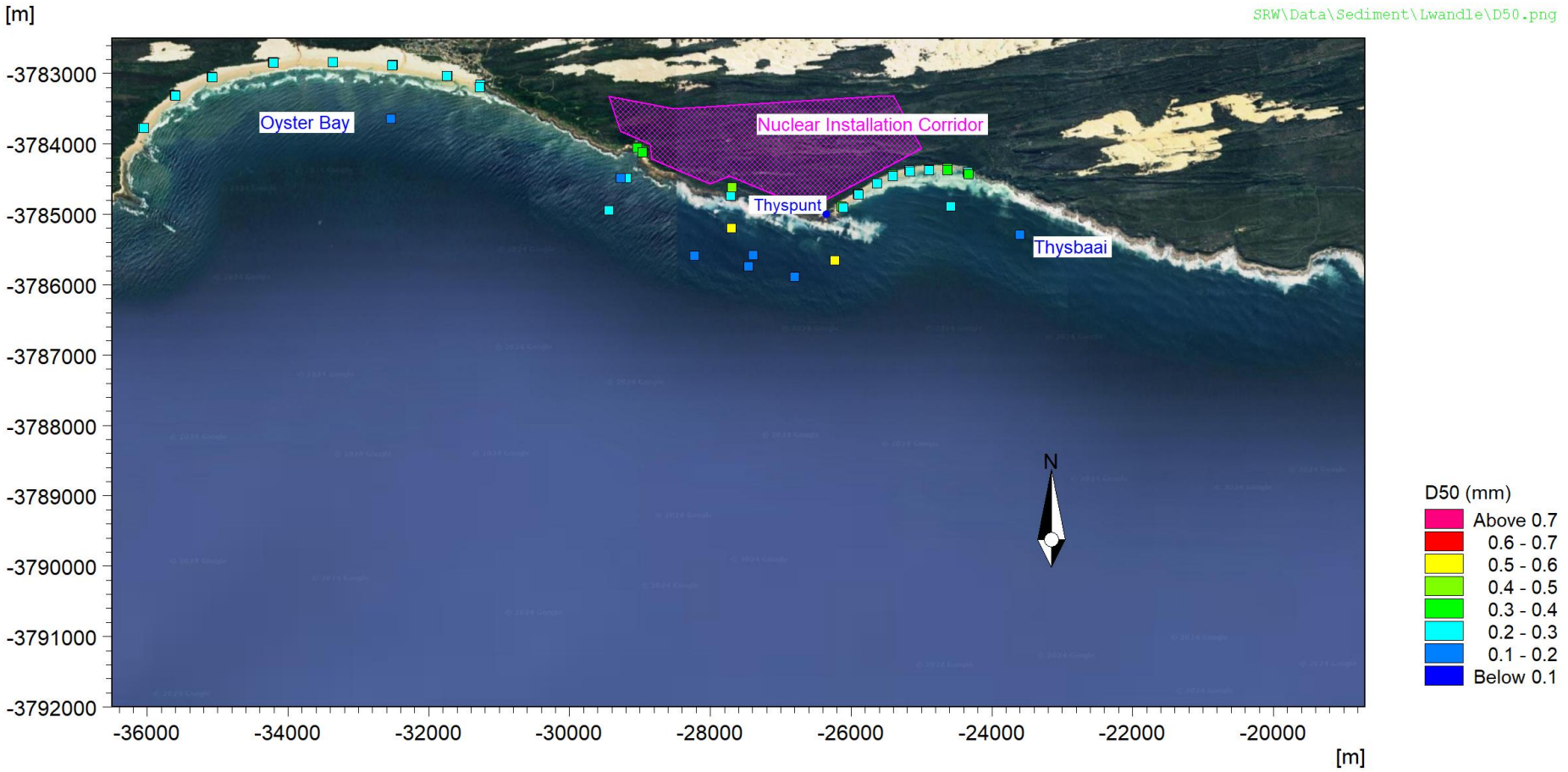


Figure 5.9-8: Measured Sediment Grain Size Offshore and Along the Beach.

CONTROLLED DISCLOSURE

When downloaded from the EDS database, this document is uncontrolled and the responsibility rests with the user to ensure it is in line with the authorised version on the database.

5.9.9 Hydrographic Conditions

This section characterises the hydrographic conditions at the site based on measurements and numerical modelling. These hydrographic conditions are used as inputs to the sediment transport modelling, flooding from the sea, and thermal plume dispersion, as described in the subsections that follow.

5.9.9.1 Tidal Levels

Water levels have been measured in a shallow rock gulley at Site C using a levelled pressure sensor corrected for atmospheric pressure. Details of the locations, instruments, sampling intervals, dates and length of valid data are provided in ***Subsection 5.9.6.1***. The data from February 2008 to March 2019 (6.02 y) was used in the tidal analysis.

The instrument was deployed within the breaker zone, a region that is subject to time-varying changes in the mean water level due to wave set-up. The local wave set-up at the measurement location in the gully was quantified using a coupled spectral wave and two-dimensional (2D) hydrodynamic model which simulates the time-varying wave refraction, wave breaking and associated radiation stress gradients which generate wave set-up. Details of the model description, setup, cases modelled, and calibration are provided in ***Appendix 5.9.A.1***. The wave set-up was calculated as the difference between the modelled water levels at the measurement location and in a depth of -40 m msl offshore of the site. ***Figure 5.9-9*** presents the measured water levels before and after the correction for wave set-up, as well as the modelled wave set-up levels used for the correction.

CONTROLLED DISCLOSURE

When downloaded from the EDS database, this document is uncontrolled and the responsibility rests with the user to ensure it is in line with the authorised version on the database.



Figure 5.9-9: Measured Hourly Water Levels at Thyspunt.

A tidal harmonic analysis was performed on the wave set-up corrected water levels using the MIKE 21 tidal analysis and prediction toolbox (DHI, 2024p) to obtain the tidal constituents that characterise the astronomical tide at the site. The Mean Level (ML) at Thyspunt was calculated as the arithmetic average of the water levels over the measurement period. The level is representative of a baseline date of 2013.5, the approximate mid-point of the dataset.

The resulting main tidal constituents and predicted tidal levels are provided in ***Table 5.9-9*** and ***Table 5.9-10***. Tides along the entire South African coastline are semi-diurnal and microtidal.

CONTROLLED DISCLOSURE

When downloaded from the EDS database, this document is uncontrolled and the responsibility rests with the user to ensure it is in line with the authorised version on the database.

Table 5.9-9: Tidal Constituents at Thyspunt (Baseline Date is 2013.5).

Constituent Symbol	Constituent Name	Amplitude	Phase
		(m)	(°)
Z0	Elevation of ML above msl	0.206	0.00
M2	Principal lunar semi-diurnal	0.539	101.89
S2	Principal solar semi-diurnal	0.278	129.10
N2	Larger lunar elliptic semi-diurnal	0.106	96.09
K2	Luni-solar semi-diurnal	0.095	127.01
K1	Luni-solar diurnal	0.071	168.64
NU2	Larger lunar evectional constituent	0.020	93.00
P1	Principal solar diurnal	0.019	162.35
MU2	Variational semi-diurnal	0.018	82.75
O1	Principal lunar diurnal	0.018	288.68
2N2	Lunar elliptical semidiurnal second-order	0.015	82.71
L2	Smaller lunar elliptic semi-diurnal	0.015	102.14
S1	Solar diurnal	0.013	234.600
Q1	Larger lunar elliptic diurnal	0.011	272.72
T2	Larger solar elliptic semi-diurnal	0.010	141.30
SSA	Solar semi-annual long-period	0.009	241.24
SA	Solar annual long-period	0.009	312.66
M4	Shallow water overtides of principal lunar	0.009	234.71
MF	Lunar fortnightly long-period	0.009	281.30
H1	Solar semi-diurnal	0.007	64.44
OO1	Lunar diurnal	0.006	244.14
SK3	Not available	0.006	201.77
MSF	Lunisolar synodic fortnightly	0.006	164.46
M3	Lunar terdiurnal	0.006	37.03
J1	Smaller lunar elliptic diurnal	0.006	187.44
ETA2	Not available	0.006	161.37
H2	Not available	0.006	265.11
MM	Lunar monthly long-period	0.006	41.69
R2	Not available	0.005	162.19
MN4	Shallow water quarter diurnal	0.005	195.86
MS4	Not available	0.005	274.56

CONTROLLED DISCLOSURE

When downloaded from the EDS database, this document is uncontrolled and the responsibility rests with the user to ensure it is in line with the authorised version on the database.

Table 5.9-10: Predicted Tidal Levels at Thyspunt (Baseline Date is 2013.5).

Parameter	Level (m msl)
Highest Astronomical Tide (HAT)	1.406
Mean High Water Springs (MHWS)	1.061
Mean High Water Neaps (MHWN)	0.468
Mean Level (ML)	0.206
Mean Low Water Neaps (MLWN)	-0.037
Mean Low Water Springs (MLWS)	-0.632
Lowest Astronomical Tide (LAT)	-0.873

The US NRC's recommended initial tidal water level to apply for storm surge and tsunami run-up calculations in deterministic studies is the 90th percentile high tide (NRC, 2009). This is defined as the high tide level that is exceeded by 10 per cent of the high tides over a continuous 19 y period. For low water calculations the 10th percentile low tide is the recommended initial level. The predicted tides at the site were used to calculate the following initial tidal levels:

- 90th percentile high tide = +1.08 m msl;
- 10th percentile low tide = -0.65 m msl.

5.9.9.2 Storm Surge

Storm surge is for the purpose of this report defined as the influence of meteorological effects such as winds and barometric pressure that result in the actual sea level being above or below the predicted astronomical tide level. The storm surge events have durations of hours to days and can thus be extracted from hourly tidal measurements. In this report water level fluctuations with shorter periods between 8 and 60 minutes that can be extracted from 1 to 3-minute tidal measurements are referred to as long waves and are described in ***Subsection 5.9.9.3***.

The measured storm surge at Thyspunt was calculated by subtracting the predicted tidal water levels from the measured water levels corrected for wave set-up. It is important to note that although wave set-up is an important component of the maximum water level at the site during storm events, the storm wave run-up modelling conducted in this study to determine the maximum water levels (see ***Subsection 5.9.12***) implicitly includes wave set-up. Thus, to include the wave set-up in the storm surge analysis would lead to double counting of this component. Time-series of the measured

CONTROLLED DISCLOSURE

When downloaded from the EDS database, this document is uncontrolled and the responsibility rests with the user to ensure it is in line with the authorised version on the database.

water levels corrected for wave set-up, the predicted tidal water levels, and storm surge are presented in ***Figure 5.9-10***.

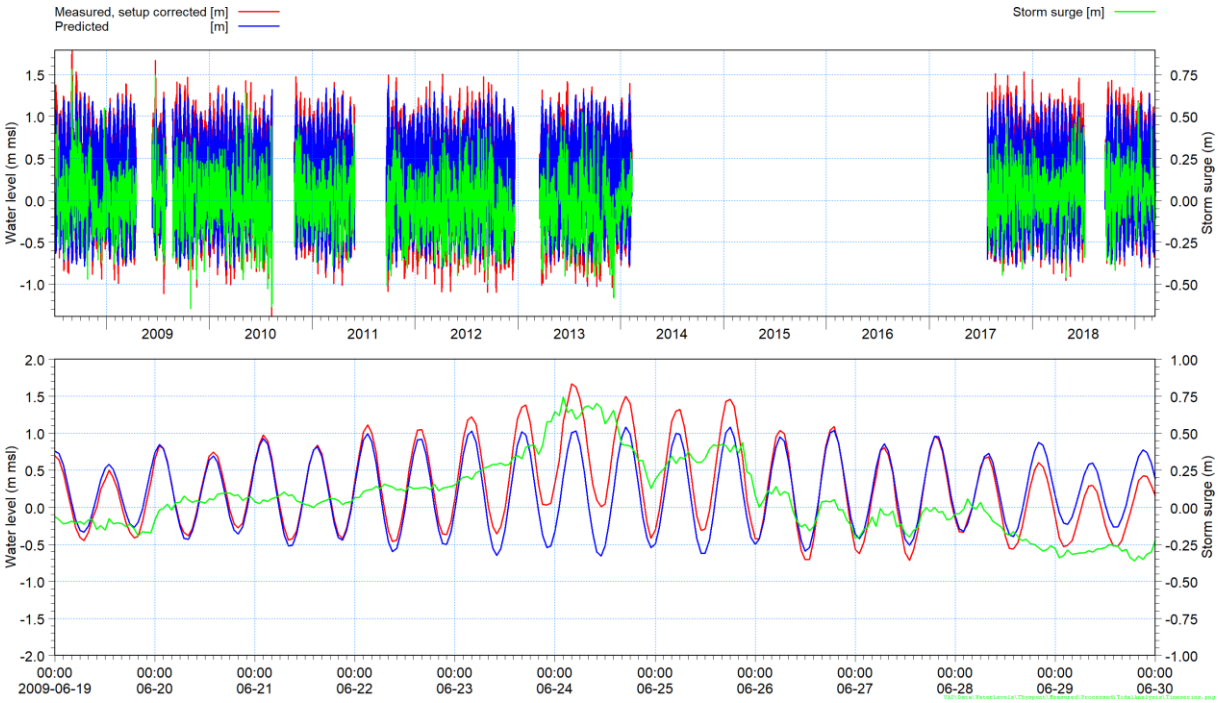


Figure 5.9-10: Measured Water Level, Predicted Tide and Storm Surge at Thyspunt for the Entire Dataset (Top) and Detail for a Storm Event in 2009 (Bottom).

In addition to the measurements at Site C, measured hourly water levels at Gqeberha (formerly Port Elizabeth) from 1978 to 2023 was kindly provided by the Hydrographer of the South African Navy (who is not responsible for any transcription errors or errors due to calculations using the data). A linear regression fitted to the annual average water level over the measured period indicated a trend of 2.0 mm/y, which was removed prior to further analysis. A tidal analysis and prediction were undertaken on the detrended data as described in ***Subsection 5.9.9.1***. Predicted tidal water levels were subtracted from the measured water levels at Gqeberha to obtain the storm surge. A high-pass filter with a frequency of 1.85E-5 Hz (period of 15 hours) was used to remove residual tidal signals in the storm surge time-series, which likely occurred due to timing errors in the data. The measured water level, predicted tide and filtered storm surge at Gqeberha are plotted in ***Figure 5.9-11***.

CONTROLLED DISCLOSURE

When downloaded from the EDS database, this document is uncontrolled and the responsibility rests with the user to ensure it is in line with the authorised version on the database.

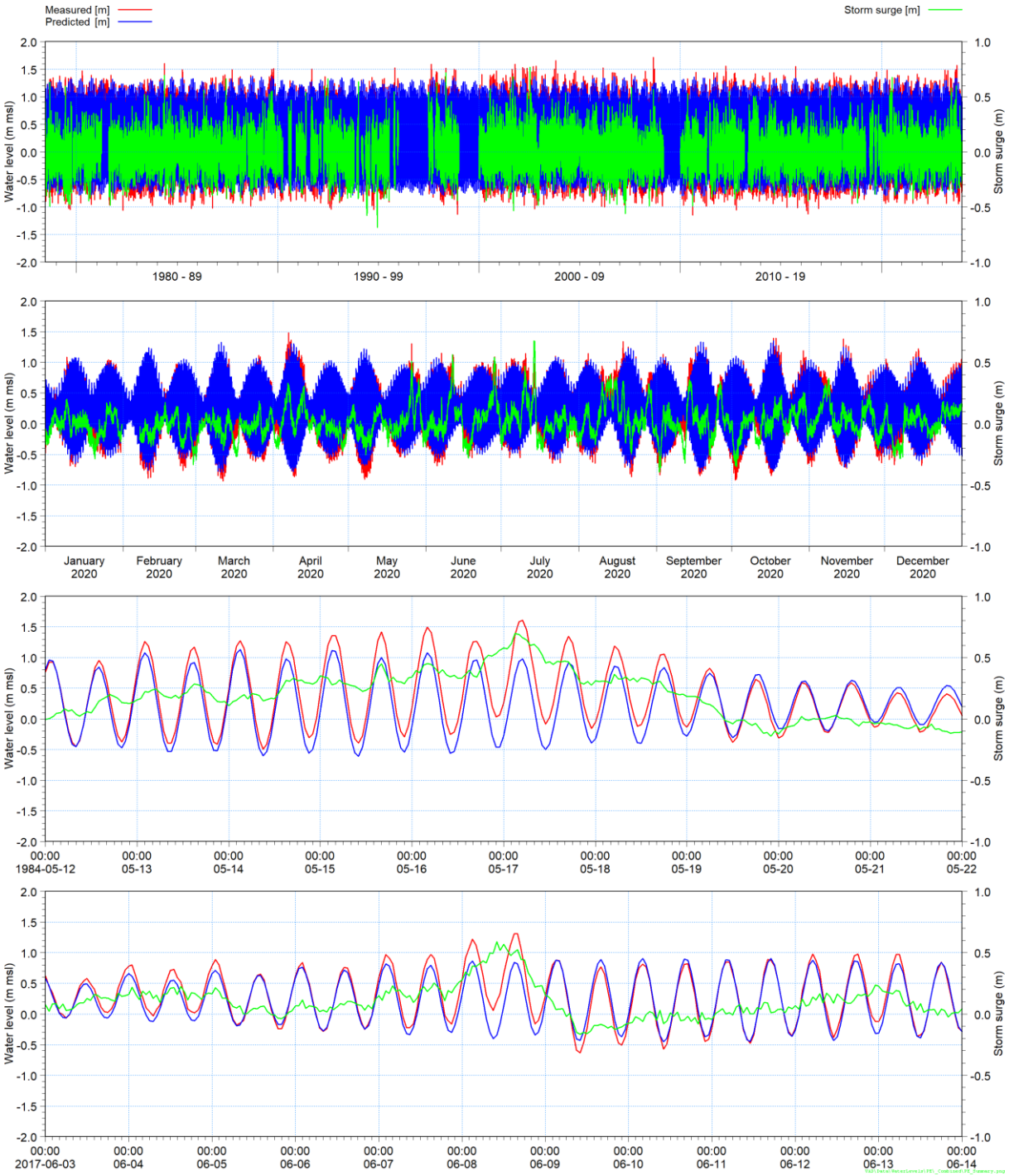


Figure 5.9-11: Measured Water Level, Predicted Tide and Storm Surge at Gqeberha (Port Elizabeth) for the Entire Dataset (Top), Detail for 2020 (Top Middle), the May 1984 Storm (Bottom Middle) and the June 2017 Storm (Bottom).

CONTROLLED DISCLOSURE

When downloaded from the EDS database, this document is uncontrolled and the responsibility rests with the user to ensure it is in line with the authorised version on the database.

For the analysis of extreme storm surge, the Gqeberha dataset was preferred over the water levels measured at Site C due to the longer duration of the data (38 y vs 6 y). The Thyspunt site is situated on an exposed coastline facing approximately south-westwards, while the Gqeberha tide gauge is in the Port of Port Elizabeth in the lee of Cape Recife, which is sheltered from the south-west but exposed to the east. The differences in exposure and orientation between the two sites results in a difference in wind-driven storm surge. ***Figure 5.9-12*** presents a scatter comparison of the storm surge at the aforementioned sites.

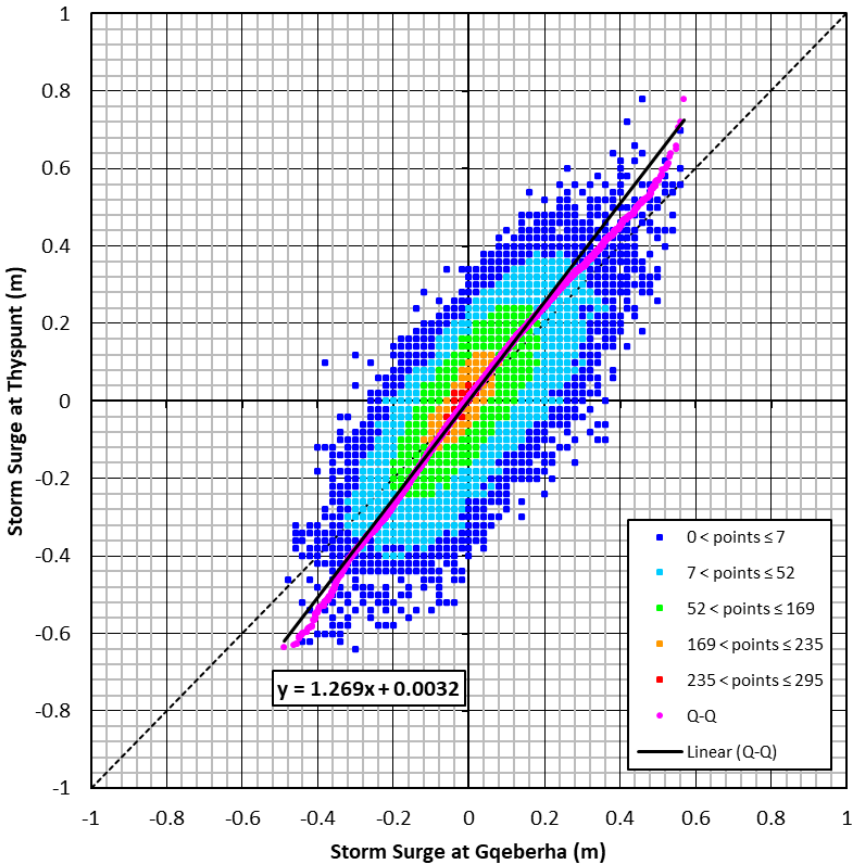


Figure 5.9-12: Scatter Comparison of Measured Storm Surge at Thyspunt and Gqeberha for the Overlapping Period.

Figure 5.9-12 shows reasonable agreement between the measured storm surge at Thyspunt and Gqeberha. The good correlation indicates that storm surge events were typically experienced at both sites simultaneously, while the linear trend line fitted to the Q-Q curve indicates that the measured storm surge at Thyspunt is approximately 27% larger than that at Gqeberha.

The storm surge measured at Gqeberha was scaled using the above correction and used to estimate the extreme storm surge at Thyspunt. An

CONTROLLED DISCLOSURE

When downloaded from the EDS database, this document is uncontrolled and the responsibility rests with the user to ensure it is in line with the authorised version on the database.

extreme value analysis (refer to ***Subsection 5.9.6.2*** for the methodology) was performed on the scaled positive storm surge (measured water level higher than predicted tide) and scaled negative storm surge (measured water level lower than the predicted tide). The extreme value analysis results for positive and negative storm surges are plotted in ***Figure 5.9-13*** and ***Figure 5.9-14***, respectively. The baseline date is 2001 which is the mid-point of the measurement period.

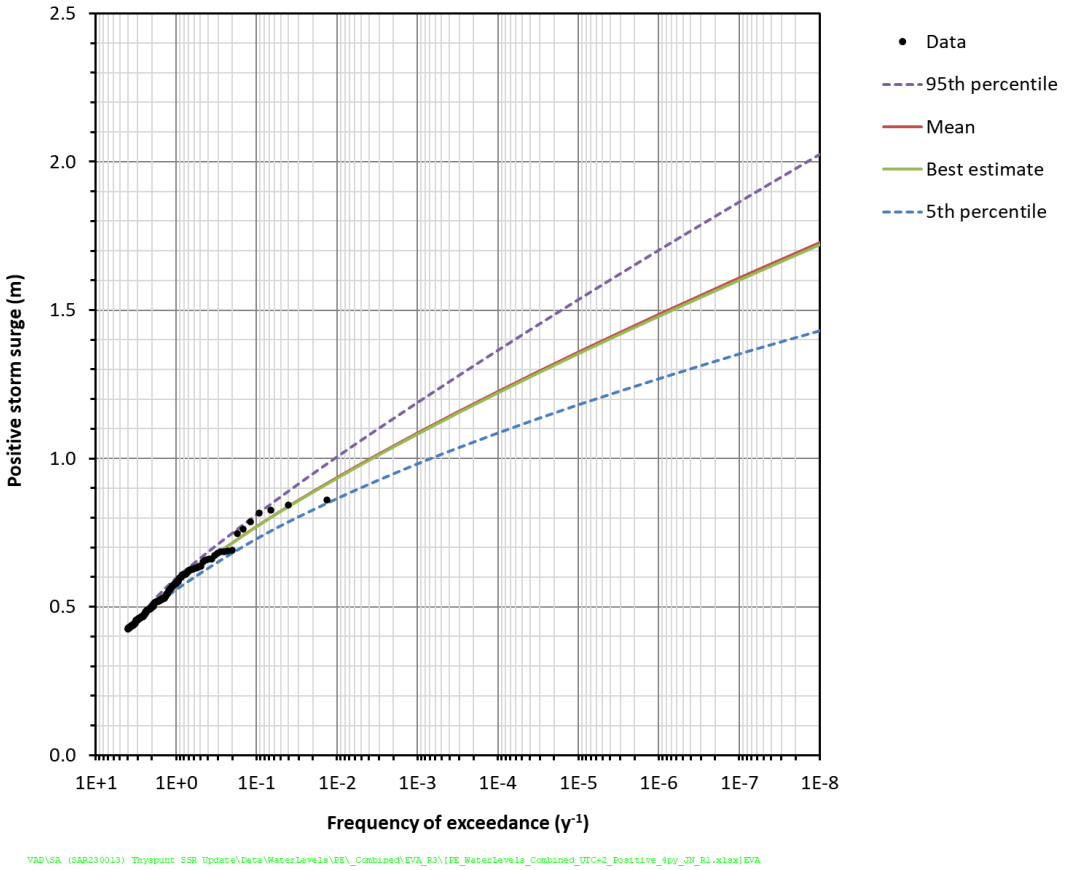


Figure 5.9-13: Extreme Value Analysis of Scaled Positive Storm Surge Residuals at Gqeberha (Baseline Date is 2001).

CONTROLLED DISCLOSURE

When downloaded from the EDS database, this document is uncontrolled and the responsibility rests with the user to ensure it is in line with the authorised version on the database.

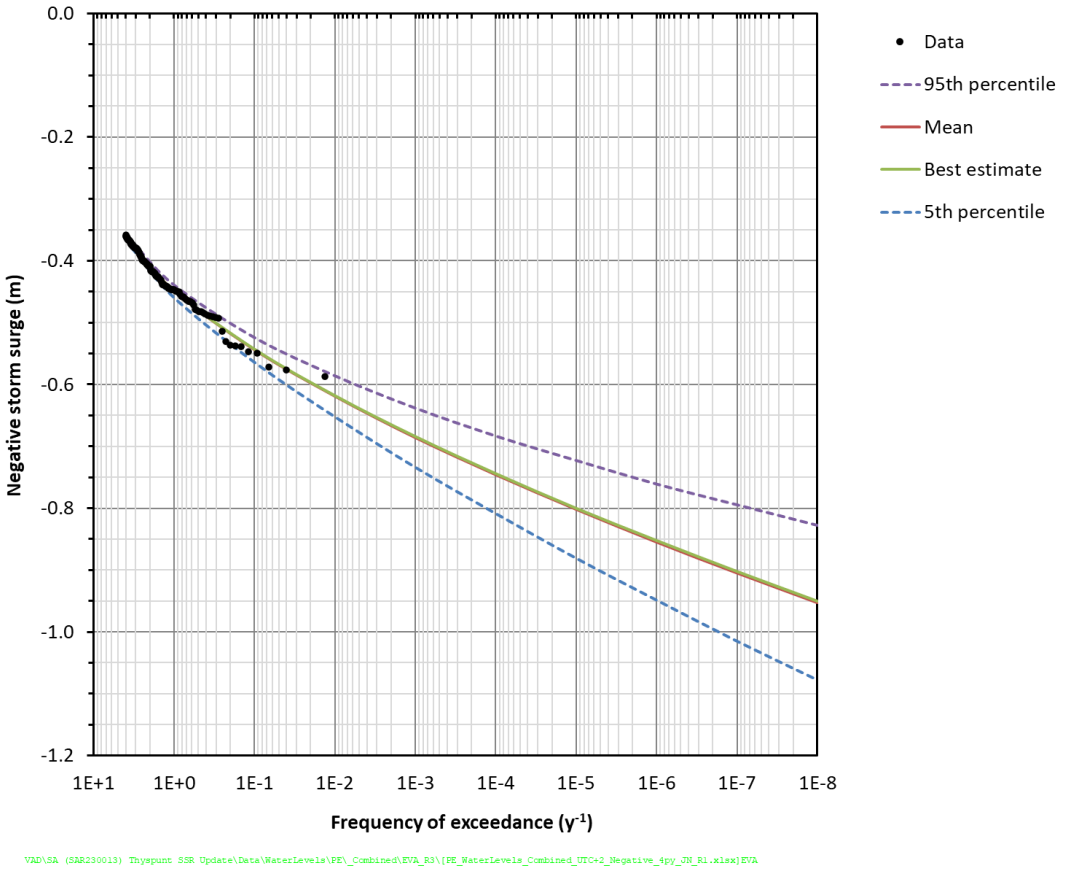


Figure 5.9-14: Extreme Value Analysis of Scaled Negative Storm Surge Residuals at Gqeberha (Baseline Date is 2001).

The positive storm surge was then adjusted for climate change (***Subsection 5.9.7***) and added to the 90% high tide (***Subsection 5.9.9.1***) and the sea level rise (***Subsection 5.9.7***) to obtain the maximum still water level at the three dates of interest, as shown in ***Table 5.9-11***. The minimum still water level was calculated in the same way except that the 10% low tide was used (***Subsection 5.9.9.1***) and sea level rise was conservatively set to zero, with the results shown in ***Table 5.9-12***.

CONTROLLED DISCLOSURE

When downloaded from the EDS database, this document is uncontrolled and the responsibility rests with the user to ensure it is in line with the authorised version on the database.

Table 5.9-11: Extreme Positive Storm Surge and Maximum Still Water Levels.

Exceedance Frequency	Uncertainty	Tide [a]	Sea Level Rise [b]					Positive Storm Surge [c]			Maximum Still Water Level				
(y^{-1})		(m msl)	(m)					(m)			(m msl)				
			2034	2114	2114 High SLR	2134	2134 High SLR	2034	2114	2134	2034	2114	2114 High SLR	2134	2134 High SLR
1E+0	5th Percentile	1.08	0.14	1.38	2.22	1.76	3.28	0.56	0.58	0.58	1.79	3.04	3.88	3.42	4.94
	Mean	1.08	0.14	1.38	2.22	1.76	3.28	0.58	0.60	0.60	1.81	3.06	3.90	3.44	4.96
	Best Estimate	1.08	0.14	1.38	2.22	1.76	3.28	0.58	0.60	0.60	1.81	3.06	3.90	3.44	4.96
	95th Percentile	1.08	0.14	1.38	2.22	1.76	3.28	0.60	0.62	0.62	1.83	3.08	3.92	3.47	4.99
1E-1	5th Percentile	1.08	0.14	1.38	2.22	1.76	3.28	0.74	0.76	0.76	1.96	3.22	4.06	3.60	5.12
	Mean	1.08	0.14	1.38	2.22	1.76	3.28	0.78	0.80	0.81	2.00	3.26	4.10	3.65	5.17
	Best Estimate	1.08	0.14	1.38	2.22	1.76	3.28	0.78	0.80	0.80	2.00	3.26	4.10	3.65	5.17
	95th Percentile	1.08	0.14	1.38	2.22	1.76	3.28	0.82	0.84	0.85	2.04	3.30	4.14	3.69	5.21
1E-2	5th Percentile	1.08	0.14	1.38	2.22	1.76	3.28	0.87	0.90	0.90	2.10	3.36	4.20	3.75	5.26
	Mean	1.08	0.14	1.38	2.22	1.76	3.28	0.94	0.97	0.98	2.17	3.43	4.27	3.82	5.34
	Best Estimate	1.08	0.14	1.38	2.22	1.76	3.28	0.94	0.97	0.97	2.17	3.43	4.27	3.82	5.34
	95th Percentile	1.08	0.14	1.38	2.22	1.76	3.28	1.02	1.04	1.05	2.24	3.50	4.34	3.89	5.41
1E-3	5th Percentile	1.08	0.14	1.38	2.22	1.76	3.28	0.99	1.02	1.03	2.22	3.48	4.32	3.87	5.39
	Mean	1.08	0.14	1.38	2.22	1.76	3.28	1.10	1.13	1.13	2.32	3.59	4.43	3.98	5.50
	Best Estimate	1.08	0.14	1.38	2.22	1.76	3.28	1.09	1.12	1.13	2.32	3.58	4.42	3.97	5.49
	95th Percentile	1.08	0.14	1.38	2.22	1.76	3.28	1.20	1.23	1.24	2.42	3.69	4.53	4.08	5.60
1E-4	5th Percentile	1.08	0.14	1.38	2.22	1.76	3.28	1.10	1.13	1.13	2.32	3.59	4.43	3.98	5.50
	Mean	1.08	0.14	1.38	2.22	1.76	3.28	1.24	1.27	1.28	2.46	3.73	4.57	4.12	5.64
	Best Estimate	1.08	0.14	1.38	2.22	1.76	3.28	1.23	1.27	1.28	2.46	3.73	4.57	4.12	5.64
	95th Percentile	1.08	0.14	1.38	2.22	1.76	3.28	1.38	1.42	1.43	2.60	3.88	4.72	4.27	5.79
1E-5	5th Percentile	1.08	0.14	1.38	2.22	1.76	3.28	1.19	1.23	1.23	2.42	3.69	4.53	4.08	5.60
	Mean	1.08	0.14	1.38	2.22	1.76	3.28	1.37	1.41	1.42	2.60	3.87	4.71	4.26	5.78
	Best Estimate	1.08	0.14	1.38	2.22	1.76	3.28	1.37	1.40	1.41	2.59	3.86	4.70	4.26	5.77
	95th Percentile	1.08	0.14	1.38	2.22	1.76	3.28	1.55	1.59	1.61	2.78	4.05	4.89	4.45	5.97
1E-6	5th Percentile	1.08	0.14	1.38	2.22	1.76	3.28	1.28	1.32	1.33	2.50	3.78	4.62	4.17	5.69
	Mean	1.08	0.14	1.38	2.22	1.76	3.28	1.50	1.54	1.55	2.72	4.00	4.84	4.39	5.91
	Best Estimate	1.08	0.14	1.38	2.22	1.76	3.28	1.49	1.53	1.55	2.72	3.99	4.83	4.39	5.91
	95th Percentile	1.08	0.14	1.38	2.22	1.76	3.28	1.72	1.77	1.78	2.94	4.23	5.07	4.62	6.14
1E-7	5th Percentile	1.08	0.14	1.38	2.22	1.76	3.28	1.37	1.40	1.41	2.59	3.86	4.70	4.25	5.77
	Mean	1.08	0.14	1.38	2.22	1.76	3.28	1.63	1.67	1.68	2.85	4.13	4.97	4.52	6.04
	Best Estimate	1.08	0.14	1.38	2.22	1.76	3.28	1.62	1.66	1.67	2.84	4.12	4.96	4.51	6.03
	95th Percentile	1.08	0.14	1.38	2.22	1.76	3.28	1.88	1.94	1.95	3.11	4.40	5.24	4.79	6.31
1E-8	5th Percentile	1.08	0.14	1.38	2.22	1.76	3.28	1.44	1.48	1.49	2.67	3.94	4.78	4.34	5.86
	Mean	1.08	0.14	1.38	2.22	1.76	3.28	1.75	1.79	1.81	2.97	4.25	5.09	4.65	6.17
	Best Estimate	1.08	0.14	1.38	2.22	1.76	3.28	1.74	1.79	1.80	2.96	4.24	5.09	4.64	6.16
	95th Percentile	1.08	0.14	1.38	2.22	1.76	3.28	2.05	2.10	2.12	3.27	4.56	5.40	4.96	6.48

Notes:

(a) 90th percentile high tide, baseline date is 2013.5.
(b) Baseline date is 2013.5. The 2134 High SLR scenario incorporates processes which are deeply uncertain but cannot be ruled out.
(c) Baseline date is 2001.

CONTROLLED DISCLOSURE

When downloaded from the EDS database, this document is uncontrolled and the responsibility rests with the user to ensure it is in line with the authorised version on the database.

Table 5.9-12: Extreme Negative Storm Surge and Minimum Still Water Levels.

Exceedance Frequency	Uncertainty	Tide [a]	Sea Level Rise [b]			Negative Storm Surge [c]			Maximum Still Water Level		
(y^{-1})		(m msl)	(m)			(m)			(m msl)		
			2034	2114	2134	2034	2114	2134	2034	2114	2134
1E+0	5th Percentile	-0.65	0.00	0.00	0.00	-0.46	-0.48	-0.48	-1.11	-1.13	-1.13
	Mean	-0.65	0.00	0.00	0.00	-0.45	-0.47	-0.47	-1.10	-1.12	-1.12
	Best Estimate	-0.65	0.00	0.00	0.00	-0.45	-0.47	-0.47	-1.10	-1.12	-1.12
	95th Percentile	-0.65	0.00	0.00	0.00	-0.44	-0.46	-0.46	-1.09	-1.11	-1.11
1E-1	5th Percentile	-0.65	0.00	0.00	0.00	-0.57	-0.59	-0.60	-1.22	-1.24	-1.25
	Mean	-0.65	0.00	0.00	0.00	-0.55	-0.56	-0.57	-1.20	-1.21	-1.22
	Best Estimate	-0.65	0.00	0.00	0.00	-0.55	-0.56	-0.57	-1.20	-1.21	-1.22
	95th Percentile	-0.65	0.00	0.00	0.00	-0.53	-0.54	-0.55	-1.18	-1.19	-1.20
1E-2	5th Percentile	-0.65	0.00	0.00	0.00	-0.66	-0.68	-0.69	-1.31	-1.33	-1.34
	Mean	-0.65	0.00	0.00	0.00	-0.63	-0.64	-0.65	-1.28	-1.29	-1.30
	Best Estimate	-0.65	0.00	0.00	0.00	-0.62	-0.64	-0.65	-1.27	-1.29	-1.30
	95th Percentile	-0.65	0.00	0.00	0.00	-0.59	-0.61	-0.62	-1.24	-1.26	-1.27
1E-3	5th Percentile	-0.65	0.00	0.00	0.00	-0.74	-0.76	-0.78	-1.39	-1.41	-1.43
	Mean	-0.65	0.00	0.00	0.00	-0.69	-0.71	-0.72	-1.34	-1.36	-1.37
	Best Estimate	-0.65	0.00	0.00	0.00	-0.69	-0.71	-0.72	-1.34	-1.36	-1.37
	95th Percentile	-0.65	0.00	0.00	0.00	-0.65	-0.66	-0.67	-1.30	-1.31	-1.32
1E-4	5th Percentile	-0.65	0.00	0.00	0.00	-0.82	-0.84	-0.85	-1.47	-1.49	-1.50
	Mean	-0.65	0.00	0.00	0.00	-0.75	-0.77	-0.79	-1.40	-1.42	-1.44
	Best Estimate	-0.65	0.00	0.00	0.00	-0.75	-0.77	-0.79	-1.40	-1.42	-1.44
	95th Percentile	-0.65	0.00	0.00	0.00	-0.69	-0.71	-0.72	-1.34	-1.36	-1.37
1E-5	5th Percentile	-0.65	0.00	0.00	0.00	-0.89	-0.91	-0.93	-1.54	-1.56	-1.58
	Mean	-0.65	0.00	0.00	0.00	-0.81	-0.83	-0.85	-1.46	-1.48	-1.50
	Best Estimate	-0.65	0.00	0.00	0.00	-0.81	-0.83	-0.85	-1.46	-1.48	-1.50
	95th Percentile	-0.65	0.00	0.00	0.00	-0.73	-0.75	-0.76	-1.38	-1.40	-1.41
1E-6	5th Percentile	-0.65	0.00	0.00	0.00	-0.96	-0.99	-1.00	-1.61	-1.64	-1.65
	Mean	-0.65	0.00	0.00	0.00	-0.86	-0.89	-0.90	-1.51	-1.54	-1.55
	Best Estimate	-0.65	0.00	0.00	0.00	-0.86	-0.88	-0.90	-1.51	-1.53	-1.55
	95th Percentile	-0.65	0.00	0.00	0.00	-0.77	-0.79	-0.80	-1.42	-1.44	-1.45
1E-7	5th Percentile	-0.65	0.00	0.00	0.00	-1.03	-1.05	-1.07	-1.68	-1.70	-1.72
	Mean	-0.65	0.00	0.00	0.00	-0.91	-0.94	-0.96	-1.56	-1.59	-1.61
	Best Estimate	-0.65	0.00	0.00	0.00	-0.91	-0.94	-0.95	-1.56	-1.59	-1.60
	95th Percentile	-0.65	0.00	0.00	0.00	-0.80	-0.83	-0.84	-1.45	-1.48	-1.49
1E-8	5th Percentile	-0.65	0.00	0.00	0.00	-1.09	-1.12	-1.14	-1.74	-1.77	-1.79
	Mean	-0.65	0.00	0.00	0.00	-0.96	-0.99	-1.01	-1.61	-1.64	-1.66
	Best Estimate	-0.65	0.00	0.00	0.00	-0.96	-0.99	-1.00	-1.61	-1.64	-1.65
	95th Percentile	-0.65	0.00	0.00	0.00	-0.84	-0.86	-0.87	-1.49	-1.51	-1.52

Notes:

(a) 10th percentile low tide, baseline date is 2013.5.
(b) Conservatively set to zero. The 2134 High SLR scenario is therefore not included in this table.
(c) Baseline date is 2001.

CONTROLLED DISCLOSURE

When downloaded from the EDS database, this document is uncontrolled and the responsibility rests with the user to ensure it is in line with the authorised version on the database.

These still water levels (defined as the water level in the absence of waves) were used as inputs to the sediment transport, flooding from the sea and integrity of cooling water supply, as described in the subsections below.

5.9.9.3 Long Waves

Long waves are, for the purpose of this report, defined as fluctuations in still water level with periods between 8 and 60 min. Long waves typically include: edge waves, bound waves, tsunamis (generated by geophysical phenomena such as earthquakes) and meteo-tsunamis (generated by atmospheric pressure fluctuations). Seiches typically also have periods in this range but can only occur in enclosed water bodies, which is not applicable to the open coastline at the Thyspunt site. The other type of waves described in this report are wind waves with periods between 3 s and 25 s, which are described in ***Subsection 5.9.9.8***.

Meteo-tsunamis can produce similar wave patterns to tsunamis, i.e., a sequence of wave trains with a wave period of 10 to 20 min. On 21 August 2008 a series of water level fluctuations was measured on the west and south coasts of South Africa, with the largest amplitude of approximately 0.7 m measured at Port Nolloth (see ***Figure 5.9-15*** and ***Figure 5.9-16***). The measurement of atmospheric pressure fluctuations at Port Nolloth coinciding with the onset of this event provides compelling evidence that this was a meteo-tsunami (CGS, 2008).

CONTROLLED DISCLOSURE

When downloaded from the EDS database, this document is uncontrolled and the responsibility rests with the user to ensure it is in line with the authorised version on the database.

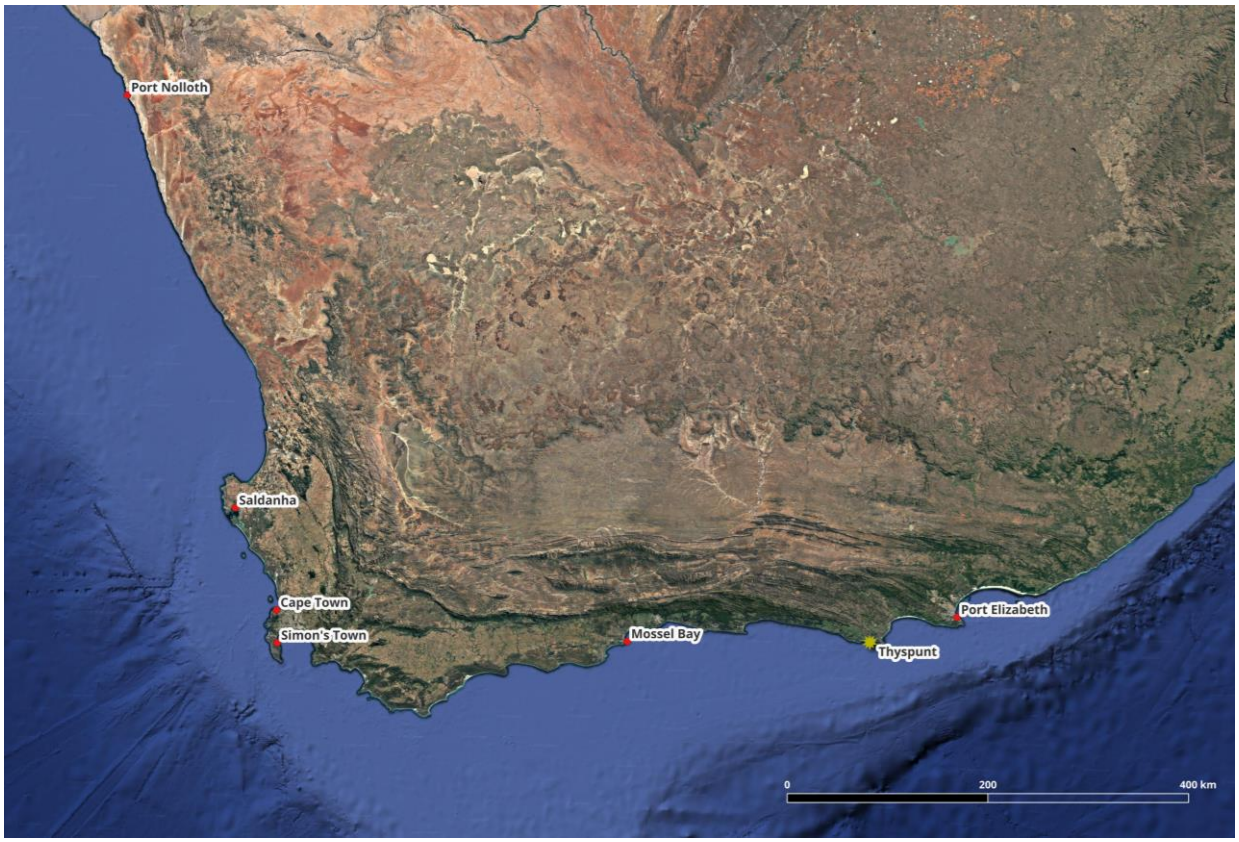


Figure 5.9-15: Locations of Tide Gauges

CONTROLLED DISCLOSURE

When downloaded from the EDS database, this document is uncontrolled and the responsibility rests with the user to ensure it is in line with the authorised version on the database.

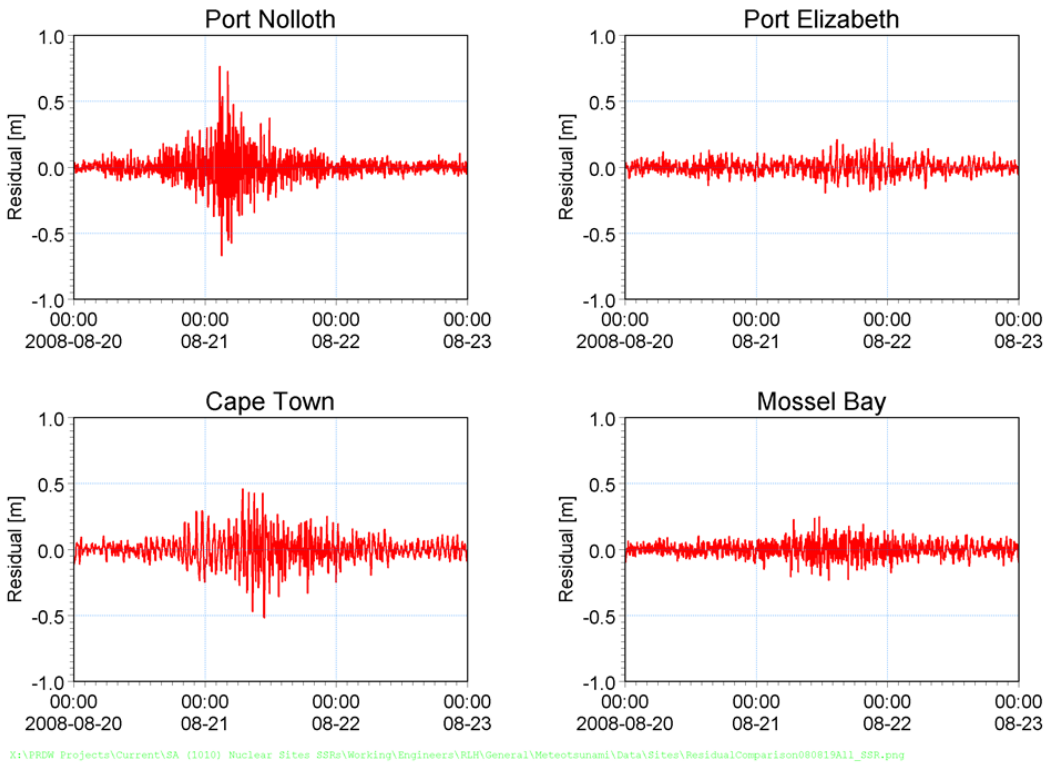


Figure 5.9-16: Propagation of a Meteo-Tsunami Event Measured Along the South African Coast

An analysis of available South African analogue tidal records from 1958 to 1986 (Wijnberg, 1993) identified several long wave events, the largest having an amplitude of 0.6 m measured at Port Nolloth on 1 June 1986.

All the available high frequency (1- or 3-minute) digital data from tide gauges at Cape Town and Port Elizabeth (up to 2024) and Port Nolloth, Simon's Town, and Mossel Bay (up to 2011) have been processed to determine the occurrence and severity of long waves (see ***Figure 5.9-15*** for these locations). The data has been kindly provided by the Hydrographer of the South African Navy (who is not responsible for any transcription errors or errors due to calculations using the data). PRDW undertook the following processing of the measured water surface elevation data to ensure the data quality was fit for purpose:

- comparison of measured water surface elevation to the predicted tide to identify and correct levelling issues;
- removal of spikes, defined as a large water surface elevation change occurring for one time step only;
- intercomparison of data from different measurement sites to confirm extreme events;

CONTROLLED DISCLOSURE

When downloaded from the EDS database, this document is uncontrolled and the responsibility rests with the user to ensure it is in line with the authorised version on the database.

- identification of typical signatures of long wave events;
- identification of known events (reported tsunamis, meteo-tsunamis and storms).

Considering that the long waves have been defined as having periods from 8 to 60 min, and the high frequency tidal data are measured at either 1- or 3-min intervals, this provides either 3 or 8 points per wave period for the shortest wave period of 8 min.

The water level residuals (difference between the measured data and a 60 min running mean) have been extracted at each tide gauge. Since these high frequency digital tidal recordings are available only from 2005, the data for each tide gauge were combined into one longer time-series based on the assumption that the long wave events at each location are independent, thus creating a data set with a duration of 41.2 y. ***Figure 5.9-16*** indicates that although the meteo-tsunami event propagates along the coast, it is significantly larger near the source location (in this case Port Nolloth) compared to the other tide gauge locations, supporting the assumption of independence.

An extreme value analysis (refer to ***Subsection 5.9.6.2*** for the methodology) was then performed on the positive and negative long wave amplitudes. The extreme value analysis results are plotted in ***Figure 5.9-17*** and ***Figure 5.9-18***. The baseline date is 2014.5 which is the middle of the measurement period.

CONTROLLED DISCLOSURE

When downloaded from the EDS database, this document is uncontrolled and the responsibility rests with the user to ensure it is in line with the authorised version on the database.

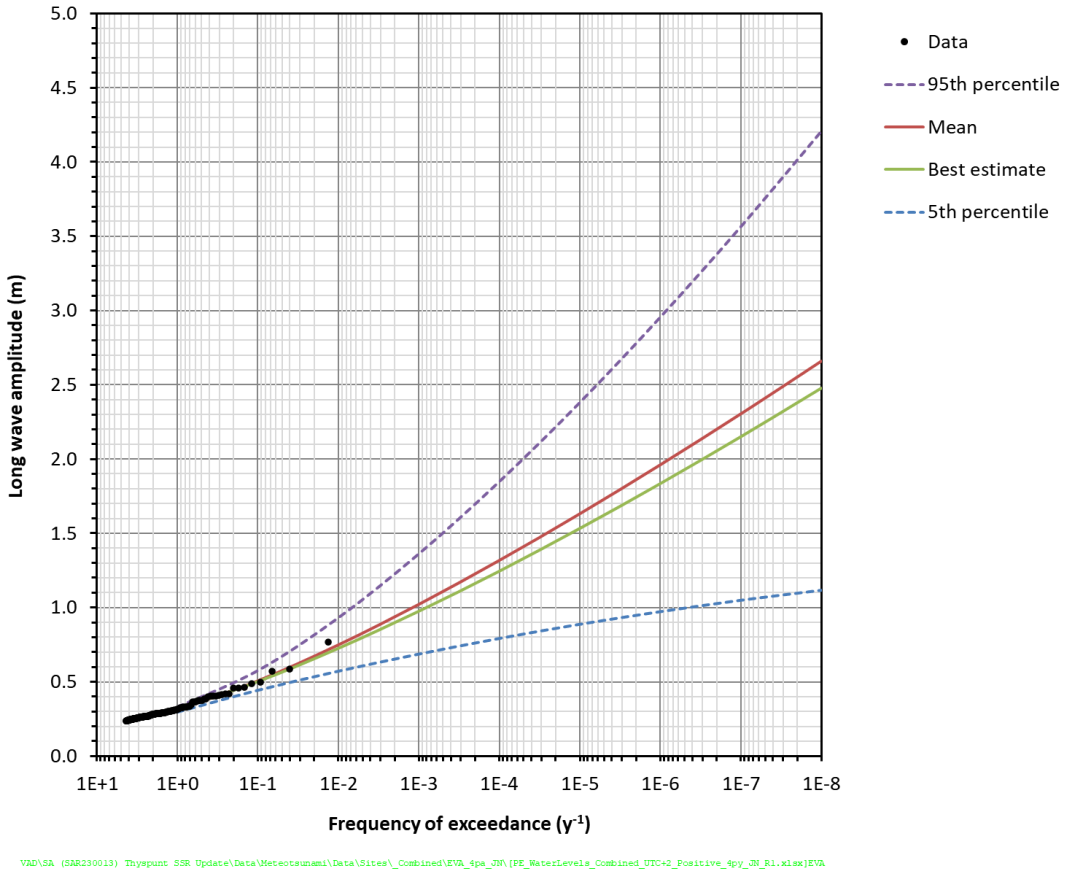


Figure 5.9-17: Extreme Value Analysis of Positive Long Wave Amplitude (Baseline Date is 2014.5).

CONTROLLED DISCLOSURE

When downloaded from the EDS database, this document is uncontrolled and the responsibility rests with the user to ensure it is in line with the authorised version on the database.

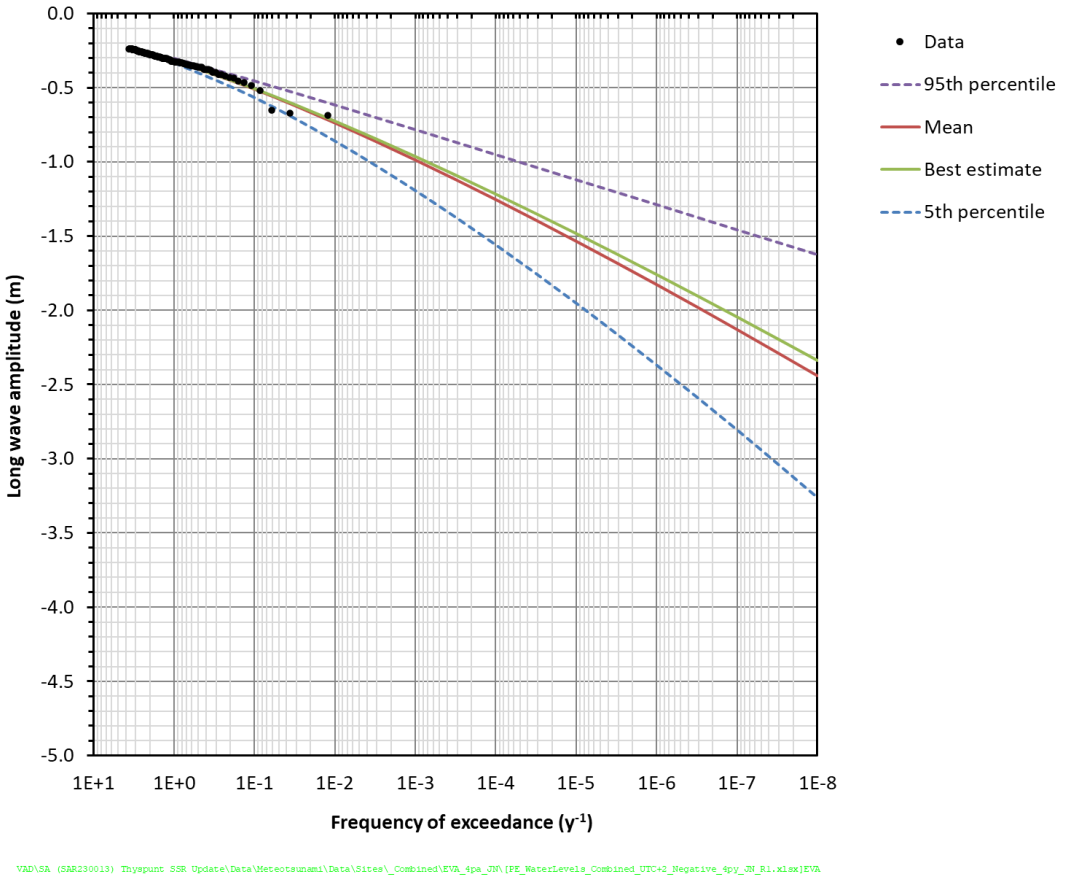


Figure 5.9-18: Extreme Value Analysis of Negative Long Wave Amplitude (Baseline Date is 2014.5).

The long wave amplitudes were then adjusted for climate change (***Subsection 5.9.7***) and are shown in ***Table 5.9-13***.

CONTROLLED DISCLOSURE

When downloaded from the EDS database, this document is uncontrolled and the responsibility rests with the user to ensure it is in line with the authorised version on the database.

Table 5.9-13: Extreme Long Wave Amplitudes.

Exceedance Frequency	Uncertainty	Positive Long Wave Amplitude			Negative Long Wave Amplitude		
(y^{-1})		(m)			(m)		
		2034	2114	2134	2034	2114	2134
1E+0	5th Percentile	0.30	0.31	0.31	-0.33	-0.34	-0.35
	Mean	0.31	0.32	0.32	-0.32	-0.33	-0.33
	Best Estimate	0.32	0.33	0.33	-0.32	-0.33	-0.33
	95th Percentile	0.33	0.34	0.34	-0.31	-0.31	-0.32
1E-1	5th Percentile	0.44	0.46	0.46	-0.57	-0.59	-0.59
	Mean	0.51	0.53	0.53	-0.51	-0.53	-0.53
	Best Estimate	0.50	0.52	0.52	-0.51	-0.53	-0.53
	95th Percentile	0.58	0.59	0.60	-0.46	-0.47	-0.47
1E-2	5th Percentile	0.57	0.59	0.59	-0.87	-0.89	-0.90
	Mean	0.75	0.78	0.78	-0.74	-0.76	-0.77
	Best Estimate	0.73	0.75	0.75	-0.73	-0.75	-0.76
	95th Percentile	0.94	0.96	0.97	-0.62	-0.64	-0.64
1E-3	5th Percentile	0.69	0.71	0.71	-1.20	-1.23	-1.24
	Mean	1.03	1.06	1.06	-0.99	-1.02	-1.03
	Best Estimate	0.98	1.01	1.02	-0.97	-1.00	-1.00
	95th Percentile	1.37	1.41	1.42	-0.79	-0.81	-0.81
1E-4	5th Percentile	0.80	0.82	0.82	-1.57	-1.61	-1.62
	Mean	1.33	1.36	1.37	-1.26	-1.30	-1.31
	Best Estimate	1.25	1.29	1.30	-1.22	-1.26	-1.27
	95th Percentile	1.86	1.91	1.92	-0.96	-0.98	-0.99
1E-5	5th Percentile	0.89	0.92	0.92	-1.96	-2.02	-2.03
	Mean	1.64	1.69	1.70	-1.55	-1.59	-1.60
	Best Estimate	1.54	1.59	1.60	-1.49	-1.53	-1.54
	95th Percentile	2.39	2.46	2.48	-1.13	-1.16	-1.17
1E-6	5th Percentile	0.98	1.00	1.01	-2.38	-2.45	-2.47
	Mean	1.98	2.03	2.04	-1.84	-1.89	-1.90
	Best Estimate	1.85	1.90	1.91	-1.77	-1.82	-1.83
	95th Percentile	2.97	3.06	3.08	-1.29	-1.33	-1.34
1E-7	5th Percentile	1.05	1.08	1.09	-2.82	-2.90	-2.92
	Mean	2.32	2.38	2.40	-2.14	-2.20	-2.22
	Best Estimate	2.16	2.22	2.24	-2.06	-2.11	-2.13
	95th Percentile	3.59	3.69	3.71	-1.47	-1.51	-1.52
1E-8	5th Percentile	1.12	1.15	1.16	-3.28	-3.37	-3.40
	Mean	2.68	2.75	2.77	-2.46	-2.53	-2.54
	Best Estimate	2.49	2.56	2.58	-2.35	-2.42	-2.43
	95th Percentile	4.23	4.35	4.38	-1.63	-1.68	-1.69

Since long waves (including meteo-tsunamis) can produce similar wave patterns and associated run-up and drawdown to geological tsunamis, i.e., a sequence of wave trains with a wave period of 10 to 20 min, the extreme

CONTROLLED DISCLOSURE

When downloaded from the EDS database, this document is uncontrolled and the responsibility rests with the user to ensure it is in line with the authorised version on the database.

positive long wave amplitudes were compared to the geological tsunami results as described in ***Subsection 5.9.13***. The maximum positive long wave amplitude is 4.38 m for the 1E-8 y^{-1} exceedance 95th percentile (***Table 5.9-13***). This is significantly less than the run-up height of approximately 13 m above antecedent water level anticipated for Thyspunt due to a volcanic flank collapse tsunamis (refer ***Subsection 5.9.13.5***). The long waves (including meteo-tsunamis) are thus anticipated to be enveloped by the other tsunami types and are not analysed further. This should be confirmed once an updated Tsunami Hazard Analysis (THA) has been undertaken for Thyspunt.

5.9.9.4 Currents

Currents have been measured at Site A (water depth -13.2 m msl) and at Site B (water depth -30.8 m msl). Details of the locations, instruments, sampling intervals, dates and length of valid data are provided in ***Subsection 5.9.6.1***.

The surface and bottom currents are presented below as time-series (***Figure 5.9-19*** and ***Figure 5.9-20***), current roses (***Figure 5.9-21***) and statistics (***Table 5.9-14***). Note that current direction is the direction towards which the current is flowing, measured clockwise from true north.

CONTROLLED DISCLOSURE

When downloaded from the EDS database, this document is uncontrolled and the responsibility rests with the user to ensure it is in line with the authorised version on the database.

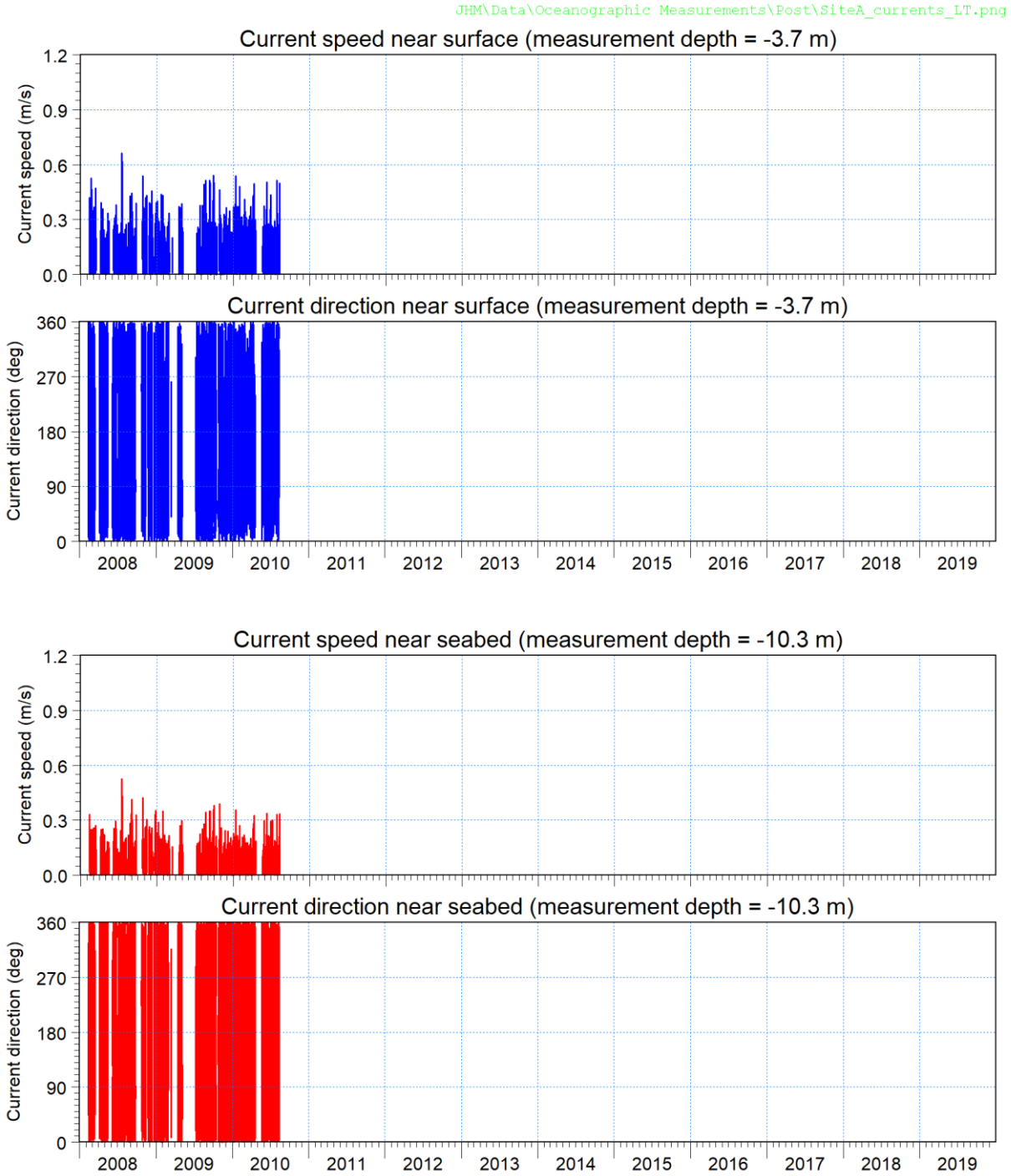


Figure 5.9-19: Time-Series of Measured Currents at Site A (Water Depth -13.2 m msl).

CONTROLLED DISCLOSURE

When downloaded from the EDS database, this document is uncontrolled and the responsibility rests with the user to ensure it is in line with the authorised version on the database.

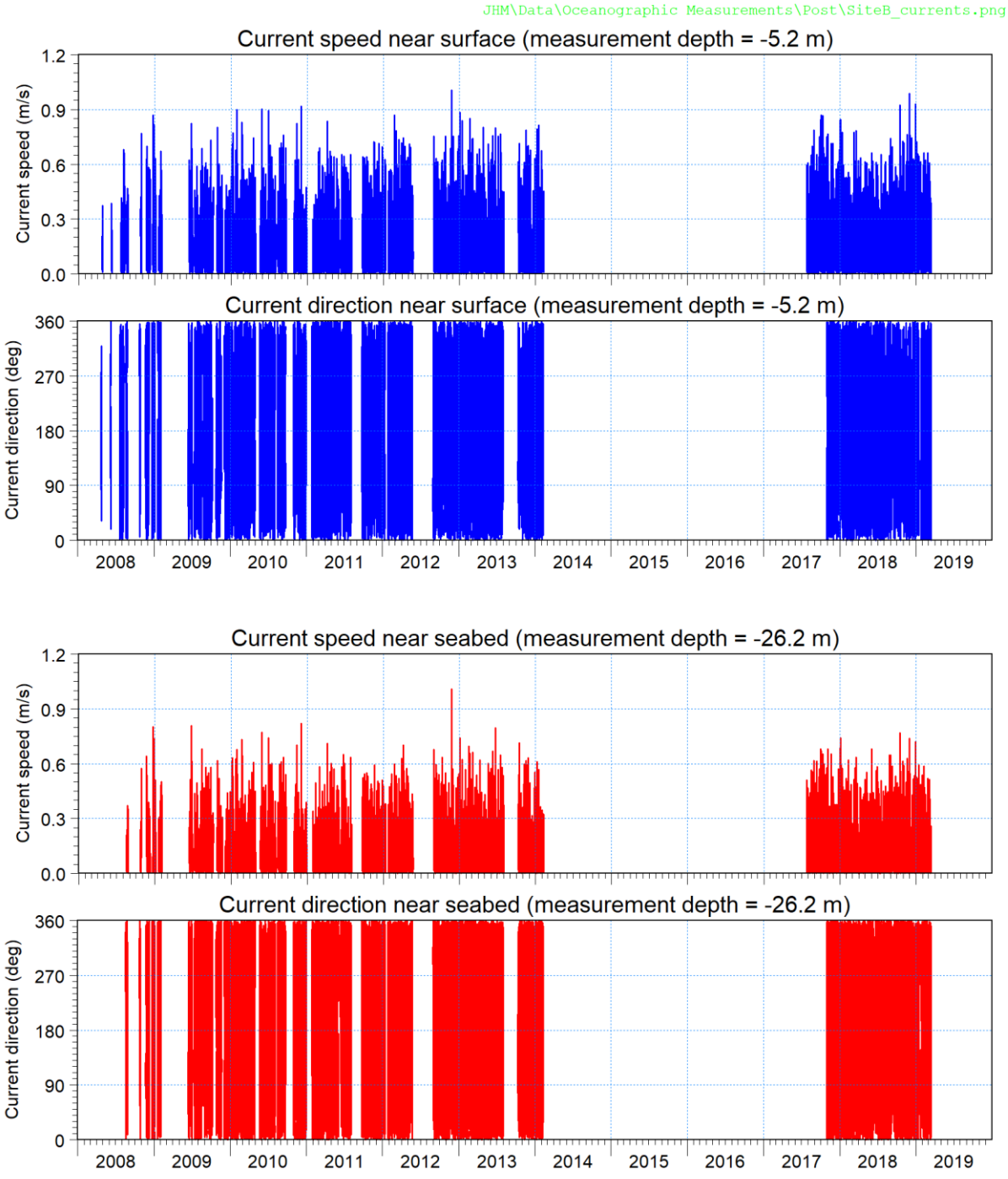


Figure 5.9-20: Time-Series of Measured Currents at Site B (Water Depth -30.8 m msl).

CONTROLLED DISCLOSURE

When downloaded from the EDS database, this document is uncontrolled and the responsibility rests with the user to ensure it is in line with the authorised version on the database.

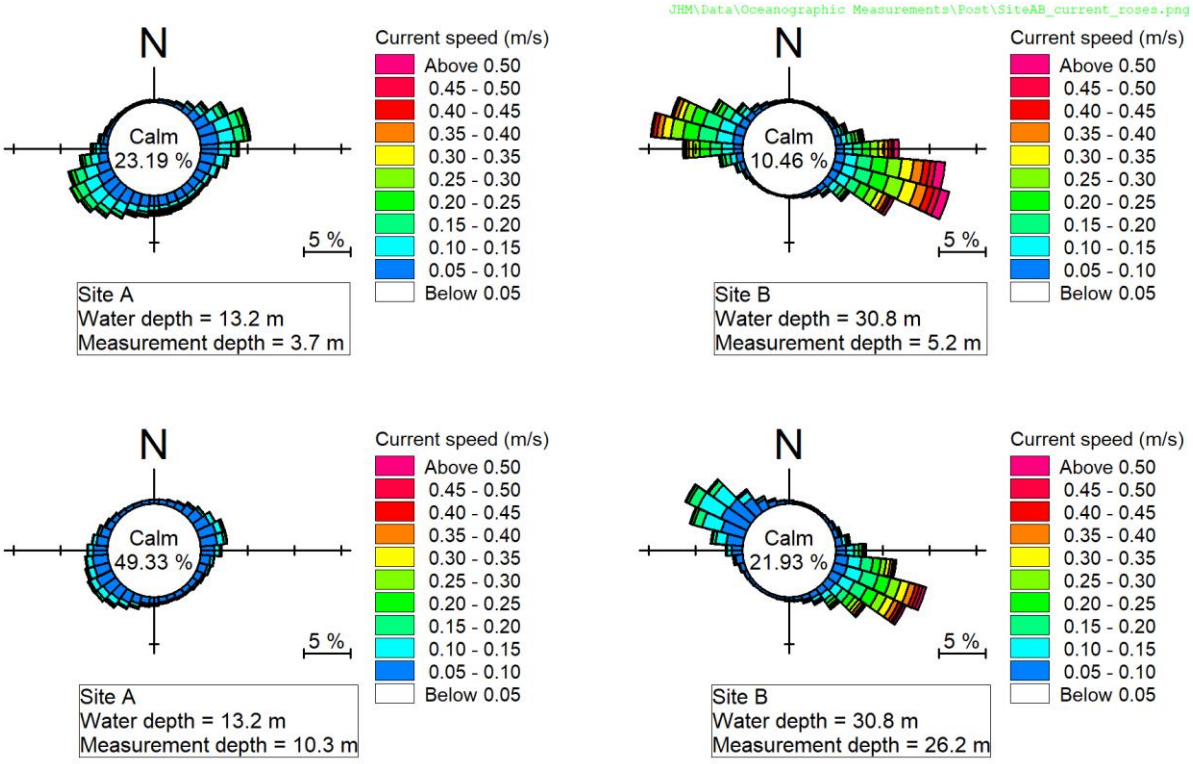


Figure 5.9-21: Measured Current Roses at Sites A and B.

Table 5.9-14: Summary of Measured Current Speeds.

Percentile	Site A (Water Depth -13.2 m msl)		Site B (Water Depth -30.8 m msl)	
	Near Surface (-3.7 m msl)	Near Seabed (-10.3 m msl)	Near Surface (-5.2 m msl)	Near Seabed (-26.2 m msl)
(%)	(m/s)			
0	0.00	0.00	0.00	0.00
1	0.01	0.01	0.01	0.01
2	0.01	0.01	0.02	0.01
5	0.02	0.01	0.03	0.02
10	0.03	0.02	0.05	0.03
20	0.05	0.03	0.08	0.05
30	0.06	0.03	0.11	0.06
40	0.07	0.04	0.14	0.08
50	0.09	0.05	0.17	0.10
60	0.10	0.06	0.20	0.12
70	0.12	0.07	0.24	0.15
80	0.15	0.09	0.30	0.19
90	0.19	0.12	0.38	0.27
95	0.23	0.14	0.45	0.35
98	0.29	0.18	0.54	0.44
99	0.33	0.21	0.61	0.49
100	0.66	0.53	1.01	1.01

CONTROLLED DISCLOSURE

When downloaded from the EDS database, this document is uncontrolled and the responsibility rests with the user to ensure it is in line with the authorised version on the database.

The current speeds are moderate (<1 m/s), with higher speeds near the surface. The currents are predominantly driven by the wind and Agulhas Current as well as waves in the nearshore or during large storm events. The surface and seabed currents at Site A are predominantly either south-westerly driven by easterly winds, or north-easterly driven by westerly winds and wave storms, which are more prevalent in winter. The surface and seabed currents at Site B are predominantly either easterly to south-easterly due to westerly winds, or westerly to north-westerly due to easterly winds. The bottom current directions at Site B are rotated clockwise relative to the surface currents by Ekman effects, which leads to upwelling of cold water during easterly winds.

An extreme value analysis (refer to ***Subsection 5.9.6.2*** for the methodology) was performed on the 10-minute depth-averaged current speeds measured at Site B, which has 5.26 y of data and is the longest available current dataset. The currents measured at 0.5 m intervals in the water column were used to calculate the depth-averaged current using vector averaging. The results are plotted in ***Figure 5.9-22***. The baseline date is 2013 which is the middle of the measurement period. As expected, when extrapolating this short-duration 5.26 y dataset to an exceedance frequency of 1E-8 y^{-1}, the percentiles indicate a high level of uncertainty. It is noted that only the best estimate (and not the percentiles) has been used to calculate the suspended sand concentrations in ***Subsection 5.9.11.8***.

The extreme current speeds were then adjusted for climate change (***Subsection 5.9.7***) and are presented in ***Table 5.9-15***.

CONTROLLED DISCLOSURE

When downloaded from the EDS database, this document is uncontrolled and the responsibility rests with the user to ensure it is in line with the authorised version on the database.

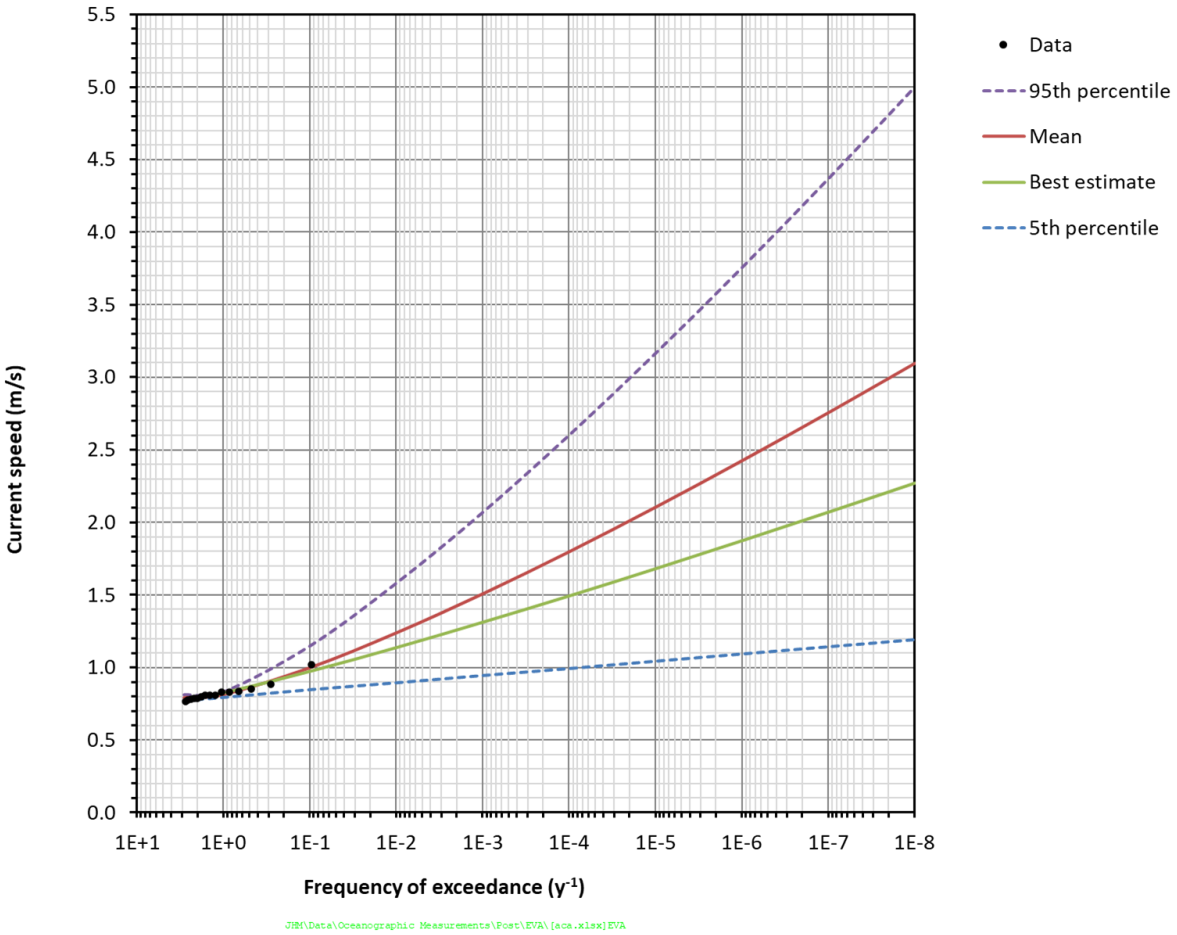


Figure 5.9-22: Extreme Value Analysis of Depth-Averaged Current Speed at Site B (Depth -30.8 m msl) (Baseline Date is 2013).

CONTROLLED DISCLOSURE

When downloaded from the EDS database, this document is uncontrolled and the responsibility rests with the user to ensure it is in line with the authorised version on the database.

Table 5.9-15: Extreme Depth-Averaged Current Speed at Site B Including Climate Change (Water Depth -30.8 m msl).

Exceedance Frequency	Uncertainty	Current Speed		
(y^{-1})		(m/s)		
		2034	2114	2134
1E+0	5th Percentile	0.80	0.82	0.82
	Mean	0.82	0.84	0.84
	Best Estimate	0.83	0.85	0.85
	95th Percentile	0.84	0.86	0.86
1E-1	5th Percentile	0.85	0.87	0.88
	Mean	1.01	1.03	1.03
	Best Estimate	0.98	1.00	1.01
	95th Percentile	1.16	1.18	1.19
1E-2	5th Percentile	0.90	0.92	0.93
	Mean	1.25	1.28	1.28
	Best Estimate	1.14	1.17	1.18
	95th Percentile	1.59	1.63	1.64
1E-3	5th Percentile	0.95	0.97	0.98
	Mean	1.52	1.55	1.56
	Best Estimate	1.32	1.35	1.36
	95th Percentile	2.08	2.13	2.14
1E-4	5th Percentile	1.00	1.02	1.03
	Mean	1.81	1.85	1.86
	Best Estimate	1.50	1.54	1.54
	95th Percentile	2.62	2.68	2.69
1E-5	5th Percentile	1.05	1.07	1.08
	Mean	2.12	2.17	2.18
	Best Estimate	1.69	1.73	1.74
	95th Percentile	3.19	3.26	3.28
1E-6	5th Percentile	1.10	1.13	1.13
	Mean	2.44	2.50	2.51
	Best Estimate	1.89	1.93	1.94
	95th Percentile	3.78	3.86	3.89
1E-7	5th Percentile	1.15	1.18	1.18
	Mean	2.77	2.84	2.85
	Best Estimate	2.08	2.13	2.14
	95th Percentile	4.39	4.50	4.52
1E-8	5th Percentile	1.20	1.23	1.23
	Mean	3.11	3.19	3.20
	Best Estimate	2.28	2.34	2.35
	95th Percentile	5.03	5.14	5.17

The measured currents were used to calibrate the 3D hydrodynamic model as described in ***Appendix 5.9.A.7***. The best estimate extreme currents

CONTROLLED DISCLOSURE

When downloaded from the EDS database, this document is uncontrolled and the responsibility rests with the user to ensure it is in line with the authorised version on the database.

were used to calculate the suspended sand concentrations in ***Subsection 5.9.11.8***.

5.9.9.5 Seawater Temperature

Seawater temperatures have been measured at Sites A, B and C. Details of the locations, instruments, sampling intervals, dates and length of valid data are provided in ***Subsection 5.9.6.1***.

The temperatures are presented below as time-series (***Figure 5.9-23)*** and for sites with sufficiently long durations as seasonal statistics (***Table 5.9-16*** and ***Table 5.9-17***).

CONTROLLED DISCLOSURE

When downloaded from the EDS database, this document is uncontrolled and the responsibility rests with the user to ensure it is in line with the authorised version on the database.

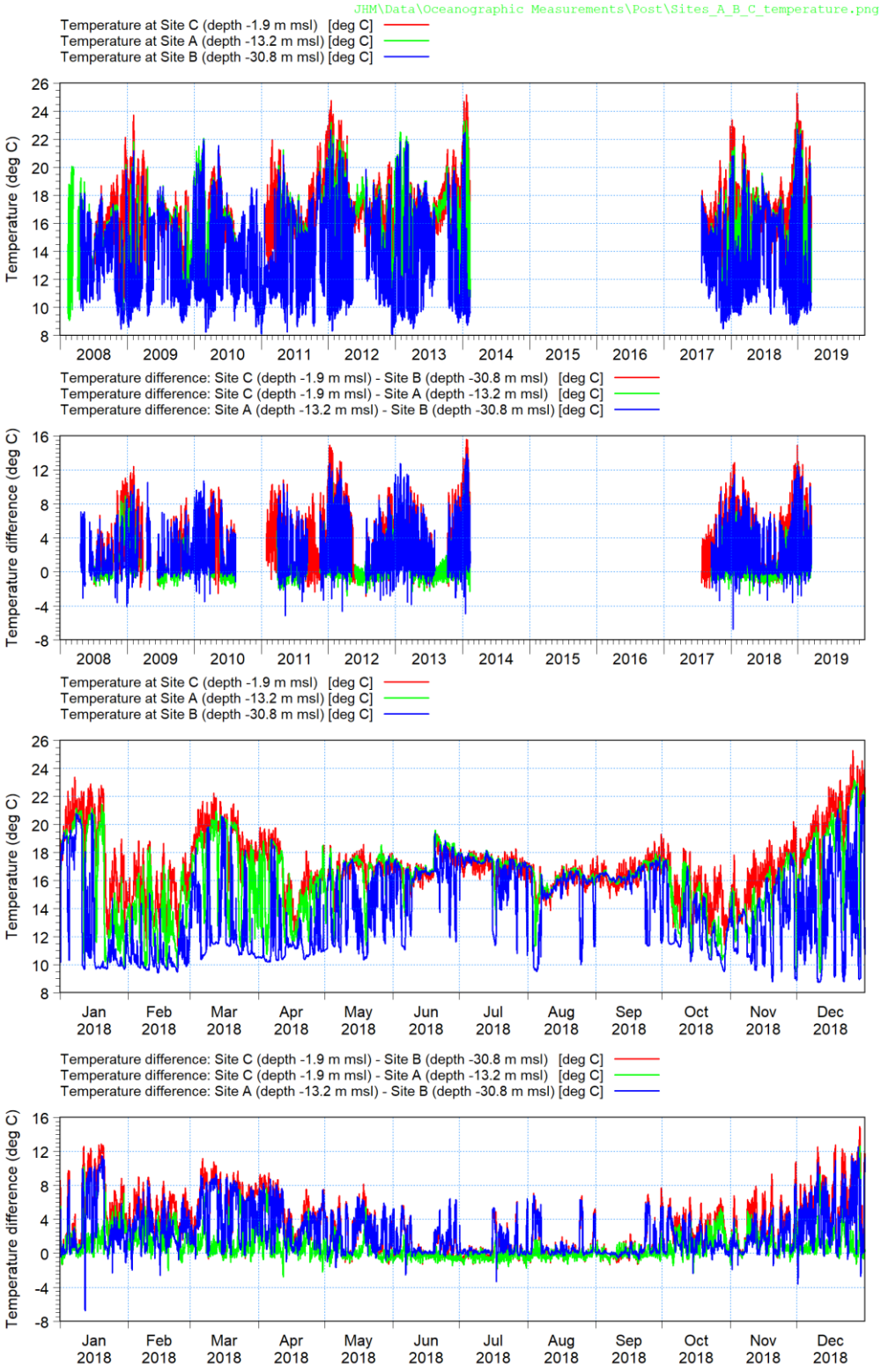


Figure 5.9-23: Time-Series of Measured Seawater Temperatures and Stratification at All Sites. Bottom Plots Show the Results for 2018 in More Detail.

CONTROLLED DISCLOSURE

When downloaded from the EDS database, this document is uncontrolled and the responsibility rests with the user to ensure it is in line with the authorised version on the database.

Table 5.9-16: Statistics of Measured Hourly Seawater Temperature.

Percentile	Site C (Water Depth -1.9 m msl)	Site A (Water Depth -13.2 m msl)	Site B (Water Depth -30.8 m msl)
(%)	(°C)		
0	9.66	8.82	7.93
1	11.88	9.70	8.77
2	12.39	10.00	8.96
5	13.19	10.73	9.36
10	14.11	11.62	9.76
20	15.13	13.30	10.44
30	15.75	14.83	11.02
40	16.22	15.75	11.72
50	16.65	16.36	12.96
60	17.11	16.89	14.60
70	17.63	17.40	15.84
80	18.37	18.06	16.61
90	19.72	19.33	17.58
95	20.96	20.55	18.55
98	22.05	21.48	19.89
99	22.58	22.03	20.70
100	25.28	23.35	22.73

Table 5.9-17: Seasonal Percentiles of Measured Seawater Temperature Stratification.

Location	Summer			Autumn			Winter			Spring		
	5%	50%	95%	5%	50%	95%	5%	50%	95%	5%	50%	95%
	(°C)											
Temperature difference: Site C (-1.9 m msl) – Site A (-13.2 m msl)	-0.30	1.77	6.13	-0.76	0.31	4.24	-1.07	-0.28	1.05	-0.64	0.42	3.40
Temperature difference: Site C (-1.9 m msl) – Site B (-30.8 m msl)	0.38	5.33	11.68	-0.50	4.17	9.00	-0.92	0.18	4.89	-0.47	1.83	7.08
Temperature difference: Site A (-13.2 m msl) – Site B (-30.8 m msl)	0.02	2.53	9.76	-0.07	2.84	8.18	-0.23	0.33	4.77	-0.15	0.94	5.60

The temperatures in the vicinity of Thyspunt display a distinct seasonality. Temperatures in summer are significantly more variable than in winter, with solar heating (resulting in higher temperatures) and upwelling events (resulting in lower temperatures) occurring most frequently during summer. There is generally a decrease in temperature with increasing depth below the water surface, although in some cases, especially in winter, the temperatures at Site C are colder than Site A due to atmospheric cooling in the gully. The stratification between the different water depths shows a seasonal trend, with the sea being stratified during summer and being more isothermal during winter.

CONTROLLED DISCLOSURE

When downloaded from the EDS database, this document is uncontrolled and the responsibility rests with the user to ensure it is in line with the authorised version on the database.

The temperature measurements at Site B contain only 6.79 y of valid data. To increase the robustness of an extreme value analysis, the dataset was extended using measurements from a thermistor string deployed at Middelbank in the Tsitsikamma Marine Protected Area, approximately 80 km west of the Thyspunt site. The dataset includes measured seawater temperature at several depths at one location between July 1997 to November 2011 with a total of 13.16 y of valid data. Details of the thermistor string location and depths are shown in ***Figure 5.9-24*** and ***Table 5.9-18***. A comparison of the temperatures measured at Site B (-30.8 m msl) and Middelbank (-27 m msl) is shown in ***Figure 5.9-25*** to ***Figure 5.9-27***.

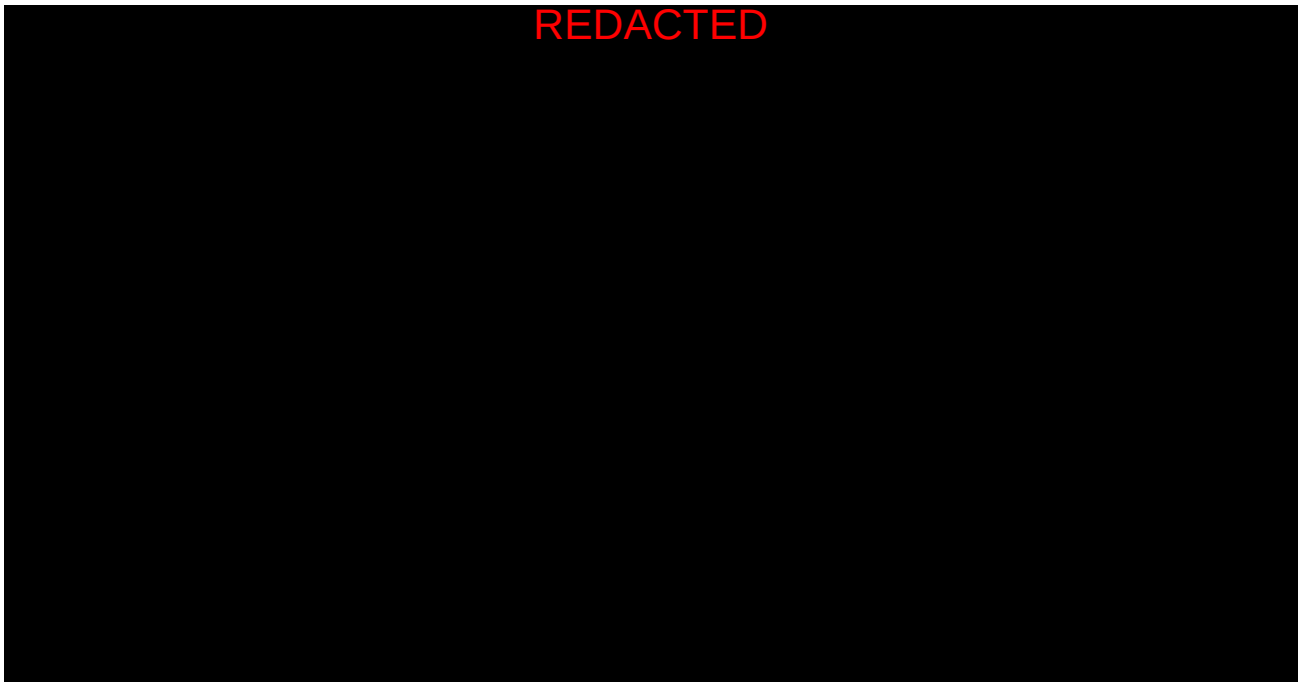


Figure 5.9-24: Location of Thermistor String at Middelbank.

Table 5.9-18: Location and Depth of Thermistor String at Middelbank.

REDACTED

CONTROLLED DISCLOSURE

When downloaded from the EDS database, this document is uncontrolled and the responsibility rests with the user to ensure it is in line with the authorised version on the database.

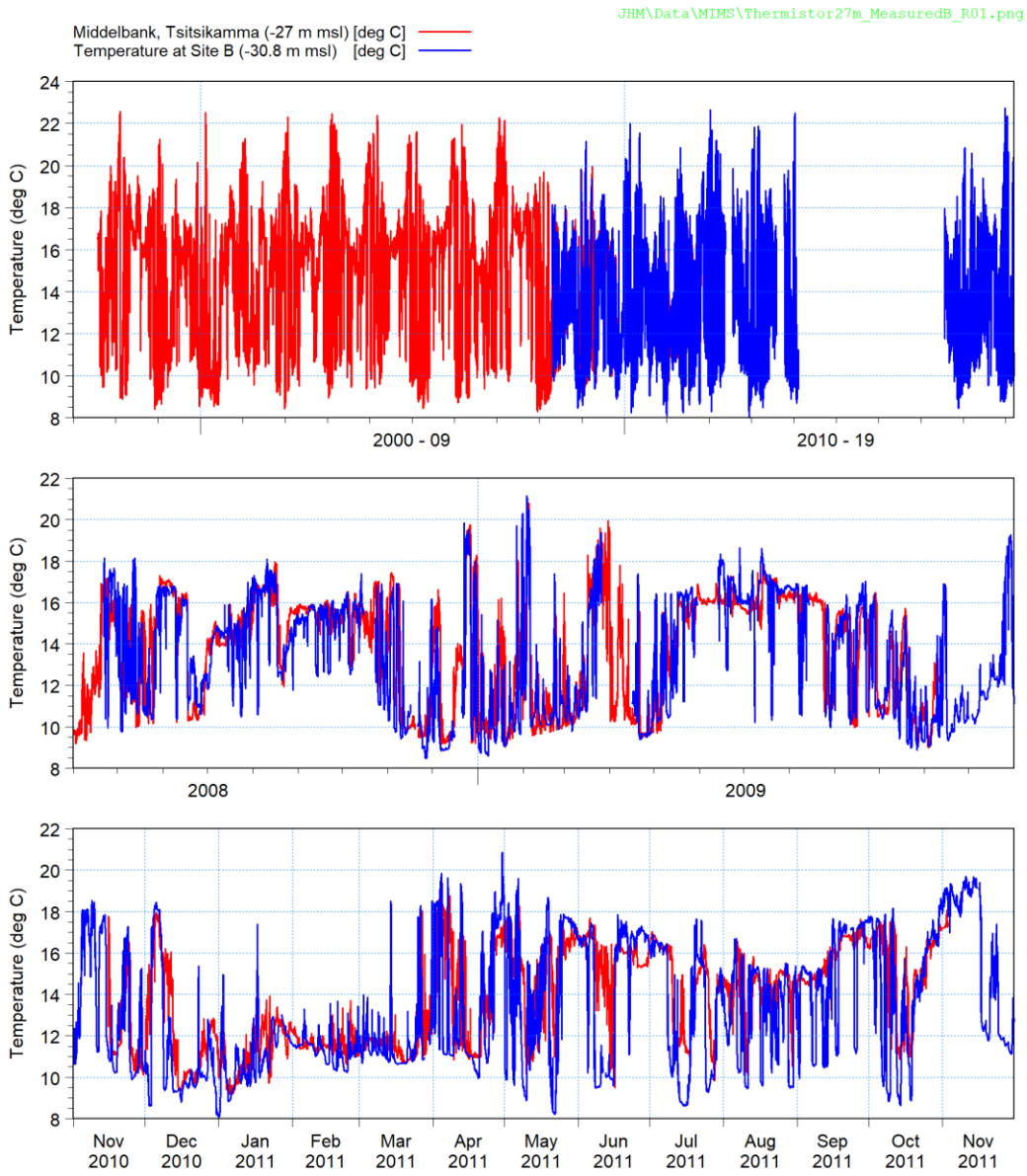
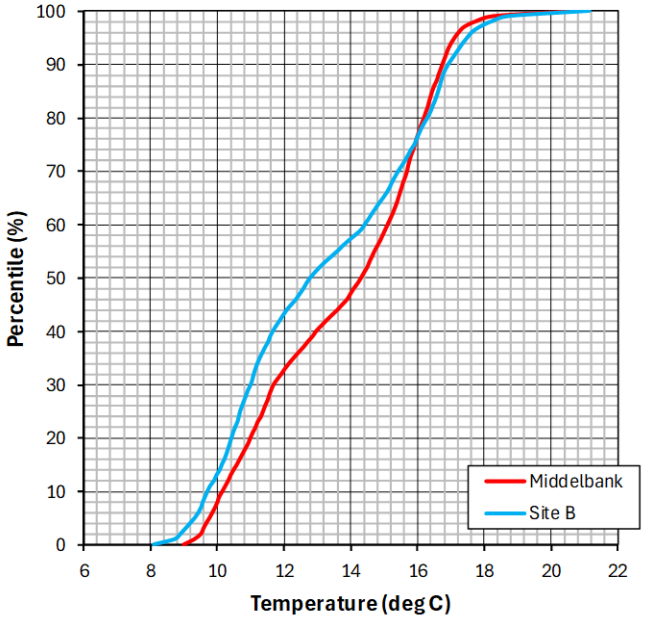


Figure 5.9-25: Time-Series of Seawater Temperatures Measured at Site B and Middelbank.

CONTROLLED DISCLOSURE

When downloaded from the EDS database, this document is uncontrolled and the responsibility rests with the user to ensure it is in line with the authorised version on the database.



Percentile	Middelbank (-27 m msl)	Site B (-30.8 m msl)
(%)	(°C)	
0	9.01	8.09
1	9.32	8.71
2	9.52	8.89
5	9.78	9.32
10	10.16	9.70
20	11.00	10.42
30	11.70	11.00
40	12.97	11.66
50	14.31	12.78
60	15.10	14.42
70	15.68	15.42
80	16.19	16.30
90	16.74	16.92
95	17.11	17.49
98	17.73	18.21
99	18.26	18.71
100	20.81	21.15

Figure 5.9-26: Percentile Comparison of the Seawater Temperatures Measured at Site B and Middelbank for the Overlapping Period Between 2008 and 2011.

CONTROLLED DISCLOSURE

When downloaded from the EDS database, this document is uncontrolled and the responsibility rests with the user to ensure it is in line with the authorised version on the database.

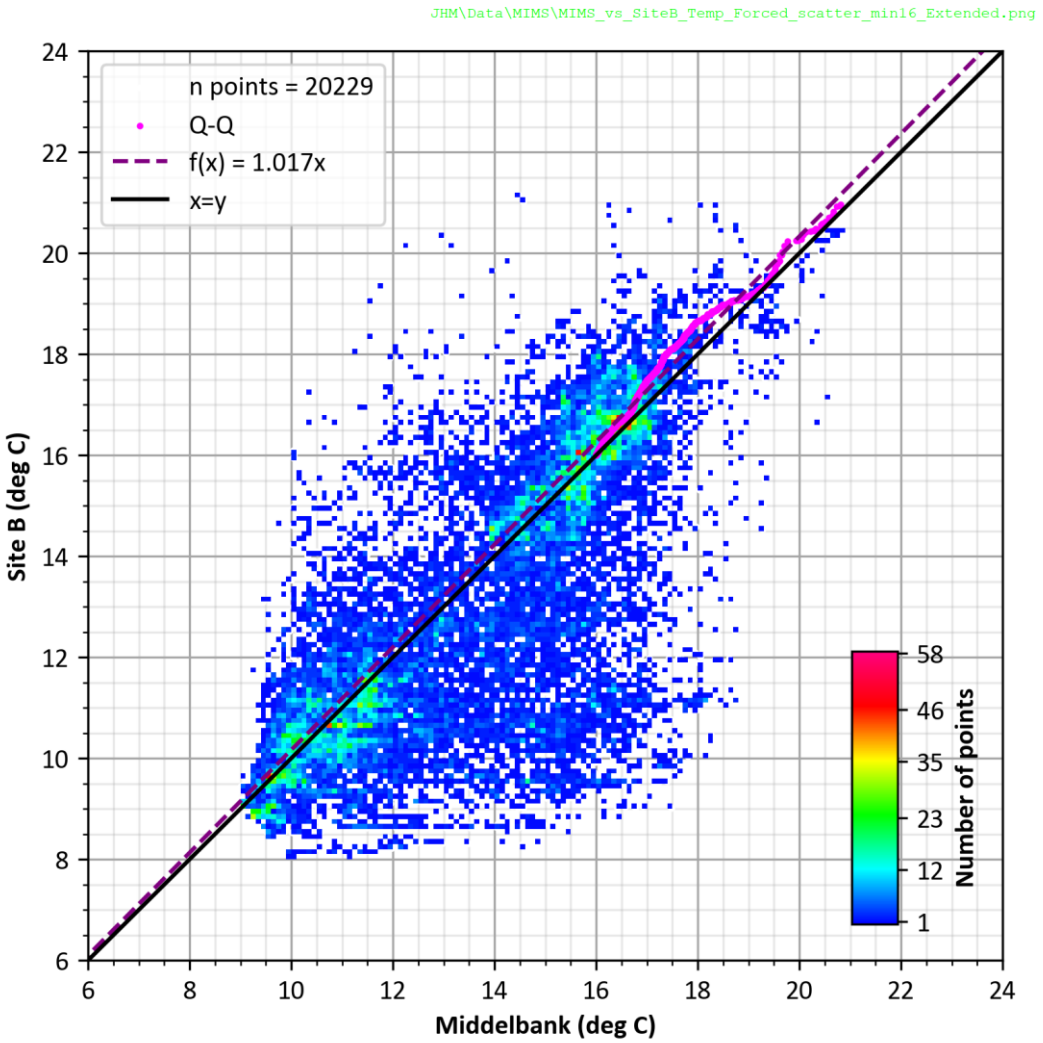


Figure 5.9-27: Scatterplot and Q-Q Comparison of the Seawater Temperature Measured at Site B and Middelbank.

Figure 5.9-25 to ***Figure 5.9-27*** show that there is a good correlation between the temperatures at the two locations. The linear fit of the Q-Q for temperatures greater than 16°C (***Figure 5.9-27***) indicates that the temperature measurements at Middelbank provide a good representation of extreme temperatures at Site B, and can thus be used to extend the Site B dataset used in the extreme value analysis.

Figure 5.9-28 shows the time-series of the hourly combined seawater temperatures at Site B and Middelbank along with the events used for the extreme value analysis.

CONTROLLED DISCLOSURE

When downloaded from the EDS database, this document is uncontrolled and the responsibility rests with the user to ensure it is in line with the authorised version on the database.

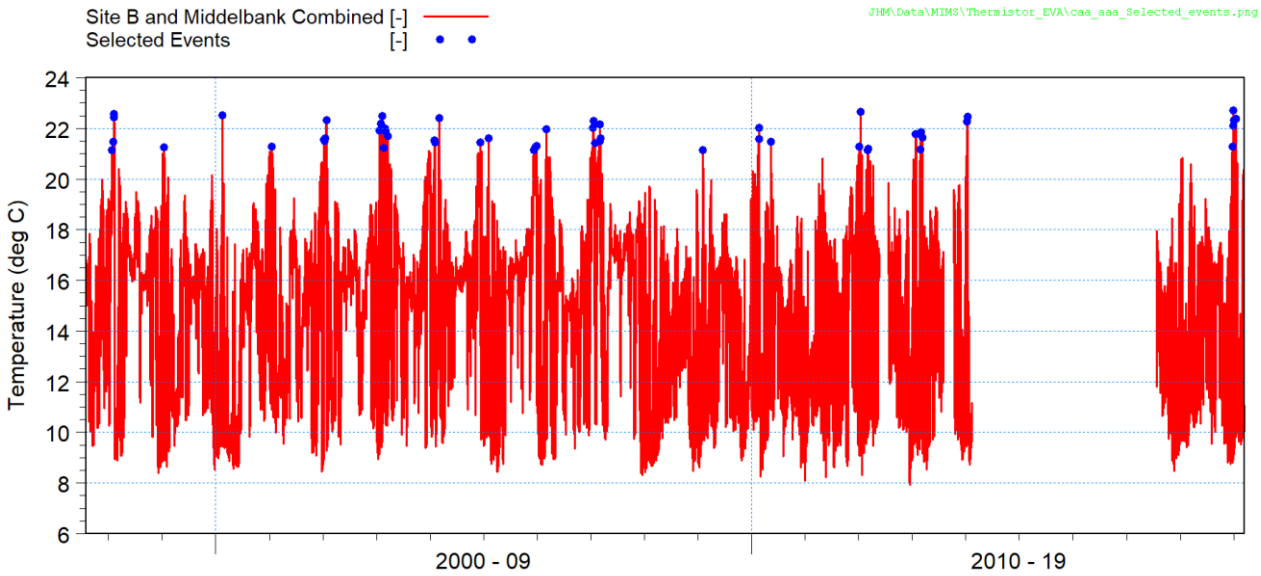


Figure 5.9-28: Time-Series of the Combined Seawater Temperatures at Site B (Water Depth -30.8 m msl) and Middelbank (Water Depth -27 m msl) Used for the EVA. The Blue Dots Show the Events Selected for the EVA, i.e., the Extreme Value Series.

An extreme value analysis (refer to ***Subsection 5.9.6.2*** for the methodology) was performed on the combined measured seawater temperatures at Site B and Middelbank, which has a total of 17.68 y of data. The results are plotted in ***Figure 5.9-13***. The baseline date is 2008 which is approximately the middle of the measurement period.

CONTROLLED DISCLOSURE

When downloaded from the EDS database, this document is uncontrolled and the responsibility rests with the user to ensure it is in line with the authorised version on the database.

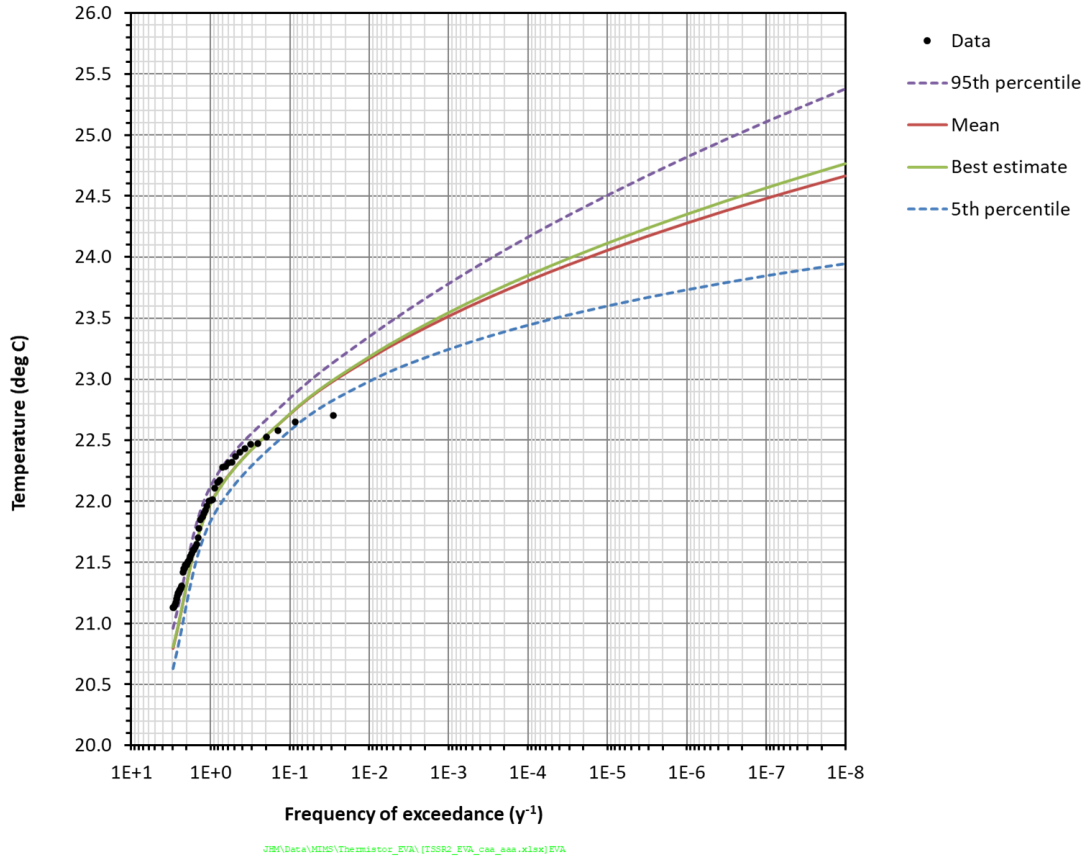


Figure 5.9-29: Extreme Value Analysis of Seawater Temperatures at Site B (Water Depth -30.8 m msl) and Middelbank (Water Depth -27 m msl) (Baseline Date is 2008).

Site B in a water depth of -30.8 m msl is representative of the seawater intakes for the new NIs, which consider intake tunnels extending to a water depth of -30 m msl. The extreme seawater temperatures at these intake depths have been estimated based on the measured temperatures at the site as shown in ***Table 5.9-16***.

The extreme maximum seawater temperatures were then adjusted for climate change (***Subsection 5.9.7***) and are presented in ***Table 5.9-19***. These extreme temperatures will be combined with the thermal plume recirculation temperatures (***Subsection 5.9.16.6***) to obtain the maximum temperatures at the cooling water intake (see ***Subsection 5.9.16.7***).

CONTROLLED DISCLOSURE

When downloaded from the EDS database, this document is uncontrolled and the responsibility rests with the user to ensure it is in line with the authorised version on the database.

Table 5.9-19: Extreme Maximum Seawater Temperatures.

Exceedance Frequency	Uncertainty	Water Depth -30.8 m msl		
(y^{-1})		(°C)		
		2034	2114	2134
1E+0	5th Percentile	22.33	25.17	26.18
	Mean	22.47	25.31	26.32
	Best Estimate	22.47	25.31	26.32
	95th Percentile	22.62	25.45	26.46
1E-1	5th Percentile	23.08	25.92	26.92
	Mean	23.21	26.05	27.06
	Best Estimate	23.21	26.05	27.06
	95th Percentile	23.34	26.18	27.19
1E-2	5th Percentile	23.48	26.32	27.33
	Mean	23.66	26.50	27.51
	Best Estimate	23.68	26.52	27.53
	95th Percentile	23.85	26.68	27.69
1E-3	5th Percentile	23.74	26.58	27.59
	Mean	24.01	26.85	27.86
	Best Estimate	24.04	26.88	27.89
	95th Percentile	24.28	27.12	28.13
1E-4	5th Percentile	23.94	26.78	27.79
	Mean	24.30	27.14	28.15
	Best Estimate	24.34	27.18	28.19
	95th Percentile	24.66	27.50	28.51
1E-5	5th Percentile	24.10	26.94	27.95
	Mean	24.55	27.39	28.40
	Best Estimate	24.61	27.45	28.46
	95th Percentile	25.00	27.84	28.85
1E-6	5th Percentile	24.23	27.07	28.08
	Mean	24.77	27.61	28.62
	Best Estimate	24.85	27.69	28.70
	95th Percentile	25.32	28.16	29.16
1E-7	5th Percentile	24.35	27.18	28.19
	Mean	24.98	27.81	28.82
	Best Estimate	25.06	27.90	28.91
	95th Percentile	25.61	28.44	29.45
1E-8	5th Percentile	24.45	27.28	28.29
	Mean	25.16	28.00	29.01
	Best Estimate	25.26	28.10	29.11
	95th Percentile	25.88	28.72	29.72

Regarding the possibility of ice occurring in the sea surrounding the site, the lowest seawater temperature measured in all the data sets described in this section is 7.93°C, and an extreme value analysis of the combined minimum

CONTROLLED DISCLOSURE

When downloaded from the EDS database, this document is uncontrolled and the responsibility rests with the user to ensure it is in line with the authorised version on the database.

measured temperatures at Site B and Middelbank was above 0°C at an exceedance of 1E-8 y^{-1}. On this basis ice is not anticipated to form in the sea at the site and the minimum cooling water intake temperature of -0.5°C will be met.

5.9.9.6 Salinity

Salinity has been measured at the Thyspunt site in a water depth of -30.8 m msl with instruments located 10 m and 30 m below the water surface. The salinity shows little variation (< 1 psu) and averages 35.0 psu which is in line with the global average sea surface salinity. Salinity is thus a minor safety and design parameter, in contrast to the sea temperature which is an important determinant of the efficiency of the seawater cooling system.

5.9.9.7 Suspended Sediment

To date, 66 water samples have been collected and analysed for Total Suspended Solids (TSS), which comprise both organic (e.g. algae) and inorganic (e.g. silt) particles suspended in the water column. The sampling positions and the measured TSS are plotted in ***Figure 5.9-30*** and ***Figure 5.9-31*** respectively.

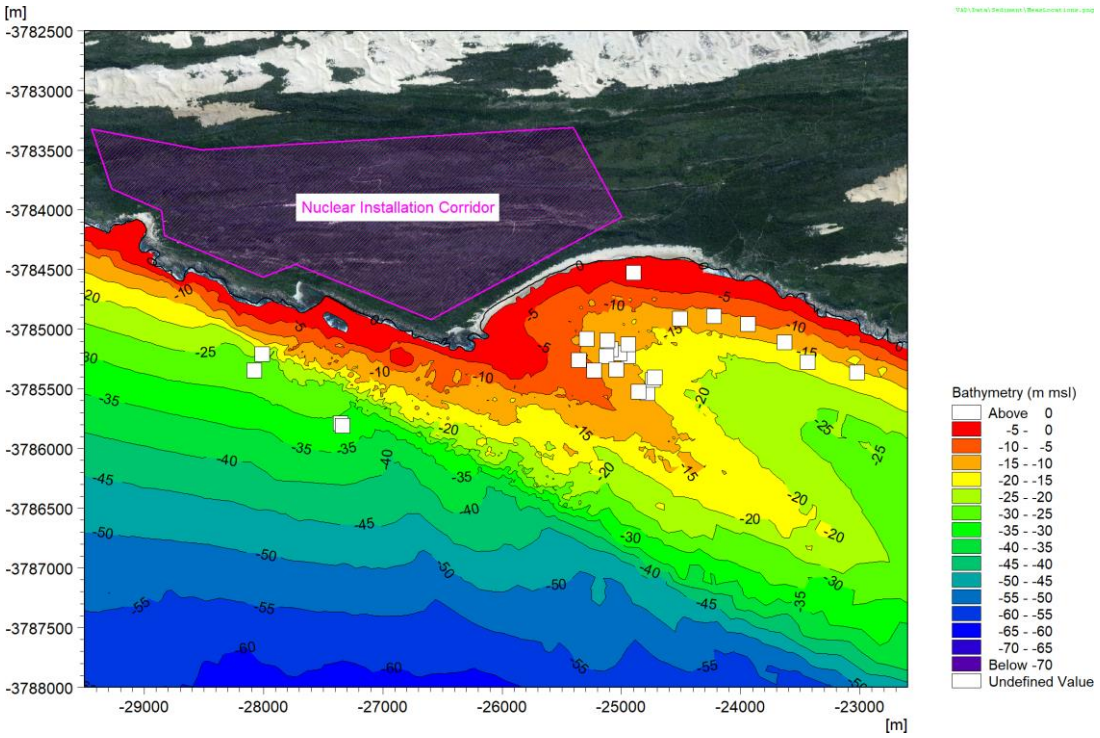


Figure 5.9-30: Total Suspended Solids Sampling Locations.

CONTROLLED DISCLOSURE

When downloaded from the EDS database, this document is uncontrolled and the responsibility rests with the user to ensure it is in line with the authorised version on the database.

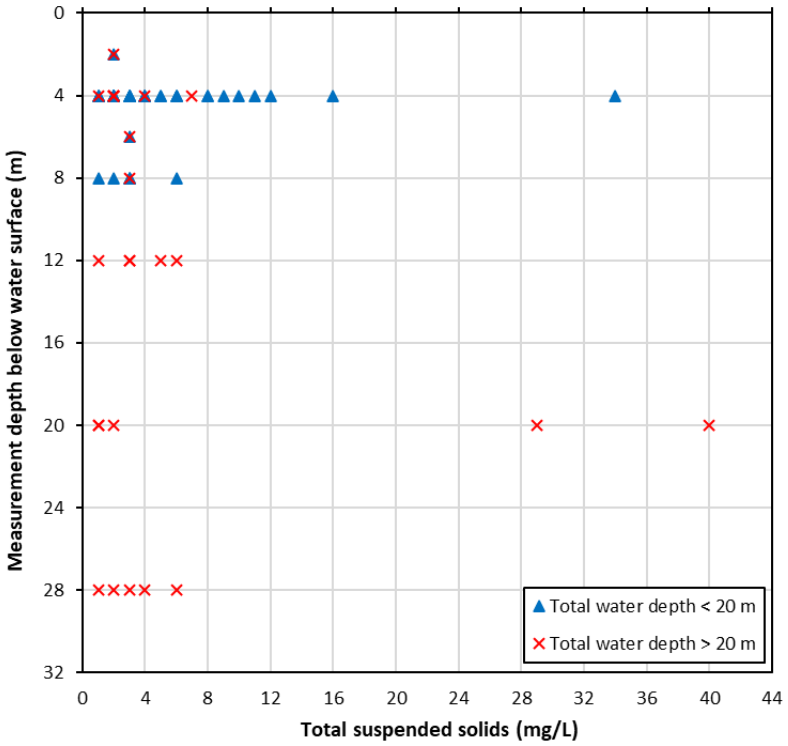


Figure 5.9-31: Total Suspended Solids Distribution in Water Column.

Table 5.9-20: Summary of Measured Total Suspended Solids.

Percentile (%)	TSS (mg/L)
0	1.0
1	1.0
5	1.0
10	1.0
20	2.0
30	2.0
40	3.0
50	3.0
60	3.0
70	4.5
80	6.0
90	9.5
95	15.0
99	36.1
100	40.0

The median, average and maximum TSS measured at the site are 3, 5 and 40 mg/L, respectively. The results show little difference in TSS concentrations between shallower inshore sampling sites and the deeper offshore sites. The TSS concentration is relatively uniform over the water column (see ***Figure 5.9-31***), implying that these are smaller cohesive

CONTROLLED DISCLOSURE

When downloaded from the EDS database, this document is uncontrolled and the responsibility rests with the user to ensure it is in line with the authorised version on the database.

sediment particles (D_{50} < 0.063 mm) rather than larger sand particles (which would show significantly higher concentrations near the seabed). Suspended sand at the intakes is calculated in ***Subsection 5.9.11.8***.

5.9.9.8 Waves

Measured waves

Waves have been measured at Site A (water depth -13.2 m msl) and at Site B (water depth -30.8 m msl). Details of the locations, instruments, sampling intervals, dates and length of valid data are provided in ***Subsection 5.9.6.1***.

The measured wave parameters are presented below as time-series (***Figure 5.9-32*** and ***Figure 5.9-33***), wave roses (***Figure 5.9-34***) and statistics (***Table 5.9-21***). H_{m0} is the significant wave height, T_p is the peak wave period, and MWD is the wave energy weighted mean wave direction. Note that wave direction is the direction from which the waves are coming, measured clockwise from true north.

CONTROLLED DISCLOSURE

When downloaded from the EDS database, this document is uncontrolled and the responsibility rests with the user to ensure it is in line with the authorised version on the database.

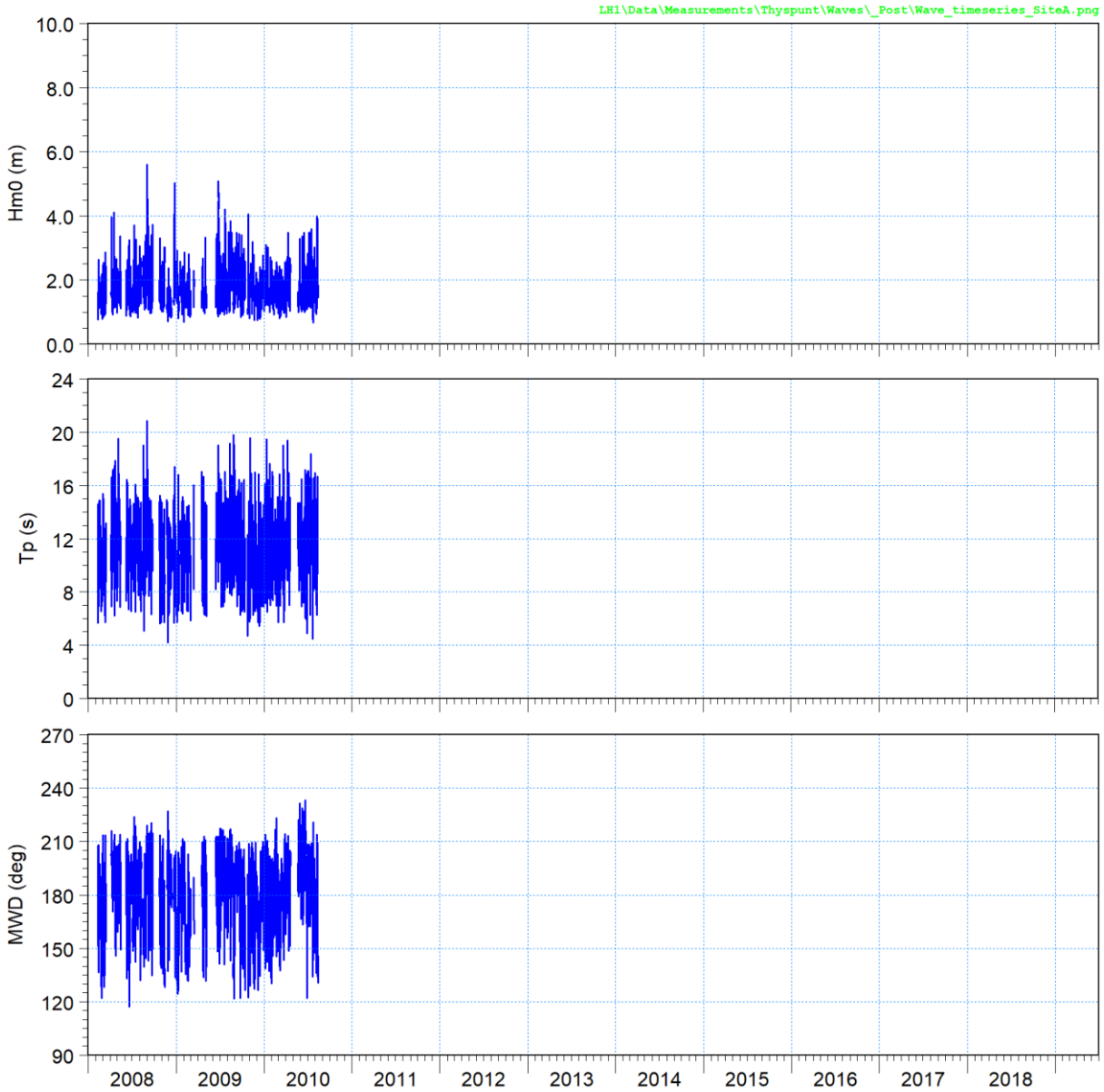


Figure 5.9-32: Time-Series of Measured Wave Parameters at Site A (Water Depth -13.2 m msl).

CONTROLLED DISCLOSURE

When downloaded from the EDS database, this document is uncontrolled and the responsibility rests with the user to ensure it is in line with the authorised version on the database.

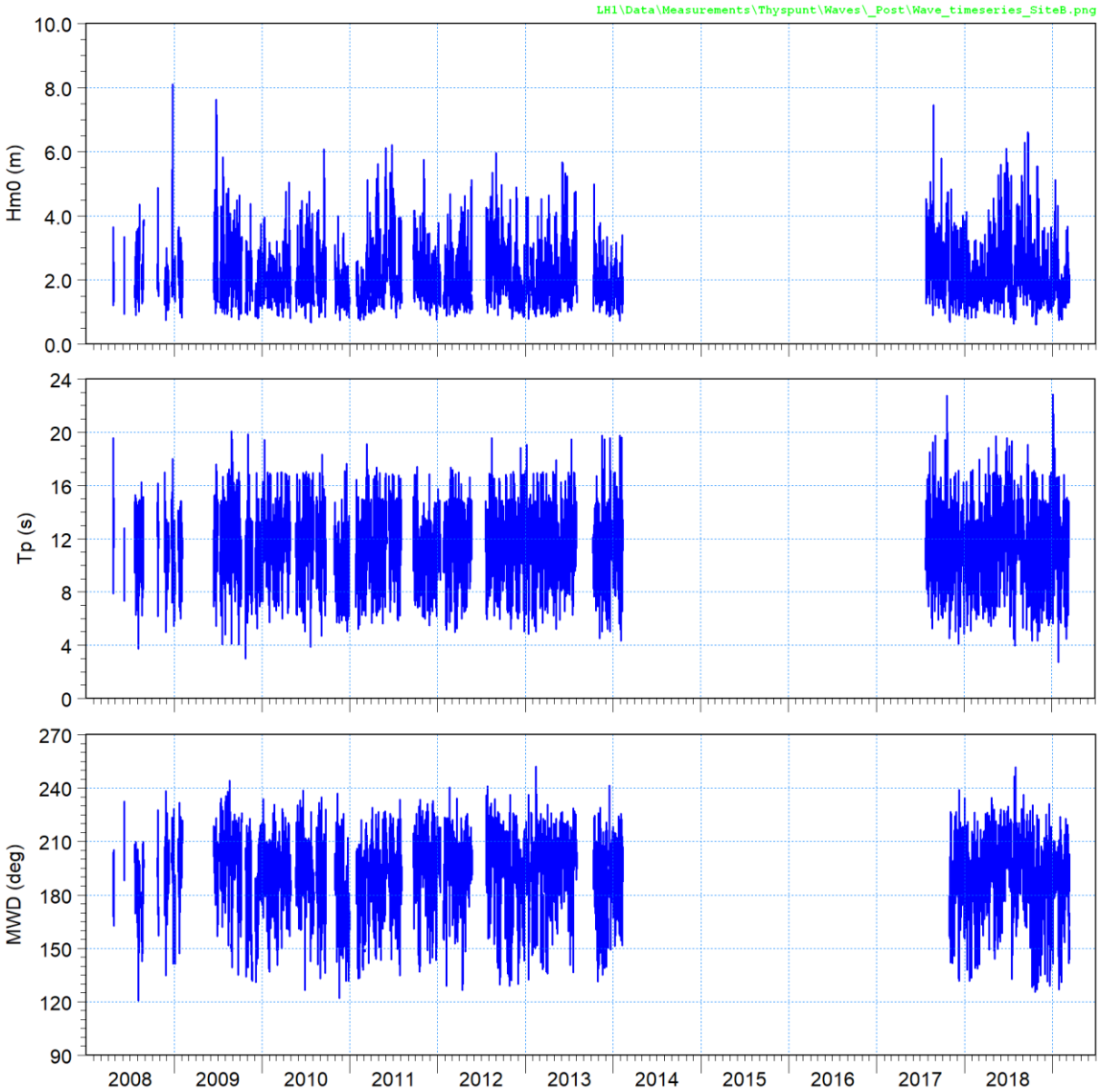


Figure 5.9-33: Time-Series of Measured Wave Parameters at Site B (Water Depth -30.8 m msl).

CONTROLLED DISCLOSURE

When downloaded from the EDS database, this document is uncontrolled and the responsibility rests with the user to ensure it is in line with the authorised version on the database.

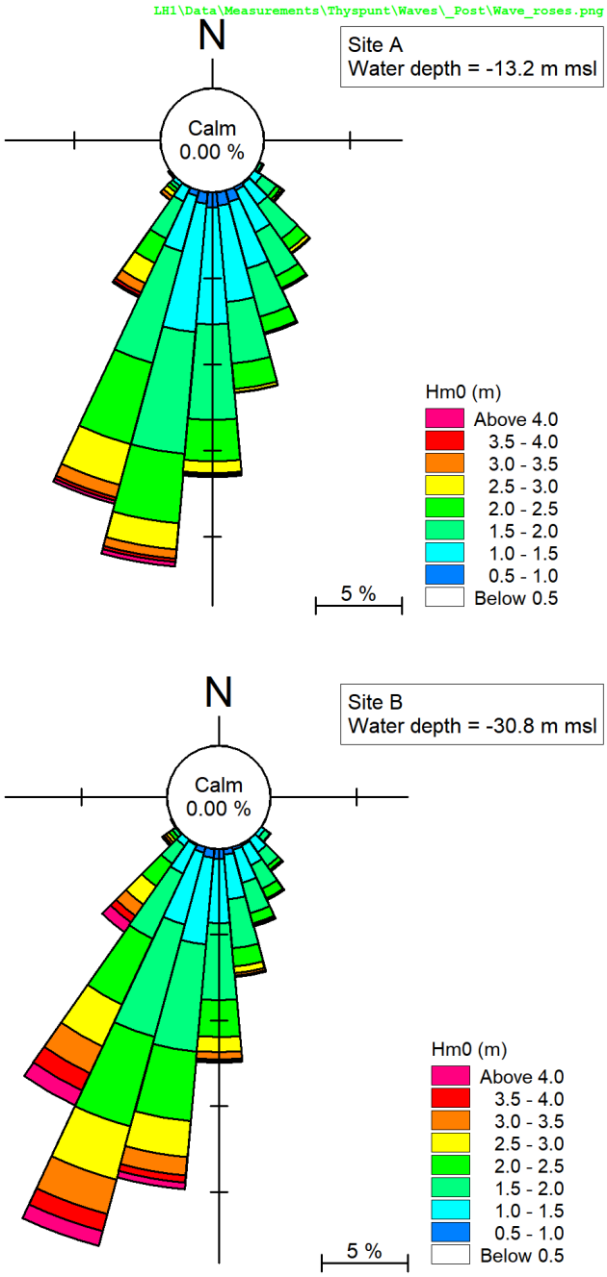


Figure 5.9-34: Wave Roses at Site A and Site B.

CONTROLLED DISCLOSURE

When downloaded from the EDS database, this document is uncontrolled and the responsibility rests with the user to ensure it is in line with the authorised version on the database.

Table 5.9-21: Summary of Measured Waves.

Percentile	Significant Wave Height (H_{m0})	
	Site A (Water Depth -13.2 m msl)	Site B (Water Depth -30.8 m msl)
(%)	(m)	(m)
0	0.66	0.62
1	0.89	0.91
5	1.03	1.11
10	1.13	1.24
20	1.29	1.43
30	1.42	1.59
40	1.54	1.74
50	1.66	1.91
60	1.80	2.11
70	1.97	2.35
80	2.18	2.68
90	2.54	3.22
95	2.87	3.71
99	3.75	4.81
100	5.60	8.10

The measured wave data indicates a rough wave climate with a median H_{m0} of 1.91 m at Site B. The maximum H_{m0} of 8.10 m was measured during a storm event on 24 December 2008. There is a significant seasonal variation in wave height, with smaller waves typically occurring during summer (December to February) and larger waves occurring during winter (June to August), although the largest event measured at Site B did occur in summer. The dominant wave direction at the site is 200° and shifts slightly westward in winter and southward in summer. These wave measurements were used to calibrate the wave refraction model described below.

Spectral wave modelling

Nearshore operational and extreme wave conditions are required as input to the modelling of sediment transport (***Subsection 5.9.11***) and storm wave run-up and drawdown (***Subsection 5.9.12***). Due to the limited duration (5.5 y) of the measured wave data at the site, offshore wave data from a global hindcast model has been transformed to the site using a spectral wave model. Details of the hindcast data, model description, setup, calibration, and cases modelled are provided in ***Appendix 5.9.A.2***. The resulting nearshore operational and extreme wave climates are reported below.

Nearshore operational wave climate

Ten years of continuous hourly waves were required as input to the 2D sediment transport analysis described in ***Subsection 5.9.11***. Ten years of offshore hindcast data (2000-2009) were thus transformed to obtain wave

CONTROLLED DISCLOSURE

When downloaded from the EDS database, this document is uncontrolled and the responsibility rests with the user to ensure it is in line with the authorised version on the database.

conditions along the 2D sediment transport model boundary. Point 1 (X = -27030, Y = -3787430, depth = -55 m msl, refer ***Figure 5.9-35***) provides representative wave conditions offshore of the Thyspunt site.

Figure 5.9-35 shows an example instantaneous wave refraction plot. ***Figure 5.9-36***, ***Figure 5.9-37*** and ***Figure 5.9-38*** present the time-series and a 3D scatterplot of 10 years of modelled spectral wave parameters at Point 1.

CONTROLLED DISCLOSURE

When downloaded from the EDS database, this document is uncontrolled and the responsibility rests with the user to ensure it is in line with the authorised version on the database.

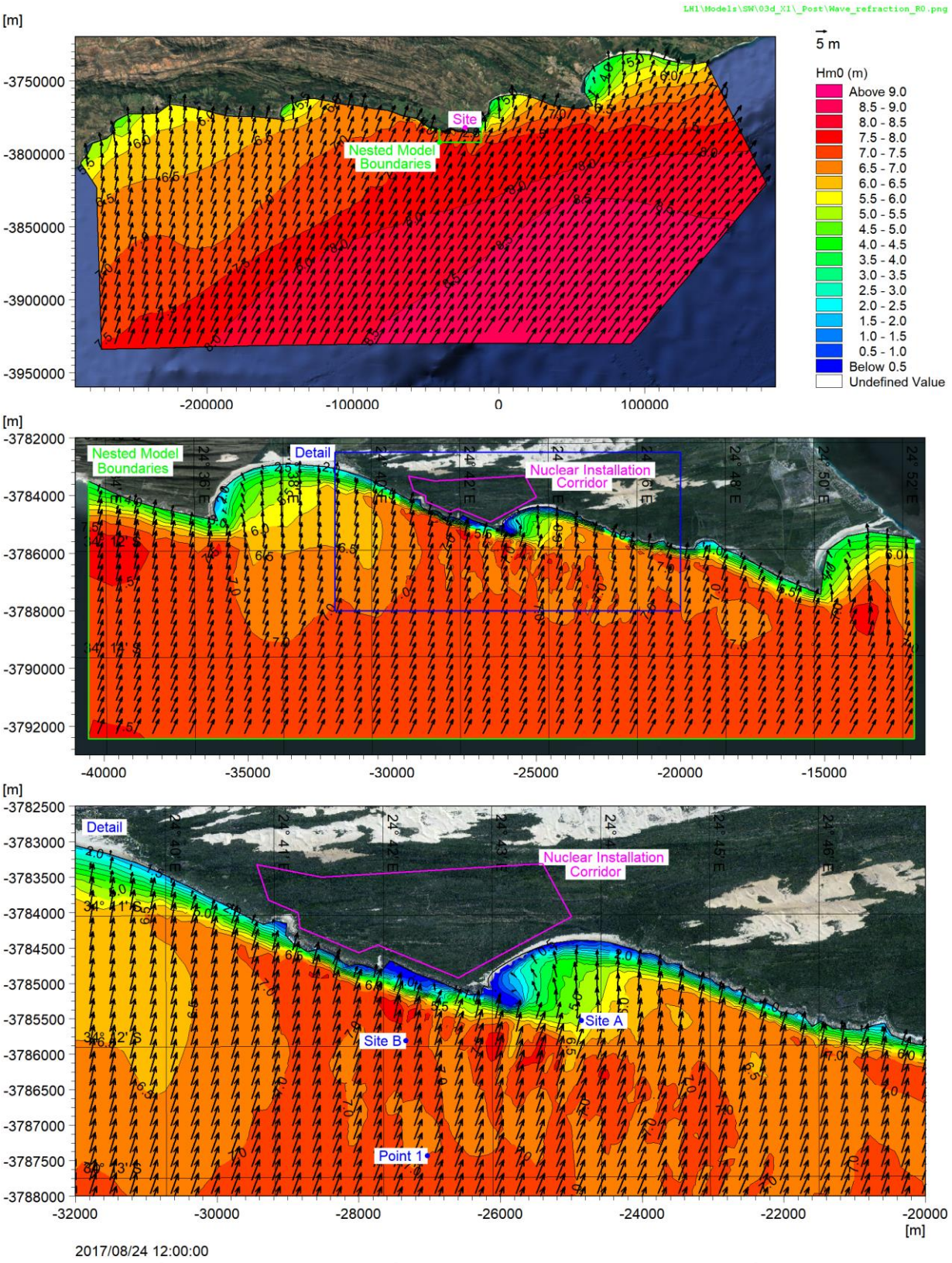


Figure 5.9-35: Example Instantaneous Wave Refraction.

CONTROLLED DISCLOSURE

When downloaded from the EDS database, this document is uncontrolled and the responsibility rests with the user to ensure it is in line with the authorised version on the database.

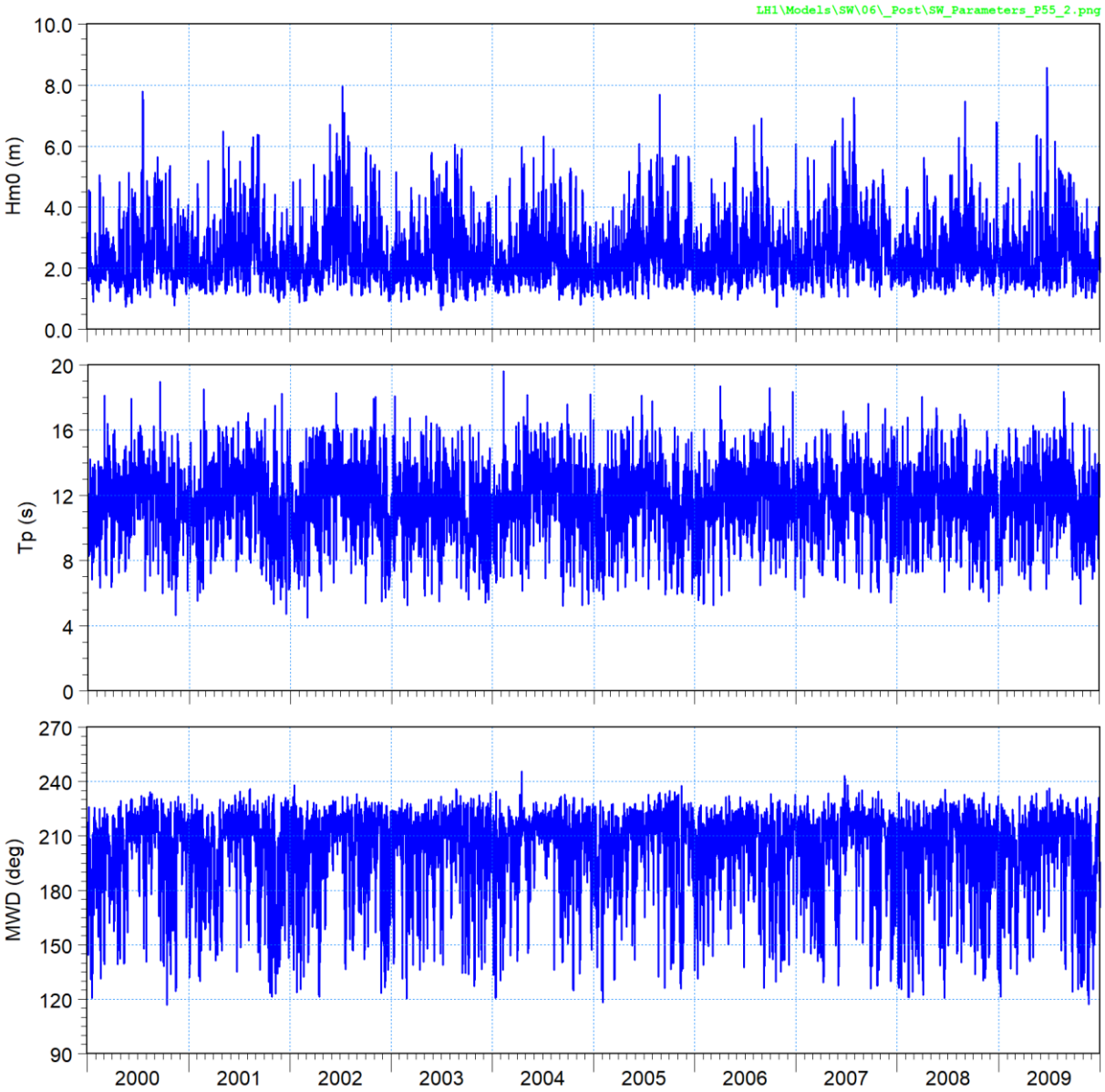


Figure 5.9-36: Time-Series of 10 Years (2000-2009) of Modelled Operational Wave Parameters at Point 1 (-55 m msl).

CONTROLLED DISCLOSURE

When downloaded from the EDS database, this document is uncontrolled and the responsibility rests with the user to ensure it is in line with the authorised version on the database.

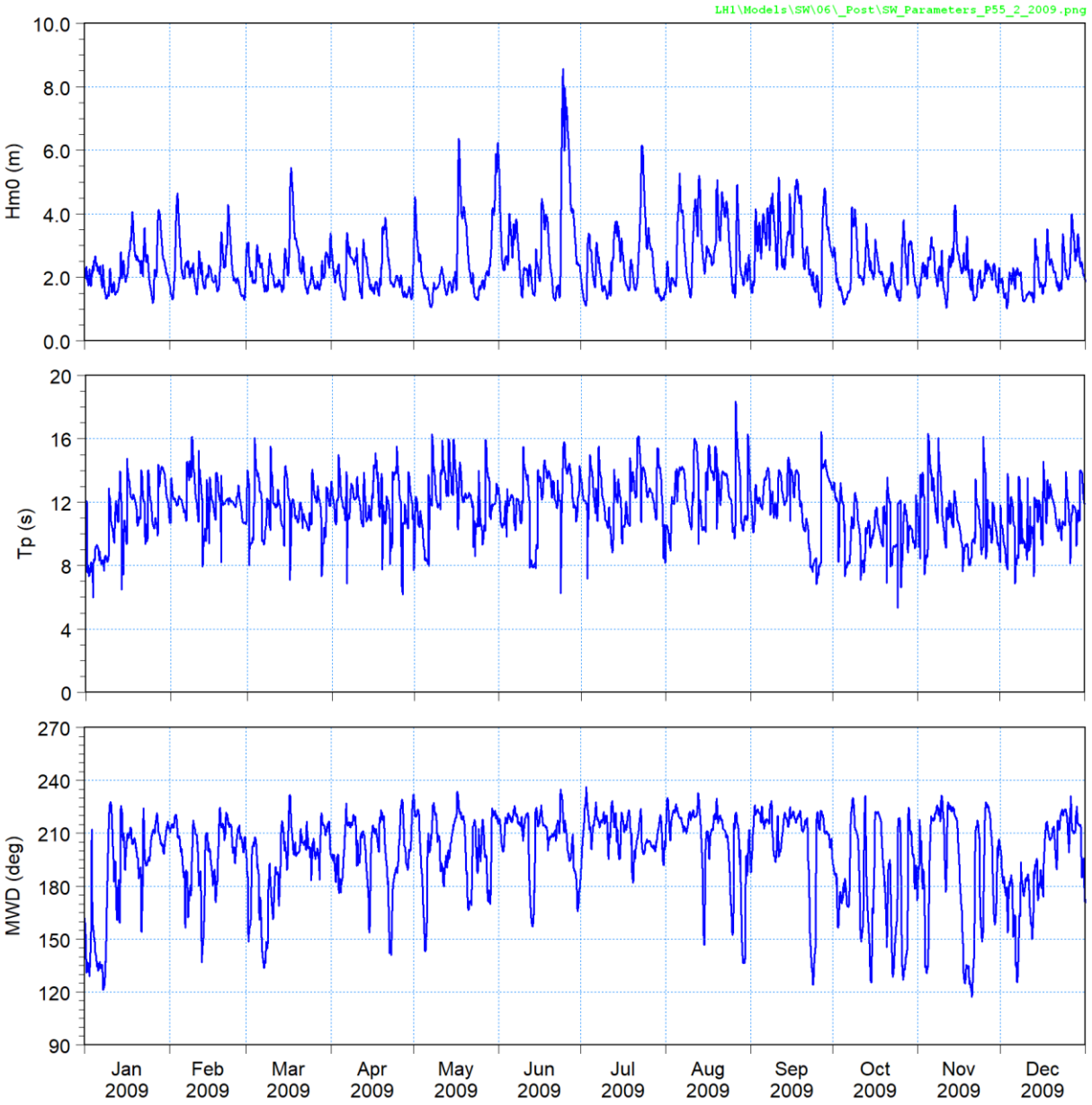


Figure 5.9-37: Time-Series of 1 Year (2009) of Modelled Operational Wave Parameters at Point 1 (-55 m msl).

CONTROLLED DISCLOSURE

When downloaded from the EDS database, this document is uncontrolled and the responsibility rests with the user to ensure it is in line with the authorised version on the database.

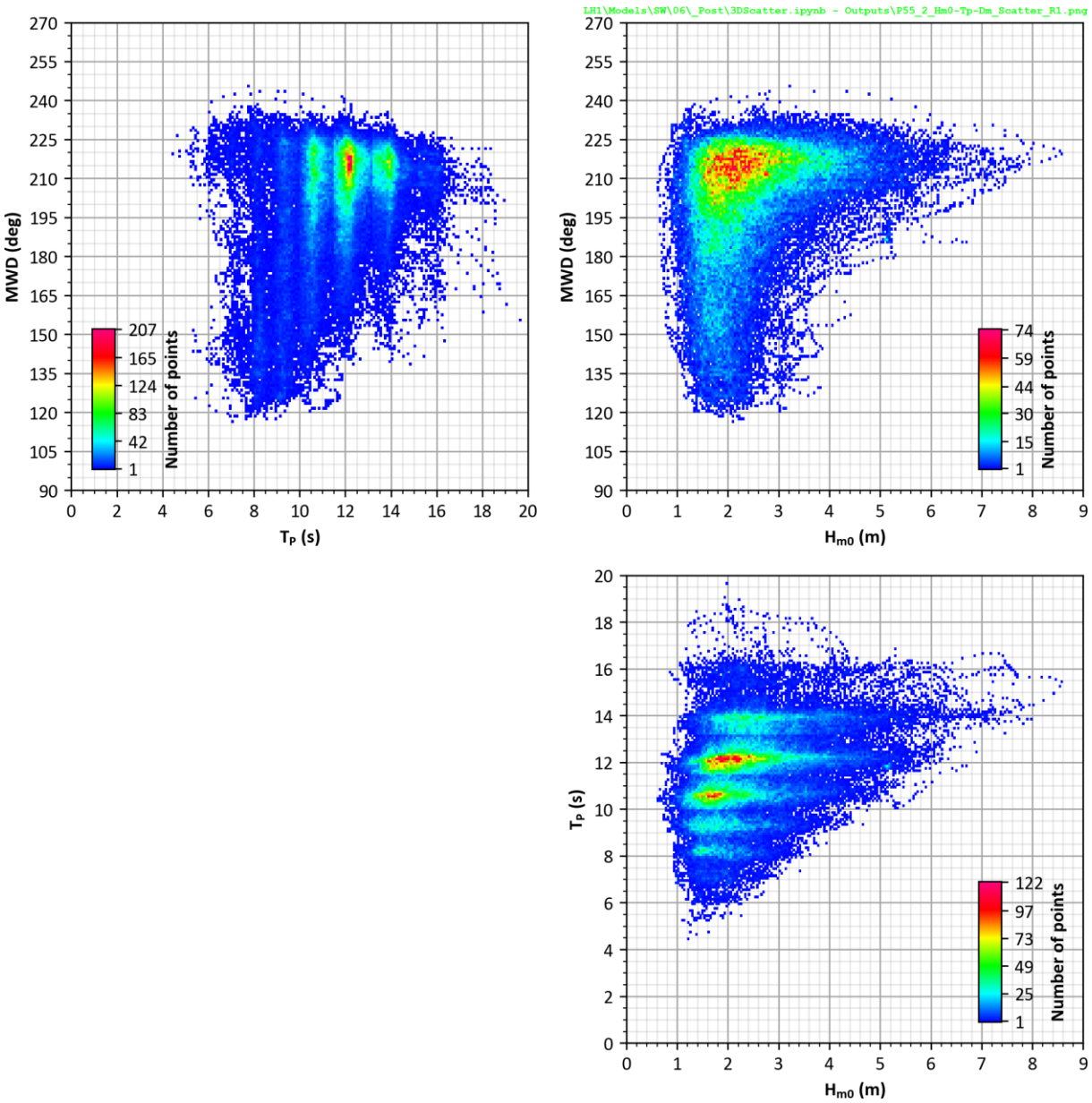


Figure 5.9-38: 3D Scatterplot of 10 Years (2000-2009) of Modelled Operational Wave Parameters at Point 1 (-55 m msl).

Two additional 10-year sets were modelled for the 2134 and 2134 High SLR scenarios at the end of the decommissioning period of the new NIs. To account for the effect of climate change the model boundary conditions were adjusted to include the rotation of wave direction (the same for both scenarios) and increase in water elevation (different for the two scenarios) as per ***Table 5.9-8***. The wave height and period were not adjusted.

CONTROLLED DISCLOSURE

When downloaded from the EDS database, this document is uncontrolled and the responsibility rests with the user to ensure it is in line with the authorised version on the database.

Nearshore extreme wave climate

To determine the nearshore extreme wave climate, 228 storm events in the 45.5-year offshore hindcast dataset were refracted to Point 1 (see ***Figure 5.9-35***) located directly in front of the site using the calibrated spectral wave model.

Scatterplots over the duration of each storm event of H_{m0} compared to T_p, MWD_p (the mean wave direction associated with the peak wave period) and DSD_p (the directional standard deviation associated with the peak wave period) are presented in the following figures:

- ***Figure 5.9-39***: scatterplot comparison of H_{m0} and T_p at Point 1, as well as the H_{m0}-T_p relationship (where the $H_{m0}^{0.5}$ factor is based on limiting the wave steepness and the 5.2 factor is a site-specific fit to the data), used to determine the extreme wave periods associated with the extreme wave heights.
- ***Figure 5.9-40***: scatterplot comparison of H_{m0} and MWD_p used to determine the extreme wave directions associated with the extreme wave heights. The 5th, 50th, and 95th percentiles of MWD_p were determined from the H_{m0}-MWD_p distribution for waves exceeding the 1 y^{-1} exceedance frequency H_{m0}. ($H_{m0} \geq 6.9$ m, ***Table 5.9-22***).
- ***Figure 5.9-41***: scatterplot comparison of H_{m0} and DSD_p used to determine the extreme wave directional distributions associated with the extreme wave heights. The 50th percentile of DSD_p was determined from the H_{m0}-DSD_p distribution for waves exceeding the 1 y^{-1} exceedance frequency H_{m0}.

CONTROLLED DISCLOSURE

When downloaded from the EDS database, this document is uncontrolled and the responsibility rests with the user to ensure it is in line with the authorised version on the database.

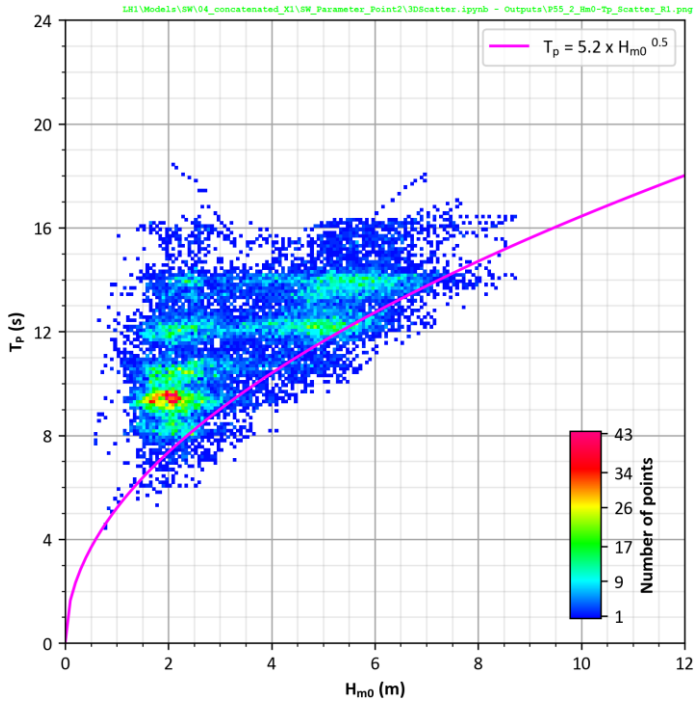


Figure 5.9-39: Scatterplot Showing Relationship between Wave Height and Period at Point 1 from Modelled Storms between 1979 and 2024.

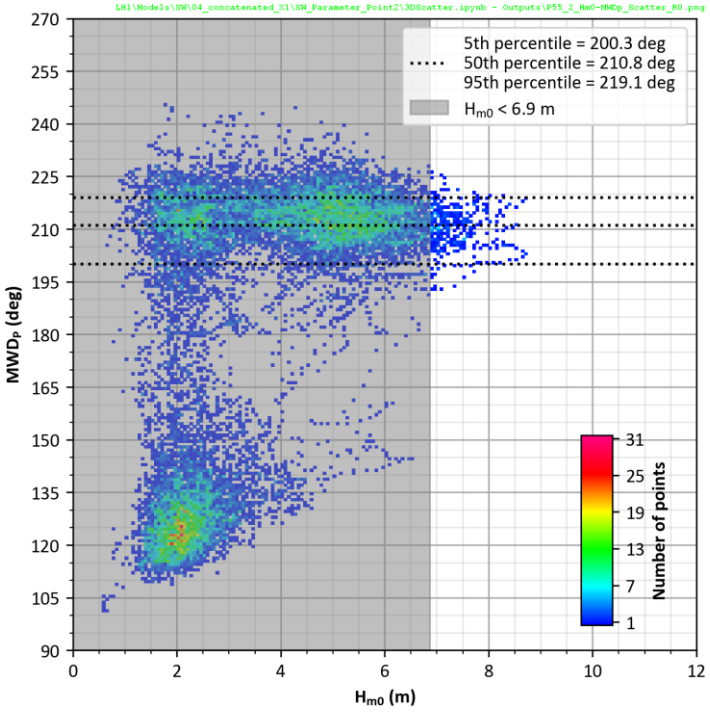


Figure 5.9-40: Scatterplot Showing Relationship between Wave Height and Direction at Point 1 from Modelled Storms between 1979 and 2024. The 5th, 50th, and 95th Percentiles of MWD_p were Determined from the H_{m0}-MWD_p Distribution for Waves Exceeding the 1 y^{-1} Exceedance Frequency H_{m0}.

CONTROLLED DISCLOSURE

When downloaded from the EDS database, this document is uncontrolled and the responsibility rests with the user to ensure it is in line with the authorised version on the database.

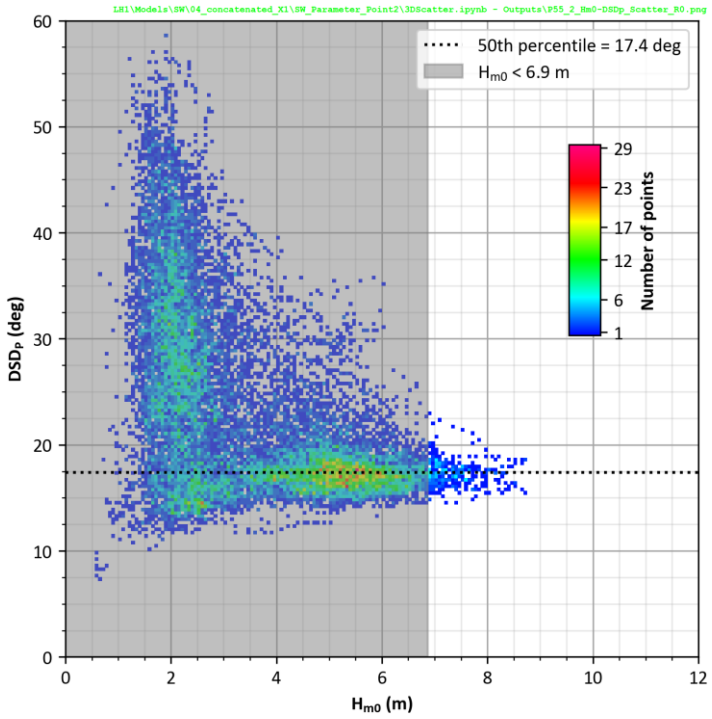
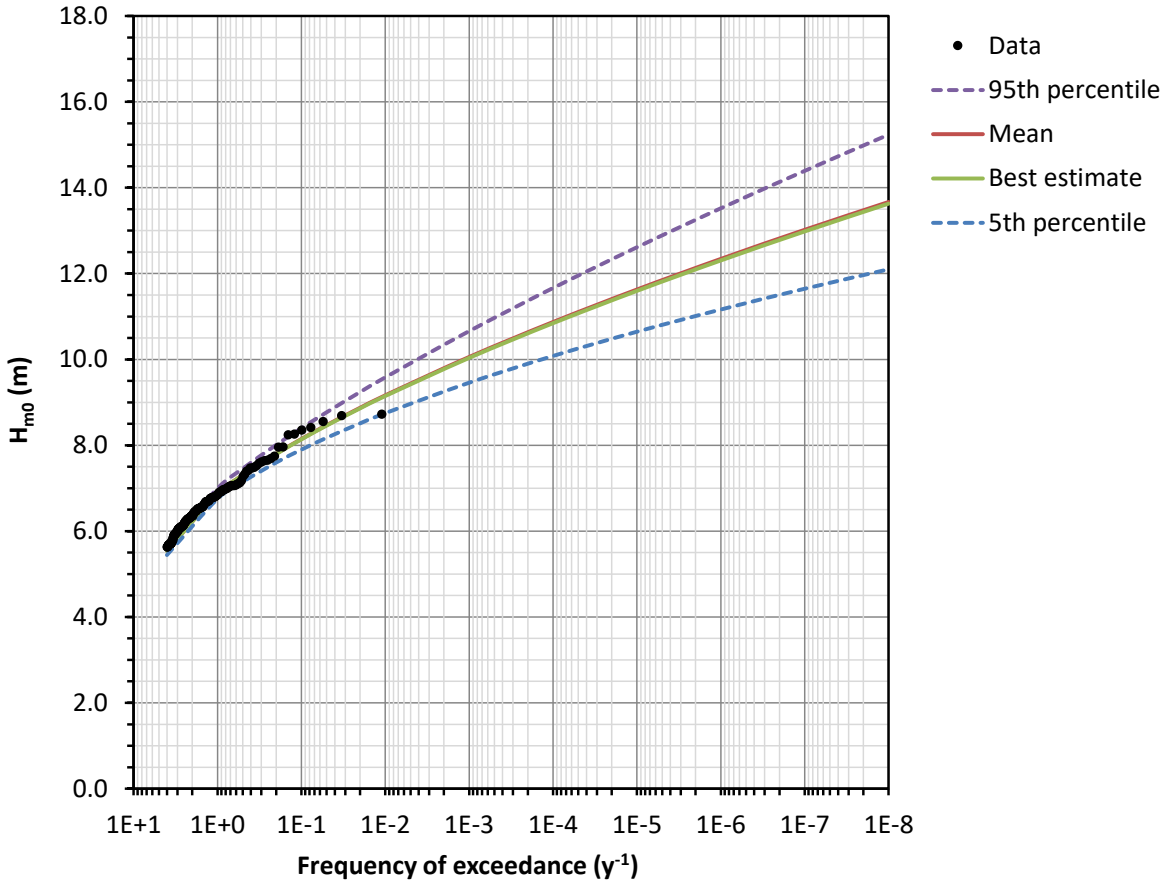


Figure 5.9-41: Scatterplot Showing Relationship between Wave Height and Directional Spreading at Point 1 from Modelled Storms between 1979 and 2024. The 50th Percentile of DSD_p was Determined from the H_{m0}-DSD_p Distribution for Waves Exceeding the 1 y^{-1} Exceedance Frequency H_{m0}.

An extreme value analysis (refer to ***Subsection 5.9.6.2*** for the methodology) was then performed on the modelled nearshore wave heights of the 228 storm events. The EVA results are presented in ***Figure 5.9-42***. The baseline date is 2001.5 which is the middle of the modelled period.

CONTROLLED DISCLOSURE

When downloaded from the EDS database, this document is uncontrolled and the responsibility rests with the user to ensure it is in line with the authorised version on the database.



LH1\Models\SW\04_concatenated_X1\SW_Parameter_Point2\EVA_R1\[SW_Spectral_Parameters_P55_2_4pa.xlsx]EVA

Figure 5.9-42: Extreme Value Analysis of Wave Height at Point 1 in a Depth of -55 m msl (Baseline Date is 2001.5).

The extreme wave heights were then adjusted for climate change (***Subsection 5.9.7***) and are presented in ***Table 5.9-22***. The associated T_p, MWD_p and DSD_p are also shown.

CONTROLLED DISCLOSURE

When downloaded from the EDS database, this document is uncontrolled and the responsibility rests with the user to ensure it is in line with the authorised version on the database.

Table 5.9-22: Extreme Wave Parameters at Point 1 in a Depth of -55 m msl.

Exceedance Frequency	Uncertainty	H_{m0}			T_p			MWD_p[(a)]			DSD_p[(b)]
								5%	50%	95%	
(y^{-1})		(m)			(s)			(°)			(°)
		2034	2114	2134	2034	2114	2134	All	All	All	All
1E+0	5th Percentile	6.9	7.2	7.3	13.6	14.0	14.0	200	211	219	17.4
	Mean	7.0	7.3	7.4	13.8	14.1	14.2	200	211	219	17.4
	Best Estimate	7.0	7.3	7.4	13.8	14.1	14.2	200	211	219	17.4
	95th Percentile	7.1	7.5	7.5	13.9	14.2	14.3	200	211	219	17.4
1E-1	5th Percentile	8.0	8.4	8.5	14.8	15.1	15.2	200	211	219	17.4
	Mean	8.3	8.7	8.8	15.0	15.3	15.4	200	211	219	17.4
	Best Estimate	8.3	8.7	8.8	15.0	15.3	15.4	200	211	219	17.4
	95th Percentile	8.6	9.0	9.0	15.2	15.6	15.6	200	211	219	17.4
1E-2	5th Percentile	8.9	9.3	9.4	15.5	15.9	16.0	200	211	219	17.4
	Mean	9.3	9.8	9.9	15.9	16.3	16.3	200	211	219	17.4
	Best Estimate	9.3	9.8	9.9	15.9	16.2	16.3	200	211	219	17.4
	95th Percentile	9.8	10.2	10.3	16.2	16.6	16.7	200	211	219	17.4
1E-3	5th Percentile	9.6	10.1	10.2	16.1	16.5	16.6	200	211	219	17.4
	Mean	10.2	10.7	10.8	16.6	17.0	17.1	200	211	219	17.4
	Best Estimate	10.2	10.7	10.8	16.6	17.0	17.1	200	211	219	17.4
	95th Percentile	10.9	11.4	11.5	17.1	17.5	17.6	200	211	219	17.4
1E-4	5th Percentile	10.3	10.7	10.9	16.7	17.0	17.1	200	211	219	17.4
	Mean	11.1	11.6	11.7	17.3	17.7	17.8	200	211	219	17.4
	Best Estimate	11.1	11.6	11.7	17.3	17.7	17.8	200	211	219	17.4
	95th Percentile	11.9	12.4	12.6	17.9	18.3	18.4	200	211	219	17.4
1E-5	5th Percentile	10.8	11.3	11.5	17.1	17.5	17.6	200	211	219	17.4
	Mean	11.9	12.4	12.5	17.9	18.3	18.4	200	211	219	17.4
	Best Estimate	11.8	12.4	12.5	17.9	18.3	18.4	200	211	219	17.4
	95th Percentile	12.9	13.4	13.6	18.6	19.1	19.2	200	211	219	17.4
1E-6	5th Percentile	11.4	11.9	12.0	17.5	17.9	18.0	200	211	219	17.4
	Mean	12.6	13.2	13.3	18.4	18.9	19.0	200	211	219	17.4
	Best Estimate	12.5	13.1	13.3	18.4	18.8	18.9	200	211	219	17.4
	95th Percentile	13.8	14.4	14.6	19.3	19.7	19.9	200	211	219	17.4
1E-7	5th Percentile	11.9	12.4	12.6	17.9	18.3	18.4	200	211	219	17.4
	Mean	13.3	13.9	14.0	18.9	19.4	19.5	200	211	219	17.4
	Best Estimate	13.2	13.8	14.0	18.9	19.3	19.5	200	211	219	17.4
	95th Percentile	14.7	15.3	15.5	19.9	20.4	20.5	200	211	219	17.4
1E-8	5th Percentile	12.3	12.9	13.0	18.3	18.7	18.8	200	211	219	17.4
	Mean	13.9	14.6	14.7	19.4	19.9	20.0	200	211	219	17.4
	Best Estimate	13.9	14.5	14.7	19.4	19.8	19.9	200	211	219	17.4
	95th Percentile	15.5	16.2	16.4	20.5	21.0	21.1	200	211	219	17.4

Notes:

(a) The 5%, 50% and 95% refer to the 5th, 50th, and 95th percentiles from the MWD_p distribution for waves exceeding the 1 y^{-1} exceedance frequency H_{m0}.

(b) DSD_p is the 50th percentile from the DSD_p distribution for waves exceeding the 1 y^{-1} exceedance frequency H_{m0}.

CONTROLLED DISCLOSURE

When downloaded from the EDS database, this document is uncontrolled and the responsibility rests with the user to ensure it is in line with the authorised version on the database.

The extreme wave climate above was used as input to the storm erosion modelling (***Subsection 5.9.11.5***), the modelling of suspended sand at the cooling water intakes (***Subsection 5.9.11.8***) and the storm wave run-up and drawdown modelling (***Subsection 5.9.12***).

5.9.9.9 Waterspouts

Waterspouts are generally divided into two categories: 'tornadic' waterspouts and fair weather waterspouts as defined below (IAEA, 2011):

- Tornadic waterspouts are tornadoes that form over water or move from land to water. They have the same characteristics as a land tornado. They are associated with severe thunderstorms, and are often accompanied by high winds and seas, large hail and frequent dangerous lightning.
- Fair weather waterspouts are generally more prevalent. They are usually less intense phenomena that form most commonly in the summer in fair and relatively calm weather. Fair weather waterspouts usually form along the dark flat bases of a line of developing cumulus clouds. They typically move slowly, if at all, since the cloud they are attached to is typically horizontally static. While many waterspouts form in the tropics, locations farther north (or south) within temperate zones also report waterspouts, such as the Great Lakes region in North America and Europe.

Waterspouts may transfer large amounts of water to the land from nearby water bodies.

The meteorological hazards associated with waterspouts are assessed in ***Section 5.8*** as part of the assessment of tornadoes. As presented in ***Section 5.8*** the 3 s gust wind speed of the highest intensity tornado in the Enhanced Fujita Scale (EF5) is >90 m/s with an average path width of 1 636 m. The most intense tornado ever recorded in South Africa was classified as EF4 (3 s wind gusts of 76 to 89 m/s and average width of 998 m). The 1E-8 exceedance frequency wind speed at the site (determined through an Extreme Value Analysis of 19 years of wind measurements at Cape St Francis) is 40.5 ± 8.0 m/s (1-hour average) and 80.2 ± 22.0 m/s (wind gust).

The potential oceanographic hazards associated with waterspouts include waves and storm surge generated by wind stress on the water surface, and these are discussed below.

The generation of waves or storm surge over large waterbodies requires sustained rather than transient wind stress and depends on the length over which the stress acts (called wind fetch). Thus, even the waves and storm

CONTROLLED DISCLOSURE

When downloaded from the EDS database, this document is uncontrolled and the responsibility rests with the user to ensure it is in line with the authorised version on the database.

surge generated by a waterspout with a sustained wind speed of 90 m/s would be limited by the fetch, owing to its small footprint. Based on the empirical relationships between wind speed, fetch, storm surge and wave height, for the 1E-8 1-hour average wind speed at the site (40.5 m/s) to generate the same wind set-up or wave height as such a tornado would require a fetch of only five times that of the tornado, which for an EF5 tornado is approximately 8 km. Extra-tropical storms responsible for generating the storm surge and waves assessed in ***Subsection 5.9.9.2*** and ***5.9.9.8*** have typical fetches in the order of 100 to 1 000 km and will thus envelope waves or storm surge due to waterspouts.

5.9.10 Joint Probability

5.9.10.1 Introduction

The numerical modelling described in ***Subsections 5.9.11*** and ***5.9.12*** requires the joint probability of the hydrographic parameters used as inputs to the models, such as waves and storm surge.

In all cases the US NRC's recommendation (NRC, 2009) is used for the initial tidal water level, i.e., for the high water cases the 90th percentile high tide and for low water cases is the 10th percentile low tide. These levels are analysed and presented in ***Subsection 5.9.9.1***.

The tidal level is combined with SLR and the storm surge to obtain the still water level, as analysed and presented in ***Table 5.9-11*** and ***Table 5.9-12***.

The joint probabilities between the following parameters are then required:

- Waves and positive storm surge:

  The storm erosion modelling (***Subsection 5.9.11.5***) and the storm wave run-up modelling (***Subsection 5.9.12***) requires the joint probability of waves and positive storm surge.
- Waves and negative storm surge:

  Modelling the extreme wave drawdown (***Subsection 5.9.12***) requires the joint probability of waves and negative storm surge.
- Waves and currents:

  Modelling the suspended sand at the cooling water intakes (***Subsection 5.9.11.8***) requires the joint probability of waves and currents.

The joint probability depends on the site-specific level of dependence between the parameters. The methodology applied for estimating the joint

CONTROLLED DISCLOSURE

When downloaded from the EDS database, this document is uncontrolled and the responsibility rests with the user to ensure it is in line with the authorised version on the database.

probabilities is described below, followed by the estimation of the joint probabilities for each of the combinations in the bullet list above.

5.9.10.2 Methodology

A methodology for calculating the joint probability and resultant impact on coastal flooding of storm surge vs wave height, storm surge vs river discharge and wave height vs river discharge is described by (Petroliagkis, et al., 2016). This methodology has been applied in this section, based on the similarity of the application and the solid theoretical basis presented in (Petroliagkis, et al., 2016). The joint (combined) exceedance frequency of two variables (e.g., storm surge and wave height) is given by:

$$F_{X,Y} = \chi \sqrt{F_X \cdot F_Y}$$ Equation 5.9.2

where:

$F_{X,Y}$ = joint exceedance frequency of two variables occurring together (y^{-1})

F_X = exceedance frequency of first variable X (y^{-1})

F_Y = exceedance frequency of second variable Y (y^{-1})

χ = dependence parameter between the first and second variables ranging between 1 when fully dependent and 0 when independent.

Equation 5.9.2 shows that once χ has been calculated, then a specified joint exceedance frequency $F_{X,Y}$ can be achieved by selecting F_X and F_Y as follows:

$$F_X = F_{X,Y}\ ;\ F_Y = \frac{F_{X,Y}}{\chi^2}$$ Equation 5.9.3

For fully dependent datasets $\chi = 1$ and thus $F_{X,Y} = F_X = Fy$, as expected. As the datasets become less dependent χ becomes less than 1 and Fy becomes larger.

The dependence parameter χ is calculated from a site-specific dataset containing simultaneous values of the first (X) and second (Y) variables. The methodology requires counting the number of events where both variables simultaneously exceed a common percentile threshold (x*, y*), which enables χ to be calculated for each percentile as shown in ***Equation 5.9.3***.

$$\chi = 2 - \frac{ln\left[\frac{\text{Number of (X,Y) such that } X \le x^* \text{ and } Y \le y^*}{\text{Total number of (X,Y)}}\right]}{\frac{1}{2} ln\left[\frac{\text{Number of } X \le x^*}{\text{Total number of X}} * \frac{\text{Number of } Y \le y^*}{\text{Total number of Y}}\right]}$$ Equation 5.9.4

CONTROLLED DISCLOSURE

When downloaded from the EDS database, this document is uncontrolled and the responsibility rests with the user to ensure it is in line with the authorised version on the database.

The largest χ is then selected from the range of percentiles representing the more extreme events, e.g., events above the 85th percentile, since only the extreme events are of interest. The applicable formulas and the full details of the methodology are provided in (Petroliagkis, et al., 2016). The following categories of dependence are defined:

Table 5.9-23: Categories of Dependence (Petroliagkis, et al., 2016).

Dependence Parameter χ	Category
X ≤ -0.06	Negative
-0.05 ≤ X ≤ 0.05	Zero
0.06 ≤ X ≤ 0.14	Low
0.15 ≤ X ≤ 0.24	Modest
0.25 ≤ X ≤ 0.34	Well
0.35 ≤ X ≤ 0.44	Strong
X ≥ 0.45	Very Strong

5.9.10.3 Waves and Positive Storm Surge

The site-specific dataset used was the hourly measured storm surge at Thyspunt (refer ***Subsection 5.9.9.2***) and the hourly measured waves at Site B (refer ***Subsection 5.9.9.8***). ***Figure 5.9-43*** shows a scatterplot of these data using 36 320 hourly data pairs, equivalent to 4.1 years. ***Figure 5.9-44*** shows the calculated dependence parameter χ of wave height and positive storm surge.

CONTROLLED DISCLOSURE

When downloaded from the EDS database, this document is uncontrolled and the responsibility rests with the user to ensure it is in line with the authorised version on the database.

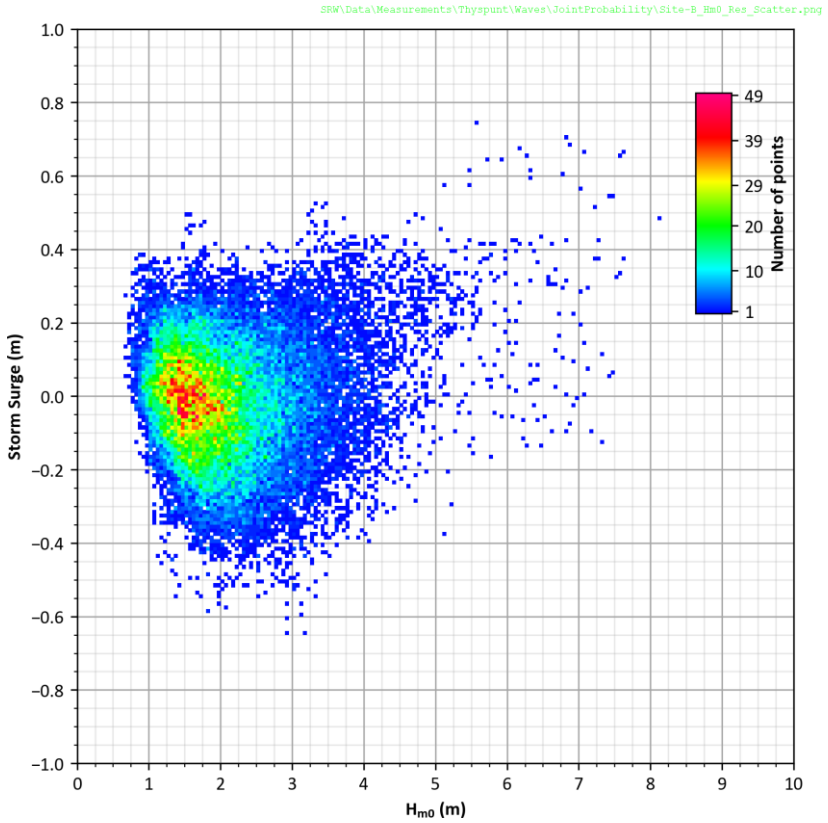


Figure 5.9-43: Scatterplot of Wave Height and Storm Surge at Thyspunt.

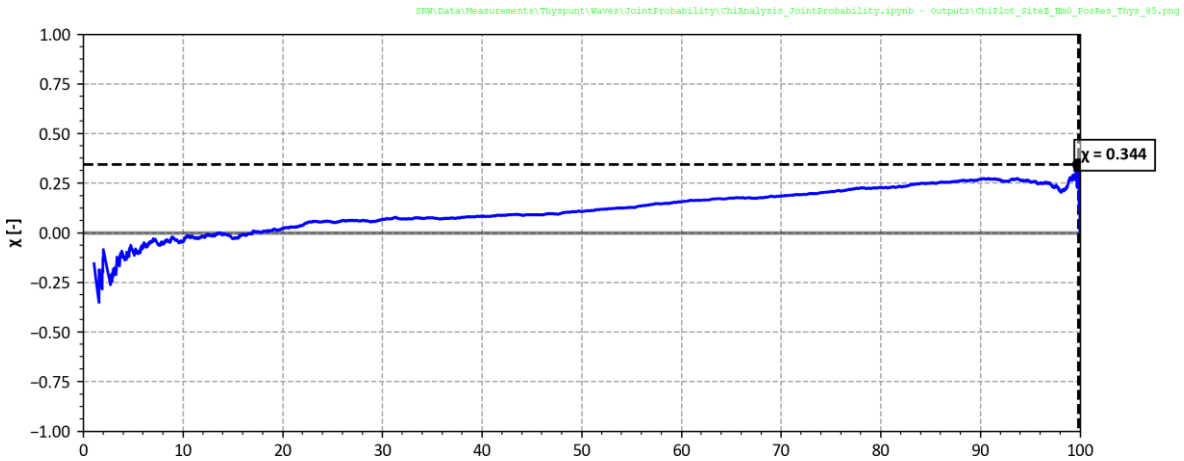


Figure 5.9-44: Dependence Parameter *χ* of Wave Height and Positive Storm Surge at Thyspunt.

The results show that χ has a maximum value of 0.344 which is categorised in ***Table 5.9-23*** as a "well" level of dependence. The reason that the correlation is not higher is that the waves are generated hundreds to thousands of kilometres offshore and do not arrive at the site at exactly the

CONTROLLED DISCLOSURE

When downloaded from the EDS database, this document is uncontrolled and the responsibility rests with the user to ensure it is in line with the authorised version on the database.

same time as the frontal weather systems which also generate the storm surge.

Equation 5.9.3 can then be used to calculate the joint exceedance frequencies as shown in ***Table 5.9-24***. For each joint exceedance frequency both combinations of storm surge and wave height have been modelled and the most conservative result has been selected.

Table 5.9-24: Joint Exceedance Frequency of Wave Height and Positive Storm Surge for χ = 0.344.

Joint Exceedance Frequency of Wave Height and Positive Storm Surge	Exceedance Frequency of Wave Height	Exceedance Frequency of Positive Storm Surge
(y^{-1})	(y^{-1})	(y^{-1})
1E-2	1E-2	8.45E-2
	8.45E-2	1E-2
1E-4	1E-4	8.45E-4
	8.45E-4	1E-4
1E-6	1E-6	8.45E-6
	8.45E-6	1E-6
1E-8	1E-8	8.45E-8
	8.45E-8	1E-8

5.9.10.4 Waves and Negative Storm Surge

Figure 5.9-43 shows the scatterplot of wave height and storm surge at Thyspunt. ***Figure 5.9-45*** shows the calculated dependence parameter χ of wave height and negative storm surge.

CONTROLLED DISCLOSURE

When downloaded from the EDS database, this document is uncontrolled and the responsibility rests with the user to ensure it is in line with the authorised version on the database.

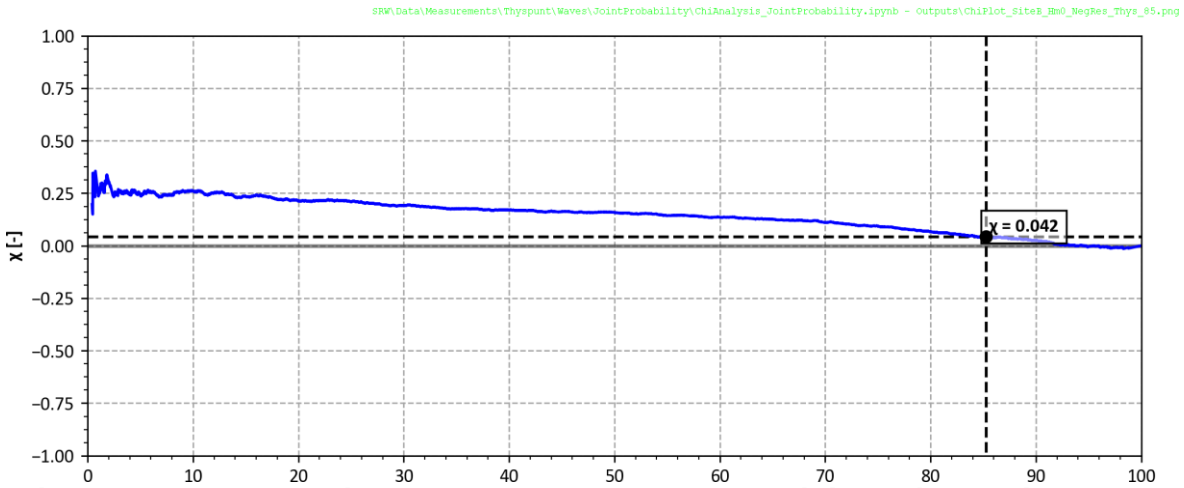


Figure 5.9-45: Dependence Parameter *χ* of Wave Height and Negative Storm Surge.

The results show that χ has a maximum value of 0.042 which is categorised in ***Table 5.9-23*** as a "zero" level of dependence. ***Equation 5.9.3*** can then be used to calculate the joint exceedance frequencies as shown in ***Table 5.9-25***. For each joint exceedance frequency both combinations of wave height and negative storm surge have been modelled and the most conservative result has been selected.

Table 5.9-25: Joint Exceedance Frequency of Wave Height and Negative Storm Surge for *χ* = 0.042.

Joint Exceedance Frequency of Wave Height and Negative Storm Surge	Exceedance Frequency of Wave Height	Exceedance Frequency of Negative Storm Surge
(y^{-1})	(y^{-1})	(y^{-1})
1E-2	1E-2	5.76
	5.76	1E-2
1E-4	1E-4	5.76E-2
	5.76E-2	1E-4
1E-6	1E-6	5.76E-4
	5.76E-4	1E-6
1E-8	1E-8	5.76E-6
	5.76E-6	1E-8

5.9.10.5 Waves and currents

The dataset used was the depth-averaged currents measured at Site B (see ***Subsection 5.9.9.4***) and the wave height measured at the same location (see ***Subsection 5.9.9.8***). ***Figure 5.9-46*** shows a scatterplot of these data

CONTROLLED DISCLOSURE

When downloaded from the EDS database, this document is uncontrolled and the responsibility rests with the user to ensure it is in line with the authorised version on the database.

using 45 564 hourly data pairs, equivalent to 5.2 years. Figure 5.9-47 shows the calculated dependence parameter χ of wave height and current speed.

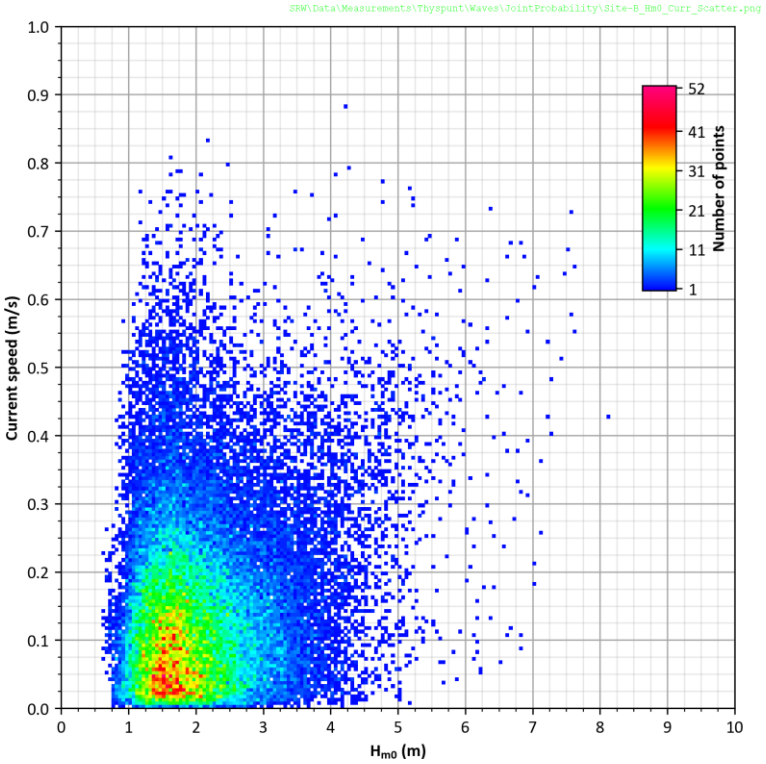


Figure 5.9-46: Scatterplot of Measured Wave Height and Depth-Averaged Current Speed at Thyspunt.

CONTROLLED DISCLOSURE

When downloaded from the EDS database, this document is uncontrolled and the responsibility rests with the user to ensure it is in line with the authorised version on the database.

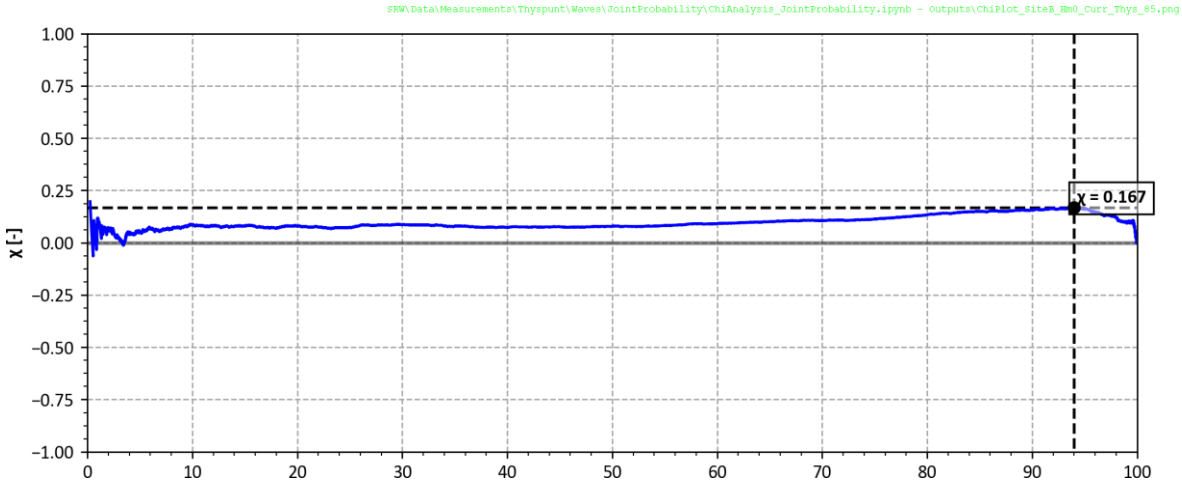


Figure 5.9-47: Dependence Parameter *χ* of Wave Height and Current Speed at Thyspunt.

The results show that χ has a maximum value above 85th percentile of 0.167, which is categorised in ***Table 5.9-23*** as a "modest" level of dependence. ***Equation 5.9.3*** can then be used to calculate the joint exceedance frequencies as shown in ***Table 5.9-26.*** For each joint exceedance frequency both combinations of wave height and current have been modelled and the most conservative result has been selected.

Table 5.9-26: Joint Exceedance Frequency of Wave Height and Current Speed for *χ* = 0.167.

Joint Exceedance Frequency of Wave Height	Exceedance Frequency of Wave Height	Exceedance Frequency of Current Speed
(y^{-1})	(y^{-1})	(y^{-1})
1E-2	1E-2	3.59E-1
	3.59E-1	1E-2
1E-4	1E-4	3.34E-3
	3.59E-3	1E-4
1E-6	1E-6	3.59E-5
	3.59E-5	1E-6
1E-8	1E-8	3.59E-7
	3.59E-7	1E-8

CONTROLLED DISCLOSURE

When downloaded from the EDS database, this document is uncontrolled and the responsibility rests with the user to ensure it is in line with the authorised version on the database.

5.9.11 Sediment Transport

In order to assess the stability of the coastline near the site, the following physical processes and timescales have been evaluated:

- Long-term coastline trends;
- The present-day sediment budget;
- Recession due to sea level rise;
- Coastline changes due to wave climate change;
- Erosion and sedimentation due to storms; and
- Erosion and sedimentation due to the cooling water outfall structure.

In addition, an analysis of suspended sand has been conducted to assess the potential for sedimentation in the intakes.

5.9.11.1 Long-Term Coastline Trends

Historical aerial images obtained from the Chief Directorate: National Geo-Spatial Information (CD:NGI) are available along the Cape St. Francis headland from 1954. ***Figure 5.9-48*** presents a composite map of the oldest historical images covering the entire area between Oyster Bay and St. Francis Bay from 1961 and a recent satellite image in August 2023 (Esri, 2024).

CONTROLLED DISCLOSURE

When downloaded from the EDS database, this document is uncontrolled and the responsibility rests with the user to ensure it is in line with the authorised version on the database.

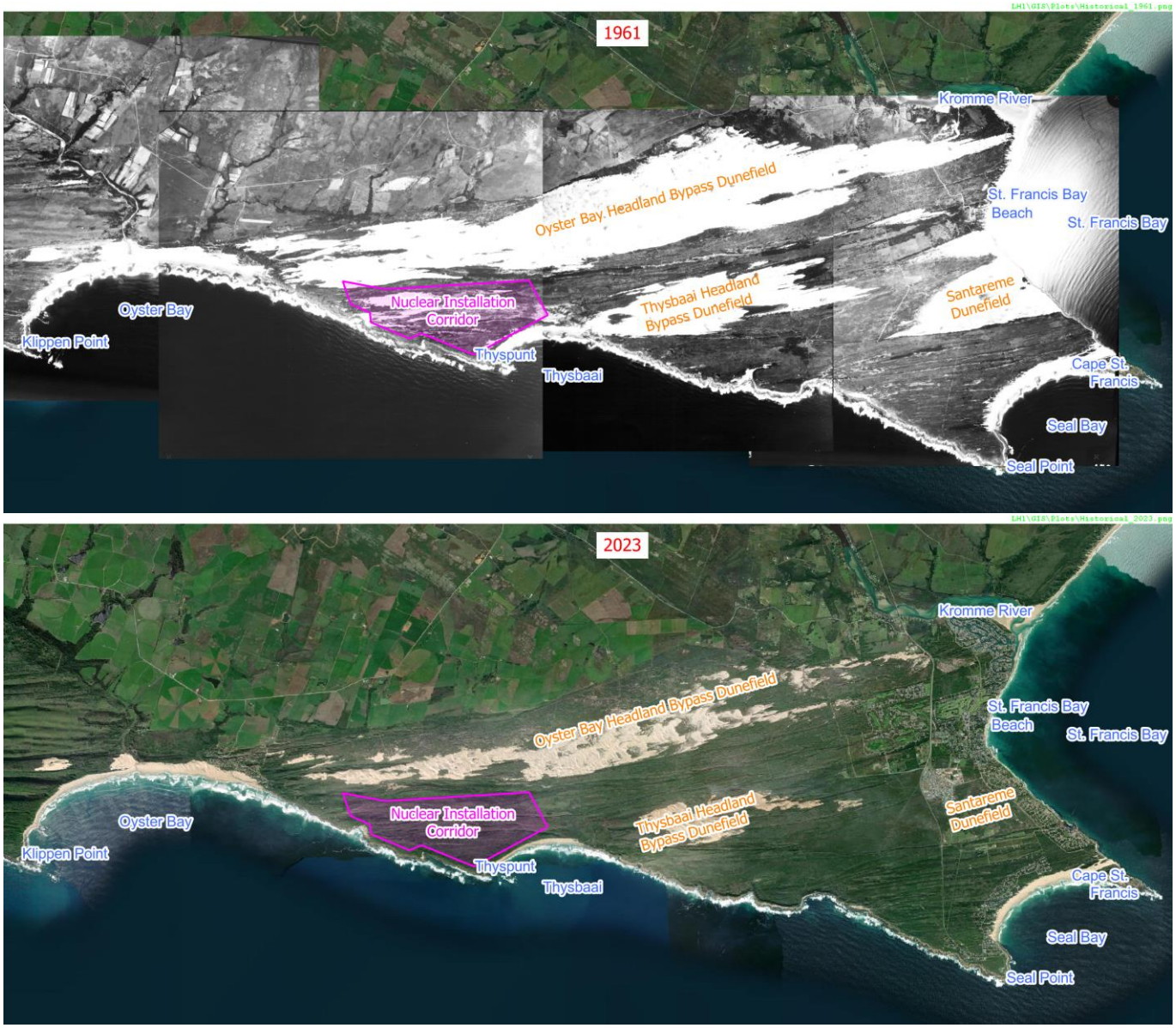


Figure 5.9-48: Historical Images of the Cape St. Francis Headland in 1961 (Top) and 2023 (Bottom).

On the Cape St. Francis headland, two large-scale headland-bypass dune corridors are recognised: the Oyster Bay Headland Bypass Dunefield (HBD) and the Thysbaai HBD, as well as the small Cape St Francis HBD system crossing the easternmost cape (see ***Figure 5.9-48***). Historically the Santareme dune field on the downwind (eastern) seaboard of the headland was present.

Historically, the aeolian (wind-driven) transport from these dune fields along with sediment deposits from the Kromme River nourished the beaches along St. Francis Bay. Although some regional eastward longshore

CONTROLLED DISCLOSURE

When downloaded from the EDS database, this document is uncontrolled and the responsibility rests with the user to ensure it is in line with the authorised version on the database.

sediment transport may have contributed to the budget, the aeolian transport was by far the largest fraction of the total sediment moving east of Cape St. Francis (WorleyParsons, 2014).

Between 1917 and 1924 approximately 100 hectares of drift sand were stabilised at the western end of the Oyster Bay HBD using the invasive species, Acacia cyclops. Between 1970 and 1980 the Santareme dune field was stabilised for the development of the Santareme Village, a holiday resort suburb in the area (Elkington, 2012). The stabilisation of the dune fields has reduced the aeolian transport potential from the area between Oyster Bay and Seal Point to supply sediment to the St. Francis Bay Beach area (WorleyParsons, 2014).

Construction of the Impofu dam upstream of Kromme River mouth, completed in 1983, has resulted in a lack of natural flushing of sediments to the coast which in turn has further reduced the volume of sand transported onto the beaches along St. Francis Bay (WorleyParsons, 2014).

Since the 1970's St. Francis Bay Beach has eroded some 40 to 50 m of which the bulk of the erosion has occurred in the post-dune stabilisation and post-dam construction era (ASR, 2006).

Figure 5.9-49 and ***Figure 5.9-50*** present historical aerial and satellite images of Oyster Bay and Thysbaai, respectively.

CONTROLLED DISCLOSURE

When downloaded from the EDS database, this document is uncontrolled and the responsibility rests with the user to ensure it is in line with the authorised version on the database.

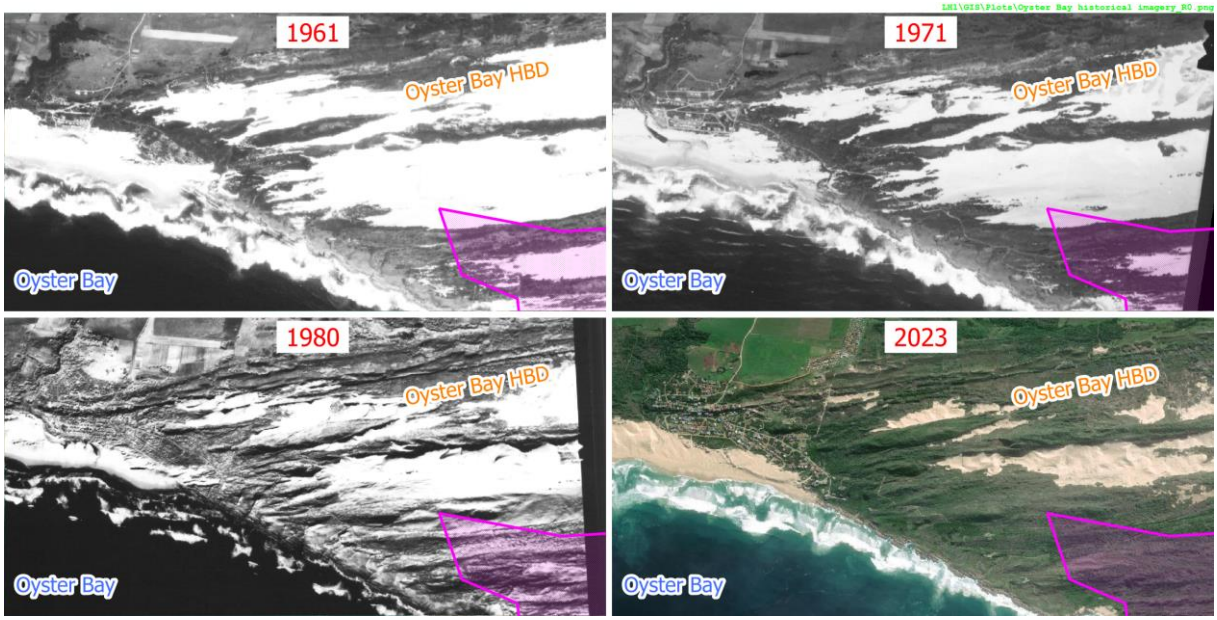


Figure 5.9-49: Historical Aerial and Satellite Images of Oyster Bay.

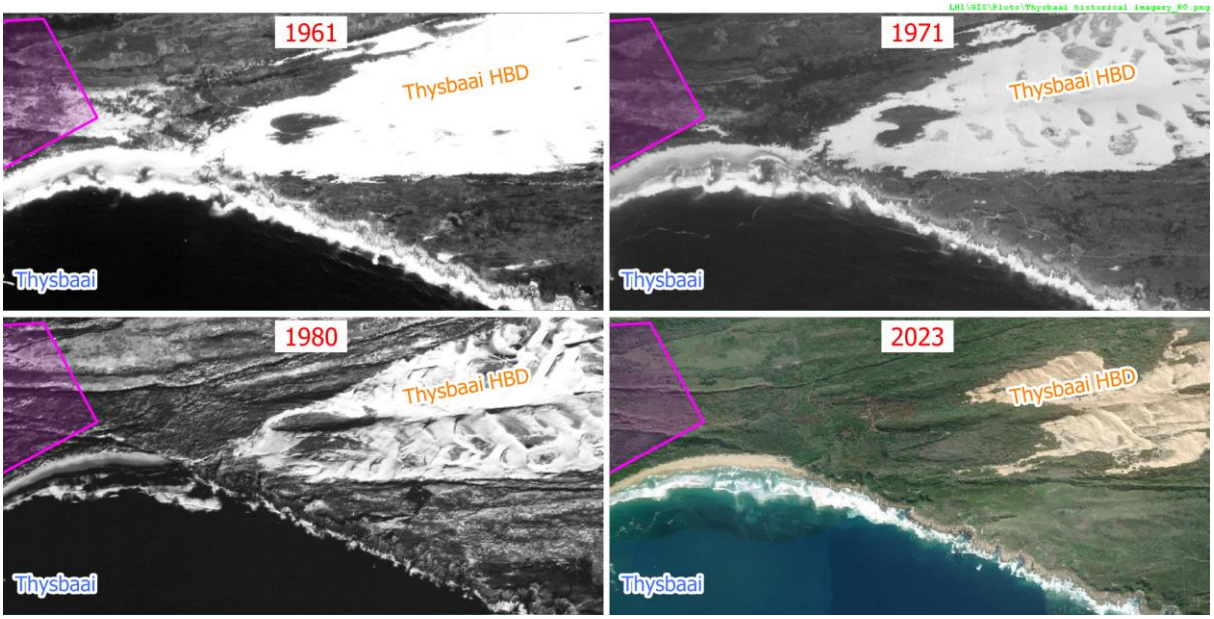


Figure 5.9-50: Historical Aerial and Satellite Images of Thysbaai.

The historical images indicate that the Oyster Bay and Thysbaai dunes were stabilised between 1971 and 1980 during which the aeolian transport losses from the beach into the HBD systems would have reduced significantly. By 2023 large areas of the Oyster Bay and Thysbaai HBD systems have become vegetated.

The long-term coastline trends at Oyster Bay and Thysbaai beaches have been analysed from beach profile surveys, LiDAR surveys, historical

When downloaded from the EDS database, this document is uncontrolled and the responsibility rests with the user to ensure it is in line with the authorised version on the database.

satellite and aerial images and the Digital Earth Africa Map Coastlines (2024) database, as discussed below.

Beach profiles have been measured since 2008 at 20 locations as part of the oceanographic monitoring programme for this SSR. Details of the profile locations, instruments, sampling intervals, dates and number of surveys are provided in ***Subsection 5.9.6.1***.

Examples of the measured beach profiles for Profiles 03, 10, 27 and 38 are shown in ***Figure 5.9-51*** to ***Figure 5.9-54*** (see ***Figure 5.9-2*** for the locations of these beach profiles). The full set of profiles is presented in the TSSR Ch 5.9 2 Yrs Oceanographic Monitoring Data report (PRDW, 2019), with the exception of the profiles surveyed in 2024. Also shown are profiles extracted from the LiDAR surveys of Thyspunt by Southern Mapping Geospatial in 2008 (SRK, 2008) and 2011 (SRK, 2011).

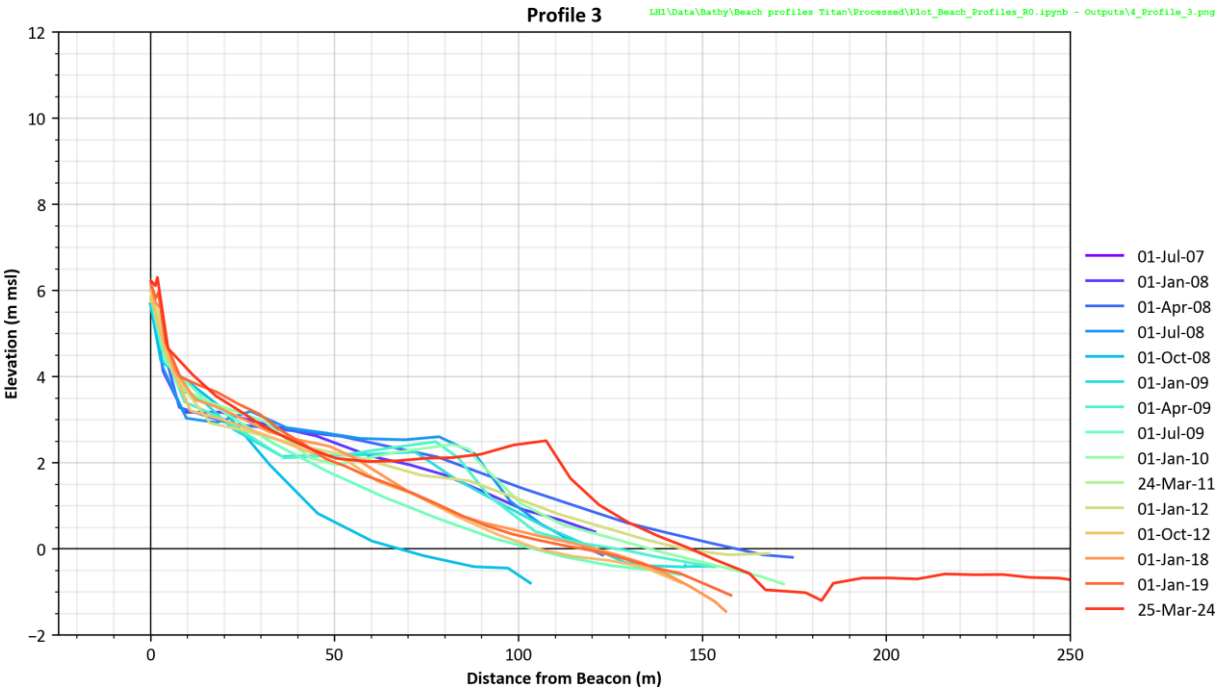


Figure 5.9-51: Measured Beach Profiles at Profile 03: Western End of Oyster Bay.

CONTROLLED DISCLOSURE

When downloaded from the EDS database, this document is uncontrolled and the responsibility rests with the user to ensure it is in line with the authorised version on the database.

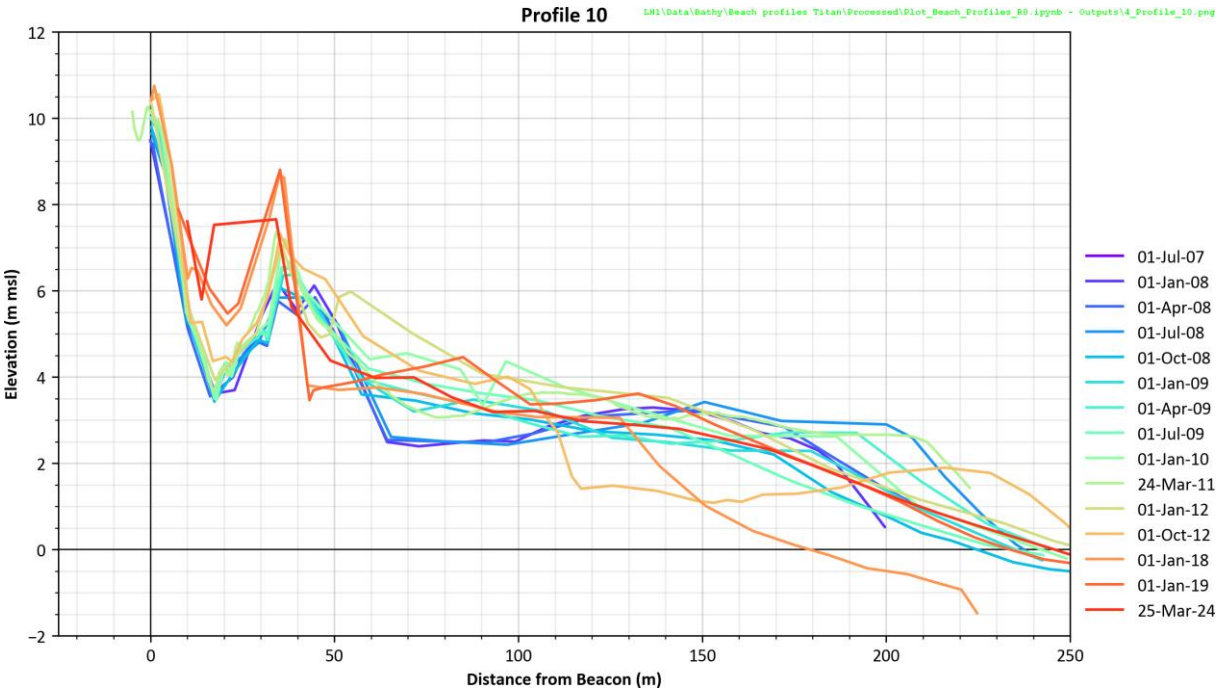


Figure 5.9-52: Measured Beach Profiles at Profile 10: Eastern End of Oyster Bay.

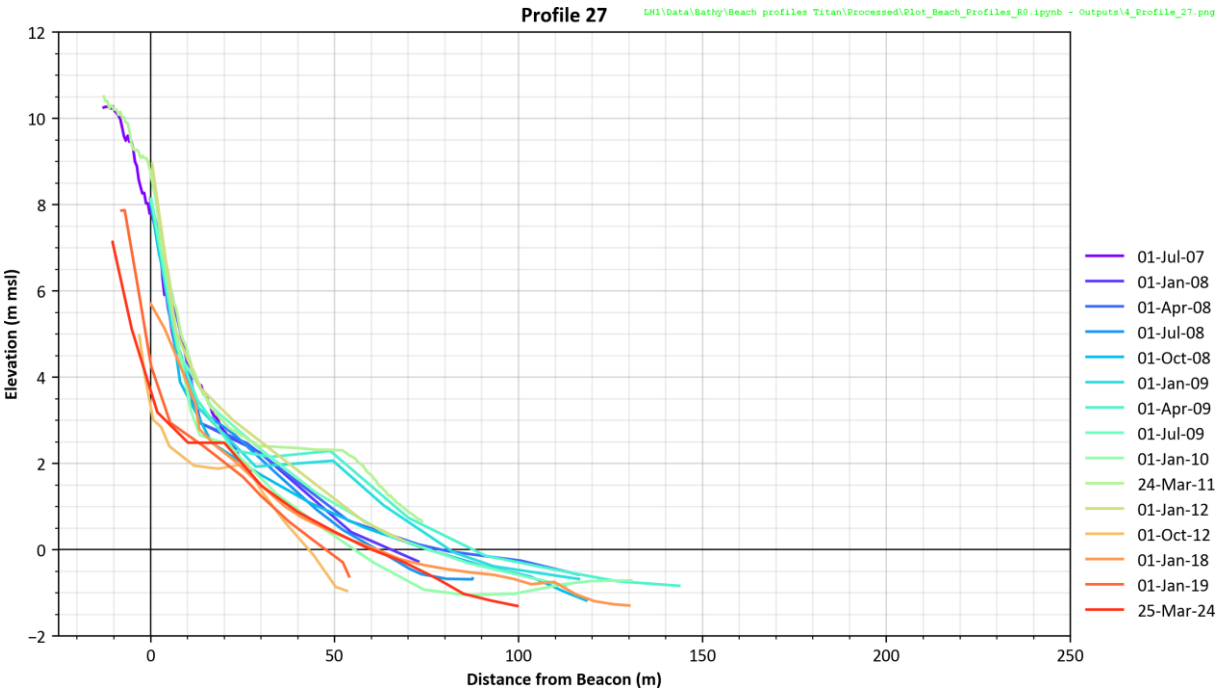


Figure 5.9-53: Measured Beach Profiles at Profile 27: Western End of Thysbaai.

CONTROLLED DISCLOSURE

When downloaded from the EDS database, this document is uncontrolled and the responsibility rests with the user to ensure it is in line with the authorised version on the database.

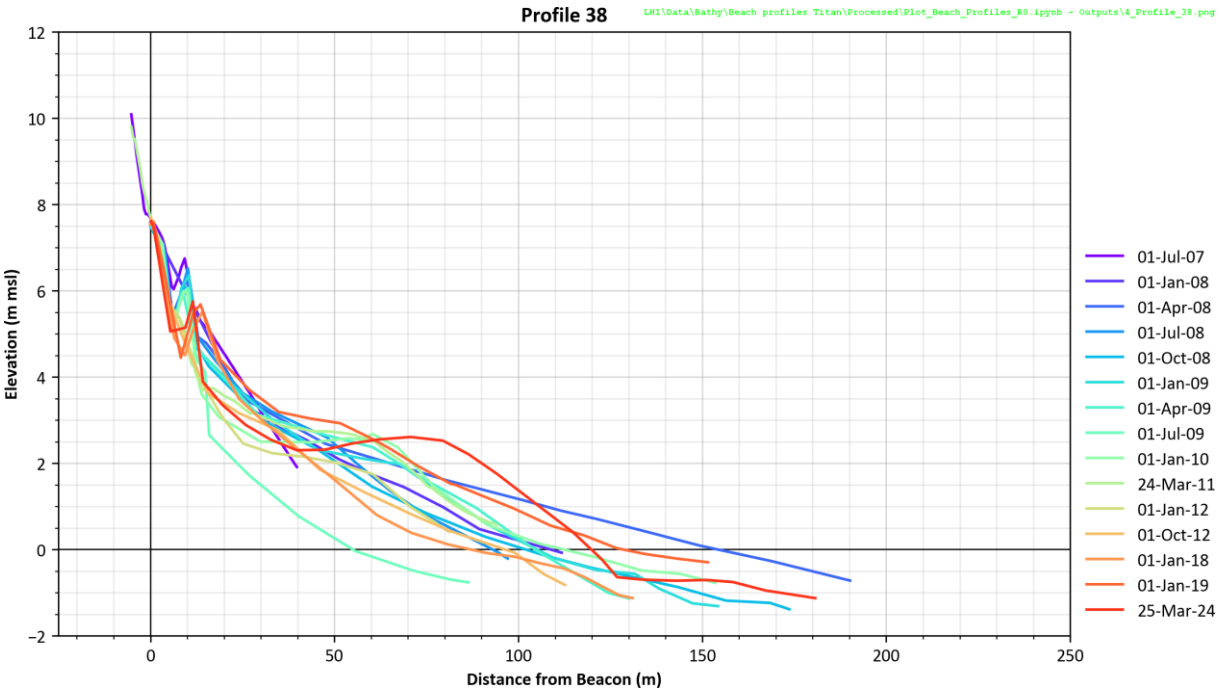


Figure 5.9-54: Measured Beach Profiles at Profile 38: Eastern End of Thysbaai.

To analyse the long-term trends, the horizontal distances from the beacon of the beach profile to the 0, +1, +2, +3, +4, +5 and +6 m msl levels on the profiles have been extracted for each of the profiles. Trend lines have been fitted to the data and the slopes of the trend lines have been used to estimate erosion/accretion rates for each profile based on the horizontal changes at these elevations. Examples are shown in ***Figure 5.9-55*** and ***Figure 5.9-56*** for the +2 m msl levels on Oyster Bay and Thysbaai, respectively.

CONTROLLED DISCLOSURE

When downloaded from the EDS database, this document is uncontrolled and the responsibility rests with the user to ensure it is in line with the authorised version on the database.

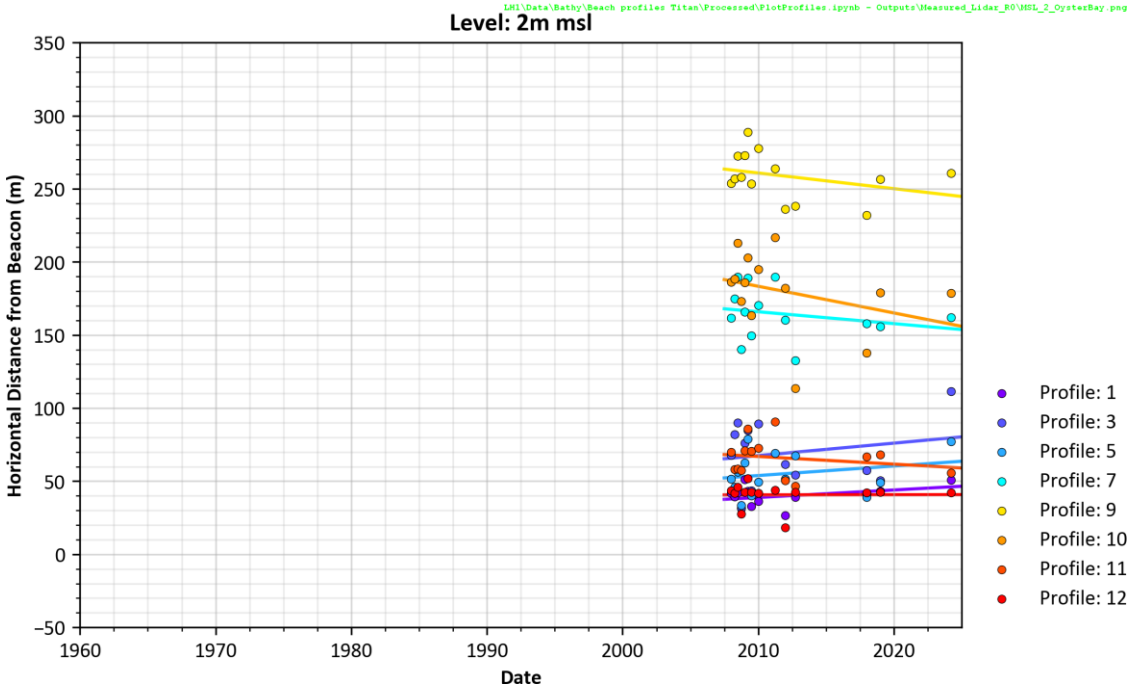


Figure 5.9-55: Horizontal Movement of the +2 m msl Level Over Time on Oyster Bay.

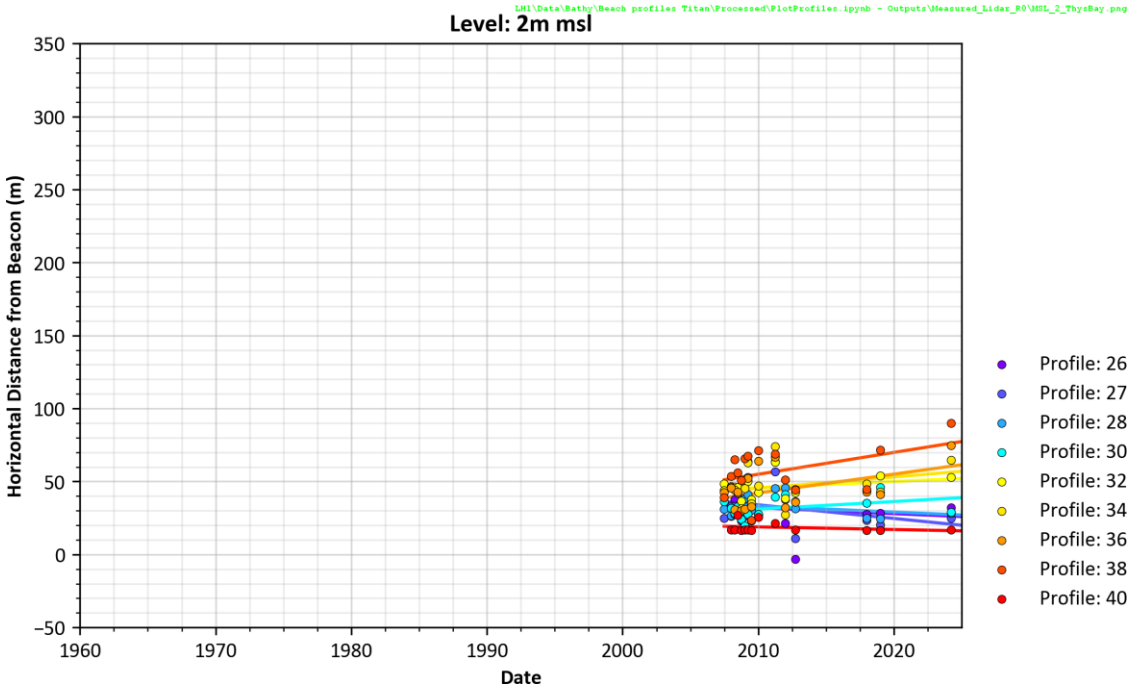


Figure 5.9-56: Horizontal Movement of the +2 m msl Level Over Time on Thysbaai.

The horizontal movement of the wetted line was extracted from aerial images from CD:NGI for 1961 to 1986, from the imagery produced with the

CONTROLLED DISCLOSURE

When downloaded from the EDS database, this document is uncontrolled and the responsibility rests with the user to ensure it is in line with the authorised version on the database.

LiDAR surveys (2008 and 2011), and from a recent satellite image (2023). In each image the previous wet/dry interface on the coastline was defined as the wetted line. Although the position of the wetted line depends on the tide, storm surge, and wave conditions in addition to variability in the position and slope of the beach profile, this data provides valuable insight into long-term stability not available from the beach profile survey data. ***Figure 5.9-57*** shows the wetted line along Oyster Bay and Thysbaai from 1961 to 2023. ***Figure 5.9-58*** and ***Figure 5.9-59*** present the horizontal movement of the wetted line along each of the surveyed beach profiles relative to the beacon of each profile.

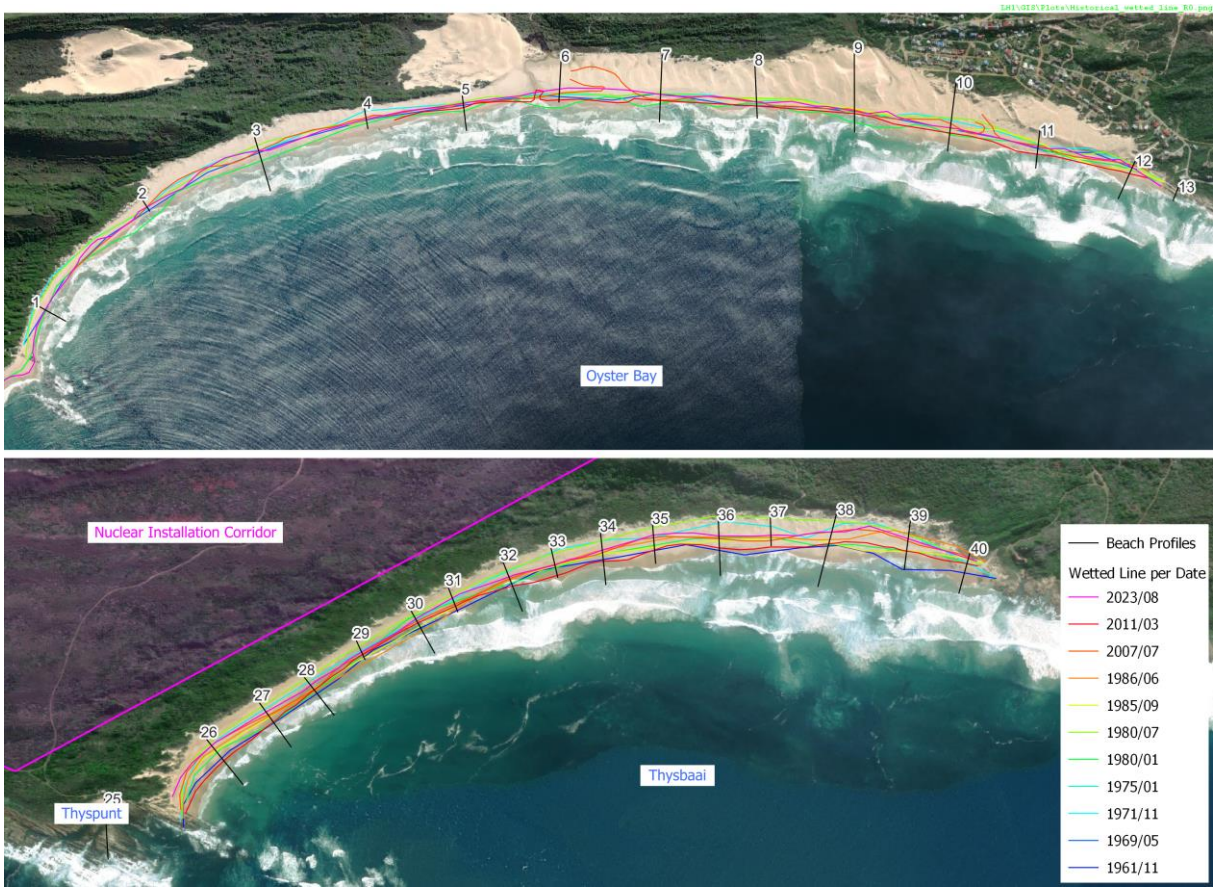


Figure 5.9-57: Historical Wetted Line Along Oyster Bay (Top) and Thysbaai (Bottom) from 1961 to 2023.

CONTROLLED DISCLOSURE

When downloaded from the EDS database, this document is uncontrolled and the responsibility rests with the user to ensure it is in line with the authorised version on the database.

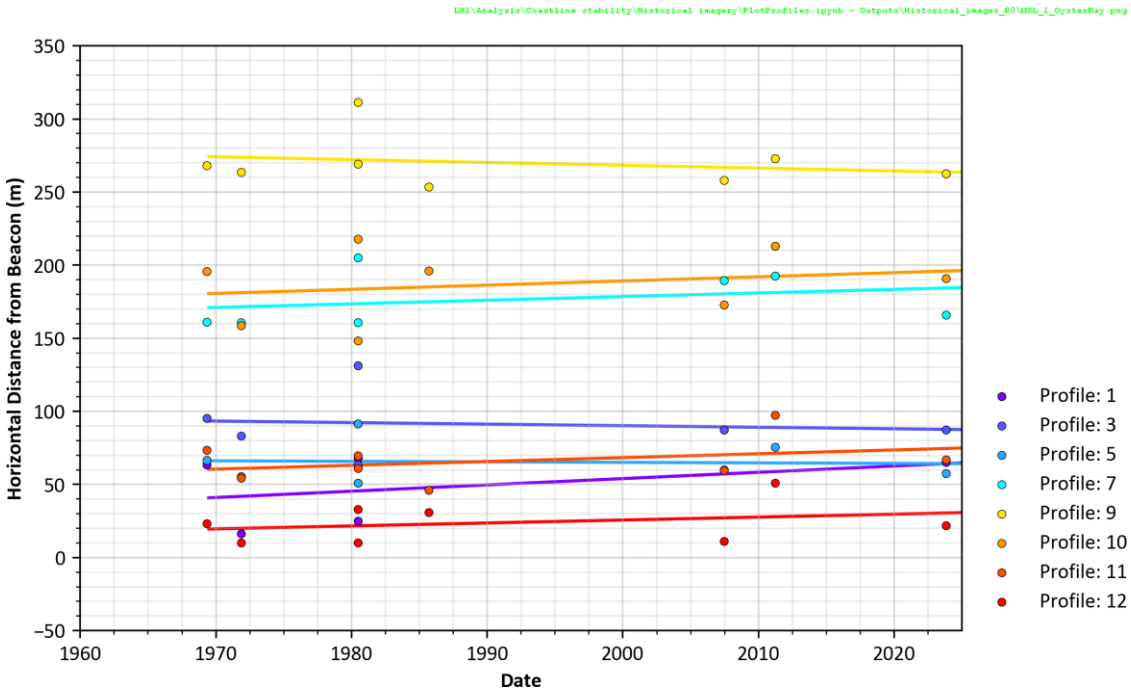


Figure 5.9-58: Horizontal Movement of the Wetted Line from Historical Images Over Time on Oyster Bay.

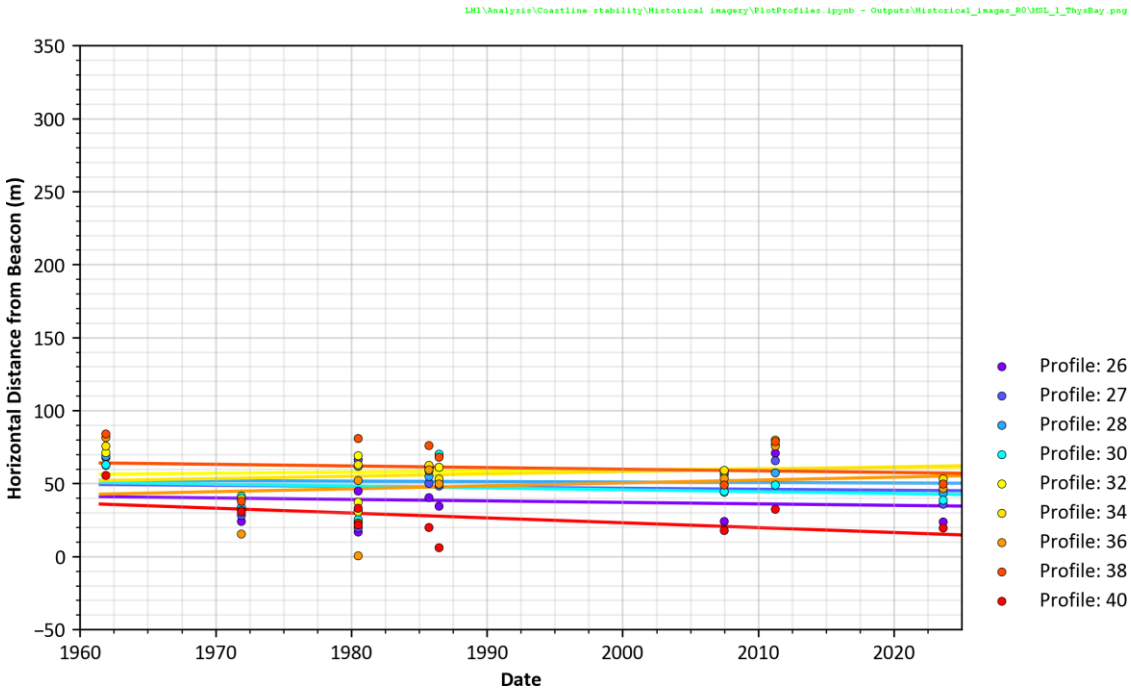


Figure 5.9-59: Horizontal Movement of the Wetted Line from Historical Images Over Time on Thysbaai.

The Digital Earth Africa Map (further referred to as DE Africa) developed by the Australian Commonwealth Scientific and Industrial Research

CONTROLLED DISCLOSURE

When downloaded from the EDS database, this document is uncontrolled and the responsibility rests with the user to ensure it is in line with the authorised version on the database.

Organisation in collaboration with Geoscience Australia, provides map-based access to spatial information for the African continent (Digital Earth Africa Map, 2024). The DE Africa Coastlines monitoring service uses Landsat Collection 2 and Sentinel-2 satellite images since 2000 to map the location of the African coastline over time, corrected to a consistent tide height of mean level (0.2 m msl). The coastline data from each image is further processed to provide the following:

- The median position of the coastline throughout each year;
- The rate of coastal change in metres per year for every 30 m along non-rocky coastlines, calculated by linear regression of the annual coastline positions against time.

The median positions of the coastline at Oyster Bay and Thyspunt were used to obtain the horizontal movement of the coastline along each of the surveyed beach profiles relative to the beacon of each profile, as shown in ***Figure 5.9-60*** and ***Figure 5.9-61***.

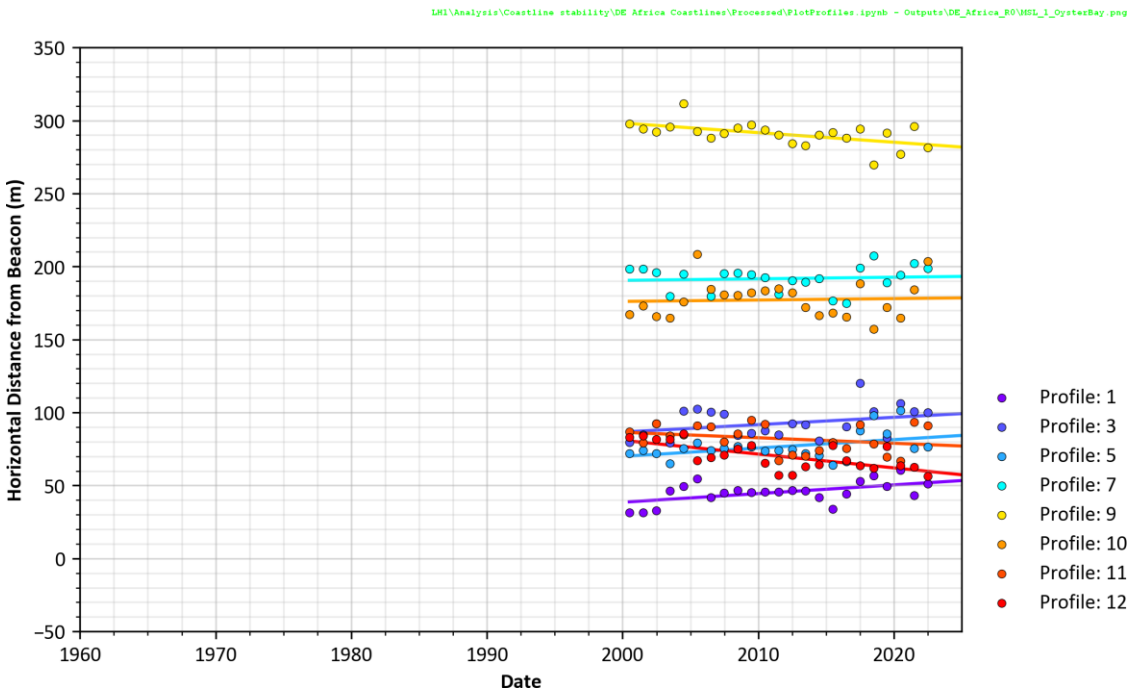


Figure 5.9-60: Horizontal Movement of the Coastline from Satellite Imagery Over Time on Oyster Bay.

CONTROLLED DISCLOSURE

When downloaded from the EDS database, this document is uncontrolled and the responsibility rests with the user to ensure it is in line with the authorised version on the database.

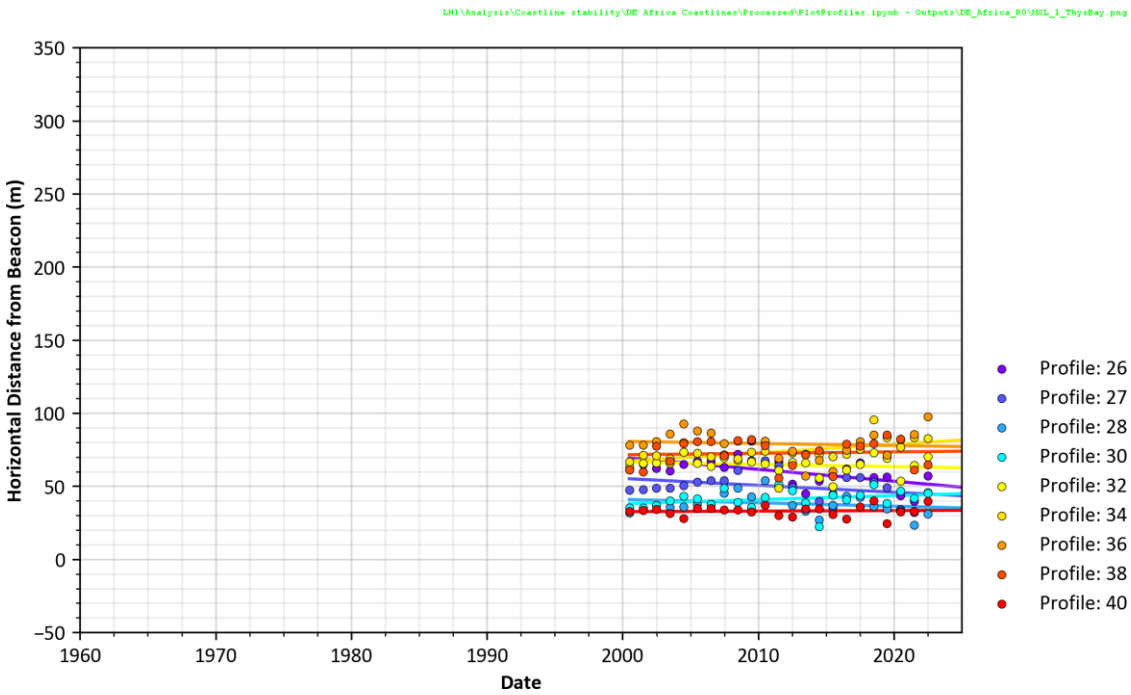


Figure 5.9-61: Horizontal Movement of the Coastline from Satellite Imagery Over Time on Thysbaai.

The average erosion/accretion rate over the 0 to +6 m msl elevations of the beach profiles was compared to the trends from the historical wetted line analysis and the DE Africa Coastlines, as shown in ***Figure 5.9-62***.

CONTROLLED DISCLOSURE

When downloaded from the EDS database, this document is uncontrolled and the responsibility rests with the user to ensure it is in line with the authorised version on the database.

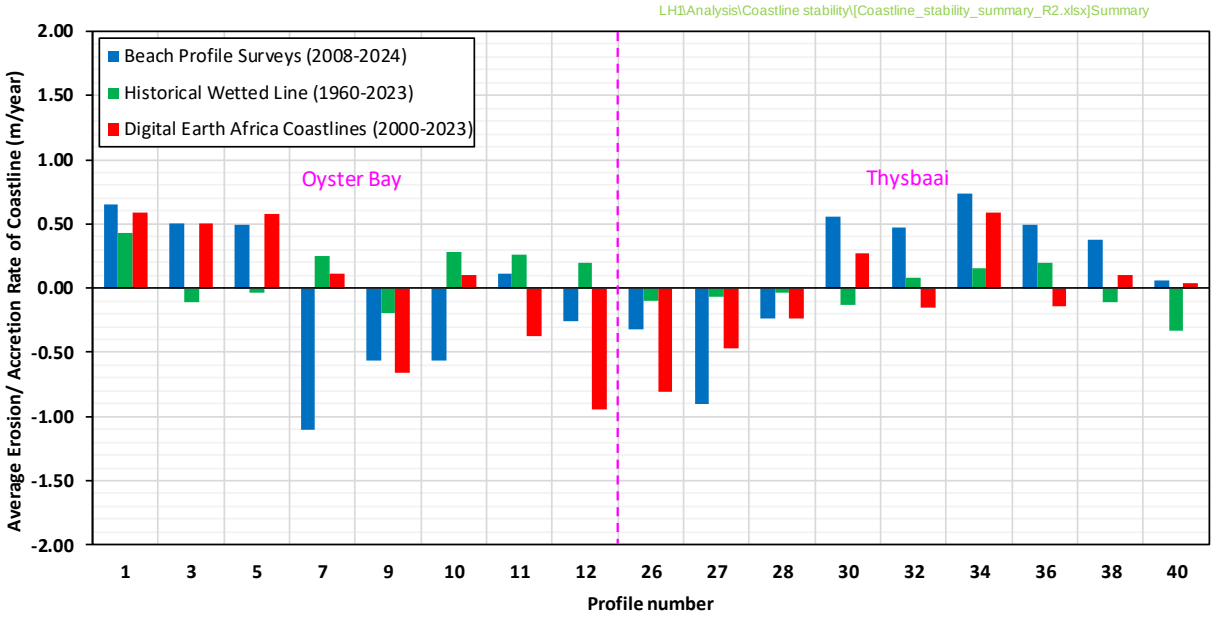


Figure 5.9-62: Long-Term Coastline Trends from Measured Beach Profile Surveys, Historical Wetted Lines from Aerial Imagery and Digital Earth Africa Coastlines (2024).

These results show the following:

- The beach profile analysis indicates trends of coastline rotation on Oyster Bay (accretion in the west and erosion in the east) and Thysbaai (erosion in the west and accretion in the east) over the recent period of 2008-2024. These trends are in reasonable agreement with the analysis of satellite imagery (Digital Earth Africa Map, 2024) over the period of 2000-2023.
- The analysis of wetted lines from historical imagery over the last 60 years (1961-2023) shows that Oyster Bay and Thysbaai have been approximately stable over the long-term. This suggests that the coastline rotations observed in the recent data are short-term or cyclical changes rather than continuous long-term trends.
- The wetted line analysis includes historical images before and after the stabilisation of the dunes at Oyster Bay and Thysbaai in the 1970's and shows no discernible systematic change in the beach stability before and after stabilisation. This supports that the stability of Thysbaai is not sensitive to aeolian losses from the beach into the Thysbaai HBD, nor to changes in sediment supply from Oyster Bay driven by aeolian losses to the Oyster Bay HBD system. Thus, the future stability of Thysbaai is not dependent on whether the HBD systems are active or inactive.

CONTROLLED DISCLOSURE

When downloaded from the EDS database, this document is uncontrolled and the responsibility rests with the user to ensure it is in line with the authorised version on the database.

- The coastline changes that have occurred at St. Francis Bay Beach are not applicable at the Oyster Bay and Thysbaai beaches. Historically, the St. Francis Bay beaches were predominantly supplied by aeolian and alluvial sediment transport whereas the Oyster Bay and Thysbaai beaches are not sensitive to aeolian transport and the budget is dominated by coastal sediment transport (discussed in ***Subsection 5.9.11.2***).
- Therefore, there is no evidence of significant long-term coastline trends at Thysbaai and no trends were applied in this SSR.

5.9.11.2 Present-Day Sediment Budget

The MIKE 21 Sand Transport model was used to determine the present-day sediment budget. The model was run for one year of morphology under the forcing of a representative year of operational waves and wind-driven currents, and considering limited sand supply due to exposed bedrock as described in ***Subsection 5.9.8***. Details of the model description, setup, calibration, and cases modelled are provided in ***Appendix 5.9.A.3.***

Figure 5.9-63 presents an example of the instantaneous waves, depth-averaged currents, surface elevation, and sediment transport during a large south westerly wave event (H_{m0} = 8.1 m on the model boundary) and a strong (20 m/s) westerly wind. The annual net transport including vectors (plotted on a log scale) are presented in ***Figure 5.9-64***, with ***Figure 5.9-65*** presenting the annual bed level change.

CONTROLLED DISCLOSURE

When downloaded from the EDS database, this document is uncontrolled and the responsibility rests with the user to ensure it is in line with the authorised version on the database.

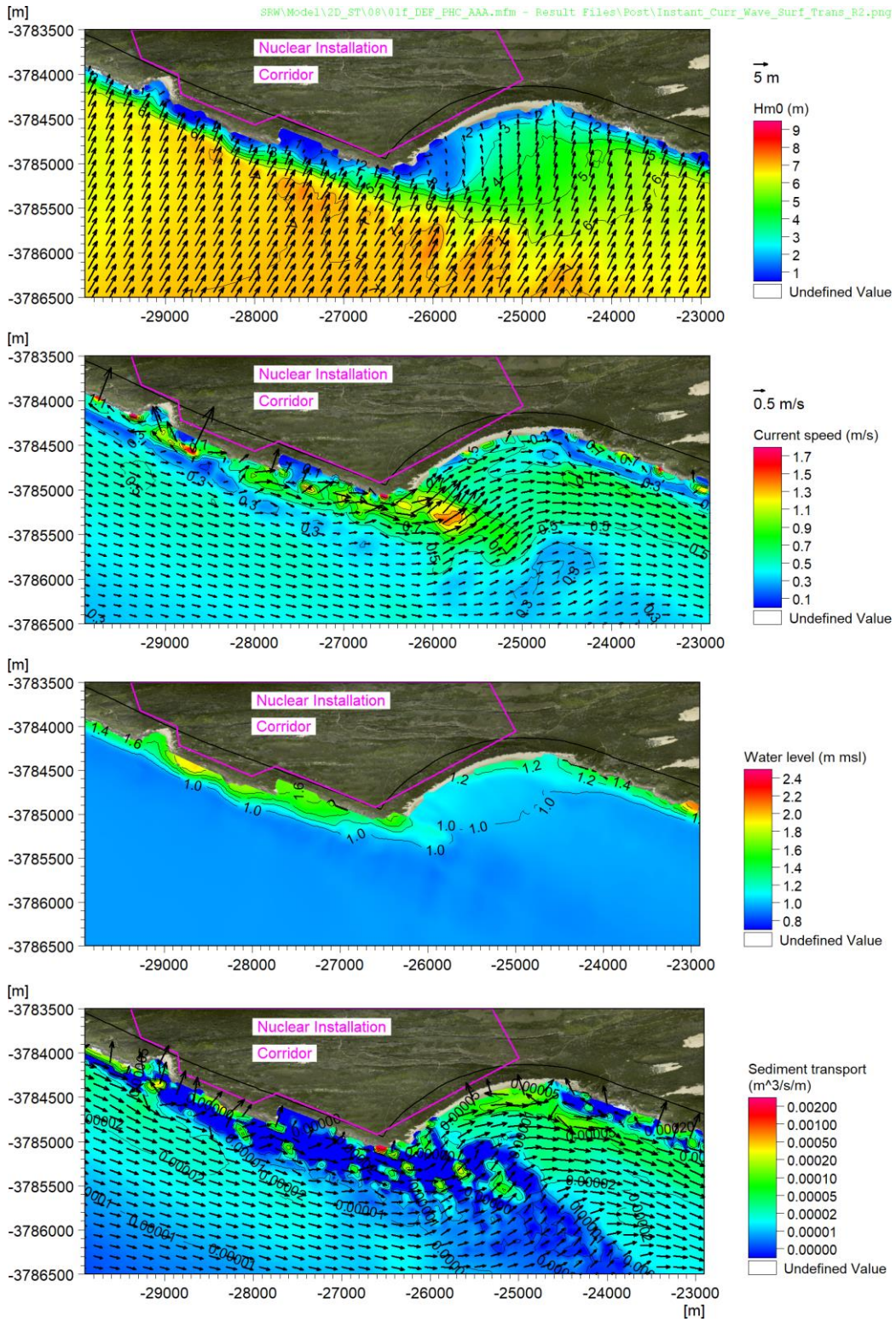


Figure 5.9-63: Example Results of Operational Conditions During a Large Wave Event Showing Instantaneous Waves, Currents, Sediment Transport, and Surface Elevation. The Sediment Transport Vectors are Plotted on a Log Scale.

CONTROLLED DISCLOSURE

When downloaded from the EDS database, this document is uncontrolled and the responsibility rests with the user to ensure it is in line with the authorised version on the database.

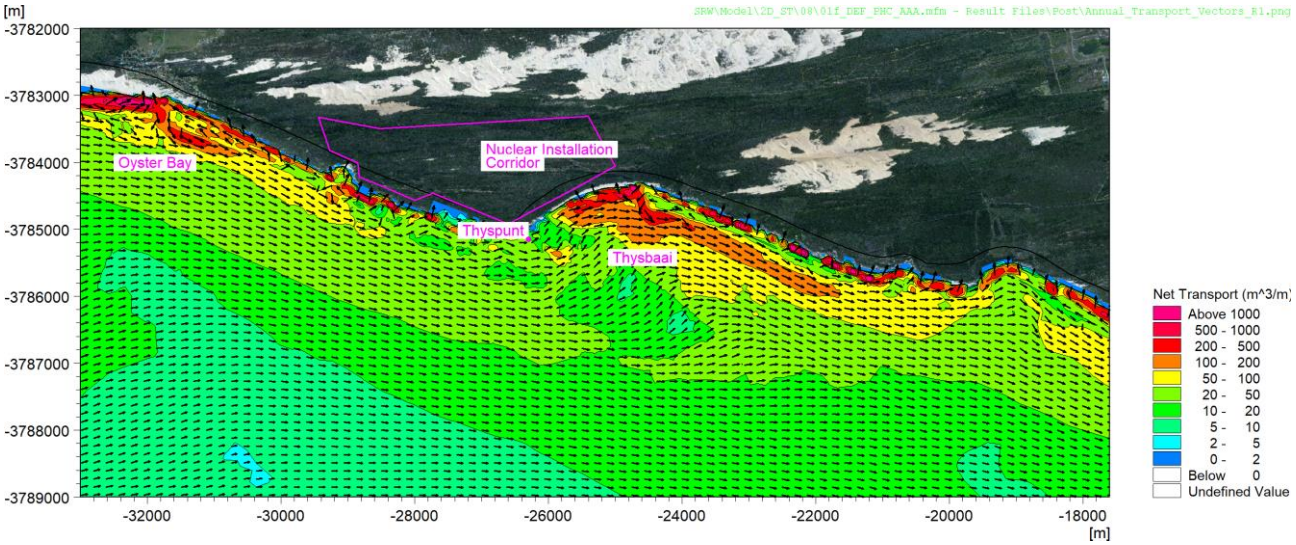


Figure 5.9-64: Annual Net Transport Including Vectors (Plotted on a Log Scale) for the Present-Day Case.

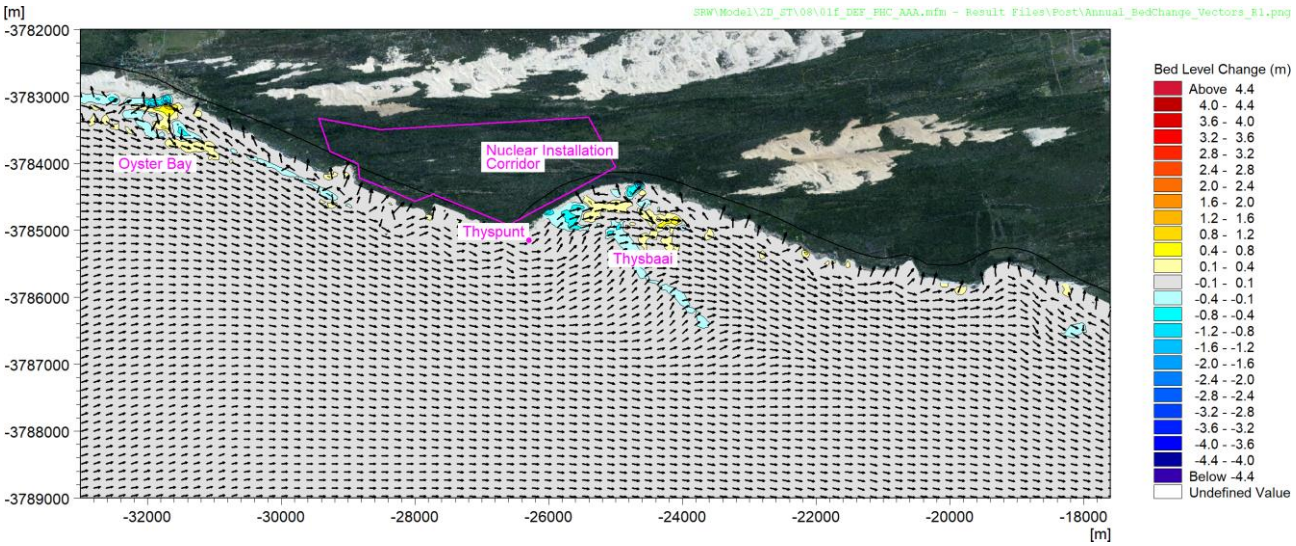


Figure 5.9-65: Annual Bed Level Change Including Annual Net Transport Vectors (Plotted on a Log Scale) for the Present-Day Case.

The sediment transport through 33 cross-shore profiles, labelled “1” to “33” in ***Figure 5.9-66*** was calculated. ***Figure 5.9-67*** presents a timeseries of the cumulative transport over the modelled year at Profiles 6 and 30. The net transports for each of the profiles shown in ***Figure 5.9-66*** are presented in ***Figure 5.9-68***. The sediment transport budget for the present day is summarised in ***Table 5.9-27***, in which the profiles have been separated into two sections: Section 1, west of Thysbaai, for profiles 1 to 15 and Section 2, east of Thysbaai, for profiles 16 to 33.

CONTROLLED DISCLOSURE

When downloaded from the EDS database, this document is uncontrolled and the responsibility rests with the user to ensure it is in line with the authorised version on the database.

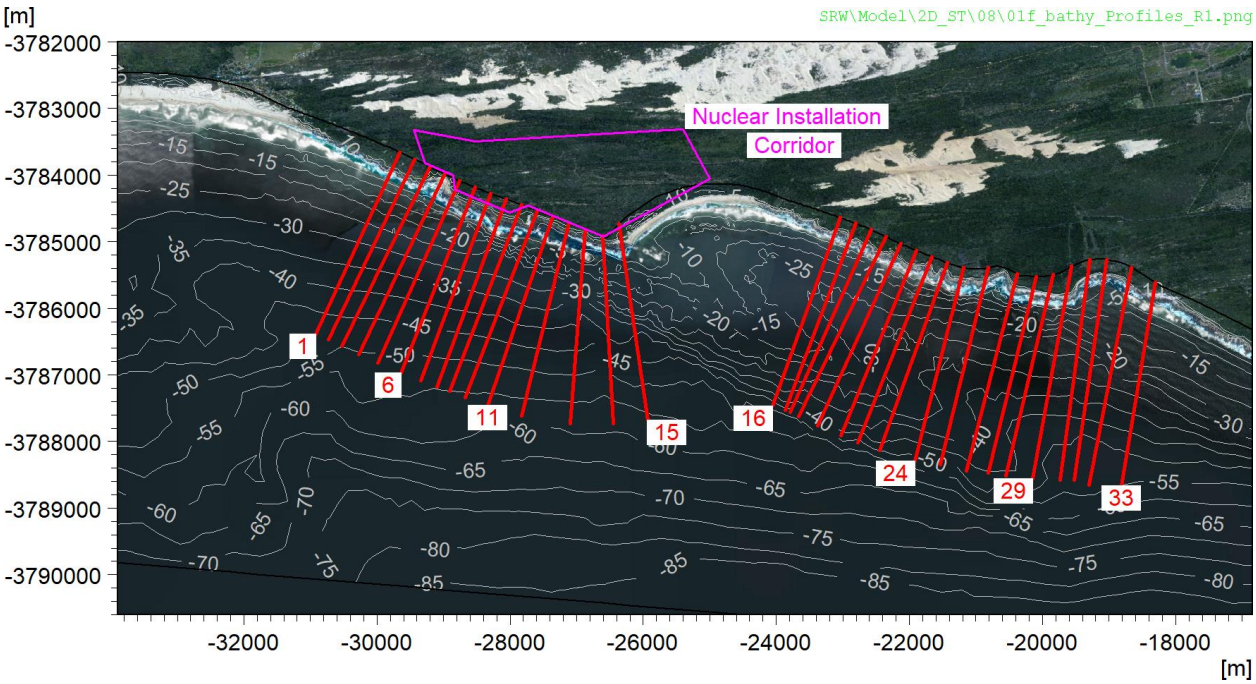


Figure 5.9-66: Location of Profiles 1 to 33 Used to Calculate the Sediment Budget at the Site.

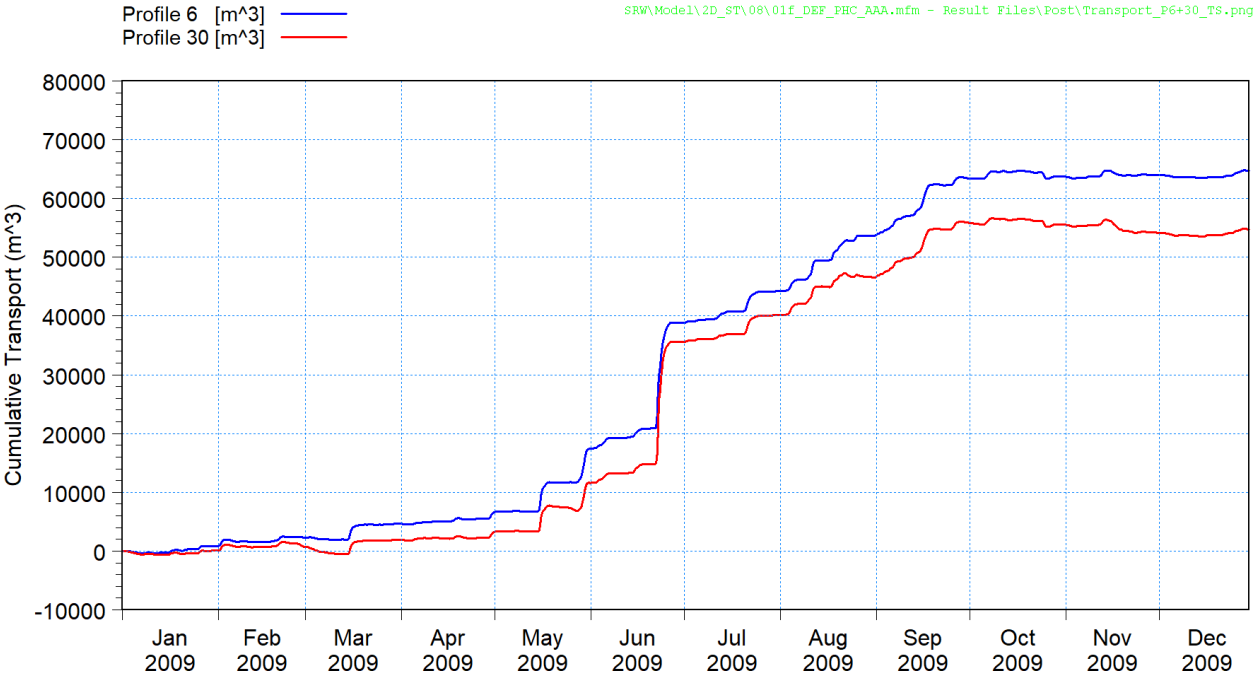


Figure 5.9-67: Cumulative Transport for Profiles 6 and 30 for the Present-Day Case. Positive Transport is Eastward.

CONTROLLED DISCLOSURE

When downloaded from the EDS database, this document is uncontrolled and the responsibility rests with the user to ensure it is in line with the authorised version on the database.

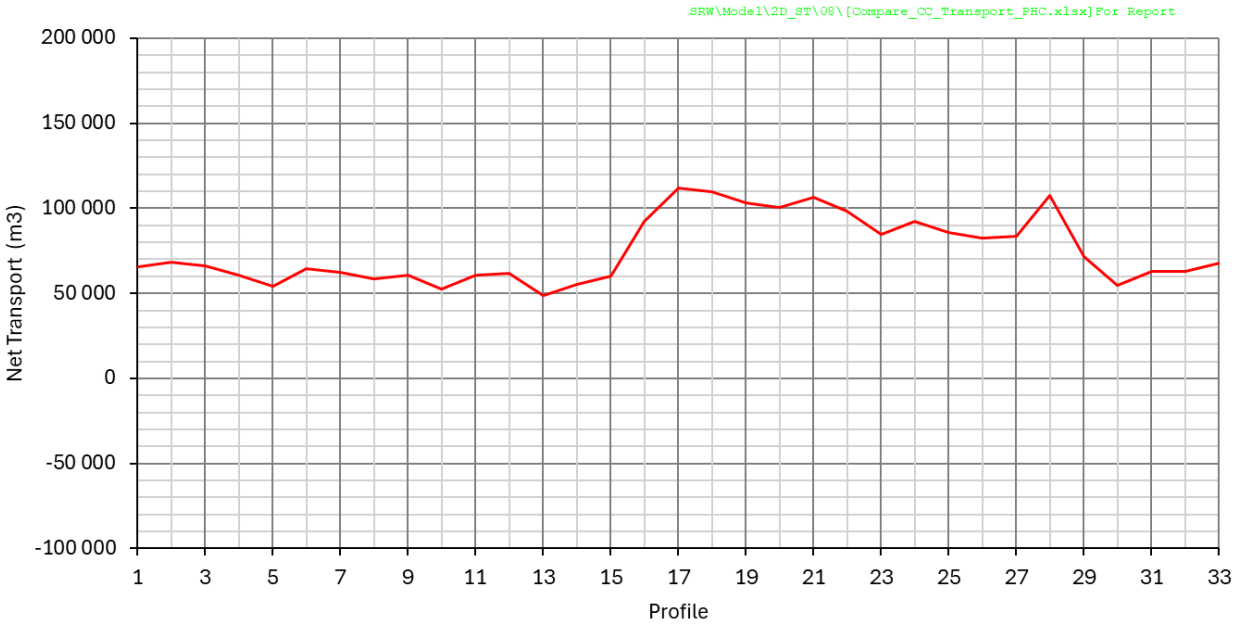


Figure 5.9-68: Net Transport per Profile for the Present-Day Case. Positive Transport is Eastward.

Table 5.9-27: Present-Day Sediment Budget.

Section	Net Transport	Gross Transport	Westward Transport	Eastward Transport
	(m^3/y)	(m^3/y)	(m^3/y)	(m^3/y)
1	60 000	80 000	10 000	70 000
2	90 000	100 000	10 000	100 000

The results indicate the following:

- The rocky coastline between Oyster Bay and Thyspunt is characterised by rip cells and limited sediment supply. Offshore of the rocks where more sand is available the net transport is eastwards due to wave and wind-driven currents.
- There is a constant net transport eastward along the coast from Oyster Bay into Thysbaai of approximately 60 000 m^3/y.
- Within Thysbaai the net transport remains eastward, although a small westward wave-driven transport eddy occurs at the beach.
- The rocky coastline east of Thysbaai has a net eastward transport as a continuation of the transport from within Thysbaai, although the transport directly against the coastline is westwards.

CONTROLLED DISCLOSURE

When downloaded from the EDS database, this document is uncontrolled and the responsibility rests with the user to ensure it is in line with the authorised version on the database.

- The model results show a net transport out of Thysbaai to the east of approximately 90 000 m^3/y but reduces back to approximately 60 000 m^3/y 2.5 km east of Thysbaai (Profiles 29 to 33).
- Overall, the transport into and out of Thysbaai is therefore approximately in balance for the representative year modelled, at a rate of between 60 000 and 90 000 m^3/y. In general, the transport through the bay is limited by the supply.
- Thysbaai beach is therefore considered to be in a state of dynamic equilibrium, which is supported by the analysis of historical trends (***Subsection 5.9.11.1***).

5.9.11.3 Recession due to Sea Level Rise

The shore response model proposed by Bruun (1962) has been applied to estimate coastline recession due to long-term sea level rise at the site. The basic assumption behind the Bruun Rule is that with a rise in sea level, the equilibrium profile of the beach and the nearshore moves upward and landward conserving both mass and the original profile according to the following assumptions:

- The upper beach erodes because of a landward translation of the profile.
- Sediment eroded from the upper beach is deposited immediately offshore, with the eroded and deposited volumes being equal.
- The rise in the nearshore seafloor is equal to the rise in sea level.

The Bruun Rule is considered as a standard approach to coastline recession in coastal engineering applications, e.g., The Coastal Engineering Manual (USACE, 2002b). There are several limitations which have been discussed in literature, e.g., Ranasinghe and Stive (2009), Shand, et al., (2013), however most of these limitations are not applicable for the application of the Bruun Rule at this site, as discussed below:

- Time is required for the equilibrium profile to be established, however, for this application the timescale of SLR at the site (see ***Table 5.9-8***) is large compared to the timescale of the beach profile reshaping processes.
- The Bruun Rule does not accommodate erosion/accretion due to gradients in alongshore sediment transport or changes in the sediment supply. However, for this application the erosion/accretion due to these processes are evaluated separately (see ***Subsections 5.9.11.1***, ***5.9.11.2***, and ***5.9.11.4***).

CONTROLLED DISCLOSURE

When downloaded from the EDS database, this document is uncontrolled and the responsibility rests with the user to ensure it is in line with the authorised version on the database.

- The Bruun Rule assumes uniform sediment size along the profile and does not account for control by hard structures such as substrate geology or adjacent headlands. For this SSR adjustments are made for substrate and exposed bedrock as described in this section, while the effect of headlands on shoreline erosion/accretion is calculated separately in ***Subsection 5.9.11.4***.
- The preservation of an equilibrium profile shape assumes a stationary wave climate. For this SSR the effects of a change in mean wave direction at the site are calculated separately in ***Subsection 5.9.11.4***.
- There is some uncertainly associated with the estimation of the slope of the active profile, which is governed by the depth of closure using empirical formulations. In this SSR the inner Hallermeier equation has been used (USACE, 2002b). The Hallermeier analytical equation is one of the most widely accepted for defining closure depths as it is based on site-specific physical characteristics and processes (Shand, et al., 2013).

D'Anna, et al., (2021) analysed the integration of SLR-driven recession into equilibrium shoreline models for a cross-shore-transport dominated coast. They demonstrated that, when Bruun's assumptions are satisfied, that the model can explicitly calculate the wave-erosion component of the SLR recession with a trend similar to the Bruun Rule.

Ranashinge, et al., (2011) developed a process-based model which provides probabilistic estimates of SLR-driven coastal recession based on the governing physical processes. Comparison of this model and the Bruun Rule for a case study at Narrabeen beach (Sydney, Australia) showed the Bruun Rule, when using the inner depth of closure method from Hallermeier, provided a conservative result, where the erosion predicted by the Bruun Rule was only exceeded by 8% of the probabilistic results.

Based on the discussion above the Bruun Rule is considered to be an appropriate and conservative method for estimating the coastline recession due to long-term sea level rise at the site and was applied specifically on the sandy coastline in Thysbaai. The rocky coastline west of Thyspunt is largely devoid of sediment in the upper beach profile, except for the presence of vegetated dunes typically above 4 m msl. These dunes do not actively participate in normal cross-shore processes since there is little to no aeolian transport and erosion can only occur during extreme storms. The Bruun Rule was therefore not applied along this section of the coastline. However, this section of the coastline does respond to extreme cross-shore storm erosion, for which the effects of sea level rise were included in ***Subsection 5.9.11.5***.

CONTROLLED DISCLOSURE

When downloaded from the EDS database, this document is uncontrolled and the responsibility rests with the user to ensure it is in line with the authorised version on the database.

Bruun's Rule has been applied in the following form (USACE, 2002b) and (Hands, 1983) (refer to ***Figure 5.9-69***):

$$x = \frac{z\,X}{Z}$$ Equation 5.9.5

where:

x = profile recession due to sea level rise

z = sea level rise

Z = vertical distance from the depth of closure (the depth at which no significant changes in seabed level occurs) to the upper point of profile adjustment (the maximum wave run-up level)

X = the corresponding horizontal distance from the depth of closure to the upper point of profile adjustment

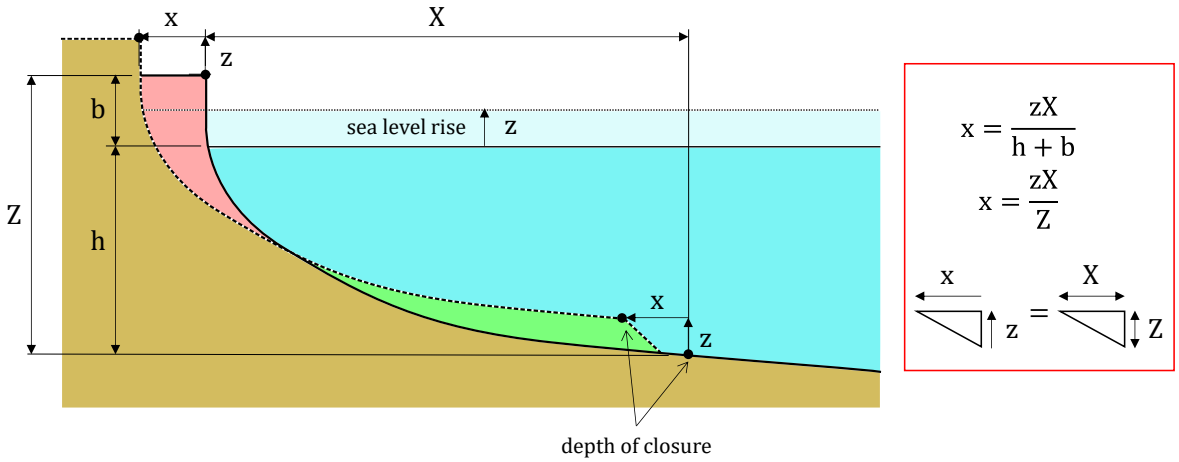


Figure 5.9-69: Schematic representation of the Bruun Rule, modified after Hands (1983).

The depth of closure was approximated using the inner Hallermeier analytical equation (USACE, 2002b):

$$d_\ell = 2.28H_e - 68.5\left(\frac{H_e^2}{gT_e^2}\right)$$ Equation 5.9.6

where:

d_ℓ = is the annual depth of closure below the mean water level

H_e = the non-breaking significant wave height that is exceeded 12 hours per year (0.137%)

T_e = the wave period associated with H_e

CONTROLLED DISCLOSURE

When downloaded from the EDS database, this document is uncontrolled and the responsibility rests with the user to ensure it is in line with the authorised version on the database.

g = gravitational acceleration (9.81 m/s^2)

The depth of closure was calculated from 10 years of modelled wave data (see ***Subsection 5.9.9.8***) at Point 2 (see ***Figure 5.9-70***) in a fairly exposed location some distance away from the shelter of the rocky outcrop with H_e = 6.57 m and T_e = 14.5 s, which yielded d_ℓ = -13.3 m msl.

More than 500 cross-shore profiles at 5 m increments along Thysbaai were interpolated from the available bathymetry and topography datasets, as well as the bedrock levels at the site (discussed in ***Section 5.9.8***). The primary data informing the upper beach slope and dunes is the 2011 LiDAR survey, which was best matched by the 2010 beach profile survey data to describe the lower beach profile. The representative baseline date for the beach profiles is thus 2011.

Figure 5.9-70 presents a plan view of the cross-shore profiles used for the coastline stability analysis. A comparison of a subset of the profiles is shown in ***Figure 5.9-71*** with chainages shifted horizontally to intersect at x = 0, z = 0 m msl for visualization of the slopes.

CONTROLLED DISCLOSURE

When downloaded from the EDS database, this document is uncontrolled and the responsibility rests with the user to ensure it is in line with the authorised version on the database.

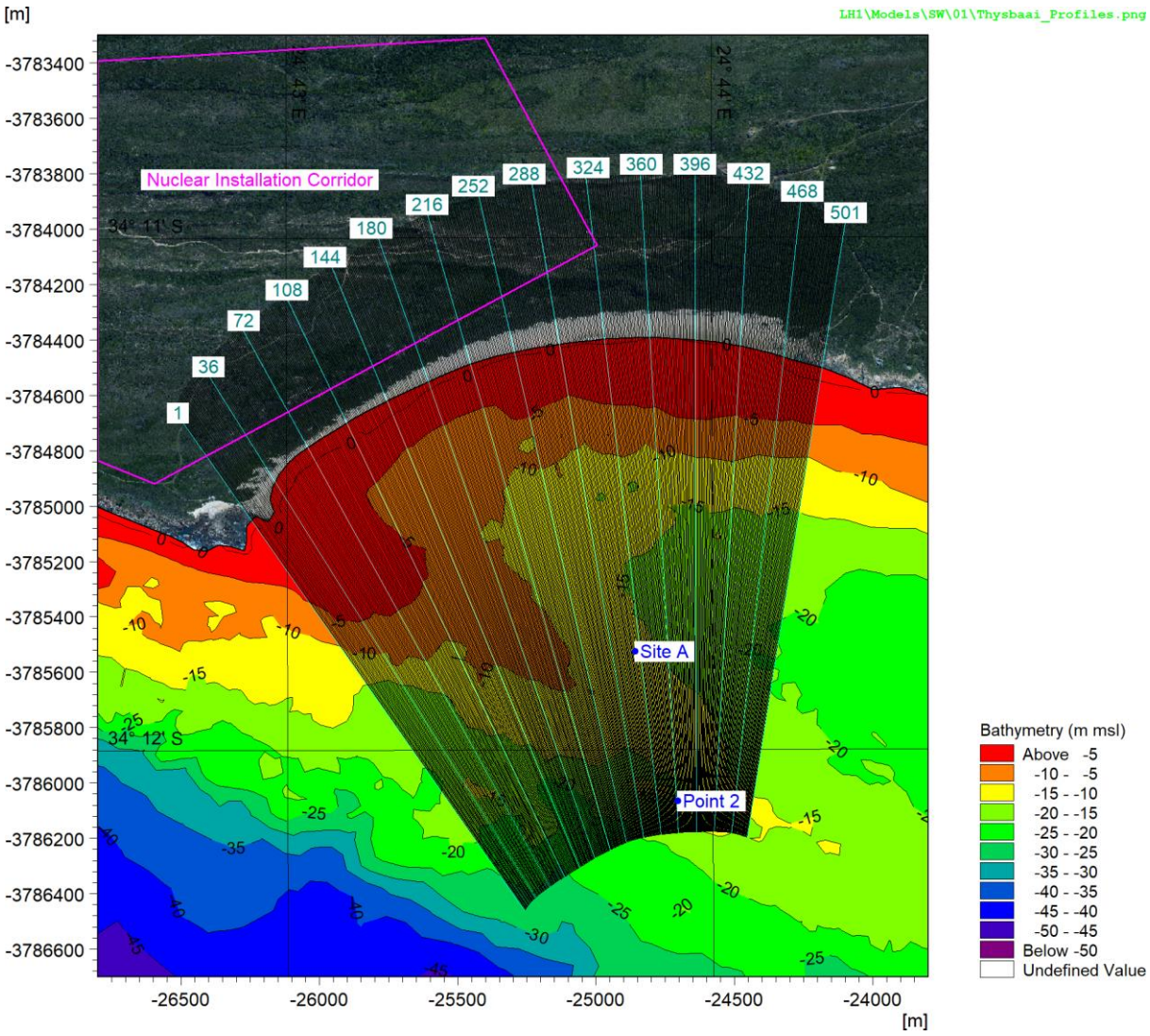


Figure 5.9-70: Plan View of Cross-Shore Profiles Used in the Coastline Stability Analysis.

CONTROLLED DISCLOSURE

When downloaded from the EDS database, this document is uncontrolled and the responsibility rests with the user to ensure it is in line with the authorised version on the database.

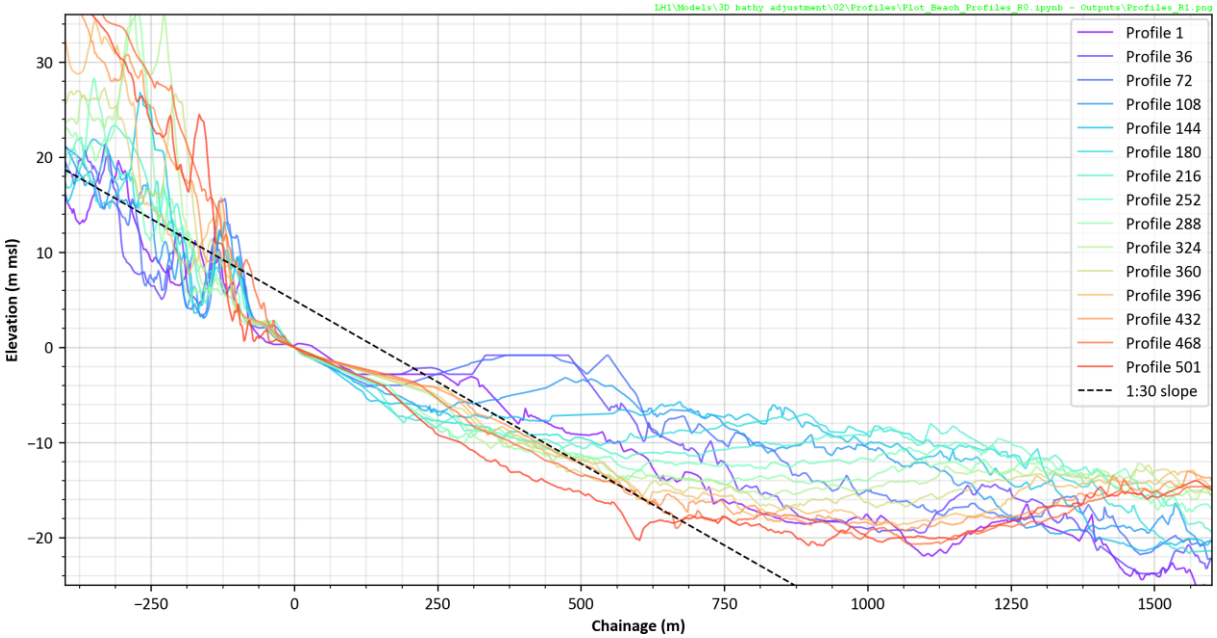


Figure 5.9-71: Comparison of Cross-Shore Profiles Along Thysbaai.

The profile slope between an average crest level of +10 m msl and the depth of closure was calculated for each profile. Many of the profiles have exposed bedrock above the depth of closure, which alters the profiles from a natural sandy beach slope and make these profiles unsuitable for the estimation of the Bruun slope. Therefore, a slope of 1 in 30 based on all profiles without exposed bedrock (Profiles 250 to 501) was used.

With the known sea level rise (***Table 5.9-8***, but adjusted to a baseline date of 2011) and profile slope, the average profile recession is expressed in ***Equation 5.9.7*** in terms of ***Equation 5.9.5***. Landward migration of the foredune due to overwash and aeolian transport is included, similar to Cowell, et al., (1992) and McCarrol, et al., (2021). For each profile the upper point of profile adjustment was thus assumed to be at the crest level of the foredune which varies along Thysbaai. Where no foredune was present, the +10 m msl contour was used.

$$x = \frac{z}{30}$$ Equation 5.9.7

Figure 5.9-72 and ***Figure 5.9-73*** illustrate examples of profile recession due to sea level rise using ***Equation 5.9.7*** for Profiles 107 and 347 for the 2134 High SLR scenario. Also shown are the cumulative coastline changes due to wave climate change (***Subsection 5.9.11.4***). There were no adjustments for long-term trends as discussed in ***Subsection 5.9.11.1***.

CONTROLLED DISCLOSURE

When downloaded from the EDS database, this document is uncontrolled and the responsibility rests with the user to ensure it is in line with the authorised version on the database.

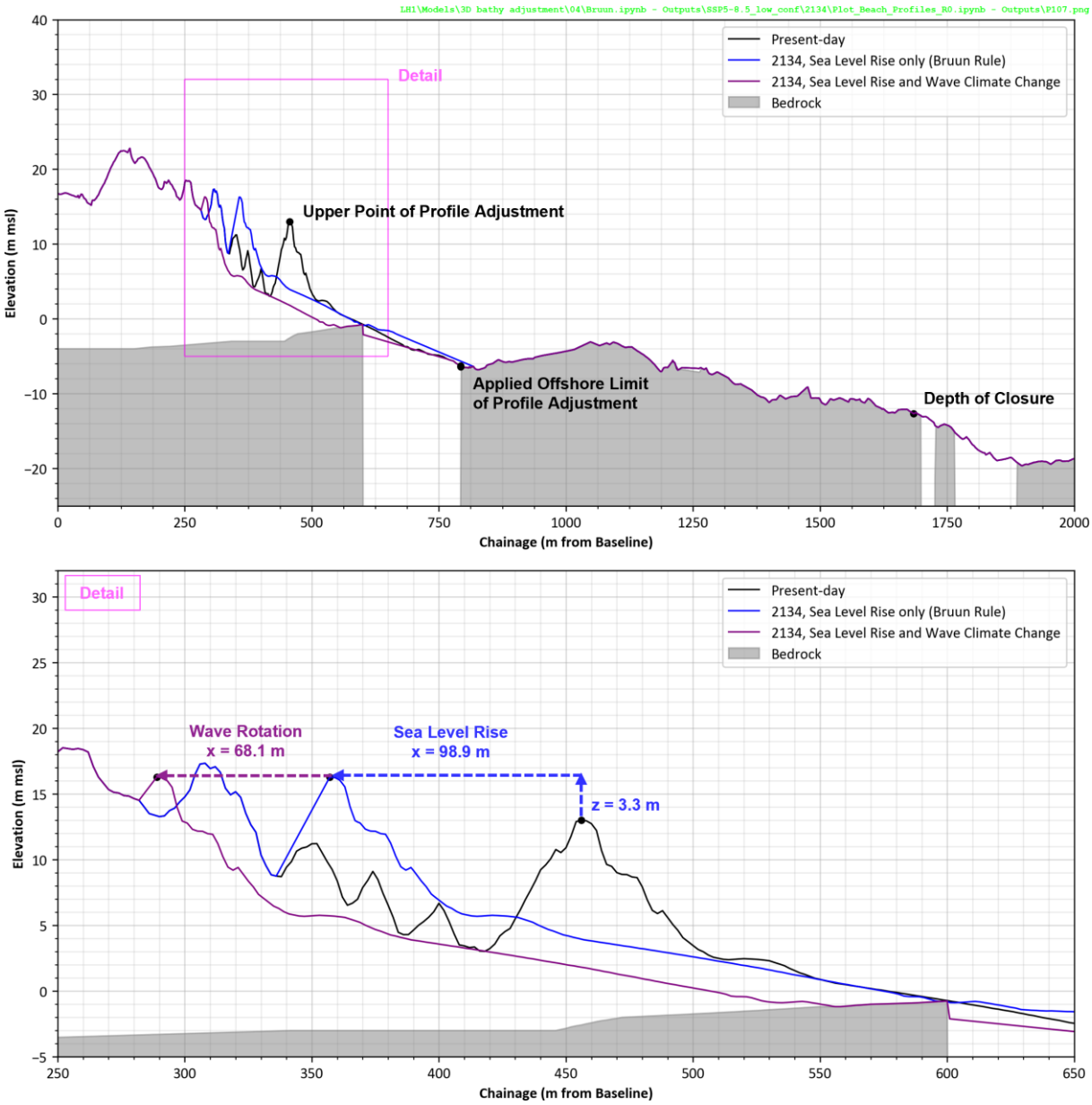


Figure 5.9-72: Example of Profile Recession due to Sea Level Rise for Profile 107 for the 2134 High SLR Scenario. Also Shown are the Cumulative Coastline Changes due to Wave Climate Change.

CONTROLLED DISCLOSURE

When downloaded from the EDS database, this document is uncontrolled and the responsibility rests with the user to ensure it is in line with the authorised version on the database.

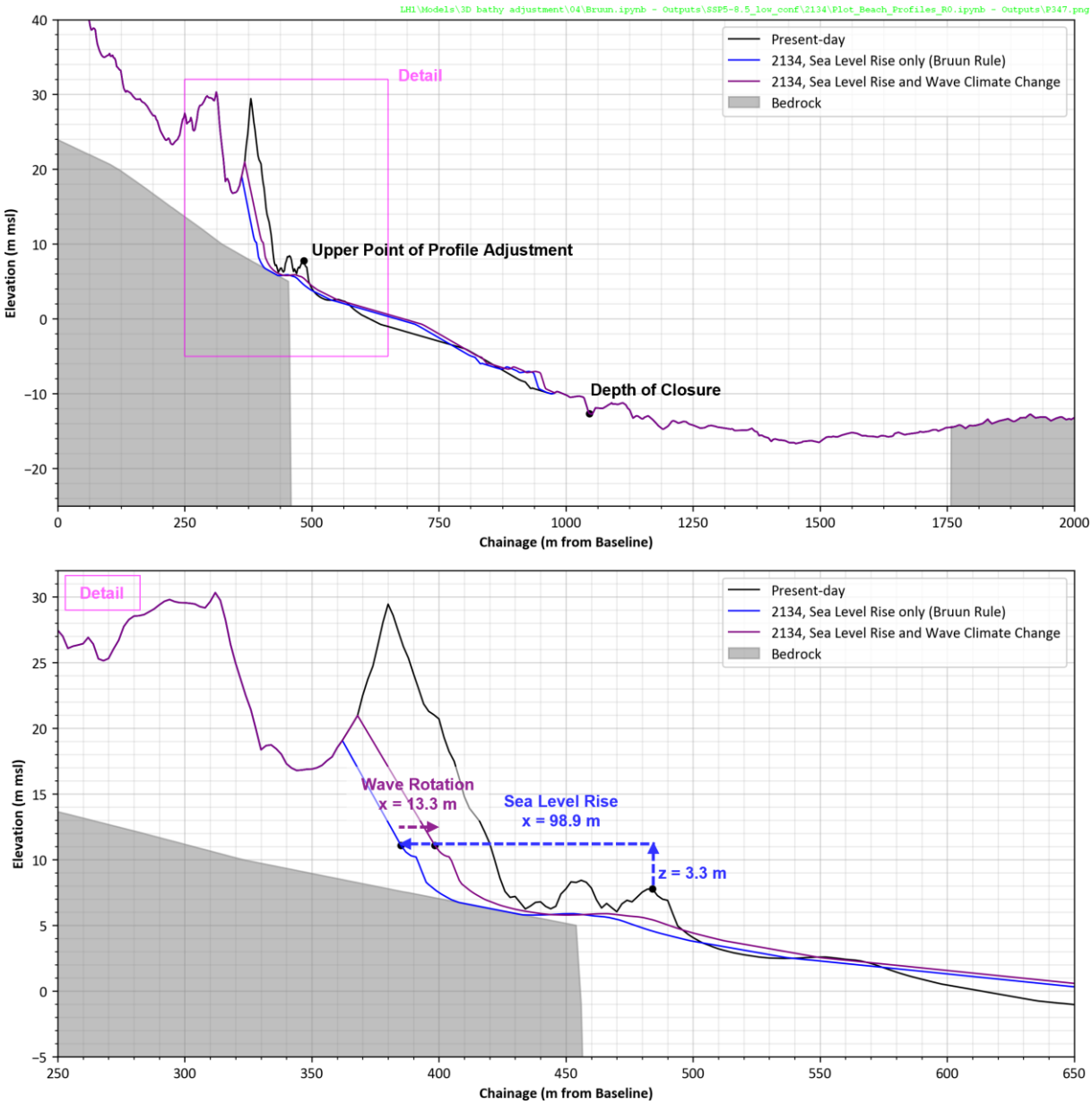


Figure 5.9-73: Example of Profile Recession due to Sea Level Rise for Profile 347 for the 2134 High SLR Scenario. Also Shown are the Cumulative Coastline Changes due to Wave Climate Change.

Figure 5.9-72 presents a typical cross-shore profile with exposed offshore bedrock landward of the depth of closure. The profile change due to sea level rise is a horizontal recession of 98.9 m and vertical rise of 3.3 m. The wave rotation adds an additional recession of 68.1 m, resulting in a horizontal recession of 158 m. The offshore portion of the profile with exposed bedrock deviates from an equilibrium sandy beach profile and would not be raised with the rest of the profile due to sea level rise. The profile adjustment is thus expected to only occur landward of the offshore

CONTROLLED DISCLOSURE

When downloaded from the EDS database, this document is uncontrolled and the responsibility rests with the user to ensure it is in line with the authorised version on the database.

bedrock, indicated in the figure as the applied offshore limit of profile adjustment. The profile adjustment is also limited by the bedrock elevation where the erosion reaches shallow bedrock at approximately -1 m msl on this profile.

Figure 5.9-73 illustrates a typical cross-shore profile without exposed offshore bedrock landward of the depth of closure. The profile change due to wave climate change is 13.1 m of horizontal accretion, which results in a combined profile recession of 85.6 m.

5.9.11.4 Coastline Changes due to Wave Climate Change

The projected climate change includes changes in wave direction and sea level rise (***Table 5.9-8***), both of which influence the nearshore wave climate which drives sediment transport. To determine the associated coastline changes, the operational 2D sediment transport model described in ***Subsection 5.9.11.2*** (details in ***Appendix 5.9.A.3***) was forced using water levels adjusted for sea level rise and the rotated wave climate (described in ***Subsection 5.9.9.8***). This was done for the 2134 and 2134 High SLR scenarios, using the corresponding adjustments for coastline recession (***Subsection 5.9.11.3***) as the initial bathymetry. In each case, ten repeat years were simulated to allow sufficient time for the sediment transport regime to reach a new equilibrium, which in reality would occur over a timescale of a century.

Figure 5.9-74 and ***Figure 5.9-75*** present the cumulative bed level change after 10 years for the 2134 and 2134 High SLR scenarios, respectively.

CONTROLLED DISCLOSURE

When downloaded from the EDS database, this document is uncontrolled and the responsibility rests with the user to ensure it is in line with the authorised version on the database.

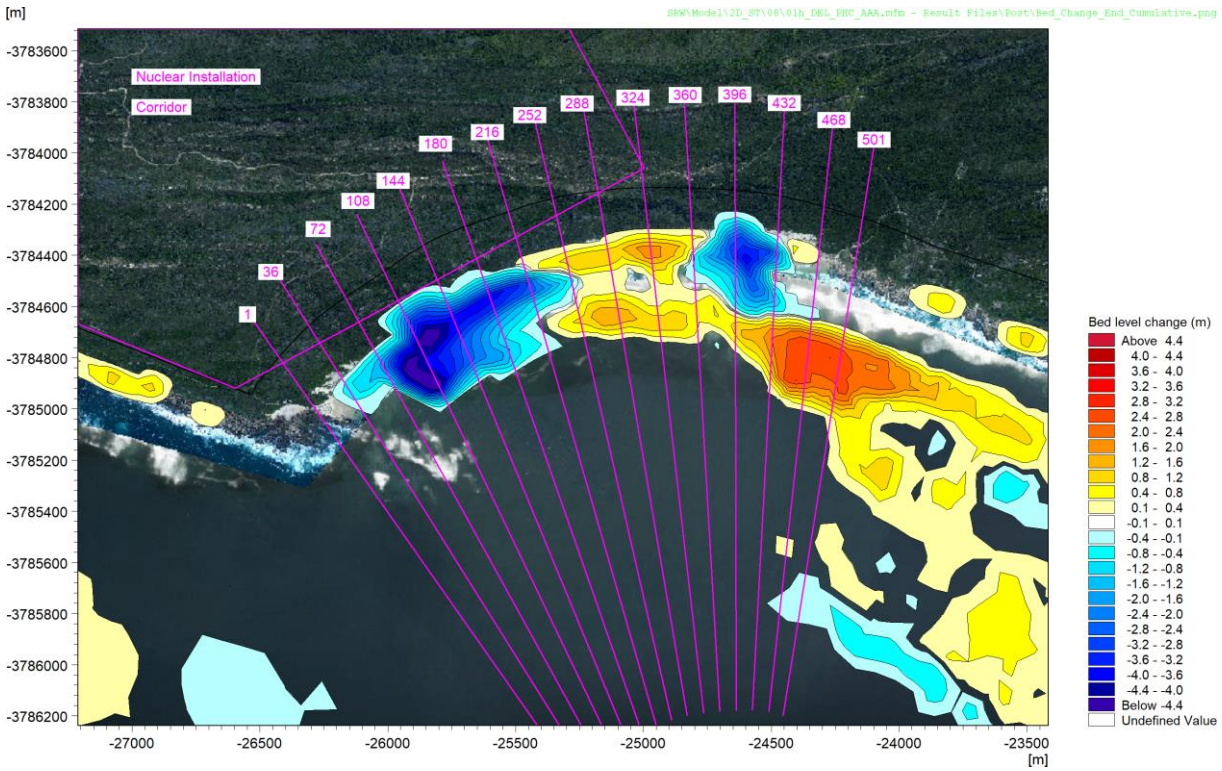


Figure 5.9-74: Cumulative Bed Level Change After 10 Years for the 2134 Scenario.

CONTROLLED DISCLOSURE

When downloaded from the EDS database, this document is uncontrolled and the responsibility rests with the user to ensure it is in line with the authorised version on the database.

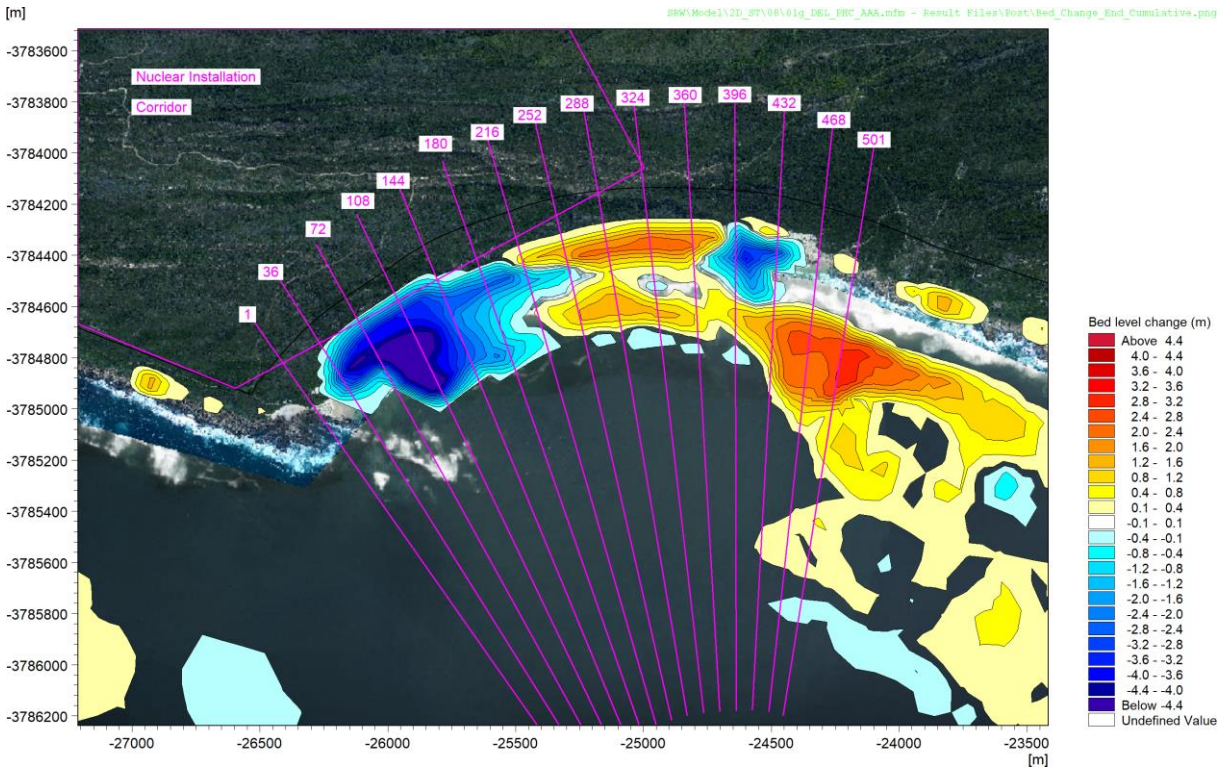


Figure 5.9-75: Cumulative Bed Level Change After 10 Years for the 2134 High SLR Scenario.

The cumulative bed level change over 10 years was extracted along each of the cross-shore profiles used in the coastline stability analysis (see ***Figure 5.9-70)***. The average vertical change along each profile up to the offshore end of profile adjustment (see ***Subsection 5.9.11.3***) was converted to a horizontal change using the profile slope of 1:30 along Thysbaai. The cumulative coastline changes over 10 years due to wave climate change for the 2134 and 2134 High SLR scenarios are presented in ***Figure 5.9-76*** and ***Figure 5.9-77***, respectively.

CONTROLLED DISCLOSURE

When downloaded from the EDS database, this document is uncontrolled and the responsibility rests with the user to ensure it is in line with the authorised version on the database.

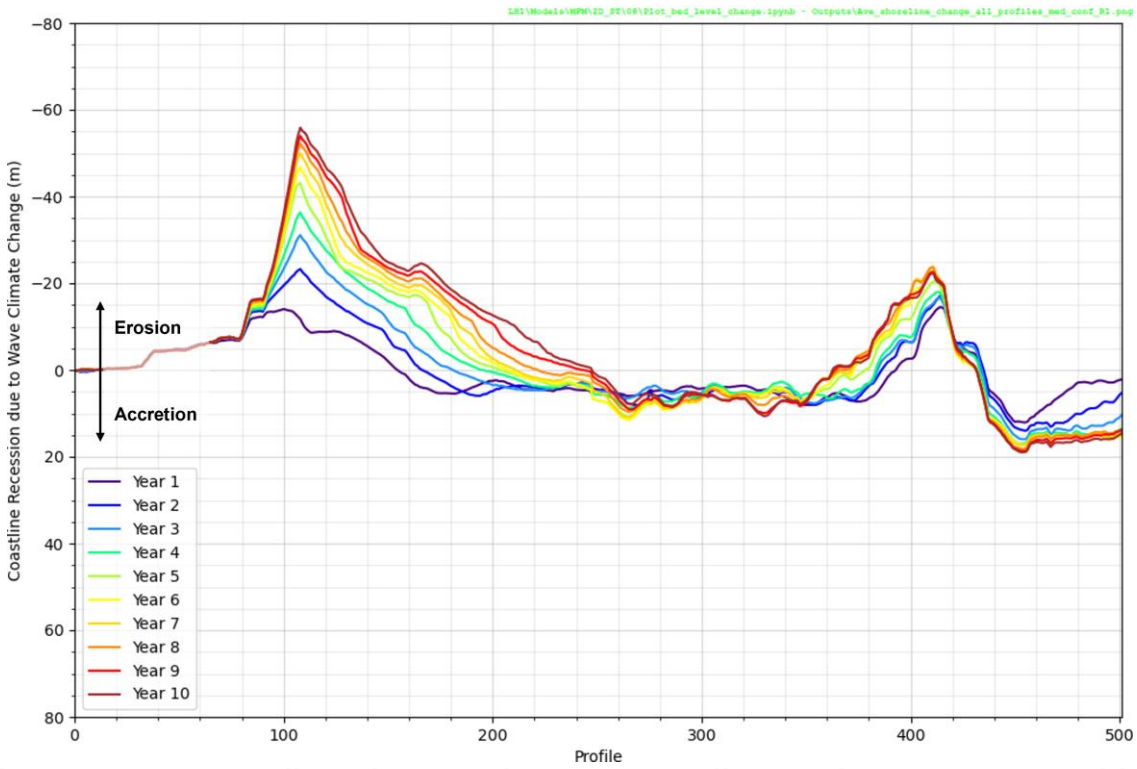


Figure 5.9-76: Coastline Changes due to Wave Climate Change: 2134. Positive Values Indicate Accretion and Negative Values Indicate Erosion.

CONTROLLED DISCLOSURE

When downloaded from the EDS database, this document is uncontrolled and the responsibility rests with the user to ensure it is in line with the authorised version on the database.

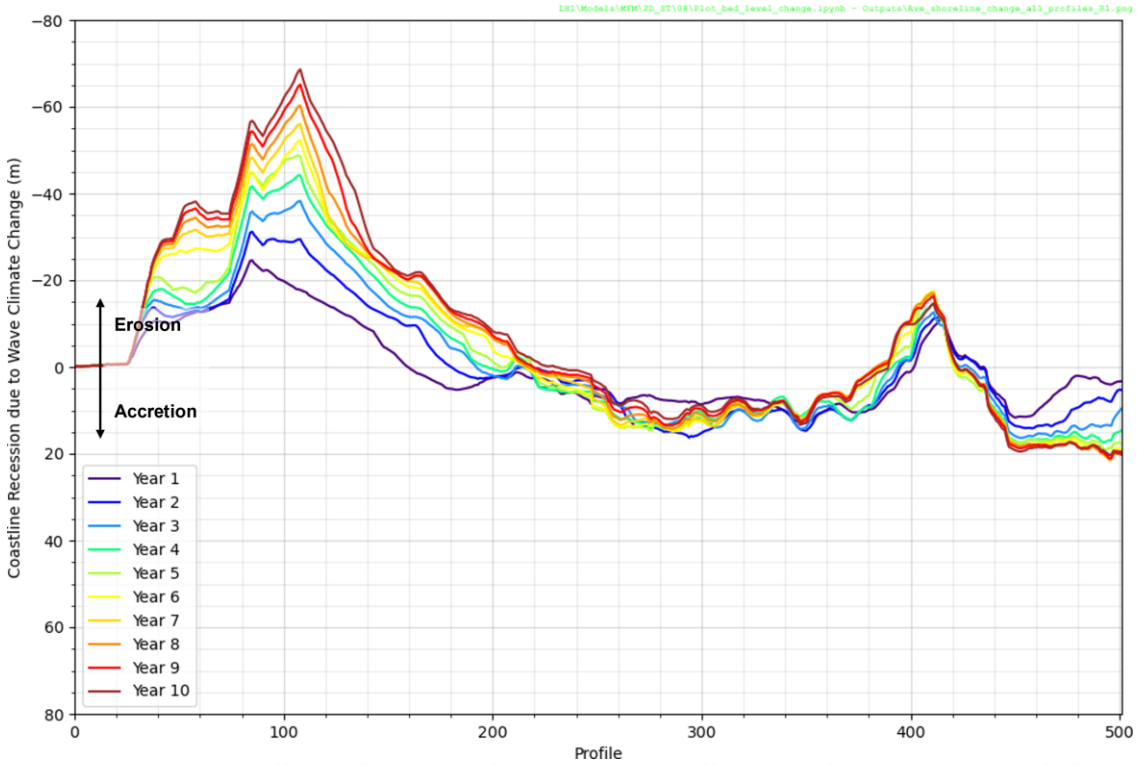


Figure 5.9-77: Coastline Changes due to Wave Climate Change: 2134 High SLR. Positive Values Indicate Accretion and Negative Values Indicate Erosion.

The results show a systematic bed level change, with erosion along the western end of Thysbaai and some accretion in east, resulting in a clockwise rotation of the beach. Both 2134 scenarios show similar trends, although the effect is enhanced for the additional sea level rise in the High SLR scenario. These results are consistent with a reduced sheltering by the Thysbaai reef under increased water levels causing an increased wave exposure of the western end of the bay. The effect of SLR is thus more dominant than the effect of the counter-clockwise rotation of the mean offshore wave direction, which if applied alone would be expected to cause a counter-clockwise rotation of the beach.

The cumulative results show that Thysbaai has reached an approximate equilibrium state after 10 years of sand transport modelling except to the west of Thysbaai (around Profiles 80 to 140) for the High SLR scenario. In reality, the estimated horizontal coastline recession will intercept the shallow bedrock on the western side of Thysbaai (see ***Figure 5.9-72***), which will interrupt the erosion. On this basis the results after 10 years are considered stable.

CONTROLLED DISCLOSURE

When downloaded from the EDS database, this document is uncontrolled and the responsibility rests with the user to ensure it is in line with the authorised version on the database.

5.9.11.5 Erosion and Sedimentation due to Storms

This section assesses the erosion of the coastline during storms, including 2D sediment transport in Thysbaai and cross-shore beach erosion along the coastline opposite the site. This erosion contributes to the total coastline erosion and increases the flooding risk.

2D Sand transport modelling

The 2D sediment transport model was used to model the effects of extreme storms on the coastline. The 1E-8 y^{-1} storm was modelled for the 2034, 2134 and 2134 High SLR scenarios. Details of the model description, setup and cases modelled are provided in ***Appendix 5.9.A.3.***

Figure 5.9-78 to ***Figure 5.9-80*** present the bed level change at the end of the 1E-8 y^{-1} storm for the three scenarios mentioned above.

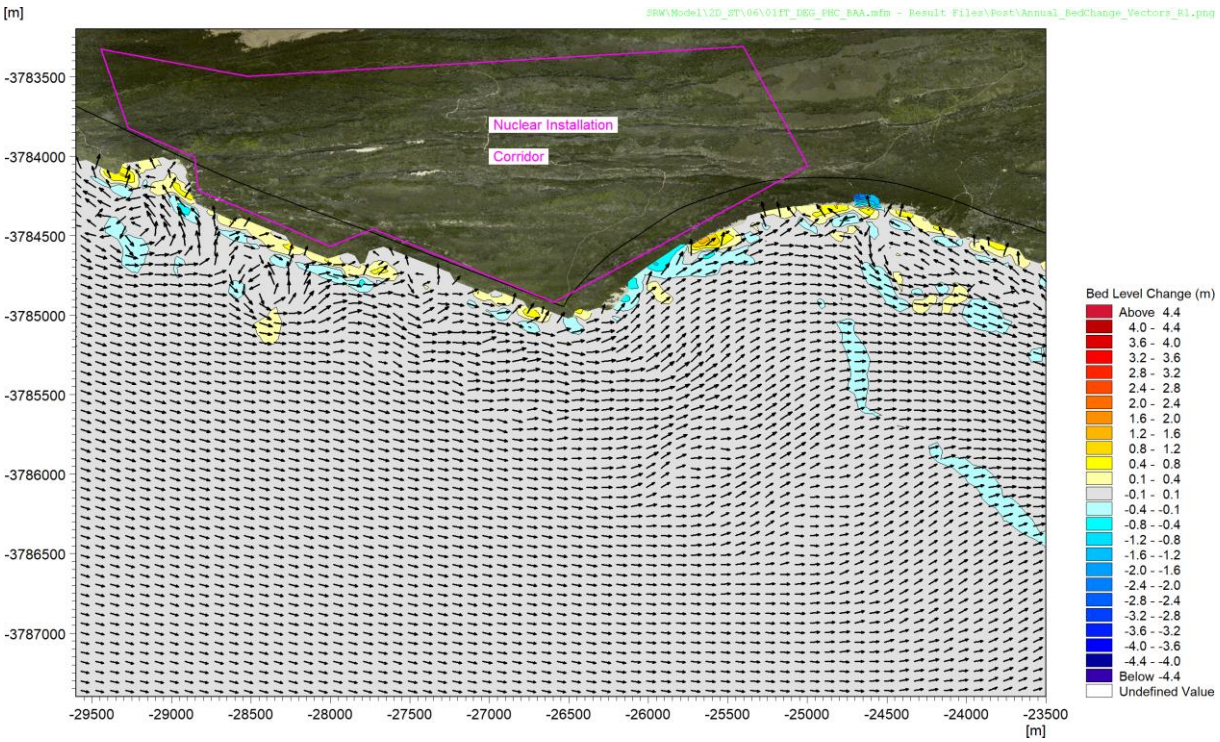


Figure 5.9-78: Bed Level Change Including Net Transport Vectors (Plotted on a Log Scale) for the 1E-8 y^{-1} 2034 Scenario.

CONTROLLED DISCLOSURE

When downloaded from the EDS database, this document is uncontrolled and the responsibility rests with the user to ensure it is in line with the authorised version on the database.

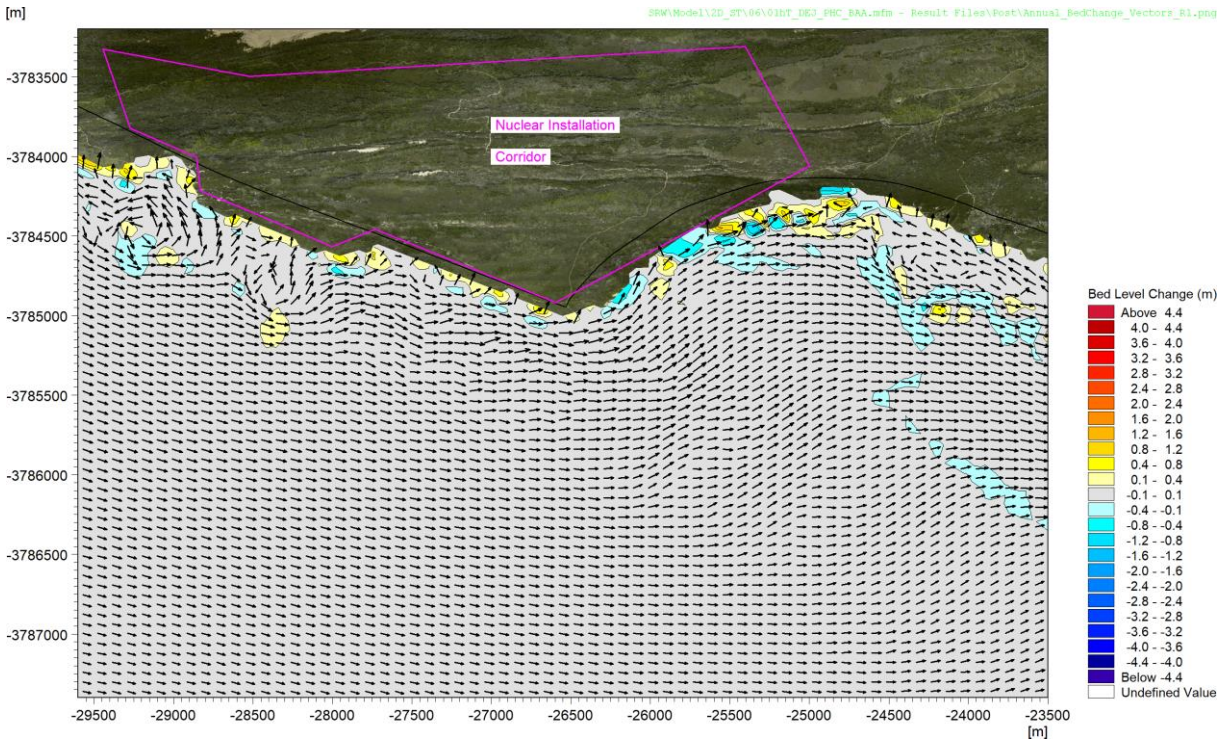


Figure 5.9-79: Bed Level Change Including Net Transport Vectors (Plotted on a Log Scale) for the 1E-8 y^{-1} 2134 Scenario.

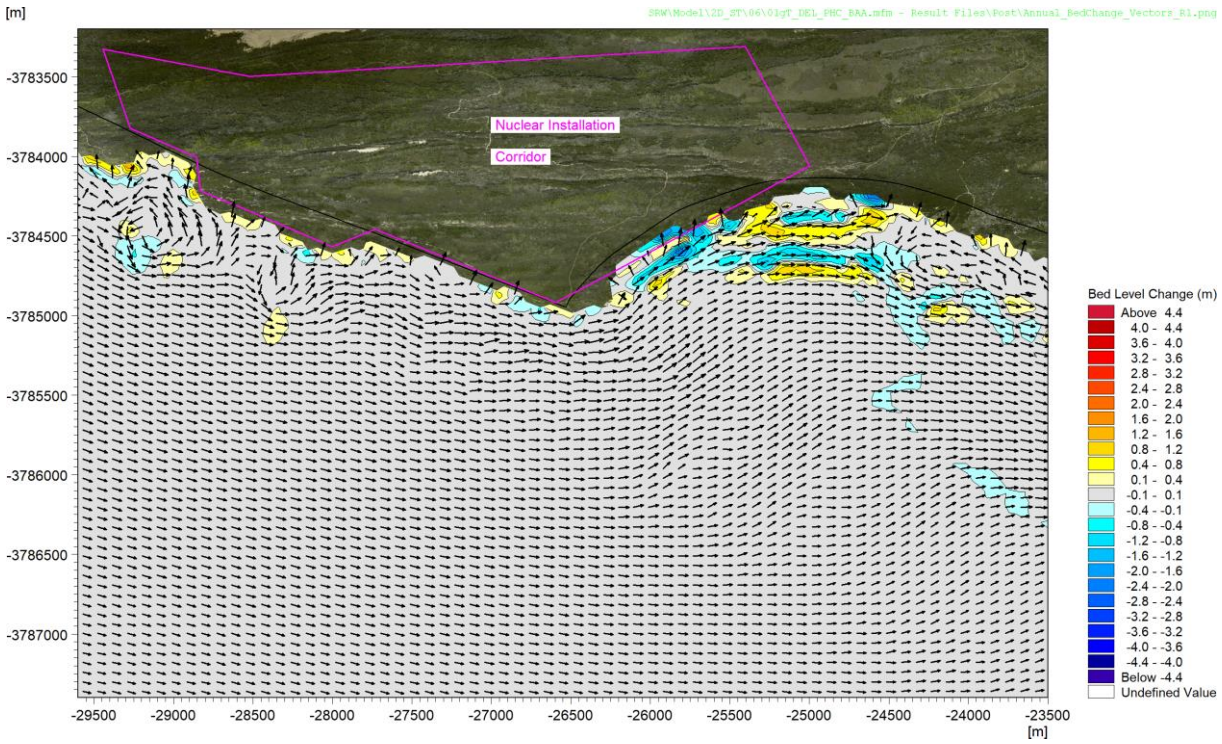


Figure 5.9-80: Bed Level Change Including Net Transport Vectors (Plotted on a Log Scale) for the 1E-8 y^{-1} 2134 High SLR Scenario.

CONTROLLED DISCLOSURE

When downloaded from the EDS database, this document is uncontrolled and the responsibility rests with the user to ensure it is in line with the authorised version on the database.

The results show that the storms generate strong eastwards sediment transport but, due to only small gradients in this transport, in none of the scenarios did the 1E-8 y^{-1} storm cause significant shoreline rotation or longshore erosion. The corresponding horizontal shoreline recession was calculated as described in ***Subsection 5.9.11.4*** which showed less than 5 m of recession due to the 1E-8 y^{-1} storms. Therefore no other extreme storm cases were modelled and 2D sand transport was not included in the overall coastline stability.

Cross-shore erosion modelling

The SBEACH (Storm-induced BEAch CHange) storm erosion model was used to simulate the erosion of the coastline in front of the site during storm events. The model was run for extreme storms with exceedance frequencies of 1E-2, 1E-4, 1E-6 and 1E-8 y^{-1} for the 2034, 2134 and 2134 High SLR scenarios. Details of the model description and cases modelled are provided in ***Appendix 5.9.A.4***. Example cross-shore erosion results are reported below.

Figure 5.9-81 and ***Figure 5.9-82*** present examples of the erosion results for the three scenarios and four storm exceedance frequencies at Profile 108 in Thysbaai (corresponding to the maximum additional recession due to wave climate change) and Profile R18 on the rocky coastline (see ***Figure 5.9-83***). In these examples the storm surge dominated joint probability case is shown.

CONTROLLED DISCLOSURE

When downloaded from the EDS database, this document is uncontrolled and the responsibility rests with the user to ensure it is in line with the authorised version on the database.

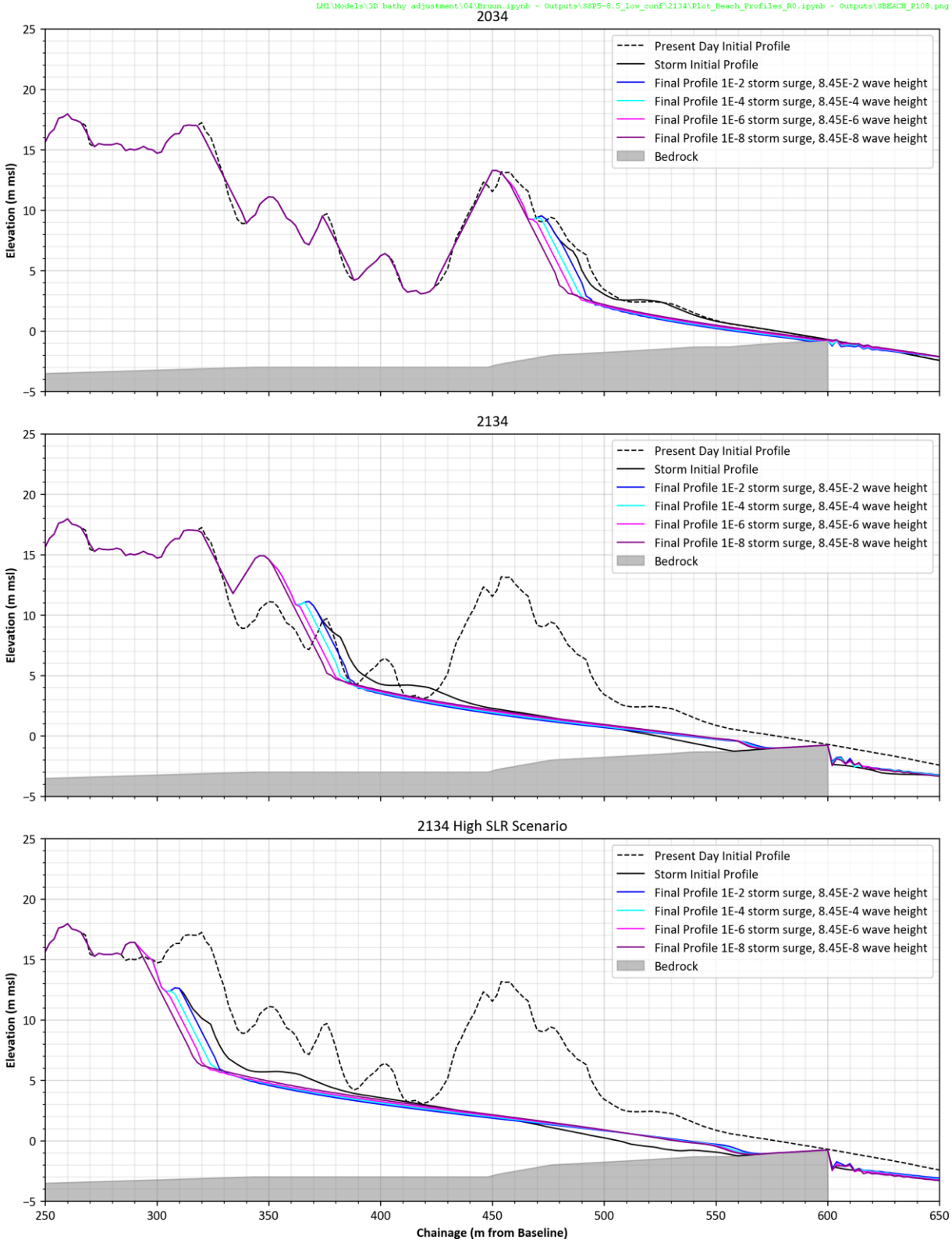


Figure 5.9-81: Profile 108 Cross-Shore Erosion Results for Storm Surge Dominant Cases.

CONTROLLED DISCLOSURE

When downloaded from the EDS database, this document is uncontrolled and the responsibility rests with the user to ensure it is in line with the authorised version on the database.

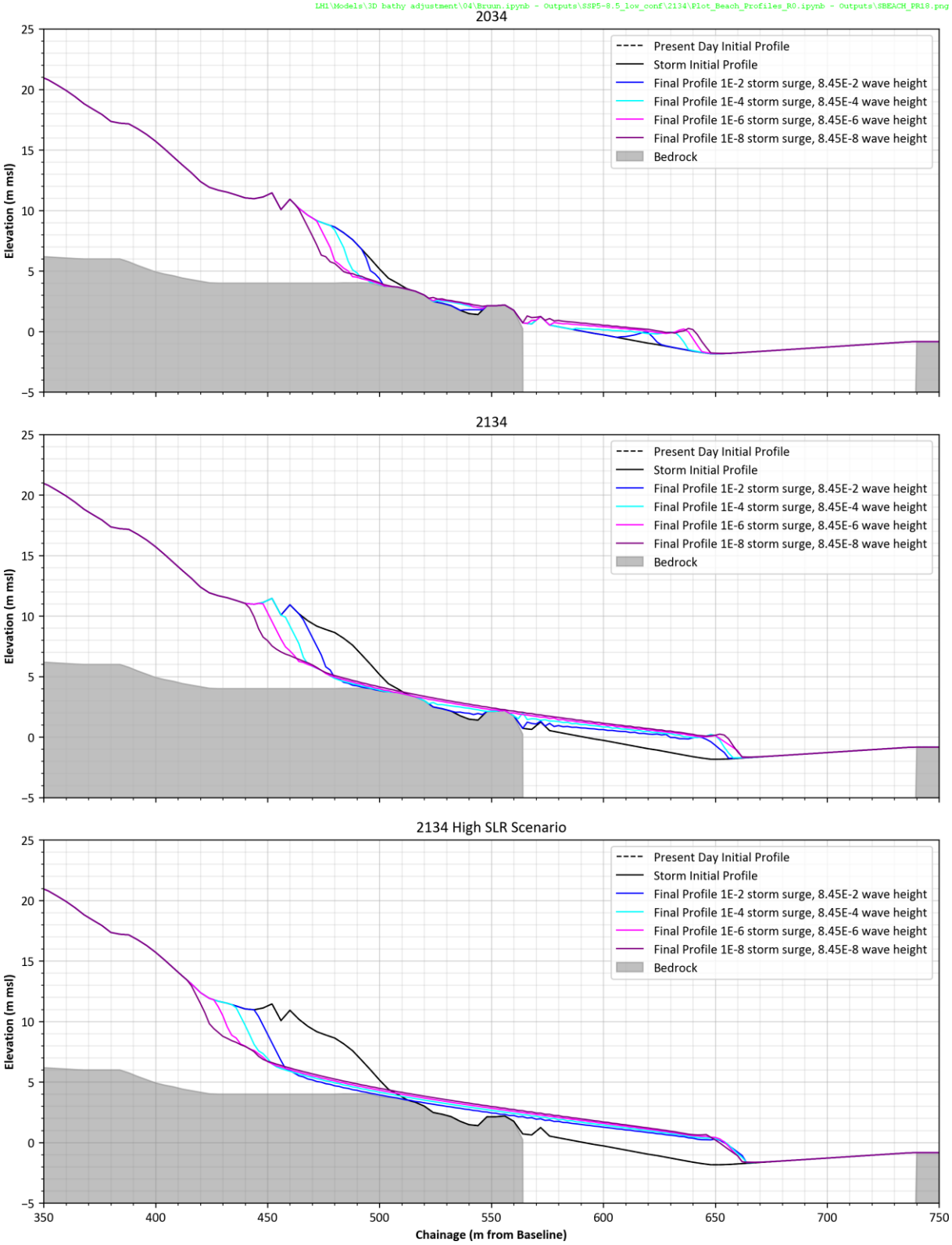


Figure 5.9-82: Profile R18 Cross-Shore Erosion Results for Storm Surge Dominant Cases.

CONTROLLED DISCLOSURE

When downloaded from the EDS database, this document is uncontrolled and the responsibility rests with the user to ensure it is in line with the authorised version on the database.

In ***Figure 5.9-81*** and ***Figure 5.9-82*** the following results are shown:

- "Present Day Initial Profile" is the beach and dune profile as measured in 2011.
- "Storm Initial Profile" is the profile prior to the storm and is the sum of the following:
    - Recession due to sea level rise (***Subsection 5.9.11.3***); and
    - Coastline changes due to wave climate change (***Subsection 5.9.11.4***).
- "Final Profile" is the profile including cross-shore erosion due to the storm at the indicated exceedance frequency.

Figure 5.9-81 shows that the cross-shore storm erosion at Profile 108 (in Thysbaai) during a 1E-8 y^{-1} storm ranges between approximately 15 m in 2034 and 20 m for the 2134 High SLR scenario. This is significantly less than the coastline changes due to combined sea level rise and wave climate change of 168 m for the 2134 High SLR scenario. ***Figure 5.9-82*** on the rocky coastline presents the cross-shore erosion of the erodible material landward of the exposed bedrock under the effects of sea level rise and storm events. The results show erosion of up to 20 m for 2034, 40 m for 2134 and 50 m for the 2134 High SLR scenario.

The cross-shore erosion of the dunes due to storm events is expected to increase the flooding potential at the site. The erosion results per scenario and exceedance frequency were bilinearly interpolated along the coastline to produce erosion maps, in each case taking the worst erosion between the joint probability combinations. The maps conservatively included only the erosion but not the associated accretion. An example of the interpolated storm erosion for the 2134 High SLR scenario and 1E-8 y^{-1} storm is shown in ***Figure 5.9-83***. The resultant coastline stability along the site is provided in ***Subsection 5.9.11.7.***

CONTROLLED DISCLOSURE

When downloaded from the EDS database, this document is uncontrolled and the responsibility rests with the user to ensure it is in line with the authorised version on the database.

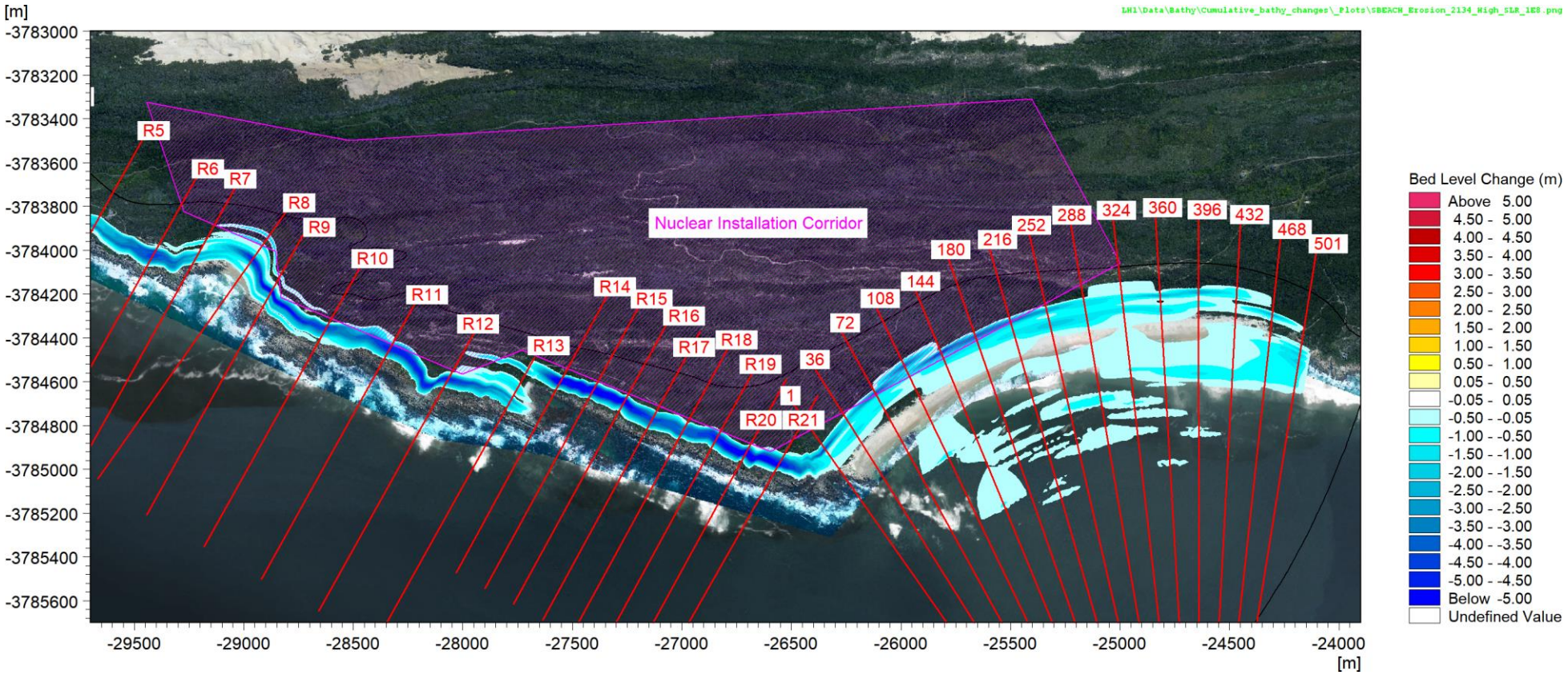


Figure 5.9-83: Interpolated Storm Erosion for the 2134 High SLR scenario and 1E-8 y^{-1} Storm.

.

CONTROLLED DISCLOSURE

When downloaded from the EDS database, this document is uncontrolled and the responsibility rests with the user to ensure it is in line with the authorised version on the database.

5.9.11.6 Erosion and Sedimentation due to Outfall Structure

The 2D sediment transport model (details in ***Appendix 5.9.A.3***) was used to investigate potential erosion and sedimentation due to inclusion of the cooling water outfall channel and associated discharge. The present-day operational case and 1E-8 y^{-1} storm were re-run with the outfall structure and cooling water discharge (445 m^3/s) included in the model.

Figure 5.9-84 and ***Figure 5.9-85*** present the bed level change (including the net transport vectors on a log scale) for the operational case and the 1E-8 y^{-1} storm, respectively.

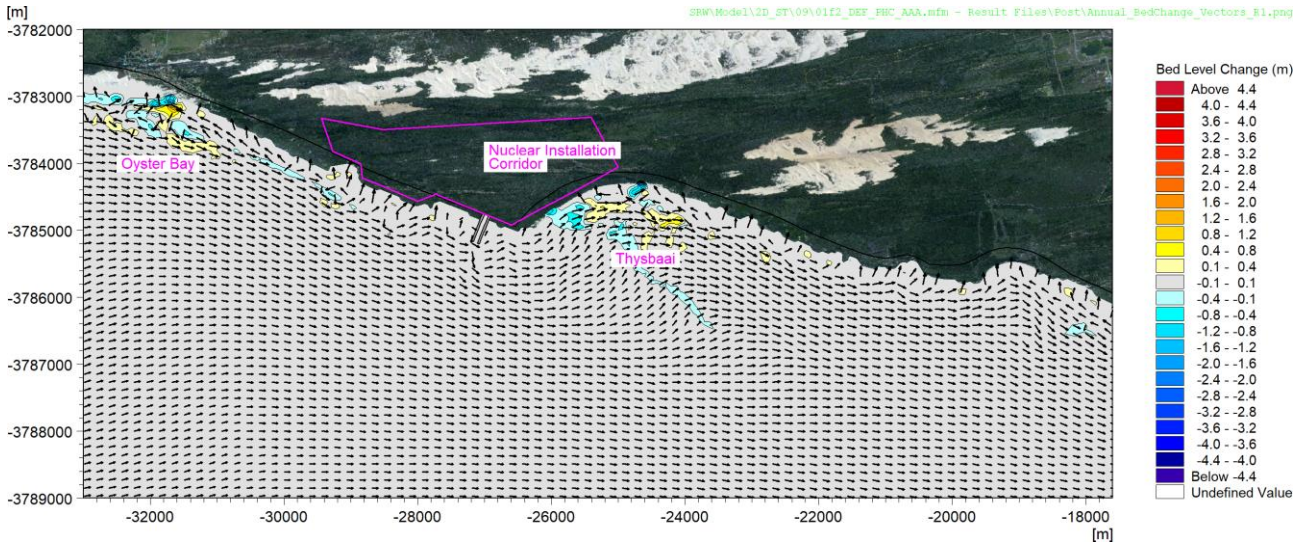


Figure 5.9-84: Annual Bed Level Change Including Annual Net Transport Vectors (Plotted on a Log Scale) for the Present-Day Operational Case Including the Outfall Structure.

CONTROLLED DISCLOSURE

When downloaded from the EDS database, this document is uncontrolled and the responsibility rests with the user to ensure it is in line with the authorised version on the database.

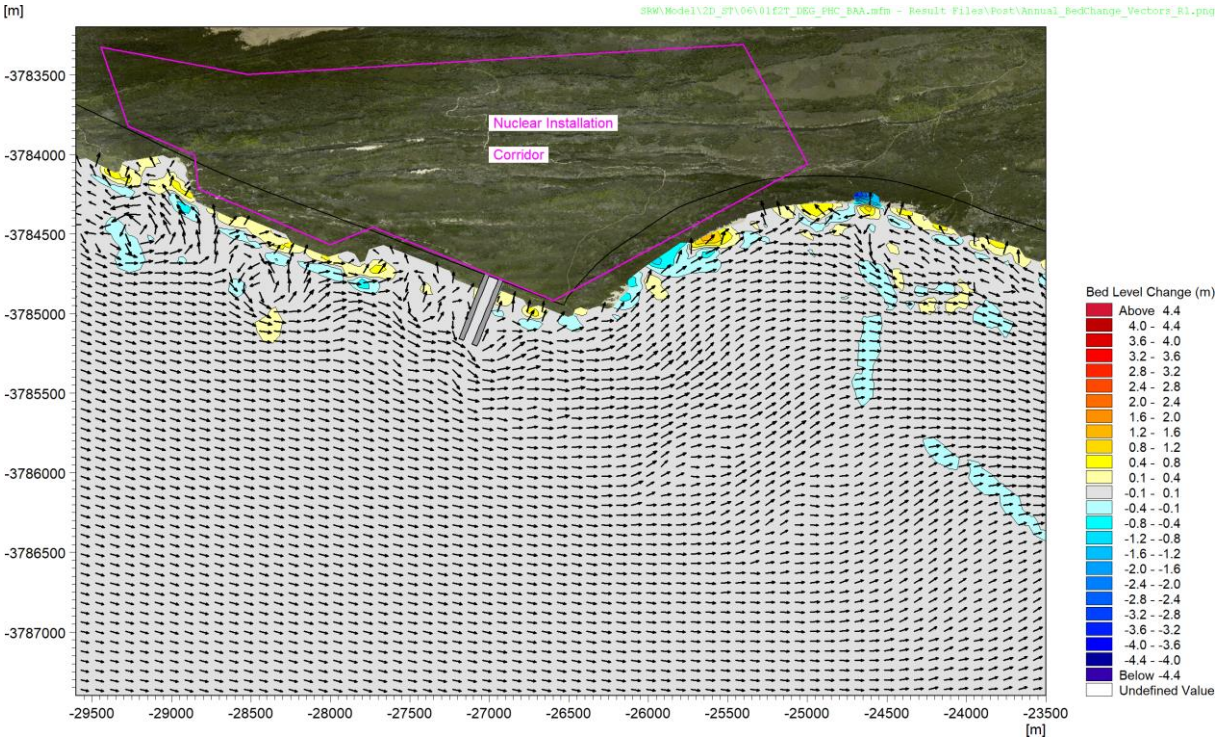


Figure 5.9-85: Bed Level Change Including Net Transport Vectors (Plotted on a Log Scale) for the 1E-8 y^{-1} 2034 Storm Case Including the Outfall Structure.

The present-day operational and storm cases showed very little influence of the outfall on the overall transport regime, with minor impacts (<0.4 m) to the transport directions directly in front of the outfall. The results showed no sedimentation or scour along the edges of the outfall structure, noting that the outfall structure is founded on rock and is thus non-erodible.

5.9.11.7 Resultant Coastline Stability

The total coastline change is the sum of the following components assessed in the subsections above:

- Recession due to sea level rise (***Subsection 5.9.11.3***);
- Coastline changes due to wave climate change (***Subsection 5.9.11.4***); and
- Cross-shore erosion (***Subsection 5.9.11.5***).

The baseline bathymetry (***Subsection 5.9.8***) was adjusted following these steps:

- Recession due to sea level rise was applied in Thysbaai for each climate change scenario. ***Figure 5.9-86***, ***Figure 5.9-87*** and ***Figure 5.9-88***

CONTROLLED DISCLOSURE

When downloaded from the EDS database, this document is uncontrolled and the responsibility rests with the user to ensure it is in line with the authorised version on the database.

present the bathymetries for the 2034, 2134 and 2134 High SLR scenarios.

- Additional changes due to wave climate change were added for each climate change scenario. ***Figure 5.9-89*** shows the 2134 High SLR scenario as an example.
- Finally, the additional changes due to cross-shore erosion were then added for each climate change scenario and exceedance frequency, in each case taking the worst erosion between the wave and storm surge dominated cases. ***Figure 5.9-90*** presents the 2134 High SLR scenario with the 1E-8 y^{-1} cross-shore storm erosion as an example.

CONTROLLED DISCLOSURE

When downloaded from the EDS database, this document is uncontrolled and the responsibility rests with the user to ensure it is in line with the authorised version on the database.

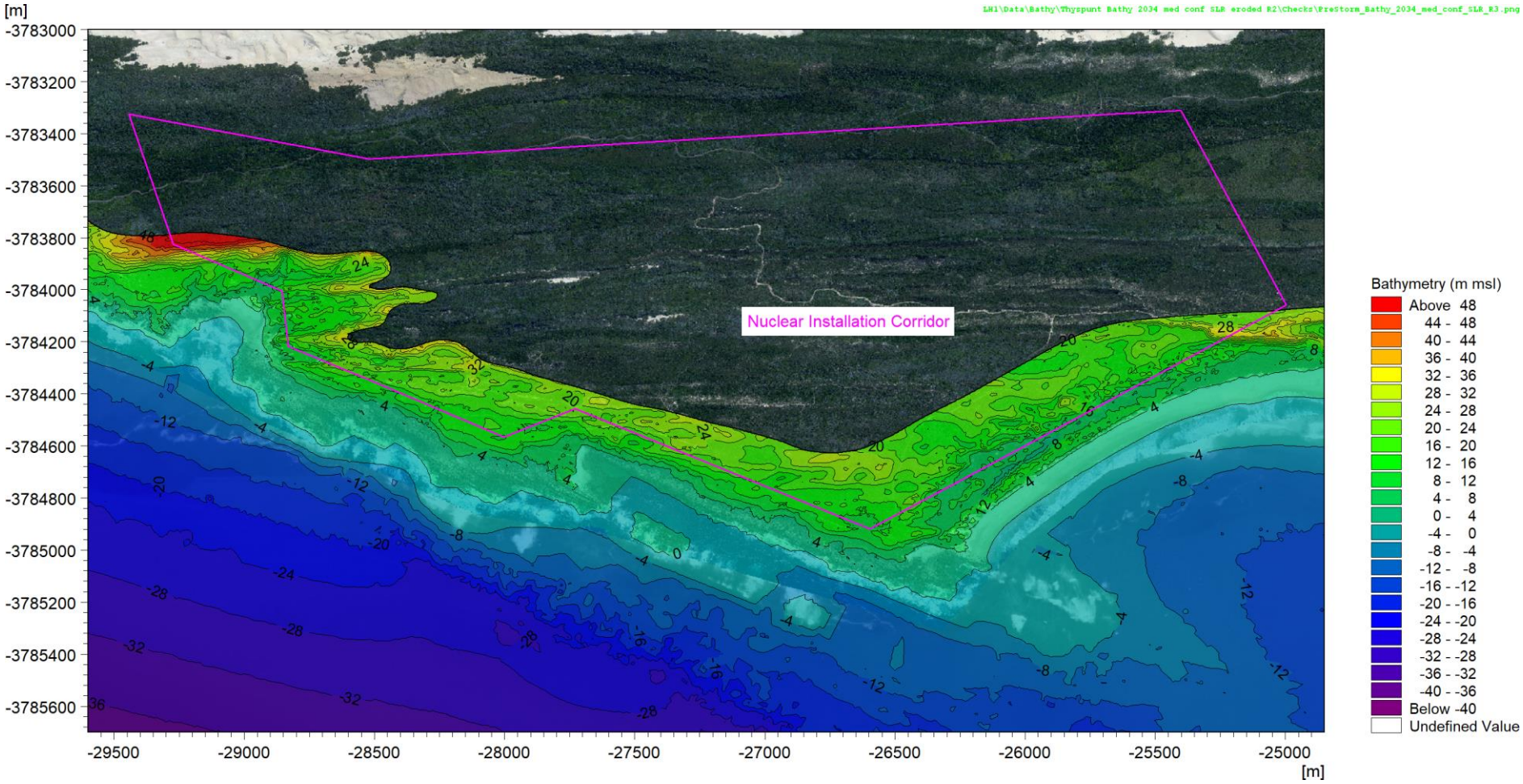


Figure 5.9-86: Pre-Storm Bathymetry Adjusted for Sea Level Rise: 2034.

CONTROLLED DISCLOSURE

When downloaded from the EDS database, this document is uncontrolled and the responsibility rests with the user to ensure it is in line with the authorised version on the database.

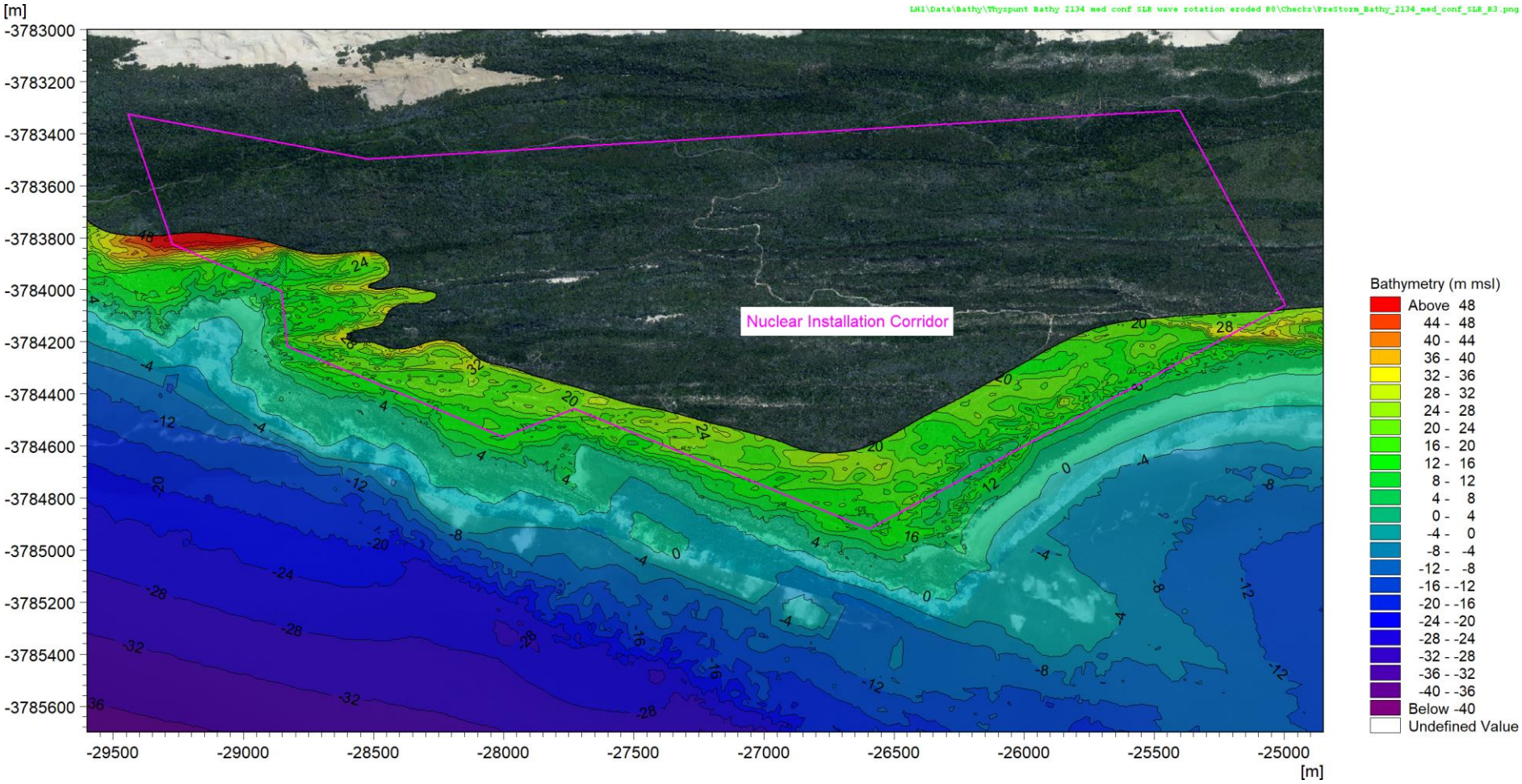


Figure 5.9-87: Pre-Storm Bathymetry Adjusted for Sea Level Rise: 2134.

CONTROLLED DISCLOSURE

When downloaded from the EDS database, this document is uncontrolled and the responsibility rests with the user to ensure it is in line with the authorised version on the database.

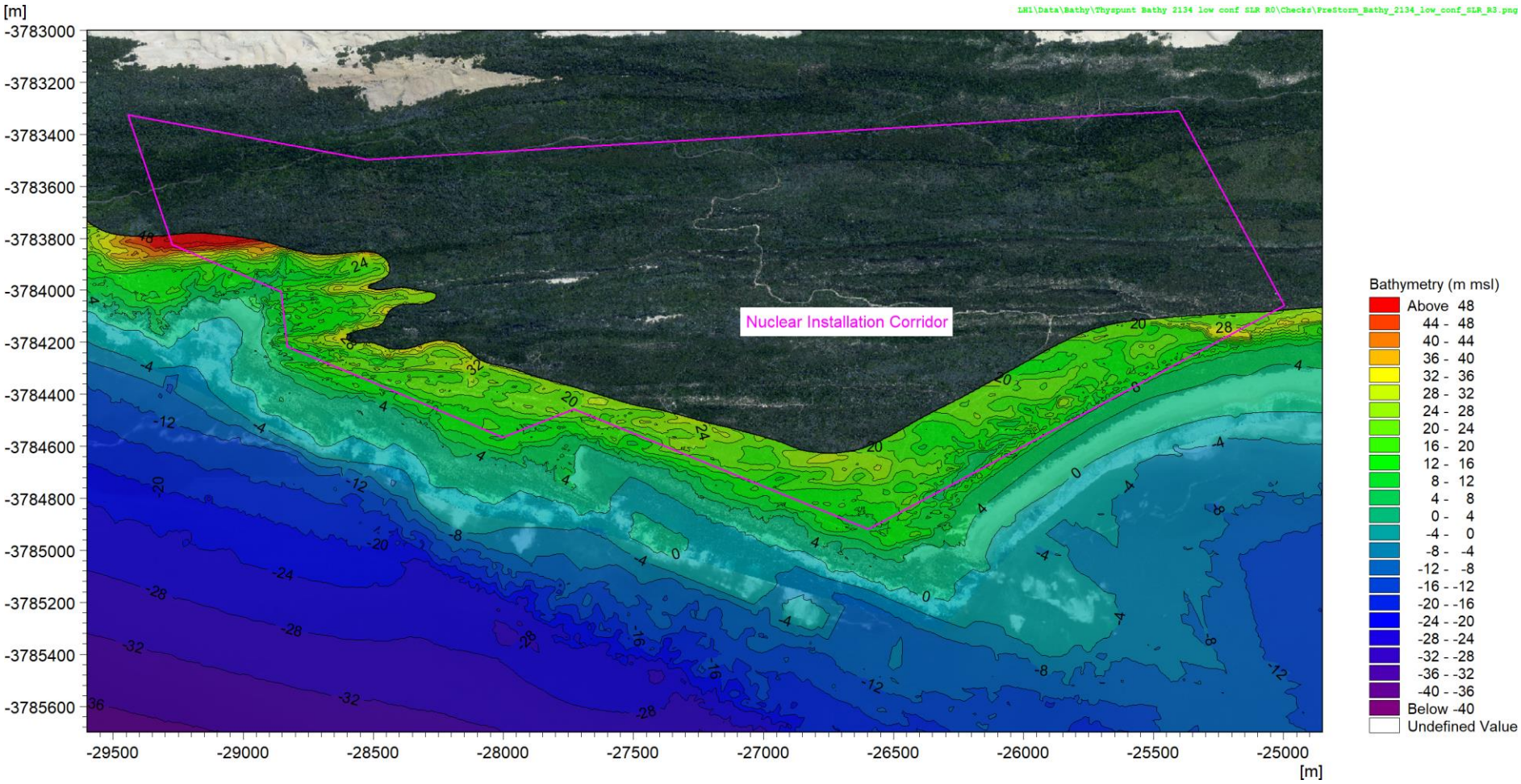


Figure 5.9-88: Pre-Storm Bathymetry Adjusted for Sea Level Rise: 2134 High SLR.

CONTROLLED DISCLOSURE

When downloaded from the EDS database, this document is uncontrolled and the responsibility rests with the user to ensure it is in line with the authorised version on the database.

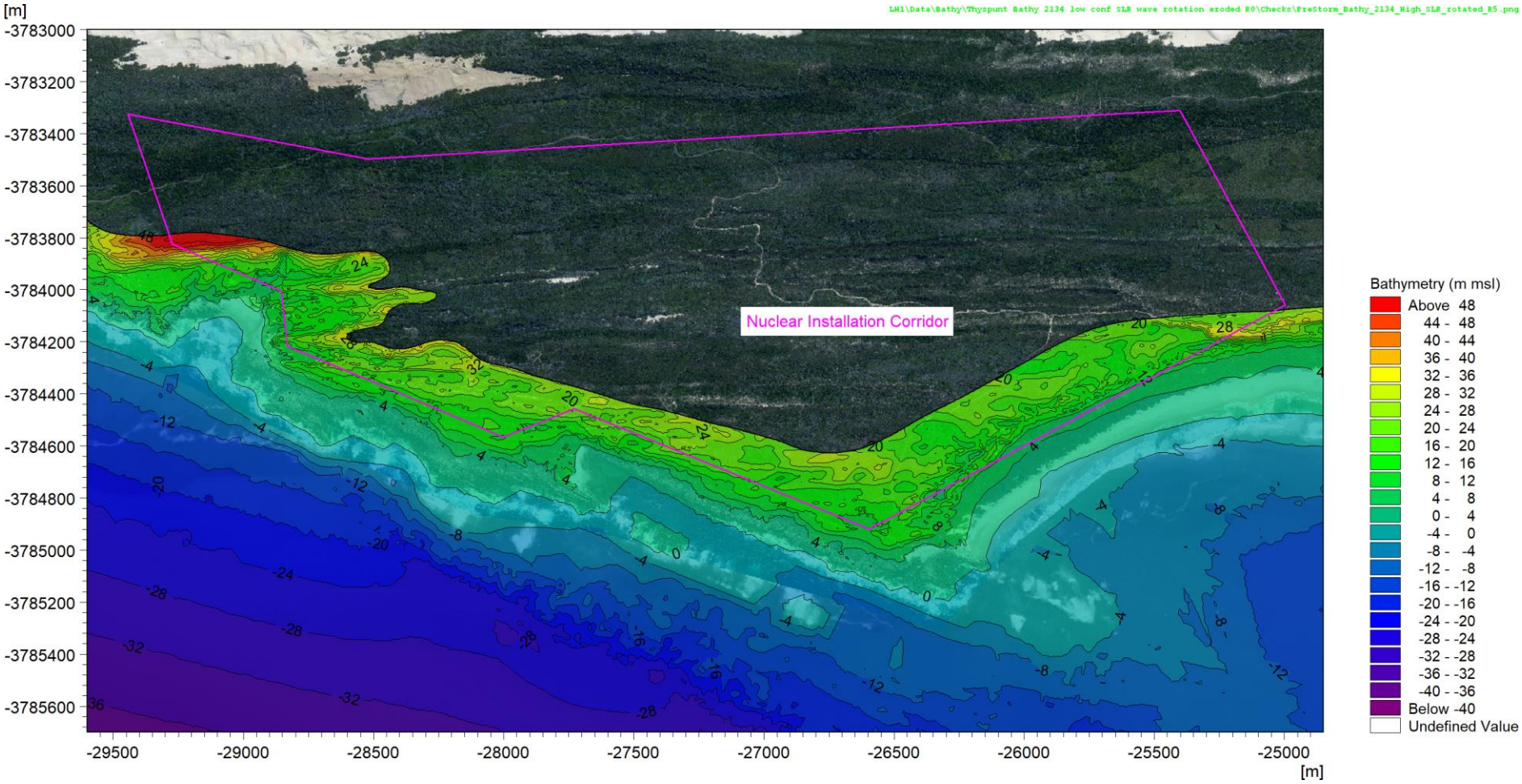


Figure 5.9-89: Pre-Storm Bathymetry Adjusted for Sea Level Rise and Wave Climate Change: 2134 High SLR.

CONTROLLED DISCLOSURE

When downloaded from the EDS database, this document is uncontrolled and the responsibility rests with the user to ensure it is in line with the authorised version on the database.

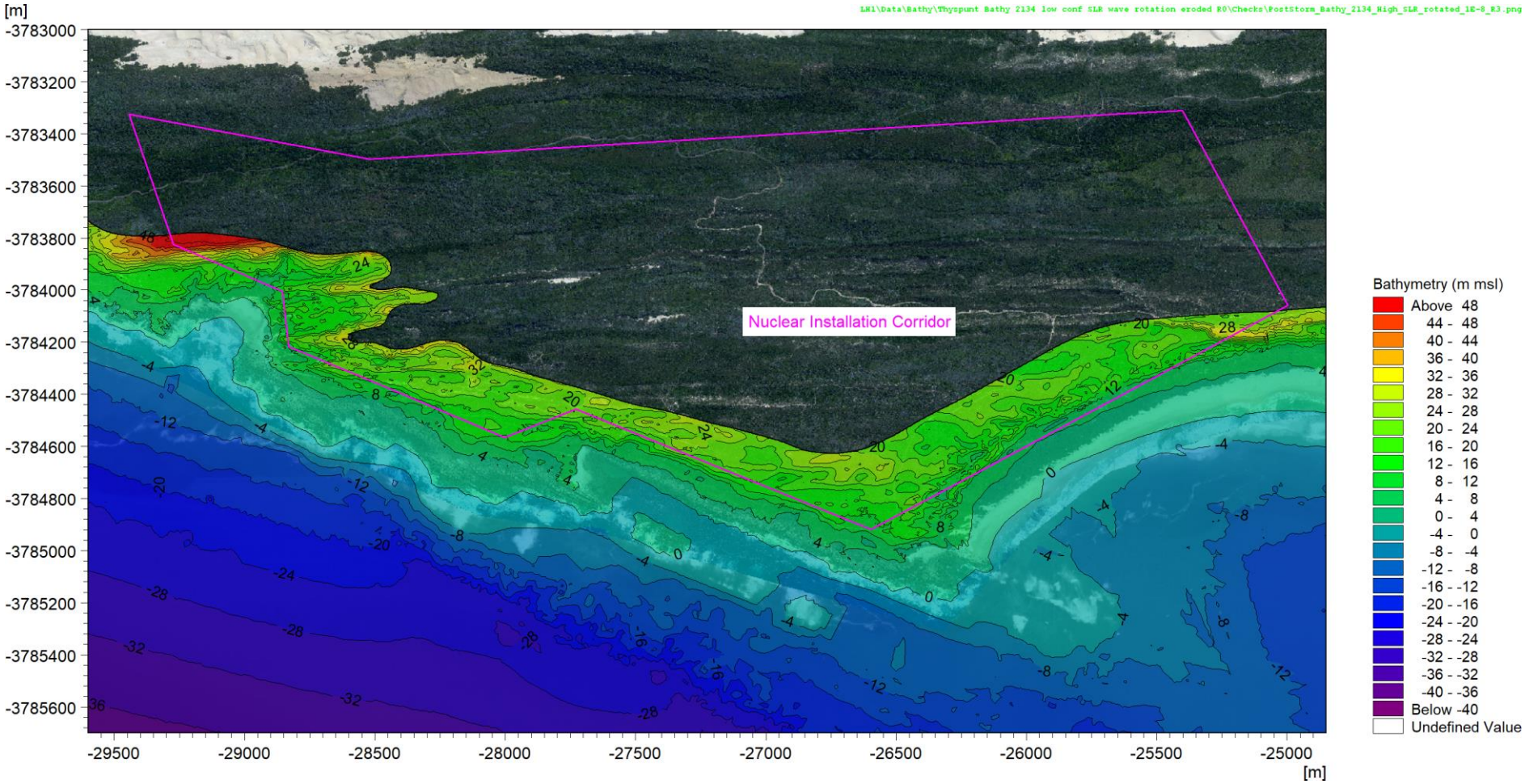


Figure 5.9-90: Post-Storm Bathymetry Adjusted for Sea Level Rise, Wave Climate Change and 1E-8 y^{-1} Storm: 2134 High SLR.

CONTROLLED DISCLOSURE

When downloaded from the EDS database, this document is uncontrolled and the responsibility rests with the user to ensure it is in line with the authorised version on the database.

The resultant bathymetries were used for the storm wave run-up and drawdown modelling (***Subsection 5.9.12***).

The erosion lines in front of the site for the 1E-2, 1E-4, 1E-5, 1E-6, 1E-7, and 1E-8 y^{-1} exceedance frequencies for all modelled climate change scenarios are plotted in ***Figure 5.9-91*** to ***Figure 5.9-93***. The erosion lines are defined as the line drawn in horizontal space demarcating the most landward extent where erosion exceeding 0.05 m occurs.

CONTROLLED DISCLOSURE

When downloaded from the EDS database, this document is uncontrolled and the responsibility rests with the user to ensure it is in line with the authorised version on the database.

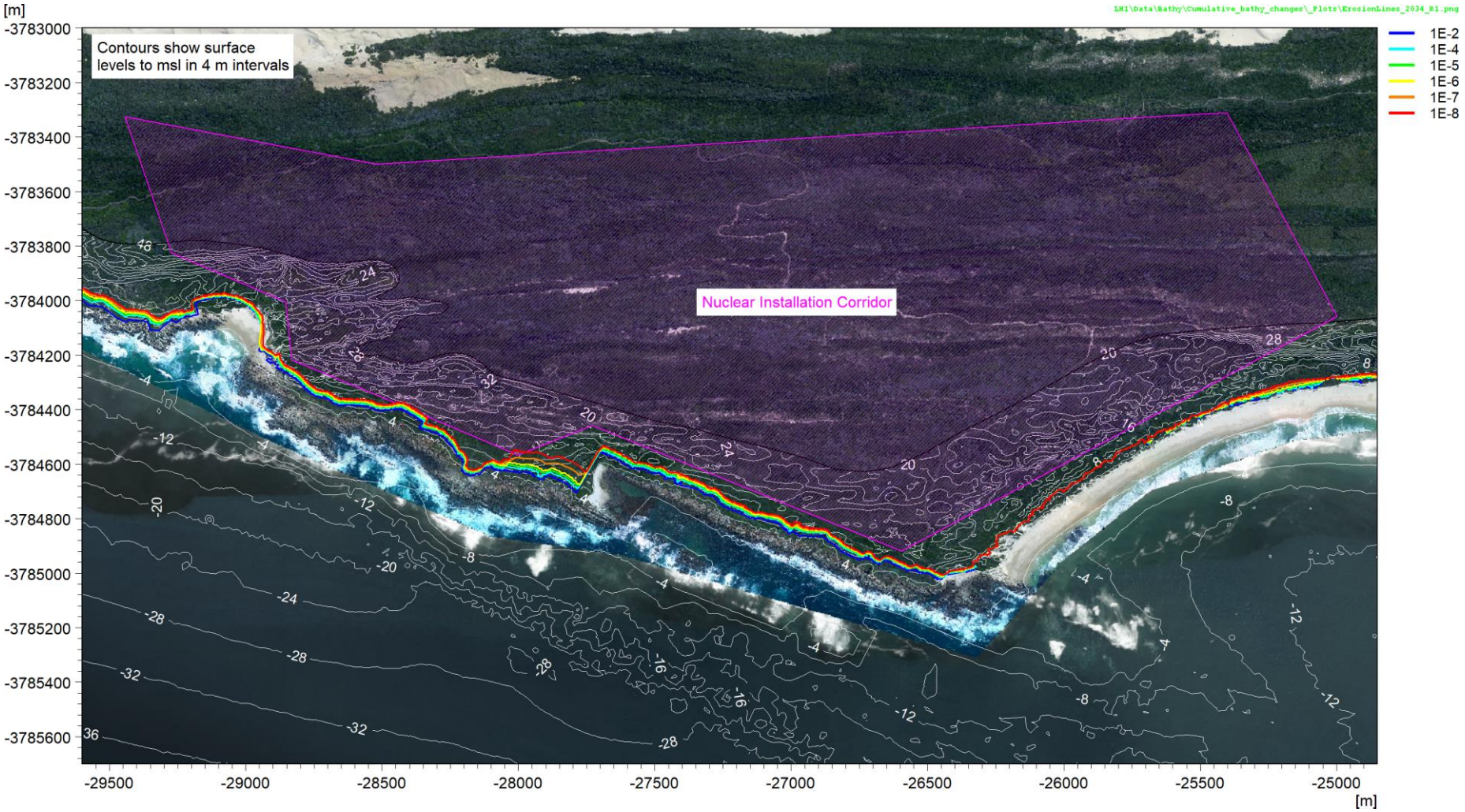


Figure 5.9-91: Erosion Lines for the Labelled Storm Frequencies: 2034. The Contours Indicate the Pre-Storm Bathymetry.

CONTROLLED DISCLOSURE

When downloaded from the EDS database, this document is uncontrolled and the responsibility rests with the user to ensure it is in line with the authorised version on the database.

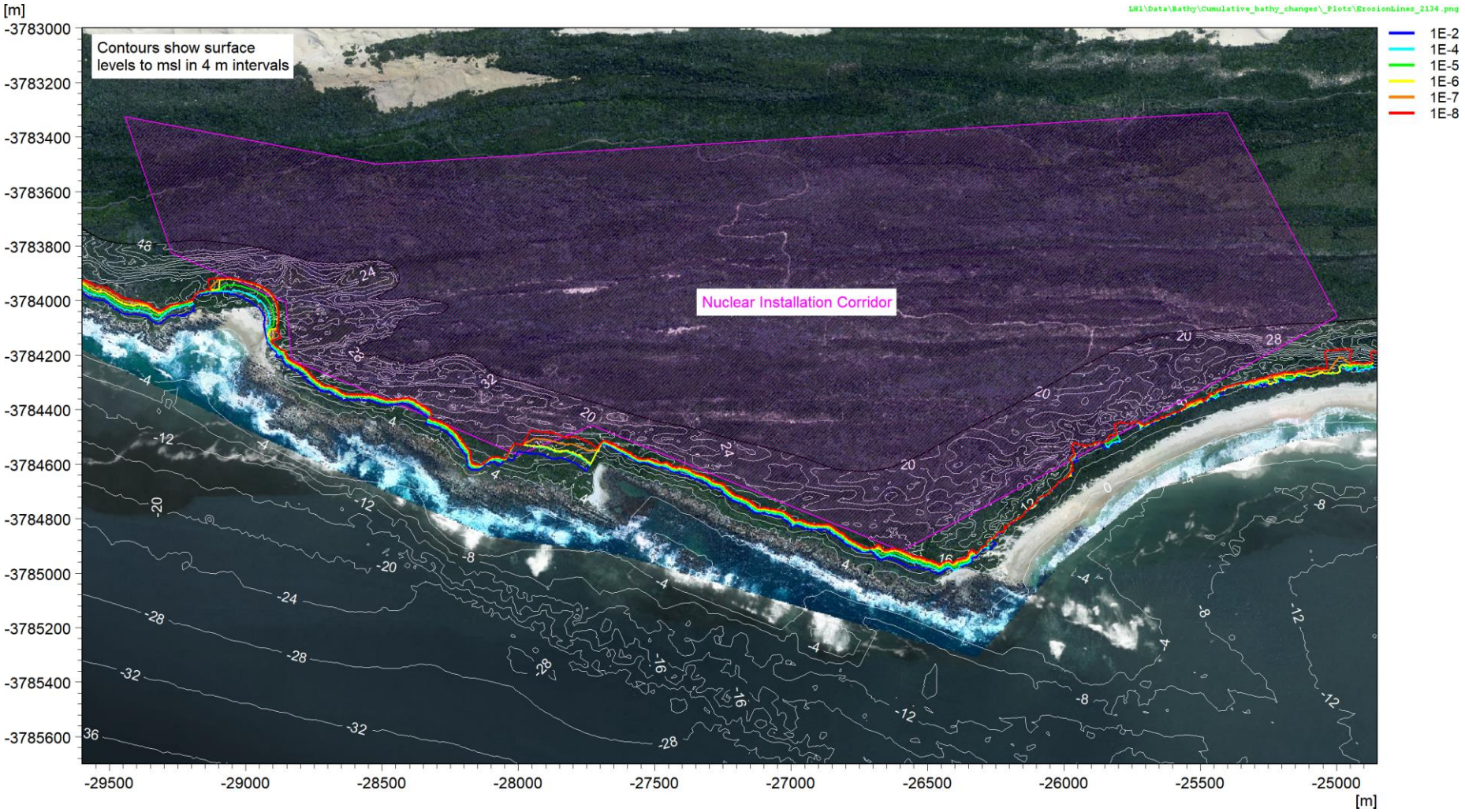


Figure 5.9-92: Erosion Lines for the Labelled Storm Frequencies: 2134. The Contours Indicate the Pre-Storm Bathymetry.

CONTROLLED DISCLOSURE

When downloaded from the EDS database, this document is uncontrolled and the responsibility rests with the user to ensure it is in line with the authorised version on the database.

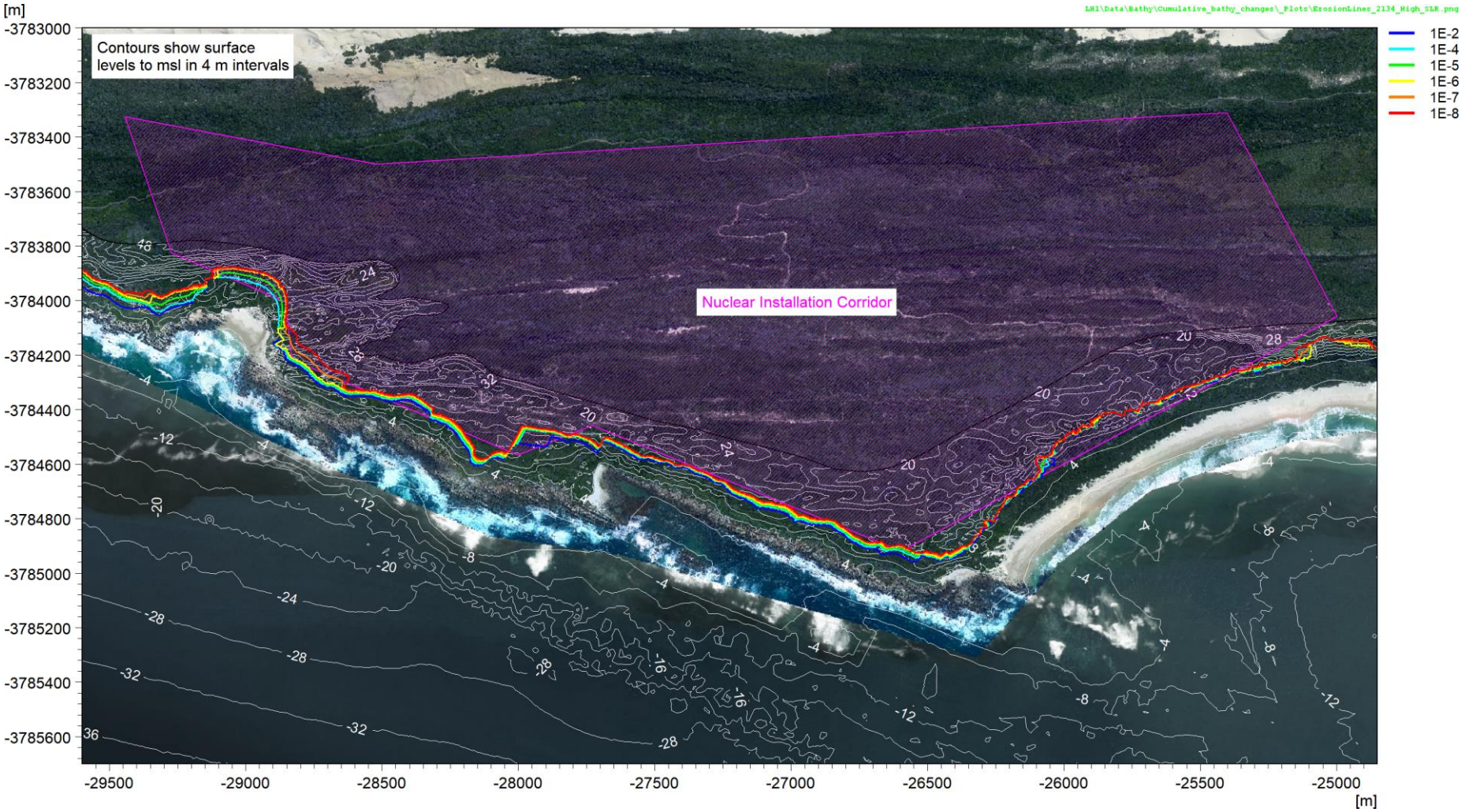


Figure 5.9-93: Erosion Lines for the Labelled Storm Frequencies: 2134 High SLR. The Contours Indicate the Pre-Storm Bathymetry.

CONTROLLED DISCLOSURE

When downloaded from the EDS database, this document is uncontrolled and the responsibility rests with the user to ensure it is in line with the authorised version on the database.

These results show the following:

- The coastline erosion increases over time due to climate change which causes sea level rise and associated coastline recession, a rotated wave climate, and increases in storm wave height and storm surge.
- The erosion is more severe in Thysbaai than on the rocky coastline in the west, driven by recession due to sea level rise and coastline changes due to wave climate change which affect sandy coastlines.
- In 2034 only the 1E-8 y^{-1} storm erosion line extends onto a small section of the Nuclear Installation Corridor near the centre of the rocky coastline west of Thyspunt.
- By 2134 the Nuclear Installation Corridor is exceeded by the erosion lines for all storms with exceedance frequencies of 1E-2 y^{-1} and lower, at a limited number of locations along the rocky coastline west of Thyspunt and within Thysbaai.
- The 2134 High SLR scenario increases the erosion along the entire site, most substantially within Thysbaai. The erosion lines for all storms with exceedance frequencies of 1E-2 y^{-1} and lower extend onto the Nuclear Installation Corridor along the majority of Thysbaai and along the westernmost half of the rocky coastline west of Thyspunt.
- Note that these erosion lines show the extent of erosion of the topography which will threaten safety related structures, systems and components (SSCs) at the site. Wave run-up and flooding due to storm waves or tsunamis may extend further inland than these erosion lines. Flooding is assessed in ***Subsections 5.9.12, 5.9.13*** and ***5.9.14***.
- Further engineering studies should be undertaken to ensure that the outfall structures can withstand the predicted coastline erosion over the operating life of the plant.

5.9.11.8 Suspended Sand at Intakes

The proposed seawater intake is a tunnel extending to approximately -30 m msl water depth, with the intake opening positioned 3 to 5 m above the seabed (see ***Subsection 5.9.16.3***). One of the design parameters will be the volume of sand drawn into the intake which will have to be removed from the proposed landside intake basin. Modelling was performed to estimate the volume of sand drawn into the intakes. The model description, setup and cases modelled are described in Appendix 5.9.A.5.

Figure 5.9-94 shows an example of the modelled vertical profile of suspended sand in a depth -30 m msl at the peak of the 1E-8 y^{-1} storm. The results show the reduction in sand concentrations with increasing distance from the seabed.

CONTROLLED DISCLOSURE

When downloaded from the EDS database, this document is uncontrolled and the responsibility rests with the user to ensure it is in line with the authorised version on the database.

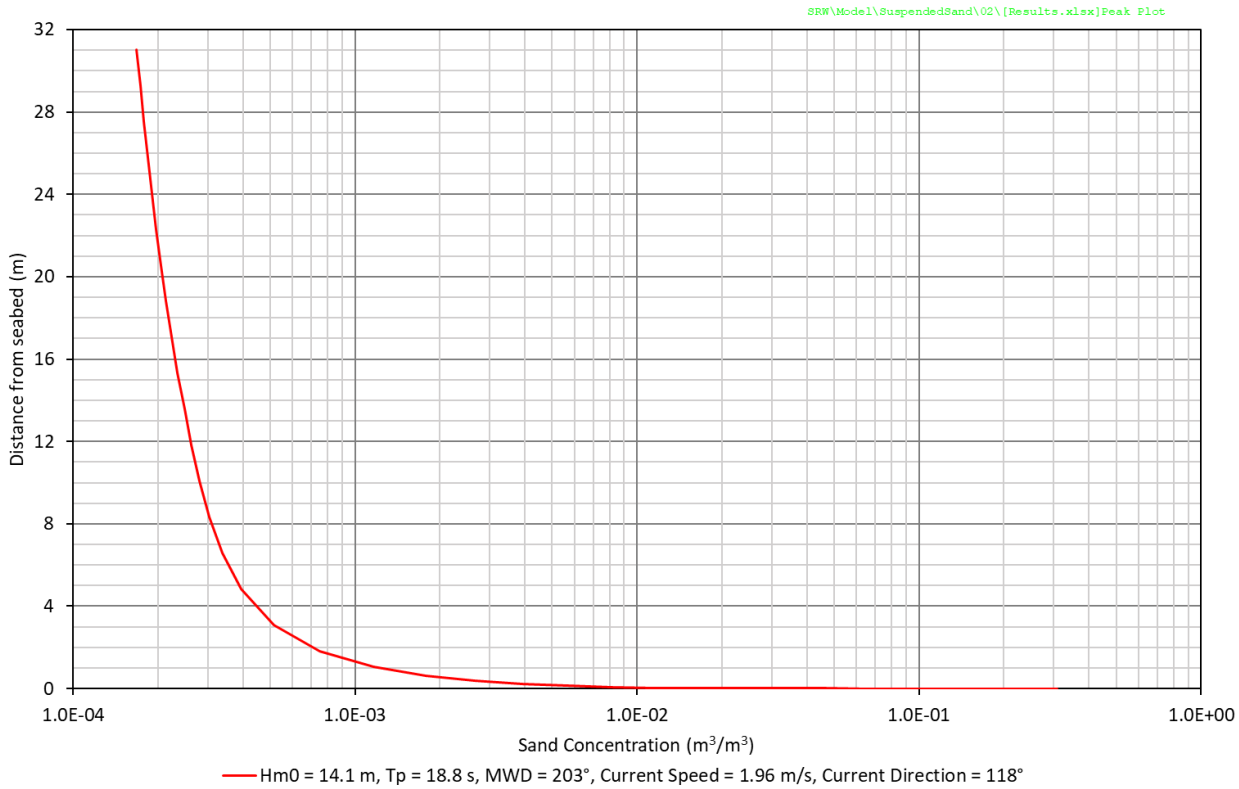


Figure 5.9-94: Example of Modelled Vertical Profile of Suspended Sand in -30 m msl at the Peak of the 1E-8 y^{-1} Storm.

The sand volumes drawn into the cooling water intake tunnels for the 10 000 MWe power station and an associated intake flow rate of 445 m^3/s are provided in ***Table 5.9-28***. Results are provided at the level of the intake openings 3 m and 5 m above the seabed, as well as 1 m above seabed. The latter accounts for the possible enhancement of sediment concentration around the intake shafts, or sand wave-induced build-up around the intake. However, it is sediment scour that is more likely around the intake structure which makes the results at 1 m above the seabed conservative.

The volumes are calculated as the suspended sand concentration at the given distance above seabed multiplied by the intake flow rate, integrated over the duration of the event, and then converted to bulk sand volume assuming a porosity of 0.4.

CONTROLLED DISCLOSURE

When downloaded from the EDS database, this document is uncontrolled and the responsibility rests with the user to ensure it is in line with the authorised version on the database.

Table 5.9-28: Sand Volume Drawn into Cooling Water Intake Tunnels for 10 000 MWe Power Station.

Exceedance Frequency (y^{-1})	Case	Units	Intake at -30 m msl		
			1 m above bed	3 m above bed	5 m above bed
-	Operational Conditions	m^3/y	2 900	690	390
10^{-2}	Storm event	m^3/event	2 500	460	290
10^{-4}	Storm event	m^3/event	10 000	2 200	1 400
10^{-5}	Storm event	m^3/event	18 000	4 100	2 700
10^{-6}	Storm event	m^3/event	30 000	7 600	5 500
10^{-7}	Storm event	m^3/event	54 000	15 000	10 000
10^{-8}	Storm event	m^3/event	96 000	28 000	21 000

Notes:

(a) These sand volumes apply for a 10 000 MWe power station and an associated intake flow rate of 445 m^3/s. They can be reduced proportionally for a lower power and flow rate.

These results show the following:

- For operational conditions the volume of sand drawn into the tunnel intakes which will have to be removed from the proposed landside intake basins is less than 2 900 m^3/y.
- A maintenance dredging programme will be required to prevent excessive sedimentation in the basin and to keep a sufficient buffer for storm events.
- For extreme storm events the sand volume increases significantly and the 1E-2 y^{-1} storm event results in similar sand volumes over the 5.4-day event as the annual maintenance dredging requirements. The intake basin will need to be designed to accommodate these sediment volumes without blocking the pumps.

5.9.12 Storm Wave Run-Up and Drawdown

5.9.12.1 Introduction

This section describes the results of the wave modelling undertaken to estimate the maximum wave run-up and drawdown due to storms at the site. The model description, set-up, calibration and cases modelled are described in ***Appendix 5.9.A.6***.

5.9.12.2 Example Outputs

Figure 5.9-95 shows an example of the progression of waves across the model domain for the 1E-8 y^{-1} wave-dominated storm case in 2034, including two profiles of the water surface elevation and orbital velocities

When downloaded from the EDS database, this document is uncontrolled and the responsibility rests with the user to ensure it is in line with the authorised version on the database.

within the domain. The following processes can be seen: wave diffraction, wave refraction, wave breaking, wave set-up and wave run-up. Profile 2 highlights the influence of the reef at approximately 1 300 m along the profile, resulting in notable dissipation of energy due to wave breaking and diffraction. This can also be seen in the plan view of water surface elevation which shows reduced wave heights along Thysbaai.

Figure 5.9-96 shows an example of the instantaneous water surface elevation and depth-averaged currents at the bay to the west of the site. The arriving wave within the bay can be seen by means of the wave crest, while notable wave run-up can be observed to the west of the bay. Several low-lying valleys that surround the bay are flooded by the arriving waves, ultimately reaching the estimated position of the Nuclear Installation Corridor.

CONTROLLED DISCLOSURE

When downloaded from the EDS database, this document is uncontrolled and the responsibility rests with the user to ensure it is in line with the authorised version on the database.

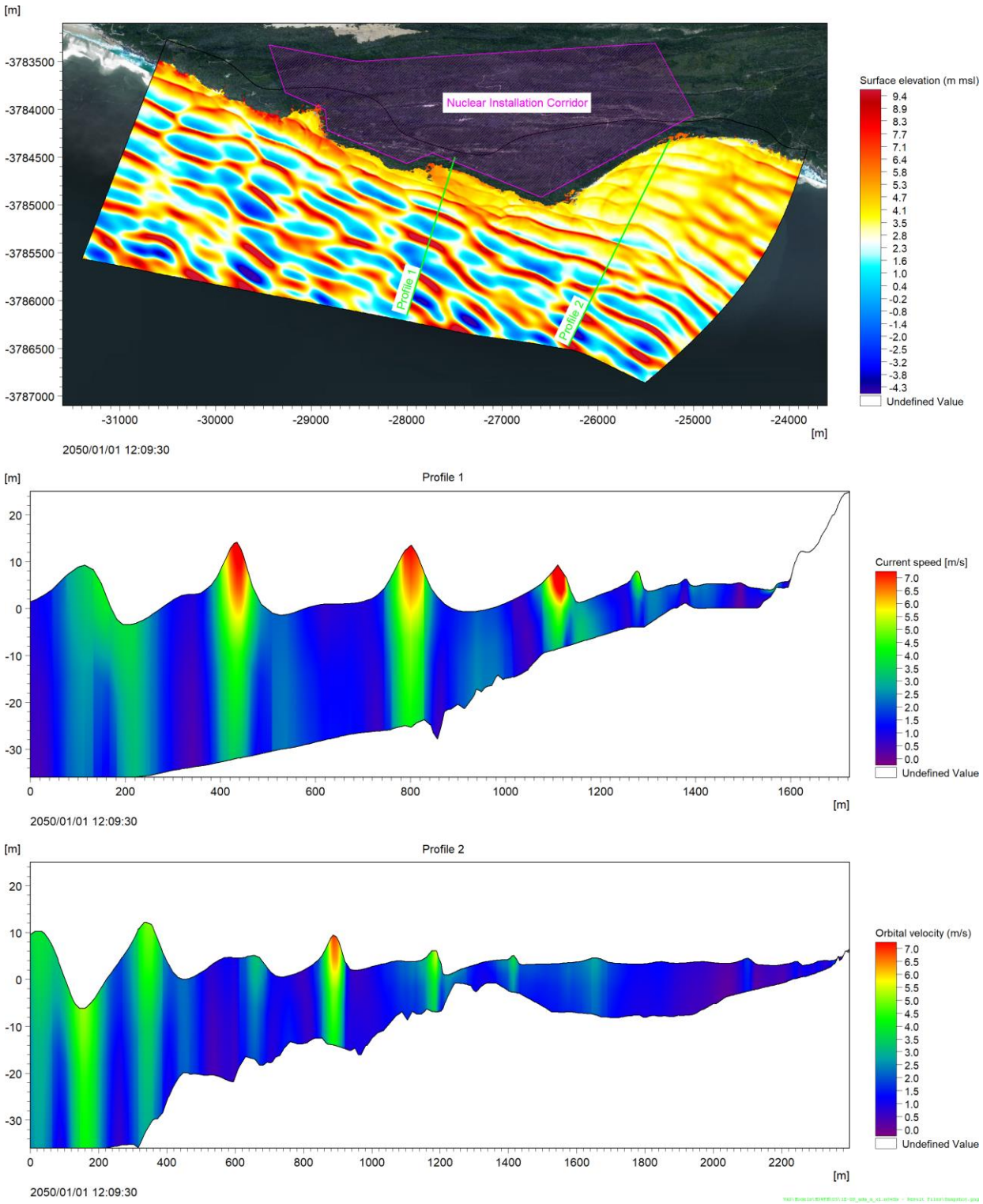


Figure 5.9-95: Instantaneous Water Surface Elevation (Top) and Profiles of Water Surface Elevation with Orbital Velocities for the 1E-8 y^{-1} Wave-Dominated Storm Case in 2034.

CONTROLLED DISCLOSURE

When downloaded from the EDS database, this document is uncontrolled and the responsibility rests with the user to ensure it is in line with the authorised version on the database.

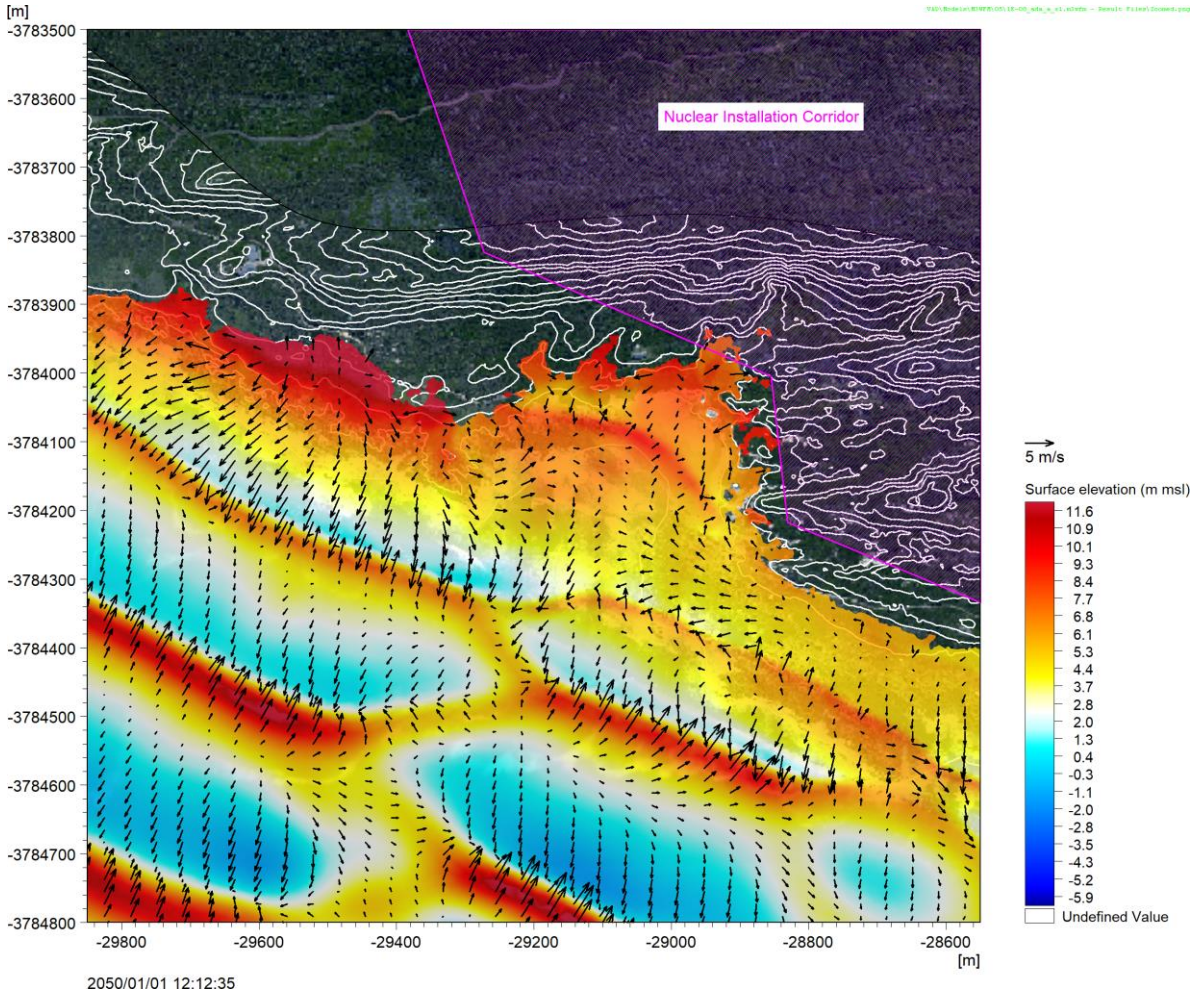


Figure 5.9-96: Instantaneous Water Surface Elevation (Contours) and Depth-Averaged Currents (Vectors) at the Bay to the West of the Site for the 1E-8 y^{1} Wave-Dominated Storm Case in 2034.

5.9.12.3 Maximum Flood Lines

The following key results were extracted from the model outputs for each case:

- The maximum flood line defined as the most landward point flooded by wave run-up (see ***Figure 5.9-97***).
- The maximum vertical run-up level, defined as the highest ground level that was flooded (see ***Figure 5.9-97***). Depending on the topography, this point may or may not coincide with the maximum flood line.
- The minimum drawdown level at the cooling water intakes at the -30 m msl depth

CONTROLLED DISCLOSURE

When downloaded from the EDS database, this document is uncontrolled and the responsibility rests with the user to ensure it is in line with the authorised version on the database.

- For each exceedance frequency, both joint probability combinations of positive storm surge and wave height were modelled. Due to the randomness inherent in wave simulations (see ***Appendix 5.9.A.6***), three seeds were simulated for each scenario. When calculating the maximum vertical run-up level, only elements that were flooded by at least two out of three simulations were considered, i.e. the median. Similarly, when calculating the minimum drawdown level, the median of the three seeds was used.

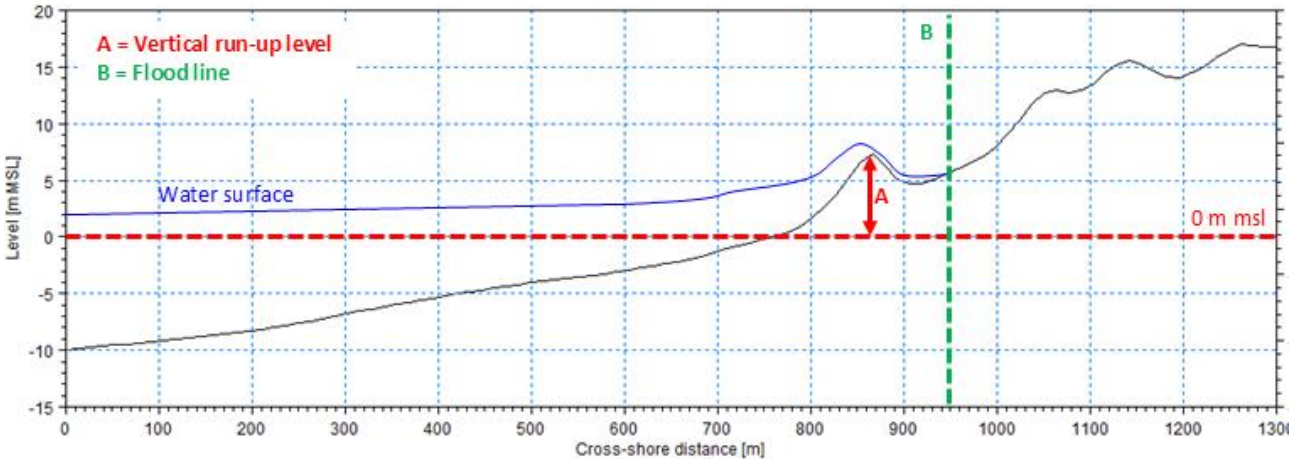


Figure 5.9-97: Definition Sketch for Vertical Run-Up Level and the Horizontal Flood Line.

Maximum flood lines for 2034, 2134 and 2134 with high sea level rise are presented in ***Figure 5.9-98***, ***Figure 5.9-99*** and ***Figure 5.9-100*** respectively. The location of the maximum vertical run-up level for each labelled frequency is indicated with markers on all figures.

CONTROLLED DISCLOSURE

When downloaded from the EDS database, this document is uncontrolled and the responsibility rests with the user to ensure it is in line with the authorised version on the database.

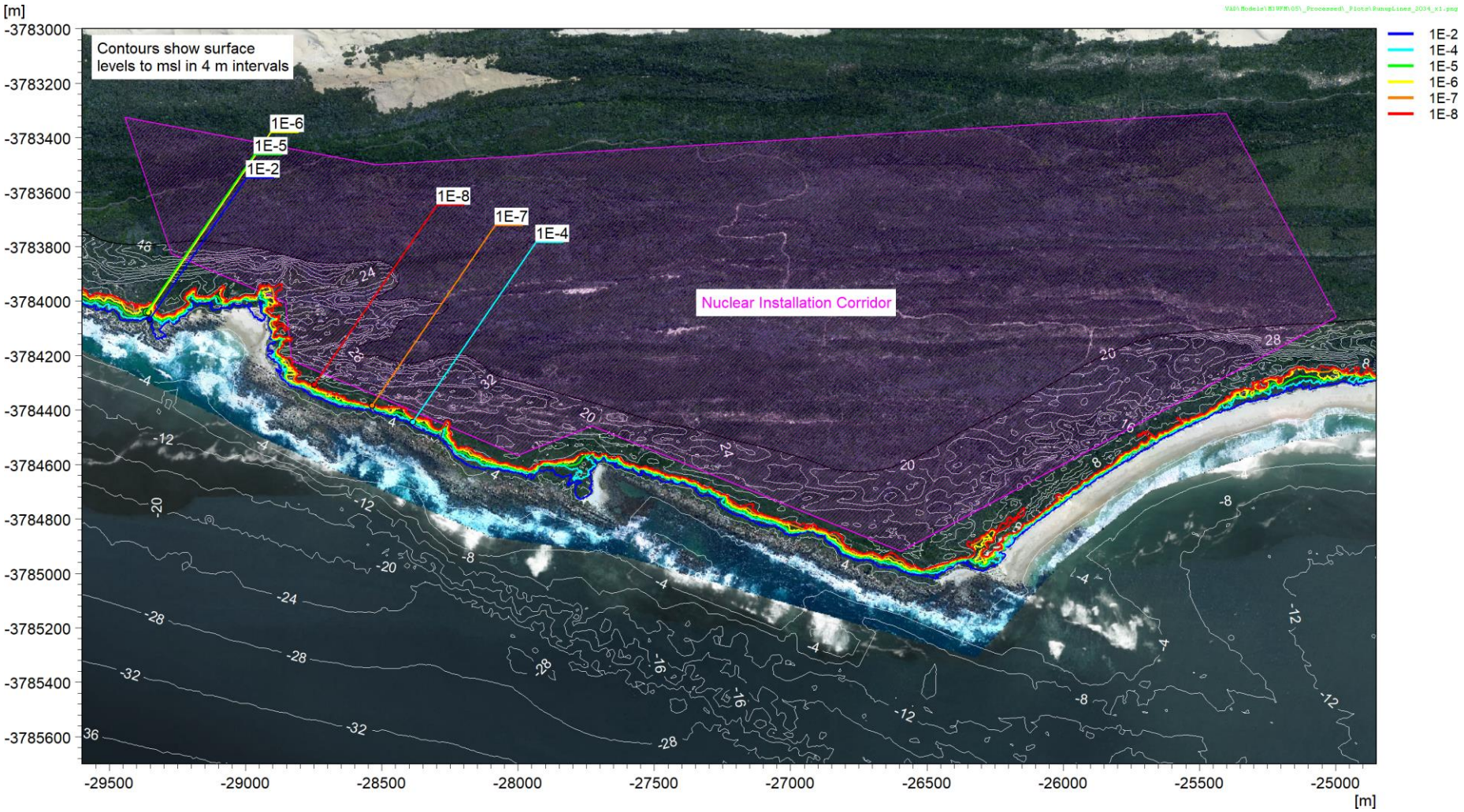


Figure 5.9-98: Maximum Flood Lines Due to Storm Wave Run-Up for the Labelled Storm Frequencies in 2034.

CONTROLLED DISCLOSURE

When downloaded from the EDS database, this document is uncontrolled and the responsibility rests with the user to ensure it is in line with the authorised version on the database.

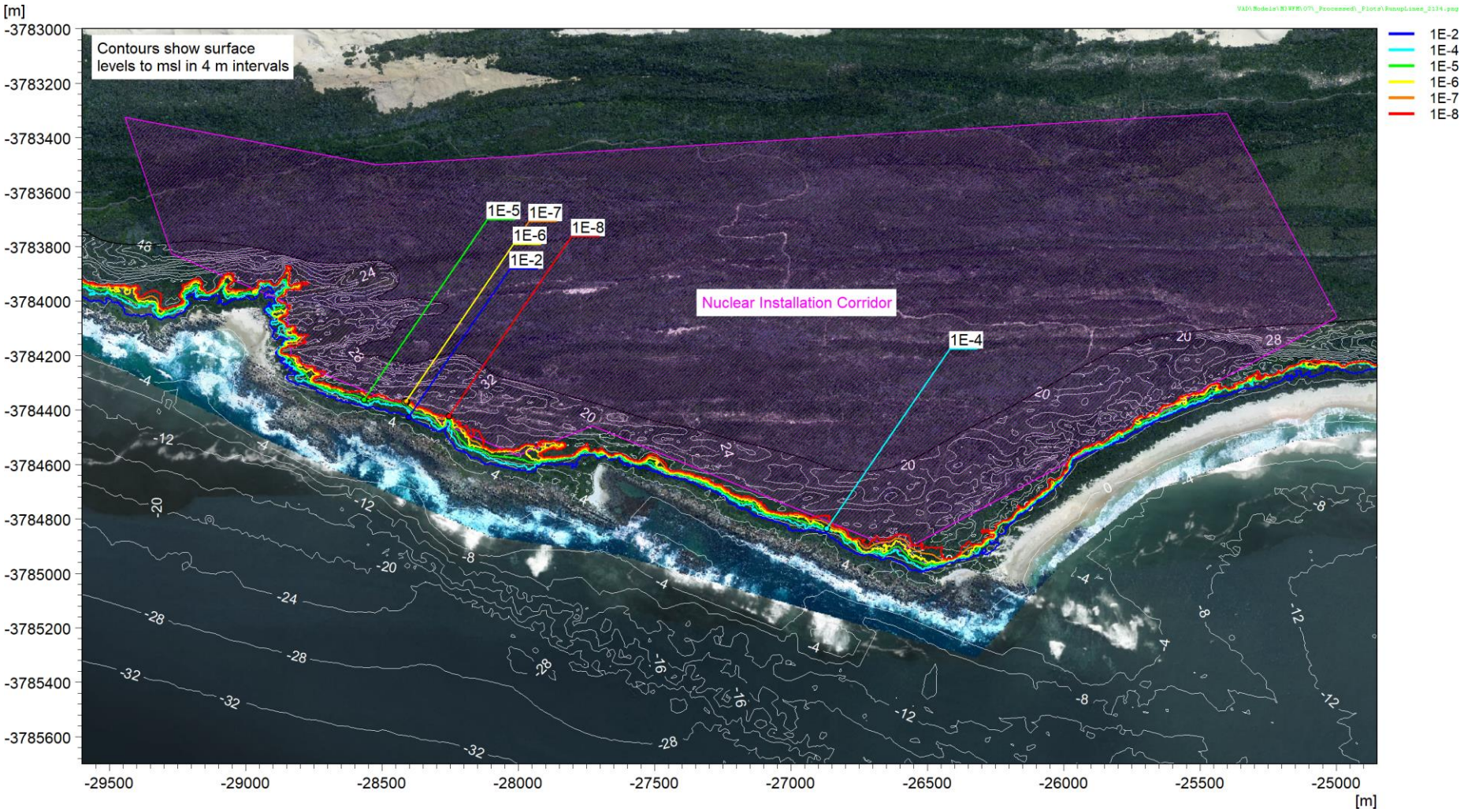


Figure 5.9-99: Maximum Flood Lines Due to Storm Wave Run-Up for the Labelled Storm Frequencies in 2134.

CONTROLLED DISCLOSURE

When downloaded from the EDS database, this document is uncontrolled and the responsibility rests with the user to ensure it is in line with the authorised version on the database.

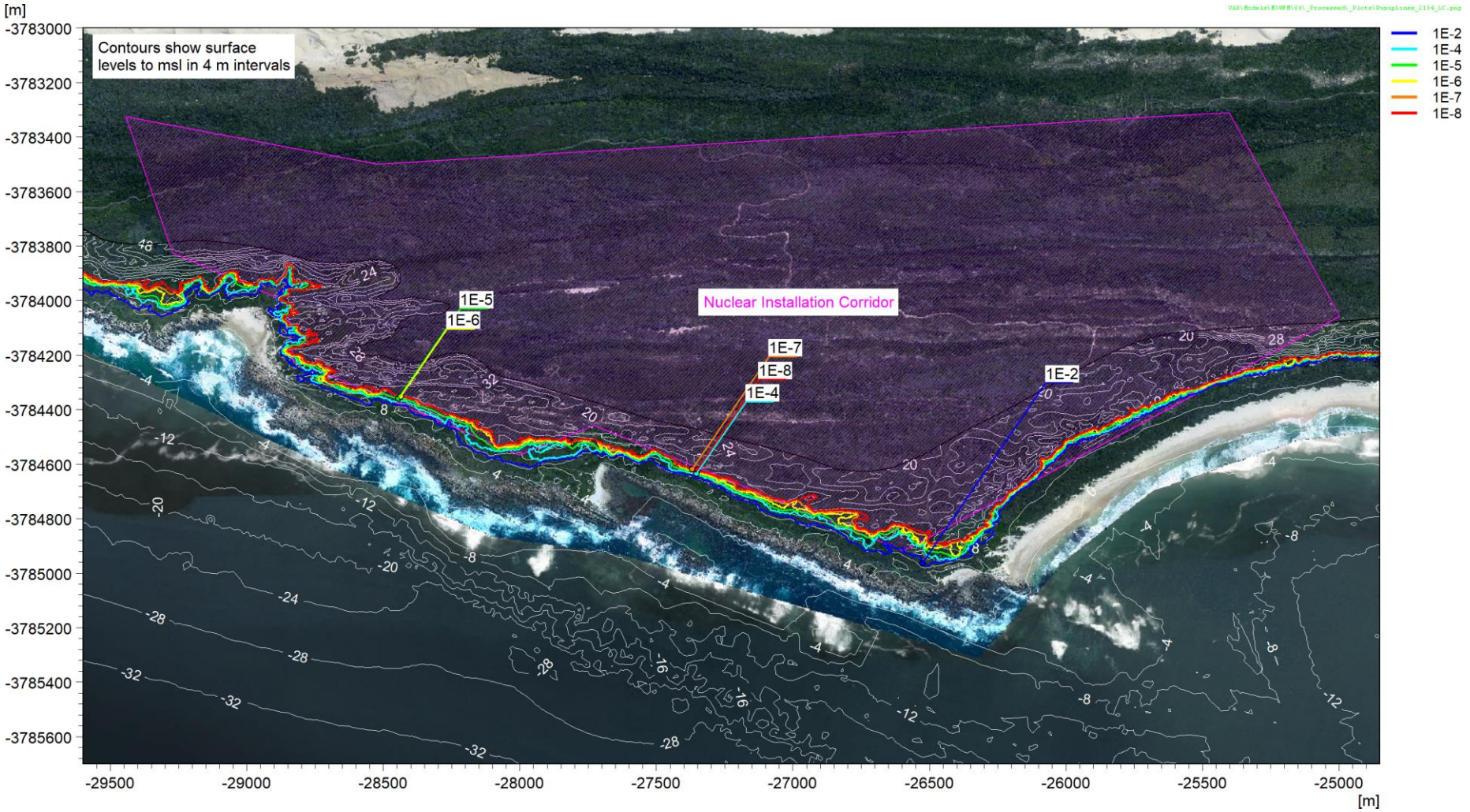


Figure 5.9-100: Maximum Flood Lines Due to Storm Wave Run-Up for the Labelled Storm Frequencies in 2134, High SLR.

CONTROLLED DISCLOSURE

When downloaded from the EDS database, this document is uncontrolled and the responsibility rests with the user to ensure it is in line with the authorised version on the database.

5.9.12.4 Maximum Vertical Run-Up

The extreme flooding results for all exceedance frequencies are provided in ***Table 5.9-29*** and plotted in ***Figure 5.9-101***. These show the maximum storm wave run-up occurring anywhere in the area shown in the flood line plots. These values also correspond with the markers presented in ***Figure 5.9-98***, ***Figure 5.9-99*** and ***Figure 5.9-100*** that indicate the location of maximum vertical run-up level for each modelled frequency. Results include the best estimate from the model results, plus the mean, 5th and 95th percentile uncertainties, which have been calculated using the uncertainty methodology described in ***Appendix 5.9.A.6***.

Table 5.9-29: Extreme Flooding Due to Storm Waves.

Exceedance Frequency	Uncertainty	Maximum Vertical Run-Up Level		
(y^{-1})		(m msl)		
		2034	2134	2134 High SLR
1E-2	5th Percentile	7.54	11.60	13.13
	Mean	8.00	12.06	13.69
	Best Estimate	7.99	12.04	13.67
	95th Percentile	8.47	12.52	14.25
1E-4	5th Percentile	9.57	12.66	15.52
	Mean	10.47	13.56	16.60
	Best Estimate	10.44	13.53	16.56
	95th Percentile	11.37	14.46	17.68
1E-5	5th Percentile	11.62	14.80	16.63
	Mean	12.74	15.92	17.97
	Best Estimate	12.70	15.89	17.93
	95th Percentile	13.86	17.05	19.32
1E-6	5th Percentile	11.64	14.95	17.96
	Mean	12.99	16.30	19.58
	Best Estimate	12.95	16.26	19.53
	95th Percentile	14.34	17.65	21.20
1E-7	5th Percentile	11.69	15.52	18.63
	Mean	13.27	17.11	20.32
	Best Estimate	13.23	17.06	20.27
	95th Percentile	14.85	18.69	22.00
1E-8	5th Percentile	11.50	15.78	19.13
	Mean	13.31	17.59	21.09
	Best Estimate	13.26	17.55	21.04
	95th Percentile	15.12	19.41	23.05

CONTROLLED DISCLOSURE

When downloaded from the EDS database, this document is uncontrolled and the responsibility rests with the user to ensure it is in line with the authorised version on the database.

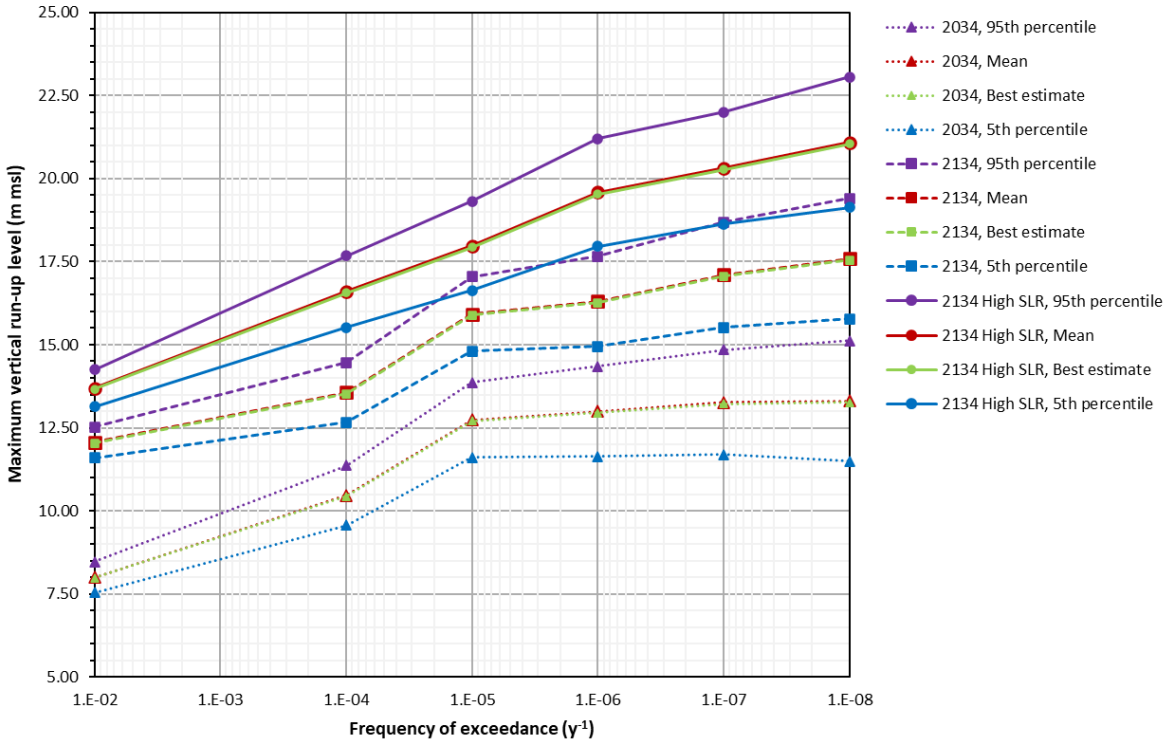


Figure 5.9-101: Vertical Run-Up Levels Due to Storm Waves.

The extreme flooding results presented above show the following:

- The flooding hazard increases over time due to climate change which causes sea level rise and associated coastline recession, a rotated wave climate, and increases in storm wave height and storm surge.
- The best estimate maximum vertical run-up level in 2034 due to the 1E-8 y^{-1} storm is 13.3 m msl, increasing to 17.6 m msl in 2134, and 21.0 m msl for the 2134 High SLR scenario.
- The maximum wave run-up for all frequencies in 2034 and both 2134 scenarios occurred along the exposed rocky coastline to the west of Thyspunt, while Thysbaai to the east of Thyspunt experienced significant landward flooding due to coastline recession.
- The flood lines extend into the estimated position of the Nuclear Installation Corridor for all three climate change scenarios. The Nuclear Installation Corridor is reached by all exceedance frequencies in 2034 except for 1E-2 y^{-1}, while all exceedance frequencies reach the corridor in both 2134 scenarios.
- The SSCs will need to be placed landward of the maximum flood lines, or alternatively protective structures such as revetments and wave walls will need to be placed in front of the SSCs. The SSCs will also need to be placed landward of the maximum erosion lines presented in ***Figure 5.9-91*** to ***Figure 5.9-93***.

CONTROLLED DISCLOSURE

When downloaded from the EDS database, this document is uncontrolled and the responsibility rests with the user to ensure it is in line with the authorised version on the database.

The warning time for these storm events is related to the wave and storm surge forecasts provided by the South African Weather Service and other forecast agencies. It is likely that an extreme storm event will be identified a number of days in advance.

As described in ***Subsection 5.9.11.5***, the duration of an extreme storm is approximately 5 days, although the maximum run-up and minimum drawdown are likely to occur over a few hours at the peak of the storm and will be associated with a group of large waves.

5.9.12.5 Minimum Vertical Drawdown

The extreme low water levels at the three proposed cooling water intakes in depths of −28.8 to −30.0 m msl (see ***Figure 5.9-104***) for all exceedance frequencies are provided in ***Table 5.9-30*** and plotted in ***Figure 5.9-102***. Uncertainties were calculated using the methodology described in ***Appendix 5.9.A.6***, but replacing drawdown for run-up.

CONTROLLED DISCLOSURE

When downloaded from the EDS database, this document is uncontrolled and the responsibility rests with the user to ensure it is in line with the authorised version on the database.

Table 5.9-30: Extreme Low Water Levels Due to Storm Waves.

Exceedance Frequency	Uncertainty	Minimum Vertical Drawdown Level at Intakes	
(y^{-1})		(m msl)	
		2034	2134
1E-2	5th Percentile	-6.09	-6.49
	Mean	-6.01	-6.43
	Best Estimate	-6.01	-6.43
	95th Percentile	-5.94	-6.37
1E-4	5th Percentile	-6.85	-7.16
	Mean	-6.70	-7.05
	Best Estimate	-6.71	-7.05
	95th Percentile	-6.56	-6.95
1E-5	5th Percentile	-7.00	-7.38
	Mean	-6.84	-7.25
	Best Estimate	-6.84	-7.25
	95th Percentile	-6.67	-7.12
1E-6	5th Percentile	-7.17	-7.59
	Mean	-6.96	-7.43
	Best Estimate	-6.97	-7.44
	95th Percentile	-6.77	-7.28
1E-7	5th Percentile	-7.41	-7.69
	Mean	-7.18	-7.50
	Best Estimate	-7.18	-7.51
	95th Percentile	-6.95	-7.33
1E-8	5th Percentile	-7.65	-7.78
	Mean	-7.39	-7.57
	Best Estimate	-7.39	-7.58
	95th Percentile	-7.13	-7.38

CONTROLLED DISCLOSURE

When downloaded from the EDS database, this document is uncontrolled and the responsibility rests with the user to ensure it is in line with the authorised version on the database.

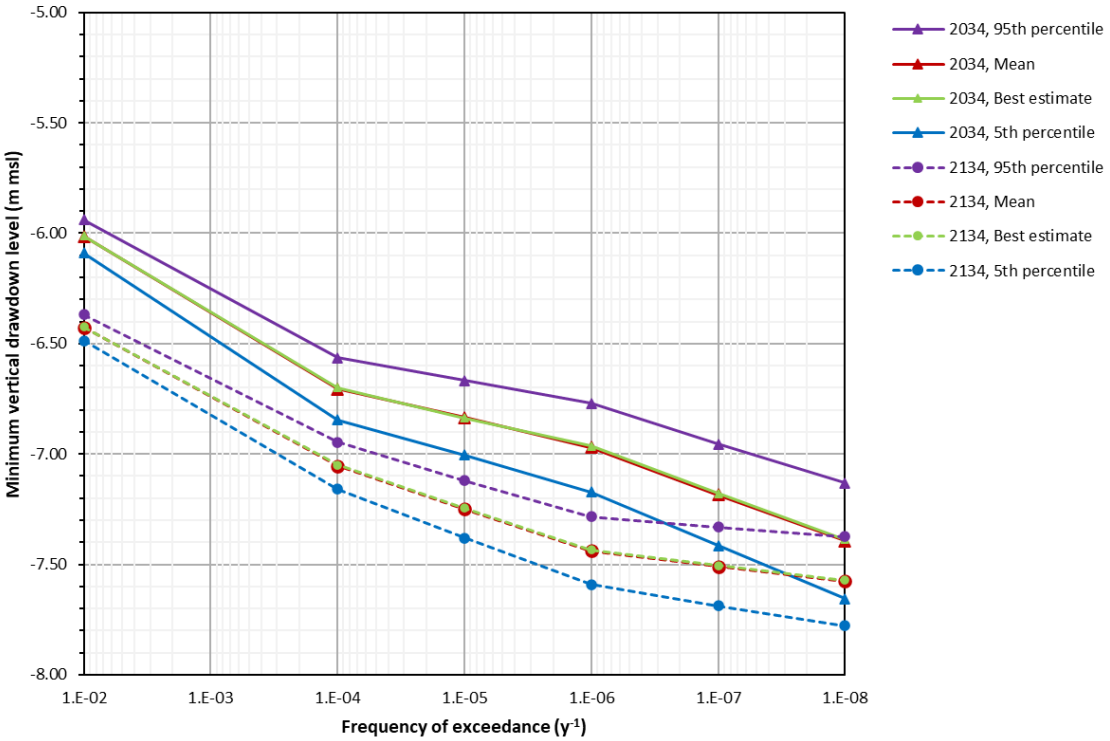


Figure 5.9-102: Extreme Low Water Levels at the Intakes Due to Storm Waves.

The extreme low water level results presented above show the following:

- The extreme low water levels do not change significantly over time, since sea level rise has conservatively been excluded, and because the coastline erosion has little impact on these low water levels.
- Drawdown levels in 2134 increase at a reduced rate with increasing frequency of exceedance due to the depth limitation of waves at the location of the intakes.
- If a tunnel intake in a depth of -30 m msl is selected for the new NIs, then the results show that the intake should be designed to accommodate a best estimate minimum water level of -7.6 m msl, which is driven by the 1E-8 y^{-1} storm event in 2134.

5.9.13 Tsunamis

5.9.13.1 Introduction

The hazards that tsunamis pose to the site include:

- Flooding from the sea; and
- Extreme low water levels at the cooling water intakes.

CONTROLLED DISCLOSURE

When downloaded from the EDS database, this document is uncontrolled and the responsibility rests with the user to ensure it is in line with the authorised version on the database.

The scope of work for this update of the SSR excluded an updated Tsunami Hazard Analysis (THA). This SSR will thus need to be updated once an updated THA has been undertaken. In the interim the following three sources of tsunami hazard information are summarised below:

- the initial Tsunami Hazard Analysis undertaken for the previous Thyspunt SSR in 2012 (Eskom, 2013);
- the deterministic Tsunami Hazard Analysis undertaken for the Duynefontyn SSR in 2022 (Eskom, 2024b); and
- the probabilistic Tsunami Hazard Analysis undertaken for the Duynefontyn SSR in 2024 (Eskom, 2024b).

5.9.13.2 Initial Tsunami Hazard Analysis Undertaken for the Previous Thyspunt SSR in 2012

An initial THA was undertaken for Section 5.9 of the previous Thyspunt SSR in 2012 (Eskom, 2013). That study assessed distant earthquake tsunamigenic sources at Sumatra (Indonesia), Karachi (Pakistan) and the South Sandwich Islands (South Atlantic Ocean). For each source region the probable maximum earthquake magnitude and the corresponding fault parameters were defined and a numerical model was then used to propagate the tsunami waves to the Thyspunt site. Based on these results the following tsunami run-up levels were recommended at the Thyspunt site:

- Tsunami run-up height of 2.5 m;
- Tsunami drawdown of -2.0 m.

These are the maximum tsunami-induced run-up height and drawdown relative to the antecedent water level, which must be added to these values to obtain the total tsunami run-up and drawdown levels.

The initial THA also assessed local tsunamigenic sources in the form of submarine slumps on the South African shelf margin in the Agulhas and Cape Town slump regions. However, since a quantitative assessment of the risk of occurrence and geometry of future slump events along the South African shelf margin was not available at this time, this assessment was qualitative only.

Based on these limitations, Section 5.9 of the previous Thyspunt SSR in 2012 (Eskom, 2013) recommended that all the outstanding tsunamigenic sources be quantified and the associated tsunami run-ups at the site modelled in a future revision of the SSR.

CONTROLLED DISCLOSURE

When downloaded from the EDS database, this document is uncontrolled and the responsibility rests with the user to ensure it is in line with the authorised version on the database.

5.9.13.3 Deterministic Tsunami Hazard Analysis Undertaken for the Duynefontyn SSR in 2022

To address the limitations of the 2012 tsunami study at the Duynefontyn site (which were the same as described for the TSSR above), a deterministic Tsunami Hazard Analysis was undertaken in 2022 as part of the update of the SSR for the Duynefontyn site (Eskom, 2024b), comprising both the existing Koeberg Nuclear Power Station (KNPS) and the planned development of new nuclear installation(s) (NIs). Although this analysis was for Duynefontyn rather than Thyspunt, the results provide valuable insights and are thus summarised below.

The scope of work of the deterministic THA was to assess the hazard due to the following tsunamigenic sources:

- Distant earthquakes;
- Local earthquakes;
- Submarine slumps;
- Submarine slides;
- Volcanoes;
- Local subaerial landslides; and
- Meteorites.

The approach was systematic and hierarchal, comprising data gathering, preliminary source characterisation, refined source characterisation, numerical modelling of tsunami propagation and sensitivity testing. The output of the deterministic THA was the Probable Maximum Tsunami (PMT) run-up, drawdown and velocity at the site.

Based on the preliminary source characterisation and tsunami propagation modelling, the following sources were screened in and assessed in more detail:

- Subduction zone interface earthquakes on the Scotia (South Sandwich Islands) subduction zone;
- Local submarine landslides on the continental slope offshore of Cape Town; and
- Volcanic flank collapse landslides from Ascension, Tristan da Cunha and Marion Islands.

The tsunami run-up results are summarised below in ***Table 5.9-31***. Although results are available for both the existing KNPS and the new NIs on the Duynefontyn site, only the results for the new NIs are presented here,

CONTROLLED DISCLOSURE

When downloaded from the EDS database, this document is uncontrolled and the responsibility rests with the user to ensure it is in line with the authorised version on the database.

as these are for the natural topography without the KNPS and are thus more similar to the Thyspunt site.

Table 5.9-31: Results of the Deterministic THA at the New NIs at the Duynefontyn Site.

Source Type	Antecedent Water Level[(a)] (m msl)			Tsunami Run-Up Height[(b)] (m)			Tsunami Run-Up Level[(c)] (m msl)		
	2021	2064	2130	2021	2064	2130	2021	2064	2130
Distant earthquakes (Scotia)	1.71	2.16	3.55	4.96	5.06	5.40	6.67	7.22	8.95
Local submarine landslides	1.71	2.16	3.55	5.09	6.03	6.53	6.80	8.19	10.08
Volcanic flank collapse (Tristan da Cunha)	1.71	2.16	3.55	11.00	11.77	12.27	12.71	13.93	15.82

Notes:
(a) The water level before the arrival of the tsunami, comprising the tide, storm surge and sea level rise.
(b) The vertical run-up height above the antecedent water level due to the tsunami.
(c) The total vertical run-up level equal to the sum of the antecedent water level and the tsunami run-up.

These results show that the PMT for the new NIs at the Duynefontyn Site is due to volcanic flank collapse at Tristan da Cunha, with a tsunami run-up height in 2130 of 12.27 m reaching a level of 15.82 m msl.

5.9.13.4 Probabilistic Tsunami Hazard Analysis Undertaken for the Duynefontyn SSR in 2024

Following on from the deterministic THA described above, a probabilistic THA was undertaken in 2024 for volcanic flank collapse tsunamis at the Duynefontyn site (Eskom, 2024b). This included all potential volcanic flank collapse tsunamigenic sources considered to be potential sources of significant tsunami for the Duynefontyn site, comprising the existing KNPS and the proposed new NIs. The outputs are the hazard curves of flood depth, water surface elevation and current speed at KNPS and the new NIs.

The location of the volcanic flank collapse sources is shown in ***Figure 5.9-103***. ***Table 5.9-32*** presents the frequency of occurrence of landslide events and the maximum subevent volume for each source.

CONTROLLED DISCLOSURE

When downloaded from the EDS database, this document is uncontrolled and the responsibility rests with the user to ensure it is in line with the authorised version on the database.

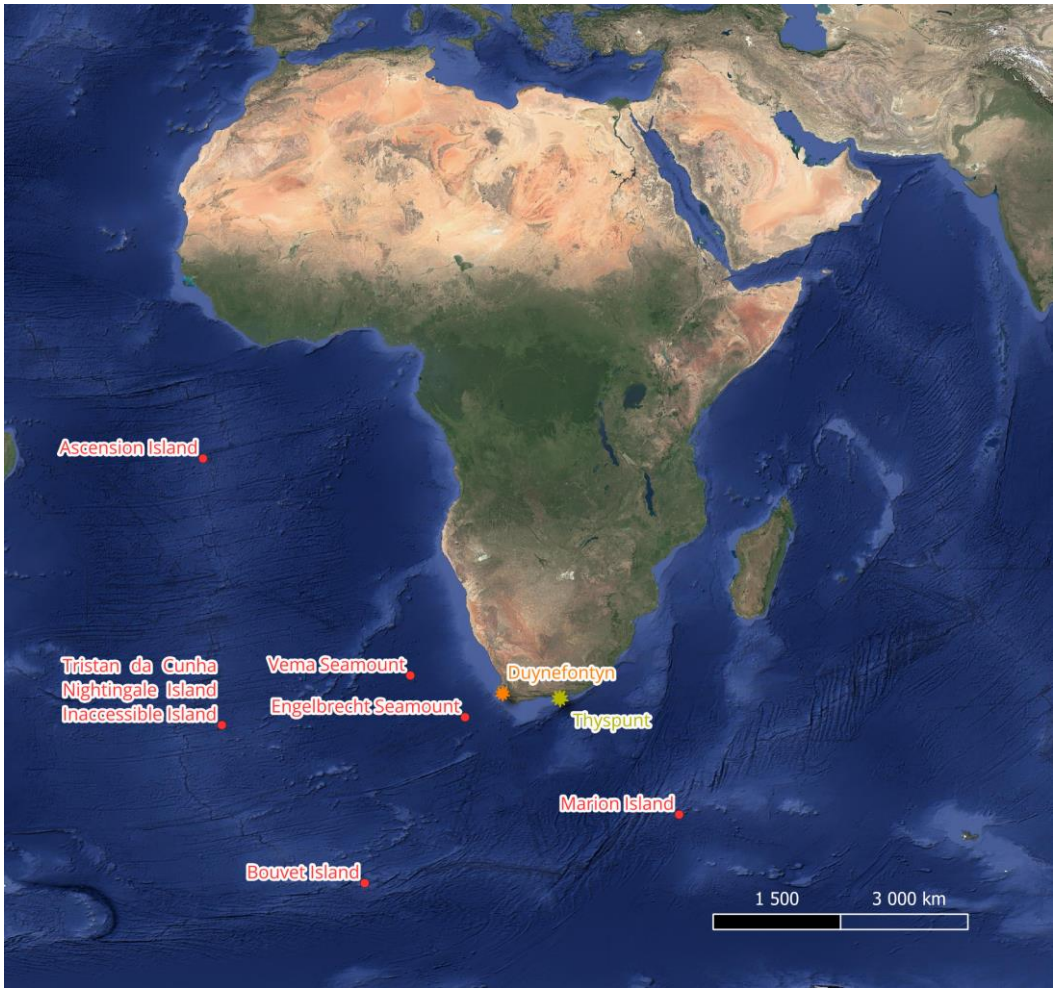


Figure 5.9-103: Location of Each Volcanic Flank Collapse Tsunami Source.

CONTROLLED DISCLOSURE

When downloaded from the EDS database, this document is uncontrolled and the responsibility rests with the user to ensure it is in line with the authorised version on the database.

Table 5.9-32: Frequency of Occurrence and Volume of Landslide Events for Each Volcanic Flank Collapse Source.

Source	Frequency of Occurrence of Landslide Events (Best Estimate) (y^{-1})	Max. Subevent Volume (km^3)
Tristan da Cunha Island	1.63E-05	107
Ascension Island	8.10E-06	107
Marion Island	8.00E-06	107
Bouvet Island	8.00E-06	80
Inaccessible Island	2.10E-06	60
Nightingale Island	2.10E-06	60
Vema Seamount	2.10E-06	60
Engelbrecht Seamount	2.10E-06	60

Following the processing of the source parameters, the landslide kinematics were run for all source scenarios and the corresponding space and time varying bathymetries generated. A propagation model was used to simulate the tsunami generation and propagation from the source to a depth of approximately 50 m offshore of the Duynefontyn site. A local flooding model was used to simulate the wave flooding at the site for multiple antecedent water levels. The results were post-processed to calculate the hazard curves at KNPS and the new NIs, with the tsunami run-up results for the new NIs shown below.

Table 5.9-33: Results of the Probabilistic THA at the New NIs at the Duynefontyn Site.

Frequency of Exceedance (Best Estimate)	Antecedent Water Level[(a)]			Tsunami Run-up Height[(b)]			Tsunami Run-up Level[(c)]		
	(m msl)			(m)			(m msl)		
(y^{-1})	2021	2064	2130	2021	2064	2130	2021	2064	2130
1E-05	1.49	1.89	3.06	3.61	4.06	5.18	5.10	5.95	8.24
1E-06	1.49	1.89	3.06	7.79	8.00	10.32	9.28	9.89	13.38
1E-07	1.49	1.89	3.06	11.35	11.51	13.10	12.84	13.41	16.16
1E-08	1.49	1.89	3.06	13.71	13.70	14.41	15.20	15.60	17.47

Notes:
(a) The water level before the arrival of the tsunami, comprising the tide, storm surge and sea level rise.
(b) The vertical run-up height above the antecedent water level due to the tsunami.
(c) The total vertical run-up level equal to the sum of the antecedent water level and the tsunami run-up.

These results show the combined hazard for all potential volcanic flank collapse tsunamigenic sources, with Tristan da Cunha dominating the hazard. These results show that the tsunami hazard due to volcanic flank collapse for a frequency of exceedance of 1E-07 in 2130 is a tsunami run-

CONTROLLED DISCLOSURE

When downloaded from the EDS database, this document is uncontrolled and the responsibility rests with the user to ensure it is in line with the authorised version on the database.

up height of 13.10 m reaching a level of 16.16 m msl. This result is consistent with the deterministic PMT results in ***Table 5.9-31***.

5.9.13.5 Conclusions and Recommendations for Tsunamis

The deterministic and probabilistic THAs undertaken for Duynefontyn showed that volcanic flank collapse caused significantly larger tsunamis at the Duynefontyn site compared to other potential tsunamigenic sources. Based on these results, it is anticipated that volcanic flank collapse will also cause the largest tsunamis at the Thyspunt site.

Although it is not possible to estimate the tsunami run-up levels at Thyspunt without a site specific THA, considering the distance between the volcanic island sources and the site (***Figure 5.9-103***), as well as the slide frequencies and volumes (***Table 5.9-32***) it is anticipated that Marion Island will likely pose the largest tsunami hazard to the Thyspunt site (among the sources assessed for Duynefontyn), and that this hazard will be comparable to the hazard posed to the Duynefontyn site by Tristan da Cunha, i.e., a tsunami run-up height of approximately 13 m above antecedent water level.

Since the initial THA for Thyspunt in 2012 did not include volcanic flank collapse sources and only considered distant earthquake sources which resulted in a tsunami run-up of only 2.5 m above antecedent water level, it will be inaccurate to use the 2012 tsunami results in this updated SSR.

For this reason, no tsunami results are presented in this SSR and the maximum run-up and drawdown are based on the storm wave results only (see ***Subsection 5.9.12***). Since tsunamis will pose a significant hazard to the site, it is recommended that an updated THA be undertaken for Thyspunt and that this SSR should then be updated once these results are available.

5.9.14 Flooding from the Sea

Flooding from the sea can occur due to:

- Storm wave run-up combined with sea level rise, high tides, positive storm surge and wave set-up, as described in ***Subsection 5.9.12***; and
- Tsunami run-up combined with sea level rise, high tides and positive storm surge.

As described in ***Subsection 5.9.13***, no tsunami results are presented in this SSR and it is recommended that an updated THA be undertaken for Thyspunt and that this SSR should then be updated once these results are available. In the interim the flooding from the sea is based on the storm wave run-up only, as described in ***Subsection 5.9.12***.

CONTROLLED DISCLOSURE

When downloaded from the EDS database, this document is uncontrolled and the responsibility rests with the user to ensure it is in line with the authorised version on the database.

5.9.15 Extreme Low Water Levels

Extreme low water levels at the cooling water intakes can occur due to:

- Storm wave drawdown combined with low tides and negative storm surge, as described in ***Subsection 5.9.12***; and
- Tsunami drawdown combined with low tides and negative storm surge.

As described in ***Subsection 5.9.13***, no tsunami results are presented in this SSR and it is recommended that an updated THA be undertaken for Thyspunt and that this SSR should then be updated once these results are available. In the interim the extreme low water levels are based on the storm wave drawdown only, as described in ***Subsection 5.9.12***.

5.9.16 Thermal Plume Dispersion

5.9.16.1 Introduction

It is proposed that the new NIs will be cooled using a once-through seawater cooling system. A conceptual layout for the seawater cooling intake and outfall system has been developed and thermal plume dispersion modelling has been performed to demonstrate the technical feasibility of the site regarding the following PPE parameters (see ***Table 5.9-3***):

- The range of water temperatures at the intake is -0.5°C to 30°C.
- The intake and the outfall configuration should not result in a net rise in the cooling water temperature. The maximum increase in the temperature (ΔT) of the recirculated water should be less than 1.5°C.

5.9.16.2 Discharge Characteristics

Chapter 3 (Overview of Planned Activities at the Site) indicates that the new NIs at the site will generate 10 000 MWe.

The cooling water discharge characteristics are given in ***Table 5.9-34***. The discharge rate was calculated using a cooling water flow rate of 76 m^3/s per 1708 MWe, with a temperature increase (ΔT) between the intake and the outfall of 12°C, as given in the PPE (see ***Table 5.9-3***).

CONTROLLED DISCLOSURE

When downloaded from the EDS database, this document is uncontrolled and the responsibility rests with the user to ensure it is in line with the authorised version on the database.

Table 5.9-34: Discharge Characteristics.

Parameter	Unit	Value
Discharge rate	m^3/s	445
ΔT	°C	12

5.9.16.3 Engineering Concept for Intake and Outfall Structures

No engineering feasibility studies were performed for the SSR and the conceptual layout thus serves only to demonstrate the technical feasibility of the layout in terms of thermal plume dispersion, recirculation and sediment transport.

The conceptual layout considers offshore tunnel intakes at a depth of −30 m msl and an outfall channel discharging at −5 m msl, based on (Eskom, 2008a). A plan view of the layout is shown in ***Figure 5.9-104***. A schematic diagram of the offshore tunnel intakes is shown in ***Figure 5.9-105***.

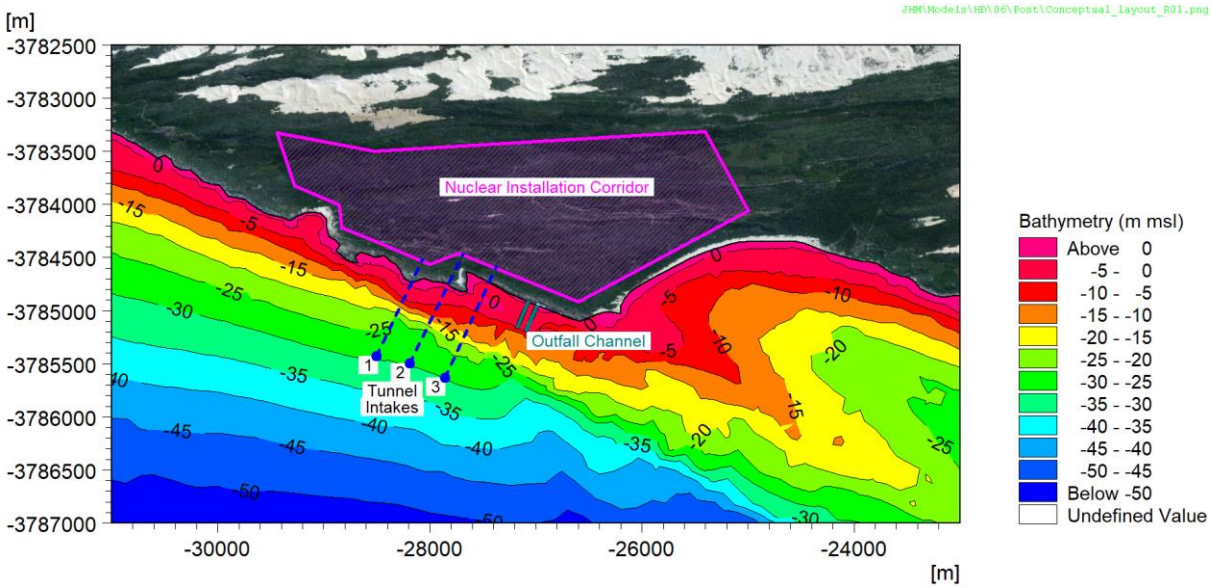


Figure 5.9-104: Tunnel Intakes and Channel Outfall.

CONTROLLED DISCLOSURE

When downloaded from the EDS database, this document is uncontrolled and the responsibility rests with the user to ensure it is in line with the authorised version on the database.

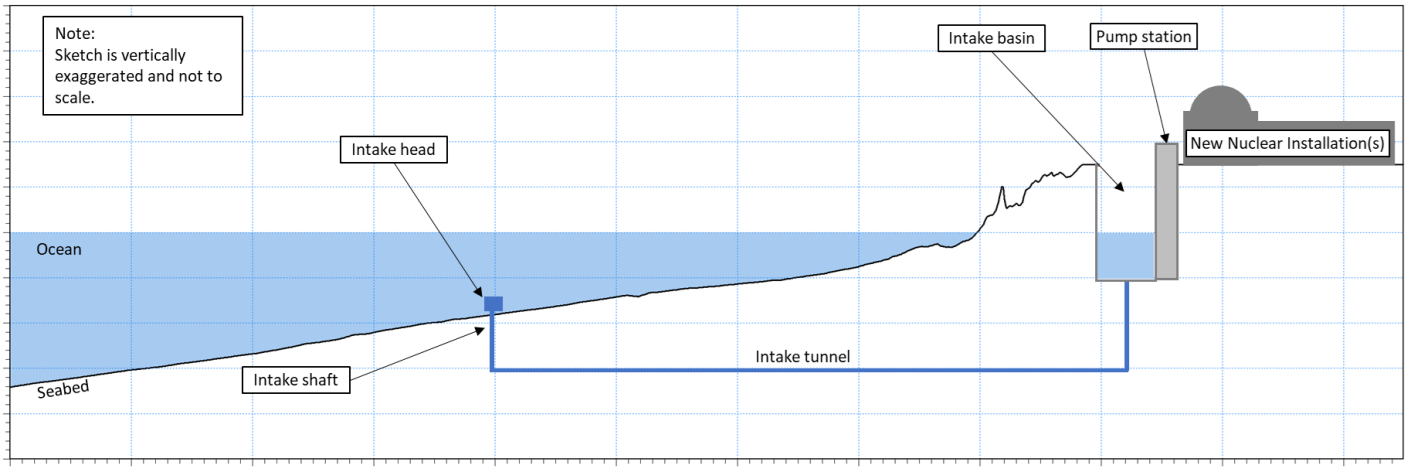


Figure 5.9-105: Schematic Diagram Showing the Main Components for an Offshore Tunnel Intake Configuration.

Figure 5.9-105 illustrates a generic cross-section identifying the main components of this configuration as follows:

- Seawater is pumped from an intake basin located on land to deliver cooling water to the new NIs. The basin will be adequately sized to ensure low current speeds and sedimentation of sand during normal operation of the nuclear installation(s). In the extreme case of a loss of the ultimate heat sink (if applicable in the case of the adopted technology), the intake basin will need to have sufficient volume for the cooling of safety related systems of the new NIs.
- An intake tunnel connects the landside intake basin to the sea. Water is abstracted via intake heads located approximately 4 m (between 3 m and 5 m) above the seabed to prevent the drawing in of large quantities of sediment (assessed in ***Subsection 5.9.11.8***).
- The tunnel diameters are designed to maintain a tunnel flow velocity of 2.5 to 3.0 m/s to avoid sedimentation.

The outfall channel is conceptualised as an emerged rubble-mound structure. The structure discharges at a minimum invert level of -2 m msl and extends approximately 270 m offshore where it slopes down to a depth of -5 m msl. The width of the channel is approximately 60 m, resulting in a discharge velocity of approximately 1.2 to 1.7 m/s for water levels corresponding to the 90th percentile high tide and the 10th percentile low tide respectively. It is important to note that this channel width is estimated for the construction and operation of a nuclear installation(s) with total electrical generating capacity of 10 000 MWe. In the event that a lower generating capacity is built as part of the Nuclear-1 project, a narrower channel would be recommended to maintain the same velocity in the channel.

CONTROLLED DISCLOSURE

When downloaded from the EDS database, this document is uncontrolled and the responsibility rests with the user to ensure it is in line with the authorised version on the database.

Details of the intake and outfall configurations for the 10 000 MWe new NI(s) are given in ***Table 5.9-35***.

Table 5.9-35: Intake and Outfall Configuration.

Parameter	Unit	Value
Discharge	m^3/s	445
Number of intake tunnels	No.	3
Intake flow per tunnel	m^3/s	148.3
Intake tunnel length from coastline	km	Intake 1: 1.0 Intake 2: 1.1 Intake 3: 1.2
Depth at intake head	m msl	Intake 1: -30.0 Intake 2: -29.8 Intake 3: -28.8
Intake height above seabed	m	4
Length of the outfall channel from the coastline	m	270
Outfall channel width	m	60
Depth at outfall head	m msl	-5
Discharge velocity at the 10th percentile low tide	m/s	1.7
Discharge velocity at the 90th percentile high tide	m/s	1.2

The intake heads are located between 700 m offshore of the head of the outfall channel to reduce recirculation, noting that the intake and buoyant outfall plume are also separated vertically.

5.9.16.4 Damage to Cooling Water Intake and Outfall Structures

In the case of offshore intake structures, the structures need to be positioned in a depth where extreme wave conditions will have no damaging impact on the structure or any of its components which might jeopardise the intake or discharge of cooling water. In the case of nearshore channel type structures armoured with rock or concrete armour units, the structure should be designed for a 'no-damage' criterion, defined as less than 5% damage.

The extreme still water level and wave conditions at the site are provided in ***Table 5.9-11*** and ***Table 5.9-22***, respectively. These environmental conditions along with the design considerations given above will need to be

When downloaded from the EDS database, this document is uncontrolled and the responsibility rests with the user to ensure it is in line with the authorised version on the database.

accounted for in the design development of the cooling water supply system.

5.9.16.5 Dispersion Modelling

Introduction

Dispersion modelling of the thermal plume was undertaken to simulate the dispersion characteristics of the site including the recirculation of heated water from the outfall back to the intake and the resultant intake temperatures. The MIKE 3 Flow Model Flexible Mesh model was used to simulate the dispersion of the thermal plume for the discharge characteristics presented in ***Subsection 5.9.16.2*** and conceptual layout presented in ***Subsection 5.9.16.3***. The dispersion was run for a full calendar year to account for the effect of seasonal variations of waves, wind, currents, and temperature on the thermal plume dispersion. Details of the model description, setup, calibration, and cases modelled are provided in ***Appendix 5.9.A.7***.

Results

The primary model output parameter is the seawater temperature in each horizontal and vertical element of the computational mesh at 1-hour intervals for the full simulated year. These results were used to calculate the change in temperature (ΔT) for the discharge case compared to a baseline case without any thermal discharge, in each element at 1-hr intervals. The 99th percentile ΔT, which is presented in the contour plots below, will be exceeded 1% of the time and is thus close to the maximum ΔT.

Figure 5.9-106 to ***Figure 5.9-111*** present examples of instantaneous ΔT and currents near the surface and seabed. ***Figure 5.9-112*** and ***Figure 5.9-113*** show the 99th percentile ΔT at surface and seabed respectively.

CONTROLLED DISCLOSURE

When downloaded from the EDS database, this document is uncontrolled and the responsibility rests with the user to ensure it is in line with the authorised version on the database.

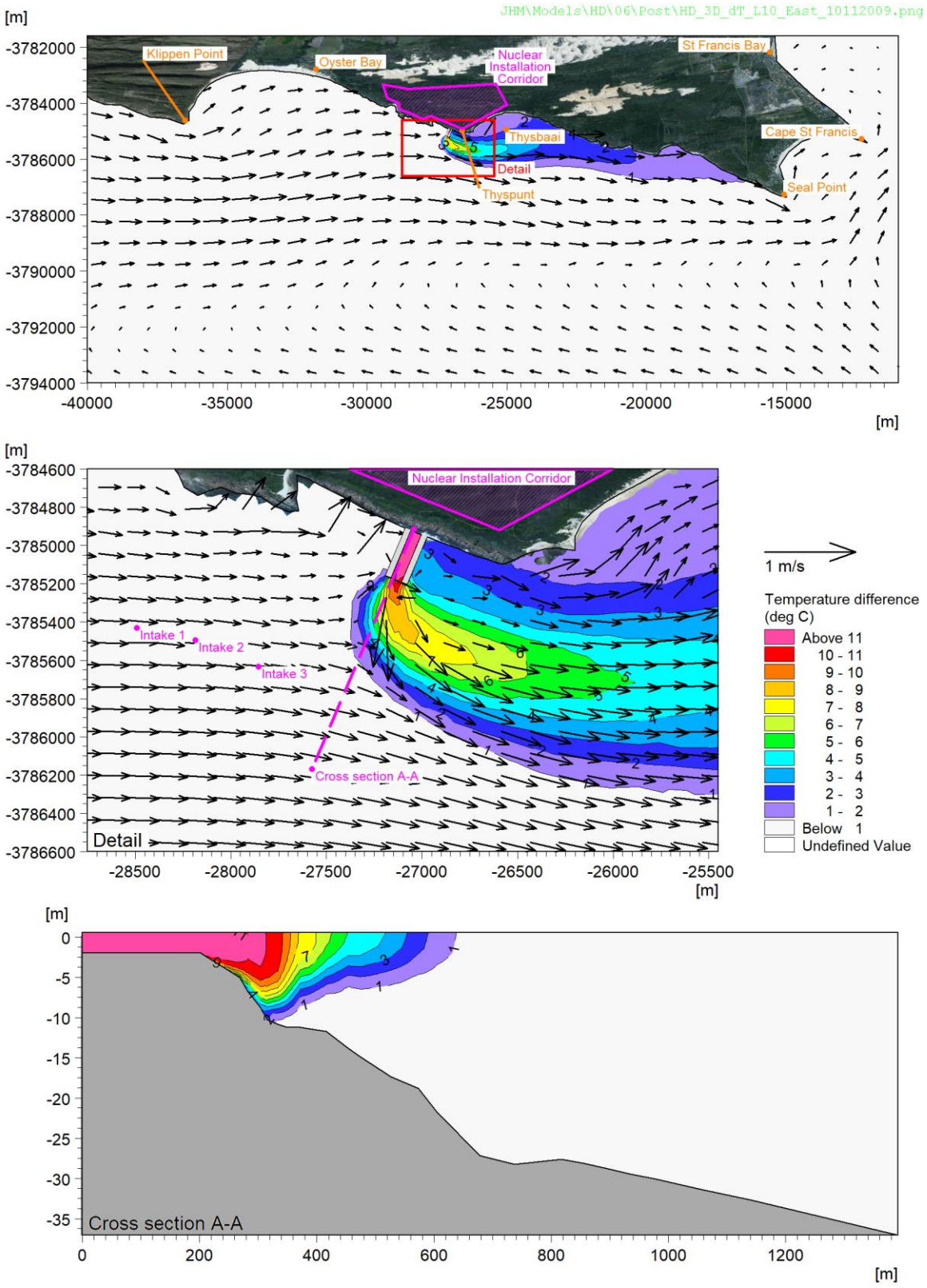


Figure 5.9-106: Example of Instantaneous ΔT and Currents Near Surface with the Plume Moving East.

CONTROLLED DISCLOSURE

When downloaded from the EDS database, this document is uncontrolled and the responsibility rests with the user to ensure it is in line with the authorised version on the database.

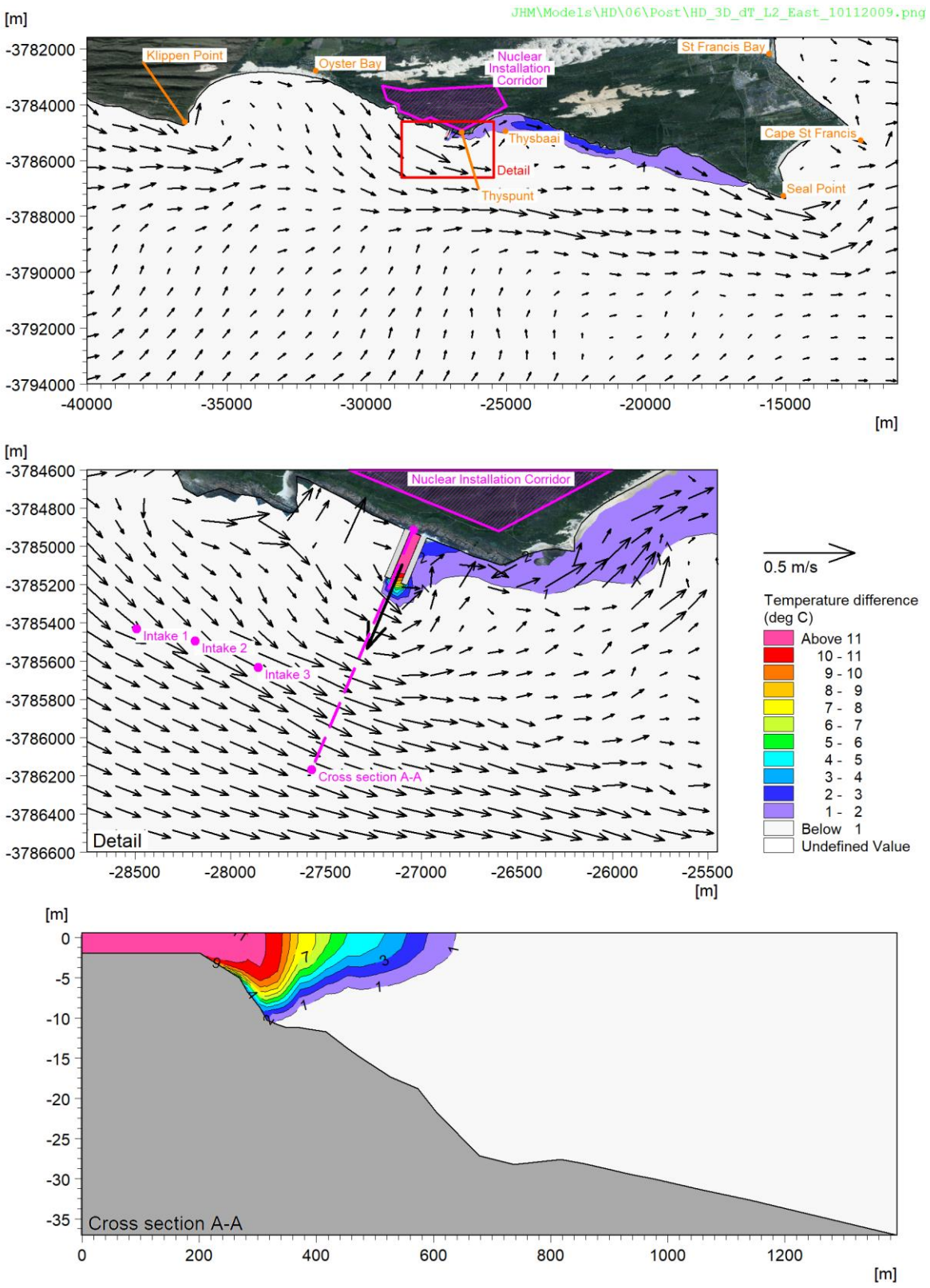


Figure 5.9-107: Example of Instantaneous ΔT and Currents Near Seabed with the Plume Moving East.

CONTROLLED DISCLOSURE

When downloaded from the EDS database, this document is uncontrolled and the responsibility rests with the user to ensure it is in line with the authorised version on the database.

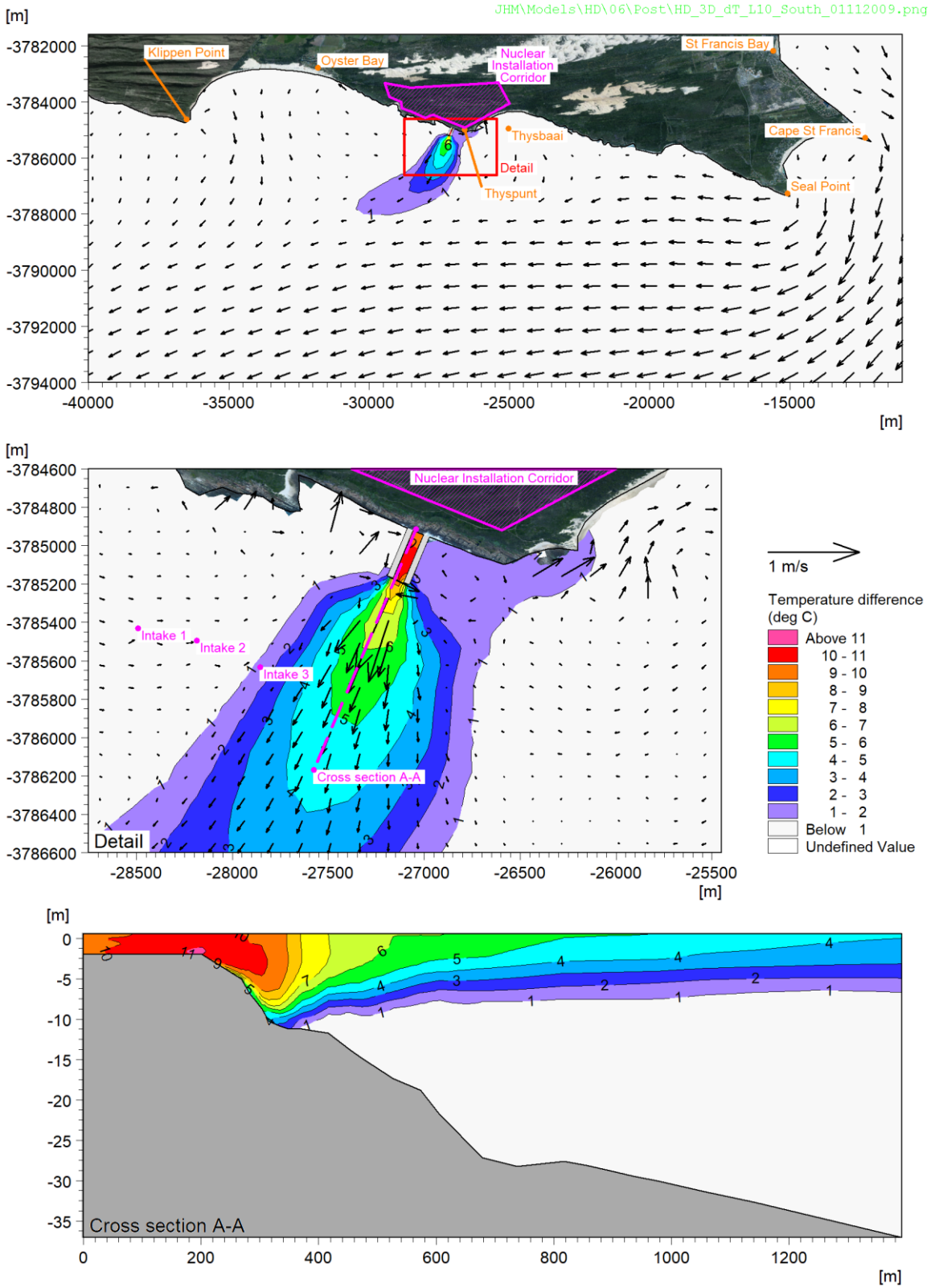


Figure 5.9-108: Example of Instantaneous ΔT and Currents Near Surface with the Plume Moving South.

CONTROLLED DISCLOSURE

When downloaded from the EDS database, this document is uncontrolled and the responsibility rests with the user to ensure it is in line with the authorised version on the database.

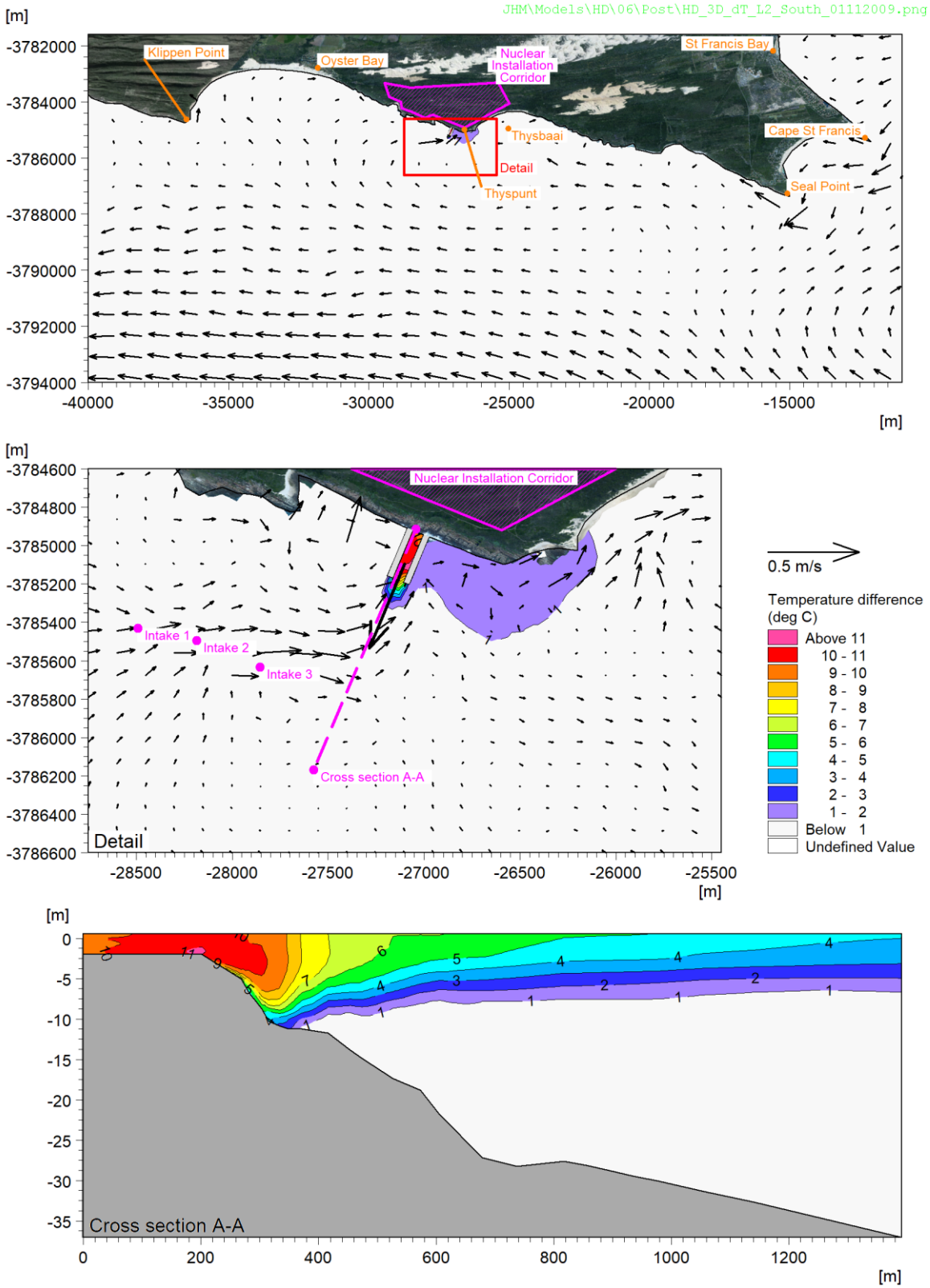


Figure 5.9-109: Example of Instantaneous ΔT and Currents Near Seabed with the Plume Moving South.

CONTROLLED DISCLOSURE

When downloaded from the EDS database, this document is uncontrolled and the responsibility rests with the user to ensure it is in line with the authorised version on the database.

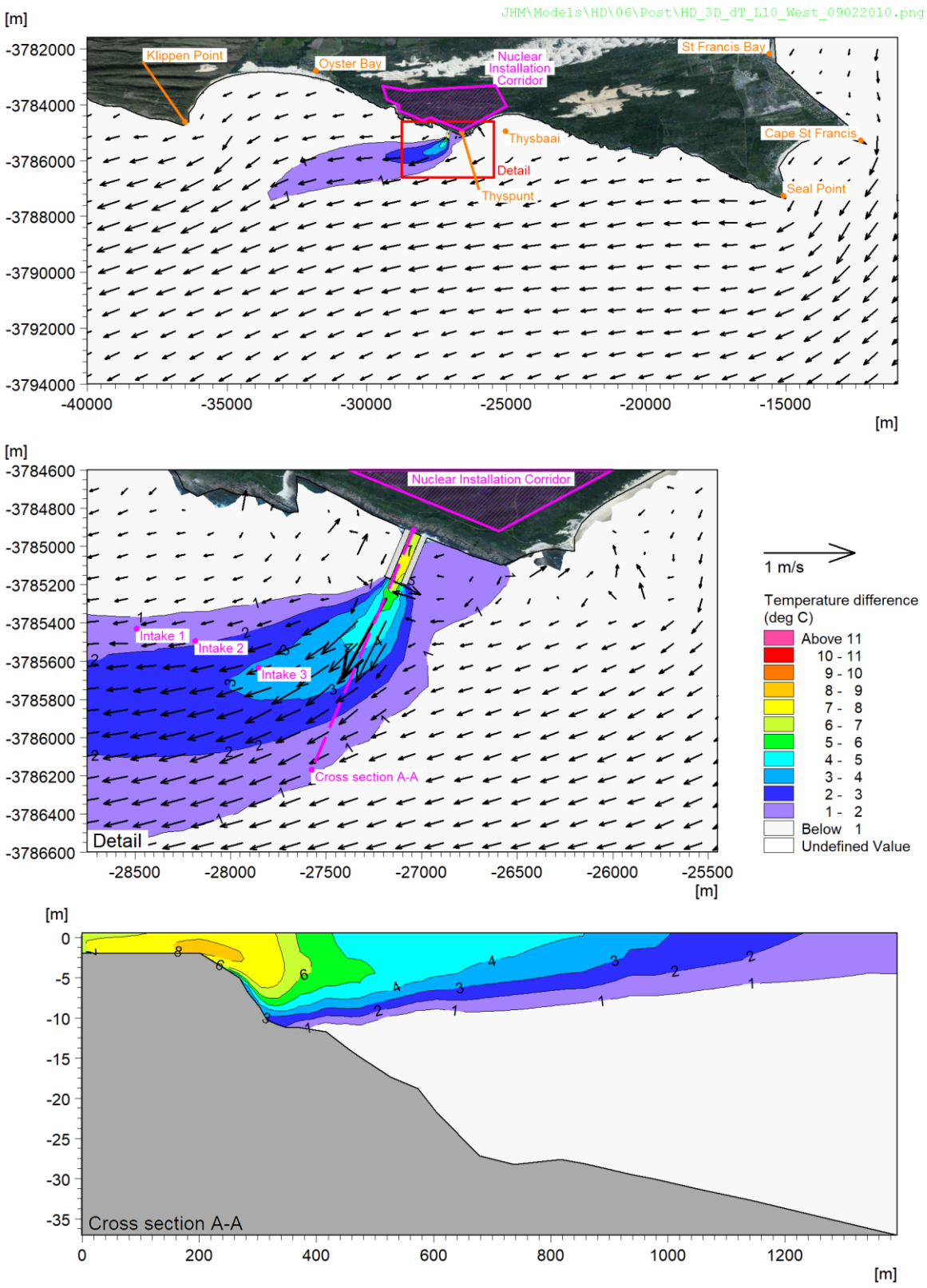


Figure 5.9-110: Example of Instantaneous ΔT and Currents Near Surface with the Plume Moving West.

CONTROLLED DISCLOSURE

When downloaded from the EDS database, this document is uncontrolled and the responsibility rests with the user to ensure it is in line with the authorised version on the database.

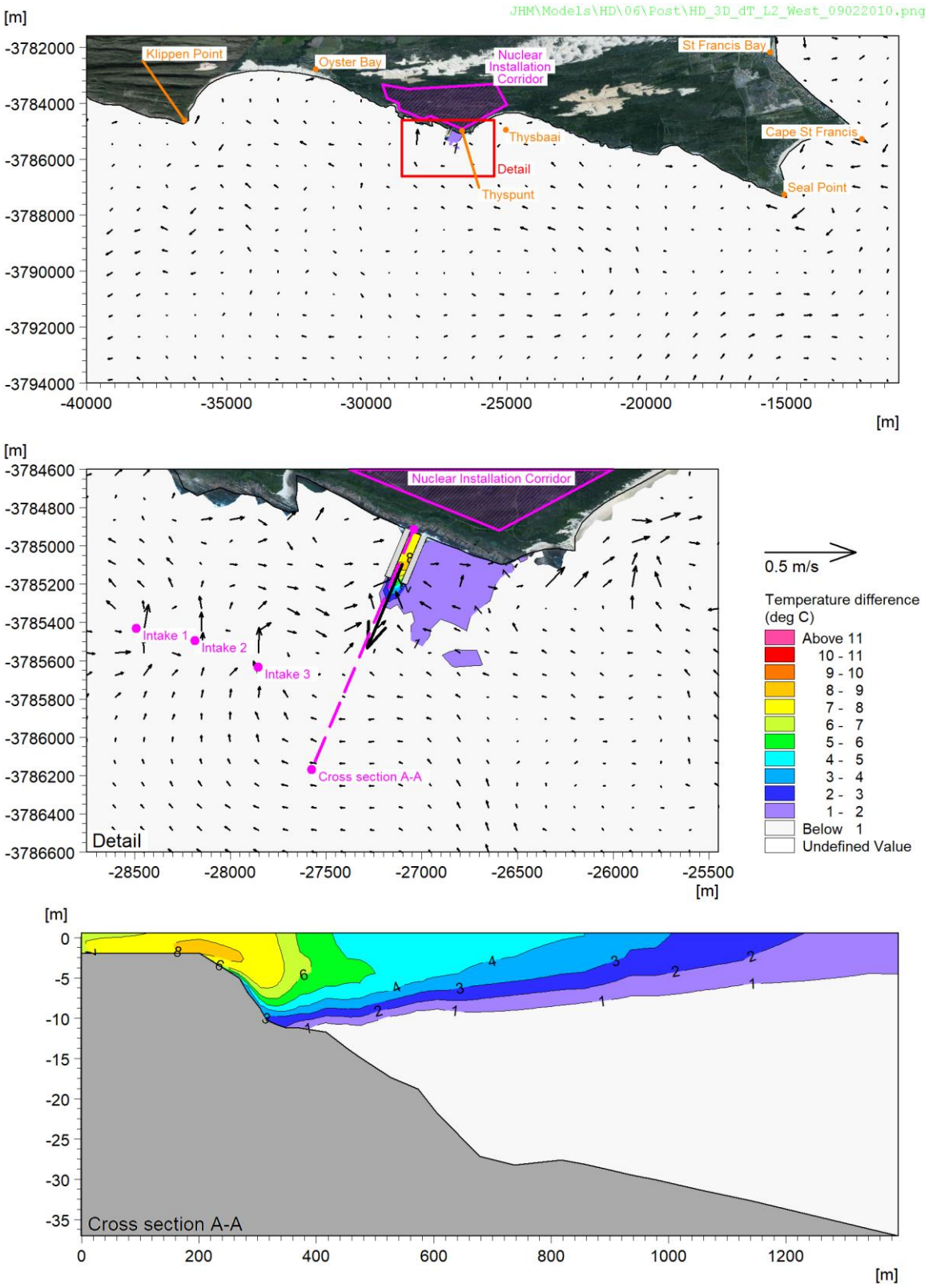


Figure 5.9-111: Example of Instantaneous ΔT and Currents Near Seabed with the Plume Moving West.

CONTROLLED DISCLOSURE

When downloaded from the EDS database, this document is uncontrolled and the responsibility rests with the user to ensure it is in line with the authorised version on the database.

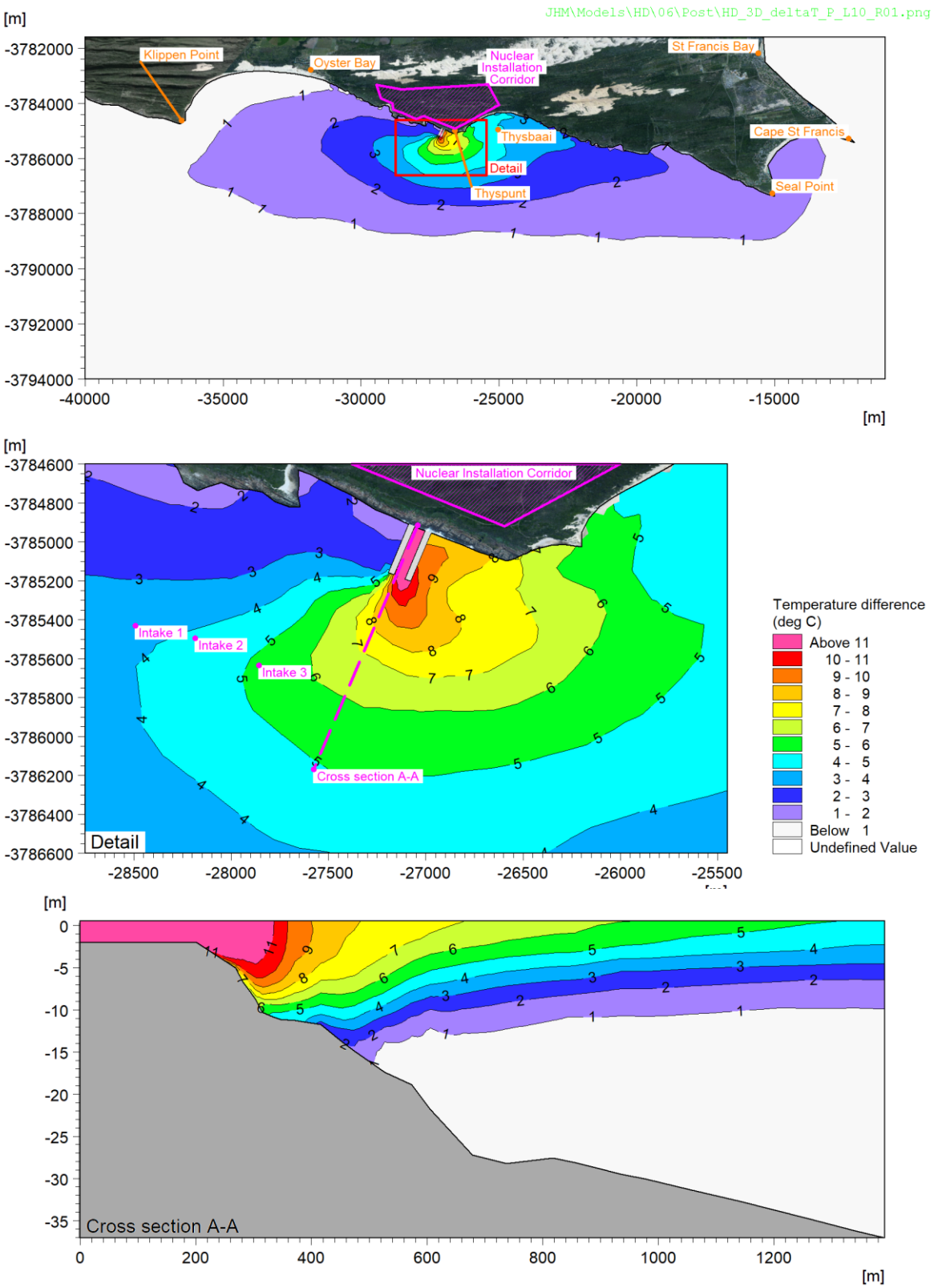


Figure 5.9-112: 99th Percentile ΔT Near Surface.

CONTROLLED DISCLOSURE

When downloaded from the EDS database, this document is uncontrolled and the responsibility rests with the user to ensure it is in line with the authorised version on the database.

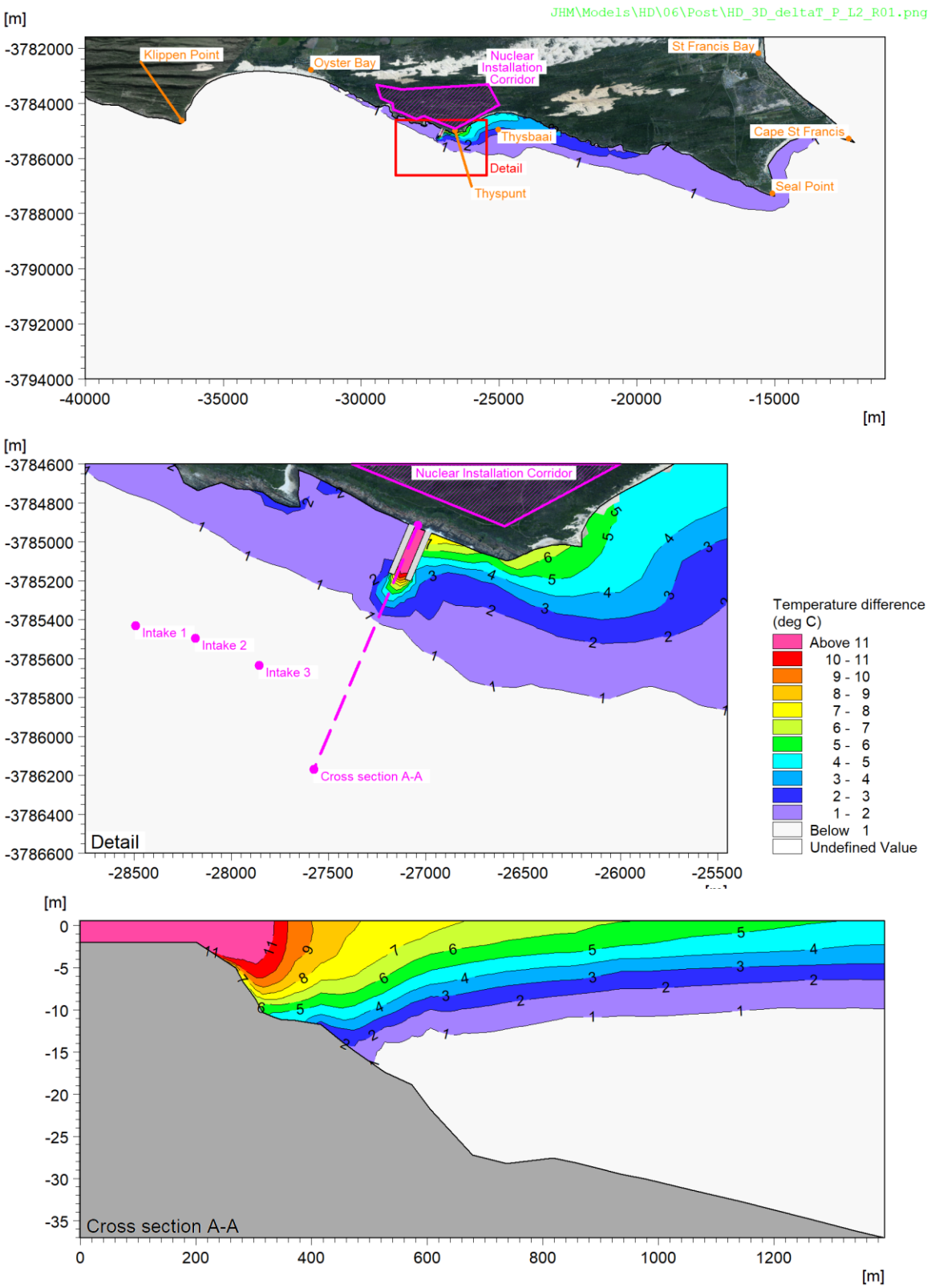


Figure 5.9-113: 99th Percentile ΔT Near Seabed.

CONTROLLED DISCLOSURE

When downloaded from the EDS database, this document is uncontrolled and the responsibility rests with the user to ensure it is in line with the authorised version on the database.

Figure 5.9-112 and ***Figure 5.9-113*** shows that due to buoyancy the highest ΔT's tend to be near the water surface.

5.9.16.6 Thermal Recirculation

The PPE specifies that the maximum ΔT of the re-circulated water should be less than 1.5°C (see ***Table 5.9-3***).

The recirculation of temperature from the discharge back to the intake is equal to the modelled ΔT at the location and depth of the intake. In ***Figure 5.9-114*** these recirculation ΔT's at the intakes are presented as percentiles for each of the intakes. ***Table 5.9-36*** summarises these results for the 50th, 95th and 99th percentiles.

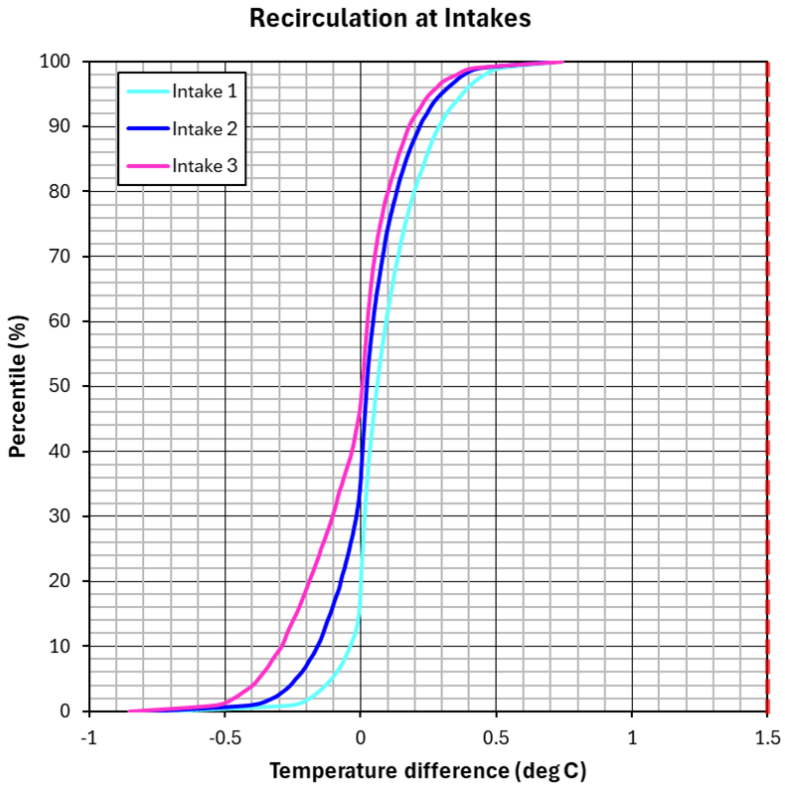


Figure 5.9-114: Recirculation at Intakes.

CONTROLLED DISCLOSURE

When downloaded from the EDS database, this document is uncontrolled and the responsibility rests with the user to ensure it is in line with the authorised version on the database.

Table 5.9-36: Recirculation at the Intakes.

Location	ΔT at Intakes (°C)		
	50th Percentile	95th Percentile	99th Percentile
Intake 1	0.06	0.38	0.51
Intake 2	0.02	0.29	0.44
Intake 3	0.01	0.25	0.41

The results above show the worst case 99th percentile ΔT at the intakes is 0.51°C, which is below the specified 1.5°C maximum allowable ΔT at the intakes. The negative values shown in **Figure 5.9-114** reflect colder water being drawn toward the intakes, reducing the temperatures compared to the baseline case.

5.9.16.7 Extreme Seawater Temperatures at Intakes

The PPE also specifies a maximum cooling water intake temperature of 30°C (see ***Table 5.9-3***). The maximum seawater temperature at the cooling water intakes will depend on:

- The intake and outfall layout, the power output and resultant ΔT due to recirculation from the outfall to the intake, as determined from the thermal plume dispersion modelling (***Table 5.9-36***),
- The extreme maximum background seawater temperature at the intake location as determined from the EVA of the site measurements adjusted for climate change (***Table 5.9-19***).

To obtain the extreme maximum seawater temperature the 99th percentile ΔT at each intake has been added to the extreme maximum background seawater temperatures. The results have been presented as the best estimate frequency to exceed 30°C at the intakes, as shown in ***Table 5.9-37*** below.

CONTROLLED DISCLOSURE

When downloaded from the EDS database, this document is uncontrolled and the responsibility rests with the user to ensure it is in line with the authorised version on the database.

Table 5.9-37: Extreme Maximum Seawater Temperatures at the Intakes (Including Recirculation).

Location	Best Estimate Frequency to Exceed 30°C at Intakes (y^{-1})		
	2034	2114	2134
Intake 1	7.8E-51	6.5E-18	7.9E-11
Intake 2	5.1E-52	1.5E-18	2.7E-11
Intake 3	2.3E-52	1.0E-18	2.0E-11

These results show that the exceedance frequency of the maximum specified PPE intake temperature of 30°C is 7.8E-51 y^{-1} (in 2034) and 7.9E-11 y^{-1} (in 2134), thus the intake temperature at the site will be less than the maximum specified in the PPE.

5.9.17 Blockage of Intakes and Biofouling

In the case of an offshore intake structure, cooling water is taken from greater depths (>15 m) compared to a basin intake. This significantly reduces the risk of blockage of the intake structure. A 'velocity cap' should be placed over the vertical terminal of the offshore intake tunnel/pipe. This converts vertical flow into horizontal flow at the intake entrance in order to reduce fish entrainment. Chlorine or other biocides should be used to keep the cooling system free of marine growth.

In case of a nearshore intake structure (basin or channel type structure), the pumphouse should be designed to limit the possibility of blockage of the intakes by drawing water at a sufficiently low level to limit risk of blockage by flotsam, fuel oil and marine flora and fauna. Suitable coarse and fine screens should be provided to prevent a sudden complete blockage. The layout and position of the basin should be designed to reduce the siltation rate of the basin and the depth of the basin should be maintained by maintenance dredging.

An offshore intake structure with tunnels connecting the seawater intake to the onshore cooling water intake basin is considered for the Thyspunt new NIs.

A study by the World Association of Nuclear Operators (WANO) (EPRI, 2008) found that in the period 2004 to 2006, there were 44 occurrences of blockages at nuclear installations. Of the 44 events, 37 of these were attributed to aquatic life, including algae, seaweed and other grasses, mussels, jellyfish, crustaceans (shrimps and crabs) and fish. The remaining blockage events were caused by depositions of sand and silt and ingress of crude oil. The risk from oil spills is addressed in ***Section 5.7*** (Nearby Transportation, Industrial and Military Facilities).

CONTROLLED DISCLOSURE

When downloaded from the EDS database, this document is uncontrolled and the responsibility rests with the user to ensure it is in line with the authorised version on the database.

The marine ecology specialist study conducted for the environmental impact assessment for the proposed site (Eskom, 2008b) indicated that the species listed in ***Table 5.9-38*** were found at the site.

Table 5.9-38: Marine Species Found at the Site.

Zones	Species
Intertidal Zone	Algae, Gastropod, Barnacle, Mussel, Giant Periwinkle, Plough Shell
Benthic Environment	Colonial Ascidians, Hydroids, Sponges, Coralline Alga
Open Water	Chokka Squid, Dusky Kob, Silver Kob, Cape Salmon, Shad, White Steenbras, Bronze Bream, Bottlenose Dolphin, Common Dolphin, Humpback Whale, Southern Right Whale

A study by the Electric Power Research Institute (EPRI, 2021) culminated in the development of a best management practices manual for preventing cooling water intake blockages. The report identifies current best practices and technology fixes for effectively addressing debris-related intake blockage events worldwide. It provides background and context of debris events at cooling water intake structures, successful and unsuccessful mitigation approaches, up-to-date procedural and best practice guidance, state-of-technology information, and detailed site audits of various power plants around the world, including KNPS. KNPS has experienced multiple jellyfish ingress events since 1997, as well as ingress of fish and Spoon Worm, as shown in ***Table 5.9-39***. These events had operational impacts such as screen failures, pump trips, and reductions in plant power output. The plant has been able to manage the production risk linked to jellyfish invasions, although there have been at least four instances over the last two decades when plant power reductions were required to deal with the events.

Table 5.9-39: Summary of Major Debris Events at KNPS Since 1997 (EPRI, 2021).

Date	Debris	Description
1997-02-12	Jellyfish	A significant inflow of jellyfish caused two trash recovery baskets to overflow, and a third was damaged, causing the recirculation of the jellyfish in the pumping station. No plant load reduction was required.
1999-05-20	Jellyfish	The inflow of jellyfish caused the activation of alarms due to the pressure loss on the level of the filter drums on the two units and high-speed activation on two drums. No plant load reduction was required.
1999-06-20	Jellyfish	A significant inflow of jellyfish resulted in cavitation of the main cooling water circulating pump. Unit electrical output was decreased to 60% on both units; Unit 2 was then shut down following a failure of the device for rotating the drum screen 2 CRF 002 TF.
2005-05-08	Jellyfish	A significant inflow of jellyfish, estimated to be at a rate of 32 tons per hour, caused tripping of a main seawater circulating water pump (1 CRF 003 PO). The event started on May 8 and continued for 12 days.

CONTROLLED DISCLOSURE

When downloaded from the EDS database, this document is uncontrolled and the responsibility rests with the user to ensure it is in line with the authorised version on the database.

Date	Debris	Description
		As a result of the event, the power output was reduced to between 60% and 70% during this period.
2008-07-28	Jellyfish	On July 28, 2008, a jellyfish migration into the plant intake basin was reported. The number of jellyfish was small, and, therefore, the event did not have any significant impact on plant power production operations (that is, the plant remained at full-power operation).
2016-04-23	Jellyfish	On April 23, 2016, Unit 1 reduced load to 70% power due to significant jellyfish ingress. The drum screen, 1 CFI 002 TF, was stationary, and the drive motor was running uncoupled. The coupling had disengaged on torque overload. At around 08h00, 1 CRF 002 PO tripped on low suction pit level. The on-duty mechanical maintenance team was called to remove the coupling cover to inspect the coupling. Jellyfish fouling of the drum screen was evident, although excessive foaming made it difficult to clearly observe the extent of the fouling.
2020-03	Fish	This event was marked with a sudden ingress of fish (suspected to be anchovies) although some jellyfish and kelp were also found in the trash baskets. The event significance was characterized by latent shortcomings of plant equipment designed to deal with the event rather than the event initiator itself. Although the observed amount of debris was within the motor's design capacity, an incorrect (lower) torque setpoint on the coupling caused the coupling to disengage. Although the remaining train was able to maintain sufficient vacuum in the main condenser to maintain the reduced electrical load, fouling of the related heat exchanger train for secondary cooling systems resulted in temperature increases, which further necessitated a complete reduction of unit output to the national transmission grid. Review of the processes and practices identified that improvements were required in the guidance available in maintenance procedures for the torque settings, as well as adjustment and renewal of drum screen components.
2022-01-19	Spoon Worm	This event occurred after publication of (EPRI, 2021). Information describing the event below is from the Marine Ingress Feedback Report (Eskom, 2022). An unusual event was declared due to ingress of marine organisms (worm-like creatures) into the cooling water intake basin. The marine ecologist that reviewed photos of the worms advised that they were likely to have been Echiurus echiurus, a species of spoon worm (Echiura). There were high swells with long periods on the day. Echuirans are mostly infaunal animals (common in soft sediments), occupying burrows in the seabed, either in the lower intertidal zone or the shallow subtidal zone. The large waves and strong currents experienced during this period may have forced the worms out of their underwater burrows and washed them ashore and into the KNPS cooling water intake basin. It is very difficult to predict whether a recurrence of an event of this nature is likely or not. Adverse environmental conditions, and the associated impact on the marine life present at that time is to a large extent unpredictable.

CONTROLLED DISCLOSURE

When downloaded from the EDS database, this document is uncontrolled and the responsibility rests with the user to ensure it is in line with the authorised version on the database.

Date	Debris	Description
		Author comment: The KNPS procedure for dealing with marine ingress was implemented and successfully mitigated affects to the nuclear cooling system. There is nothing to suggest that a more severe ingress may be expected in the future and that the KNPS procedures nor the SSC and procedures of a new NI will not be able to manage such an event.

The EPRI study concludes that there is no single solution to preventing intake blockages, and the best practice will be determined by site-specific factors, such as the type and extent of debris present, screening equipment in use, and forecasting ability at the facility. Five main categories for tackling the problem of blockages are identified (EPRI, 2021), viz:

- Routine maintenance of equipment increases its reliability when called into action during a major clogging event.
- Standard operating procedures (SOPs) provide explicit instructions to station team members on how intake event response tasks are to be implemented and should be tailored to the intake, the equipment, and the types of debris typically encountered.
- Event response teams can be used to implement the SOPs when certain events are forecasted or triggered.
- Having a debris management plan documents the actions to take prior to and/or during a debris event.
- An early warning or event forecasting system can contribute to effective management of power plant operation, reduce plant downtime, minimise damage to plant equipment, and improve safety.

The recommendations put forward by WANO and the EPRI best management practices manual will form an important and valuable input to the new NIs intake design and prevention of cooling water intake blockages through the plant life.

Biofouling has been measured at the site between July 2008 and December 2009. Asbestos plates, approximately 20 cm x 20 cm were deployed at specific depths for time periods of approximately three and six months. These plates were periodically removed, photographed and the thickness of marine growth measured.

Initially the plates were moored 3 m and 8 m below the water surface in 10 m water depth. The plates were later mounted directly on the two ADCP frames at Sites A and B (see ***Figure 5.9-1***) in depths of -13 m msl and -31 m msl, respectively. These plates were mounted approximately 0.5 m above the sea floor. Photographs of the plates after removal are shown in ***Figure 5.9-115***. The biofouling results are summarised in

When downloaded from the EDS database, this document is uncontrolled and the responsibility rests with the user to ensure it is in line with the authorised version on the database.

Table 5.9-40. To facilitate an inter-site comparison of growth rates, the corresponding results for the Duynefontyn site are included in the table.

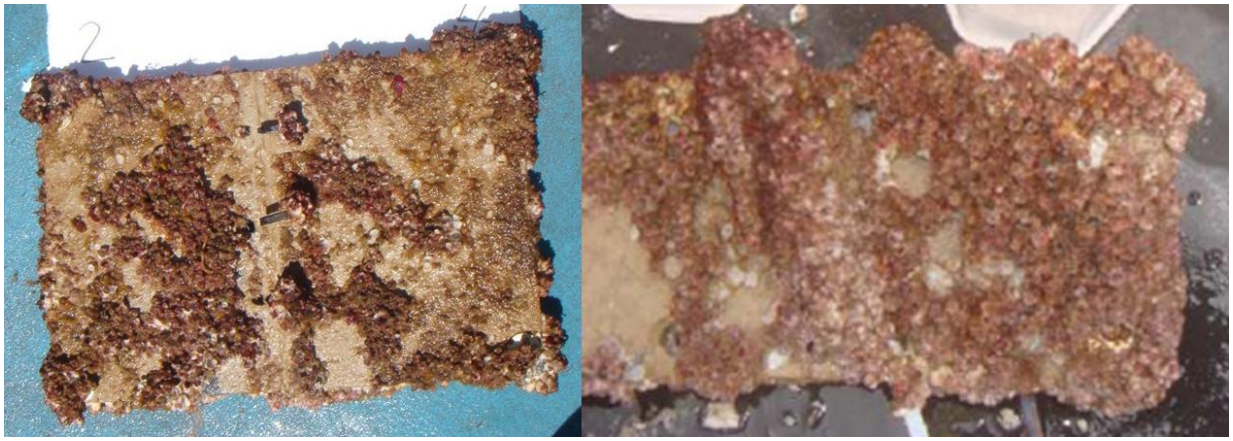


Figure 5.9-115: Thyspunt Biofouling After 3.7 Months at 3 m Depth (Left) and After 5.6 Months in 10 m Depth (Right).

Table 5.9-40: Summary of Measured Biofouling Thickness.

Site	Duration	Date Deployed	Date Retrieved	Depth Below Surface	Average Biofouling Thickness	Average Rate of Growth
				(m)	(mm)	(mm/month)
Thyspunt	3.7 Months	2008/07/01	2008/10/23	3	7.5	2.0
				8	2.8	0.7
	5.6 Months	2009/06/14	2009/12/03	13	11.0	2.0
				31	7.0	1.3
Duynefontyn	5.6 Months	2008/05/01	2008/10/18	3	16.0	2.9
				8	17.5	3.1
	6.0 Months	2009/05/22	2009/11/20	10	7.0	1.2
				29	4.5	0.8
	14.0 Months	2009/05/22	2010/07/24	10	70.0	5.0

Based on the above results, the biofouling growth rate for the periods measured ranges from 1 to 2 mm/month at Thyspunt and 1 to 5 mm/month at Duynefontyn. The average biofouling growth rates at Thyspunt are comparable with those at Duynefontyn over the first six months of growth i.e. 1 to 3 mm/month. There were no samples beyond six months growth duration available for Thyspunt. It can be expected that the growth rate beyond six months will be similar at Thyspunt to what was measured at Duynefontyn i.e. 5 mm/month, as this growth rate was related to mussel growth (see ***Figure 5.9-116***) which are found at Duynefontyn and Thyspunt sites.

CONTROLLED DISCLOSURE

When downloaded from the EDS database, this document is uncontrolled and the responsibility rests with the user to ensure it is in line with the authorised version on the database.



Figure 5.9-116: Duynefontyn Biofouling After 6 Months at 8 m Depth (Left) and After 14 Months in 10 m Depth (Right).

The growth rates increase after the initiation of the “bacterial film” whereby smaller fauna and flora attach on to the surface of foreign objects, thus making the surface more amenable to the growth/habitation of larger fauna. Chlorine produced by means of electrolysis is used to keep the cooling water system at the KNPS free of marine growth, although marine growth at the pumphouse intakes has previously been a maintenance problem owing to deficiencies in the chlorination system (Eskom, 2006).

Based on the KNPS and worldwide experience (EPRI, 2021) it can be concluded that the new NIs intakes could be designed to cope with the species identified in ***Table 5.9-38*** and to minimise the risk of complete blockage of the intake.

5.9.18 Uncertainties and Future Work

The estimation of the influence of climate change has been based on the most reliable scientific information available at the time that this study was undertaken, but must be continually reassessed as new data and research results become available (at least every five years). The SSR would only need to be updated should one of the relevant climate change parameters change significantly.

The conceptual seawater cooling intakes and outfalls which have been developed and modelled for the SSR will need to be refined in the future based on an engineering feasibility study. Marine geotechnical surveys and additional numerical modelling will be required as part of future engineering design studies of the intake and outfall structures.

The scope of work for this update of the SSR excluded an updated Tsunami Hazard Analysis. Since tsunamis will pose a significant hazard to the site, it

CONTROLLED DISCLOSURE

When downloaded from the EDS database, this document is uncontrolled and the responsibility rests with the user to ensure it is in line with the authorised version on the database.

is recommended that an updated THA be undertaken for Thyspunt and that this SSR should then be updated once these results are available.

5.9.19 Monitoring Programme

A comprehensive oceanographic data collection programme has been implemented at the site and is described in ***Subsection 5.9.6.1***.

The present-day monitoring programme comprises the following:

- water level and seawater temperature measurements at Site C inside the gulley at Thyspunt in a depth of -2 m msl;
- wave, current and seawater temperature measurements at Site B in a depth of -31 m msl;
- seawater temperature measurements at Site A in a depth of -13 m msl;
- annual beach profile surveys at the 20 locations.

It is recommended that the present-day monitoring programme be continued to extend the duration of the datasets and to capture any extreme events that occur. The monitoring programme should be reviewed and updated every five years, e.g., with regard to the number, position and frequency of measurements.

5.9.20 Management System

A quality assurance programme was established to control the effectiveness of the execution of the coastal engineering and oceanography investigations, and the formulation of conclusions on the site acceptability. This conforms to the overall management system for the SSR as outlined in ***Chapter 10***.

The classification of the services and resultant quality management are described in Eskom's Technical Requirement Specification (Eskom, 2023). The classification of the products and processes related to the updating of the oceanography and coastal engineering section excluding the Tsunami Hazard Analyses determines that the quality management system of the organisation responsible for this service must comply with the Safety Level 2 requirements of RD-0034 (NNR, 2008). This requires implementation and maintenance of an effective, documented quality and safety management system as required by the Eskom specification for Quality and Safety Management Requirements for Nuclear Suppliers Level 2 (Eskom, 2018).

The detailed supporting information about this evaluation of the site and the results achieved is available and contains sufficient data to support key decisions taken, the choice of methodologies and models selected and applied, and the conclusions made. It provides the back-up for the data

CONTROLLED DISCLOSURE

When downloaded from the EDS database, this document is uncontrolled and the responsibility rests with the user to ensure it is in line with the authorised version on the database.

presented in ***Section 5.9***. A clear audit trail is provided to illustrate the conclusions reached. The data and information presented in ***Section 5.9*** forms the foundation for the peer review process of the SSR.

Prior to site work commencing, the following documents were compiled:

- Method statement;
- Project quality plan;
- Risk assessment;
- Health safety and environmental management plan.

Table 5.9-41 lists the activities carried out by the author, links of this ***Section 5.9*** to other SSR sections and chapters, and quality control requirements.

CONTROLLED DISCLOSURE

When downloaded from the EDS database, this document is uncontrolled and the responsibility rests with the user to ensure it is in line with the authorised version on the database.

Table 5.9-41: Summary of Activities, Links and Quality Requirements.

Activity	Links		Quality Requirements
	Inputs	**Outputs**	
All	***Section 3*** (Overview of Planned Activities): Plant Parameter Envelope (PPE)		
Climate change	***Section 5.8*** (Meteorology): Operational and extreme wind speeds including climate change.	***Section 5.8*** (Meteorology): Climate change alignment.	Based on best available climate science.
		Sections 5.10 (Hydrology and Hydraulics) and ***5.11*** (Geohydrology). Sea level rise.	Based on best available climate science.
Tsunamis		***Chapter 6*** (External Events). Tsunami run-up, rundown and velocity.	RD-0034 Level 1.
Hydrodynamic modelling	***Section 5.8*** (Meteorology): Wind speed and direction measurements at the site.		Calibrated instrumentation
	Section 5.13 (Geology): Bathymetry, side scan and marine geology within 8 km radius of the site.		Calibrated instrumentation
		Section 5.2 (Monitoring): Description of monitoring programme.	Calibrated instrumentation
		Chapter 6 (Evaluation of External Events): Waves, erosion and sedimentation.	RD-0034 Level 2.
Flooding		***Sections 5.10*** (Hydrology and Hydraulics) and ***5.11*** (Geohydrology): Extreme seawater levels.	RD-0034 Level 2.
		Chapter 6 (Evaluation of External Events): Climate change, tides, storm surge, seiches, wave run-up, maximum flooding sea level, minimum low sea level.	RD-0034 Level 2.
Thermal plume modelling	***Sections 5.3*** (Ecology): Biofouling.	***Section 5.6*** (Adjacent Sea Use): Thermal plume dispersion results.	RD-0034 Level 2.
		Chapter 6 (Evaluation of External Events): Extreme seawater cooling temperature.	RD-0034 Level 2.
		Chapter 7 (PIPE): Thermal plume dilution factors.	RD-0034 Level 2.

The establishment of oceanography and coastal engineering site parameters and evaluations does not lend itself to direct verification by inspections or tests that can be precisely defined and controlled. Peer

CONTROLLED DISCLOSURE

When downloaded from the EDS database, this document is uncontrolled and the responsibility rests with the user to ensure it is in line with the authorised version on the database.

review of these evaluations is therefore essential, by suitably qualified and experienced persons who are independent from those who performed the work.

Specific quality assurance/control requirements applicable to the oceanography section are:

- calibration of monitoring instruments and quality control of the data from the monitoring programme;
- correct use of the numerical models, i.e., model selection, model setup and interpretation of model results.

Detailed records of the work carried are kept by the author, i.e., calculations performed and data bases established. These include:

- oceanographic data from the monitoring programme;
- setup and calibration of numerical models;
- model V&V as per the requirements contained in NSIP02761 (Eskom, 2020) and RG-0016 (NNR, 2016b);
- post-processing of numerical model results.

Electronic records are stored in a secure central repository with regular off-site back-up procedures and subject to Eskom's approval.

The regulatory compliance matrix for ***Section 5.9*** is shown in ***Table 5.9-42***.

CONTROLLED DISCLOSURE

When downloaded from the EDS database, this document is uncontrolled and the responsibility rests with the user to ensure it is in line with the authorised version on the database.

Table 5.9-42: Regulatory Compliance Matrix.

Act/ Regulation	Section/ Regulation	Requirements/Issue	Addressed in Sub-Section
R.927: Regulations on Licensing of Sites for New Nuclear Installations (Department of Energy, 2011)	Regulation 4(5)	Natural phenomena and potential man-made hazards must be appropriately accounted for in the design of the new nuclear installation(s)	5.9.9 to 5.9.17
	Regulation 5(3)	The characteristics of the site relevant to the design assessment, risk and dose calculations, including inter alia: (a) external events; (b) meteorological data; (f) projections of the above data commensurate with the design life of the nuclear installation(s)".	5.9.7 to 5.9.17
RG-0011: Interim Guidance on the Siting of Nuclear Facilities (NNR, 2016a);	Section 6.1(1)	In the evaluation of the suitability of a site for a nuclear facility, the following aspects should be considered: a) Effects of external events occurring in the region of the particular site (natural or human induced);	5.9.7 to 5.9.17
	Section 6.1(4)	Site characteristics that may affect the safety of the nuclear facility should be investigated and assessed.	5.9.7 to 5.9.17
	Section 6.1(5)	A quality management programme should be established to control the effectiveness of the execution of the site investigations and assessments and engineering activities performed in the different stages of the site evaluation process, covering all activities that may influence safety or the derivation of parameters for the design basis.	5.9.20
	Section 6.6.3(2)	The Site Safety Report should characterise all the factors relevant to the site, including natural and human-induced external events.	5.9.7 to 5.9.17
	Section 6.6.3(3)	The Site Safety Report should include the necessary external events data in support of the safety assessment for a given facility.	5.9.7 to 5.9.17
	Section 7.1(2)	Proposed sites should be adequately investigated with respect to all the characteristics that could affect safety in relation to natural and human-induced events.	5.9.9 to 5.9.17
	Section 7.1(3)	The hazards associated with external events, which are to be considered in the design of the nuclear facility, must be determined. For an external event (or a combination of events), the parameters and the values of those parameters used to characterise the hazards must be chosen so that they can be used readily in the design of the nuclear facility.	5.9.10, 5.9.11.7, 5.9.14, 5.9.15, 5.9.16.7
	Section 7.1(5)	Prehistorical, historical and instrumental information and records, as applicable, of the occurrences and severity of those important natural phenomena or human-induced situations/activities should be collected for the region and carefully analysed for reliability, accuracy and completeness.	5.9.6.1
	Section 7.1(6)	Appropriate methodologies should be adopted for establishing the hazards from important external phenomena.	5.9.6
	Section 7.1(7)	The methodologies used should be the current and state of the art, and should be justified as being compatible with the characteristics of the region.	5.9.6
	Section 7.1(8)	Preferential consideration should be given to applicable probabilistic methodologies.	5.9.6

CONTROLLED DISCLOSURE

When downloaded from the EDS database, this document is uncontrolled and the responsibility rests with the user to ensure it is in line with the authorised version on the database.

Act/ Regulation	Section/ Regulation	Requirements/Issue	Addressed in Sub-Section
	Section 7.1(9)	It should be noted that probabilistic hazard curves are generally required to conduct external event PSAs.	5.9.6
	Section 7.1(10)	The size of the region, to which a method for establishing the hazards associated with major external phenomena is to be applied, should be large enough to include all the features and areas that could be of significance in the determination of the natural and human-induced phenomena under consideration and for the characteristics of the event.	5.9.8
	Section 7.1(11)	All natural events that have a frequency of occurrence of more than the minimum safety goal defined in PP-0014 (i.e. about 10^{-7} per year) should be considered. Natural phenomena, which may exist or can occur in the region of a proposed site, should be identified and classified as per their impact on plant safety. Design bases should be derived for each credible event and credible combination of events by adopting appropriate methodologies.	5.9.6, 5.9.10, 5.9.11.7, 5.9.14, 5.9.15, 5.9.16.7
	Section 7.1(15)	The evaluation of site characteristics to determine design basis parameters should include considerations for exceedance of design basis and/or design extension conditions.	5.9.6.2
	Section 7.1(16)	The evaluation of site characteristics to determine design basis parameters should take into account changes of hazards (both natural and human induced) with regards to the design life of the facility.	5.9.7
	Section 7.2.2(1)	Meteorological events/parameters to be considered for evaluation of design bases include: …, storm surge, cooling water temperature, …	5.9.9.2, 5.9.9.5
	Section 7.2.3(2)	Coastal sites should be assessed for: high tides, cyclones/storm surge, wind-induced waves, precipitation, tsunami-generated waves, etc. Appropriate combinations of these phenomena should also be considered.	5.9.9.1, 5.9.9.2, 5.9.9.8, 5.9.13, 5.9.10
	Section 7.2.3(3)	The design basis should take into account the highest water level reached at the site during the above events. Other associated parameters like the duration of flood, flow conditions, warning time for flood and the height and period of waves, if relevant, should also be estimated.	5.9.12, 5.9.13, 5.9.14
	Section 7.2.3(4)	Suitable meteorological, hydrological and topographical data, including data on relevant bodies of water, should be collected. Uncertainty and data inadequacy, if any, should be taken into consideration when deriving the design basis value of the flood water level. The design basis' highest water level at the site should be arrived at by using appropriate flood routing models.	5.9.6.1, 5.9.8, 5.9.12, 5.9.13
	Section 7.2.3(9)	The potential for seiches in enclosed bodies of water should be examined for inland sites located close to such bodies of water.	5.9.12, 5.9.13, 5.9.14
	Section 7.2.3(10)	Coastal sites should be examined for potential flooding caused by a surge due to cyclones, wind-induced waves as well as tsunami waves.	5.9.9.2, 5.9.9.8, 5.9.12, 5.9.13, 5.9.14
	Section 7.2.3(11)	Wave run-up should also be considered taking into account any amplification due to the coastal configuration adjacent to the site.	5.9.12
	Section 7.2.3(12)	Bathymetry and topography data of the coastal region should be collected and utilised.	5.9.6.1, 5.9.8

CONTROLLED DISCLOSURE

When downloaded from the EDS database, this document is uncontrolled and the responsibility rests with the user to ensure it is in line with the authorised version on the database.

Act/ Regulation	Section/ Regulation	Requirements/Issue	Addressed in Sub-Section
	Section 7.2.3(13)	The region should be evaluated to determine the potential for tsunamis that could affect the safety of nuclear facilities on the site. The hazards associated with tsunamis should include potential drawdown and run-up as well as hydrodynamic forces, if applicable.	5.9.13
	Section 7.2.3(14)	Design basis earthquake should be arrived at with data of earthquakes resulting from a tsunami wave landing at the site using appropriate hydrological and numerical models.	5.9.13
	Section 7.2.3(15)	The frequency of occurrence, magnitude and height of regional tsunamis should be estimated. On the basis of the available data for the region, prehistorical and historical, and comparison with similar regions that have been well studied, all potential tsunamigenic sources and their maximum potential should be identified and used in determining the possible hazards associated with tsunamis. Appropriate models should be used in the evaluation and should take into account any amplification due to the coastal configuration adjacent to the site.	5.9.13
	Section 7.2.4(12)	For coastal sites, the potential for shore instability due to erosion or sedimentation should be investigated.	5.9.11
	Section 7.2.4(14)	The potential for the loss of ultimate heat sink of a nuclear facility should be analysed. If the potential exists, the site should be considered unsuitable unless a reliable and practical engineering solution is available.	5.9.11.8, 5.9.15, 5.9.16.7, 5.9.18
	Section 8.4.3(1)(a)	The general shore and bottom configuration in the region, and unique features of the shoreline in the vicinity of the discharge. Data on bathymetry out to a distance of several kilometres, and data on the amount and character (transport, deposition and resuspension) of sediments in the shallow shelf waters.	5.9.8, 5.9.9.7
	Section 8.4.3(1)(b)	Speeds, temperatures and directions of any near shore currents that could affect the dispersion of discharged radioactive material. Measurements should be made at appropriate depths and distances, depending on the bottom profile and the location of the point of discharge.	5.9.9.4
	Section 8.4.3(1)(c)	The duration of stagnation and characteristics of current reversals.	5.9.9.4
	Section 8.4.3(1)(d)	The thermal stratification of water layers and its variation with time, including the position of the thermocline and its seasonal changes.	5.9.9.5
	Section 8.6.3(1)(b)	Hydrological, physical, physicochemical and biological characteristics governing the transport, diffusion and retention of radioactive materials.	5.9.8, 5.9.9.4, 5.9.9.5
	Section 10.4(11)	Physical protection systems that are exposed to anticipated weather and environmental conditions or probable maximum flood conditions should be identified and considered in determining any challenges or impediments to designs.	5.9.14
	Section 10.4(12)	Changes to the topography of the site caused by low water conditions should be considered for determining if resulting conditions would present challenges or impediments to the design of engineered and administrative security controls.	5.9.11, 5.9.15

CONTROLLED DISCLOSURE

When downloaded from the EDS database, this document is uncontrolled and the responsibility rests with the user to ensure it is in line with the authorised version on the database.

Act/ Regulation	Section/ Regulation	Requirements/Issue	Addressed in Sub-Section
	Section 11.1(1)	The site characteristics relevant to the nuclear facility that are considered in the safety requirements and that are pertinent to licensing and safe operation should be monitored for the period of applicability of the NSL, or until the NL is superseded by the construction licence.	5.9.6.1, 5.9.19
	Section 11.1(4)	The data obtained should be used as a baseline in future investigations.	5.9.6.1

5.9.21 Conclusions

5.9.21.1 Climate Change

The effect of climate change on all relevant oceanographic and coastal engineering parameters has been included. The primary guidance is taken from the latest publications from the Intergovernmental Panel for Climate Change (IPCC), along with peer-reviewed journal articles where IPCC projections are outdated or unavailable. For each parameter the baseline date was taken as the middle of the period of available data at the site. Projections derived from literature were converted relative to the baseline date for each parameter. The effect of climate change was evaluated over both the operating life and the decommissioning period of the proposed new NIs at the site. ***Table 5.9-43*** shows the climate change values applied.

SLR projections were extracted for the upper end of the likely range (83rd percentile) for the SSP5-8.5 emissions scenario. This projection incorporates only those processes in which the AR6 has at least medium confidence. To inform decision making for stakeholders with a low risk tolerance, the AR6 also presents high-end sea level projections, which incorporate processes which are deeply uncertain but cannot be ruled out. This projection for the SSP5-8.5 scenario was considered as a high-end sea level rise scenario for only the 2134 date, and is referred to as the '2134 High SLR' scenario throughout ***Section 5.9***.

The estimation of the influence of climate change has been based on the most reliable scientific information available at the time that this study was undertaken, but must be continually reassessed as new data and research results become available (at least every five years). The SSR would only need to be updated should one of the relevant climate change parameters change significantly.

CONTROLLED DISCLOSURE

When downloaded from the EDS database, this document is uncontrolled and the responsibility rests with the user to ensure it is in line with the authorised version on the database.

Table 5.9-43: Climate Change Applied for Each Oceanographic Parameter and Date.

Parameter	Description	Scenario	Units	Baseline date	2034	2114	2134
Sea level rise	Regional relative sea level rise	SSP5-8.5 83rd percentile	m	2013.5	0.14	1.38	1.76
		SSP5-8.5 High SLR 83rd percentile	m	2013.5	0.18	2.22	3.28
Seawater temperature	Sea surface temperature	RCP8.5 mean, (No uncertainty ranges available)	°C	2008.0	0.50	3.34	4.35
Storm surge	Extreme positive	RCP8.5, 95th percentile	%	2001.0	1.07	3.85	4.56
	Extreme negative		%	2001.0	1.07	3.85	4.56
Long waves	Extreme positive	RCP8.5, 95th percentile	%	2014.5	0.63	3.40	4.10
	Extreme negative		%	2014.5	0.63	3.40	4.10
Wave height	Extreme in deep water offshore	RCP8.5 mean, (No uncertainty ranges available)	%	2001.5	1.91	6.62	7.80
	Mean in deep water offshore		%	2004.5	0.0	0.0	0.0
Wave period	Extreme in deep water offshore	RCP8.5 mean, (No uncertainty ranges available)	%	2001.5	Base on H_{m0}-T_P relationship		
	Mean in deep water offshore		%	2004.5	0.0	0.0	0.0
Wave direction	Extreme in deep water offshore	RCP8.5 mean, (No uncertainty ranges available)	deg, pos clockwise	2001.5	Not available		
	Mean in deep water offshore			2004.5	-1.1	-4.0	-4.8
Current speed	Extreme depth-averaged wave-driven longshore current	RCP8.5 mean, (No uncertainty ranges available)	%	2013.0	0.61	2.91	3.48

5.9.21.2 Nearshore Waves

The best estimate extreme nearshore wave climate at a depth of -55 m msl in front of the site is provided in ***Table 5.9-44***. H_{m0} is the significant wave height (the mean of the highest one-third of waves), T_p is the peak wave direction, MWD_p is the mean wave direction associated with the peak wave period and DSD_p is the directional standard deviation (a measure of the directional spreading) associated with the peak wave period.

CONTROLLED DISCLOSURE

When downloaded from the EDS database, this document is uncontrolled and the responsibility rests with the user to ensure it is in line with the authorised version on the database.

Table 5.9-44: Extreme Wave Parameters at a Depth of -55 m msl in Front of the Site.

Exceedance Frequency	H_{m0}			T_p			MWD_p	DSD_p
(y^{-1})	(m)			(s)			(°)	(°)
	2034	2114	2134	2034	2114	2134	All	All
10^{-2}	9.3	9.8	9.9	15.9	16.2	16.3	211	17.4
10^{-4}	11.1	11.6	11.7	17.3	17.7	17.8	211	17.4
10^{-5}	11.8	12.4	12.5	17.9	18.3	18.4	211	17.4
10^{-6}	12.5	13.1	13.3	18.4	18.8	18.9	211	17.4
10^{-7}	13.2	13.8	14.0	18.9	19.3	19.5	211	17.4
10^{-8}	13.9	14.5	14.7	19.4	19.8	19.9	211	17.4

These results indicate a rough wave climate that will need to be accounted for in the design of all coastal structures at the site during the SAR and engineering design phases, e.g., intake structures, outfall structures and revetments.

5.9.21.3 Coastline Stability

The best estimate coastline stability at the site has been assessed including sea level rise, wave climate change and cross-shore storm erosion. The maximum horizontal erosion lines in front of the new NIs for 2034, 2134 and 2134 with high sea level rise are provided in ***Figure 5.9-91***, ***Figure 5.9-92***, and ***Figure 5.9-93***, respectively.

- The coastline erosion increases over time due to climate change which causes sea level rise and associated coastline recession, a rotated wave climate, and increases in storm wave height and storm surge.
- The erosion is more severe in Thysbaai than on the rocky coastline in the west, driven by recession due to sea level rise and coastline changes due to wave climate change which affect sandy coastlines.
- In 2034 only the 1E-8 y^{-1} storm erosion line extends onto a small section of the Nuclear Installation Corridor near the centre of the rocky coastline west of Thyspunt.
- By 2134 the Nuclear Installation Corridor is exceeded by the erosion lines for all storms with exceedance frequencies of 1E-2 y^{-1} and lower, at a limited number of locations along the rocky coastline west of Thyspunt and within Thysbaai.
- The 2134 High SLR scenario increases the erosion along the entire site, most substantially within Thysbaai. The erosion lines for all storms with exceedance frequencies of 1E-2 y^{-1} and lower extend onto the Nuclear Installation Corridor along the majority of Thysbaai and along the westernmost half of the rocky coastline west of Thyspunt.

CONTROLLED DISCLOSURE

When downloaded from the EDS database, this document is uncontrolled and the responsibility rests with the user to ensure it is in line with the authorised version on the database.

- It will thus be necessary to move the position of the new NIs landward, or to design appropriate coastal protection such as revetments.
- Note that these erosion lines show the extent of erosion of the topography which will threaten safety related structures, systems and components (SSCs) at the site. Wave run-up and flooding due to storm waves or tsunamis may extend further inland than these erosion lines. Flooding is discussed below.
- Further engineering studies should be undertaken to ensure that the outfall structures can withstand the predicted coastline erosion over the operating life of the plant.

5.9.21.4 Flooding from the Sea

Flooding from the sea can occur due to:

- Storm wave run-up combined with sea level rise, high tides, positive storm surge and wave set-up; and
- Tsunami run-up combined with sea level rise, high tides and positive storm surge.

No tsunami results are presented in this SSR and it is recommended that an updated THA be undertaken for Thyspunt and that this SSR should then be updated once these results are available. In the interim the flooding from the sea is based on the storm wave run-up only, as described below.

Maximum flood lines for 2034, 2134 and 2134 with high sea level rise are presented in ***Figure 5.9-98***, ***Figure 5.9-99*** and ***Figure 5.9-100*** respectively. The location of the maximum vertical run-up level for each labelled frequency is indicated with markers on all figures. The extreme flooding results for all exceedance frequencies are provided in ***Table 5.9-45***.

CONTROLLED DISCLOSURE

When downloaded from the EDS database, this document is uncontrolled and the responsibility rests with the user to ensure it is in line with the authorised version on the database.

Table 5.9-45: Extreme Flooding Due to Storm Waves.

Exceedance Frequency	Uncertainty	Maximum Vertical Run-Up Level		
(y^{-1})		(m msl)		
		2034	2134	2134 High SLR
1E-2	5th Percentile	7.54	11.60	13.13
	Mean	8.00	12.06	13.69
	Best Estimate	7.99	12.04	13.67
	95th Percentile	8.47	12.52	14.25
1E-4	5th Percentile	9.57	12.66	15.52
	Mean	10.47	13.56	16.60
	Best Estimate	10.44	13.53	16.56
	95th Percentile	11.37	14.46	17.68
1E-5	5th Percentile	11.62	14.80	16.63
	Mean	12.74	15.92	17.97
	Best Estimate	12.70	15.89	17.93
	95th Percentile	13.86	17.05	19.32
1E-6	5th Percentile	11.64	14.95	17.96
	Mean	12.99	16.30	19.58
	Best Estimate	12.95	16.26	19.53
	95th Percentile	14.34	17.65	21.20
1E-7	5th Percentile	11.69	15.52	18.63
	Mean	13.27	17.11	20.32
	Best Estimate	13.23	17.06	20.27
	95th Percentile	14.85	18.69	22.00
1E-8	5th Percentile	11.50	15.78	19.13
	Mean	13.31	17.59	21.09
	Best Estimate	13.26	17.55	21.04
	95th Percentile	15.12	19.41	23.05

- The flooding hazard increases over time due to climate change which causes sea level rise and associated coastline recession, a rotated wave climate, and increases in storm wave height and storm surge.
- The best estimate maximum vertical run-up level in 2034 due to the 1E-8 y^{-1} storm is 13.3 m msl, increasing to 17.6 m msl in 2134, and 21.0 m msl for the 2134 High SLR scenario.
- The maximum wave run-up for all frequencies in 2034 and both 2134 scenarios occurred along the exposed rocky coastline to the west of Thyspunt, while Thysbaai to the east of Thyspunt experienced significant landward flooding due to coastline recession.
- The flood lines extend into the estimated position of the Nuclear Installation Corridor for all three climate change scenarios. The Nuclear Installation Corridor is reached by all exceedance frequencies modelled

CONTROLLED DISCLOSURE

When downloaded from the EDS database, this document is uncontrolled and the responsibility rests with the user to ensure it is in line with the authorised version on the database.

in 2034 except for 1E-2 y^{-1}, while all exceedance frequencies modelled reach the corridor in both 2134 scenarios.

- The SSCs will need to be placed landward of the maximum flood lines, or alternatively protective structures such as revetments and wave walls will need to be placed in front of the SSCs. The SSCs will also need to be placed landward of the maximum erosion lines presented in ***Figure 5.9-91*** to ***Figure 5.9-93***.

5.9.21.5 Extreme Low Water Levels

Extreme low water levels at the cooling water intakes can occur due to:

- Storm wave drawdown combined with low tides and negative storm surge; and
- Tsunami drawdown combined with low tides and negative storm surge.

No tsunami results are presented in this SSR and it is recommended that an updated THA be undertaken for Thyspunt and that this SSR should then be updated once these results are available. In the interim the extreme low water levels are based on the storm wave drawdown only, as described below.

The extreme low water levels at the three proposed cooling water intakes in depths of −28.8 to −30.0 m msl for all exceedance frequencies are provided in ***Table 5.9-46***.

CONTROLLED DISCLOSURE

When downloaded from the EDS database, this document is uncontrolled and the responsibility rests with the user to ensure it is in line with the authorised version on the database.

Table 5.9-46: Extreme Low Water Levels Due to Storm Waves.

Exceedance Frequency	Uncertainty	Minimum Vertical Drawdown Level at Intakes	
(y^{-1})		(m msl)	
		2034	2134
1E-2	5th Percentile	-6.09	-6.49
	Mean	-6.01	-6.43
	Best Estimate	-6.01	-6.43
	95th Percentile	-5.94	-6.37
1E-4	5th Percentile	-6.85	-7.16
	Mean	-6.70	-7.05
	Best Estimate	-6.71	-7.05
	95th Percentile	-6.56	-6.95
1E-5	5th Percentile	-7.00	-7.38
	Mean	-6.84	-7.25
	Best Estimate	-6.84	-7.25
	95th Percentile	-6.67	-7.12
1E-6	5th Percentile	-7.17	-7.59
	Mean	-6.96	-7.43
	Best Estimate	-6.97	-7.44
	95th Percentile	-6.77	-7.28
1E-7	5th Percentile	-7.41	-7.69
	Mean	-7.18	-7.50
	Best Estimate	-7.18	-7.51
	95th Percentile	-6.95	-7.33
1E-8	5th Percentile	-7.65	-7.78
	Mean	-7.39	-7.57
	Best Estimate	-7.39	-7.58
	95th Percentile	-7.13	-7.38

- The extreme low water levels do not change significantly over time, since sea level rise has conservatively been excluded, and because the coastline erosion has little impact on these low water levels.
- Drawdown levels in 2134 increase at a reduced rate with increasing frequency of exceedance due to the depth limitation of waves at the location of the intakes.
- If a tunnel intake in a depth of -30 m msl is selected for the new NIs, then the results show that the intake should be designed to accommodate a best estimate minimum water level of -7.6 m msl, which is driven by the 1E-8 y^{-1} storm event in 2134.

CONTROLLED DISCLOSURE

When downloaded from the EDS database, this document is uncontrolled and the responsibility rests with the user to ensure it is in line with the authorised version on the database.

5.9.21.6 Thermal Plume Dispersion and Recirculation

It is proposed that the new NIs will be cooled using a once-through seawater cooling system. A conceptual layout for the seawater cooling intake and outfall system has been developed and thermal plume dispersion modelling has been performed to demonstrate the technical feasibility of the site. The concept considers offshore tunnel intakes at a depth of −30 m msl and an outfall channel discharging at −5 m msl.

The PPE specifies that the maximum ΔT of the re-circulated cooling water between the discharge and the intake should be less than 1.5°C.

The modelled recirculation ΔT's at the intakes are presented in ***Table 5.9-47***.

Table 5.9-47: Recirculation at the Intakes.

Location	ΔT at Intakes (°C)		
	50th Percentile	95th Percentile	99th Percentile
Intake 1	0.06	0.38	0.51
Intake 2	0.02	0.29	0.44
Intake 3	0.01	0.25	0.41

- The results above show the worst case 99th percentile ΔT at the intakes is 0.51°C, which is below the specified 1.5°C maximum allowable ΔT at the intakes.

5.9.21.7 Extreme Seawater Temperatures

The PPE also specifies a maximum cooling water intake temperature of 30°C. The maximum seawater temperature at the cooling water intakes will depend on:

- The intake and outfall layout, the power output and resultant ΔT due to recirculation from the outfall to the intake; and
- The extreme maximum background seawater temperature at the intake location and climate change.

The best estimate frequency to exceed 30°C at the intakes is presented in ***Table 5.9-48***.

CONTROLLED DISCLOSURE

When downloaded from the EDS database, this document is uncontrolled and the responsibility rests with the user to ensure it is in line with the authorised version on the database.

Table 5.9-48: Extreme Maximum Seawater Temperatures at the Intakes (Including Recirculation).

Location	Best Estimate Frequency to Exceed 30°C at Intakes (y^{-1})		
	2034	2114	2134
Intake 1	7.8E-51	6.5E-18	7.9E-11
Intake 2	5.1E-52	1.5E-18	2.7E-11
Intake 3	2.3E-52	1.0E-18	2.0E-11

- These results show that the exceedance frequency of the maximum specified PPE intake temperature of 30°C is 7.8E-51 y^{-1} (in 2034) and 7.9E-11 y^{-1} (in 2134), thus the intake temperature at the site will be less than the maximum specified in the PPE.

5.9.21.8 Sedimentation at Intakes

The proposed seawater intake is a tunnel extending to approximately -30 m msl water depth, with the intake opening positioned 3 to 5 m above the seabed. Modelling was performed to estimate the volume of sand drawn into the intakes which will have to be removed from the proposed landside intake basin. The results presented in ***Table 5.9-49*** are conservatively based on the suspended sediment concentrations 1 m above seabed.

Table 5.9-49: Sand Volume Drawn into Cooling Water Intake Tunnels.

Exceedance Frequency (y^{-1})	Case	Units	Intake at -30 m msl		
			1 m above bed	3 m above bed	5 m above bed
-	Operational Conditions	m^3/y	2 900	690	390
10^{-2}	Storm event	m^3/event	2 500	460	290
10^{-4}	Storm event	m^3/event	10 000	2 200	1 400
10^{-5}	Storm event	m^3/event	18 000	4 100	2 700
10^{-6}	Storm event	m^3/event	30 000	7 600	5 500
10^{-7}	Storm event	m^3/event	54 000	15 000	10 000
10^{-8}	Storm event	m^3/event	96 000	28 000	21 000

Notes:

(a) These sand volumes apply for a 10 000 MWe power station and an associated intake flow rate of 445 m^3/s. They can be reduced proportionally for a lower power and flow rate.

- For operational conditions the volume of sand drawn into the tunnel intakes which will have to be removed from the proposed landside intake basins is less than 2 900 m^3/y.

CONTROLLED DISCLOSURE

When downloaded from the EDS database, this document is uncontrolled and the responsibility rests with the user to ensure it is in line with the authorised version on the database.

- A maintenance dredging programme will be required to prevent excessive sedimentation in the basin and to keep a sufficient buffer for storm events.
- For extreme storm events the sand volume increases significantly and the 1E-2 y^{-1} storm event results in similar sand volumes over the 5.4-day event as the annual maintenance dredging requirements. The intake basin will need to be designed to accommodate these sediment volumes without blocking the pumps.

5.9.21.9 Blockage of Intakes and Biofouling

Based on the KNPS and worldwide experience it can be concluded that the new NIs intakes could be designed to cope with the marine species found at the site and to minimise the risk of complete blockage of the intake.

Chlorine or other biocides should be used to keep the cooling system free of marine growth.

The recommendations put forward by WANO and the EPRI best management practices manual will form an important and valuable input to the new NIs intake design and prevention of cooling water intake blockages through the plant life.

CONTROLLED DISCLOSURE

When downloaded from the EDS database, this document is uncontrolled and the responsibility rests with the user to ensure it is in line with the authorised version on the database.

5.9.22 References

ASR, 2006. *St Francis Bay Beach Project: Feasibility Study. Investigations into the Application of Multi-Purpose Reefs at St Francis Beach for Coastal Protection and Amenity Enhancement.,* Raglan, New Zealand: ASR Ltd.

Bruun, P., 1962. Sea Level Rise as a Cause of Shore Erosion. *J. Waterways Harbors Div,* 88(1), pp. 117-132.

CGS, 2008. *Potential Sources of Tsunami along the South African Coast. CGS Report Number: 2008-0220,* Bellville: Council for Geoscience.

Claassen, D., Wit, D. & M, 2017. Site-specific geoscientific characterization of Thyspunt, South Africa – an area identified for the proposed construction of a nuclear power plant. *South African Journal of Geology,* 120(4), pp. 459-476.

Cowell, P. J., Roy, P. & Jones, R., 1992. Shoreface translation model: computer simulation of coastal-sand-body response to sea level rise. *Mathematics and Computers in Simulation,* 33(5-6), p. 603–608.

D'Anna, M. et al., 2021. Reinterpreting the Bruun Rule in the Context of Equilibrium Shoreline Models. *Journal of Marine Science and Engineering,* 9(974).

Department of Energy, 2011. *R.927: The Regulations on Licencing of Sites for New Nuclear Installations. Government Gazette No. 34735,* Pretoria: Department of Energy.

DHI, 2024a. *Extreme Value Analysis, User Guide. DHI A/S, Hørsholm, Denmark.* [Online]
Available at:
https://manuals.mikepoweredbydhi.help//2024/General/EVA_UserGuide.pdf

DHI, 2024b. *Extreme Value Analysis, Technical Reference and Documentation. DHI A/S, Hørsholm, Denmark.* [Online]
Available at:
https://manuals.mikepoweredbydhi.help//2024/General/EVA_SciDoc.pdf

DHI, 2024c. *MIKE 21 Flow Model FM, User Guide. DHI A/S, Hørsholm, Denmark.* [Online]
Available at:
https://manuals.mikepoweredbydhi.help//2024/Coast_and_Sea/MIKE_FM_HD_2D.pdf

CONTROLLED DISCLOSURE

When downloaded from the EDS database, this document is uncontrolled and the responsibility rests with the user to ensure it is in line with the authorised version on the database.

DHI, 2024d. *MIKE 21 Flow Model FM, Scientific Documentation. DHI A/S, Hørsholm, Denmark.* [Online]
Available at:
https://manuals.mikepoweredbydhi.help//2024/Coast_and_Sea/MIKE_21_Flow_FM_Scientific_Doc.pdf

DHI, 2024e. *MIKE 21 Spectral Waves FM, User Guide. DHI A/S, Hørsholm, Denmark.* [Online]
Available at:
https://manuals.mikepoweredbydhi.help//2024/Coast_and_Sea/MIKE21SW.pdf

DHI, 2024f. *MIKE 21 Spectral Waves FM, Scientific Documentation. DHI A/S, Hørsholm, Denmark.* [Online]
Available at:
https://manuals.mikepoweredbydhi.help//2024/Coast_and_Sea/M21SW_Scientific_Doc.pdf

DHI, 2024g. *MIKE 21 Flow Model FM Sand Transport Module, User Guide. DHI A/S, Hørsholm, Denmark.* [Online]
Available at:
https://manuals.mikepoweredbydhi.help//2024/Coast_and_Sea/MIKE_FM_ST_2D.pdf

DHI, 2024h. *MIKE 21 Flow Model FM Sand Transport Module, Scientific Documentation. DHI A/S, Hørsholm, Denmark.* [Online]
Available at:
https://manuals.mikepoweredbydhi.help//2024/Coast_and_Sea/MIKE_FM_ST_Scientific_Doc.pdf

DHI, 2024i. *Littoral Processes FM, User Guide. DHI A/S, Hørsholm, Denmark.* [Online]
Available at:
https://manuals.mikepoweredbydhi.help//2024/Coast_and_Sea/MIKE_FM_LP.pdf

DHI, 2024j. *Littoral Processes FM, Scientific Documentation. DHI A/S, Hørsholm, Denmark.* [Online]
Available at:
https://manuals.mikepoweredbydhi.help//2024/Coast_and_Sea/LittoralProcessesFM_ScientificDoc.pdf

DHI, 2024k. *MIKE 3 Wave Model FM, Hydrodynamic Module and Sand Transport, User Guide. DHI A/S, Hørsholm, Denmark.* [Online]
Available at:
https://manuals.mikepoweredbydhi.help/2024/Coast_and_Sea/MIKE_FM_Wave.pdf

CONTROLLED DISCLOSURE

When downloaded from the EDS database, this document is uncontrolled and the responsibility rests with the user to ensure it is in line with the authorised version on the database.

DHI, 2024l. *MIKE 3 Wave Model FM, Hydrodynamic Module, Scientific Documentation. DHI A/S, Hørsholm, Denmark.* [Online]
Available at:
https://manuals.mikepoweredbydhi.help/2024/Coast_and_Sea/MIKE_3_Wave_FM_Scientific_Doc.pdf

DHI, 2024m. *MIKE 3 Flow Model FM, User Guide. DHI A/S, Hørsholm, Denmark.* [Online]
Available at:
https://manuals.mikepoweredbydhi.help//2024/Coast_and_Sea/MIKE_FM_HD_3D.pdf

DHI, 2024n. *MIKE 3 Flow Model FM, Scientific Documentation. DHI A/S, Hørsholm, Denmark.* [Online]
Available at:
https://manuals.mikepoweredbydhi.help//2024/Coast_and_Sea/MIKE_3_Flow_FM_Scientific_Doc.pdf

DHI, 2024o. *MIKE C-MAP Electronic Charts Database. DHI A/S, Hørsholm, Denmark,* Hørsholm, Denmark: DHI A/S.

DHI, 2024p. *MIKE 21 Tidal Analysis and Prediction Module, Scientific Documentation.* [Online]
Available at:
https://manuals.mikepoweredbydhi.help/2024/Coast_and_Sea/TideTools_Scientific_Doc.pdf

Digital Earth Africa Map, 2024. *Coastlines.* [Online]
Available at: https://maps.digitalearth.africa
[Accessed 2024].

DTU, 2010. *Improvement in global ocean tide model in shallow water regions,* Copenhagen, Denmark: Technical University of Denmark.

ECMWF, 2024. *European Centre for Medium-Range Weather Forecasts: ERA5.* [Online]
Available at: https://cds.climate.copernicus.eu/datasets/reanalysis-era5-single-levels?tab=overview
[Accessed 2024].

Elkington, L., 2012. *Morphology, Patterns and Processes in the Oyster Bay Headland Bypass Dunefield, South Africa,* Grahamstown, South Africa: Department of Geology, Rhodes University.

EPRI, 2008. *Best Management Practices for Preventing Cooling Water Intake Blockage. 1016319,* Palo Alto, California: Electric Power Research Institute.

CONTROLLED DISCLOSURE

When downloaded from the EDS database, this document is uncontrolled and the responsibility rests with the user to ensure it is in line with the authorised version on the database.

EPRI, 2021. *Best Management Practices Manual for Preventing Cooling Water Intake Blockages. 3002019660,* Palo Alto, California: Electric Power Research Institute.

Eskom, 2006. *Koeberg Site Safety Report. Chapter 6, Oceanography and Cooling Supply. Rev 3,* Johannesburg: Eskom.

Eskom, 2008a. *Cooling Water Intake and Outfall Works for the Eskom Nuclear 1 Sites - Conceptual Arrangements. Nuclear Programmes Department Nuclear-1, Document No. 300-9,* Johannesburg: Eskom.

Eskom, 2008b. *Environmental Impact Assessment for the Proposed Nuclear Power Station ('Nuclear-1') and Associated Infrastructure - Marine Ecology Study,* Johannesburg: Eskom.

Eskom, 2011. *External Hazards Requirements for New Nuclear Installations. Unique Identifier 238-1503. Rev 1,* Johannesburg: Eskom.

Eskom, 2013. *Site Safety Report for Thyspunt. Section 5.9: Oceanography and Coastal Engineering. Rev 0.,* Johannesburg: Eskom.

Eskom, 2018. *Quality and Safety Management Requirements for Nuclear Suppliers Level 2. Unique Identifier: 238-102. Rev 1,* Johannesburg: Eskom.

Eskom, 2020. *Specification for Validation and Verification Tasks for Simulation Models used in Nuclear Siting. Unique Identifier: NSIP02761. Rev 1,* Johannesburg: Eskom.

Eskom, 2022. *Koeberg Nuclear Power Station: KORC Feedback, Marine Ingress into Intake Basin, Jana Uys, 7 February 2022,* Cape Town: Eskom.

Eskom, 2023. *Revision and Update of the Site Safety Report for Thyspunt. Technical Requirement Specification, Unique Identifier: NSIP04251. Rev2,* Johannesburg: Eskom.

Eskom, 2024a. *Plant Parameter Envelope. Document Identifier: NSIP03179,* Johannesburg: Eskom.

Eskom, 2024b. *Duynefontyn Site Safety Report. Section 5.9, Oceanography and Coastal Engineering. Rev 3,* Johannesburg: Eskom.

Eskom, In Progress. *Technical Specification for Site Safety Reports: Section 5.9 Oceanography and Coastal Engineering. Revision 3,* Johannesburg: Eskom.

CONTROLLED DISCLOSURE

When downloaded from the EDS database, this document is uncontrolled and the responsibility rests with the user to ensure it is in line with the authorised version on the database.

Esri, 2024. *Esri World Imagery Wayback.* [Online]
Available at: https://livingatlas.arcgis.com/wayback
[Accessed 04 2024].

Fugro, 2006. *Geophysical Survey Report for Thyspunt. Eskom Site Surveys South Africa. Report no. MZ581za-01-RPT-04-01,* Cape Town, South Africa: Fugro Survey Africa (Pty) Ltd.

Fugro, 2007. *Geophysical Survey Report for Thyspunt Inshore Site Survey for Eskom, South Africa. Report no. MZ639za-01-RPT-02-01,* Cape Town, South Africa: Fugro Survey Africa (Pty) Ltd.

Hands, E., 1983. *The Great Lakes as a Test Model for Profile Responses to Sea-Level Changes.* s.l.:CRC Press.

HYCOM, 2024. *Hybrid Coordinate Ocean Model.* [Online]
Available at:
https://tds.hycom.org/thredds/catalogs/GLBv0.08/expt_53.X.html
[Accessed 2024].

IAEA, 2004. *Safety Standards Series, NS-G-1.9. Design of the Reactor Coolant System and Associated Systems in Nuclear Power Plants,* Vienna: International Atomic Energy Agency.

IAEA, 2011. *Safety Standards Series. SSG-18. Meteorological and Hydrological Hazards in Site Evaluation for Nuclear Installations,* Vienna: International Atomic Energy Agency.

IMOS, 2024. *Integrated Marine Observing System: Surface Waves.* [Online]
Available at: https://imos.org.au/facilities/srs/surface-waves/
[Accessed 2024].

IPCC, 2021. *Climate Change 2021: The Physical Science Basis. Contribution of Working Group I to the Sixth Assessment Report of the Intergovermental Panel on Climate Change.,* Cambridge, United Kingdom and New York, NY, USA: Cambridge University Press.

McCarrol, R. et al., 2021. A rules-based shoreface translation and sediment budgeting tool for estimating coastal change: ShoreTrans. *Marine Geology,* Volume 435.

Meucci, A. et al., 2020. Projected 21st century changes in extreme wind-wave events.. *Science Advances,* Issue 6, pp. 1-9.

CONTROLLED DISCLOSURE

When downloaded from the EDS database, this document is uncontrolled and the responsibility rests with the user to ensure it is in line with the authorised version on the database.

Morim, J., Hemer, M. & Wang, X. L., 2019. Robustness and uncertainties in global multivariate wind-wave climate projections.. *Nature Climate Change,* Issue 9, pp. 711-718.

Morim, J. et al., 2020. A global ensemble of ocean wave climate projections from CMIP5-driven models. *Scientific Data,* Volume 7.

NCEP, 2024. *WAVEWATCH III® Hindcast and Reanalysis Archives.* [Online]
Available at: https://polar.ncep.noaa.gov/waves/hindcasts/
[Accessed 2024].

NNR, 2008. *RD-0034: Quality and Safety Management Requirements for Nuclear Installations. Rev 0.,* Centurion: National Nuclear Regulator.

NNR, 2014. *PP-0014: Position Paper on Consideration of External Events for New Nuclear Installations. Rev. 0.,* Centurion: National Nuclear Regulator.

NNR, 2016a. *RG-0011: Interim Guidance on the Siting of Nuclear Facilities,* Centurion: National Nuclear Regulator.

NNR, 2016b. *RG-0016: Guidance on the Verification and Validation of Evaluation and Calculation Models used in Safety and Design Analyses. Rev 0.,* Centurion: National Nuclear Regulator.

NRC, 1976. *Regulatory Guide 1.102. Flood Protection for Nuclear Power Plants.,* Washington DC: US Nuclear Regulatory Commission.

NRC, 1977. *Regulatory Guide 1.59. Design Basis Floods for Nuclear Power Plants. Rev. 2. (errata published in 1980).,* Washington DC: US Nuclear Regulatory Commission.

NRC, 1978. *Regulatory Guide 1.70, Standard Format and Content of Safety Analysis Reports for Nuclear Power Plants. Rev. 3,* Washington DC: US Nuclear Regulatory Commission.

NRC, 2007a. *Combined License Applications for Nuclear Power Plants. Regulatory Guide 1.206,* Washington DC: US Nuclear Regulatory Commission.

NRC, 2007b. *Standards Review Plan. NUREG-0800, Part 2.4.5, Probable Maximum Surge and Seiche Flooding,* Washington DC: US Nuclear Regulatory Commission.

NRC, 2007c. *NUREG-0800. Part 2.4.6. Probable Maximum Tsunami Hazards,* Washington DC: US Nuclear Regulatory Commission.

CONTROLLED DISCLOSURE

When downloaded from the EDS database, this document is uncontrolled and the responsibility rests with the user to ensure it is in line with the authorised version on the database.

NRC, 2007d. *Standards Review Plan. NUREG-0800, Part 2.4.11. Low Water Considerations,* Washington DC: US Nuclear Regulatory Commission.

NRC, 2009. *Tsunami Hazard Assessment at Nuclear Power Plant Sites in the United States of America. Final Report. NUREG/CR-6966,* Richland, WA: United States Nuclear Regulatory Commission.

NRC, 2011. *Design-Basis Flood Estimation for Site Characterization at Nuclear Power Plants in the United States of America. NUREG/CR-7046 (PNNL-20091),* Washington DC: US Nuclear Regulatory Commission.

NRC, 2015. *Regulation 1.27. Ultimate Heat Sink for Nuclear Power Plants. Rev. 3,* Washington DC: US Nuclear Regulatory Commission.

NRC, 2016. *Tsunami Hazard Assessment: Best Modeling Practices and State-of-the-Art Technology. NUREG/CR-7223,* Washington DC: US Nuclear Regulatory Commission.

Petroliagkis, T. I., Voukouvalas, E., Disperati, J. & Bildot, J., 2016. *Joint Probabilities of Storm Surge, Significant Wave Height and River Discharge Components of Coastal Flooding Events. EUR 27824 EN. doi:10.2788/677778,* Italy: European Union.

PRDW, 2019. *Thyspunt SSR Ch 5.9: 2 Yrs Oceanographic Monitoring Data, S2052-01-RP-CE-002-R0,* Cape Town: PRDW.

PRDW, 2022a. *Duynefontyn SSR Ch 5.9: V&V Report. S2052-QP-QM-022-R2,* Cape Town: PRDW.

PRDW, 2022b. *Duynefontyn Tsunami Hazard Analysis (DTHA). Report S2052-07-RP-CE-001-R4,* Cape Town: PRDW.

Ranasinghe, R., Callaghan, D. & Stive, M., 2011. Estimating Coastal Recession due to Sea Level Rise: Beyond the Bruun Rule. *Climatic Change.*

Ranasinghe, R. & Stive, M. J. F., 2009. Rising Seas and Retreating Coastlines. *Climatic Change,* Volume 97, p. 465–468.

Shand, T. et al., 2013. A Review of Shoreline Response Models to Changes in Sea Level. *Coasts and Ports Australasian Conference.*

SRK, 2008. *LiDAR Survey,* Cape Town: SRK Consulting.

SRK, 2011. *Thyspunt: Project Lidar Survey Report. Report no. SGP2011_06,* Cape Town, South Africa: SRK Consulting.

CONTROLLED DISCLOSURE

When downloaded from the EDS database, this document is uncontrolled and the responsibility rests with the user to ensure it is in line with the authorised version on the database.

Tritan Survey cc, 2008. *Bantams Klip and Thys Punt: Installation and Calibration Report,* Cape Town: Tritan Survey.

Tritan Survey, 2024. *Technical Survey Report. Report No. 10425,* Cape Town, South Africa: Tritan Survey (Pty) Ltd.

USACE, 1989. *SBEACH: Numerical Model for Simulating Storm-Induced Beach Change. Report 1: Empirical Foundation and Model Development. Technical Report CERC-89-9,* Vicksburg, Mississippi, USA: US Army Corps of Engineers.

USACE, 1990. *SBEACH: Numerical Model for Simulating Storm-Induced Beach Change. Report 2: Numerical Formulation and Model Tests. Technical Report CERC-89-9,* Vicksburg, Mississippi, USA: US Army Corps of Engineers.

USACE, 1996a. *SBEACH-32 Interface User's Manual,* s.l.: US Army Corps of Engineers.

USACE, 1996b. *SBEACH: Numerical Model for Simulating Storm-Induced Beach Change. Report 4: Cross-Shore Transport Under Random Waves and Model Validation with SUPERTANK and Fleld Data. Technical Report CERC-89-9,* Vicksburg, Mississippi, USA: US Army Corps of Engineers.

USACE, 2002a. *Coastal Engineering Manual: Part II Chapter 4 - Surf Zone Hydrodynamics,* Washington DC, USA: US Army Corps of Engineers.

USACE, 2002b. *Coastal Engineering Manual: Part IV Chapter 3 - Coastal Morphodynamics,* Washington DC, USA: US Army Corps of Engineers.

Van Gent, M. et al., 2008. Large-scale dune erosion tests to study the influence of wave periods. *Coastal Engineering,* Volume 55, pp. 1041-1051.

Vousdoukas, M. I. et al., 2018. Global probabilistic projections of extreme sea levels show intensification of coastal flood hazard. *Nature Communications,* Volume 9, pp. 1-12.

Wijnberg, A. R., 1993. *Design Sea Levels for Southern Africa: A Probabilistic Approach. PhD Dissertation,* Cape Town: University of Cape Town.

WorleyParsons, 2014. *Investigation of the St. Francis Bay Spit and Beach Erosion Problems: Review of Previous Studies and Investigations and Assessment of Potential Remedial Options. Report no. 278960-00-CS-REP-0001-Rev 1 ,* Bellville, South Africa: WorleyParsons RSA.

CONTROLLED DISCLOSURE

When downloaded from the EDS database, this document is uncontrolled and the responsibility rests with the user to ensure it is in line with the authorised version on the database.

CONTROLLED DISCLOSURE

When downloaded from the EDS database, this document is uncontrolled and the responsibility rests with the user to ensure it is in line with the authorised version on the database.

APPENDIX 5.9.A: NUMERICAL MODEL DETAILS

CONTENTS

5.9.A.1 Coupled Spectral Waves and 2D Hydrodynamic Modelling 5.9-237
5.9.A.1.1 Introduction 5.9-237
5.9.A.1.2 Model Description 5.9-237
5.9.A.1.3 Model Setup 5.9-237
5.9.A.1.4 Cases Modelled 5.9-238
5.9.A.1.5 Calibration 5.9-239
5.9.A.2 Spectral Wave Modelling 5.9-241
5.9.A.2.1 Introduction 5.9-241
5.9.A.2.2 Offshore Hindcast Wave Data 5.9-241
5.9.A.2.3 Offshore Hindcast Wind Data 5.9-247
5.9.A.2.4 Model Description 5.9-252
5.9.A.2.5 Model Setup 5.9-253
5.9.A.2.6 Model Calibration 5.9-256
5.9.A.2.7 Cases Modelled 5.9-261
5.9.A.3 2D Sediment Transport Modelling 5.9-263
5.9.A.3.1 Introduction 5.9-263
5.9.A.3.2 Model Description 5.9-263
5.9.A.3.3 Model Setup 5.9-264
5.9.A.3.4 Model Calibration 5.9-268
5.9.A.3.5 Cases Modelled 5.9-268
5.9.A.4 Cross-shore Erosion Modelling 5.9-272
5.9.A.4.1 Introduction 5.9-272
5.9.A.4.2 Model Description 5.9-272
5.9.A.4.3 Cases Modelled 5.9-273
5.9.A.5 Littoral Processes Modelling 5.9-277
5.9.A.5.1 Introduction 5.9-277
5.9.A.5.2 Model Description 5.9-277
5.9.A.5.3 Model Setup 5.9-277
5.9.A.5.4 Cases Modelled 5.9-278
5.9.A.6 Wave Run-Up Modelling 5.9-280
5.9.A.6.1 Introduction 5.9-280

CONTROLLED DISCLOSURE

When downloaded from the EDS database, this document is uncontrolled and the responsibility rests with the user to ensure it is in line with the authorised version on the database.

5.9.A.6.2 Model Description 5.9-280
5.9.A.6.3 Model Setup 5.9-281
5.9.A.6.4 Model Calibration 5.9-284
5.9.A.6.5 Cases Modelled 5.9-293
5.9.A.6.6 Uncertainty in Modelled Wave Run-Up 5.9-294
5.9.A.7 Hydrodynamic Modelling 5.9-296
5.9.A.7.1 Introduction 5.9-296
5.9.A.7.2 Model Description 5.9-296
5.9.A.7.3 Model Setup 5.9-297
5.9.A.7.4 Model Calibration 5.9-302

CONTROLLED DISCLOSURE

When downloaded from the EDS database, this document is uncontrolled and the responsibility rests with the user to ensure it is in line with the authorised version on the database.

FIGURES

Figure 5.9.A-1: Coupled Spectral Wave and 2D Hydrodynamic Model Mesh. Also Shown are Boundaries of the Wave Set-Up Model Mesh. 5.9-238

Figure 5.9.A-2: Time-Series of 3D and 2D Modelled Wave Set-Up.....5.9-240

Figure 5.9.A-3: Scatterplot and Q-Q Comparison of the 3D and 2D Modelled Wave Set-Up. 5.9-240

Figure 5.9.A-4: Locations of Available Offshore Hindcast Wave Data and Offshore Measured Wave Data.....5.9-243

Figure 5.9.A-5: Scatterplot and Q-Q Comparison of Unscaled (Left) and Scaled (Right) NCEP Reanalysis Hindcast H_{m0} and Measured Satellite Altimeter H_{m0} of All NCEP Nodes Used in the Model. 5.9-244

Figure 5.9.A-6: Scatterplot and Q-Q Comparison of Unscaled NCEP Production (Left) and Forecast Multi-1 (Right) Hindcast H_{m0} and Measured Satellite Altimeter H_{m0} of All NCEP Nodes Used in the Model. 5.9-245

Figure 5.9.A-7: Scatterplot and Q-Q Comparison of Unscaled (Left) and Scaled (Right) NCEP Forecast GFSv16 Hindcast H_{m0} and Measured Satellite Altimeter H_{m0} of All NCEP Nodes Used in the Model. 5.9-246

Figure 5.9.A-8: Scatterplot Comparison of Modelled and Measured Wave Heights at the FA Platform Location (Water Depth -113 m msl).....5.9-247

Figure 5.9.A-9: Locations of Available Offshore Hindcast Wind Data and Measured Wind Data.....5.9-248

Figure 5.9.A-10: Wave Rose Comparison of Modelled and Measured Wind at the FA Platform (6 June 1996 to 2 August 2012) and Airshed WS (10 January 2008 to 13 March 2019). 5.9-250

Figure 5.9.A-11: Scatterplot Comparison of Modelled and Measured Wind Speed at the FA Platform for 14.1 Years of Valid Data Overlap. 5.9-251

Figure 5.9.A-12: Scatterplot Comparison of Modelled and Measured Wind Speed at the Airshed WS for 5.4 Years of Valid Data Overlap. 5.9-251

Figure 5.9.A-13: Regional and Nested Model Mesh Used for the Production and Forecast Wave Modelling. 5.9-254

Figure 5.9.A-14: Regional and Nested Model Bathymetry Used for the Production and Forecast Wave Modelling. 5.9-255

Figure 5.9.A-15: Time-Series Comparison of Modelled and Measured Spectral Wave Parameters at Site A. 5.9-257

Figure 5.9.A-16: Time-Series Comparison of Modelled and Measured Spectral Wave Parameters at Site B. 5.9-258

CONTROLLED DISCLOSURE

When downloaded from the EDS database, this document is uncontrolled and the responsibility rests with the user to ensure it is in line with the authorised version on the database.

Figure 5.9.A-17: Wave Rose Comparison of Modelled and Measured Waves at Site A (11 February 2008 to 12 August 2010) and Site B (21 April 2008 to 14 March 2019). 5.9-259

Figure 5.9.A-18: Scatterplot Comparison of Measured and Modelled Wave Height at Site A for 1.8 Years of Valid Data Overlap (11 February 2008 to 12 August 2010).5.9-260

Figure 5.9.A-19: Scatterplot Comparison of Measured and Modelled Wave Height at Site B for 5.5 Years of Valid Data Overlap (21 April 2008 to 14 March 2019). ..5.9-261

Figure 5.9.A-20: Bathymetry Used for 2D Sediment Transport Modelling. 5.9-264

Figure 5.9.A-21: Mesh Used for 2D Sediment Transport Modelling. 5.9-265

Figure 5.9.A-22:Non-Erodible Bed for the 2D ST Model Shown in Red. 5.9-267

Figure 5.9.A-23: Exceedance Curve of H_{m0} at Point 1 for 2009 Compared to All Data from 2000 to 2009. .....5.9-269

Figure 5.9.A-24: Wave Rose of H_{m0} at Point 1 and MWD for 2009 Compared to All Data from 2000 to 2009.....5.9-269

Figure 5.9.A-25: Exceedance Curve of Wind Speed at the Site for 2009 Compared to All Data from 2000 to 2009.....5.9-270

Figure 5.9.A-26: Wind Rose at the Site for 2009 Compared to All Data from 2000 to 2009. .....5.9-270

Figure 5.9.A-27: Storm Duration Analysis Based on 182 Nearshore Storms. The Synthetic Tide For 2013.5 (Excluding Storm Surge and Sea Level Rise) is Shown for Reference.....5.9-274

Figure 5.9.A-28: Plan View of Cross-Shore Profiles Used for Cross-Shore Erosion Modelling. Also Shown are the Offshore End of Each Profile (Squares). 5.9-276

Figure 5.9.A-29: MIKE 3 Wave Model Domain and Bathymetry.....5.9-282

Figure 5.9.A-30: Detail of MIKE 3 Wave Model Mesh and Bathymetry Around the Gulley Containing Site C. 5.9-283

Figure 5.9.A-31: Scatter Comparison Between Measured and Modelled Wave Crest Levels at Site C for the 24 August 2017 Storm.....5.9-285

Figure 5.9.A-32: Time-Series of Measured and Modelled Water Surface Elevations at Site C for Two Hours During the 24 August 2017 Storm. 5.9-286

Figure 5.9.A-33: Measured and Modelled Frequency Spectra at Site C During the 24 August 2017 Storm.....5.9-287

Figure 5.9.A-34: Scatter Comparison Between Measured and Modelled Wave Crest Levels for the 24 June 2018 Storm.....5.9-288

Figure 5.9.A-35: Time-Series of Measured and Modelled Water Surface Elevations at Site C for Two Hours During the 24 June 2018 Storm. 5.9-289

CONTROLLED DISCLOSURE

When downloaded from the EDS database, this document is uncontrolled and the responsibility rests with the user to ensure it is in line with the authorised version on the database.

Figure 5.9.A-36: Measured and Modelled Frequency Spectra at Site C During the 24 June 2018 Storm. 5.9-290

Figure 5.9.A-37: Maximum Modelled Water Surface Elevation During 9 September 2023 Storm and Measured Debris Line. 5.9-291

Figure 5.9.A-38: Comparison of the Vertical Ground Level Along the Measured Debris Line and Modelled Wave Run-Up Line for the 3 September 2023 Storm. Note That 0 m Chainage Refers to the Start of the Measured Debris Line in Figure 5.9.A-37, Increasing in Chainage from West to East. 5.9-292

Figure 5.9.A-39: Scatter Plot of Modelled Wave Run-Up Height Versus Wave Height (H_{m0}) Applied at the Model Boundary at -55 m msl. 5.9-295

Figure 5.9.A-40: Regional Model Domain and Bathymetry. 5.9-298

Figure 5.9.A-41: Regional Model Mesh. 5.9-298

Figure 5.9.A-42: Nested Model Domain and Bathymetry. 5.9-300

Figure 5.9.A-43: Detail of the Nested Model Mesh. 5.9-301

Figure 5.9.A-44: Time-Series Comparison of Modelled and Measured Water Surface Elevations at Site C (Depth -1.9 m msl). 5.9-303

Figure 5.9.A-45: Scatterplot and Q-Q Comparison of Modelled and Measured Water Surface Elevation at Site C (Depth -1.9 m msl). 5.9-303

Figure 5.9.A-46: Time-Series Comparison of Modelled and Measured Current Speed and Direction at Site A (Depth -13.2 m msl) for July 2009 to December 2009. .5.9-305

Figure 5.9.A-47: Time-Series Comparison of Modelled and Measured Current Speed and Direction at Site A (Depth -13.2 m msl) for January 2010 to June 2010.....5.9-306

Figure 5.9.A-48: Time-Series Comparison of Modelled and Measured Current Speed and Direction at Site B (Depth -30.8m msl) for July 2009 to December 2009. ..5.9-307

Figure 5.9.A-49: Time-Series Comparison of Modelled and Measured Current Speed and Direction at Site B (Depth -30.8 m msl) for January 2010 to June 2010.....5.9-308

Figure 5.9.A-50: Current Rose Comparison of Modelled and Measured Currents at Site A (1 July 2009 to 30 June 2010). 5.9-309

Figure 5.9.A-51: Current Rose Comparison of Modelled and Measured Currents at Site B (1 July 2009 to 30 June 2010). 5.9-310

Figure 5.9.A-52: Percentile Comparisons of Modelled and Measured Current Speeds at Site A and B (1 July 2009 to 30 June 2010). 5.9-311

Figure 5.9.A-53: Time-Series Comparison of Modelled and Measured Near-Seabed Seawater Temperatures at Site C, A and B. 5.9-313

Figure 5.9.A-54: Percentile Comparisons of Modelled and Measured Seawater Temperatures at Site C, A, and B (left), and Temperature Differences Between the Sites (right). 5.9-314

CONTROLLED DISCLOSURE

When downloaded from the EDS database, this document is uncontrolled and the responsibility rests with the user to ensure it is in line with the authorised version on the database.

TABLES

Table 5.9.A-1: 2D Coupled Spectral Wave and Hydrodynamic Model Settings. 5.9-238

Table 5.9.A-2: Summary of Available Offshore Hindcast Wave Data. 5.9-242

Table 5.9.A-3: Available Offshore Measured Wave Data. 5.9-246

Table 5.9.A-4: Summary of Available Offshore Hindcast Wind Data. 5.9-248

Table 5.9.A-5: Available Offshore Measured Wind Data. 5.9-249

Table 5.9.A-6: Summarised Boundary Conditions at -55 m msl for Modelled Wave Dominated Storm Scenarios.....5.9-275

Table 5.9.A-7: Summarised Boundary Conditions at -55 m msl for Modelled Storm Surge Dominated Storm Scenarios. 5.9-275

Table 5.9.A-8: SBEACH Model Setup Parameters.....5.9-276

Table 5.9.A-9: Joint Probability Best Estimate Extreme Currents for 2034. .....5.9-279

Table 5.9.A-10: Bottom Roughness Applied in Wave Model. 5.9-284

Table 5.9.A-12: Summarised Boundary Conditions at -36 m msl for Modelled Wave Dominated Storm Scenarios.....5.9-293

Table 5.9.A-13: Summarised Boundary Conditions at -36 m msl for Modelled Storm Surge Dominated Storm Scenarios. 5.9-294

CONTROLLED DISCLOSURE

When downloaded from the EDS database, this document is uncontrolled and the responsibility rests with the user to ensure it is in line with the authorised version on the database.

5.9.A.1 Coupled Spectral Waves and 2D Hydrodynamic Modelling

5.9.A.1.1 Introduction

A 2D coupled spectral wave and hydrodynamic model was used for the following purposes:

- To provide a continuous time-series of wave set-up used for the correction of measured water levels at Site C (***Subsection 5.9.9.1***).
- To transform extreme storm waves from Point 1 in -55 m msl to nearshore locations for the modelling of cross-shore beach erosion (***Subsection 5.9.11.5***), suspended sediment (***Subsection 5.9.11.8***), and storm wave run-up and drawdown (***Subsection 5.9.12***).

5.9.A.1.2 Model Description

The coupled model utilised the MIKE 21 Spectral Waves model (see ***Appendix 5.9.A.2***) and the MIKE 21 Flow Hydrodynamic model (see ***Appendix 5.9.A.7***). The details of the physical processes and numerical implementation are provided in the model documentation (see ***Table 5.9-7***), while details of the sensitivity testing and V&V are provided in the V&V Report (PRDW, 2022a).

5.9.A.1.3 Model Setup

Figure 5.9.A-1 shows the mesh and bathymetry used to transform extreme storm waves from Point 1 (-55 m msl) to various locations as required for the cross-shore beach erosion and suspended sediment modelling. The model bathymetry is derived from the generic dataset described in ***Subsection 5.9.8***. The bathymetry was truncated to a depth of -55 m msl to apply the extreme wave conditions along a constant water depth. A smaller, localised mesh was used to determine the wave set-up and is indicated in ***Figure 5.9.A-1***.

CONTROLLED DISCLOSURE

When downloaded from the EDS database, this document is uncontrolled and the responsibility rests with the user to ensure it is in line with the authorised version on the database.

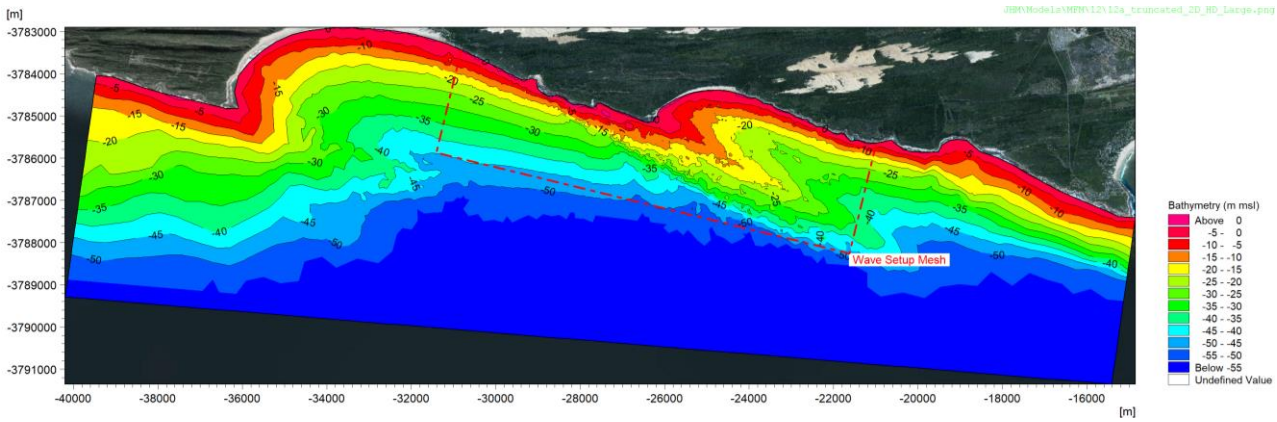


Figure 5.9.A-1: Coupled Spectral Wave and 2D Hydrodynamic Model Mesh. Also Shown are Boundaries of the Wave Set-Up Model Mesh.

The settings applied to this model were as in ***Appendix 5.9.A.2.5*** and ***Appendix 5.9.A.7.3*** except for the settings and boundary condition information given in ***Table 5.9.A-1***.

Table 5.9.A-1: 2D Coupled Spectral Wave and Hydrodynamic Model Settings.

Model	Settings	Wave Set-Up	Extreme Storm Waves
Spectral Wave Model	Boundary conditions	Space-varying parameters extracted from SW model (***Appendix 5.9.A.2***).	Space-constant parameters from EVA at Point 1
	Formulation	Parametric	Fully spectral
	Timestep	60 minutes	20 minutes
2D Hydrodynamic Model	Boundary conditions	Space-varying predicted tide from DTU10 (refer to ***Appendix 5.9.A.7.3***).	Space-constant synthetic tide time-series (refer to ***Appendix 5.9.A.4.3***)
	Bed resistance	Spatial map based on exposed rock (***Subsection 5.9.8***) using a Manning's M value of 43.4 $m^{1/3}/s$ in sandy areas and 20 $m^{1/3}/s$ in rocky areas.	

No additional forcings were applied and the hydrodynamic density was assumed to be barotropic.

5.9.A.1.4 Cases Modelled

5.9.A.1.4.1 Continuous Simulation for Wave Set-Up Correction

The coupled model was run for the full duration of available measurements at Site C between February 2008 and March 2019 to produce a continuous time-series of wave set-up used to correct the water levels measured in the shallow rock gulley at Site C.

CONTROLLED DISCLOSURE

When downloaded from the EDS database, this document is uncontrolled and the responsibility rests with the user to ensure it is in line with the authorised version on the database.

5.9.A.1.4.2 Discrete storm cases

The model was run for extreme storms with exceedance frequencies of 1E-2, 1E-4, 1E-6 and 1E-8 y^{-1} for the 2034, 2134 and 2134 High SLR scenarios. For each exceedance frequency the cases included the joint probability combinations for waves and storm surge.

5.9.A.1.5 Calibration

The spectral wave model has been calibrated to measurements at Site A and Site B as described in ***Appendix 5.9.A.2***. The modelled absolute water levels have been calibrated to measurements at Site C as described in ***Appendix 5.9.A.7***. A validation of the modelling of the wave set-up in the coupled model is presented here.

The modelled wave set-up was calculated as the difference between the modelled water levels at the measurement location (Site C) and in a depth of -40 m offshore of the site. ***Figure 5.9.A-2*** and ***Figure 5.9.A-3*** present the comparison between the 2D and 3D modelled wave set-up.

CONTROLLED DISCLOSURE

When downloaded from the EDS database, this document is uncontrolled and the responsibility rests with the user to ensure it is in line with the authorised version on the database.

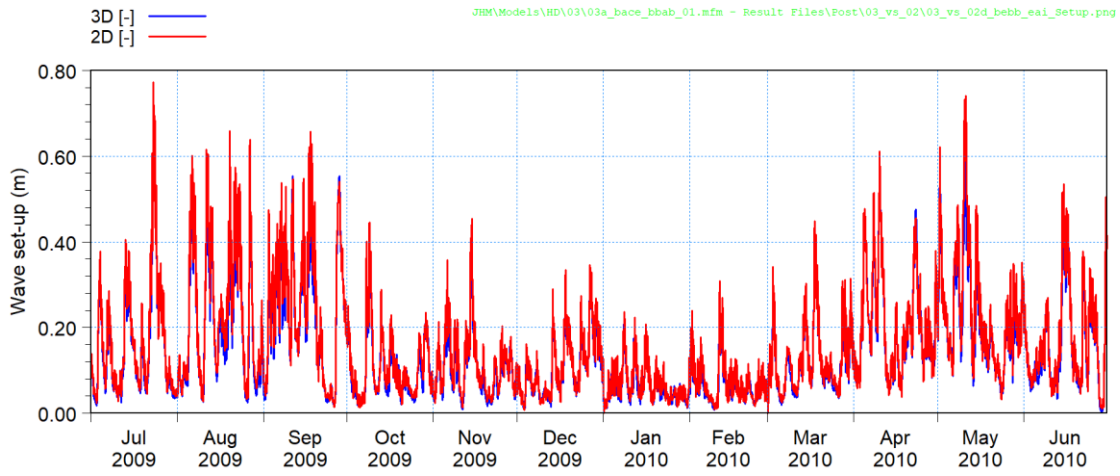


Figure 5.9.A-2: Time-Series of 3D and 2D Modelled Wave Set-Up.

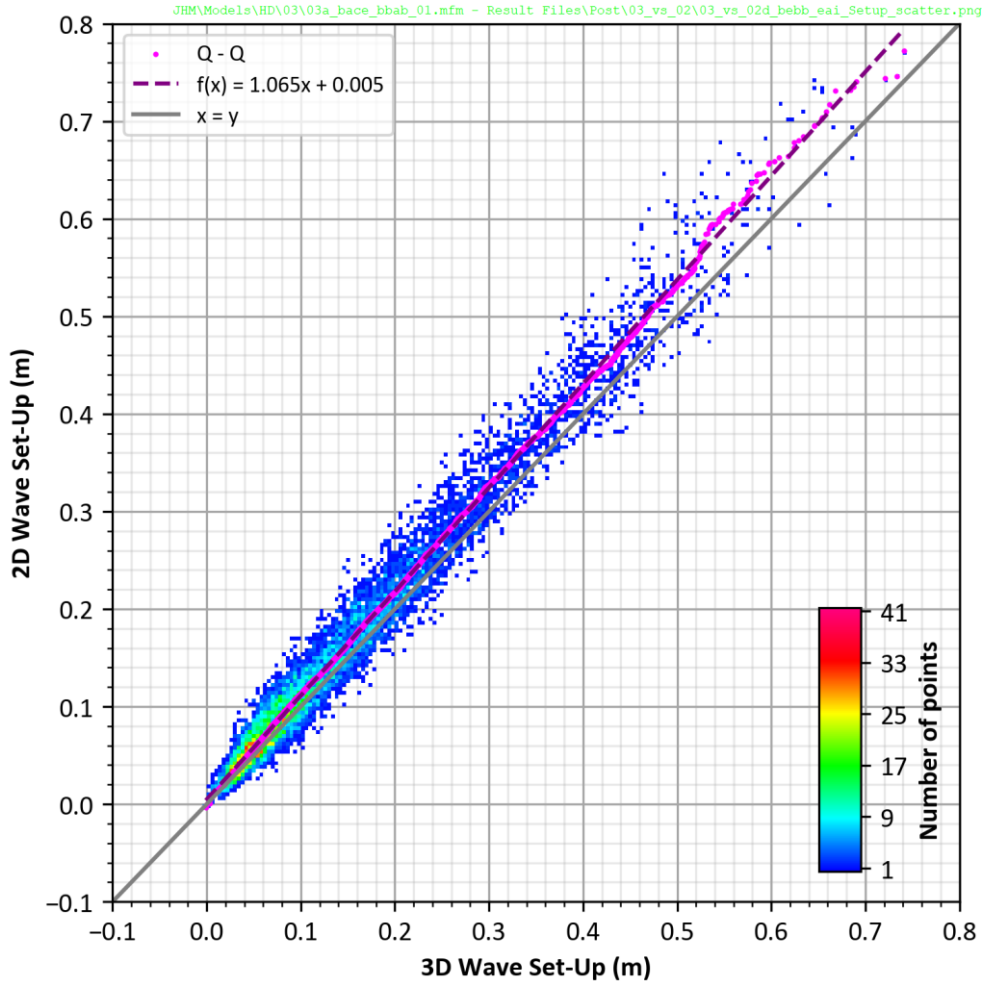


Figure 5.9.A-3: Scatterplot and Q-Q Comparison of the 3D and 2D Modelled Wave Set-Up.

CONTROLLED DISCLOSURE

When downloaded from the EDS database, this document is uncontrolled and the responsibility rests with the user to ensure it is in line with the authorised version on the database.

The results show a good agreement between the models and that the 2D model tends to overpredict the wave set-up by approximately 6%.

5.9.A.2 Spectral Wave Modelling

5.9.A.2.1 Introduction

The Spectral Wave Model was used to transform the offshore wave climate (>200 m water depth) to the nearshore wave climate (<55 m water depth) in front of the Thyspunt site. The nearshore wave climate was used to define the hydrographic conditions for design purposes (***Subsection 5.9.9***), and as input to the 2D sediment transport modelling (***Subsection 5.9.A.3***), cross-shore erosion modelling (***Subsection 5.9.A.4***), suspended sediment modelling (***Subsection 5.9.A.5***), and wave run-up modelling (***Subsection 5.9.A.6***).

5.9.A.2.2 Offshore Hindcast Wave Data

5.9.A.2.2.1 Available data

Due to the limited duration (5.5 y) of the measured wave data at the site, offshore wave data from a global hindcast model has been transformed to the site using a spectral wave model. The scaling and validation of the offshore hindcast data is described in this subsection.

Global hindcast wave data is freely available from the US National Oceanic and Atmospheric Administration's (NOAA) National Centers for Environmental Prediction (NCEP). The NCEP data is produced using the WAVEWATCH III multi-grid spectral wave model. Three datasets are currently available (NCEP, 2024):

- Reanalysis (1979-2009): A 31 year hindcast generated from the NCEP Climate Forecast System Reanalysis and Reforecast (CFSRR) homogeneous dataset of hourly high-resolution winds.
- Production (2005 to 2019): A hindcast dataset produced by rerunning the model from the operational wind fields to produce best-estimate nowcast datasets.
- Forecast (2007 to 2024): Archived dataset of ocean wave nowcasts and predictions using operational and assimilated NCEP atmospheric products as input. The global Multi-1 wave model is available up to mid-March 2021 with a new configuration of the global wave model coupled to GFSv16 available from mid-March 2021 to present.

The Reanalysis and Production datasets comprise wave partition data on a 1 degree geographical grid at hourly intervals, while the Forecast datasets are available on a 0.5 degree geographical grid at 3-hourly intervals for the

CONTROLLED DISCLOSURE

When downloaded from the EDS database, this document is uncontrolled and the responsibility rests with the user to ensure it is in line with the authorised version on the database.

Multi-1 model and hourly for the GFSv16 model. The wave partition data characterises the sea state by identifying wave parameters (H_{m0}, T_p, MWD, and DSD) for each of a variable number of peaks in the 2D wave spectrum. The wave partition data has been used to reconstitute the full 2D spectrum at each node and time step. In addition, the NCEP datasets also include space and time varying 10 m wind fields.

Table 5.9.A-2 summarises the available offshore hindcast data as used for the operational and extreme wave transformation. ***Figure 5.9.A-4*** shows the closest nodes available to the site from the three datasets. Note that latitudes of the NCEP Production dataset are offset by 0.5 degrees.

Table 5.9.A-2: Summary of Available Offshore Hindcast Wave Data.

Dataset	Resolution		Dates Available	Dates Used in Models	
	Spatial (°)	Temporal (h)		Operational	Extremes
Reanalysis	1	1	1979 - 2009	2000 – 2009	1979 - 2009
Production	1	1	2005 – 2019	N/A	2010 - May 2019
Forecast Multi-1	0.5	3	2007 - 2021	N/A	June 2019 – March 2021
Forecast GFSv16	0.5	1	2021 - 2024	N/A	March 2021 – June 2024

CONTROLLED DISCLOSURE

When downloaded from the EDS database, this document is uncontrolled and the responsibility rests with the user to ensure it is in line with the authorised version on the database.

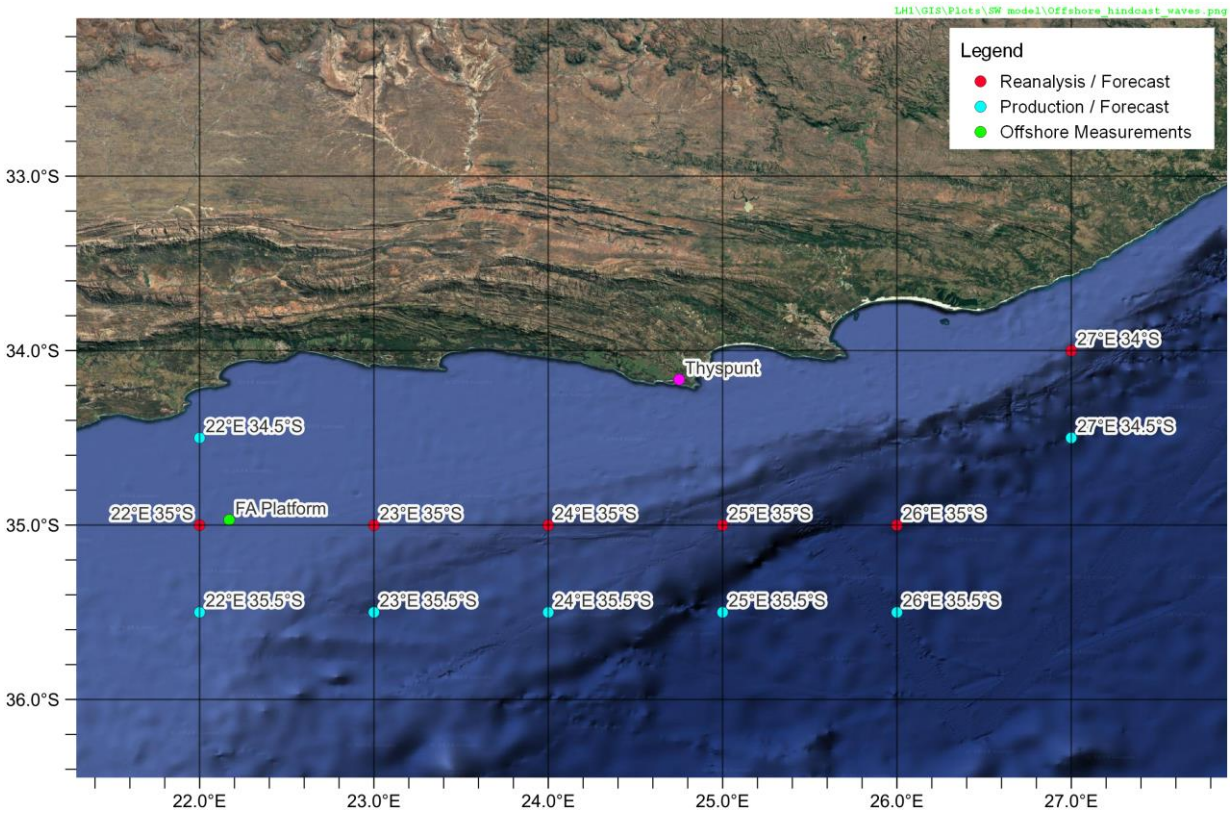


Figure 5.9.A-4: Locations of Available Offshore Hindcast Wave Data and Offshore Measured Wave Data.

5.9.A.2.2.2 Calibration

The hindcast wave heights applied on the spectral wave model boundary were calibrated against measured satellite altimeter wave heights obtained from Australia's Integrated Marine Observing System (IMOS) from 1985 to 2024 (IMOS, 2024). Each NCEP node used on the model boundary was compared to the altimeter data lying within a half-degree radius of the node (0.25-degree radius for the Forecast datasets). ***Figure 5.9.A-5*** shows the quantile-quantile (Q-Q) comparison of the unscaled and scaled scatter data of all the NCEP Reanalysis nodes used in the model.

CONTROLLED DISCLOSURE

When downloaded from the EDS database, this document is uncontrolled and the responsibility rests with the user to ensure it is in line with the authorised version on the database.

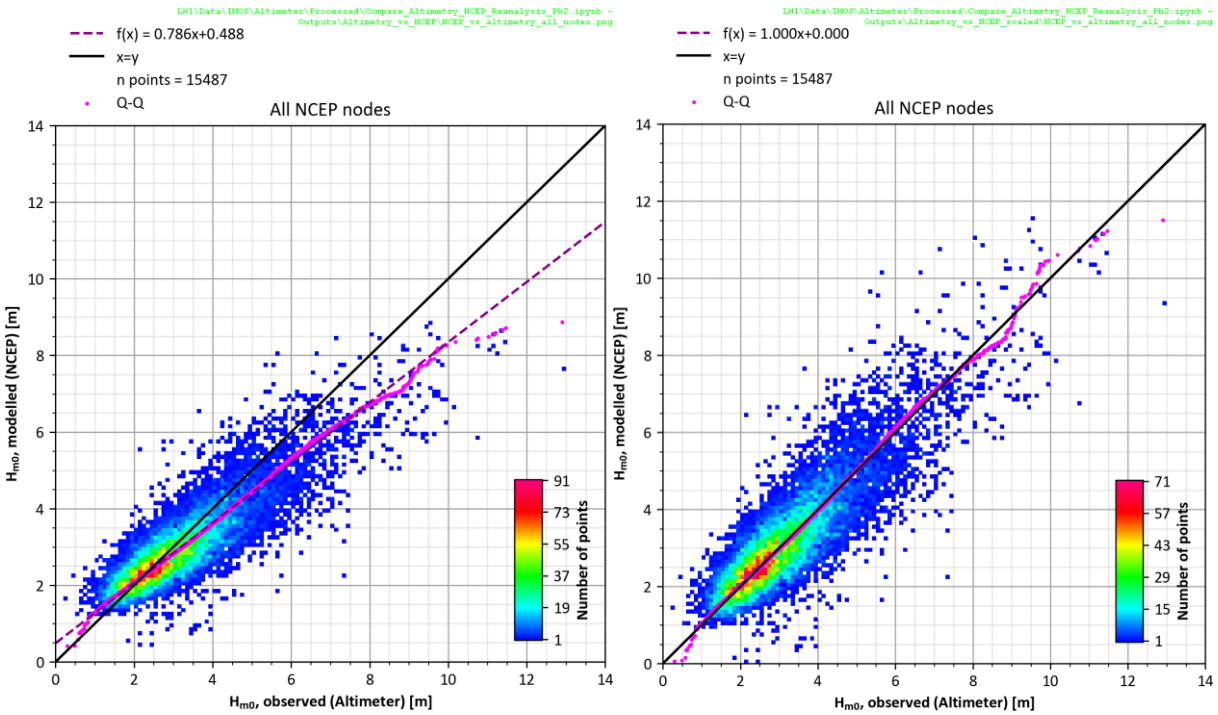


Figure 5.9.A-5: Scatterplot and Q-Q Comparison of Unscaled (Left) and Scaled (Right) NCEP Reanalysis Hindcast H_{m0} and Measured Satellite Altimeter H_{m0} of All NCEP Nodes Used in the Model.

The Reanalysis dataset was scaled using a two-part linear function, fitted to the Q-Q distributions, to produce a better fit of modelled hindcast and measured altimeter wave heights:

$$y = 1.26 \cdot x - 0.60, \quad x \leq 6.9 \text{ m}$$
$$y = 1.72 \cdot x - 3.75, \quad x > 6.9 \text{ m}$$

Equation 5.9.A.1

where:

x = Unscaled NCEP offshore wave height (m)

y = Scaled NCEP offshore wave height (m)

The NCEP Production and Forecast Multi-1 datasets had an adequate comparison to the satellite altimeter wave heights as shown in ***Figure 5.9.A-6*** and were therefore left unscaled.

CONTROLLED DISCLOSURE

When downloaded from the EDS database, this document is uncontrolled and the responsibility rests with the user to ensure it is in line with the authorised version on the database.

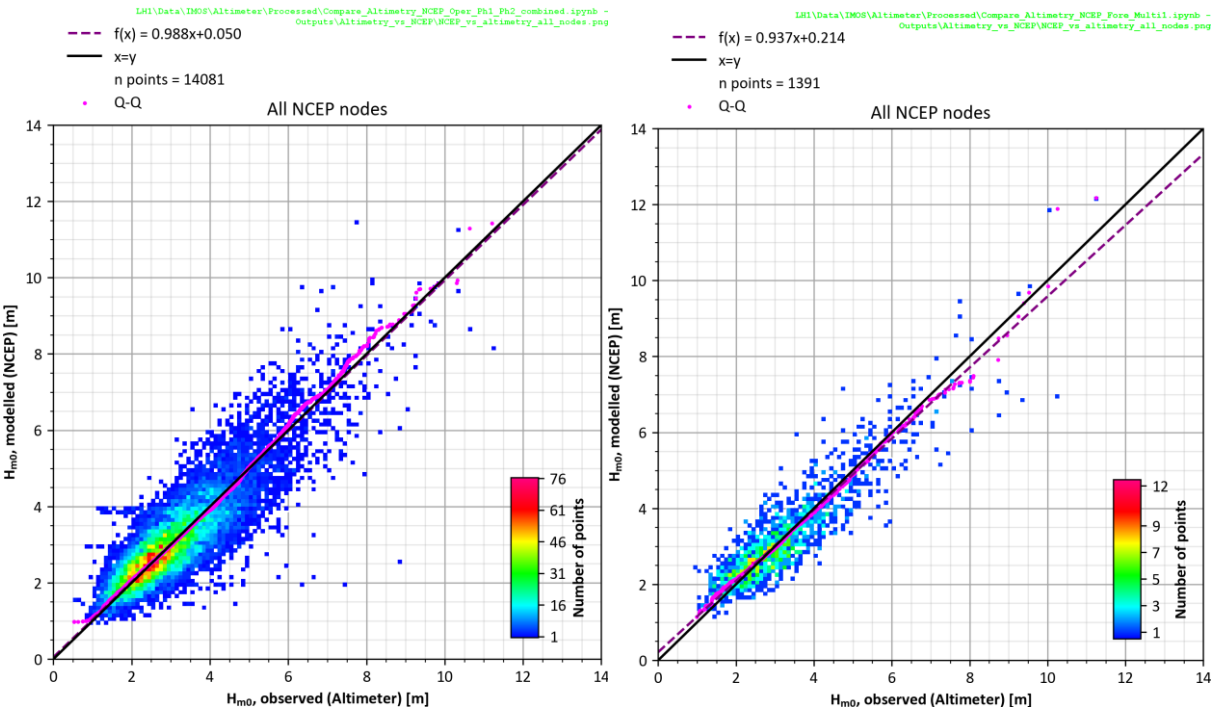


Figure 5.9.A-6: Scatterplot and Q-Q Comparison of Unscaled NCEP Production (Left) and Forecast Multi-1 (Right) Hindcast H_{m0} and Measured Satellite Altimeter H_{m0} of All NCEP Nodes Used in the Model.

The Forecast GFSv16 dataset required scaling as shown in ***Figure 5.9.A-7*** using a one-part linear equation:

$$y = 1.12\,x - 0.16$$ Equation 5.9.A.2

CONTROLLED DISCLOSURE

When downloaded from the EDS database, this document is uncontrolled and the responsibility rests with the user to ensure it is in line with the authorised version on the database.

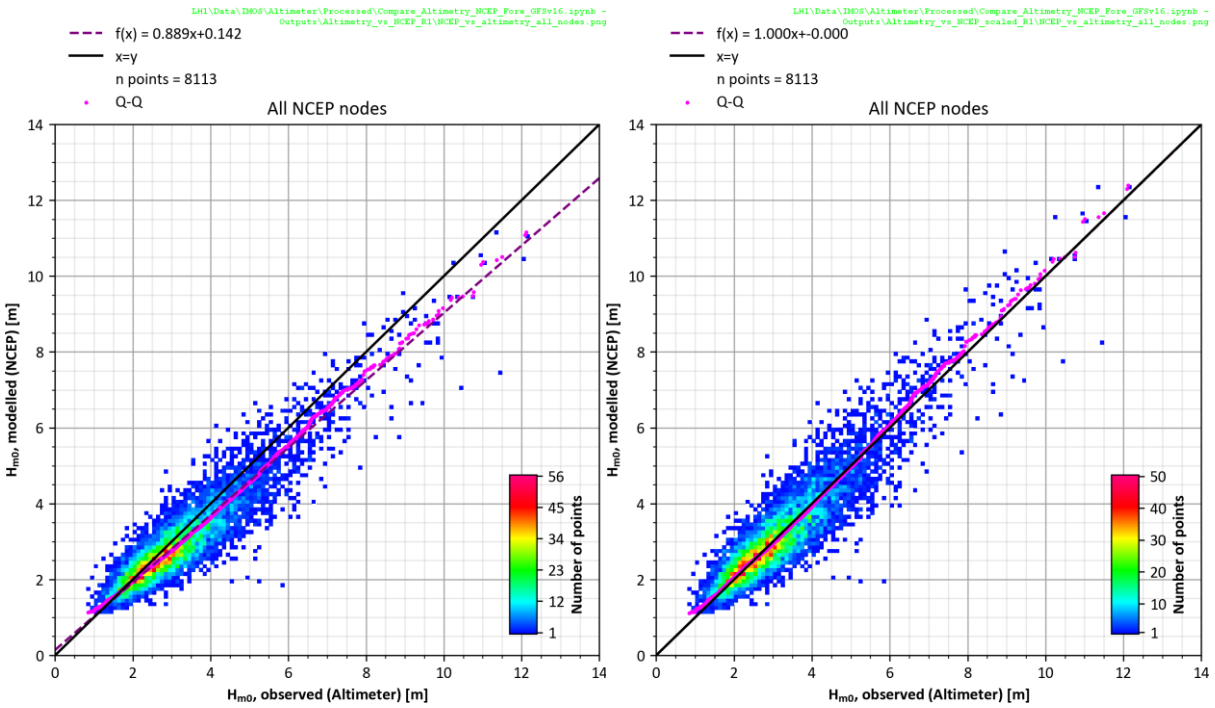


Figure 5.9.A-7: Scatterplot and Q-Q Comparison of Unscaled (Left) and Scaled (Right) NCEP Forecast GFSv16 Hindcast H_{m0} and Measured Satellite Altimeter H_{m0} of All NCEP Nodes Used in the Model.

5.9.A.2.2.3 Validation

Subsequent to the boundary calibration, the NCEP wave heights were compared to wave measurements in deep water at the oil production platform in the F-A gas field (further referred to as the FA Platform), situated offshore of Mossel Bay. Details of the dataset are given in ***Table 5.9.A-3*** with the location shown in ***Figure 5.9.A-4***.

Table 5.9.A-3: Available Offshore Measured Wave Data.

Location	Position	Water Depth (m msl)	Instrument	Parameters	Sampling Interval	Date Range
FA Platform	22.17°E, 34.97°S	-113.0	WaMoS system (Wave Radar)	Time domain significant wave height (H_s), T_p, MWD	3 min	1 Oct 2007 – 2 Aug 2012

The WaMoS measurements were averaged to calculate the 1-hour averaged wave height for comparison against the NCEP data.

The vector components of the NCEP wave height and direction were bilinearly interpolated to the FA Platform location using the wave conditions from the four closest nodes. ***Figure 5.9.A-8*** presents a scatterplot comparison of measured wave heights and the scaled NCEP Reanalysis

When downloaded from the EDS database, this document is uncontrolled and the responsibility rests with the user to ensure it is in line with the authorised version on the database.

(October 2007 – December 2009) and unscaled Production (January 2010 – August 2012) datasets at the FA Platform where the data overlap.

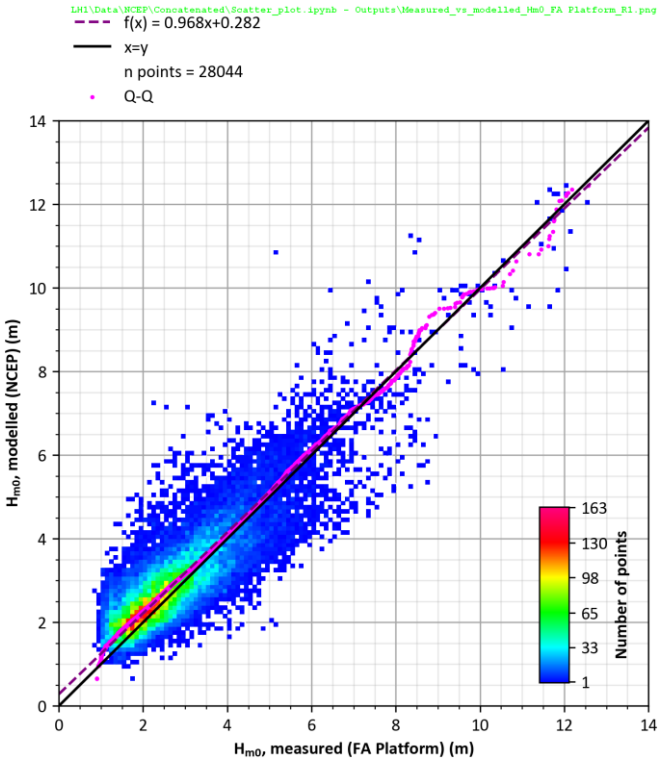


Figure 5.9.A-8: Scatterplot Comparison of Modelled and Measured Wave Heights at the FA Platform Location (Water Depth -113 m msl).

Overall, the modelled H_{m0} correlates very well to the measured wave heights as shown by the Q-Q plot, whilst the scatter indicates that some individual events are either offset in time, under-estimated or over-estimated. The calibrated NCEP hindcast wave data is therefore considered to provide a sufficiently accurate characterisation of the wave climate offshore of the site.

5.9.A.2.3 Offshore Hindcast Wind Data

Wind data is required as input to the spectral wave, 2D sediment transport and hydrodynamic modelling as described in ***Subsections 5.9.A.2.5, 5.9.A.3*** and ***5.9.A.6***. Due to the limited duration (5.4 y) and single onshore location of the measured wind data at the site (the measurement programme is detailed in ***Subsection 5.9.6.1***), wind data from a global hindcast model was applied as a space and time-varying wind field over the model domain. The validation of the offshore hindcast data is described in this subsection.

Global hindcast wind data is freely available from the US NOAA's NCEP WAVEWATCH III CFS hindcast dataset (NCEP, 2024). The CFSRR dataset (1979-2010) comprises modelled wind speed and direction on a

CONTROLLED DISCLOSURE

When downloaded from the EDS database, this document is uncontrolled and the responsibility rests with the user to ensure it is in line with the authorised version on the database.

0.31 degree geographical grid at hourly intervals at 10 m above surface level, while the CFSv2 dataset (2011-2024) is available on a 0.20 degree geographical grid.

Table 5.9.A-4 summarises the available offshore hindcast data used as wind forcing on the spectral wave model. ***Figure 5.9.A-9*** shows the CFSRR and CFSv2 nodes available close to the site.

Table 5.9.A-4: Summary of Available Offshore Hindcast Wind Data.

Dataset	Resolution		Dates Available	Dates Used in Models	
	Spatial (°)	Temporal (h)		Operational	Extremes
CFSRR	0.31	1	1979 - 2010	2000 - 2009	1979 - 2010
CFSv2	0.20	1	2011 – 2024	N/A	2011 – June 2024

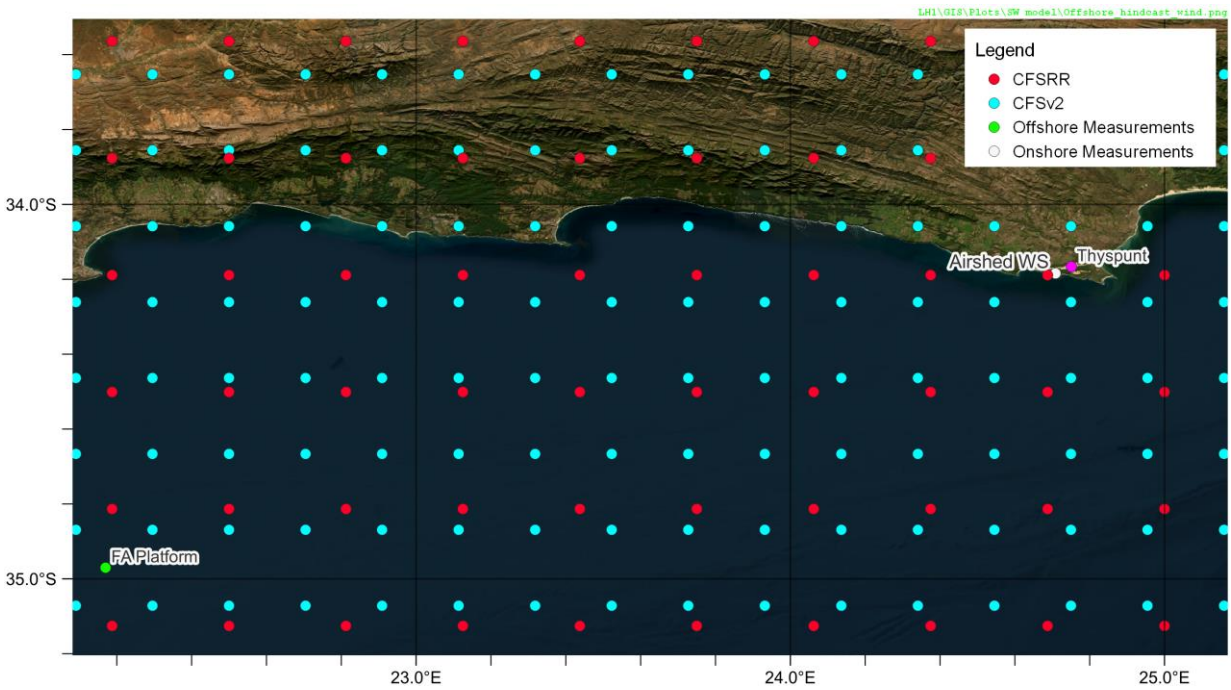


Figure 5.9.A-9: Locations of Available Offshore Hindcast Wind Data and Measured Wind Data.

The hindcast wind speed and direction applied over the model domain were compared to the nearest available offshore wind measurements, which are at the FA Platform approximately 280 km west of the site. Details of the dataset are given in ***Table 5.9.A-5*** with the location shown in ***Figure 5.9.A-9***. The hindcast data was also compared to onshore wind measurements at the Airshed Weather Station (further referred to as Airshed WS) shown in ***Figure 5.9.A-9***.

CONTROLLED DISCLOSURE

When downloaded from the EDS database, this document is uncontrolled and the responsibility rests with the user to ensure it is in line with the authorised version on the database.

Table 5.9.A-5: Available Offshore Measured Wind Data.

Location	Position	Instrument Height Above Surface (m):	Parameters	Sampling Interval	Date Range
FA Platform	22.17°E, 34.97°S	112.0	Wind speed and direction	1 h averaged up to 26 Sept 2007, then 3 min	6 Jun 1996 – 2 Aug 2012

The FA Platform data was adjusted to 10 m above surface level for comparison to the hindcast modelled wind data. The data from October 2007 to August 2012 was averaged to calculate the 1-hour averaged wind data to have a sampling interval for both measured datasets at the FA Platform.

The velocity components of the hindcast wind speed and direction were bilinearly interpolated to the FA Platform and Airshed WS locations using the wind data from the four closest nodes. Wind roses of the measured and modelled data are presented in ***Figure 5.9.A-10*** and scatterplot comparisons in ***Figure 5.9.A-11*** (FA Platform) and ***Figure 5.9.A-12*** (Airshed WS) where the data overlap.

CONTROLLED DISCLOSURE

When downloaded from the EDS database, this document is uncontrolled and the responsibility rests with the user to ensure it is in line with the authorised version on the database.

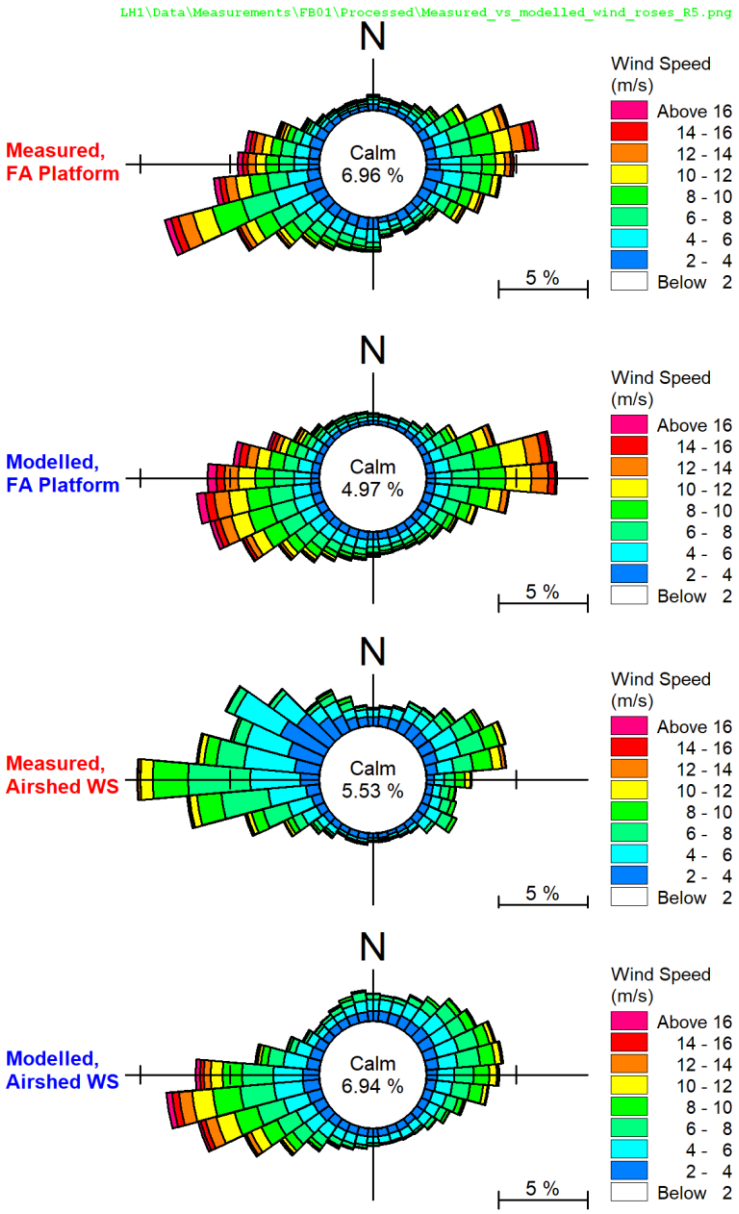


Figure 5.9.A-10: Wave Rose Comparison of Modelled and Measured Wind at the FA Platform (6 June 1996 to 2 August 2012) and Airshed WS (10 January 2008 to 13 March 2019).

CONTROLLED DISCLOSURE

When downloaded from the EDS database, this document is uncontrolled and the responsibility rests with the user to ensure it is in line with the authorised version on the database.

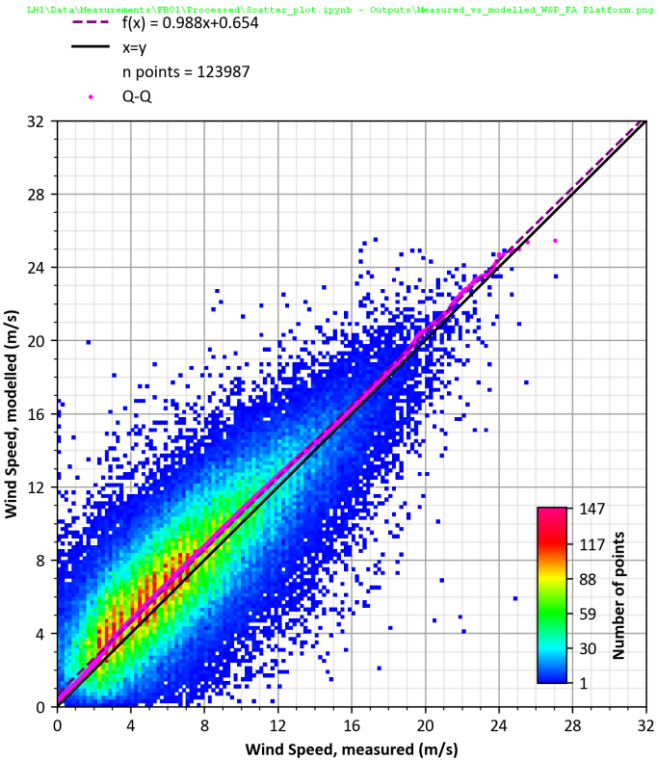


Figure 5.9.A-11: Scatterplot Comparison of Modelled and Measured Wind Speed at the FA Platform for 14.1 Years of Valid Data Overlap.

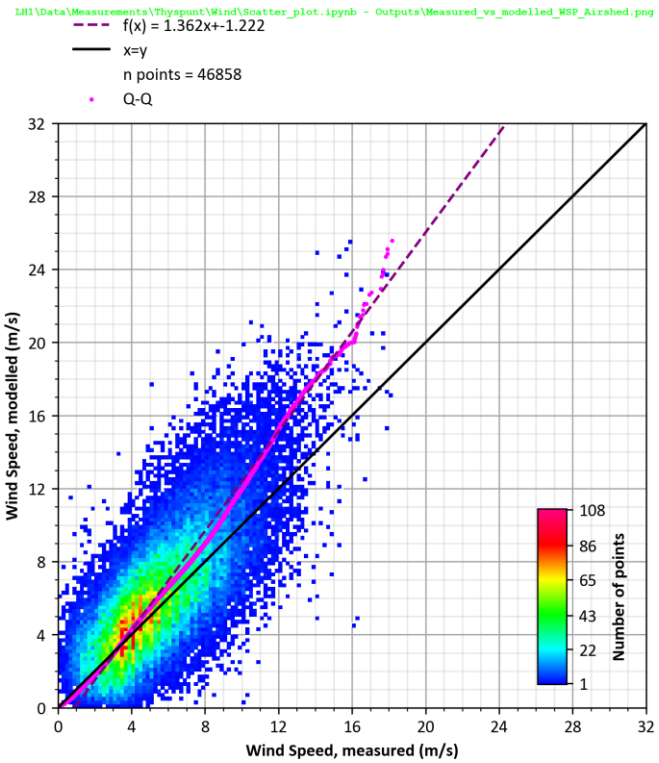


Figure 5.9.A-12: Scatterplot Comparison of Modelled and Measured Wind Speed at the Airshed WS for 5.4 Years of Valid Data Overlap.

CONTROLLED DISCLOSURE

When downloaded from the EDS database, this document is uncontrolled and the responsibility rests with the user to ensure it is in line with the authorised version on the database.

The comparison at the FA Platform shows an overall good agreement between the model and measurements as evidenced by the Q-Q comparison, while the scatter in the figure indicates some individual events are either offset in time, under-estimated or over-estimated.

The CFS model overestimates the stronger wind speeds measured at the Airshed WS location but agrees well with the operational wind speeds (< 8 m/s). The modelled wind directions from the west are approximately 10°less than the measurements. This deviation from the measurements is likely due to the coarse spatial resolution of the hindcast model that cannot resolve the coastal topography and the wind speed gradient due to wind shear at the land-sea interface. This effect is less important for model applications where the wind field over the open ocean is of primary importance.

Based on the comparison at the two measurement locations, the CFS hindcast wind data was deemed adequate to be applied as wind forcing on the wave model. Sufficient accuracy of the CFS model will be confirmed through the calibration of the models using this wind forcing, which include the spectral wave model (***Subsection 5.9.A.2.6***), the 3D hydrodynamic model (***Subsection 5.9.A.7***), and the 2D sediment transport model (***Subsection 5.9.A.3***).

5.9.A.2.4 Model Description

The MIKE 21 Spectral Waves (SW) Flexible Mesh model was used for the wave transformation modelling. The model consisted of a regional model and a nested wave model. The details of the physical processes and numerical implementation are provided in the model documentation (see ***Table 5.9-7***), while details of the sensitivity testing and V&V are provided in the V&V Report (PRDW, 2022a).

The model simulates the growth, decay and transformation of wind-generated waves and swells in offshore and coastal areas using unstructured meshes. The model includes the following physical phenomena:

- Wind-wave generation;
- Non-linear wave-wave interaction;
- Dissipation due to whitecapping;
- Dissipation due to bottom friction;
- Dissipation due to depth-induced wave breaking;
- Refraction and shoaling due to depth variations;
- The effect of time-varying water depth.

CONTROLLED DISCLOSURE

When downloaded from the EDS database, this document is uncontrolled and the responsibility rests with the user to ensure it is in line with the authorised version on the database.

5.9.A.2.5 Model Setup

Figure 5.9.A-13 and ***Figure 5.9.A-14*** show the mesh and bathymetry of the regional and nested models used for the Production and Forecast hindcast wave refraction modelling. Note that the Reanalysis hindcast data necessitated a different regional model mesh to align the offshore boundaries with the NCEP nodes.

CONTROLLED DISCLOSURE

When downloaded from the EDS database, this document is uncontrolled and the responsibility rests with the user to ensure it is in line with the authorised version on the database.

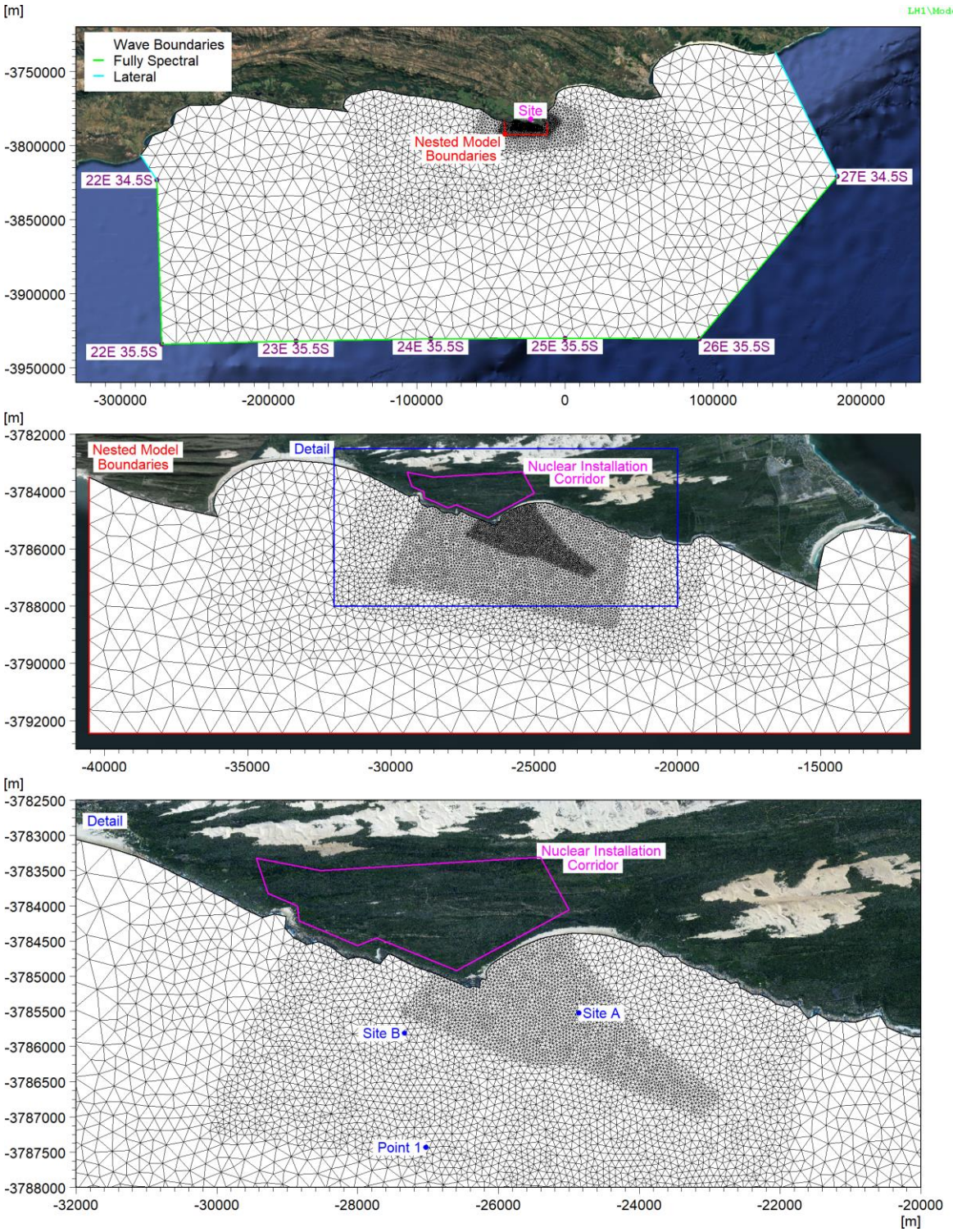


Figure 5.9.A-13: Regional and Nested Model Mesh Used for the Production and Forecast Wave Modelling.

CONTROLLED DISCLOSURE

When downloaded from the EDS database, this document is uncontrolled and the responsibility rests with the user to ensure it is in line with the authorised version on the database.

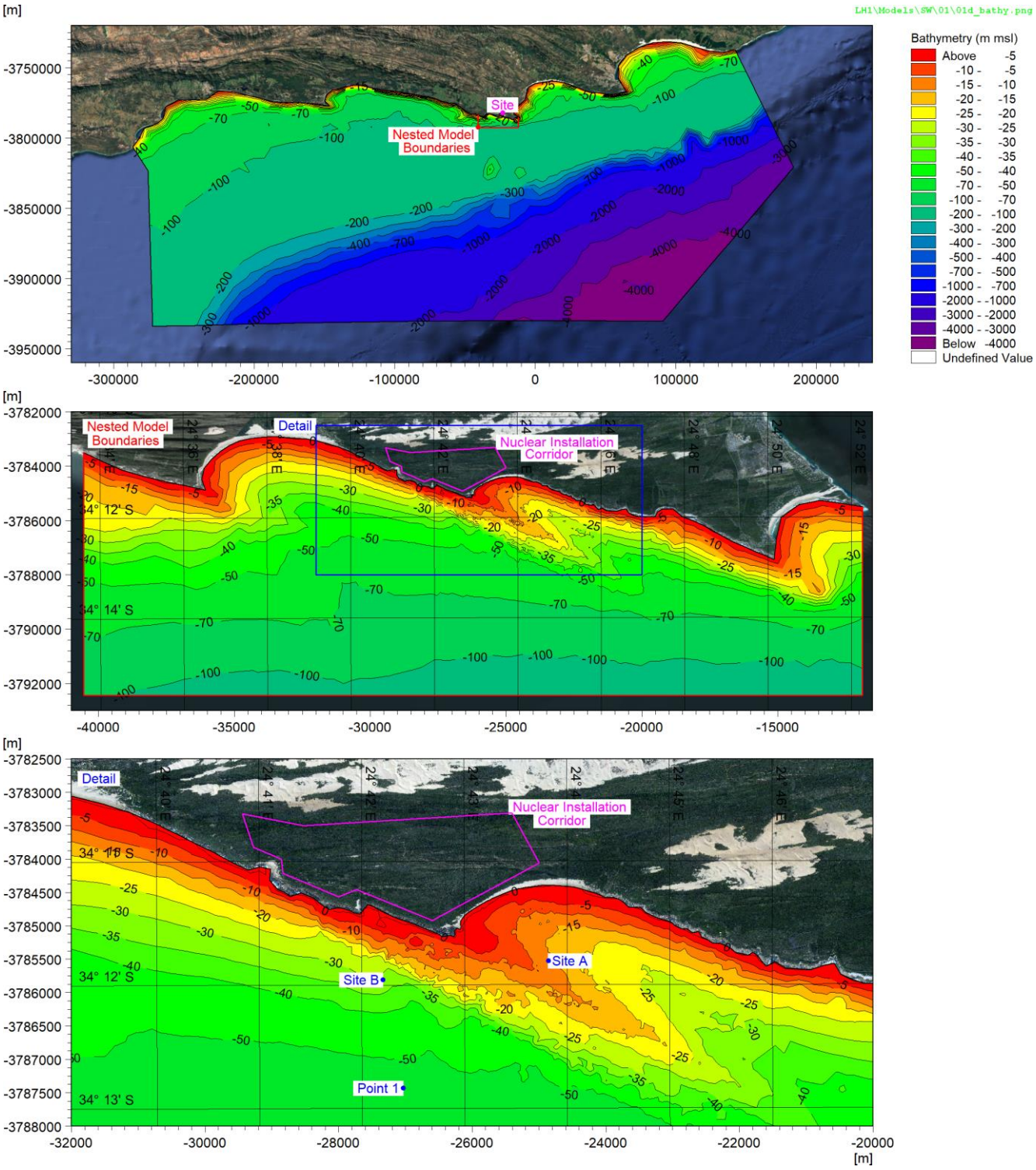


Figure 5.9.A-14: Regional and Nested Model Bathymetry Used for the Production and Forecast Wave Modelling.

The model bathymetry is derived from the generic dataset described in ***Subsection 5.9.8***.

CONTROLLED DISCLOSURE

When downloaded from the EDS database, this document is uncontrolled and the responsibility rests with the user to ensure it is in line with the authorised version on the database.

The hindcast spectral wave data was applied along the offshore boundaries of the regional model with lateral wave boundaries connecting the spectral boundaries to land at the western and eastern extents of the domain (see ***Figure 5.9.A-13***). The CFS wind data was applied as a space and time varying wind field over the model domain. The coupled formulation of air-sea interaction was used for the wind-wave generation. The regional model was run in the fully spectral, instationary formulation.

Bottom friction was modelled using a spatially varying Nikuradse roughness of k_N = 0.02 m in sandy areas and 0.60 m in rocky areas. Predicted tidal levels at the Port of Port Elizabeth was applied as a time-varying water level over the model domain.

The nested model was forced using the same model settings, CFS wind data, bottom friction and water levels as the regional model. The uncoupled formulation of air-sea interaction was used for the wind-wave generation. The wave boundary conditions were extracted from the regional wave model and were applied as time and space-varying wave spectra. The model was run in the fully spectral and quasi-stationary mode, which assumes fetch-limited wind-wave generation and sea states which are stationary in time, which is appropriate for the nested model with a maximum fetch of 15 km between the boundaries and the site.

5.9.A.2.6 Model Calibration

The nearshore operational waves were validated against measurements available at Site A and Site B (the measurement programme is detailed in ***Subsection 5.9.6.1***). The measured and modelled data had 1.8 years of valid data overlap (11 February 2008 to 12 August 2010) at Site A and 5.5 years of valid data overlap (21 April 2008 to 14 March 2019) at Site B.

Figure 5.9.A-15 and ***Figure 5.9.A-16*** show time-series comparisons of modelled and measured spectral wave parameters at Site A and Site B respectively. Wave roses are presented in ***Figure 5.9.A-17*** and scatterplot comparisons in ***Figure 5.9.A-18*** (Site A) and ***Figure 5.9.A-19*** (Site B) where the data overlap.

CONTROLLED DISCLOSURE

When downloaded from the EDS database, this document is uncontrolled and the responsibility rests with the user to ensure it is in line with the authorised version on the database.

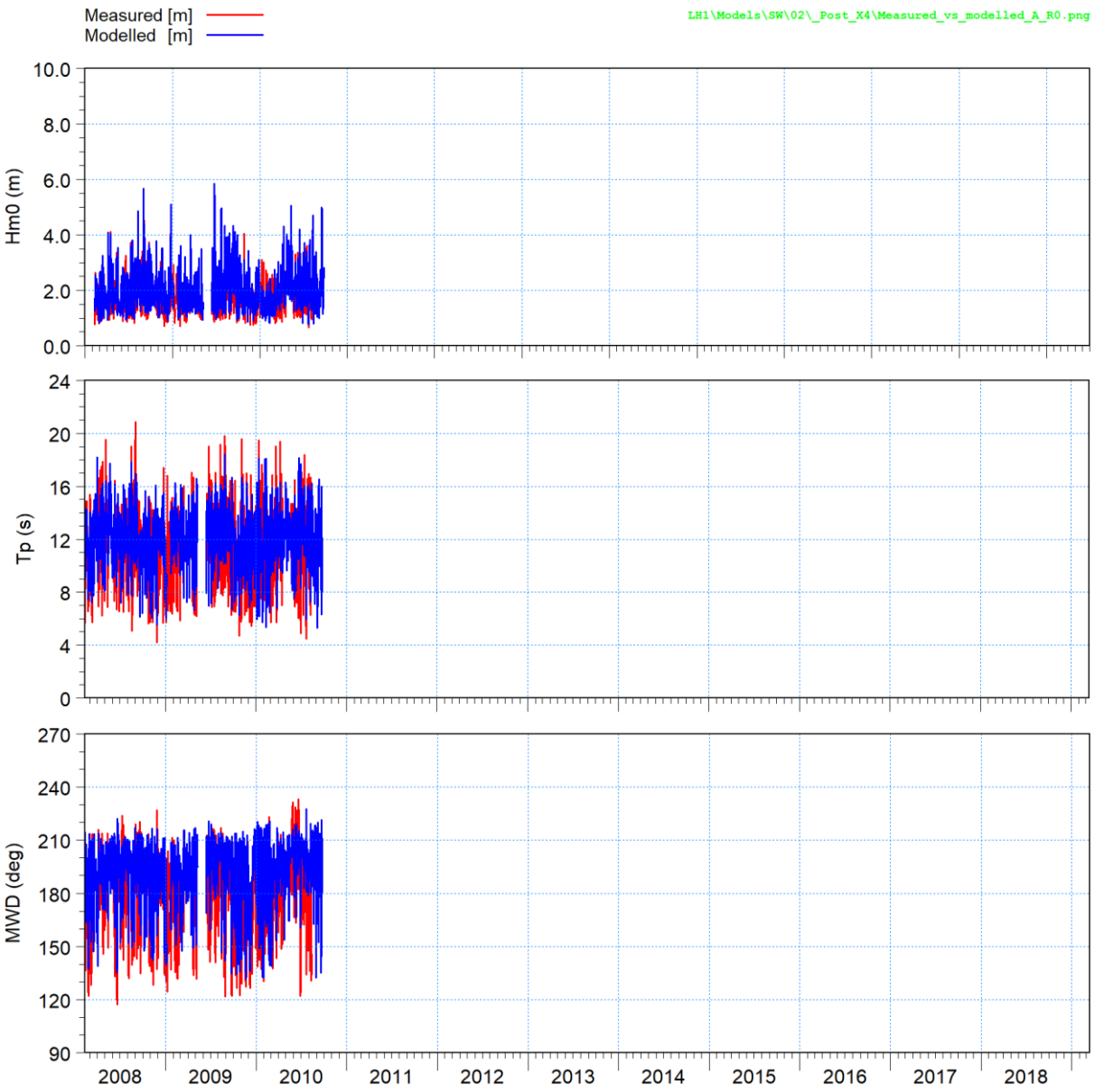


Figure 5.9.A-15: Time-Series Comparison of Modelled and Measured Spectral Wave Parameters at Site A.

CONTROLLED DISCLOSURE

When downloaded from the EDS database, this document is uncontrolled and the responsibility rests with the user to ensure it is in line with the authorised version on the database.

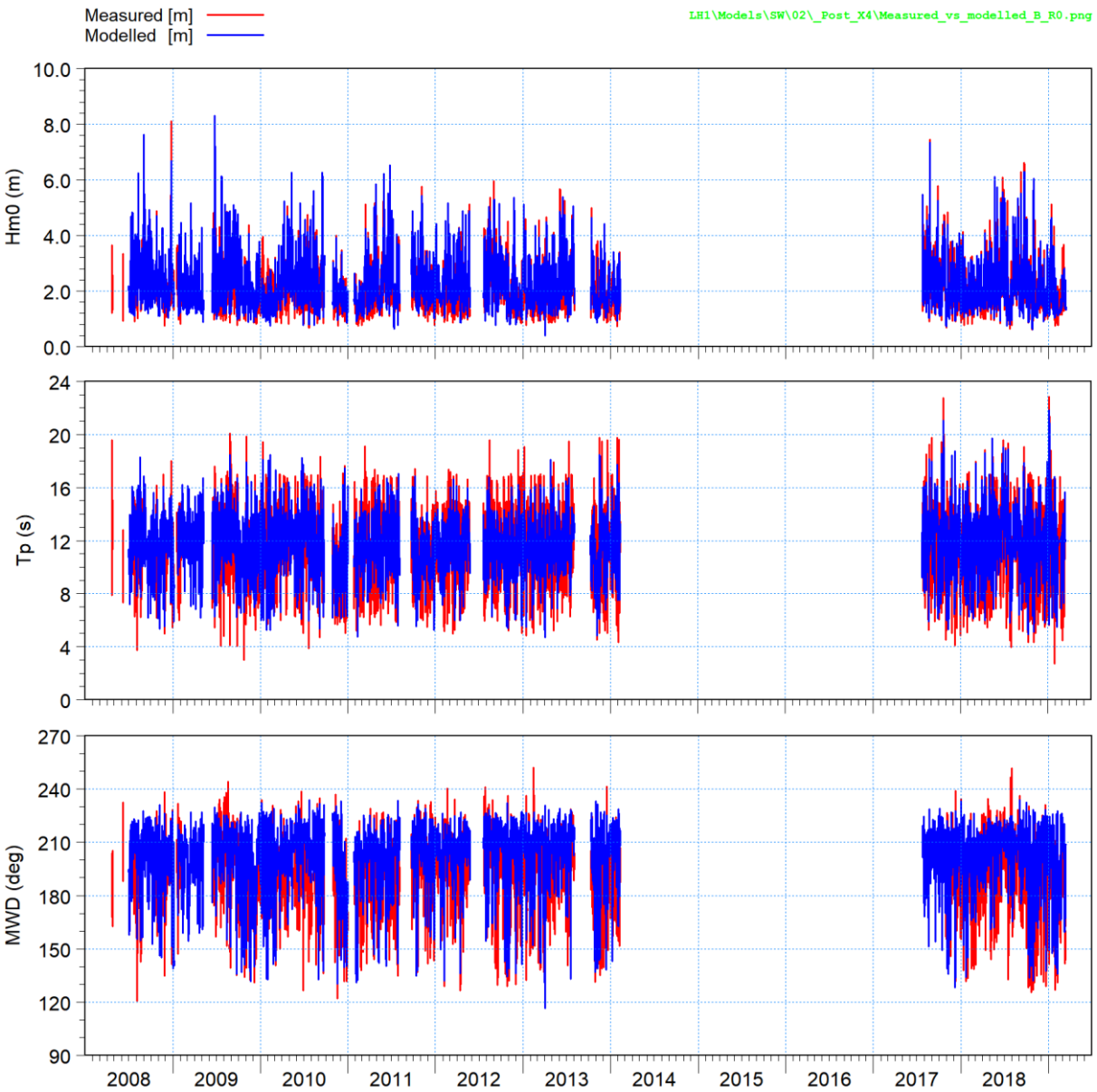


Figure 5.9.A-16: Time-Series Comparison of Modelled and Measured Spectral Wave Parameters at Site B.

CONTROLLED DISCLOSURE

When downloaded from the EDS database, this document is uncontrolled and the responsibility rests with the user to ensure it is in line with the authorised version on the database.

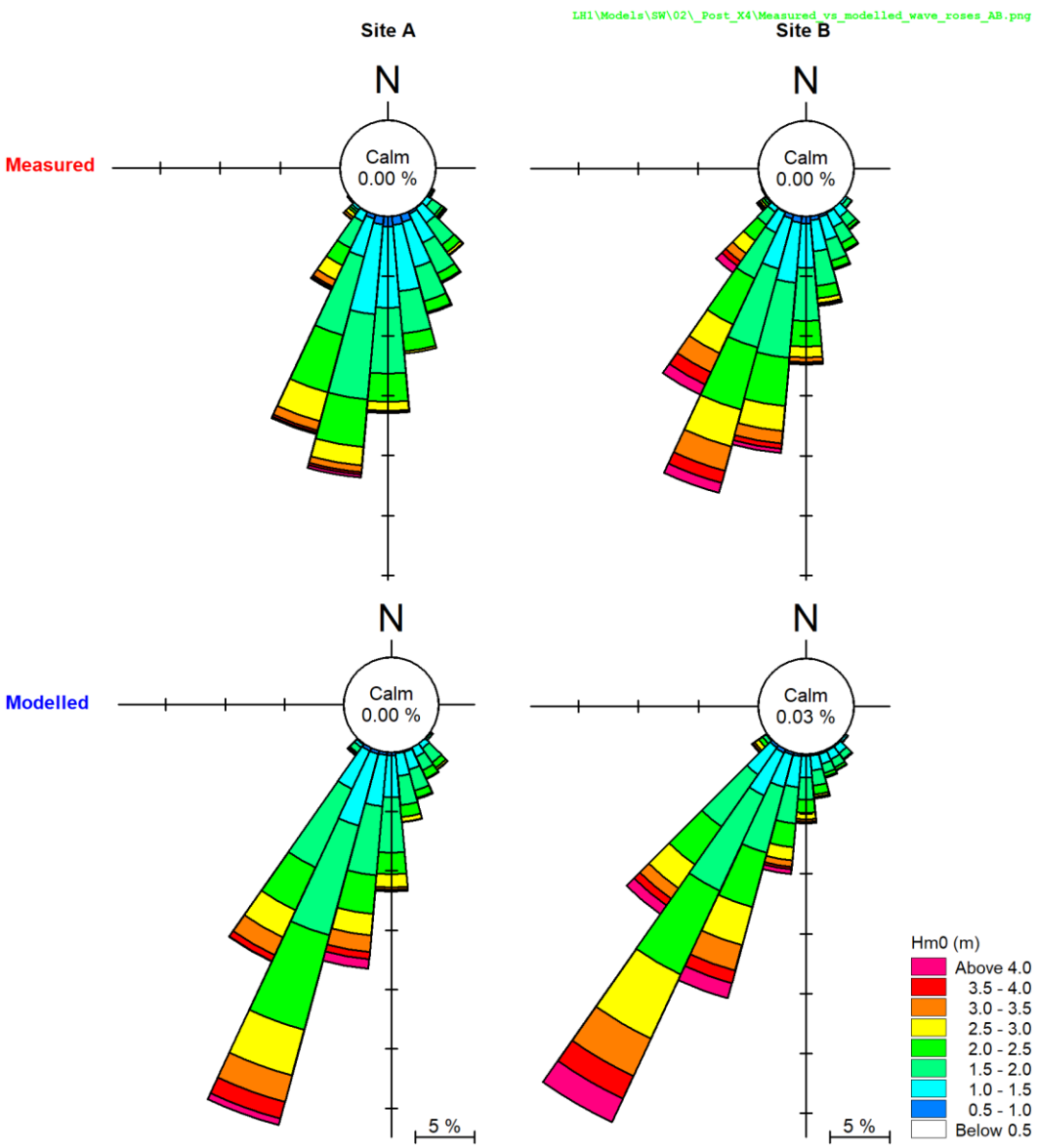


Figure 5.9.A-17: Wave Rose Comparison of Modelled and Measured Waves at Site A (11 February 2008 to 12 August 2010) and Site B (21 April 2008 to 14 March 2019).

CONTROLLED DISCLOSURE

When downloaded from the EDS database, this document is uncontrolled and the responsibility rests with the user to ensure it is in line with the authorised version on the database.

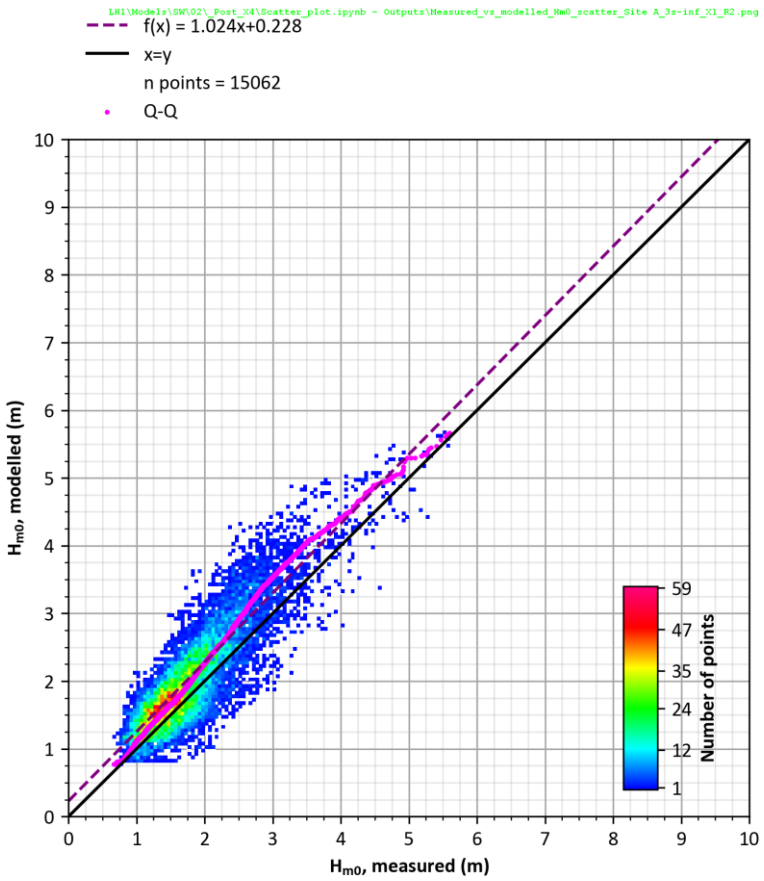


Figure 5.9.A-18: Scatterplot Comparison of Measured and Modelled Wave Height at Site A for 1.8 Years of Valid Data Overlap (11 February 2008 to 12 August 2010).

CONTROLLED DISCLOSURE

When downloaded from the EDS database, this document is uncontrolled and the responsibility rests with the user to ensure it is in line with the authorised version on the database.

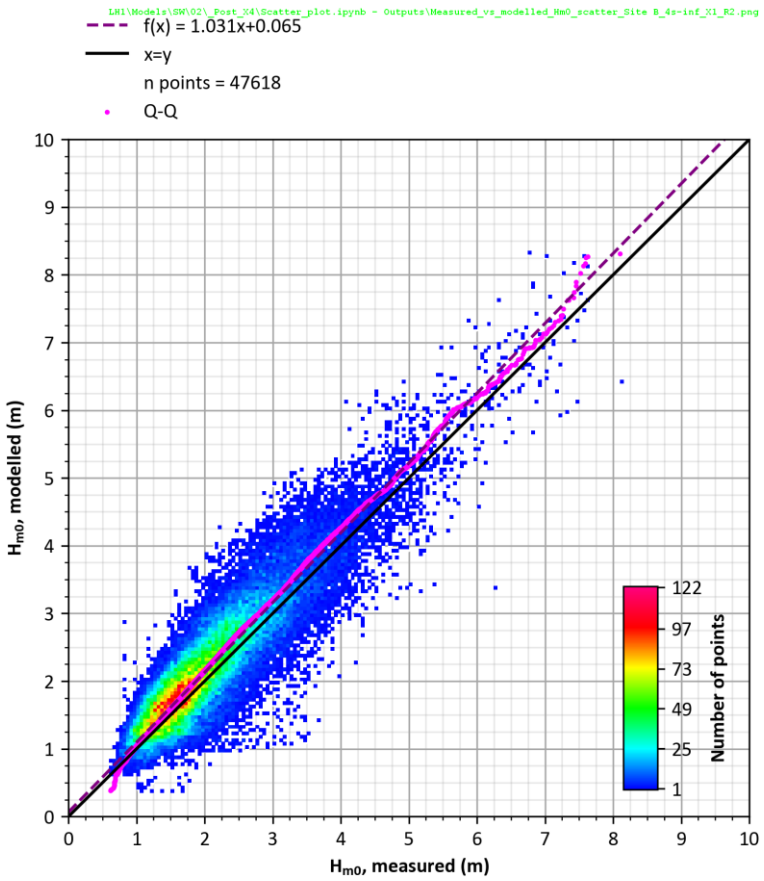


Figure 5.9.A-19: Scatterplot Comparison of Measured and Modelled Wave Height at Site B for 5.5 Years of Valid Data Overlap (21 April 2008 to 14 March 2019).

The results above show that the wave model accurately reproduces the spectral wave parameters at both sites with a small bias of overprediction of the nearshore wave heights. The comparison shows that the wave model is sufficiently calibrated for determining nearshore wave conditions at the Thyspunt site. The good calibration of wave heights at both locations confirms the suitability of the applied bottom friction and breaker parameter, which strongly affect wave energy dissipation over the reef at Site A but not Site B. The comparison also confirms the use of the CFS hindcast wind as wind forcing on the spectral wave model.

5.9.A.2.7 Cases Modelled

Ten years of hourly operational waves were required as input to the 2D sediment transport modelling described in ***Subsection 5.9.A.3***. The most recent ten years of the NCEP Reanalysis dataset (2000-2009) were modelled. Two additional 10-year sets were modelled for the 2134 and 2134 High SLR scenarios at the end of the decommissioning period of the new NIs. To account for the effect of climate change the model boundary

CONTROLLED DISCLOSURE

When downloaded from the EDS database, this document is uncontrolled and the responsibility rests with the user to ensure it is in line with the authorised version on the database.

conditions were adjusted to include the rotation of wave direction by rotating the offshore wave spectra, and the increase in water elevation due to SLR as per ***Table 5.9-8***. The wave height and period were not adjusted for climate change as per ***Table 5.9-8***.

For the evaluation of the extreme wave climate, modelling the full 45.5 y of available data was not necessary. Rather, a series of storms with large wave heights were selected from a time-series of hindcast wave data at the offshore node closest to the project site. The storm peaks were identified using the ‘peaks over threshold’ or ‘partial duration series’ method, with the threshold defined as the value that was exceeded five times per year on average, resulting in a total selection of 228 storm events. Each of the 228 storm events were then modelled for a duration of 24 hours before and 24 hours after the offshore storm peak.

CONTROLLED DISCLOSURE

When downloaded from the EDS database, this document is uncontrolled and the responsibility rests with the user to ensure it is in line with the authorised version on the database.

5.9.A.3 2D Sediment Transport Modelling

5.9.A.3.1 Introduction

2D sediment transport modelling was conducted to simulate the nearshore sediment transport regime in the vicinity of Thysbaai. The results were used to determine the present-day sediment budget (***Subsection 5.9.11.2***), quantify coastline changes due to wave climate change (***Subsection 5.9.11.4***), assess the erosion and sedimentation due to storms (***Subsection 5.9.11.5***), and to investigate potential erosion and sedimentation due to inclusion of the cooling water outfall channel and associated discharge (***Subsection 5.9.11.6***).

5.9.A.3.2 Model Description

The MIKE 21 Sand Transport model was used for the sediment transport modelling. The details of the physical processes and numerical implementation are provided in the model documentation (see ***Table 5.9-7***), while details of the sensitivity testing and V&V are provided in the V&V Report (PRDW, 2022a).

The Sand Transport model calculates the transport of non-cohesive sediment (grain size > 0.063 mm) based on the combination of flow conditions from the hydrodynamic module (***Appendix 5.9.A.7***) and wave conditions from the spectral wave module (***Appendix 5.9.A.2***). For the case of combined waves and currents, sediment transport rates are derived by linear interpolation in a sediment transport lookup table. The values in the table are calculated by the quasi three-dimensional sediment transport model (STPQ3D). The STPQ3D model calculates the instantaneous and time-averaged hydrodynamics and sediment transport in two horizontal directions. As the model calculates the bed load and the suspended load separately, the values in the sediment transport table are the total load.

The temporal and vertical variations of shear stress, turbulence, flow velocity and sediment concentrations are resolved in the model. The time evolution of the boundary layer due to combined wave/current motion is solved by means of an integrated momentum approach. The force balance includes contributions from the near bed wave orbital motion, forces associated with wave breaking (gradients of radiation stresses) and the water level gradient.

The morphological development can be included by updating the bathymetry for every time step with the net sedimentation in each cell, which is based on the divergence of the sediment transport field and the porosity of the seabed. In order to reduce computer time, the morphological development can be sped up by multiplying the bed level change by a speed-up factor. A varying sand layer thickness can be specified as the start

CONTROLLED DISCLOSURE

When downloaded from the EDS database, this document is uncontrolled and the responsibility rests with the user to ensure it is in line with the authorised version on the database.

condition for the simulation. This option is used when simulating sand transport in areas with rock bed present (i.e. cases with non-erodible bed and limited sand supply). It is possible to include the effect of slope failure on the morphological update of the bathymetry. The slope failure mechanism will come into effect if the local bed slope becomes steeper than a specified angle of repose.

5.9.A.3.3 Model Setup

5.9.A.3.3.1 Bathymetry and Mesh

Figure 5.9.A-20 and ***Figure 5.9.A-21*** show the bathymetry and computational mesh of the model used for the 2D sediment transport modelling.

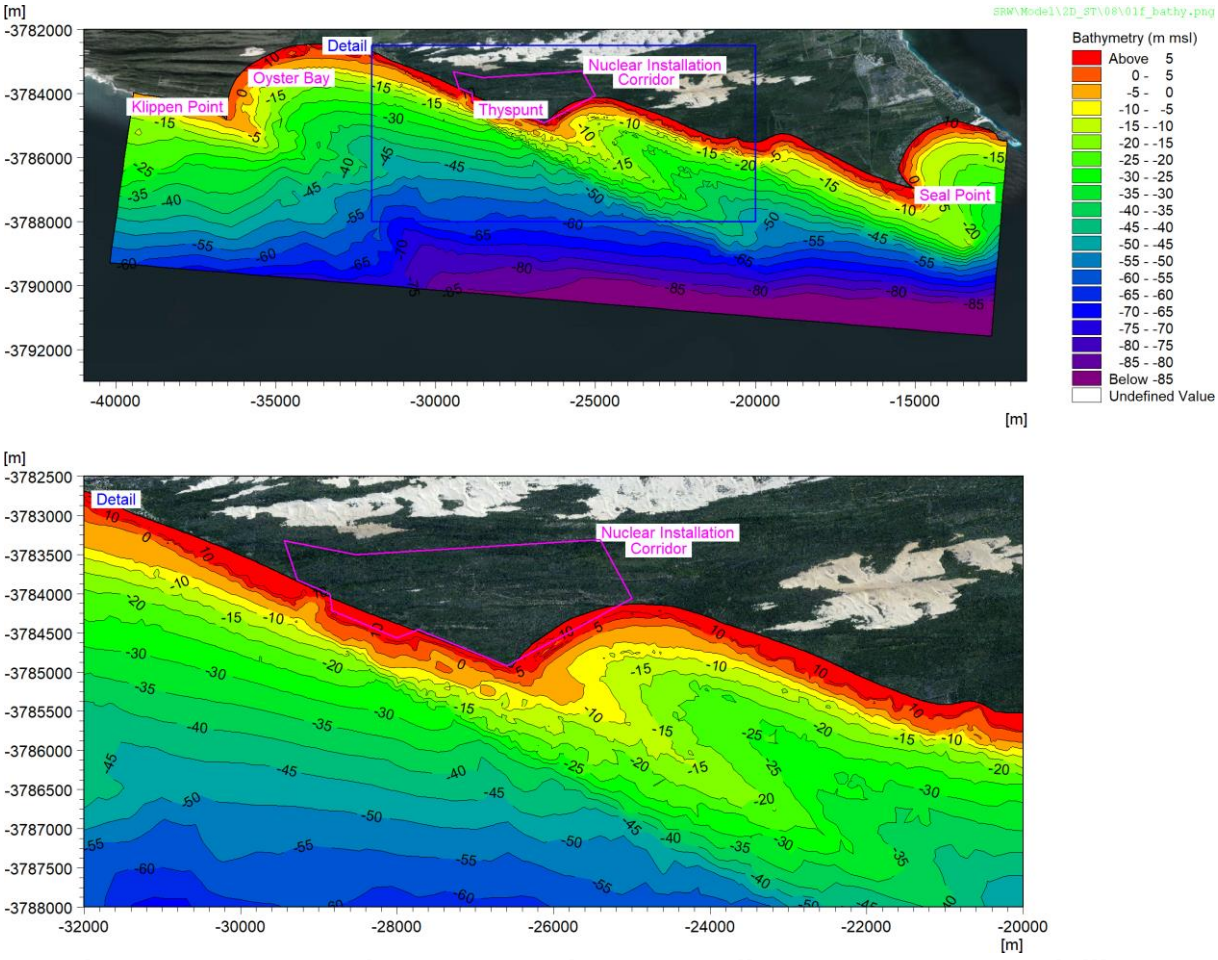


Figure 5.9.A-20: Bathymetry Used for 2D Sediment Transport Modelling.

CONTROLLED DISCLOSURE

When downloaded from the EDS database, this document is uncontrolled and the responsibility rests with the user to ensure it is in line with the authorised version on the database.

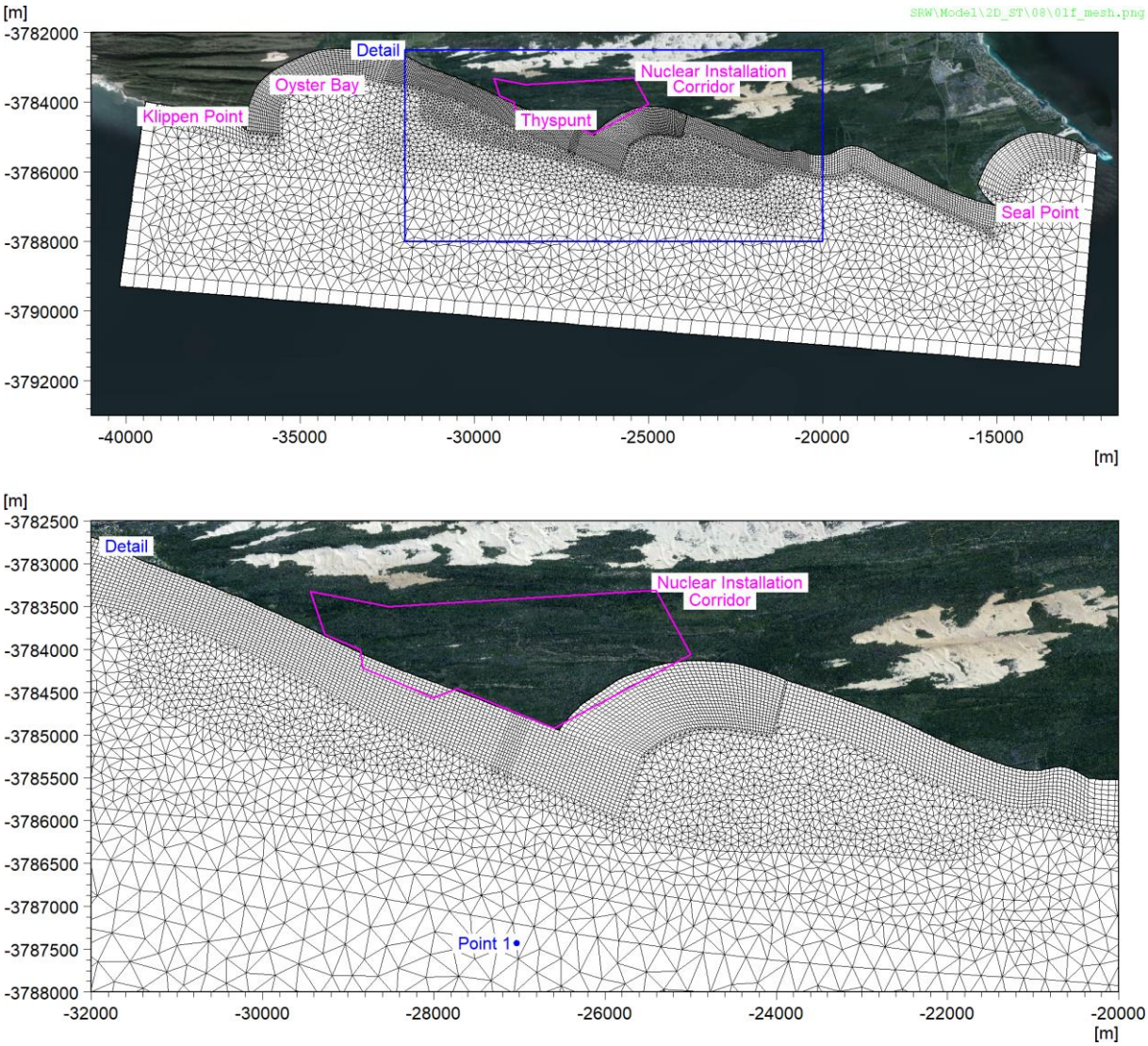


Figure 5.9.A-21: Mesh Used for 2D Sediment Transport Modelling.

The eastern and western boundaries of the mesh extend approximately 5.5 km offshore of the coast to depths ranging between -70 m msl and -90 m msl. The computational mesh comprised of triangles and quadrangles with resolutions varying between 400 m offshore to 45 m in areas of interest.

The model bathymetry is derived from the generic dataset described in ***Subsection 5.9.8***. For the simulation of extreme storm events, the model bathymetry was truncated to a depth of -55 m msl in alignment with the depth of the characterised nearshore extreme wave conditions at Point 1 (***Figure 5.9-35***).

The future cases included the bathymetry adjustments due to the Bruun Rule (see ***Subsection 5.9.11.3***) but not including any storm erosion.

CONTROLLED DISCLOSURE

When downloaded from the EDS database, this document is uncontrolled and the responsibility rests with the user to ensure it is in line with the authorised version on the database.

5.9.A.3.3.2 Boundary Conditions and Model Settings

The spectral wave model was run in the quasi-stationary, parametric formulation with no additional wind generation applied. The wave boundary conditions were applied as follows:

- For the operational cases, space-varying wave parameters were extracted from the spectral wave model (described in ***Appendix 5.9.A.2***) and applied along all model boundaries.
- For the extreme storm cases, wave parameters were applied along the offshore model boundary, with lateral boundaries along the east and west boundaries.

Bottom friction was modelled using a Nikuradse roughness of 0.02 m in sandy areas and 0.6 m in rocky areas, in alignment with the calibrated nested wave model described in ***Appendix 5.9.A.2.6***. Water levels were obtained through a direct coupling with the hydrodynamic model.

Time-varying water levels were applied along all three boundaries of the 2D hydrodynamic model using the predicted tide at Thyspunt (see ***Subsection 5.9.9.1***). Wave-driven currents and water levels were modelled using wave radiation stresses obtained through a direct coupling with the wave model. Bed resistance was modelled using a Chezy number of 50 $m^{1/2}/s$ for sandy areas and 20 $m^{1/2}/s$ on the rocky areas. Wind-driven currents were included in the operational model using the CFS hindcast wind data (described in ***Appendix 5.9.A.2.3***) and a wind friction coefficient C_d of 0.002425, but not for the extreme storms as these are wave-dominated and the associated wind is not known. Horizontal eddy viscosity was modelled using the Smagorinsky formulation. For the cases where the outfall structure was modelled, the outflow from the outfall was included to account for its effect on the hydrodynamics.

A median sediment grain diameter of D_{50} = 0.29 mm and a grading coefficient of $(D_{84}/D_{16})^{1/2}$ = 1.3 were used based on the available sediment data described in ***Subsection 5.9.8***. A space-varying initial bed thickness was used to specify a non-erodible bed on the offshore rocky reefs and rocky shorelines. ***Figure 5.9.A-22*** presents the areas with a non-erodible bed. Slope failure was included in the sandy areas of the model by specifying an angle of repose of 5.7 degrees, corresponding to a 1:10 slope on the upper beaches, with an angle of repose of 1.9 degrees, corresponding to 1:30 slope on the lower sections of the beaches down to the depth of closure.

CONTROLLED DISCLOSURE

When downloaded from the EDS database, this document is uncontrolled and the responsibility rests with the user to ensure it is in line with the authorised version on the database.

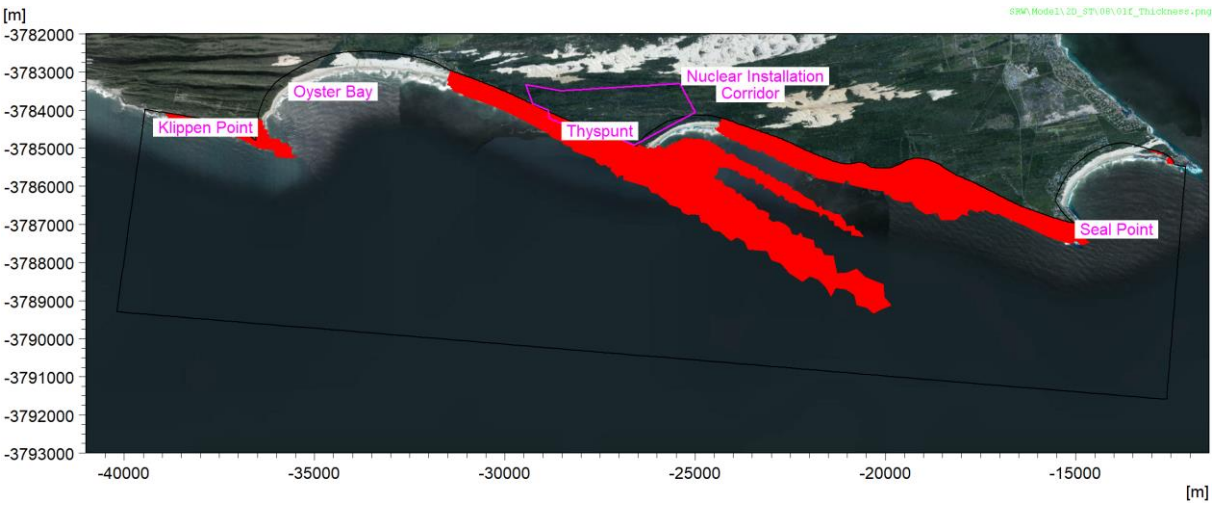


Figure 5.9.A-22:Non-Erodible Bed for the 2D ST Model Shown in Red.

Morphological updating of the bed was included to account for the effects of changes in the bed level on the hydrodynamics and waves. To enable the simulation of 2D morphology over a full year, a morphological speed-up factor of three was used, allowing a full year of morphology to be simulated over approximately four months of hydrodynamics. This required the year of hourly wave conditions to be compressed into 20-minute time steps and the spectral wave model was run at the same interval. The hourly wind forcing applied on the hydrodynamic model was compressed in the same way. The tidal water level boundary condition was not compressed, as the four-month period provided sufficient sampling of the spring-neap cycles and acceleration of the tide may generate unnatural tidal currents. No speed-up factor was used for the extreme storm events.

The STPQ3D model (described in ***Appendix 5.9.A.5***) was used to generate the transport tables used in the sand transport model using the following input parameters:

- Critical Shields' parameter = 0.05;
- Bed ripples were excluded;
- Streaming was excluded;
- Bed slope effects were excluded;
- Cross-shore processes were excluded;
- Stokes' 1st order wave theory was used;
- Deterministic bed concentration formulation was used; and
- Wave breaker index = 0.8.

CONTROLLED DISCLOSURE

When downloaded from the EDS database, this document is uncontrolled and the responsibility rests with the user to ensure it is in line with the authorised version on the database.

5.9.A.3.4 Model Calibration

While there was no site-specific calibration data available, the present-day sediment budget is sensible and consistent with literature and the analysis of long-term coastline trends presented in ***Subsection 5.9.11.1***. This, combined with the model calibration at Port Elizabeth (approximately 90 km east of the Thyspunt site) and at Duynefontyn presented in V&V Report (PRDW, 2022a), provides confidence that the model is sufficiently calibrated for the purposes of this study.

5.9.A.3.5 Cases Modelled

Operational and extreme cases were modelled in the 2D sediment model.

The operational cases were modelled for a representative year which was repeated until a stable model was reached. The representative year of 2009 was selected by comparing the exceedances of the H_{m0} and the wave roses at Point 1 (-55 m msl, see ***Figure 5.9-35***). A similar assessment was done on the wind to ensure both primary forcings were representative. ***Figure 5.9.A-23*** and ***Figure 5.9.A-24*** present the wave exceedance curves and roses while ***Figure 5.9.A-25*** and ***Figure 5.9.A-26*** present the wind exceedance curves and roses.

CONTROLLED DISCLOSURE

When downloaded from the EDS database, this document is uncontrolled and the responsibility rests with the user to ensure it is in line with the authorised version on the database.

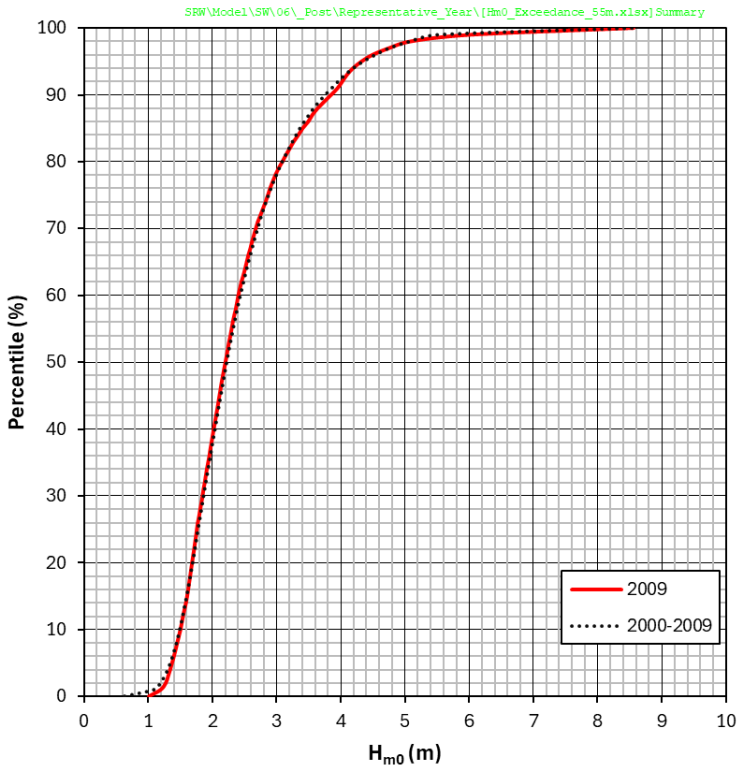


Figure 5.9.A-23: Exceedance Curve of H_{m0} at Point 1 for 2009 Compared to All Data from 2000 to 2009.

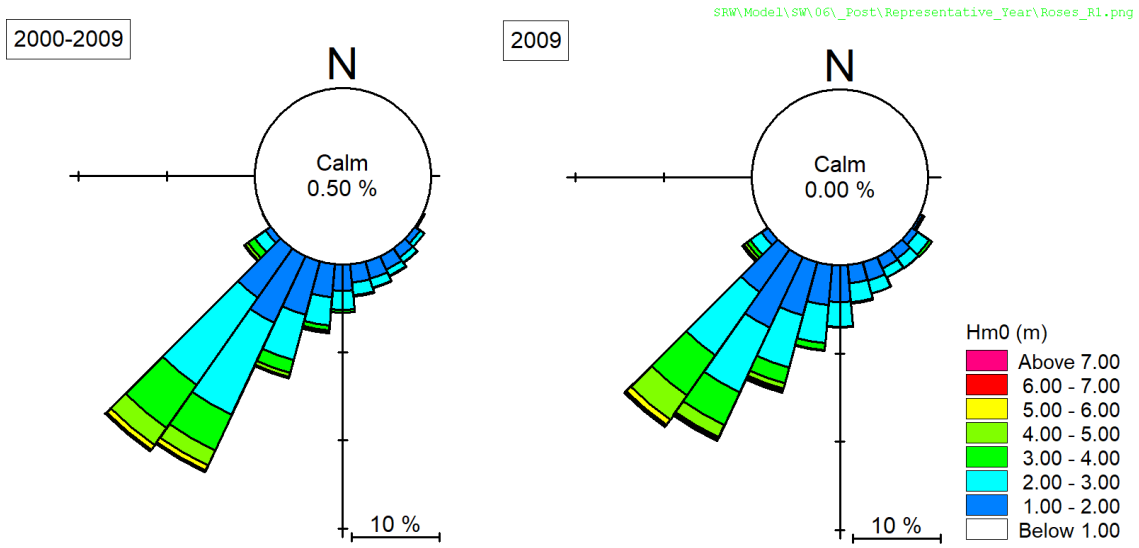


Figure 5.9.A-24: Wave Rose of H_{m0} at Point 1 and MWD for 2009 Compared to All Data from 2000 to 2009.

CONTROLLED DISCLOSURE

When downloaded from the EDS database, this document is uncontrolled and the responsibility rests with the user to ensure it is in line with the authorised version on the database.

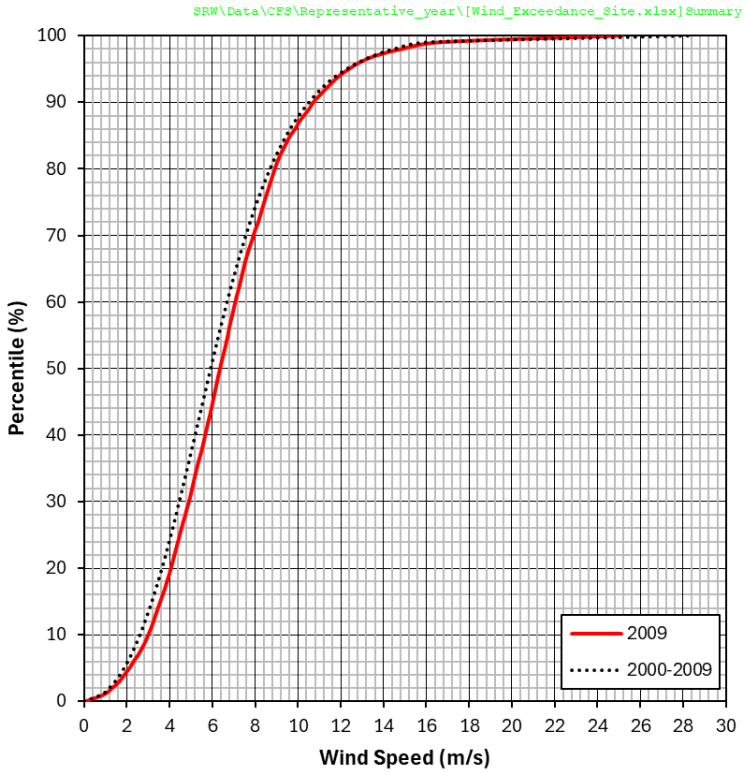


Figure 5.9.A-25: Exceedance Curve of Wind Speed at the Site for 2009 Compared to All Data from 2000 to 2009.

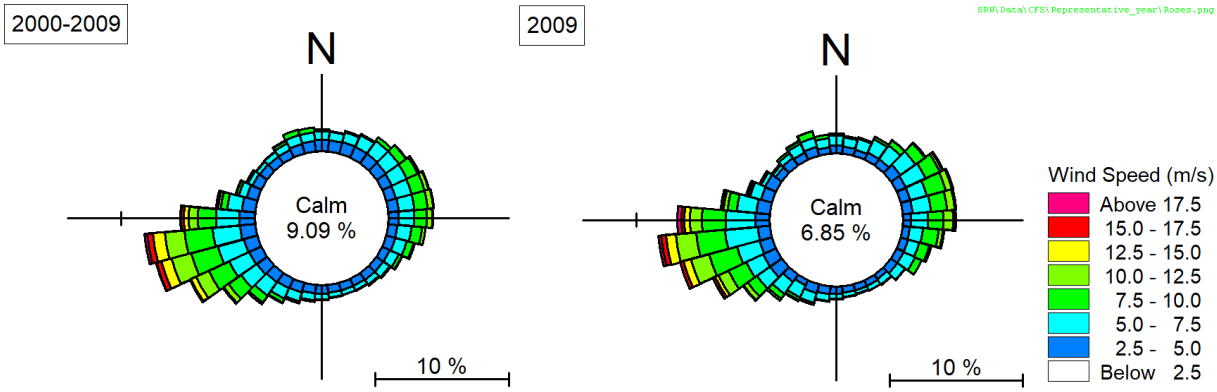


Figure 5.9.A-26: Wind Rose at the Site for 2009 Compared to All Data from 2000 to 2009.

The present-day sediment budget was modelled for four repeat years to initialise the model. The stable model was then used to assess the stability of the coastline under the future water levels and nearshore wave climate obtained from the spectral wave model (***Appendix 5.9.A.1***). Ten repeat years were simulated to allow sufficient time for the sediment transport regime to reach a new equilibrium, which in reality would occur over a

CONTROLLED DISCLOSURE

When downloaded from the EDS database, this document is uncontrolled and the responsibility rests with the user to ensure it is in line with the authorised version on the database.

timescale of a century. Two future scenarios were assessed: 2134 and 2134 High SLR.

The extreme storms were initialised with the bed levels and thicknesses at the end of the respective present-day and future operational simulations. The extreme storm cases modelled were the 1E-8 y^{-1} storm for the present day, and the 2134 and 2134 High SLR cases. As the 1E-8 y^{-1} storms showed little impact on the stable coastline for all cases, the smaller storms were not modelled. The joint probability between the waves and storm surge was accounted for as described in ***Subsection 5.9.10***. The waves were combined with the positive storm surge as shown in ***Table 5.9.A-6*** and ***Table 5.9.A-7*** where for example the 1E-8 y^{-1} wave is combined with the 8.45E-8 y^{-1} storm surge and vice versa.

Finally, the following simulations were run to investigate potential erosion and sedimentation due to inclusion of the cooling water outfall channel and associated discharge (the layout and discharge are described in ***Subsection 5.9.16***):

- One year of present-day operational conditions for comparison with the present-day sediment transport regime;
- Present day extreme 1E-8 y^{-1} storm; and
- Future 2134 High SLR extreme 1E-8 y^{-1} storm.

CONTROLLED DISCLOSURE

When downloaded from the EDS database, this document is uncontrolled and the responsibility rests with the user to ensure it is in line with the authorised version on the database.

5.9.A.4 Cross-shore Erosion Modelling

5.9.A.4.1 Introduction

This section describes the cross-shore erosion modelling conducted to determine erosion of the beach and dunes at the site during extreme storm events (***Subsection 5.9.11.5***).

5.9.A.4.2 Model Description

The SBEACH (Storm-induced BEAch CHange) storm erosion model was used to simulate the erosion of the coastline in front of the site during storm events.

The details of the physical processes and numerical implementation are provided in the model documentation (see ***Table 5.9-7***), while details of the model setup, sensitivity testing, and V&V are provided in the V&V Report (PRDW, 2022a).

The model consists of a wave model and a beach response model. The wave model calculates the transformation of wave height and direction at user specified grid points along the beach profile, taking into account the effects of wave refraction, shoaling and dissipation due to depth-induced breaking. Water level variations due to wave- and wind-induced setup are also included in the wave model. The formulation of the wave model is based on the solution of best practice deterministic equations.

The beach response model is empirically based, with the underlying assumptions and relationships derived from observations made from prototype-scale laboratory experiments. The model assumes the conservation of sediment across the profile (longshore processes are considered to be uniform and neglected in calculating profile change). The direction and rate of cross-shore transport is determined from the local wave, water level, beach profile and sediment properties, and the equation describing the conservation of beach material is solved to compute profile change as a function of time.

The model was validated against four physical model tests, two cases selected from the SUPERTANK experiments (USACE, 1996b) and two cases from the Delta Flume tests (Van Gent, et al., 2008). The model generally showed a good agreement to the measured profiles above the still water level (SWL) which is important in the context of flooding and erosion. Further details of the model V&V are provided in the V&V Report (PRDW, 2022a).

CONTROLLED DISCLOSURE

When downloaded from the EDS database, this document is uncontrolled and the responsibility rests with the user to ensure it is in line with the authorised version on the database.

5.9.A.4.3 Cases Modelled

The model was run for extreme storms with exceedance frequencies of 1E-2, 1E-4, 1E-6 and 1E-8 y^{-1}. The model was run for the 2034, 2134, and 2134 High SLR climate change scenarios to include the effect of climate change on waves, water levels and coastline stability.

The model boundary conditions were obtained from a coupled spectral wave and 2D hydrodynamic model (refer to ***Subsection 5.9.A.2***) forced with the extreme wave parameters (H_{m0}, T_p, MWD_p and DSD_p), combined with the extreme maximum still water levels (comprising a synthetic tide, sea level rise and storm surge). The synthetic tide was generated using a semi-diurnal signal with a fixed tidal range of 1.73 m (10th percentile low tide to 90th percentile high tide) and a maximum elevation equal to the extreme maximum still water level. The peak of the synthetic tide time-series was aligned with the peak of the wave height.

The storm duration was predicted by fitting a two-part Gaussian storm time-series to 182 hindcast storms at Point 1, used to derive the nearshore extreme wave climate (refer to ***Subsection 5.9.9.8***). Since no correlation was observed between the wave height peak and duration of the storm a constant duration was used for all storms. The storm duration was based on the 95th percentile time required for the wave height to increase from the average wave height to the storm peak and then to reduce back to the average height. The resulting storm has a duration of 130 hours (5.4 days). ***Figure 5.9.A-27*** compares the schematized wave height time-series of 4 example storms to the 182 storms. Also shown is an example synthetic tide signal. The corresponding time-series of peak wave period was calculated using the H_{m0}-T_p relationship at the site (***Figure 5.9-39***), with a minimum peak wave period of 10 s, which is the typical T_p corresponding to an average H_{m0} of 2.5 m.

CONTROLLED DISCLOSURE

When downloaded from the EDS database, this document is uncontrolled and the responsibility rests with the user to ensure it is in line with the authorised version on the database.

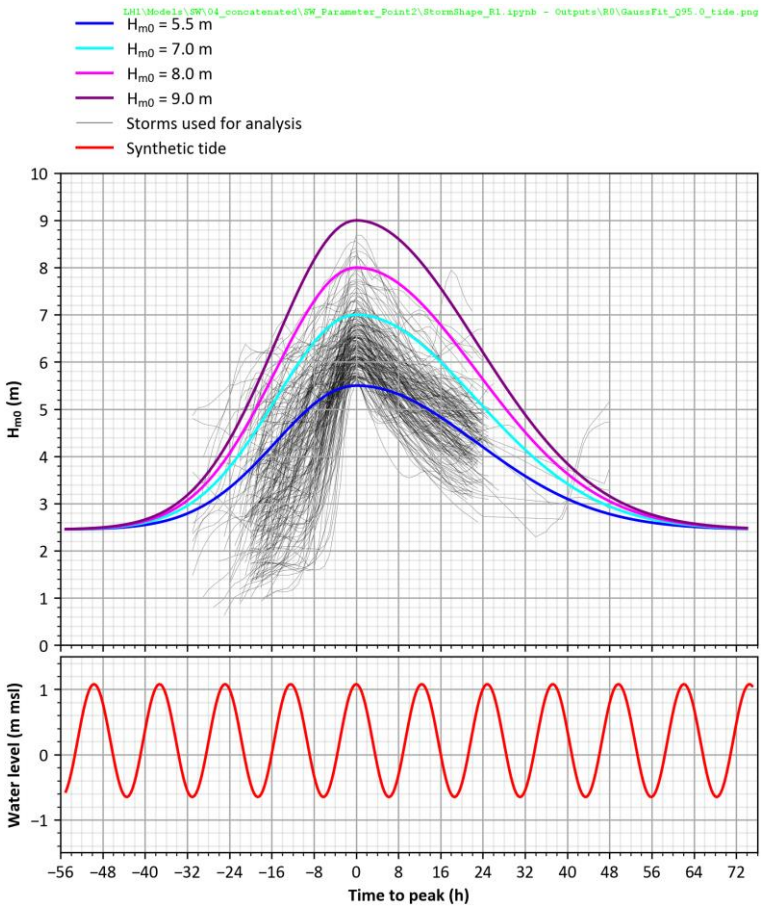


Figure 5.9.A-27: Storm Duration Analysis Based on 182 Nearshore Storms. The Synthetic Tide For 2013.5 (Excluding Storm Surge and Sea Level Rise) is Shown for Reference.

The joint probability between the waves and storm surge was accounted for as described in ***Subsection 5.9.10***. The waves were combined with the positive storm surge as shown in ***Table 5.9.A-6*** and ***Table 5.9.A-7*** where for example the 1E-4 y^{-1} wave is combined with the 8.45E-4 y^{-1} storm surge and vice versa. For each joint probability both combinations of storm surge and wave height were modelled. The total number of cases modelled was thus 3 climate change scenarios × 4 exceedance frequencies × 2 joint probability combinations = 24 cases per profile.

CONTROLLED DISCLOSURE

When downloaded from the EDS database, this document is uncontrolled and the responsibility rests with the user to ensure it is in line with the authorised version on the database.

Table 5.9.A-6: Summarised Boundary Conditions at -55 m msl for Modelled Wave Dominated Storm Scenarios.

Exceedance Frequency	Maximum Still Water Level			H_{m0}			T_p			MWD_p	DSD_p
(y^{-1})	(m msl)			(m)			(s)			(°)	(°)
	2034	2134	2134 High SLR	2034	2134	2134 High SLR	2034	2134	2134 High SLR	All	All
1E-2	2.01	3.66	5.18	9.3	9.9	9.9	15.9	16.3	16.3	211	17.4
1E-4	2.33	3.98	5.50	11.1	11.7	11.7	17.3	17.8	17.8	211	17.4
1E-6	2.60	4.27	5.78	12.5	13.3	13.3	18.4	18.9	18.9	211	17.4
1E-8	2.85	4.52	6.04	13.9	14.7	14.7	19.4	19.9	19.9	211	17.4

Table 5.9.A-7: Summarised Boundary Conditions at -55 m msl for Modelled Storm Surge Dominated Storm Scenarios.

Exceedance Frequency	Maximum Still Water Level			H_{m0}			T_p			MWD_p	DSD_p
(y^{-1})	(m msl)			(m)			(s)			(°)	(°)
	2034	2134	2134 High SLR	2034	2134	2134 High SLR	2034	2134	2134 High SLR	All	All
1E-2	2.17	3.82	5.34	8.4	8.9	8.9	15.0	15.5	15.5	211	17.4
1E-4	2.46	4.12	5.64	10.3	10.9	10.9	16.7	17.2	17.2	211	17.4
1E-6	2.72	4.39	5.91	11.9	12.6	12.6	17.9	18.4	18.4	211	17.4
1E-8	2.96	4.64	6.16	13.3	14.0	14.0	19.0	19.5	19.5	211	17.4

Fifteen cross-shore profiles at 180 m increments along Thysbaai and 21 profiles at 180 m to 350 m increments along the rocky coastline west of Thyspunt were modelled, which are shown in ***Figure 5.9.A-28***. The rocky profiles are labelled R1 to R21 and the seaward ends of the profiles are indicated. Along Thysbaai, the seaward ends of the profiles vary between the -18 m msl depth contour at the more exposed profiles in the east to the -4.2 m msl contour in the west, which was chosen such that the complex refraction, shoaling and breaking of waves on the reef would be modelled mainly in the 2D spectral waves model. On the rocky coastline the profiles extend to the -20 m msl contour. A constant grid size of 2 m was used for each profile.

CONTROLLED DISCLOSURE

When downloaded from the EDS database, this document is uncontrolled and the responsibility rests with the user to ensure it is in line with the authorised version on the database.

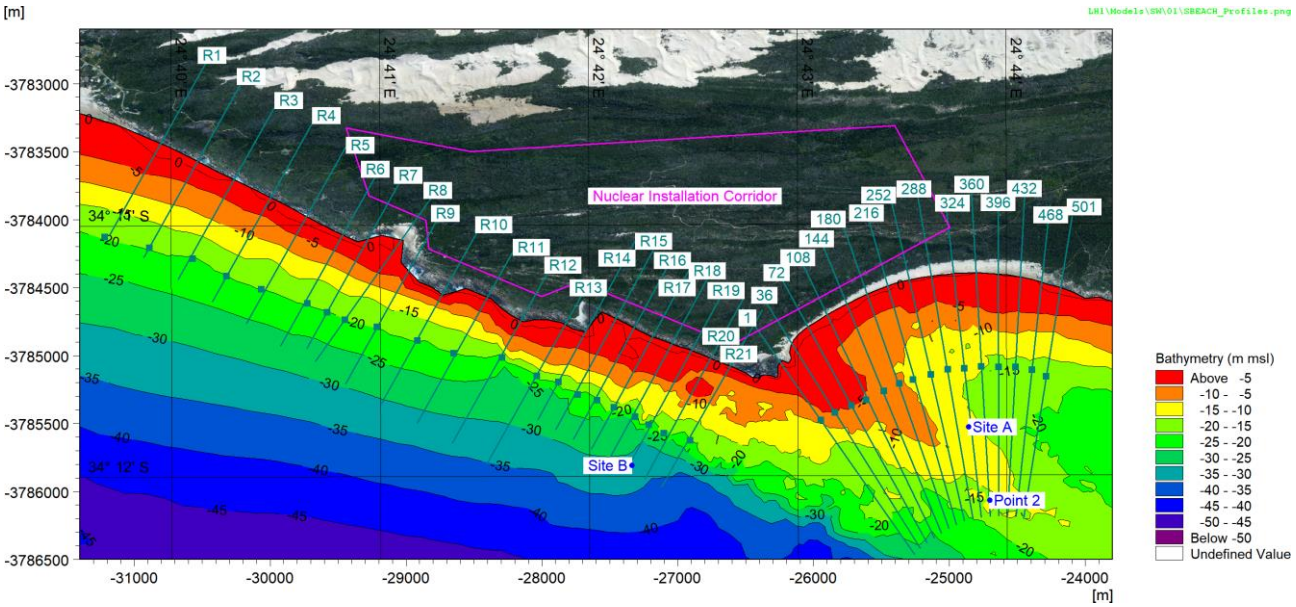


Figure 5.9.A-28: Plan View of Cross-Shore Profiles Used for Cross-Shore Erosion Modelling. Also Shown are the Offshore End of Each Profile (Squares).

The H_{m0}, T_p and water level used to force the cross-shore erosion model were extracted from the coupled wave and 2D hydrodynamic model at the offshore end of the cross-shore profiles, and the wave direction, prescribed as the angle of wave attack, was calculated as the angle between the MWD and the shore-normal for each profile. The model setup parameters were based on calibrated parameters from the V&V and site-specific data (median grain size, avalanching slope, seawater temperature) and are summarised in ***Table 5.9.A-8***. Details of the model calibration parameters are provided in the V&V Report (PRDW, 2022a).

Table 5.9.A-8: SBEACH Model Setup Parameters.

Setup Parameter	Input
Land surf zone depth	0.1 m
Median grain size (representative of upper beach and dune)	0.2 mm
Maximum slope prior to avalanching	30°
Transport rate coefficient	2E-6 m^4/N
Overwash transport parameter	0.005
Coefficient for slope-dependent term	0.003 m^2/s
Transport rate decay coefficient	0.5
Seawater temperature	17°C

CONTROLLED DISCLOSURE

When downloaded from the EDS database, this document is uncontrolled and the responsibility rests with the user to ensure it is in line with the authorised version on the database.

5.9.A.5 Littoral Processes Modelling

5.9.A.5.1 Introduction

Littoral processes modelling was conducted to model the suspended sand concentrations at the cooling water intakes (***Subsection 5.9.11.8***) and to generate the sediment transport tables used in the 2D sediment transport modelling (***Appendix 5.9.A.3***).

5.9.A.5.2 Model Description

The MIKE Littoral Processes model was used. The details of the physical processes and numerical implementation are provided in the model documentation (see ***Table 5.9-7***), while details of the sensitivity testing and V&V are provided in the V&V Report (PRDW, 2022a).

The model solves the vertical diffusion equation on an intrawave period grid to provide a detailed description of the suspended sand concentration both vertically and over the wave period.

The temporal and vertical variations of shear stress, turbulence, flow velocity and sediment concentrations are resolved in the model. The time evolution of the boundary layer due to combined wave/current motion is solved by means of an integrated momentum approach. The force balance includes contributions from the near bed wave orbital motion, forces associated with wave breaking (gradients of radiation stresses) and the water level gradient.

The model accounts for graded sediment by dividing the grading curve into a number of size classes, calculating the sediment transport for each class and then averaging to obtain the total transport rate.

The model output is the time-averaged vertical profile of suspended sand concentration. The model only simulates non-cohesive sand with grain sizes greater than 0.063 mm.

5.9.A.5.3 Model Setup

The model was set up to include the effects of waves and currents at arbitrary angles, breaking waves, Stokes 5th order wave theory, ripple-covered bed and graded bed material. The sediment is divided into 30 size fractions based on a log-normal grading curve characterized by the median grain diameter D_{50} and the sediment grading defined by $(D_{84}/D_{16})^{0.5}$.

A sensitivity test was done to determine the appropriate dominant factor for the extreme cases: water level, current, or waves. It was found that the waves were the dominant factor compared to currents and water levels. The

When downloaded from the EDS database, this document is uncontrolled and the responsibility rests with the user to ensure it is in line with the authorised version on the database.

water levels had minimal impact in a 30 m water depth at the intakes and therefore, the water level was fixed to a 90th percentile tidal variation for the extreme storms. As the wave conditions were dominant, the wave dominated joint probability between waves and currents was applied. The joint probability currents applied are presented in ***Table 5.9.A-9***.

5.9.A.5.4 Cases Modelled

The sediment properties were based on the measured seabed samples closest to the proposed intakes, resulting in D_{50} = 0.185 mm and a sediment grading of 1.25 based on the available sediment data near the intakes as described in ***Subsection 5.9.8***.

The proposed seawater intakes were modelled in a -30 m msl water depth, with the 10 000 MWe associated intake flow rates of 445 m^3/s.

The modelled cases included normal operational conditions and for four extreme storm events with exceedance frequencies of 1E-2, 1E-4, 1E-6 and 1E-8 y^{-1}, as described below:

- The operational conditions were based on 5.2 years of depth-averaged currents measured at Site B and the wave parameters measured at the same location. These conditions were applied at the -30 m msl depth.
- The operational model was run for the full 5.2 years of data with a constant water level of ML.
- For the extreme storm events the joint exceedance frequency between waves and currents was accounted for as described in ***Subsection 5.9.10***, where for example the 1E-4 y^{-1} dominant wave is combined with the 3.59E-3 y^{-1} current. The combinations of wave height and current are shown in ***Table 5.9.A-9***.
- The extreme dominant waves applied were extracted from the results of the coupled hydrodynamic and spectral wave model (see ***Appendix 5.9.A.1***). Each storm event has a synthetic shape with a duration of 5.4 days, as described in ***Appendix 5.9.A.4***.
- The extreme currents in -30 m msl were based on an extreme value analysis of the measured currents at Site B and followed the shape of the synthetic wave storm from a minimum of the median current speed up to the corresponding extreme current speed at the peak of the wave height.
- A 90th percentile tidal variation was applied for the duration of the extreme storm runs, with the peak of the high tide aligned with the peak of the storm.

CONTROLLED DISCLOSURE

When downloaded from the EDS database, this document is uncontrolled and the responsibility rests with the user to ensure it is in line with the authorised version on the database.

Table 5.9.A-9: Joint Probability Best Estimate Extreme Currents for 2034.

Joint Exceedance Frequency [y^{-1}]	Wave Exceedance Frequency [y^{-1}]	Current Exceedance Frequency [y^{-1}]	Current speed [m/s]
1E-2	1E-2	3.59E-1	0.89
1E-4	1E-4	3.59E-3	1.22
1E-6	1E-6	3.59E-5	1.59
1E-8	1E-8	3.59E-7	1.97

CONTROLLED DISCLOSURE

When downloaded from the EDS database, this document is uncontrolled and the responsibility rests with the user to ensure it is in line with the authorised version on the database.

5.9.A.6 Wave Run-Up Modelling

5.9.A.6.1 Introduction

This section describes the wave modelling undertaken to estimate the maximum wave run-up and drawdown due to storms at the site (***Subsection 5.9.12***).

5.9.A.6.2 Model Description

The MIKE 3 Wave model was used for the wave run-up and drawdown modelling. The details of the physical processes and numerical implementation are provided in the model documentation (see ***Table 5.9-7***), while details of the model setup, sensitivity testing, and V&V are provided in the V&V Report (PRDW, 2022a).

The MIKE 3 Wave is a phase-resolving wave model based on the 3D Navier-Stokes equations. An unstructured (flexible) mesh is used in the horizontal dimension with sigma layers in the vertical. The model includes the following processes:

- Wave refraction;
- Wave diffraction;
- Bottom friction;
- Non-linear wave transformation;
- Surf and swash zone hydrodynamics;
- Wave breaking and run-up;
- Wave overtopping;
- Coastal flooding;
- Wave transmission (and reflection) through porous structures.

The model is based on the numerical solution of the three-dimensional incompressible Reynolds-averaged Navier-Stokes equations. Thus, the model consists of continuity and momentum equations, and it is closed by a k-ε turbulence closure scheme in the vertical and horizontal. The free surface is accounted for using a sigma coordinate transformation approach. The spatial discretization of the governing equations in conserved form is performed using a cell-centred finite volume method. The time integration is performed using a semi-implicit scheme. The vertical convective and diffusion terms are discretized using an implicit scheme to remove the stability limitations associated with the vertical resolution. The remaining terms are discretised using a second-order explicit Runge-Kutta scheme. The projection method is employed for the non-hydrostatic pressure. The

CONTROLLED DISCLOSURE

When downloaded from the EDS database, this document is uncontrolled and the responsibility rests with the user to ensure it is in line with the authorised version on the database.

interface convective fluxes are calculated using a HLLC approximate Riemann solver. This shock-capturing scheme enables robust and stable simulation of flows involving shocks or discontinuities such as bores and hydraulic jumps. This is essential for modelling of waves in the breaking zone or porous structures. The numerical dissipation accounts for the dissipation in the breaking waves.

5.9.A.6.3 Model Setup

The model domain and bathymetry are shown in ***Figure 5.9.A-29*** and ***Figure 5.9.A-30*** respectively. The wave generation line was placed along the -36 m msl contour, with the offshore boundary extending seaward of this for a minimum of 300 m to accommodate the wave relaxation zone for wave generation and absorption. The bathymetry behind the generation line was artificially flattened to -36 m msl to aid in the stability of the wave generation. The model extends landwards to approximately +30 m msl.

The model mesh comprises triangles with a resolution varying between approximately 15 m offshore and approximately 5 m nearshore. This resulted in a resolution of approximately 11 points per wavelength in the surf-zone. The vertical mesh comprises three sigma layers with the bottom layer comprising 50%, the middle layer 30% and the surface layer 20% of the water column.

CONTROLLED DISCLOSURE

When downloaded from the EDS database, this document is uncontrolled and the responsibility rests with the user to ensure it is in line with the authorised version on the database.

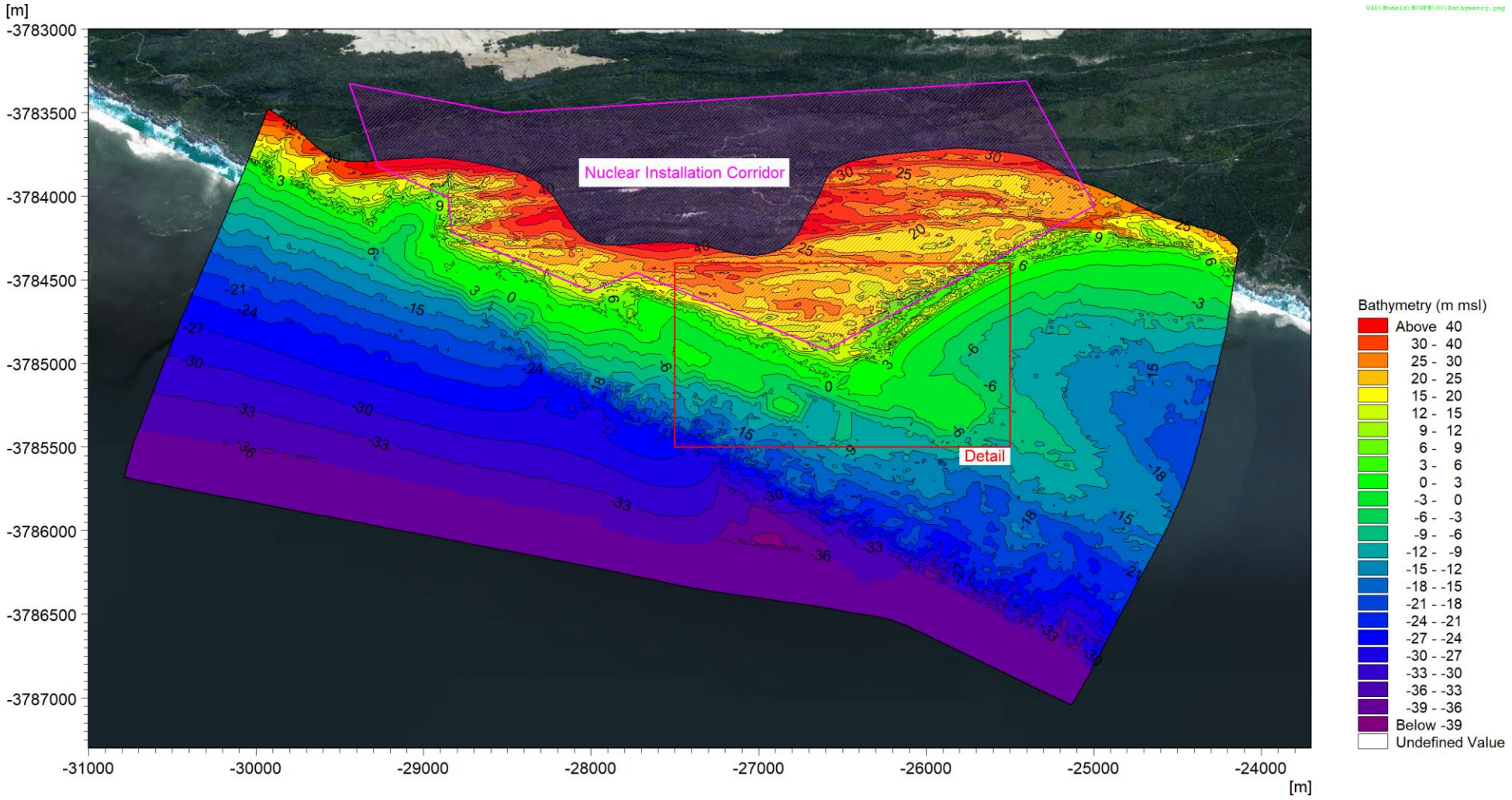


Figure 5.9.A-29: MIKE 3 Wave Model Domain and Bathymetry

CONTROLLED DISCLOSURE

When downloaded from the EDS database, this document is uncontrolled and the responsibility rests with the user to ensure it is in line with the authorised version on the database.

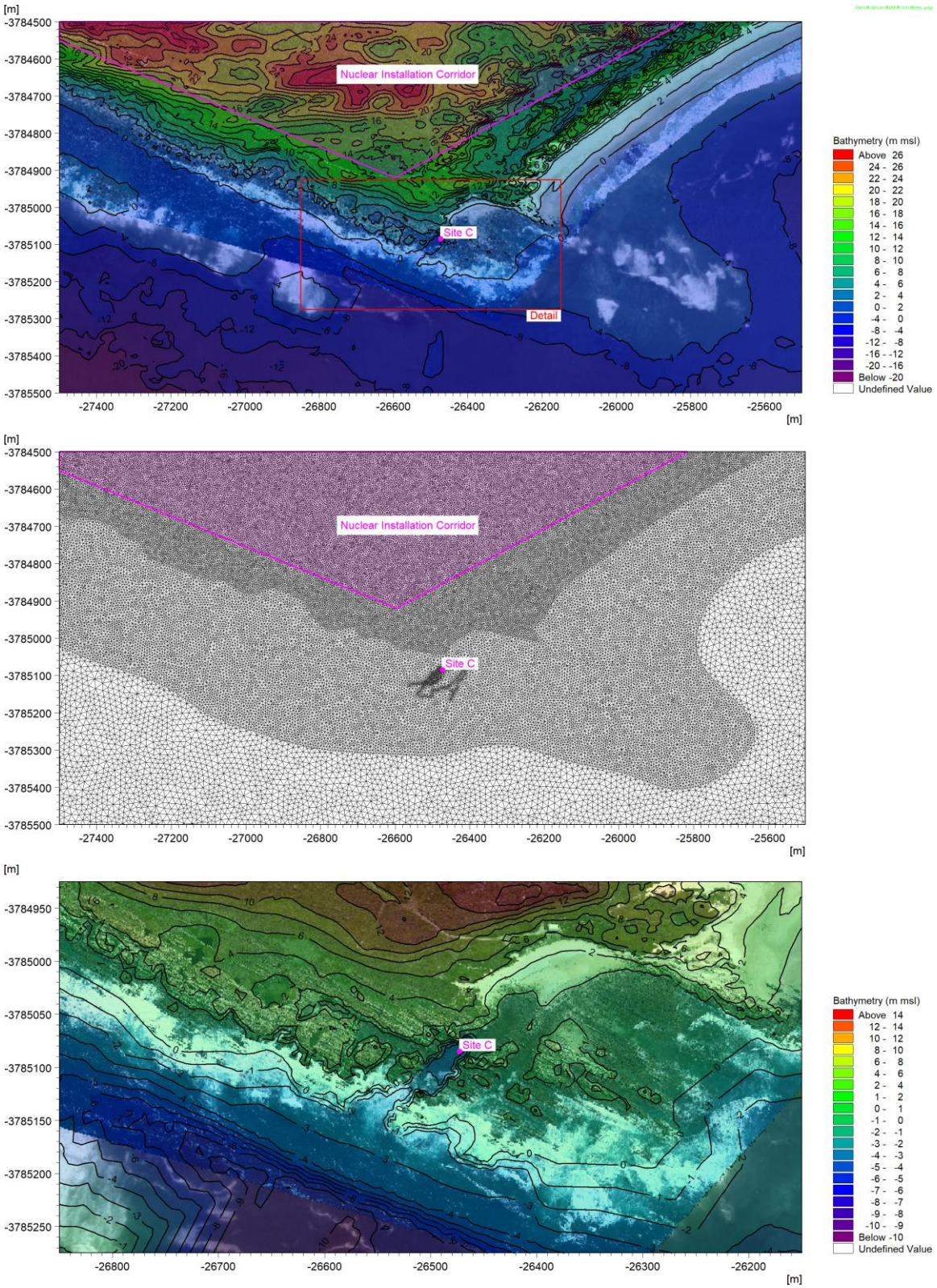


Figure 5.9.A-30: Detail of MIKE 3 Wave Model Mesh and Bathymetry Around the Gulley Containing Site C.

CONTROLLED DISCLOSURE

When downloaded from the EDS database, this document is uncontrolled and the responsibility rests with the user to ensure it is in line with the authorised version on the database.

Three base bathymetries were applied for the three years modelled (2034, 2134 and 2134 incorporating high sea level rise). All modelled periods required adjustments to the existing coastline and bathymetry to account for climate change (sea level rise and wave rotation) as described in ***Subsection 5.9.11***. Bathymetry adjustments for additional erosion during extreme storms relevant to each modelled date were applied for each modelled frequency (1E-2, 1E-4, 1E-6 and 1E-8 y^{-1}), resulting in a total of twelve different bathymetries used in the model runs. The bathymetry adjustments are presented in ***Subsection 5.9.11.7***. Minor adjustments were made to the mesh extents for the 2034 and 2134 scenarios to optimise simulation efficiency, however this did not influence the final result.

For each land/seabed surface type in the model domain, the corresponding Manning roughness was estimated from literature as described in detail in (PRDW, 2022b). These were then converted to a roughness height (k_s) for use in the MIKE 3 Wave model, as shown in ***Table 5.9.A-10***.

Table 5.9.A-10: Bottom Roughness Applied in Wave Model.

Surface Cover Type	Manning's M [(a)] ($m^{1/3}/s$)	Roughness Height k_s [(b)] (m)
Sandy seabed	32	0.25
Vegetated areas	26	0.869
Rubble-mound rock structures	20	4.196

Notes:

(a) Manning's M is the reciprocal of the generally used Manning's n. Larger values of Manning's M correspond to lower bed roughness.

(b) k_s can be related to M through the equation $M = \frac{25.4}{k_s^{1/6}}$ (DHI, 2024m).

5.9.A.6.4 Model Calibration

The numerical model was calibrated against high frequency (1 Hz) measured water levels at Site C within the gulley (see ***Table 5.9-6***) during a storm event on 24 August 2017. Although the storm peaked at H_{m0} = 7.5 m (as measured at Site B in a depth of -30 m msl, refer ***Figure 5.9-1***), the waves at the closest high tide were modelled: H_{m0} = 7.0 m and T_p = 19.6 s at -30 m msl, to allow comparison to the most stable water levels measured, considering that the water level in the model is constant for each sea state. The input boundary water level for the model was adjusted such that the average modelled water level at Site C matched the average measured water level calculated over the simulated period. The model was run for 2 hours.

Three random seeds were simulated and compared to the measured water levels. The random seeds are used to generate the random phasing of the wave train for the given wave spectrum. ***Figure 5.9.A-31*** presents a scatter

CONTROLLED DISCLOSURE

When downloaded from the EDS database, this document is uncontrolled and the responsibility rests with the user to ensure it is in line with the authorised version on the database.

comparison between the largest 5% of measured and modelled wave crest levels while ***Figure 5.9.A-32*** presents a time-series comparing measured and modelled water surface elevations at Site C for all modelled seeds. A comparison of measured and modelled wave spectra is shown in ***Figure 5.9.A-33***.

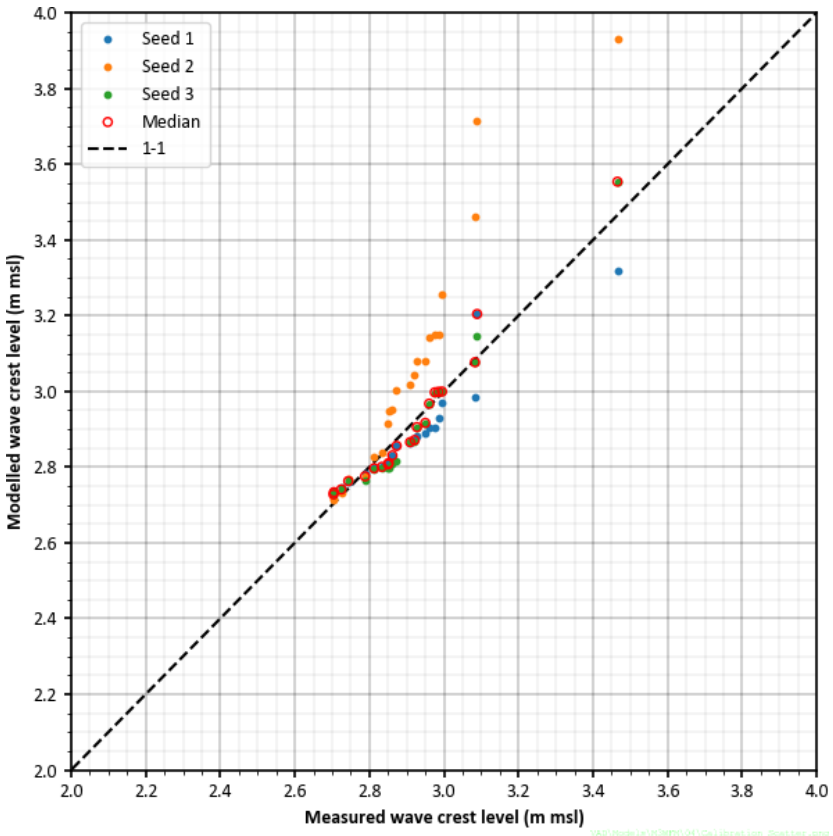


Figure 5.9.A-31: Scatter Comparison Between Measured and Modelled Wave Crest Levels at Site C for the 24 August 2017 Storm.

Figure 5.9.A-31 highlights the variability of the largest wave crests between simulated random seeds, showing that the model result can depend on the random seed chosen. This is to be expected as the exact wave train that occurred during this period is not replicated, nor the exact water levels as the offshore boundary level is fixed rather than a varying tide. Seed 2 is generally over-predicted (by 0.46 m at the maximum crest level) while Seed 1 is generally under-predicted (by 0.15 m at the maximum crest level). Seed 3 is generally well correlated to measured wave crests. The median modelled crest levels of the three seeds show satisfactory agreement to measurements with an over-prediction of 0.08 m at the maximum crest level.

CONTROLLED DISCLOSURE

When downloaded from the EDS database, this document is uncontrolled and the responsibility rests with the user to ensure it is in line with the authorised version on the database.

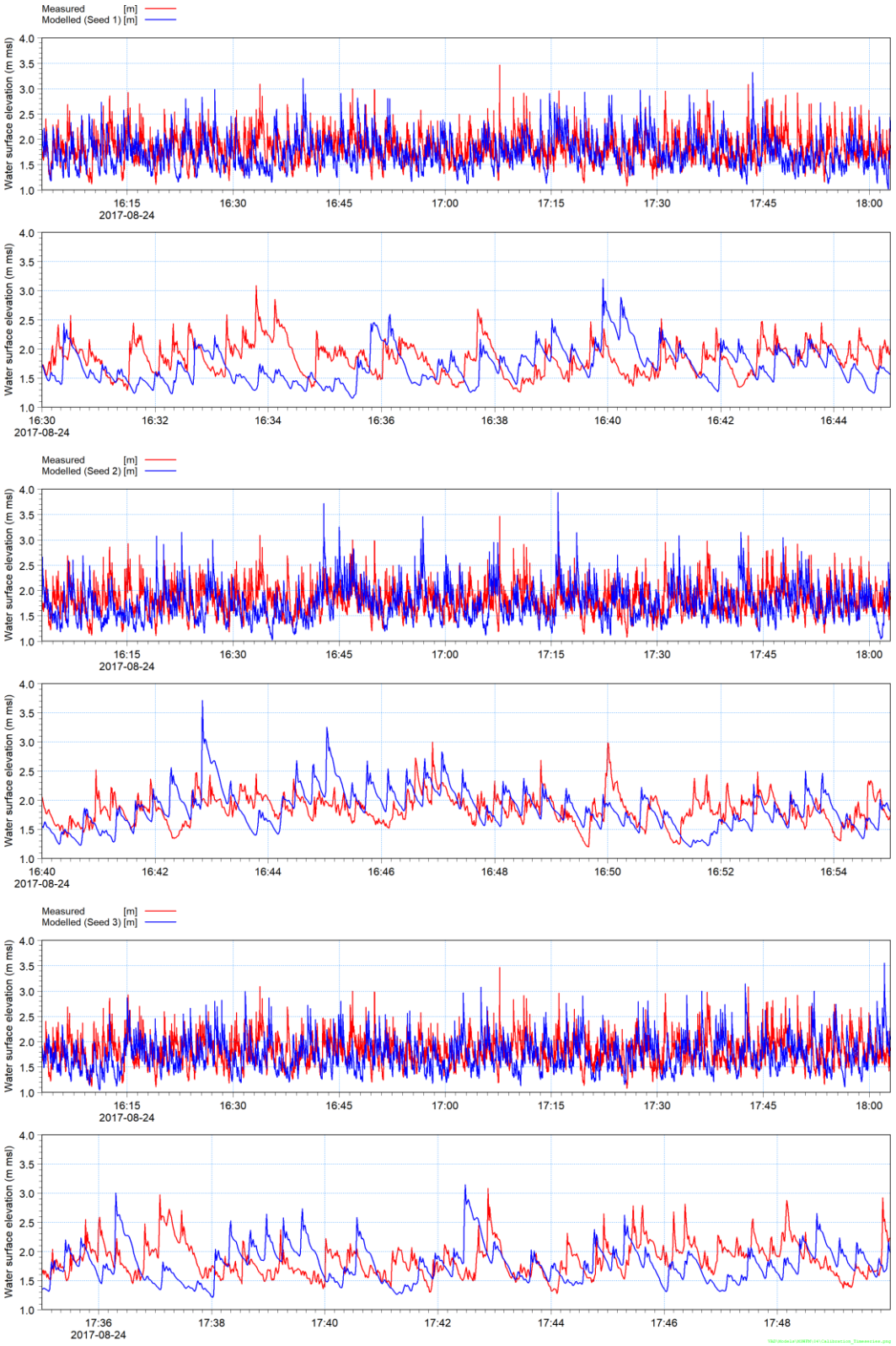


Figure 5.9.A-32: Time-Series of Measured and Modelled Water Surface Elevations at Site C for Two Hours During the 24 August 2017 Storm.

CONTROLLED DISCLOSURE

When downloaded from the EDS database, this document is uncontrolled and the responsibility rests with the user to ensure it is in line with the authorised version on the database.

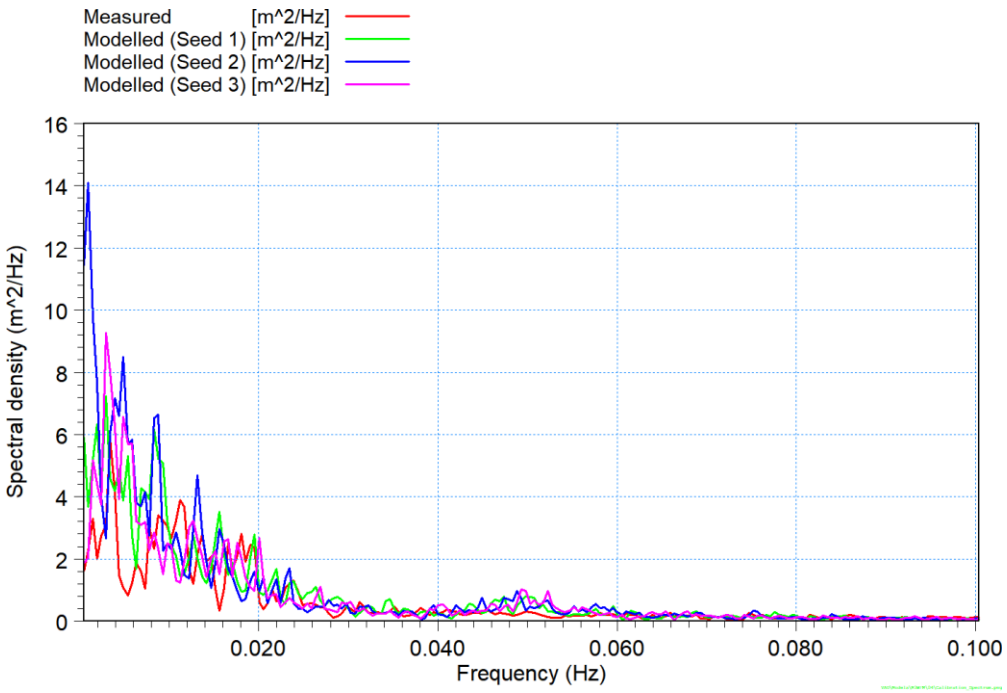


Figure 5.9.A-33: Measured and Modelled Frequency Spectra at Site C During the 24 August 2017 Storm.

The time-series plots in ***Figure 5.9.A-32*** show that the range of the modelled water levels is similar to the measurements. Note that there is no expectation that modelled water levels will match the measurements exactly due to the water level time-series applied at the model boundary being generated from the specified wave spectrum using random phasing. Modelled water levels, however, replicate the trends observed in the measurements such as wave steepness, wave asymmetry, wave set-up/surf-beat due to groups of larger waves and wave drawdown. Measured and modelled wave spectra also show good agreement throughout the frequency range presented. The over-prediction of the largest crest levels for Seed 2 in ***Figure 5.9.A-31*** may be attributed to the high density of wave energy at low frequencies (<0.005 Hz), otherwise known as bound long waves. A group of short-crested waves arriving at the same time as the crest of a bound long wave would result in a high number of large wave crests at Site C, explaining the general over-prediction of crest levels for Seed 2.

The numerical model was also calibrated against measured water levels at Site C (see ***Table 5.9-6***) during a storm event on 24 June 2018. The storm peaked at H_{m0} = 6.1 m, T_p = 13.4 s at -30 m msl, and coincided with the high tide. The model was run for 2 hours.

As with the 2017 storm, three random seeds were tested and compared to the measured water levels. ***Figure 5.9.A-34*** presents a scatter comparison between the largest 5% of measured and modelled wave crest levels while ***Figure 5.9.A-35*** presents a time-series comparing measured and modelled

When downloaded from the EDS database, this document is uncontrolled and the responsibility rests with the user to ensure it is in line with the authorised version on the database.

water surface elevations at Site C for all modelled seeds followed by measured and modelled wave spectra shown in ***Figure 5.9.A-36***.

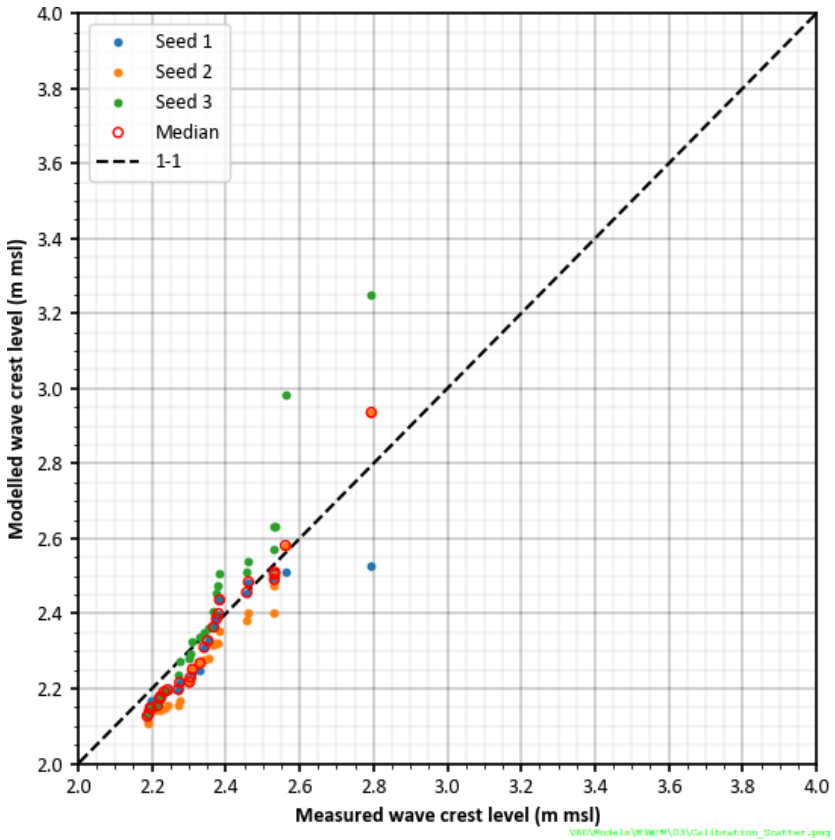


Figure 5.9.A-34: Scatter Comparison Between Measured and Modelled Wave Crest Levels for the 24 June 2018 Storm.

Similar to the results shown in ***Figure 5.9.A-31***, ***Figure 5.9.A-34*** highlights the level of variability of the largest wave crests between simulated random seeds. Simulations for the 2018 storm do however exhibit a lower variability at lower crest levels, with the largest differences observed for the largest wave crest. The median modelled crest levels for the three seeds show satisfactory agreement to measurements with an over-prediction of 0.14 m at the maximum crest level.

CONTROLLED DISCLOSURE

When downloaded from the EDS database, this document is uncontrolled and the responsibility rests with the user to ensure it is in line with the authorised version on the database.

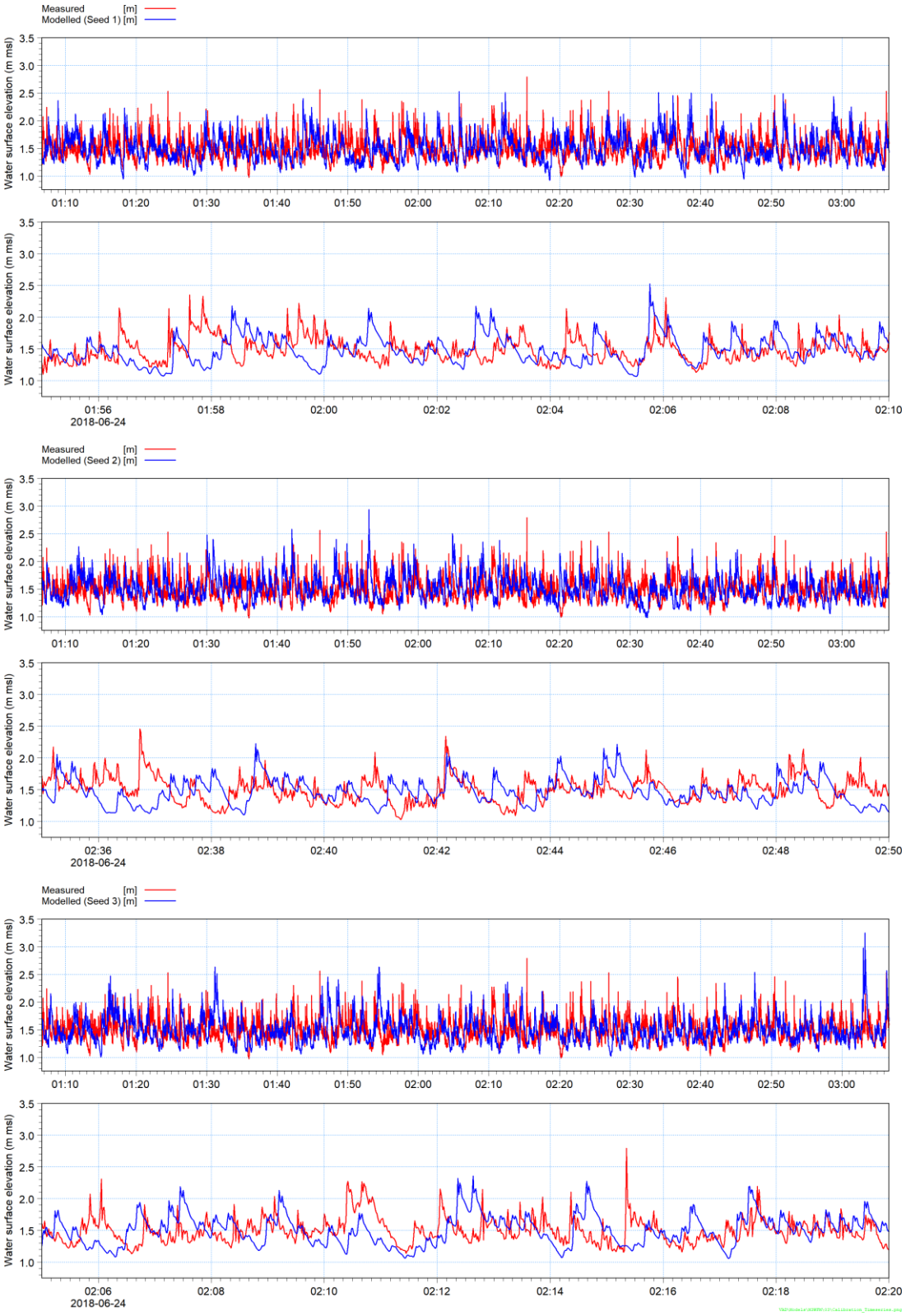


Figure 5.9.A-35: Time-Series of Measured and Modelled Water Surface Elevations at Site C for Two Hours During the 24 June 2018 Storm.

CONTROLLED DISCLOSURE

When downloaded from the EDS database, this document is uncontrolled and the responsibility rests with the user to ensure it is in line with the authorised version on the database.

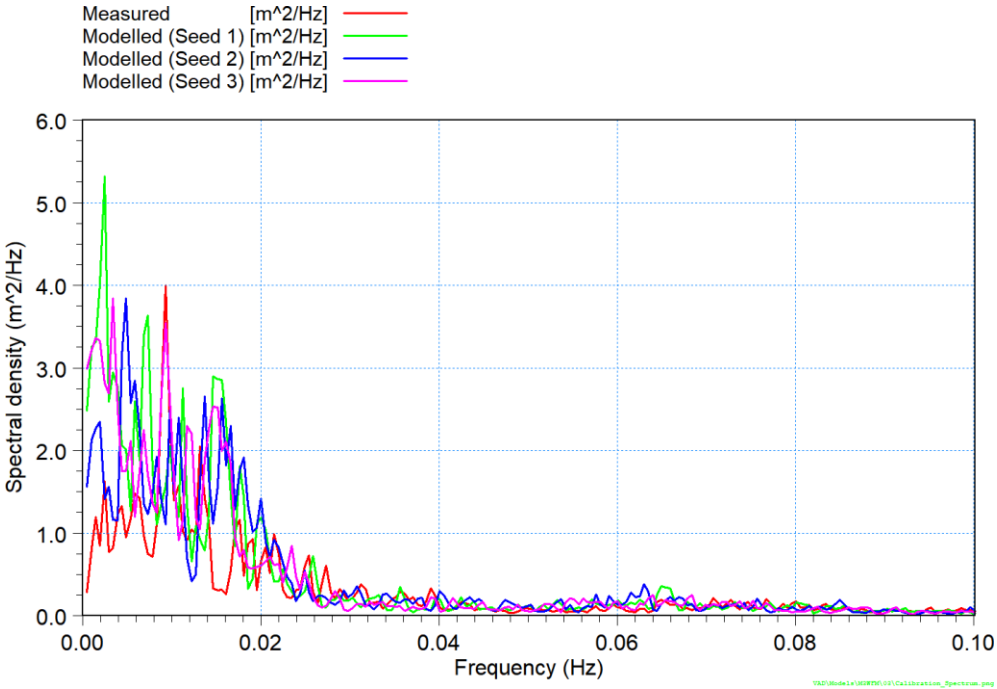


Figure 5.9.A-36: Measured and Modelled Frequency Spectra at Site C During the 24 June 2018 Storm.

The time-series plots in ***Figure 5.9.A-35*** show that the range and shape of the modelled water levels is similar to the measurements. Measured and modelled wave spectra also show good agreement throughout the frequency range presented. Seed 3 successfully replicates the peak in wave energy at 0.008 Hz that is observed in the measured spectrum, however as with Seed 1, the simulation produced more energy at low frequencies than the measurements. Although Seed 3 incorporates less long-wave energy than Seed 1, the overprediction of the largest two wave crests, seen in ***Figure 5.9.A-34***, occurs during the same event towards the end of the simulation (see ***Figure 5.9.A-35***) that likely corresponds to the arrival of a long wave.

The modelled run-up level was also calibrated against the debris line measured on the Thysbaai beach in March 2024 (see ***Subsection 5.9.6.1***). The model was used to simulate the wave run-up during the storm of 9 September 2023 (H_{m0} = 8.3 m and T_p = 16.5 s at -36 m msl), which is the largest storm that occurred at the site in the last five years and thus the most likely to have defined the debris line. The storm peak occurred during a low tide, therefore the waves at the closest high tide were modelled: H_{m0} = 7.9 m and T_p = 16.1 s at -36 m msl, which is the time most likely to have caused the maximum run-up on the beach, thereby defining the wave run-up debris line measured on site. The model was run for 2 hours. The model bathymetry was derived from the generic dataset described in ***Subsection 5.9.8***, i.e. not including any adjustments for climate change or storm erosion.

CONTROLLED DISCLOSURE

When downloaded from the EDS database, this document is uncontrolled and the responsibility rests with the user to ensure it is in line with the authorised version on the database.

Three random seeds were simulated to account for the variability in boundary water levels due to the random seed. The maximum run-up line was calculated as the most shoreward extent of mesh cells that were inundated by at least two out of three simulations, i.e., the median. ***Figure 5.9.A-37*** shows a spatial comparison of the modelled wave run-up along with the measured debris line. Additionally, the vertical level of the modelled wave run-up was compared against the vertical level of the debris line, shown in ***Figure 5.9.A-38***. Note that due to differences in length of the measured and modelled debris lines due to undulations along the line, the chainage of the modelled debris line was normalised to equal the measured chainage in ***Figure 5.9.A-38***.

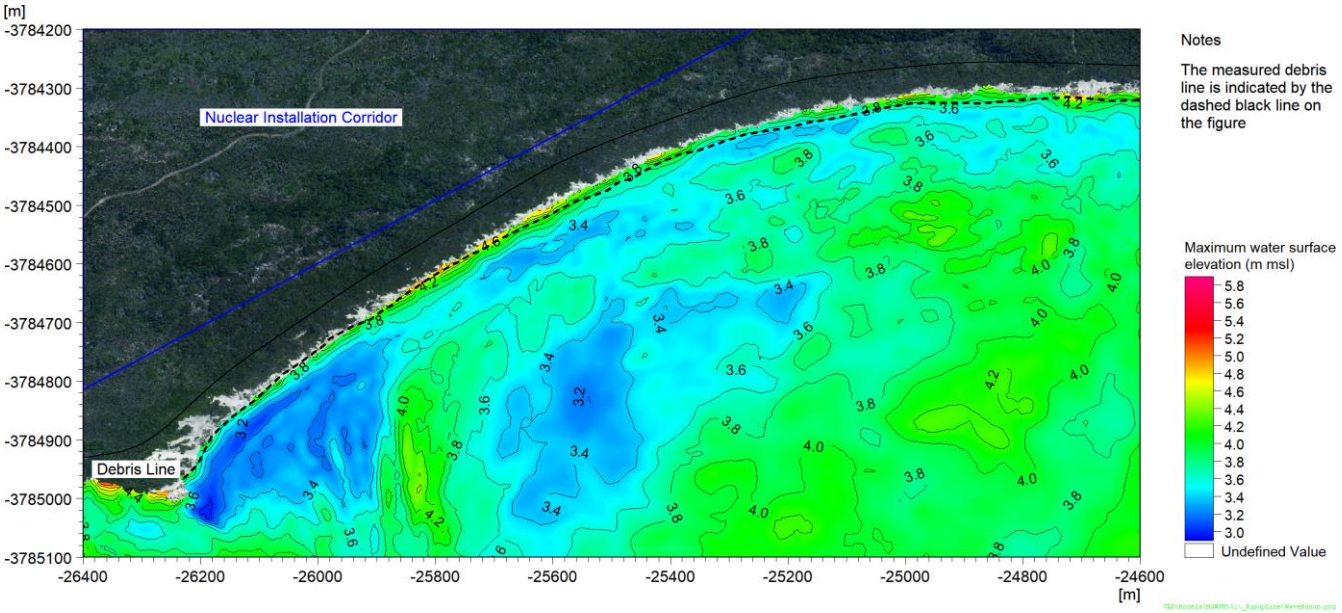


Figure 5.9.A-37: Maximum Modelled Water Surface Elevation During 9 September 2023 Storm and Measured Debris Line.

CONTROLLED DISCLOSURE

When downloaded from the EDS database, this document is uncontrolled and the responsibility rests with the user to ensure it is in line with the authorised version on the database.

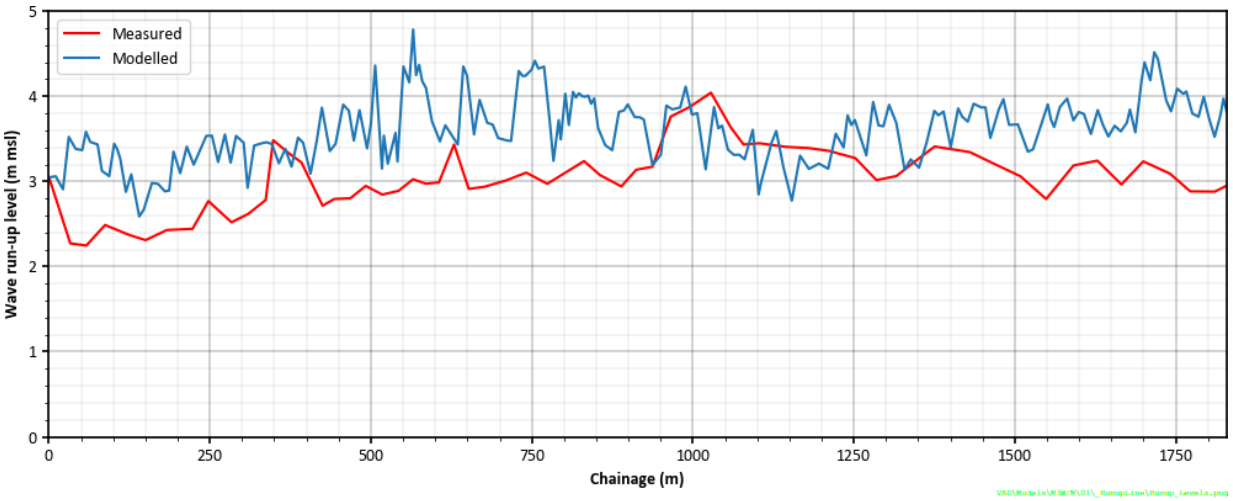


Figure 5.9.A-38: Comparison of the Vertical Ground Level Along the Measured Debris Line and Modelled Wave Run-Up Line for the 3 September 2023 Storm. Note That 0 m Chainage Refers to the Start of the Measured Debris Line in Figure 5.9.A-37, Increasing in Chainage from West to East.

The modelled wave run-up shows good agreement with the measured debris line, particularly towards the west of the domain presented in ***Figure 5.9.A-37***. The modelled wave run-up is generally shoreward of the measured debris line from the middle to the east of the domain presented. Differences between measured and modelled run-up can be explained by localised changes in the beach between the 2011 LiDAR survey used in the model and the 2023 modelled storm, which showed erosion along this section of the bay. Additionally, shorelines are highly dynamic due to factors such as aeolian (wind-blown) and longshore sediment transport, thereby introducing a level of uncertainty to the measured debris line. The comparison of vertical levels presented in ***Figure 5.9.A-38*** shows that the model generally overpredicts the wave run-up along the coastline by approximately 0.5 m on average. The model is able to replicate the increase in vertical level with increasing chainage observed in the measurements. This is due to the eastern coastline receiving less sheltering from the reefs located to the west. This is also evidenced by the maximum surface elevation, showing a maximum of 3.4 m msl in the west compared to 4.2 m msl in the east. Overall, the model shows reasonable capability in reproducing the measured debris line while also producing a conservative result.

The results above show that the model is capable of simulating the water levels at the site with sufficient accuracy, and that using the median of three seeds provides a sufficiently robust result.

CONTROLLED DISCLOSURE

When downloaded from the EDS database, this document is uncontrolled and the responsibility rests with the user to ensure it is in line with the authorised version on the database.

5.9.A.6.5 Cases Modelled

The model was run for extreme storms with exceedance frequencies of 1E-2, 1E-4, 1E-6 and 1E-8 y^{-1}. The model was run for the 2034, 2134, and 2134 High SLR climate change scenarios to include the effect of climate change on waves, water levels and coastline stability.

The model boundary conditions are the extreme wave parameters (H_{m0}, T_p, MWD and DSD), combined with the extreme maximum still water levels (comprising tide, sea level rise and storm surge).

The joint probability between the waves and storm surge was accounted for as described in ***Subsection 5.9.9.9***. For the extreme wave run-up simulations, the waves were combined with the positive storm surge as shown in ***Table 5.9-24***, where for example the 1E-4 y^{-1} wave is combined with the 8.45E-4 y^{-1} storm surge and vice versa. The best estimate values were used in the modelling and are summarised for all modelled joint probability combinations for wave dominated (***Table 5.9.A-11***) and storm surge dominated (***Table 5.9.A-12***) scenarios.

The coupled spectral wave and 2D hydrodynamic model, described in ***Appendix 5.9.A.1***, was used to obtain boundary conditions for the MIKE 3 Wave model at a depth of -36 m msl. This is due to the model results used to produce the extreme wave parameters in ***Table 5.9-22*** being obtained at -55 m msl. ***Table 5.9.A-11*** and ***Table 5.9.A-12*** summarise the boundary conditions for modelled wave and storm surge dominated scenarios respectively.

Table 5.9.A-11: Summarised Boundary Conditions at -36 m msl for Modelled Wave Dominated Storm Scenarios.

Exceedance Frequency	Maximum Still Water Level			H_{m0}			T_p			MWD			DSD		
(y^{-1})	(m msl)			(m)			(s)			(°)			(°)		
	2034	2134	2134 High SLR	2034	2134	2134 High SLR	2034	2134	2134 High SLR	2034	2134	2134 High SLR	2034	2134	2134 High SLR
10^{-2}	2.01	3.66	5.18	9.20	9.72	9.71	16.00	16.15	16.16	208.4	208.4	208.5	16.75	16.73	16.77
10^{-4}	2.33	3.98	5.50	10.95	11.62	11.61	16.71	17.96	17.96	208.2	208.2	208.3	16.69	16.69	16.74
10^{-6}	2.60	4.27	5.78	12.49	13.17	13.16	18.46	18.62	18.62	208.0	208.1	208.2	16.52	16.53	16.58
10^{-8}	2.85	4.52	6.04	13.80	14.65	14.64	18.79	19.30	19.31	207.9	208.0	208.1	16.49	16.54	16.59

CONTROLLED DISCLOSURE

When downloaded from the EDS database, this document is uncontrolled and the responsibility rests with the user to ensure it is in line with the authorised version on the database.

Table 5.9.A-12: Summarised Boundary Conditions at -36 m msl for Modelled Storm Surge Dominated Storm Scenarios.

Exceedance Frequency	Maximum Still Water Level			H_{m0}			T_p			MWD			DSD		
(y^{-1})	(m msl)			(m)			(s)			(°)			(°)		
	2034	2134	2134 High SLR	2034	2134	2134 High SLR	2034	2134	2134 High SLR	2034	2134	2134 High SLR	2034	2134	2134 High SLR
10^{-2}	2.17	3.82	5.34	8.21	8.72	8.71	14.55	15.64	15.64	208.6	208.6	208.7	16.93	16.91	16.96
10^{-4}	2.46	4.12	5.64	10.15	10.76	10.75	16.26	16.54	16.54	208.3	208.3	208.4	16.69	16.75	16.79
10^{-6}	2.72	4.39	5.91	11.83	12.49	12.48	18.14	18.46	18.46	208.1	208.1	208.2	16.62	16.57	16.62
10^{-8}	2.96	4.64	6.16	13.19	13.95	13.95	18.63	18.84	18.85	208.0	208.0	208.1	16.49	16.55	16.60

For each joint probability, both combinations of storm surge and wave height were modelled. The total number of cases modelled was thus 3 dates × 4 exceedance frequencies × 2 joint probability combinations = 24 cases for run-up.

The waves in the model were generated at the -36 m msl contour. A JONSWAP spectrum was used with a gamma of 3.3. The specified wave parameters are used by the model to generate a sea state by applying random phases and directions. The duration of each simulation was set to two hours. This allowed at least 410 waves to be simulated including a range of wave groups.

5.9.A.6.6 Uncertainty in Modelled Wave Run-Up

One of the outputs of the wave modelling is the maximum storm wave run-up level occurring anywhere on the site. The methodology described below was used to estimate the uncertainty in these modelled run-up levels.

The modelled run-up level can be expressed as follows:

$$R = (S + a) + (bH + c) \qquad \text{Equation 5.9.A.3}$$

Where:

R = modelled run-up level (m msl)

S = storm surge applied on model boundary (m)

H = H_{m0} applied on model boundary (m)

a = constant water level on boundary = tide level + SLR (m msl)

b,c = constants calculated from the model results

The uncertainties in the storm surge and H_{m0} are known from the respective EVA analyses and for a given exceedance frequency these uncertainties

CONTROLLED DISCLOSURE

When downloaded from the EDS database, this document is uncontrolled and the responsibility rests with the user to ensure it is in line with the authorised version on the database.

are normally distributed (refer ***Subsections 5.9.6.2, 5.9.9.2 and 5.9.9.8)***. The joint probability between storm surge and H_{m0} is presented in ***Subsection 5.9.10.3*** indicting a "well" level of dependence with $\chi = 0.344$, which is equivalent to a correlation coefficient $\rho = 0.53$ (Petroliagkis, et al., 2016).

The run-up is thus the sum of two correlated normally distributed random variables and is thus also normally distributed with the following mean μ and standard deviation σ:

$$\mu_R = (\mu_S + a) + (b\mu_H + c) \qquad \text{Equation 5.9.A.4}$$

$$\sigma_R = \sqrt{\sigma_S^2 + b^2\sigma_H^2 + 2\rho\sigma_S b\sigma_H} \qquad \text{Equation 5.9.A.5}$$

The uncertainty in the run-up can then be described by the 5th and 95th percentiles calculated as μ_R - *1.645* σ_R *and* μ_R + *1.645* σ_R, respectively.

The constants *b* and *c* are obtained from the linear regression fit through the model results as shown in ***Figure 5.9.A-39***, where the wave run-up height r is calculated as *r = R – (S + a)*.

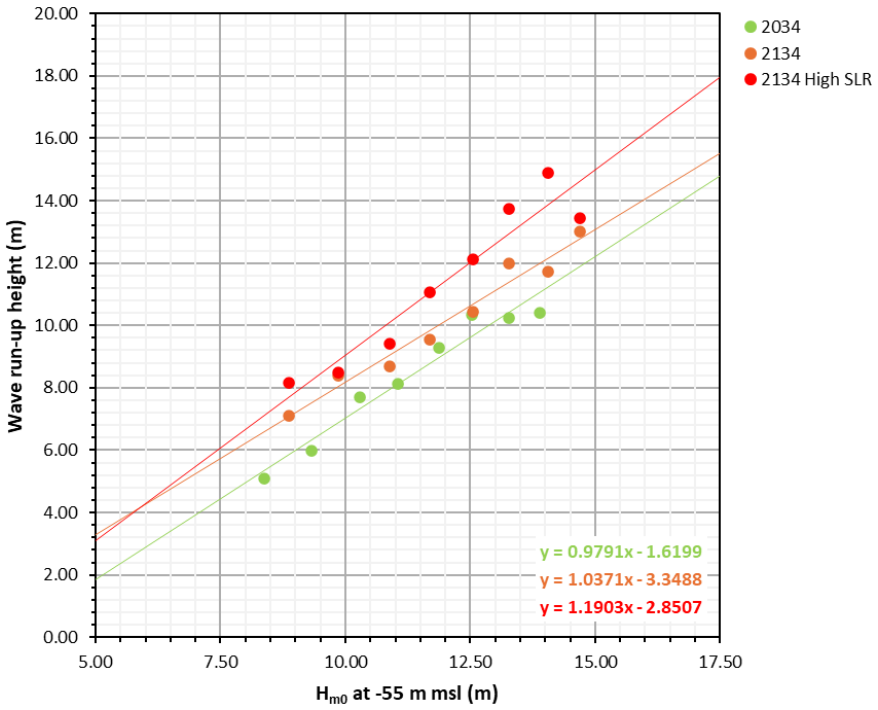


Figure 5.9.A-39: Scatter Plot of Modelled Wave Run-Up Height Versus Wave Height (H_{m0}) Applied at the Model Boundary at -55 m msl.

The results for the maximum run-up including uncertainties are presented in ***The*** extreme flooding results for all exceedance frequencies are provided in ***Table 5.9-29*** and plotted in ***Figure 5.9-101.*** These show the maximum

When downloaded from the EDS database, this document is uncontrolled and the responsibility rests with the user to ensure it is in line with the authorised version on the database.

storm wave run-up occurring anywhere in the area shown in the flood line plots. These values also correspond with the markers presented in ***Figure 5.9-98***, ***Figure 5.9-99*** and ***Figure 5.9-100*** that indicate the location of maximum vertical run-up level for each modelled frequency. Results include the best estimate from the model results, plus the mean, 5th and 95th percentile uncertainties, which have been calculated using the uncertainty methodology described in ***Appendix 5.9.A.6.***

Table 5.9-29. The extreme flooding results for all exceedance frequencies are provided in ***Table 5.9-29*** and plotted in ***Figure 5.9-102***. These show the maximum storm wave run-up occurring anywhere in the area shown in the flood line plots. These values also correspond with the markers presented in ***Figure 5.9-99***, ***Figure 5.9-100*** and ***Figure 5.9-101*** that indicate the location of maximum vertical run-up level for each modelled frequency. Results include the best estimate from the model results, plus the mean, 5th and 95th percentile uncertainties, which have been calculated using the uncertainty methodology described above.

5.9.A.7 Hydrodynamic Modelling

5.9.A.7.1 Introduction

Hydrodynamic modelling was conducted to simulate the dispersion of the thermal plume from the once-through seawater cooling system of the new NIs (***Subsection 5.9.16***).

5.9.A.7.2 Model Description

The MIKE 3 Flow Model Flexible Mesh was used for the thermal plume dispersion modelling. The details of the physical processes and numerical implementation are provided in the model documentation (see ***Table 5.9-7***), while details of the sensitivity testing and V&V are provided in the V&V Report (PRDW, 2022a).

The model is based on the numerical solution of the three-dimensional incompressible Reynolds averaged Navier-Stokes equations invoking the assumptions of Boussinesq and of hydrostatic pressure. The model consists of the continuity, momentum, temperature, salinity and density equations and is closed by a k-ε vertical turbulence closure scheme. Horizontal eddy viscosity is modelled with the Smagorinsky formulation.

The time integration of the shallow water equations and the transport equations is performed using a semi-implicit scheme, where the horizontal terms are treated explicitly and the vertical terms are treated implicitly. In the vertical direction a sigma-coordinate transformation which can be combined with z-layers is used, while the geometrical flexibility of the

CONTROLLED DISCLOSURE

When downloaded from the EDS database, this document is uncontrolled and the responsibility rests with the user to ensure it is in line with the authorised version on the database.

unstructured flexible mesh comprising triangles or quadrangles is utilised in the horizontal plane.

The model includes the following physical phenomena:

- Currents due to tides;
- Currents due to wind stress on the water surface;
- Currents due to density gradients;
- Currents due to regional currents applied on the boundary;
- Currents due to waves; the second order stresses due to breaking of short period waves are included using the radiation stresses computed in the Spectral Wave model;
- Coriolis forcing;
- Bottom friction;
- Flooding and drying;
- Sources and sinks; and
- Heat exchange.

5.9.A.7.3 Model Setup

The hydrodynamic model consisted of a larger coarser regional model and a smaller refined nested model.

5.9.A.7.3.1 Regional Model

The regional model domain and bathymetry are shown in ***Figure 5.9.A-40***. The mesh is comprised of quadrilateral elements at the offshore boundaries with a resolution of 6 000 m, and triangles with a resolution varying between approximately 6 000 m offshore to approximately 100 m at the outfall. The vertical mesh comprises 20 sigma layers with equal thicknesses up to a depth of -500 m and is followed with 15 z-layers with thickness values varying between 300 m and 40 m. ***Figure 5.9.A-41*** shows the mesh used in the regional model.

CONTROLLED DISCLOSURE

When downloaded from the EDS database, this document is uncontrolled and the responsibility rests with the user to ensure it is in line with the authorised version on the database.

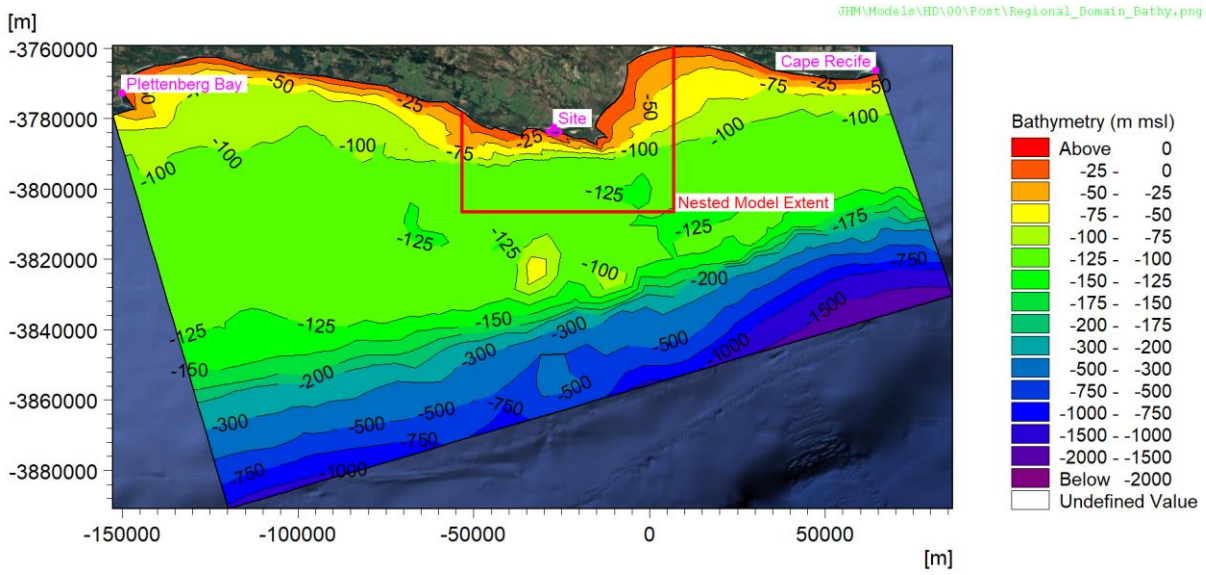


Figure 5.9.A-40: Regional Model Domain and Bathymetry.

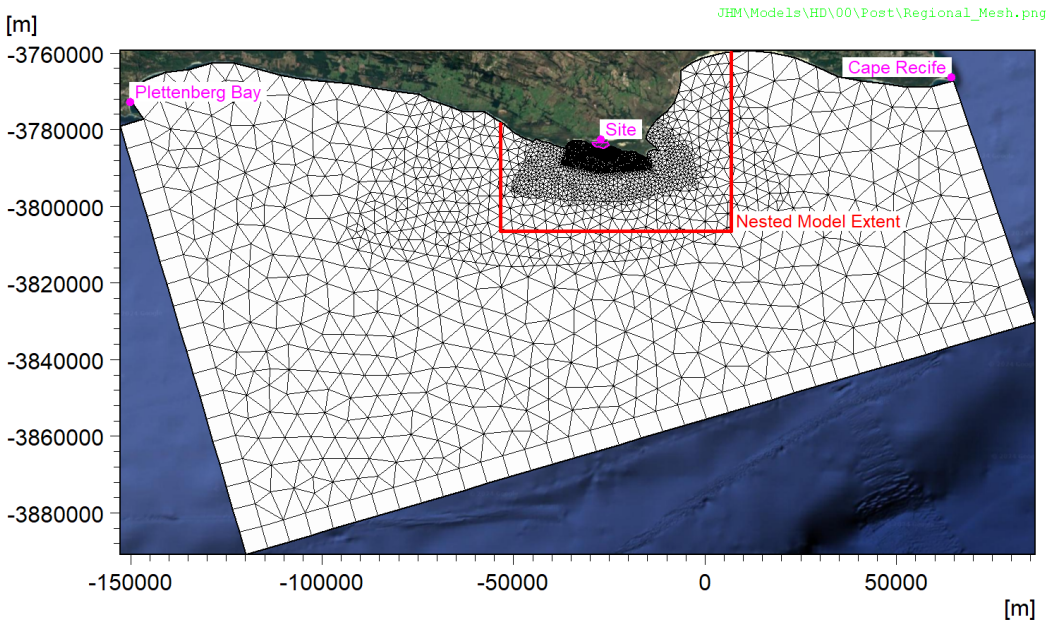


Figure 5.9.A-41: Regional Model Mesh.

The model bathymetry is derived from the generic dataset described in ***Subsection 5.9.8***. The following boundary conditions and forcings were applied in the model:

- Non-tidal water levels, ocean currents, seawater temperature and salinity were extracted from the 3D HYbrid Coordinate Ocean Model

CONTROLLED DISCLOSURE

When downloaded from the EDS database, this document is uncontrolled and the responsibility rests with the user to ensure it is in line with the authorised version on the database.

(HYCOM) global ocean circulation model and applied along the offshore boundaries (HYCOM, 2024). As part of the model calibration, the ocean currents, seawater temperature and salinity vertical grids were compressed to increase stratification.

- Predicted tides and currents were available from the DTU10 global tide model (DTU, 2010) and were applied along the offshore boundaries in addition to the non-tidal water levels and currents. A vertical correction of 0.2543 m was applied to the predicted tidal levels to convert the datum to msl.
- Space varying, hourly offshore hindcast wind data from the CFS model (see ***Appendix 5.9.A.2.3***) was applied over the model domain with a wind friction coefficient C_d of 0.002425. A constant pressure of 1013 hPa was included.
- Heat exchange between the water and the atmosphere was included in the model. The heat exchange includes the physical processes of latent heat, sensible heat, short wave radiation and long wave radiation.
- Space and time varying humidity, air temperature, short wave radiation and long wave radiation data was extracted from the EMCWF ERA5 model.

The vertical eddy viscosity was computed using the k-ε vertical turbulence closure scheme, while the vertical eddy dispersion was set to 0.1 times the vertical eddy viscosity. This scaling factor was applied to compensate for additional vertical mixing caused by the use of only 35 vertical layers and the associated smoothing of the vertical density gradients. The bed resistance was modelled using a constant roughness height of 0.03 m. The density was modelled as a function of temperature and salinity.

5.9.A.7.3.2 Nested Model

The model domain and bathymetry are shown in ***Figure 5.9.A-42***. The mesh is comprised of quadrilateral elements at the offshore boundaries with a resolution of 1 000 m, and triangles with a resolution varying between approximately 1 000 m offshore to approximately 80 m at the outfall. The vertical mesh comprises ten equidistant sigma layers. ***Figure 5.9.A-43*** shows an example detail view of the mesh used.

CONTROLLED DISCLOSURE

When downloaded from the EDS database, this document is uncontrolled and the responsibility rests with the user to ensure it is in line with the authorised version on the database.

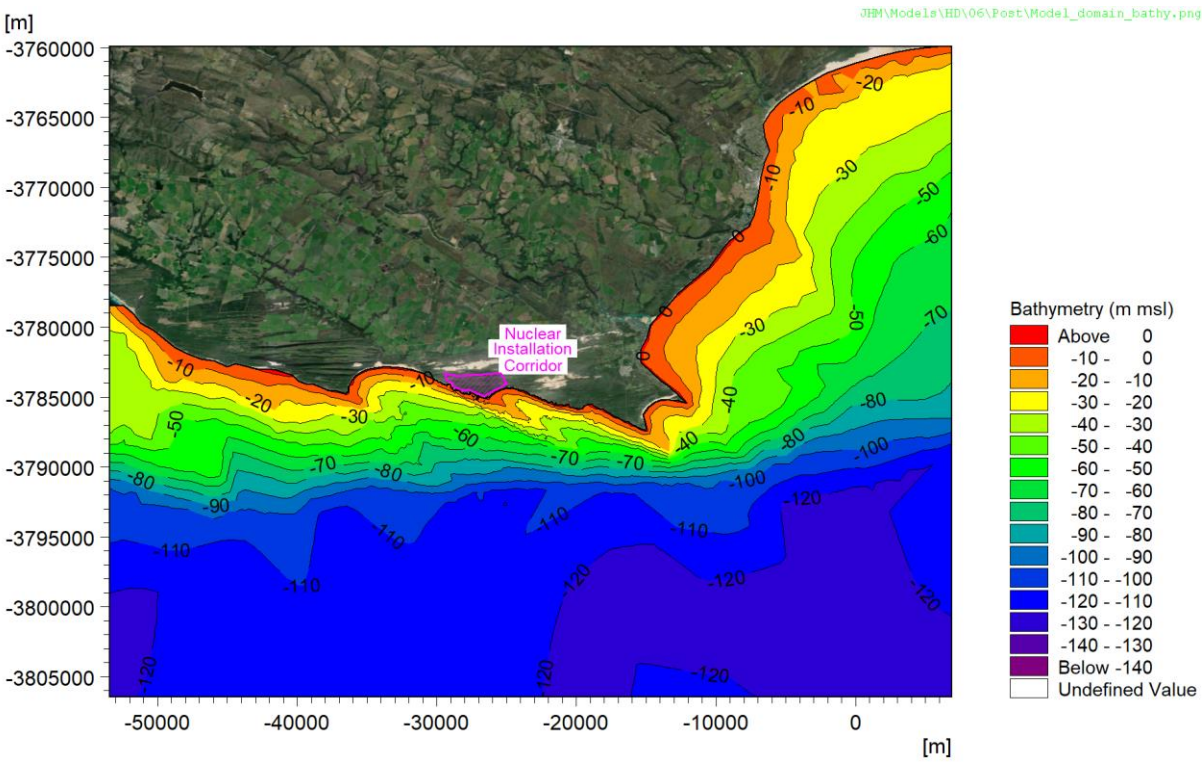


Figure 5.9.A-42: Nested Model Domain and Bathymetry.

CONTROLLED DISCLOSURE

When downloaded from the EDS database, this document is uncontrolled and the responsibility rests with the user to ensure it is in line with the authorised version on the database.

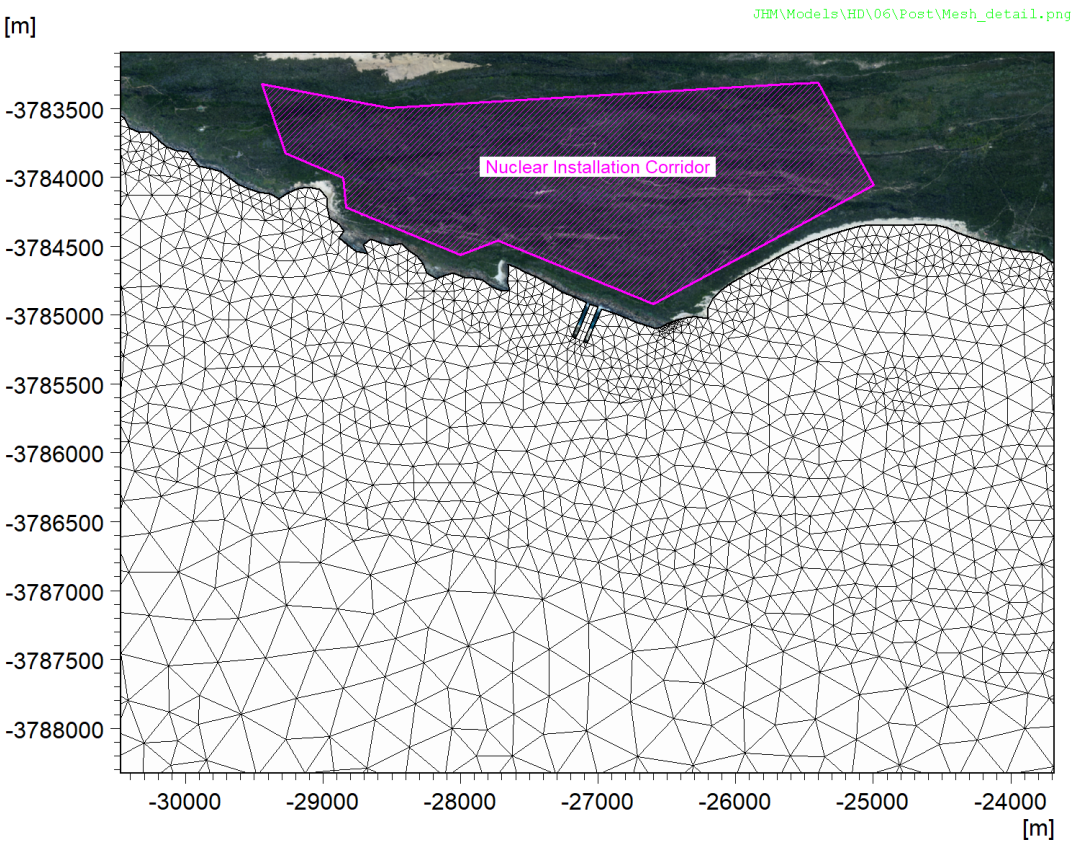


Figure 5.9.A-43: Detail of the Nested Model Mesh.

The boundary conditions and forcings applied to the model was similar to those applied to the regional model with the following exceptions:

- Water levels, currents, seawater temperature and salinity were extracted from the regional model results and applied along the offshore boundaries using Flather boundary conditions.
- As part of the model calibration, depth- and time-varying adjustments were made to the temperature boundary conditions to increase stratification during the summer months.
- A time-varying, space-constant vertical correction for atmospheric pressure fluctuations was applied to the boundary water levels, based on the barometric pressure measurements at the site (the measurement programme is detailed in ***Subsection 5.9.6.1***) and a typical seawater density of 1025 kg/m^3. Where there were gaps in the measurements, the pressure data was filled using sea level pressure from the European Centre for Medium-Range Weather Forecasts (EMCWF) ERA5 global atmospheric model (ECMWF, 2024).
- An additional 0.124 m was included in the water levels to account for the difference between mean level and mean sea level at Thyspunt. A

CONTROLLED DISCLOSURE

When downloaded from the EDS database, this document is uncontrolled and the responsibility rests with the user to ensure it is in line with the authorised version on the database.

water level offset was noted during calibration and an additional 0.1066 m was added to the water levels.

- Wave-driven currents were included using a coupled spectral wave model based on the calibrated parameters presented in ***Appendix 5.9.A.1***. The wave model was run in the fully spectral, quasi-stationary formulation.

The bed resistance was modelled using a roughness height of 0.04 m in sandy areas. In areas with exposed rough bedrock the roughness height was increased to 4 m in alignment with the bed roughness parameters presented in ***Appendix 5.9.A.6***.

The intakes and outfall were modelled using an intake connected to a simple discharge source at the landward end of the outfall channel. The discharge is dynamically coupled to the intakes so that the discharge temperature is the intake temperature plus ΔT.

5.9.A.7.4 Model Calibration

The hydrodynamic model was calibrated against current and temperature measurements available at Sites A and B, and against temperature and water surface elevation measurements at Site C (the measurement programme and the site locations are detailed in ***Subsection 5.9.6.1***).

The model was run for a full year between 1 July 2009 and 30 June 2010, which allowed the calibration to be performed against the data collected during this period of good overall data coverage. The calibration model was run for a baseline scenario, i.e. without any thermal discharges.

The modelled water surface elevation was compared to the measurements at Site C (-1.9 m msl). ***Figure 5.9.A-44*** and ***Figure 5.9.A-45*** present the comparison of the modelled and measured water surface elevation at Site C.

CONTROLLED DISCLOSURE

When downloaded from the EDS database, this document is uncontrolled and the responsibility rests with the user to ensure it is in line with the authorised version on the database.

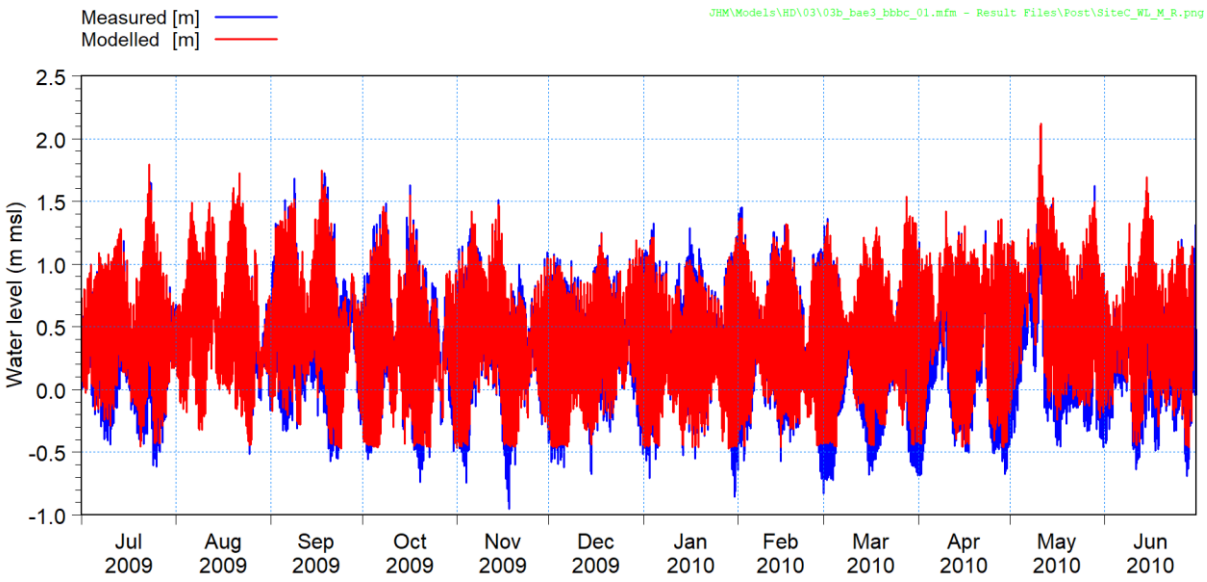


Figure 5.9.A-44: Time-Series Comparison of Modelled and Measured Water Surface Elevations at Site C (Depth -1.9 m msl).

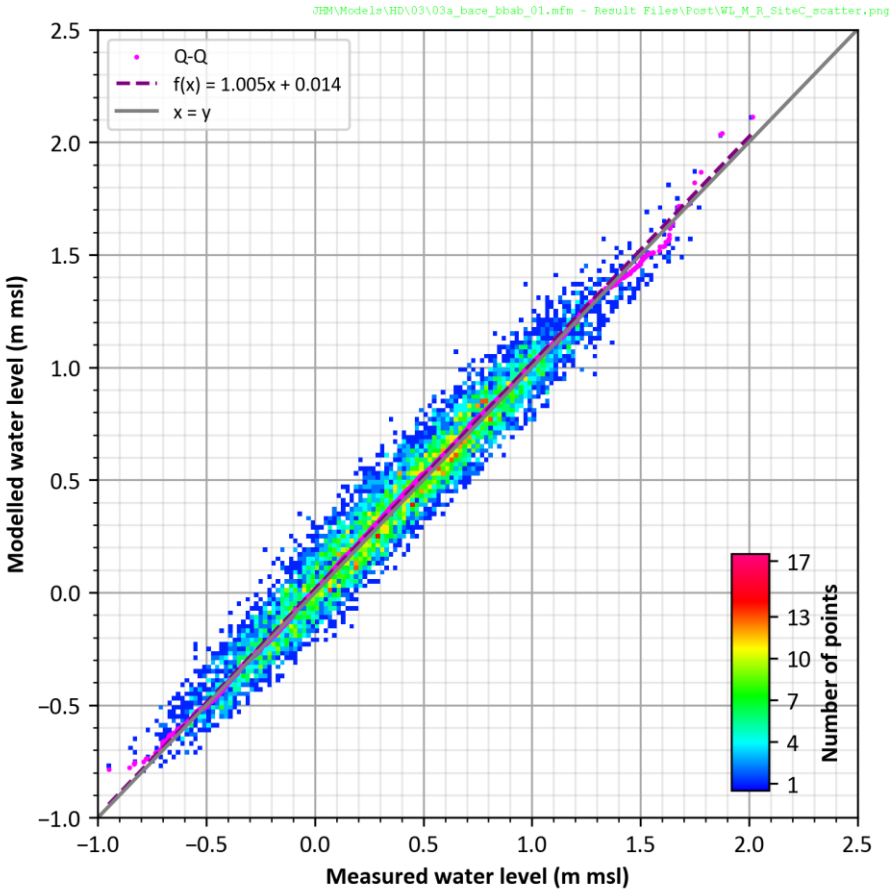


Figure 5.9.A-45: Scatterplot and Q-Q Comparison of Modelled and Measured Water Surface Elevation at Site C (Depth -1.9 m msl).

CONTROLLED DISCLOSURE

When downloaded from the EDS database, this document is uncontrolled and the responsibility rests with the user to ensure it is in line with the authorised version on the database.

These results show that the model is able to accurately simulate the water surface elevations at Site C. This includes the effects of tides, storm surge, wave set-up and regional currents on the water surface elevation.

The modelled currents were compared to the measured near-seabed and near-surface currents at Site A (-13.2 m msl) and Site B (-30.8 m msl). Figure 5.9.A-46 to Figure 5.9.A-49 present time-series comparisons of modelled and measured current speed and direction at Site A and B respectively. Current rose comparisons for Site A and B follow in Figure 5.9.A-50 and Figure 5.9.A-51. Percentile comparisons of current speeds for both sites are shown in ***Figure 5.9.A-52***. Note the roses and percentiles only include the timesteps where the modelled and measured data overlap.

CONTROLLED DISCLOSURE

When downloaded from the EDS database, this document is uncontrolled and the responsibility rests with the user to ensure it is in line with the authorised version on the database.

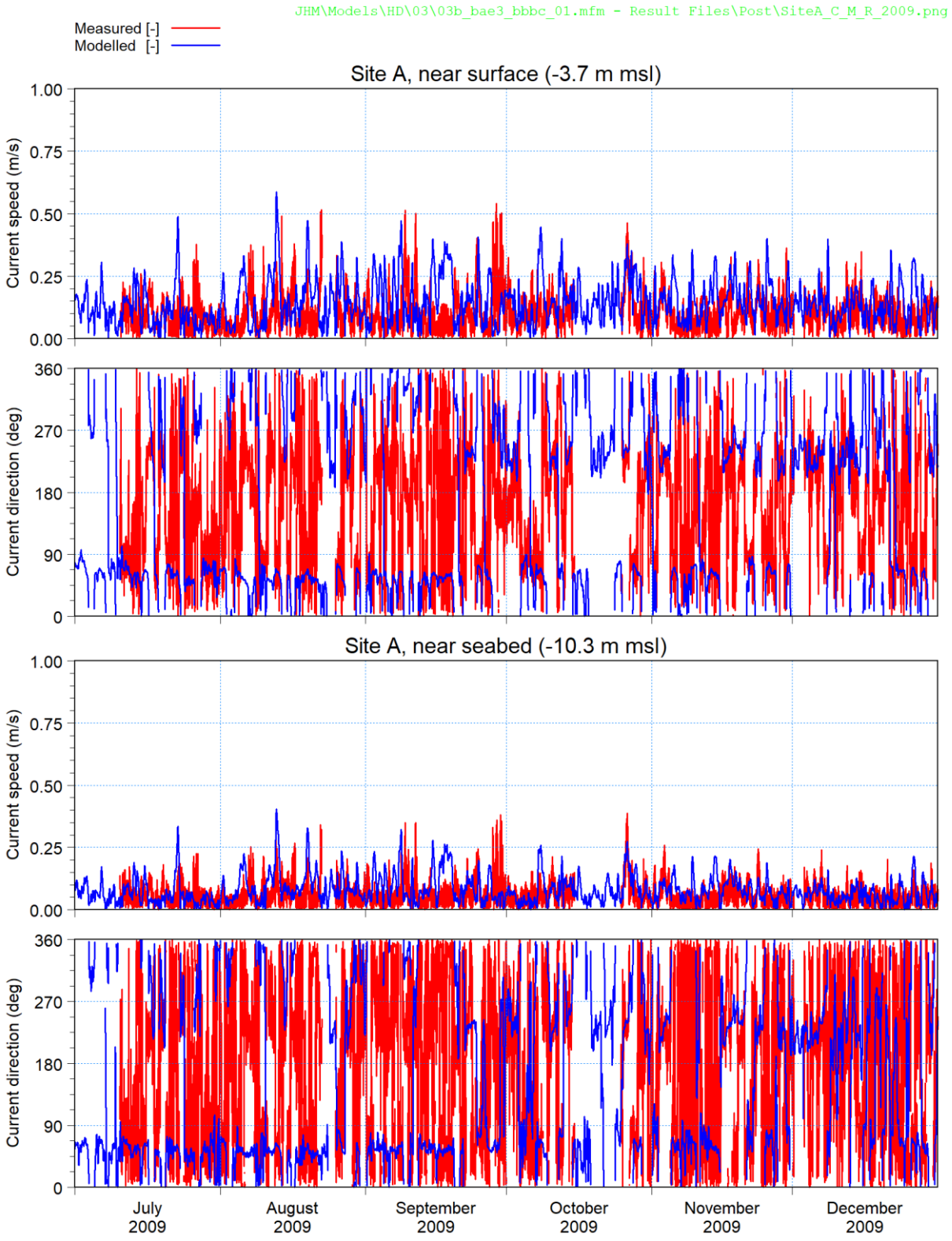


Figure 5.9.A-46: Time-Series Comparison of Modelled and Measured Current Speed and Direction at Site A (Depth -13.2 m msl) for July 2009 to December 2009.

CONTROLLED DISCLOSURE

When downloaded from the EDS database, this document is uncontrolled and the responsibility rests with the user to ensure it is in line with the authorised version on the database.

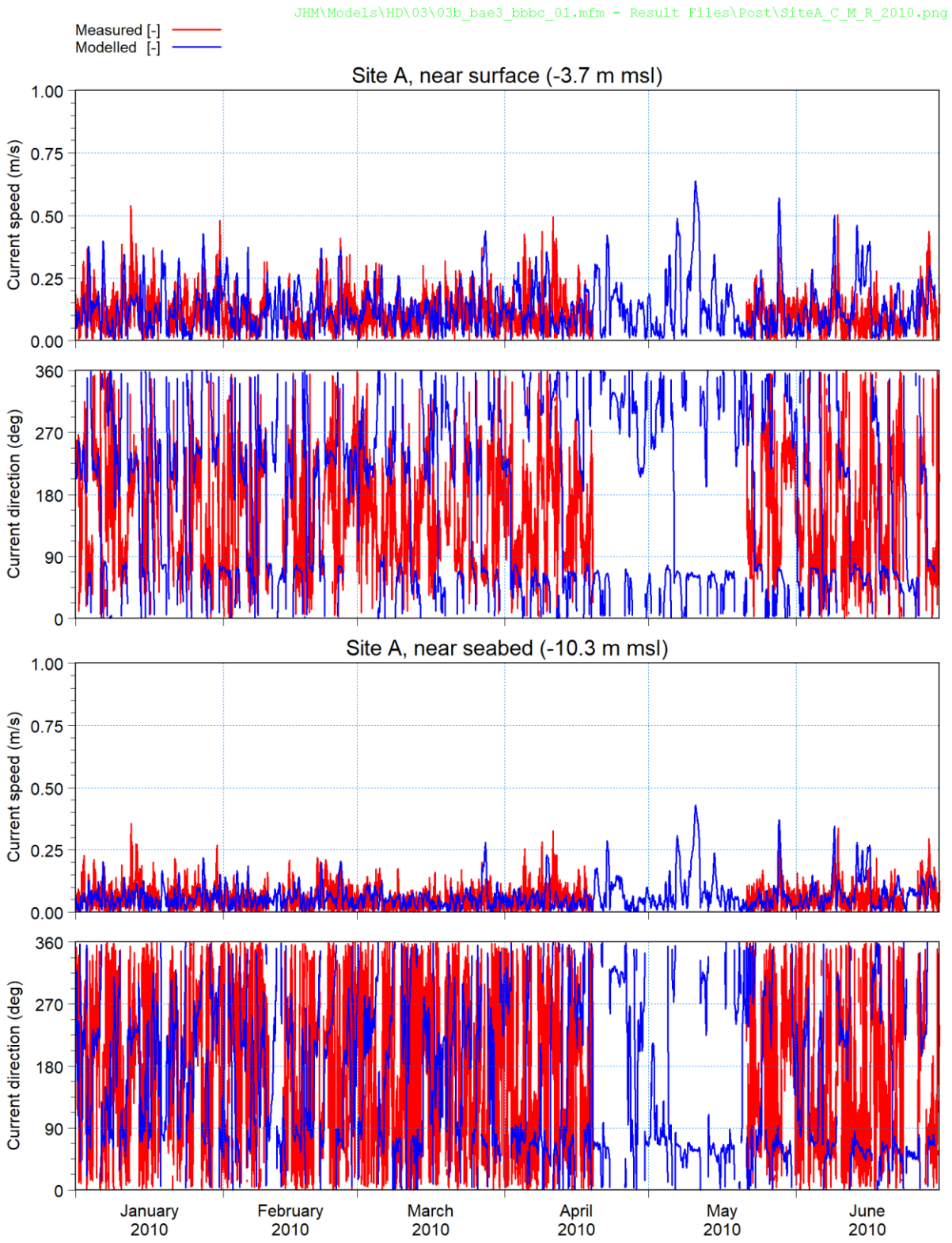


Figure 5.9.A-47: Time-Series Comparison of Modelled and Measured Current Speed and Direction at Site A (Depth -13.2 m msl) for January 2010 to June 2010.

CONTROLLED DISCLOSURE

When downloaded from the EDS database, this document is uncontrolled and the responsibility rests with the user to ensure it is in line with the authorised version on the database.

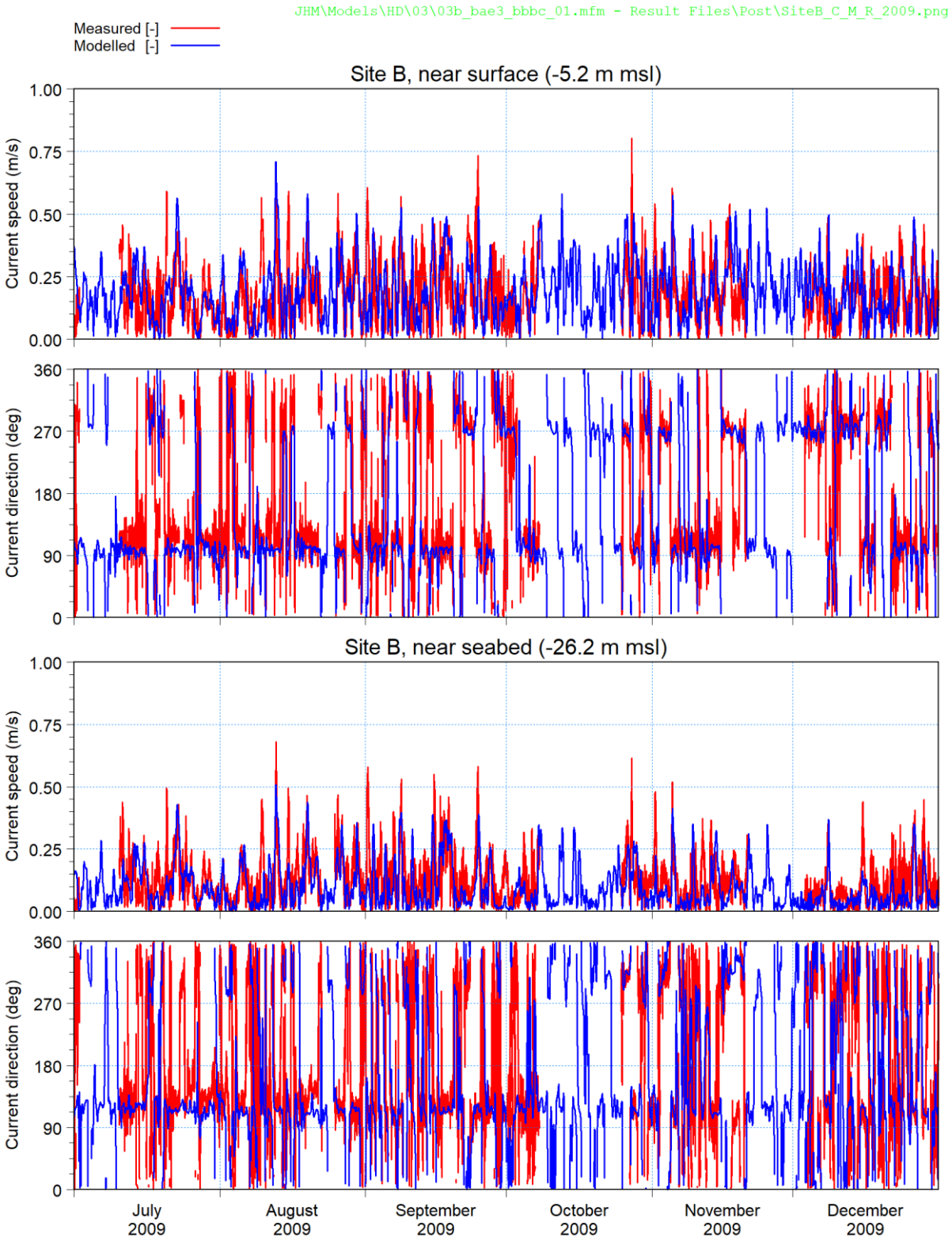


Figure 5.9.A-48: Time-Series Comparison of Modelled and Measured Current Speed and Direction at Site B (Depth -30.8m msl) for July 2009 to December 2009.

CONTROLLED DISCLOSURE

When downloaded from the EDS database, this document is uncontrolled and the responsibility rests with the user to ensure it is in line with the authorised version on the database.

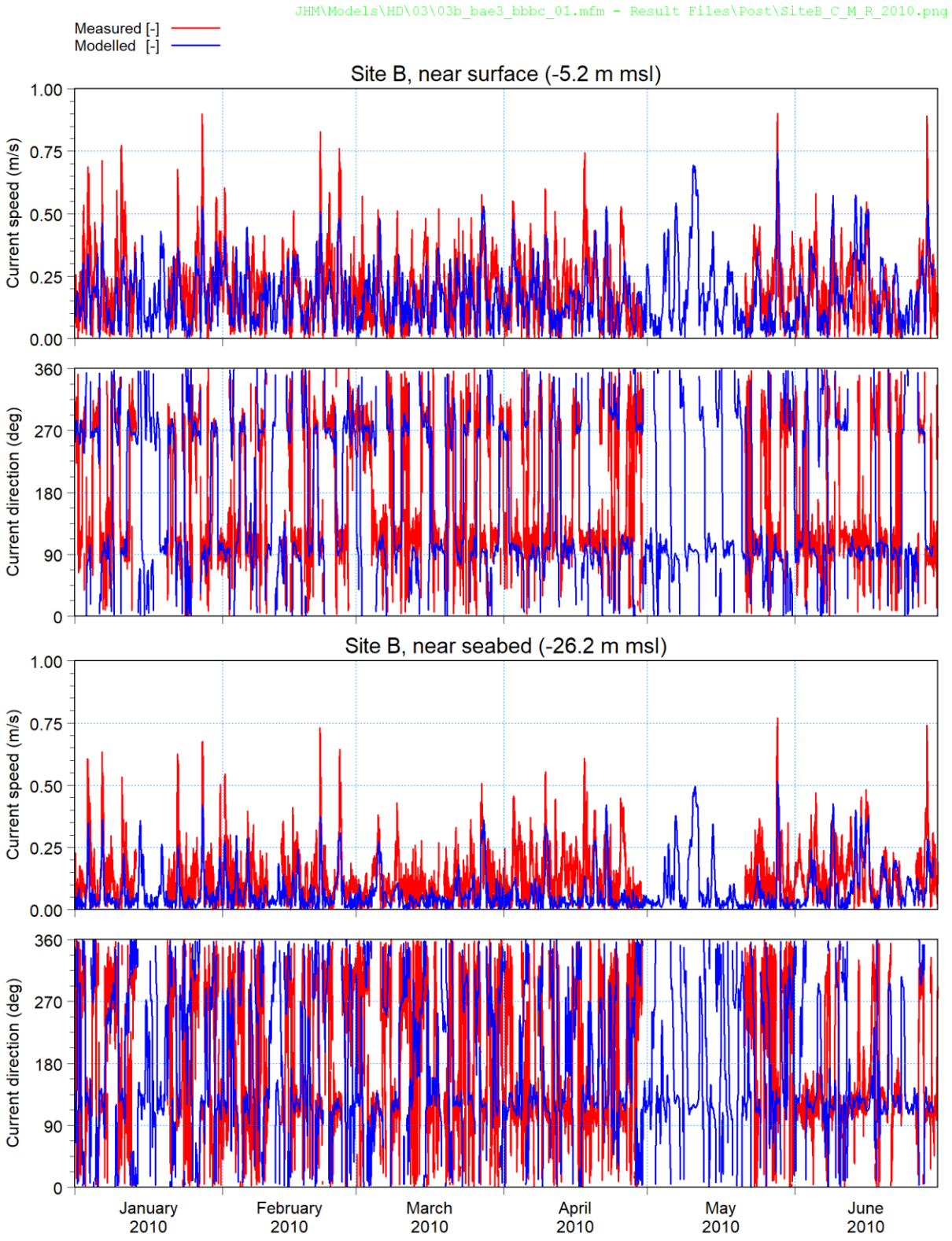


Figure 5.9.A-49: Time-Series Comparison of Modelled and Measured Current Speed and Direction at Site B (Depth -30.8 m msl) for January 2010 to June 2010.

CONTROLLED DISCLOSURE

When downloaded from the EDS database, this document is uncontrolled and the responsibility rests with the user to ensure it is in line with the authorised version on the database.

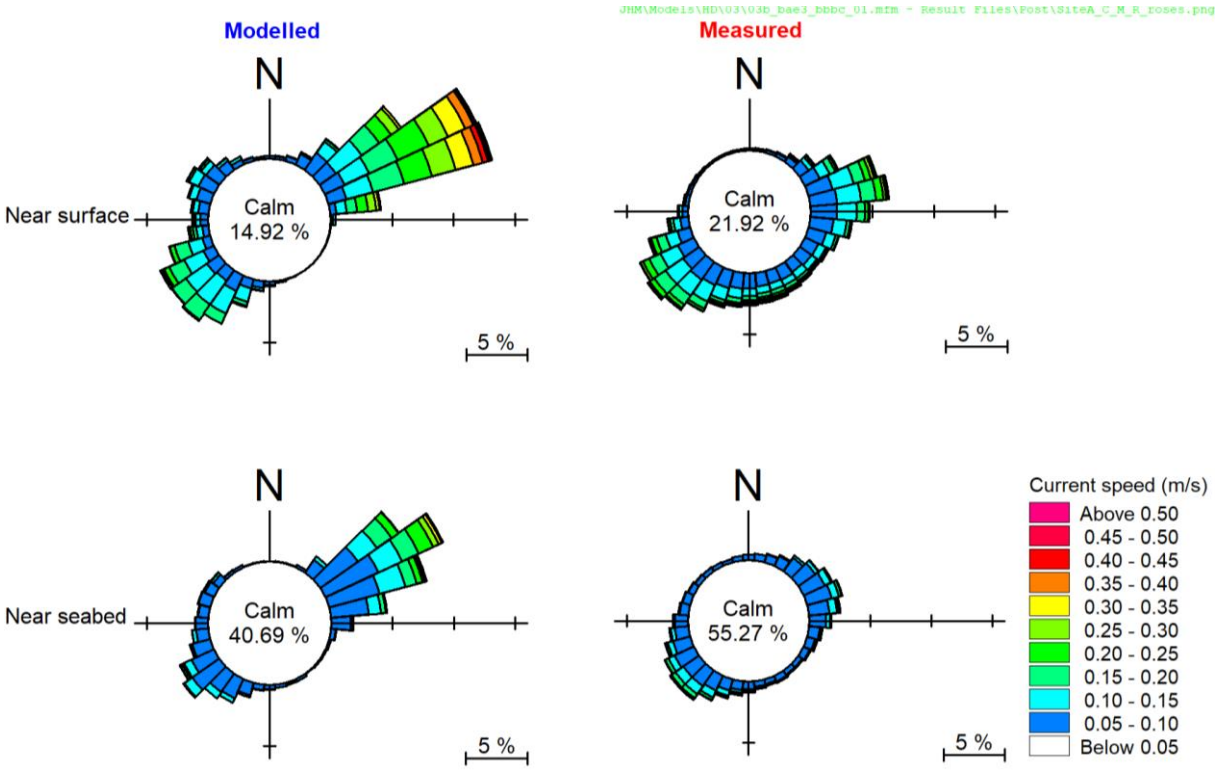


Figure 5.9.A-50: Current Rose Comparison of Modelled and Measured Currents at Site A (1 July 2009 to 30 June 2010).

CONTROLLED DISCLOSURE

When downloaded from the EDS database, this document is uncontrolled and the responsibility rests with the user to ensure it is in line with the authorised version on the database.

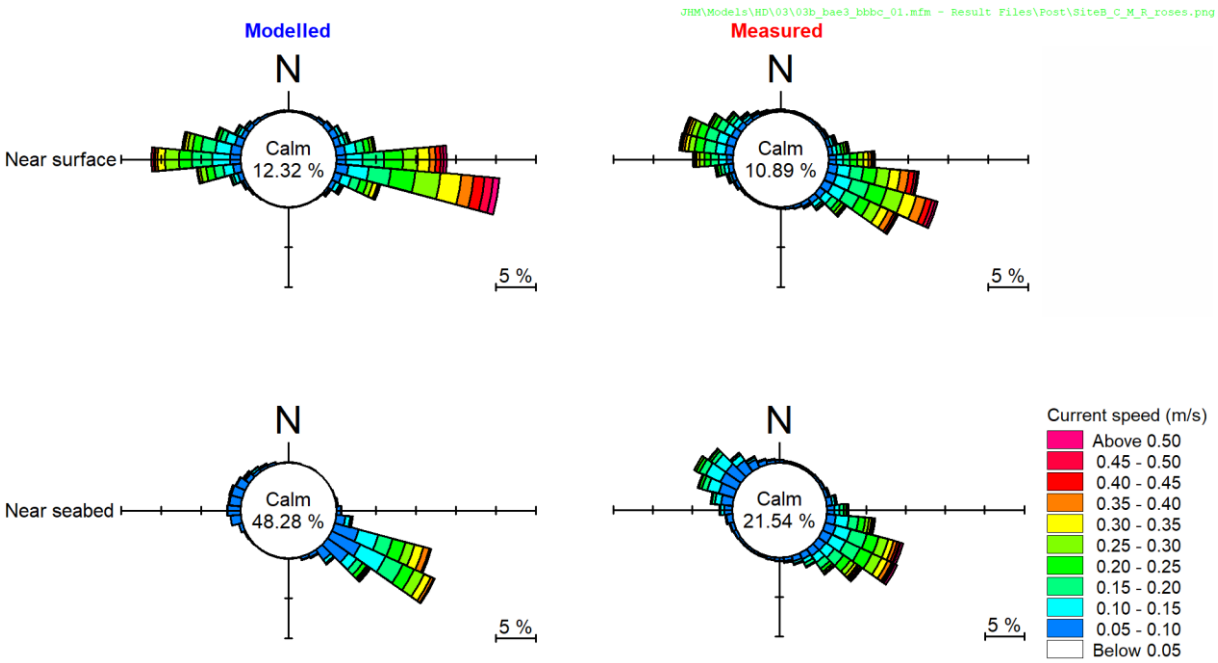


Figure 5.9.A-51: Current Rose Comparison of Modelled and Measured Currents at Site B (1 July 2009 to 30 June 2010).

CONTROLLED DISCLOSURE

When downloaded from the EDS database, this document is uncontrolled and the responsibility rests with the user to ensure it is in line with the authorised version on the database.

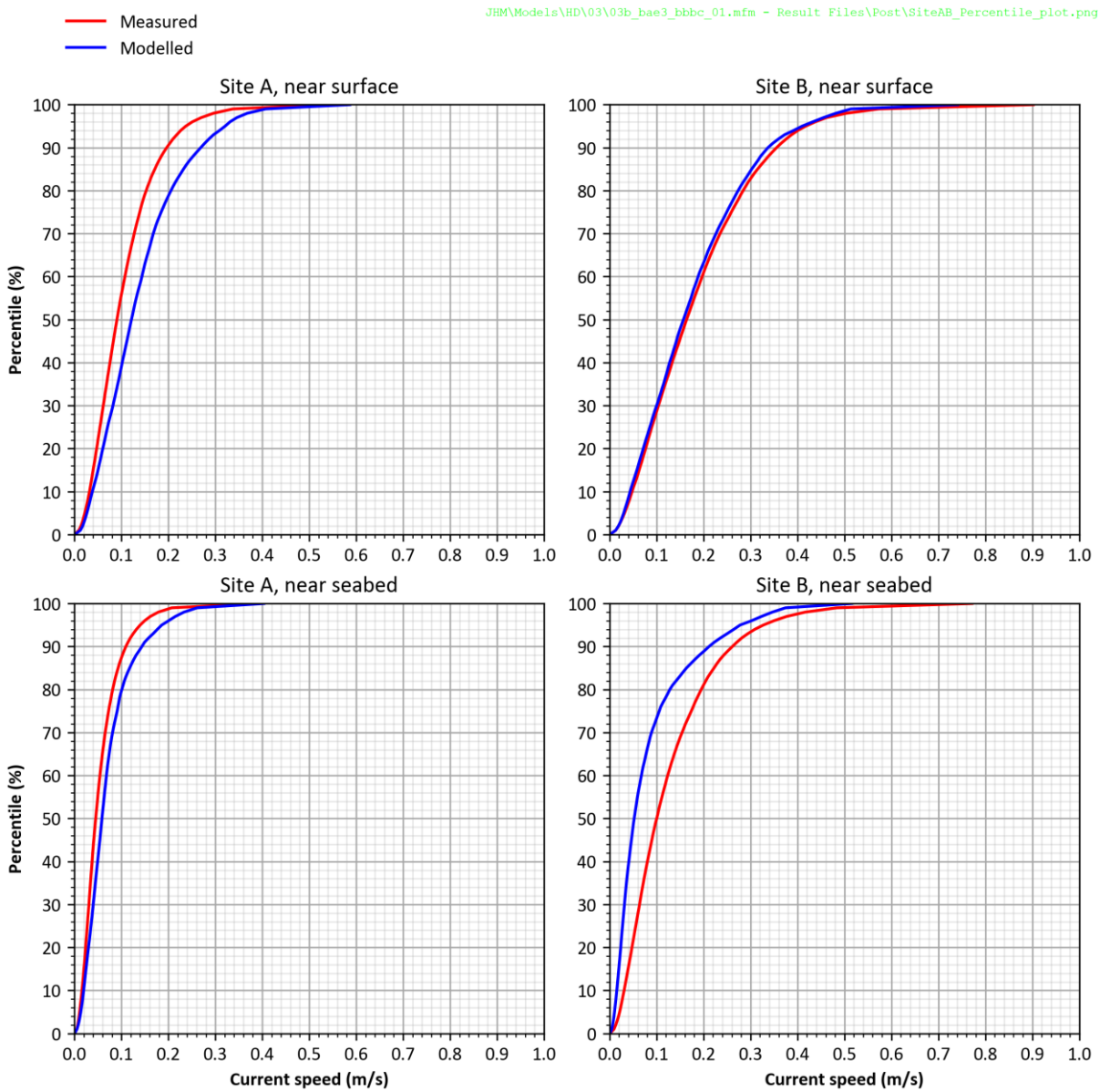


Figure 5.9.A-52: Percentile Comparisons of Modelled and Measured Current Speeds at Site A and B (1 July 2009 to 30 June 2010).

The model tends to slightly overpredict the operational currents at Site A, particularly near the surface. The modelled directions reproduce both primary measured directions well at both depths. The near-surface current speeds at Site B are resolved accurately but some of the extreme events are still underpredicted. Near the seabed, the modelled currents are somewhat underpredicted. The near-seabed directions correlate well, but the model produces fewer currents in the north-westerly direction. The modelled near-surface currents also correlate well but are slightly rotated anticlockwise. Overall the model proved to be capable of simulating the operational currents in three dimensions.

CONTROLLED DISCLOSURE

When downloaded from the EDS database, this document is uncontrolled and the responsibility rests with the user to ensure it is in line with the authorised version on the database.

The modelled temperatures were compared to seabed measurements at Site C (-1.9 m msl), A (-13.2 msl) and B (-30.8 m msl).

Figure 5.9.A-53 presents a time-series comparison of modelled and measured near-seabed seawater temperatures at Site C, A and B. Percentile comparisons of modelled and measured seawater temperatures at Site C, A, and B are shown in ***Figure 5.9.A-54***. Also shown are temperature differences between the three sites. Considering the range of depths (-1.9 m msl to -30.8 m msl) the temperature differences serve as a proxy to temperature stratification in the water column.

CONTROLLED DISCLOSURE

When downloaded from the EDS database, this document is uncontrolled and the responsibility rests with the user to ensure it is in line with the authorised version on the database.

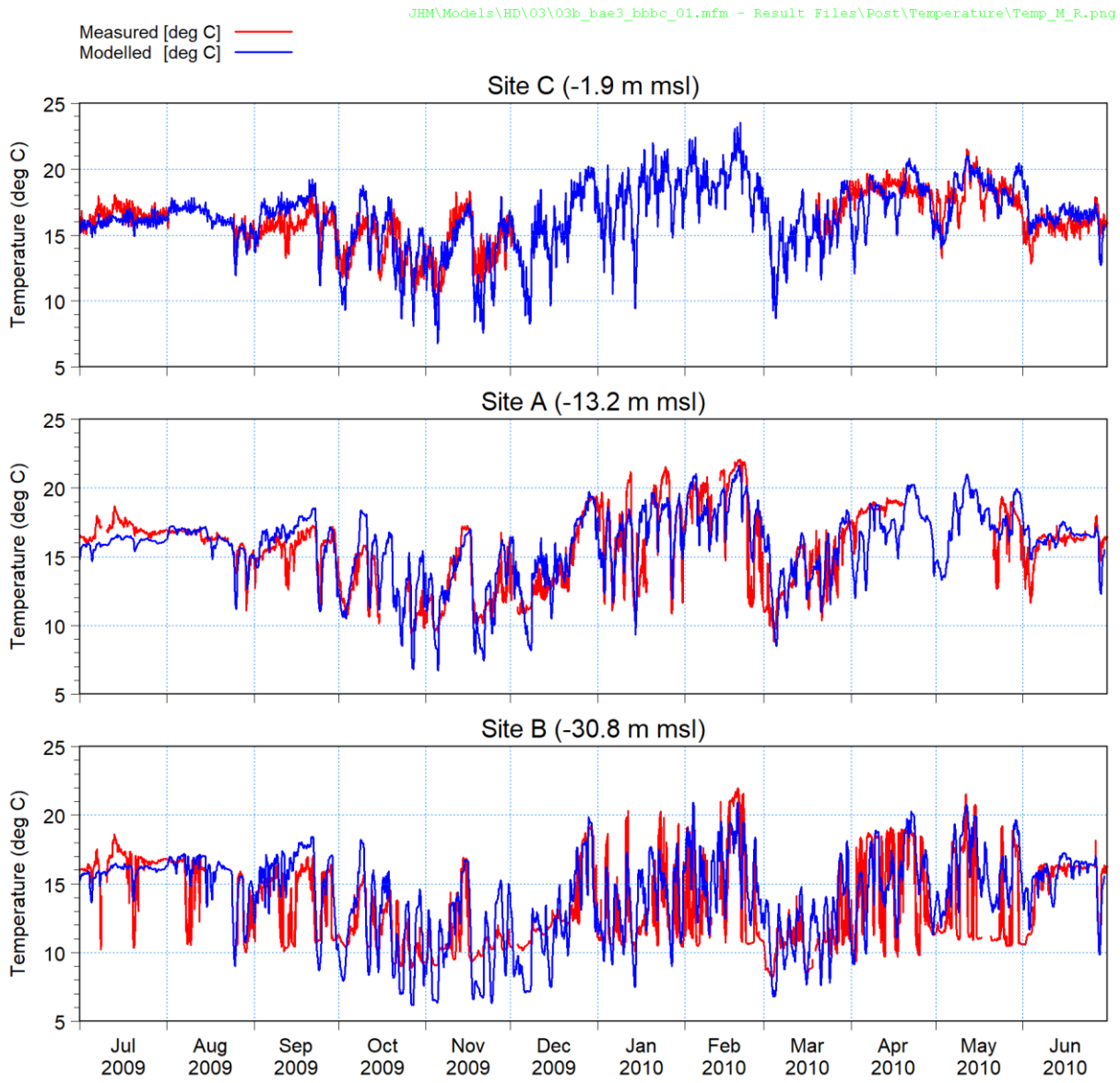


Figure 5.9.A-53: Time-Series Comparison of Modelled and Measured Near-Seabed Seawater Temperatures at Site C, A and B.

CONTROLLED DISCLOSURE

When downloaded from the EDS database, this document is uncontrolled and the responsibility rests with the user to ensure it is in line with the authorised version on the database.

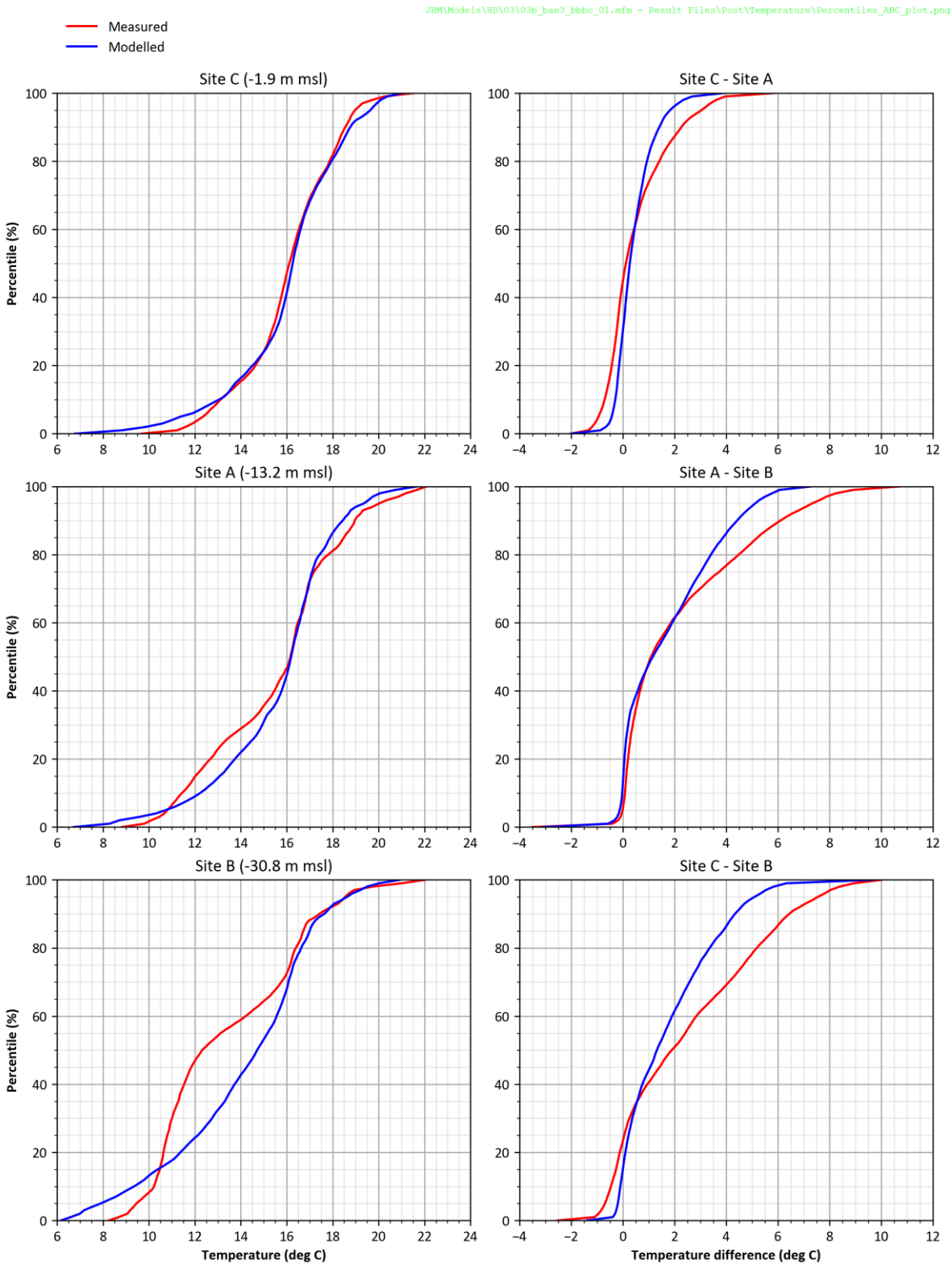


Figure 5.9.A-54: Percentile Comparisons of Modelled and Measured Seawater Temperatures at Site C, A, and B (left), and Temperature Differences Between the Sites (right).

CONTROLLED DISCLOSURE

When downloaded from the EDS database, this document is uncontrolled and the responsibility rests with the user to ensure it is in line with the authorised version on the database.

From the time-series and percentile plots it can be observed that the model is able to predict the mean trend in seawater temperatures and the majority of the upwelling and heating events. However, the modelled temperatures at Site C are at times more variable than the measurements while the modelled temperatures at the deeper Site B underrepresents the variability at times. The temperature distributions show an excellent agreement at Site C and a good agreement at Site A. At Site B the warm temperatures show good agreement, while the measured cold temperatures show a more discrete distribution than the model. As a result, the model tends to underpredict the higher stratification, mostly between Site C and Site B but overall, the modelled and measured stratifications show a good comparison.

CONTROLLED DISCLOSURE

When downloaded from the EDS database, this document is uncontrolled and the responsibility rests with the user to ensure it is in line with the authorised version on the database.